Vol. 17. No 4, 2015

ISSN 1507-2711
Cena: 25 zł (w tym 5% VAT)

EKSPLOATACJA I NIEZAWODNOŚĆ
MAINTENANCE AND RELIABILITY

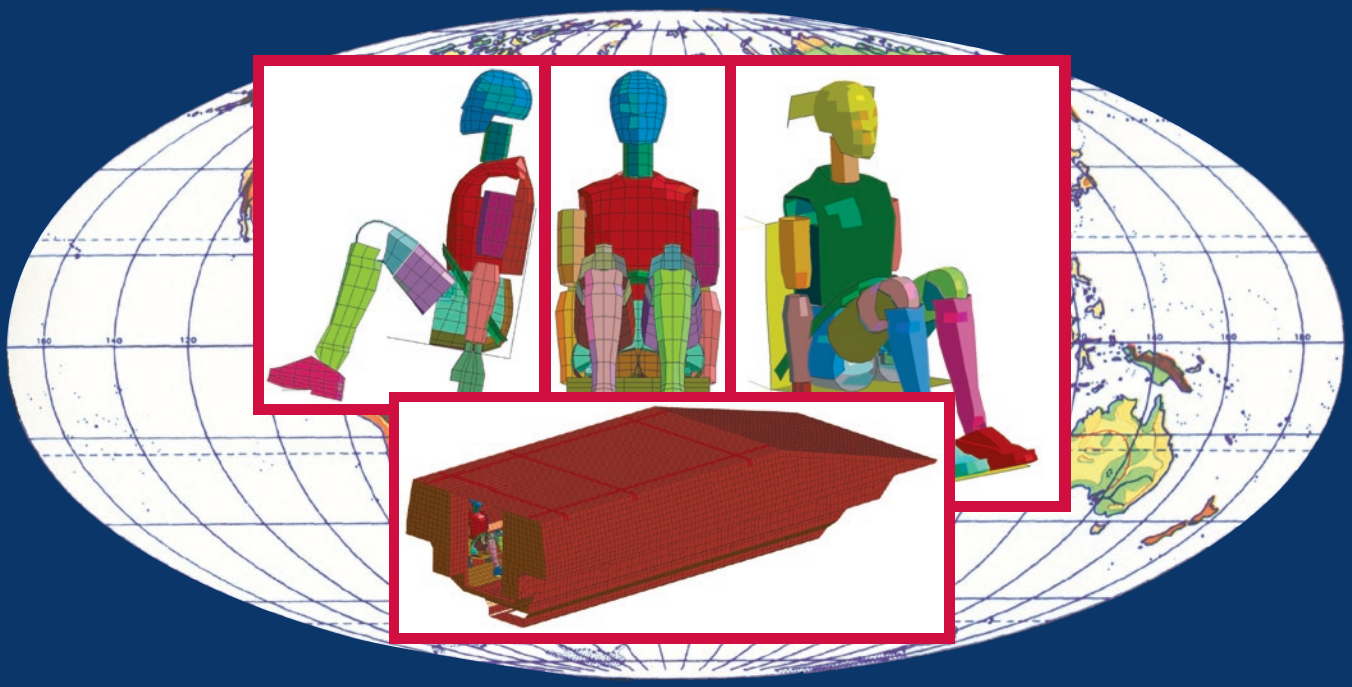

Polskie Naukowo Techniczne Towarzystwo Eksploatacyjne
Warszawa

Polish Maintenance Society
Warsaw

Co-financed by the Minister of Science and Higher Education

The Journal is indexed and abstracted in the Journal Citation Reports (JCR Science Edition), Scopus, Science Citation Index Expanded (SciSearch®) and Index Copernicus International.

The Quarterly appears on the list of journals credited with a high impact factor by the Polish Ministry of Science and Higher Education and is indexed in the Polish Technical Journal Contents database – BAZTECH and the database of the Digital Library Federation.

All the scientific articles have received two positive reviews from independent reviewers.

Our IF is 0,986

Editorial staff:	Dariusz Mazurkiewicz, PhD, DSc (Eng), Associate Professor (Editor-in-Chief, Secretary of the Scientific Board) Tomasz Klepka, PhD, DSc (Eng), Associate Professor (Deputy Editor-in-Chief) Teresa Błachnio-Krolopp, MSc (Eng) (Editorial secretary) Andrzej Koma (Typesetting and text makeup) Krzysztof Olszewski, PhD (Eng) (Webmaster)
Publisher:	Polish Maintenance Society, Warsaw
Scientific patronage:	Polish Academy of Sciences Branch in Lublin
Address for correspondence:	"Eksploatacja i Niezawodność" – Editorial Office ul. Nadbystrzycka 36, 20-618 Lublin, Poland e-mail: office@ein.org.pl http://www.ein.org.pl/
Circulation:	550 copies

Science and Technology

BĘDKOWSKI B, MADEJ J. **The innovative design concept of thermal model for the calculation of the electromagnetic circuit of rotating electrical machines**. Eksploatacja i Niezawodnosc – Maintenance and Reliability 2015; 17 (4): 481–486, http://dx.doi.org/10.17531/ein.2015.4.1.

Operating parameters and reliability of rotating electrical machines are connected to a large extent with their thermal state. The high temperature of these devices has an impact on the life of such elements as bearings, windings, andalso efficiency and possibility of their use. More often, during the analysis of the existingand new designs of electrical machines,the thermal and mechanical calculations are carried out. The finite element method which uses spatial models is commonly used in such calculations. The correct formulation of boundary conditionsand the appropriate model simplifications are the key problems. Parameters calibration of thecalculation model in order to obtain adequate calculations results to the actual device operation is necessary to performed. The innovative conception for determining the thermal parameters of the numerical model for the most complex structure of electrical machinery, which is the electromagnetic circuit, is presented in this paper. During the preparation of the thermal spatial computational models of rotating electrical machines, this method can be used. The proposed simplified monolithic model of the electromagnetic circuit with base on simple experiment calibration method allows to preparethe effective computational model which can be successfully applied in the programs which use the finite element method.

BĘDKOWSKI B, MADEJ J. **Innowacyjna koncepcja budowy obliczeniowego modelu cieplnego dla obwodu elektromagnetycznego wirujących maszyn elektrycznych**. Eksploatacja i Niezawodnosc – Maintenance and Reliability 2015; 17 (4): 481–486, http://dx.doi.org/10.17531/ein.2015.4.1.

Parametry eksploatacyjne oraz niezawodność wirujących maszyn elektrycznychzwiązane są w znacznymstopniu z ich stanem cieplnym. Wysoka temperatura tych urządzeń ma wpływ na żywotność takich elementów jakłożyska, uzwojenie, oraz sprawność i możliwości ich zastosowania. Podczas analizy istniejących konstrukcji maszyn elektrycznych oraz na etapie projektowania nowychprowadzone sącoraz częściejobliczeniawytrzymałościowe i termiczne.Przy obliczeniach takich powszechnie stosowana jest metoda elementów skończonych wykorzystująca przestrzenne modele obliczeniowe, w których zagadnieniem kluczowym jest sformułowanie poprawnych warunków brzegowych oraz przyjęcie właściwych uproszczeń. W celu otrzymania wyniku adekwatnego do rzeczywistej pracy analizowanego urządzenia niezbędne jest przeprowadzenie kalibracji parametrów modelu obliczeniowego. W niniejszej pracy przedstawiono innowacyjną koncepcję określania parametrów cieplnych modelu numerycznego dla najbardziej złożonej struktury maszyn elektrycznych, jaką jest obwód elektromagnetyczny. Metoda ta ma zastosowanie podczas budowy przestrzennych termicznych modeli obliczeniowych wirujących maszyn elektrycznych. Zaproponowany uproszczony monolityczny model obwodu elektromagnetycznego wraz z metodą jego kalibracji za pomocą prostego doświadczenia pozwala na szybkie przygotowanie efektywnegomodelu obliczeniowego, który z powodzeniem może być użyty w programach wykorzystującychmetodę elementów skończonych.

ZHOU J, HUANG N, SUN X, XING L, ZHANG S. **Network resource reallocation strategy based on an improved capacity-load model**. Eksploatacja i Niezawodnosc – Maintenance and Reliability 2015; 17 (4): 487–495, http://dx.doi.org/10.17531/ein.2015.4.2.

Network resource reallocation is a common way to help restore performance of network systems subject to cascading failures. Majority of current network resource allocation strategies either give little regard to or make impractical assumptions about the relationship between capacity and load of network nodes, despite this relationship is closely related to the propagation of network failures. In this work we present and verify an improved nonlinear network capacity-load model based on the actual relation between network capacity and load. According to the verified model and realistic dynamic characteristics of network loads, we propose a new network resource reallocation strategy for networks under attacks from the perspective of maintenance. The strategy aims to effectively reallocate new capacity to network nodes after cascading failures occur. Both theoretical analysis and empirical studies are performed on three typical types of complex networks. Results show that the proposed network resource reallocation strategy is more efficient in mitigating devastating impact of cascading failures on network performance, in comparison to other three existing network resource reallocation strategies.

ZHOU J, HUANG N, SUN X, XING L, ZHANG S. **Strategia realokacji zasobów sieciowych oparta o udoskonalony model przepustowości-obciążenia**. Eksploatacja i Niezawodnosc – Maintenance and Reliability 2015; 17 (4): 487–495, http://dx.doi.org/10.17531/ein.2015.4.2.

Realokacja zasobów sieci jest powszechnym sposobem, stosowanym w celu przywrócenia działania systemów sieciowych objętych awariami kaskadowymi. Większość współczesnych strategii alokacji zasobów sieciowych kładzie mały nacisk lub czyni niepraktyczne założenia dotyczące zależności między przepustowością i obciążeniem węzłów sieci, choć zależność ta jest ściśle związana z rozchodzeniem się awarii sieci. W niniejszej pracy przedstawiono i zweryfikowano udoskonalony nieliniowy model przepustowości-obciążenia sieci na podstawie rzeczywistej relacji między przepustowością sieci i jej obciążeniem. Na podstawie zweryfikowanych modelu i realistycznych cech dynamicznych obciążeń sieciowych, proponujemy nową strategię realokacji zasobów dla sieci poddawanych atakom z perspektywy utrzymania ruchu. Celem strategii jest skuteczna realokacja nowej przepustowości węzłom sieci po wystąpieniu kaskadowych awarii. Przeprowadzono zarówno teoretyczne analizy, jak i badania empiryczne na trzech typowych rodzajach sieci złożonych. Wyniki pokazują, że proponowana strategia realokacji zasobów sieci jest bardziej skuteczna w zwalczaniu niszczącego wpływu kaskadowych awarii na przepustowość sieci w porównaniu do pozostałych trzech wykorzystywanych strategii realokacji zasobów sieciowych.

PŁONKA S, ZABORSKI A. **Operational wear of the neck of spindle coating in cooperation with yarn**. Eksploatacja i Niezawodnosc – Maintenance and Reliability 2015; 17 (4): 496–503, http://dx.doi.org/10.17531/ein.2015.4.3.

The article presents results of research on the operating time of the neck of spindle coating with collapse balloon crown of a ring spinning frame in cooperation with yarn under industrial conditions in the form of histograms. Adopting the change of the diameter of the cylindrical part of the neck of spindle coating is the wear criterion $\Delta d \geq 0{,}5$ mm. The assessment of the spindle neck operating time was performed in cooperation with a mixture of fibres: 70÷80% wool fibres with the addition of 10÷20% of polyester fibres, which causes the greatest wear. The research included measurements with the use of the metric method of the wear of the neck coating of a spindles made of the EN AW-2024 alloy (AlCu4Mg1), which were subjected to finishing operation with abrasive cloth, grain number 80, and then 150 and polished with desilted sandpaper and, in the second variant - they were subjected to burnishing. In addition, roundness deviations of the cylindrical part of the neck of spindle coating were measured at equal distances from face of the crown, using a Talyrond 365 roundness tester. Next, on the basis of the roundness outlines obtained, an outline of the cylindricity of the neck of spindle coating burnished before and after the operating time was prepared. Also, measurements of the topography of the surface of the neck of spindle coating were performed before and after the operating time. An analysis of the cylindricity outline and the surface topography confirms that the outer surface of the surface layer along the length and circumference of the neck of spindle coating in cooperation with yarn is subject to uneven wear. The assessment of the topography of the wearing surface and micro-photographs of the side surface of the helical groove lead to the conclusion that the wear of the neck of spindle coating made of the AlCu4Mg1 occurs mostly as a result of abrasive wear.

PŁONKA S, ZABORSKI A. **Zużycie eksploatacyjne szyjki okładziny wrzecion przędzalniczych przy współpracy z przędzą**. Eksploatacja i Niezawodnosc – Maintenance and Reliability 2015; 17 (4): 496–503, http://dx.doi.org/10.17531/ein.2015.4.3.

W artykule zamieszczono wyniki badań czasu pracy szyjki okładziny wrzecion z nasadką antybalonową przędzarki obrączkowej przy współpracy z przędzą, w warunkach przemysłowych, w postaci histogramów. Przyjmując jako kryterium zużycia zmianę średnicy, części walcowej, szyjki okładziny $\Delta d \geq 0{,}5$ mm. Ocenę czasu pracy szyjki przeprowadzono przy współpracy z mieszanką włókien: 70÷80% włókien wełny z dodatkiem 30÷20% włókien poliestrowych, powodującą największe zużycie. Badania objęły pomiary, metodą metryczną, zużycia szyjki okładziny wrzecion wykonanych ze stopu EN AW-2024 (AlCu4Mg1) poddanych obróbce wykończeniowej przez szlifowanie płótnem ściernym o numerze ziarna 80, a następnie 150 oraz polerowanie papierem ściernym odmulonym, jak również w drugim wariancie - operacji nagniatania. Ponadto wykonano pomiary odchyłki okrągłości części walcowej szyjki okładziny, w równych odległościach od czoła nasadki, za pomocą okrągłościomierza Taylrond 365. Następnie na podstawie uzyskanych zarysów okrągłości sporządzono zarys walcowości szyjki okładziny wrzeciona nagniatanej przed i po czasie eksploatacji. Wykonano również pomiary topografii powierzchni szyjki okładziny wrzecion przędzalniczych, przed i po okresie eksploatacji. Analiza zarysu walcowości i topografii powierzchni potwierdzają, że powierzchnia zewnętrzna warstwy wierzchniej, na długości i obwodzie szyjki okładziny, przy współpracy z przędzą ulega nierównomiernemu zużyciu. Ocena topografii powierzchni zużycia oraz mikrofotografii powierzchni bocznej rowka śrubowego skłaniają do stwierdzenia, że zużycie szyjki okładzin wrzecion ze stopu AlCu4Mg1 następuje przede wszystkim w wyniku zużycia ściernego.

LU Z, ZHOU J, LI N. **Maintainability fuzzy evaluation based on maintenance task virtual simulation for aircraft system**. Eksploatacja i Niezawodnosc – Maintenance and Reliability 2015; 17 (4): 504–512, http://dx.doi.org/10.17531/ein.2015.4.4.

Maintainability is a significant design characteristic of civil aircraft system that has great effect on system availability, life cycle cost and operation safety. A virtual ma-

LU Z, ZHOU J, LI N. **Ocena obsługiwalności oparta na teorii zbiorów rozmytych bazująca na wirtualnej symulacji zadań konserwacyjnych systemów samolotu**. Eksploatacja i Niezawodnosc – Maintenance and Reliability 2015; 17 (4): 504–512, http://dx.doi.org/10.17531/ein.2015.4.4.

Obsługiwalność jest ważną cechą konstrukcyjną systemów stosowanych w samolotach cywilnych, która ma ogromny wpływ na gotowość systemu, koszty eksploatacji i

intenance environment is constructed to support maintainability concurrent design of aircraft system, the evaluation method of maintainability attribute is proposed based on maintenance task virtual simulation or maintainability checklist, and then system maintainability comprehensive evaluation is proposed based on fuzzy theory. A case study, which is maintainability evaluation of a nose landing gear system in civil aircraft, shows the effectiveness of the method presented herein.

BARNAT W. **Numerical examination of the influence of headrest use on the body of a soldier in a vehicle loaded with a 25 kg side load**. Eksploatacja i Niezawodnosc – Maintenance and Reliability 2015; 17 (4): 513–518, http://dx.doi.org/10.17531/ein.2015.4.5.

The issue of specialist vehicle crews' impulse resistance is described in many articles and standardization documents. These publications concern mainly explosives of smaller size. In case of sizeable explosives between 25 and 1000 kg, specialist literature is very poor. In most cases, the existing literature presents the influence of an explosive placed under the vehicle's wheel or body. The following paper focuses on the influence of a 25 kg charge placed on the side of the vehicle on the organism of a soldier staying inside. In this paper the numerical analysis results of the vehicle−explosion mechanical system have been presented. The explosion has1 been modeled using the CONWEP function. The numerical analysis has been carried out in LS-DYNA software. The vehicle has been described by Lagrange elements. The article presents results of numerical calculations for the elements of a combat vehicle's bearing structure charged with an impact generated by an explosion of a big charge placed to the side of the vehicle, at the distance of 5 m from the sideboard, at the height of 1 m. Unfortunately, the method used does not allow for taking into account the phenomena occurring as a result of the wave reflecting off the ground.

DZIUBAK T, SZWEDKOWICZ S. **Operating properties of non-woven fabric panel filters for internal combustion engine inlet air in single and two-stage filtration systems**. Eksploatacja i Niezawodnosc – Maintenance and Reliability 2015; 17 (4): 519–527. http://dx.doi.org/10.17531/ein.2015.4.6.

The parameters of basic filter media used in inlet air systems of internal combustion engines of motor vehicles are presented. Performance properties of the air filters defining their basic parameters are discussed. The effects of single and two-stage filtration systems on performance, including filter medium dust capacity are presented. The methods and conditions for testing non-woven fabric filters in single and two-stage filtration systems were developed. Filter separation efficiency and flow resistance characteristic curves for non-woven fabric filters as a function of dust capacity were determined. Dust capacity of tested non-woven fabrics was determined for allowable flow resistance values. The effects of fractional composition of dust downstream of the inertial filter on reduction of dust capacity of non-woven fabrics in two-stage filtration systems were shown.The advantages including improvement in service life and reduction of wear of engine components due to use of inertial filter as the first filtration stage are presented.

BIAŁAS K, BUCHACZ A. **Active reduction of vibration of mechatronic systems**. Eksploatacja i Niezawodnosc – Maintenance and Reliability 2015; 17 (4): 528–534, http://dx.doi.org/10.17531/ein.2015.4.7.

In the work presented methods of reduction of vibration of mechanical systems using active elements, as well as examples of the implementation of the active reduction of vibration. Also presents a structural-parametric synthesis, which is defined as the design of active mechanical systems with specific requirements. These requirements apply to the value of the frequency of vibration of these systems. Presented at work considerations relate to illustrate the possible implementation of the physical elements of active using electrical components. In the active subsystems can also be used elements in other environments. To examine their effectiveness should be obtained analysis and check what are the interactions subsystems on the primary system.

NIWAS R, KADYAN MS, KUMAR J. **Probabilistic analysis of two reliability models of a single-unit system with preventive maintenance beyond warranty and degradation**. Eksploatacja i Niezawodnosc – Maintenance and Reliability 2015; 17 (4): 535–543, http://dx.doi.org/10.17531/ein.2015.4.8.

This paper presents two reliability models of a single-unit system with the concept of preventive maintenance (PM) beyond warranty and degradation. In both the models, repair of any failure during warranty is cost-free to the users, provided failures are not due to the negligence of users. There is a single repairman who always remains with the system. Beyond warranty, the unit goes under PM and works as new after PM (in both models). In model-1, the unit works as new after its repair beyond warranty whereas; in model-2, the unit becomes degraded. After failure, the degraded unit is replaced by a new one. The failure time of the system follows negative exponential distribution while PM, replacement and repair time distributions are taken as arbitrary with different probability density functions. Supplementary variable technique is

bezpieczeństwo pracy W przedstawionych badaniach stworzono wirtualne środowisko eksploatacji wspierające łatwość obsługi systemów lotniczych; zaproponowana metoda oceny atrybutu obsługiwalności oparta jest o wirtualną symulację zadań konserwacyjnych lub listę kontrolną obsługiwalności. Następnie zaproponowano kompleksową ocenę obsługiwalności systemu opartą o teorię zbiorów rozmytych. Studium przypadku, analizujące obsługiwalność systemu podwozia części nosowej cywilnego samolotu, pokazuje skuteczność metody przedstawionej w niniejszym artykule.

BARNAT W. **Numeryczne badanie wpływu zastosowania zagłówka na ciało żołnierza znajdującego się w pojeździe obciążonym ładunkiem bocznym 25 kg**. Eksploatacja i Niezawodnosc – Maintenance and Reliability 2015; 17 (4): 513–518, http://dx.doi.org/10.17531/ein.2015.4.5.

Problematyka odporności udarowej załóg pojazdów specjalnych jest opisywana w wielu artykułach i dokumentach standaryzacyjnych. Publikacje te głównie dotyczą małych wielkości ładunków wybuchowych oddziałujących na pojazd. W przypadku dużych ładunków, o wielkości od 25 do 1000 kg, literatura tematu jest bardzo uboga. Istniejące pozycje literaturowe odnoszą się do oddziaływania ładunku umieszczonego pod kołem lub kadłubem pojazdu. W pracy przedstawiono wpływ wielkości ładunku 25 kg umieszczonego z boku pojazdu na organizm żołnierza znajdującego się w nim. Przedsięwzięcie to zrealizowano za pomocą analizy numerycznej układu mechanicznego pojazd-wybuch. Wybuch został zamodelowany funkcją CONWEP. Numeryczną analizę przeprowadzono przy użyciu oprogramowania LS-DYNA. Pojazd został opisany elementami Lagrange'a. W artykule przedstawiono wyniki obliczeń numerycznych elementów struktury nośnej wozu bojowego obciążonej udarem wygenerowanym przez eksplozję dużego ładunku wybuchowego umieszczonego z boku w odległości 5 m od burty pojazdu na wysokości 1 m. Zastosowana metoda nie pozwala na uwzględnienie zjawisk Macha zachodzących podczas odbicia fali od podłoża.

DZIUBAK T, SZWEDKOWICZ S. **Właściwości eksploatacyjne włókninowych przegród filtracyjnych powietrza wlotowego silników spalinowych pracujących w układach jedno- i dwustopniowych**. Eksploatacja i Niezawodnosc – Maintenance and Reliability 2015; 17 (4): 519–527. http://dx.doi.org/10.17531/ein.2015.4.6.

Przedstawiono parametry podstawowych materiałów filtracyjnych powietrza wlotowego silników pojazdów mechanicznych. Omówiono właściwości eksploatacyjne filtru powietrza i określające je podstawowe parametry. Przedstawiono wpływ warunków filtracji jednostopniowej i dwustopniowejna właściwości eksploatacyjne, a w tym na chłonność materiału filtracyjnego.Opracowano metodykę i warunki badań włóknin filtracyjnych pracujących w warunkach filtracji jednostopniowej i dwustopniowej. Wyznaczono charakterystyki skuteczności filtracji i oporów przepływu włóknin filtracyjnych w zależności od współczynnika chłonności pyłu. Dla dopuszczalnej wartości oporu przepływu wyznaczonowartości współczynnika chłonności pyłu badanych włóknin. Wykazano wpływ składu frakcyjnego pyłu za filtrem bezwładnościowym na zmniejszenie wartości współczynnika chłonności pyłu włóknin pracujących w warunkach filtracji dwustopniowej. Przedstawiono korzyści w postaci wydłużenia czasu eksploatacji i minimalizacji zużycia elementów silnika wynikające z stosowania filtru bezwładnościowego, jako pierwszego stopnia filtracji powietrza.

BIAŁAS K, BUCHACZ A. **Aktywna redukcja drgań układów mechatronicznych**. Eksploatacja i Niezawodnosc – Maintenance and Reliability 2015; 17 (4): 528–534, http://dx.doi.org/10.17531/ein.2015.4.7.

W pracy zaprezentowano metody redukcji drgań układów mechanicznych przy użyciu elementów aktywnych, jak również przykłady realizacji aktywnej redukcji drgań. Przedstawiono również syntezę strukturalno-parametryczna, która rozumiana jest jako projektowanie aktywnych układów mechanicznych o żądanych wymaganiach. Wymagania te dotyczą wartości częstości drgań tych układów. Przedstawione w pracy rozważania dotyczą zilustrowania możliwych realizacji fizycznych elementów aktywnych przy użyciu elementów elektrycznych. W podukładach aktywnych można stosować również elementy z innych środowisk. Aby zbadać ich skuteczność należy dokonać analizy otrzymanych układów oraz sprawdzić jakie są wzajemne oddziaływania podukładów na układ podstawowy.

NIWAS R, KADYAN MS, KUMAR J. **Analiza probabilistyczna dwóch modeli niezawodności systemu jednoelementowego wykorzystujących pojęcia pogwarancyjnej obsługi profilaktycznej oraz degradacji**. Eksploatacja i Niezawodnosc – Maintenance and Reliability 2015; 17 (4): 535–543, http://dx.doi.org/10.17531/ein.2015.4.8.

W artykule przedstawiono dwa modele niezawodności systemu jednoelementowego wykorzystujące pojęcia pogwarancyjnej obsługi profilaktycznej oraz degradacji. Oba modele zakładają, że w okresie gwarancyjnym użytkownik nie ponosi żadnych kosztów związanych z naprawą uszkodzeń, chyba że uszkodzenie powstało wskutek zaniedbania ze strony użytkownika. Obsługi są wykonywane przez jedną ekipę remontową, która zawsze pozostaje na stanowisku. Po upływie okresu gwarancyjnego, urządzenie podlega obsłudze profilaktycznej i po jej przeprowadzeniu działa jak nowe (w obu modelach). Model 1 zakłada, że element po naprawie pogwarancyjnej działa jak nowy, natomiast w Modelu 2, element ulega degradacji. Zdegradowany element, który uległ uszkodzeniu,

adopted to derive the expressions for some economic measures such as reliability, mean time to system failure (MTSF), availability and profit function. Using Abel's lemma, the behaviour of the system in steady-state has been examined. To highlight the behaviour of reliability and profit function, numerical results are considered for particular values of various parameters and repair cost. Profit comparison of both the models is also made to see the usefulness of the concept of degradation.

zostaje wymieniony na nowy. Rozkład czasu uszkodzenia jest rozkładem wykładniczym ujemnym, a rozkłady czasu obsługi profilaktycznej, wymiany i naprawy są traktowane jako arbitralne, o różnych funkcjach gęstości prawdopodobieństwa. Zastosowana technika dodatkowej zmiennej pozwoliła na wyprowadzenie wyrażeń dla niektórych miar ekonomicznych, takich jak niezawodność, średni czas do uszkodzenia systemu (MTSF), gotowość i funkcja zysków. Zachowanie systemu w stanie ustalonym badano z wykorzystaniem lematu Abela. Aby przedstawić zachowanie funkcji niezawodności i zysków, analizowano wyniki numeryczne dla poszczególnych wartości różnych parametrów oraz kosztów naprawy. Porównanie zyskowności badanych modeli umożliwiło weryfikację przydatności pojęcia degradacji.

LONKWIC P, RÓŻYŁO P, DĘBSKI H. **Numerical and experimental analysis of the progressive gear body with the use of finite-element method**. Eksploatacja i Niezawodnosc – Maintenance and Reliability 2015; 17 (4): 544–550, http://dx.doi.org/10.17531/ein.2015.4.9.

The article presents the results of experimental and numerical simulations of the braking process of new type CHP 2000 progressive gear roller. The gear which is a main element of the friction drive lift safety during braking is exposed to overloading connected with changeable weight loading the gear. Reliable operation of the braking system of the lift, especially in emergency situations, is the basis for the safe operation of these devices. Presented in this paper progressive gear design solution was subjected to tests on test stand and simulations numerical aimed at confirming the required strength and proper functionality of structures subjected to operational loads. Numerical analysis simulation was gear roller displacement during braking from the neutral position to the maximum displacement and the impact load on the alternating stress levels in the gripper elements. The results of numerical calculations verified by experimental studies, analyzing braking distance. The instrument used was a commercial numerical package for calculations using the finite element method – a program Abaqus®.

LONKWIC P, RÓŻYŁO P, DĘBSKI H. **Badania numeryczne i doświadczalne konstrukcji chwytacza progresywnego z wykorzystaniem metody elementów skończonych**. Eksploatacja i Niezawodnosc – Maintenance and Reliability 2015; 17 (4): 544–550, http://dx.doi.org/10.17531/ein.2015.4.9.

W artykule zaprezentowano wyniki badań eksperymentalnych oraz symulacji numerycznych procesu hamowania rolki chwytacza progresywnego nowego typu CHP 2000. Chwytacz będący głównym elementem bezpieczeństwa dźwigu ciernego podczas hamowania narażony jest na przeciążenia związane ze zmienną masą obciążającą układ hamowania. Niezawodna praca układu hamowania dźwigu, zwłaszcza w sytuacjach awaryjnych, stanowi podstawę bezpiecznej eksploatacji tych urządzeń. Zaprezentowane w artykule rozwiązanie konstrukcyjne chwytacza progresywnego poddane zostało próbom stanowiskowym oraz symulacjom numerycznym, mającym na celu potwierdzenie wymaganej wytrzymałości oraz właściwej funkcjonalności konstrukcji poddanej obciążeniom eksploatacyjnym. Analizie numerycznej poddano symulację przemieszczenia rolki chwytacza w trakcie hamowaniaz pozycji neutralnej do pozycji maksymalnego przemieszczenia oraz wpływ zmiennego obciążenia na poziom naprężeń w elementach chwytacza. Wyniki obliczeń numerycznych weryfikowano badaniami eksperymentalnymi, poddając analizie długość drogi hamowania. Zastosowanym narzędziem numerycznym był komercyjny pakiet do obliczeń z wykorzystaniem metody elementów skończonych – program Abaqus®.

LI X, JIA Y, WANG P, ZHAO J. **Renewable warranty policy for multiple-failure-mode product considering different maintenance options**. Eksploatacja i Niezawodnosc – Maintenance and Reliability 2015; 17 (4): 551–560, http://dx.doi.org/10.17531/ein.2015.4.10.

Along with the advancement of manufacturing techniques, the quality of the spares for product is likely to be improved during the warranty period. There can be two types of spares, i.e. low-quality spares and high-quality spares for replacement maintenance. And the manufacturers (customers) may have to decide whether or not to provide (buy) the warranty considering upgrading maintenance. This paper presents a renewing warranty policy considering three maintenance options for products with multiple failure modes. The cost and availability models of these maintenance options are proposed. Of these options, upgrading maintenance is taken into account with the assumption that the warrantied item will be upgraded one time during the warranty cycle. After upgrading maintenance, the high-quality spares are used to replace the failed item. By minimizing the ratio between cost and availability of the product, the optimal upgrading opportunity is obtained. In the numerical example, the results of these options are presented. Monte Carlo simulation results are compared with the analytical results to demonstrate the correctness and efficiency of the proposed models considering upgrading maintenance. The renewing warranty policy considering upgrading maintenance policy is compared with the one without considering upgrading maintenance. The results show that the former is better than the latter in some cases. The sensitivity of the cost model and availability model to different parameters is analyzed at last.

LI X, JIA Y, WANG P, ZHAO J. **Polityka odnawiania gwarancji dla produktówo mnogich przyczynach uszkodzeń uwzględniająca różne opcje obsługi**. Eksploatacja i Niezawodnosc – Maintenance and Reliability 2015; 17 (4): 551–560, http://dx.doi.org/10.17531/ein.2015.4.10.

Wraz z postępem techniki produkcji, wzrasta prawdopodobieństwo, że jakość części zamiennych do produktu ulegnie poprawie w przeciągu okresu gwarancyjnego. Istnieją dwa rodzaje części zamiennych: części zamienne niskiej i wysokiej jakości. Producenci (klienci) mogą być zmuszeni podjąć decyzję czy objąć produkt gwarancją (wykupić gwarancję) zapewniającą konserwację modernizacyjną. W artykule przedstawiono politykę odnawiania gwarancji z uwzględnieniem trzech różnych opcji obsługi produktów narażonych na mnogie przyczyny uszkodzeń. Zaproponowano modele kosztów i gotowości dla omawianych opcji obsługi. Spośród badanych opcji, do dalszej analizy wybrano konserwację modernizacyjną zakładającą, że element podlegający gwarancji zostanie poddany jednokrotnej modernizacji podczas cyklu gwarancyjnego. Po wykonaniu konserwacji modernizacyjnej, uszkodzony element zastępuje się częściami zamiennymi wysokiej jakości. Minimalizując stosunek kosztów do gotowości produktu, uzyskuje się optymalną możliwość modernizacji Przykład numeryczny przedstawia wyniki uzyskane dla omawianych opcji. Wyniki symulacji Monte Carlo porównano z wynikami analitycznymi w celu wykazania prawidłowości i efektywności proponowanych modeli uwzględniających konserwację modernizacyjną. Politykę odnawiania gwarancji uwzględniającą konserwację modernizacyjną porównano z polityką, która takiej konserwacji nie uwzględnia. Wyniki pokazują, że pierwsza z tych opcji jest w niektórych przypadkach korzystniejsza od drugiej. Badania wieńczy analiza czułości modelu kosztów i modelu gotowości na różne parametry.

DRÓŻDŻ K. **Adaptive control of the drive system with elastic coupling using fuzzy Kalman filter with dynamic adaptation of selected coefficients**. Eksploatacja i Niezawodnosc – Maintenance and Reliability 2015; 17 (4): 561–568, http://dx.doi.org/10.17531/ein.2015.4.11.

In the paper issues related to damping of torsional vibrations in electric drive systems with elastic joint with changeable inertia of the load machine using an adaptive control structure are presented. In order to state variables estimation of a drive system, the extended Kalman filter with a dynamic adaptation of selected coefficients has been applied. Adaptation of selected coefficients of the Kalman filter's covariance matrix ensures an improvement of the state variables and parameter estimation quality of the considered drive system with changeable inertia. The element implementing the adaptation is a fuzzy system, whose input signals are a current estimated value of a time constant of the load machine and a processed signal of an absolute value of difference between the electromagnetic and shaft torques. Theoretical considerations and simulation studies have been verified by tests with laboratory set-up.

DRÓŻDŻ K. **Sterowanie adaptacyjne układu napędowego z połączeniem sprężystym wykorzystujące rozmyty filtr Kalmana z dynamiczną adaptacją wybranych współczynników**. Eksploatacja i Niezawodnosc – Maintenance and Reliability 2015; 17 (4): 561–568, http://dx.doi.org/10.17531/ein.2015.4.11.

W artykule przedstawiono zagadnienia związane z tłumieniem drgań skrętnych w elektrycznych układach napędowych z połączeniem sprężystym o zmiennym momencie bezwładności maszyny roboczej poprzez zastosowanie struktury sterowania adaptacyjnego. W celu odtwarzania zmiennych stanu rozpatrywanego układu wykorzystano zmodyfikowany algorytm rozszerzonego filtru Kalmana z dynamiczną adaptacją wybranych współczynników. Adaptacja współczynników macierzy kowariancji zapewnia poprawę jakości estymacji zmiennych stanu i parametru układu w obecności zmiennego momentu bezwładności. Elementem realizującym wspomnianą adaptację jest system rozmyty, którego sygnałami wejściowymi są aktualna estymowana wartość stałej czasowej maszyny roboczej oraz przetworzony sygnał modułu różnicy pomiędzy momentami elektromagnetycznym i skrętnym. Rozważania teoretyczne i badania symulacyjne zostały zweryfikowane przez testy na stanowisku rzeczywistym.

GLOWACZ A. **Recognition of acoustic signals of induction motor using FFT, SMOFS-10 and LSVM**. Eksploatacja i Niezawodnosc – Maintenance and Reliability 2015; 17 (4): 569–574, http://dx.doi.org/10.17531/ein.2015.4.12.

A correct diagnosis of electrical circuits is very essential in industrial plants. An article deals with a recognition method of early fault detection of induction motor. The described approach is based on patterns recognition. Acoustic signals of specific induction motor are analyzed patterns. Acoustic signals include information about motor state. The analysis of the patterns was conducted for three states of induction motor using Fast Fourier Transform (FFT), shortened method of frequencies selection (SMoFS-10) and Linear Support Vector Machine (LSVM). The results of calculations suggest that the method is efficient and can be also used for diagnostic purposes.

GLOWACZ A. **Rozpoznawanie sygnałów akustycznich silnika indukcyjnego z zastosowaniem FFT, SMOFS-10 i LSVM**. Eksploatacja i Niezawodnosc – Maintenance and Reliability 2015; 17 (4): 569–574, http://dx.doi.org/10.17531/ein.2015.4.12.

Prawidłowa diagnostyka obwodów elektrycznych jest bardzo istotna w zakładach przemysłowych. Artykuł zajmuje się metodą rozpoznawania stanów przedawaryjnych silnika indukcyjnego. Opisane podejście jest oparte na rozpoznawaniu wzorców. Sygnały akustyczne określonego silnika indukcyjnego są badanymi wzorcami. Sygnały akustyczne zawierają informację o stanie silnika. Analiza wzorców została przeprowadzona dla trzech stanów silnika indukcyjnego używając FFT, skróconej metody wyboru częstotliwości (SMoFS-10) i liniowej maszyny wektorów wspierających (LSVM). Wyniki obliczeń sugerują, że metoda jest skuteczna i może być również zastosowana dla celów diagnostycznych.

JAKUBOWSKI R. **Evaluation of performance properties of two combustor turbofan engine**. Eksploatacja i Niezawodnosc – Maintenance and Reliability 2015; 17 (4): 575–581, http://dx.doi.org/10.17531/ein.2015.4.13.

This article presents issues connected with modification of a bypass engine with an additional combustion chamber placed between the high pressure and low pressure turbines. At the beginning, on the basis of scientific literature analysis possible benefits were pointed out which follow from modification of a turbofan aircraft engine. First of all, the attention was drawn to a possibility to limit the gas temperature in the exhaust area of a combustion chamber, which helps to reduce NOx in relation to currently used aircraft engines. Then, a design solution scheme of a two combustor engine was presented. It was discussed how this solution modifies the engine cycle. The assumptions and the adopted limitations in the stage of preparing a numerical model of the engine were presented. The main parameters of the engine operating which were used to estimate its functional qualities were characterized. On the bases of an existing high bypass ratio turbofan engine and the assumptions concerning the influence of the mentioned modification of the engine to its internal characteristics performance properties of a two combustor engine in variable performance conditions were determined: for different speeds and flight altitudes. The results were graphically illustrated in the charts in the form of dependences of thrust, specific thrust, fuel consumption and specific fuel consumption vs. the flight speed for different altitudes. In the discussion of the obtained results performance characteristics for standard a high bypass ratio turbofan engine were referred to. On this basis possible benefits which follow from exploitation of the two combustor engine were shown. This engine is characterized by better performance characteristics in comparison to a conventional turbofan engine in the range of transonic velocity. It was pointed out that despite a little higher specific fuel consumption in take-off conditions it can be more economic in further exploitation cycle, which in the case of the aircraft for which it is dedicated, takes place mostly at a transonic velocity at the altitude of about 11 km.

JAKUBOWSKI R. **Ocena właściwości eksploatacyjnychdwuprzepływowego silnika turbinowego z dwiema komorami spalania**. Eksploatacja i Niezawodnosc – Maintenance and Reliability 2015; 17 (4): 575–581, http://dx.doi.org/10.17531/ein.2015.4.13.

W artykule przedstawiono zagadnienia związane z modyfikacją silnika dwuprzepływowego o dodatkową komorę spalania usytuowaną pomiędzy turbiną wysokiego i niskiego ciśnienia. Na wstępie, na podstawie analizy literatury, wskazano możliwe korzyści wynikające z zastosowania takiej modyfikacji lotniczego silnika dwuprzepływowego. Przede wszystkim zwrócono uwagę na możliwość ograniczenia maksymalnej temperatury spalin w przekroju wylotowym komory spalania w silniku tego typu, przez co istnieje możliwość istotnej redukcji NOx w odniesieniu do współcześnie eksploatowanych silników lotniczych. Następnie przedstawiono schemat rozwiązania konstrukcyjnego silnika z dwiema komorami spalania. Omówiono, jak takie rozwiązanie modyfikuje obieg silnika. Przedstawiono założenia i przyjęte ograniczenia na etapie przygotowywania modelu numerycznego silnika oraz scharakteryzowano główne parametry pracy silnika, które wykorzystano do oceny jego właściwości eksploatacyjnych. Na bazie danych istniejącego silnika dwuprzepływowego o dużym stopniu dwuprzepływowości oraz przyjętych założeń odnośnie wpływu omawianej modyfikacji silnika na jego charakterystyki wewnętrzne, wyznaczono osiągi silnika z dwiema komorami spalania w zmieniających się warunkach eksploatacji tj. dla różnej prędkości i wysokości lotu. Wyniki zilustrowano graficznie na wykresach w postaci zależności ciągu, ciągu jednostkowego, zużycia paliwa i jednostkowego zużycia paliwa od prędkości lotu dla różnych wysokości. W dyskusji uzyskanych wyników odniesiono się do charakterystyk eksploatacyjnych dla standardowych silników dwuprzepływowych o dużym stopniu dwuprzepływowości. Na tej podstawie wykazano możliwe korzyści wynikające z eksploatacji silnika z dwiema komorami spalania. Silnik ten cechuje korzystniejszy przebieg charakterystyk eksploatacyjnych od klasycznego silnika dwuprzepływowego w zakresie prędkości okołodźwiękowych. Zaznaczono, że pomimo nieco wyższych wartości jednostkowego zużycia paliwa w warunkach startowych, może on być ekonomiczniejszy w całym cyklu eksploatacyjnym, który w przypadku statków powietrznych do których jest dedykowany, odbywa się w zdecydowanej większości czasu z prędkością okołodźwiękową na wysokości ok 11 km.

BRIŠ R, GRUNT O. **QRA of accidental events initiated by leaks causing a fire in process industries**. Eksploatacja i Niezawodnosc – Maintenance and Reliability 2015; 17 (4): 582–590, http://dx.doi.org/10.17531/ein.2015.4.14.

Risk to safety of personnel in process industries is normally modelled by the application of Event Trees, where the risk is defined as a product of event frequency and its consequences. This method is steady state whilst the actual event is time dependent. For example, gas release is an event comprising the size of gas cloud being released, probabilities of ignition, fire or explosion, fatality, escalation to new releases and fire and/or explosion, and the probability of fatality, all varying with time. This paper brings new perspective, how the risk to safety of personnel could be evaluated in dynamic context. A new approach is presented whereby the time-dependent events and the time-dependent probability of fatality are modelled by means of the analytical computation method based on modeling of different accident scenarios by use of the directed acyclic graph (DAG) and Fault Tree Analysis (FTA) method. Using these methods the modeled scenarios change with relevant probabilities at defined times to configurations with appropriate probabilities of fatalities.The paper uses a realistic example from the offshore industry, where different sizes of leak have different probability characteristics. Specifically small, medium and large leaks are evaluated. Based on the dynamic evolution of the probability of fatality, it is concluded that the most dangerous leak is the large one. Probability of fatality caused by the leak increased very rapidly within first 5 minutes. At the end of 5th minute, there is approximately one order of magnitude difference in the probabilities of fatality associated with the respective leak sizes.

BRIŠ R, GRUNT O. **Ilościowa ocena ryzyka przypadkowych zdarzeń wywołanych przez nieszczelności powodujące pożary w przemyśle przetwórczym**. Eksploatacja i Niezawodnosc – Maintenance and Reliability 2015; 17 (4): 582–590, http://dx.doi.org/10.17531/ein.2015.4.14.

Zagrożenie dla bezpieczeństwa pracowników w przemyśle przetwórczym jest zwykle modelowane za pomocą drzewa zdarzeń, gdzie ryzyko jest zdefiniowane jako iloczyn częstotliwości zdarzenia i jego skutków. Metoda ta dotyczy stanu stacjonarnego, podczas gdy rzeczywiste zdarzenie jest zależne od czasu. Na przykład, ulatnianie się gazu jest zdarzeniem, które wiąże się z wielkością obłoku uwalnianego gazu, prawdopodobieństwem zapłonu, pożaru lub wybuchu, śmiertelnością, eskalacją pod kątem dalszego wycieku i pożaru i/lub wybuchu, oraz prawdopodobieństwem ofiar śmiertelnych, w każdym przypadku zależnie od czasu. Niniejsza praca pokazuje nowe podejście do tego, jak zagrożenie dla bezpieczeństwa pracowników może być rozpatrywane w kontekście dynamicznym. Nowe metoda polega na tym, iż zdarzenia zależne od czasu i zależne od czasu prawdopodobieństwo śmiertelności są modelowane za pomocą analitycznej metody obliczeń opartej na modelowaniu różnych scenariuszy wypadków przez zastosowanie skierowanego grafu acyklicznego (DAG) i metody analizy drzewa błędów (FTA). Dzięki zastosowaniu niniejszych metod, modelowane scenariusze zmieniają się wraz z odpowiednimi prawdopodobieństwami w określonych czasach na konfiguracje z właściwymi prawdopodobieństwami śmiertelności. Artykuł wykorzystuje rzeczywisty przykład z branży morskiej, gdzie różne rozmiary wycieku wykazują różne parametry prawdopodobieństwa. Szczegółowo oceniane są małe, średnie i duże wycieki. W oparciu o dynamiczną ewolucję prawdopodobieństwa ofiar śmiertelnych, należy stwierdzić, że najbardziej niebezpieczny jest duży wyciek. Prawdopodobieństwo ofiar śmiertelnych spowodowanych wyciekiem gwałtownie wzrasta w ciągu pierwszych 5 minut. Na koniec 5. minuty, występuje różnica w przybliżeniu o jeden rząd wielkości w prawdopodobieństwie śmiertelności związanej z odpowiednimi wielkościami wycieku.

WANG Y, ZHAO J, CHENG Z, YANG Z. **Integrated decision on spare parts ordering and equipment maintenance under condition based maintenance strategy**. Eksploatacja i Niezawodnosc – Maintenance and Reliability 2015; 17 (4): 591–599, http://dx.doi.org/10.17531/ein.2015.4.15.

Aiming to optimize the equipment maintenance and the spare parts ordering management jointly, a comprehensive decision model under condition based maintenance (CBM) policy is presented for a single equipment system with continuous and random deterioration. In this model, the equipment deterioration is a continuous Gamma process under a continuous condition monitoring, and the spare parts inventory is controlled by spare parts support probability. Firstly, a spare part support probability model was developed to determine the optimal spare parts stock level S, which is set to meet the requirement of a predetermined stockout probability. Secondly, the equipment replacement and spare parts ordering decision is made to optimize the equipment replacement and spare parts ordering jointly, which is based on the equipment deterioration leveland total operating cost of the system. Thirdly, an integrated decision simulation model is presented for evaluating cost rate, availability and stockout probability. Finally, a numerical example is given to illustrate the performance of this model. The results show that the optimal preventive maintenance threshold obtained from the proposed decision model can satisfy the spare parts support requirements under (S-1, S) inventory control strategy.

WANG Y, ZHAO J, CHENG Z, YANG Z. **Zintegrowany system decyzyjny dotyczący zamawiania części zamiennych i utrzymania ruchu urządzeń w ramach strategii utrzymania zależnej od bieżącego stanu technicznego**. Eksploatacja i Niezawodnosc – Maintenance and Reliability 2015; 17 (4): 591–599, http://dx.doi.org/10.17531/ein.2015.4.15.

Dążąc do jednoczesnej optymalizacji utrzymania ruchu urządzeń i zarządzania zamówieniami części zamiennych, zaproponowano kompleksowy model decyzyjny w ramach strategii utrzymania zależnej od bieżącego stanu technicznego (CBM) przeznaczony dla systemów z pojedynczym urządzeniem i ciągłym oraz losowym zużyciem. W niniejszym modelu, zużycie urządzenia jest ciągłym procesem Gamma z ciągłym monitorowaniem stanu, podczas gdy zapasy części zamiennych są kontrolowane poprzez prawdopodobieństwo wsparcia w zakresie części zamiennych. Po pierwsze, opracowano model prawdopodobieństwa wsparcia w zakresie części zamiennych w celu określenia optymalnego poziomu zapasów części zamiennych S, ustalonej aby spełnić wymogi określonego prawdopodobieństwa braku dostępności. Po drugie, przeprowadzono proces decyzyjny dotyczący wymiany urządzenia i zamawiania części zamiennych w celu jednoczesnej optymalizacji wymiany urządzenia i zamawiania części zamiennych, w oparciu o poziom zużycia urządzenia i całkowity koszt działania systemu. Po trzecie, zaprezentowano zintegrowany symulacyjny model decyzyjny dla oceny poziomu kosztów, dostępności i prawdopodobieństwa jej braku. Zasady niniejszego modelu zilustrowano przykładem numerycznym. Wyniki pokazują, że optymalny próg konserwacji zapobiegawczej uzyskany za pomocą proponowanego modelu decyzyjnego może spełnić wymagania dotyczące części zamiennych w ramach (S-1, S) strategii kontroli zapasów.

KSIĄŻKIEWICZ A, JANISZEWSKI J. **Low voltage relay contact resistance change influence by short-circuit current**. Eksploatacja i Niezawodnosc – Maintenance and Reliability 2015; 17 (4): 600–603, http://dx.doi.org/10.17531/ein.2015.4.16.

Electromagnetic relays are exposed to switching phenomena during its service life. These phenomena may include making of a short circuit, resulting in current flow of significant value for the relay contacts. This current influences the contacts surface and thus the value of the contact resistance, which is an important exploitation parameter for electromagnetic relays.The aim of the study is to analyze the impact of current flow of substantial value on the electric contact resistance of the relay contacts. Significant changes in the resistance after each switching cycle is observed.

KSIĄŻKIEWICZ A, JANISZEWSKI J. **Zmiana rezystancji zestykowej przekaźników niskiego napięcia pod wpływem działania prądów zwarciowych**. Eksploatacja i Niezawodnosc – Maintenance and Reliability 2015; 17 (4): 600–603, http://dx.doi.org/10.17531/ein.2015.4.16.

Przekaźniki elektromagnetyczne w trakcie swojej eksploatacji są narażone na niekorzystne zjawiska łączeniowe. Do narażeń tych można zaliczyć m.in. załączenie obwodu zwartego, co skutkuje przepływem prądu o znacznej wartości przez styki przekaźnika. Przepływ tego prądu, któremu w początkowej fazie może także towarzyszyć łuk elektryczny, wpływa na stan powierzchni styczek, a tym samym na wartość rezystancji zestykowej, będącej istotnym parametrem eksploatacyjnym przekaźników. Celem pracy jest analiza oddziaływania procesów załączania prądu o znacznej wartości na rezystancję zestykową przekaźników. Obserwowane są znaczne zmiany tej rezystancji po każdym cyklu łączeniowym.

KOSICKA E, KOZŁOWSKI E, MAZURKIEWICZ D. **The use of stationary tests for analysis of monitored residual processes**. Eksploatacja i Niezawodnosc – Maintenance and Reliability 2015; 17 (4): 604–609, http://dx.doi.org/10.17531/ein.2015.4.17.

Sustaining high operational efficiency of a machine park requires the use of state-of-art solutions that support both monitoring of residual processes and performing thorough analysis of thereby collected data. What meets the needs of entrepreneurs who strive for high reliability of technological infrastructure is a modern approach to maintenance prediction. The literature of the subject offers numerous studies presenting the use of various statistical models for time series prediction. The objective of this paper is to verify whether tests used in econometrics such as the augmented Dickey-Fuller test and the Kwiatkowski-Phillips-Schmidt-Shin test are suitable for failure prediction. The simulations were performed for one diagnostic parameter, i.e. temperature.

KOSICKA E, KOZŁOWSKI E, MAZURKIEWICZ D. **Wykorzystanie testów stacjonarności do analizy monitorowanych procesów resztkowych**. Eksploatacja i Niezawodnosc – Maintenance and Reliability 2015; 17 (4): 604–609, http://dx.doi.org/10.17531/ein.2015.4.17.

Utrzymanie wysokiego poziomu efektywności eksploatacyjnej parku maszynowego wymaga stosowania nowoczesnych rozwiązań wspierających monitorowanie procesów resztkowych i poddawania szczegółowej analizie uzyskanych w ten sposób informacji. Naprzeciw oczekiwaniom przedsiębiorców dotyczących utrzymywania wysokiego poziomu niezawodności infrastruktury technicznej wychodzi nowoczesne podejście w obszarze gospodarki remontowo-konserwacyjnej, jakim jest predyktywne utrzymanie ruchu. W literaturze przedmiotu wielokrotnie prezentowano wykorzystanie różnych modeli statystycznych pozwalających na prognozowanie wartości szeregów czasowych. Celem niniejszej pracy było sprawdzenie czy stosowany w ekonometrii rozszerzony test Dickeya-Fullera oraz test Kwiatkowskiego, Phillipsa, Schmidta i Shina mogą zostać użyte do predykcji zdarzeń niepożądanych jakimi są awarie. Symulację przeprowadzono dla wartości jednego parametru diagnostycznego jakim była temperatura.

HRYNIEWICZ O, KACZMAREK K, NOWAK P. **Bayes statistical decisions with random fuzzy data – an application for the Weibull distribution**. Eksploatacja i Niezawodnosc – Maintenance and Reliability 2015; 17 (4): 610–616, http://dx.doi.org/10.17531/ein.2015.4.18.

In the majority of decision models used in practice all input data are assumed to be precise. This assumption is made both for random results of measurements, and for constant parameters such as, e.g. costs related to decisions. In reality many of these values are reported in an imprecise way. When this imprecision cannot be related to randomness the fuzzy set theory yields tools for its description. It seems to be important to retain both types of uncertainty, random and fuzzy, while building mathematical models for making decisions. In the paper we propose a fuzzy-Bayesian model for making statistical decisions. In the proposed model the randomness of data is reflected in related risks, and fuzziness is described by possibility measures of dominance such as PSD (Possibility of Strict Dominance) and NSD (Necessity of Strict Dominance). The proposed model allows a decision-maker to reflect in his/hers decisions different types of uncertainty. The theoretical results have been applied in the case of reliability data described by the Weibull distribution.

HRYNIEWICZ O, KACZMAREK K, NOWAK P. **Rozmyto-bayesowski model podejmowania decyzji statystycznych – zastosowanie do rozkładu Weiulla**. Eksploatacja i Niezawodnosc – Maintenance and Reliability 2015; 17 (4): 610–616, http://dx.doi.org/10.17531/ein.2015.4.18.

W większości stosowanych w praktyce modeli decyzyjnych zakłada się, że wszystkie występujące w nich dane wejściowe są podane w sposób precyzyjny. Założenie to dotyczy zarówno losowych wyników pomiarów jak też i stałych parametrów, takich jak np. koszty podjętych decyzji. W rzeczywistości wiele z tych wartości jest podawanych w sposób nieprecyzyjny. Jeżeli taki brak precyzji nie ma charakteru losowego, to teoria zbiorów rozmytych dostarcza narzędzi do opisu tego zjawiska. Wydaje się rzeczą istotną, by przy tworzeniu matematycznych modeli podejmowania decyzji zachować oba typy niepewności: losowość i rozmytość. W pracy proponujemy rozmyto-bayesowski model podejmowania decyzji statystycznych. W proponowanym modelu losowość odpowiada za związane z podjęciem decyzji ryzyko, zaś rozmytość jest opisana przez miary możliwości dominacji, takie jak PSD (Możliwość Ścisłej Dominacji) oraz NSD (Konieczność Ścisłej Dominacji). Zaproponowany model pozwala decydentowi ująć w procesie podejmowania decyzji różne rodzaje niepewności. Rozważania teoretyczne zostały w pracy zastosowane do analizy danych niezawodnościowych opisanych rozkładem Weibulla.

ZUO F-J, YU L, MI J, LIU Z, HUANG H-Z. **Reliability analysis of gear transmission with considering failure correlation**. Eksploatacja i Niezawodnosc – Maintenance and Reliability 2015; 17 (4): 617–623, http://dx.doi.org/10.17531/ein.2015.4.19.

Reliability analysis is of great importance in engineering practices. However, reliability analysis of mechanical system under considering correlation for multiple failure modes is very difficult. Gear is the key component in many mechanical transmission systems and therefore its reliability analysis is very important. Based on the standards of strength calculation of gears and stress-strength interference theory as well as copula theory, the reliability of gear transmission with three failure modes, including gear bending fatigue, gear flank contact fatigue and flank adhesion, is analyzed. The correlation of the three failure modes is studied and reliability of their correlation is also evaluated based on the selected copula functions. The proposed method can be used to facilitate the design, manufacturing, and maintenance planning of gears.

ZUO F-J, YU L, MI J, LIU Z, HUANG H-Z. **Reliability analysis of gear transmission with considering failure correlation**. Eksploatacja i Niezawodnosc – Maintenance and Reliability 2015; 17 (4): 617–623, http://dx.doi.org/10.17531/ein.2015.4.19.

Reliability analysis is of great importance in engineering practices. However, reliability analysis of mechanical system under considering correlation for multiple failure modes is very difficult. Gear is the key component in many mechanical transmission systems and therefore its reliability analysis is very important. Based on the standards of strength calculation of gears and stress-strength interference theory as well as copula theory, the reliability of gear transmission with three failure modes, including gear bending fatigue, gear flank contact fatigue and flank adhesion, is analyzed. The correlation of the three failure modes is studied and reliability of their correlation is also evaluated based on the selected copula functions. The proposed method can be used to facilitate the design, manufacturing, and maintenance planning of gears.

SAMBORSKI S, WIECZORKIEWICZ J, RUSINEK R. **A numerical-experimental study on damaged beams dynamics**. Eksploatacja i Niezawodnosc – Maintenance and Reliability 2015; 17 (4): 624–631, http://dx.doi.org/10.17531/ein.2015.4.20.

This paper focuses on analysis of damage influence on dynamical behaviour of beams. Finite Element Method was used to simulate vibrations of beams under three variants of boundary conditions: a cantilever beam, a simply- supported beam and a symmetrically clamped beam. Analysis of natural frequencies of both intact and damaged beams was performed in order to observe the effect of damage on the beams dynamics. Next, recurrence plot technique was applied. Finally, experimental verification is performed to check the numerical results.

ZUO F-J, YU L, MI J, LIU Z, HUANG H-Z. **Reliability analysis of gear transmission with considering failure correlation**. Eksploatacja i Niezawodnosc – Maintenance and Reliability 2015; 17 (4): 617–623, http://dx.doi.org/10.17531/ein.2015.4.19.

Analiza niezawodności ma ogromne znaczenie w praktyce inżynierskiej. Jednakże, analiza niezawodności układu mechanicznego z uwzględnieniem korelacji dla mnogich przyczyn uszkodzeń jest trudnym zadaniem. Koło zębate jest kluczowym elementem w wielu przekładniach mechanicznych i dlatego analiza jego niezawodności jest niezwykle ważna. W oparciu o normy obliczania wytrzymałości kół zębatych i teorię interferencji naprężeń i wytrzymałości, a także teorię kopuł, przeanalizowano niezawodność przekładni zębatej uwzględniając trzy przyczyny uszkodzeń: zmęczenie zginające koła zębatego, zmęczenie stykowe boku zęba i przyczepność boku. Prześledzono korelację trzech przyczyn uszkodzeń i oceniono niezawodność ich korelacji na podstawie wybranych funkcji kopuł. Proponowana metoda może być stosowana w celu ułatwienia projektowania, produkcji i planowania konserwacji przekładni.

ZUO F-J, YU L, MI J, LIU Z, HUANG H-Z. **Analiza niezawodności przekładni z uwzględnieniem korelacji uszkodzeń**. Eksploatacja i Niezawodnosc – Maintenance and Reliability 2015; 17 (4): 617–623, http://dx.doi.org/10.17531/ein.2015.4.19.

Analiza niezawodności ma ogromne znaczenie w praktyce inżynierskiej. Jednakże, analiza niezawodności układu mechanicznego z uwzględnieniem korelacji dla mnogich przyczyn uszkodzeń jest trudnym zadaniem. Koło zębate jest kluczowym elementem w wielu przekładniach mechanicznych i dlatego analiza jego niezawodności jest niezwykle ważna. W oparciu o normy obliczania wytrzymałości kół zębatych i teorię interferencji naprężeń i wytrzymałości, a także teorię kopuł, przeanalizowano niezawodność przekładni zębatej uwzględniając trzy przyczyny uszkodzeń: zmęczenie zginające koła zębatego, zmęczenie stykowe boku zęba i przyczepność boku. Prześledzono korelację trzech przyczyn uszkodzeń i oceniono niezawodność ich korelacji na podstawie wybranych funkcji kopuł. Proponowana metoda może być stosowana w celu ułatwienia projektowania, produkcji i planowania konserwacji przekładni.

SAMBORSKI S, WIECZORKIEWICZ J, RUSINEK R. **Numeryczno-doświadczalne studium dynamiki belek z uszkodzeniem**. Eksploatacja i Niezawodnosc – Maintenance and Reliability 2015; 17 (4): 624–631, http://dx.doi.org/10.17531/ein.2015.4.20.

W pracy zaprezentowano analizę wpływu uszkodzenia na dynamiczne zachowanie belek. Do symulacji numerycznych użyto Metody Elementów Skończonych gdzie analizowano trzy warianty zamocowania belek: jednostronne utwierdzenie, swobodne podparcie i obustronne utwierdzenie. Przeprowadzono analizę częstości drgań własnych belki nieuszkodzonej i uszkodzonej a następnie zastosowano metodę wykresów rekurencyjnych aby zaobserwować różnice w ich zachowaniu dynamicznym. W ostatnim etapie przeprowadzono weryfikację eksperymentalną uzyskanych wyników symulacji.

Article citation info:
BĘDKOWSKI B, MADEJ J. The innovative design concept of thermal model for the calculation of the electromagnetic circuit of rotating electrical machines. Eksploatacja i Niezawodnosc – Maintenance and Reliability 2015; 17 (4): 481–486, http://dx.doi.org/10.17531/ein.2015.4.1.

Bartłomiej BĘDKOWSKI
Jerzy MADEJ

THE INNOVATIVE DESIGN CONCEPT OF THERMAL MODEL FOR THE CALCULATION OF THE ELECTROMAGNETIC CIRCUIT OF ROTATING ELECTRICAL MACHINES

INNOWACYJNA KONCEPCJA BUDOWY OBLICZENIOWEGO MODELU CIEPLNEGO DLA OBWODU ELEKTROMAGNETYCZNEGO WIRUJĄCYCH MASZYN ELEKTRYCZNYCH*

Operating parameters and reliability of rotating electrical machines are connected to a large extent with their thermal state. The high temperature of these devices has an impact on the life of such elements as bearings, windings, andalso efficiency and possibility of their use. More often, during the analysis of the existingand new designs of electrical machines,the thermal and mechanical calculations are carried out. The finite element method which uses spatial models is commonly used in such calculations. The correct formulation of boundary conditionsand the appropriate model simplifications are the key problems. Parameters calibration of thecalculation model in order to obtain adequate calculations results to the actual device operation is necessary to performed. The innovative conception for determining the thermal parameters of the numerical model for the most complex structure of electrical machinery, which is the electromagnetic circuit, is presented in this paper. During the preparation of the thermal spatial computational models of rotating electrical machines, this method can be used. The proposed simplified monolithic model of the electromagnetic circuit with base on simple experiment calibration method allows to preparethe effective computational model which can be successfully applied in the programs which use the finite element method.

Keywords: *numerical computation, thermal analysis, FEM, operation ofelectrical machines.*

Parametry eksploatacyjne oraz niezawodność wirujących maszyn elektrycznychzwiązane są w znacznymstopniu z ich stanem cieplnym. Wysoka temperatura tych urządzeń ma wpływ na żywotność takich elementów jakłożyska, uzwojenie, oraz sprawność i możliwości ich zastosowania. Podczas analizy istniejących konstrukcji maszyn elektrycznych oraz na etapie projektowania nowychprowadzone sącoraz częściejobliczeniawytrzymałościowe i termiczne.Przy obliczeniach takich powszechnie stosowana jest metoda elementów skończonych wykorzystująca przestrzenne modele obliczeniowe, w których zagadnieniem kluczowym jest sformułowanie poprawnych warunków brzegowych oraz przyjęcie właściwych uproszczeń. W celu otrzymania wyniku adekwatnego do rzeczywistej pracy analizowanego urządzenia niezbędne jest przeprowadzenie kalibracji parametrów modelu obliczeniowego. W niniejszej pracy przedstawiono innowacyjną koncepcję określania parametrów cieplnych modelu numerycznego dla najbardziej złożonej struktury maszyn elektrycznych, jaką jest obwód elektromagnetyczny. Metoda ta ma zastosowanie podczas budowy przestrzennych termicznych modeli obliczeniowych wirujących maszyn elektrycznych. Zaproponowany uproszczony monolityczny model obwodu elektromagnetycznego wraz z metodą jego kalibracji za pomocą prostego doświadczenia pozwala na szybkie przygotowanie efektywnegomodelu obliczeniowego, który z powodzeniem może być użyty w programach wykorzystującychmetodę elementów skończonych.

Słowa kluczowe*:* *obliczenia numeryczne, obliczenia cieplne, MES, eksploatacja maszyn elektrycznych.*

1. Introduction

Growing demands on the efficiency of electric motors, as well as economic aspects and diversity of application cause that in the design of electrical machines not only electrical parameters are important.The higher reliability, minimize weight and dimensions, high strength, and appropriate vibration, noise and thermal stateparameters are required from actually designed and manufactured electrical machines [1, 4-6, 10]. In other words, electrical machines should be optimized to working conditions in which they are operated. This approach necessitate development of newer and more elaborate design. At the same time in the design process of modern electrical machines the interdisciplinary knowledge in the field of electrical engineering, electronics, strength

(*) Tekst artykułu w polskiej wersji językowej dostępny w elektronicznym wydaniu kwartalnika na stronie ***www.ein.org.pl***

of materials, thermodynamics, fluid mechanics and acoustics is required from constructor.

The development of computer technology and constantly increasing computing capabilities have contributed to the development of numerical methods and increasing popularity of programs supporting the work of design engineers. Skillful use of specialized software in the design of electrical machines can increase the efficiency of project work and motor durability simultaneously reducing their weight, vibration, noise and temperature. In the available publications, it can be seen that more often to thedesign analysis of electrical machine researchers use sophisticated computational programs. In addition to the mechanical analysis, software for thermal and flowanalysis based on *FEM* and *CFD* or the Lumped Parameter Modelingis becoming more popular[2].

In the literature related to this subject, different ways of modeling and calibration of computational models and related problemscan bealso found [1, 4-8, 10, 12, 13, 15]. However, in the most recent publications Lumped Parameter Modelingmethodsare described and used to the electrical machines thermal calculations [1, 4-6].

These analyzes allow for the development of innovative solutions of designhigh efficiency electric motors, as well as designing new efficient ways of cooling. For a variety of models, it is possible to create electrical computational models on which we can perform theheat and flow calculations. The most known and developed software forthermal analysisof electrical motors is the *Motor-CAD*. It uses the method of lumped parameter modeling, but also has modules which use*FEA* and *CFD* [1, 4-8, 10, 12, 13, 15]. However, regardless of thesoftware we use to obtain correct simulation results of the thermal condition of electric machines,it is necessary toproperlyidentify the actual or replacement value of thermal parameters of the structural materials and preparing of appropriate computational model.

2. Aims and assumptions of the work

Stator is the one of main element of rotating electrical machine and itis located inside the machine. It consists of a coil made of insulated copper wires, impregnation and lamination stack. These elements createelectromagnetic circuit and they are the main source of heat and at the same time they are responsible for heat energy dissipation from the machine. However,from the point of view of computational techniques, these elements are a complex set of parts and thus adopting appropriate computational model and selecting the right parameters has a huge impact on efficiency and accuracy of the calculation results.

The purpose of this study is to determine the appropriate thermal parameters of the elementary electromagnetic circuit component which isthe part of the whole machine. These parameters will be used to build acomputational thermal model of the complete electromagnetic assembly and developing the correct method for cooling electrical machines.

Thermal properties of the electromagnetic circuit depend on the characteristics of the components as well as their production technology. The most accurate way to determine the replacement thermal properties of components is to carry out tests on samples taken from the materials used in electrical machines built according to the technology used in the manufacturing plant. Such studieswere presented in the work [3],in which the research was conducted on samples using expensive, specialized measurement stations.

This paper proposes a method for determining the thermal parameters of the electromagnetic circuit based on a simple experiment. Such an experiment is possible to carry out in each production facilities and does not require the use of highly specialized measuring equipment.

3. The preparation of the computational model of electromagnetic circuitmethod

3.1. Sampling and verification of the thermal conductivity parameter across thelamination stack

For proper thermal properties selectionof an elementary circuit, lamination stack sample made of *M400-50A* sheet, was prepared (Fig.1). This materialis commonly used in the production of electrical machines' cores. For thermal measurements, special holes in the lamination stack sample were made.

Fig. 1.Sample of the lamination stack

In the most of the publications two-dimensional heat transfer calculation, based on Lumped Parameter Modeling, can be found. Often in these calculations one-dimensional heat distribution along lamination stack is assumed. In the three-dimensional thermal analys is the thermal conductivity parameter across the lamination stack is important. The value of this parameter depends on silicone steel type, kind of insulation and lamination pressure, which is confirmed by the studies presented in [3].

For the determination of the thermal conductivity parameter across the lamination stack the simple experiment was carried out. In the next step the experiment was modeled and solved numerically. On the basis of the experiment results, the thermal parameters were determined by the cyclic numerical simulation. The obtained computational model may be used to the thermal calculation of the complete electrical machine.

During the experiment the heating plate with a power of 125 W was used. The lamination stack sample was placed on the heating plate surface after achievement the temperature of 160°C. To ensure proper contact and heat distribution between the plate and lamination stack sample, the heat carrier plate and thermal paste were used. During the experiment, the temperature was measured by Pt100 sensors at the points shown in Fig. 2. Thermovision camera which is often used to monitor the technical condition of electric machines [9, 11] was also used.

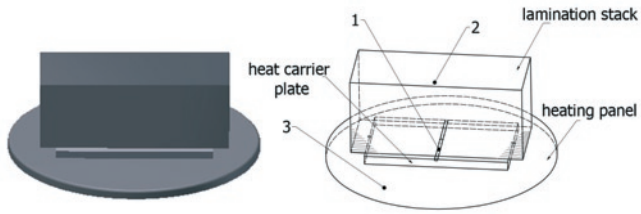

Fig. 2. Thermocouples location: 1-bottom surface of the lamination stack, 2-top surface of the lamination stack 3-heating panel surface, 4-ambient temperature

To provide heat transfer only by natural convection and radiation, the measuring position has been protected from air flow. The tempera-

ture registration continued until steady state was reached. Steady state thermogram is shown in Fig. 3.

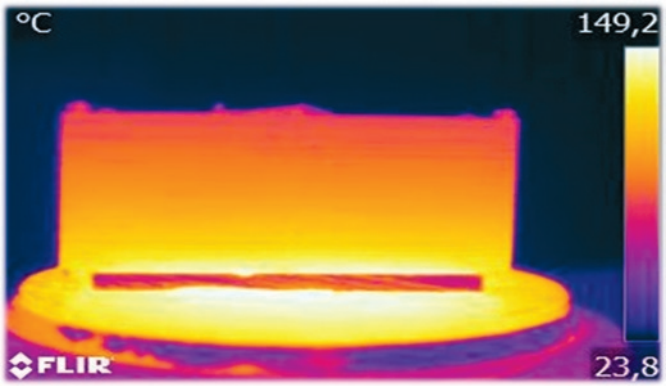

Fig. 3. Steady state thermogram of the thermal conductivity test across the lamination stack

Next the measurement position was modeled in Autodesk Inventor (Fig. 2).Prepared model was imported into Autodesk Simulation CFD to simulate the heat flow. As boundary conditions, parameters corresponding exactly to the conditions prevailing during the experiment were assumed.

They included: initial temperature of the heating plate (~160°C), the heating plate power (125 W), initial temperature of the sample which was equal to ambient temperature (~21°C), the properties of the aluminum heat carrier plate (Cp = 896 J/kgK, l = 203 W/mK) and thermal grease (Cp = 465 J/kgK, l = 0,78 W/mK). Also the phenomenon of radiation and convection were taken into account. The value of the convection parameter was assumed to 7 W/m^2.

For such prepared calculation model, in order to itscalibration, series of transient numerical simulations were performed. During calibration, the value of the thermal conductivity parameter across

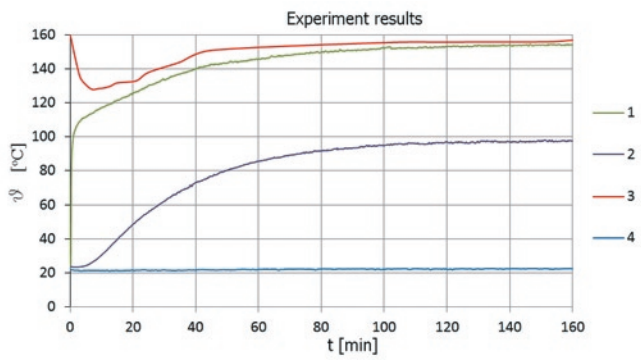

Fig. 4. Temperature distribution at the measuring points 1-4 obtained from laboratory measurements

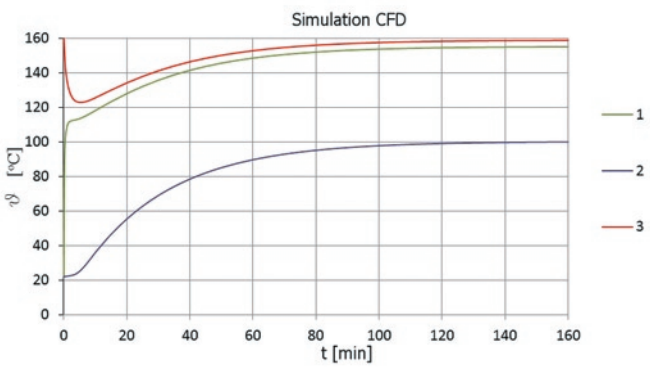

Fig. 5. Temperature distribution at the measuring points 1-3 obtained from numerical simulation

the lamination stack in the range of 1 to 5,6W/mK was changed. According to [3, 6, 13] the specific heat was set up at 490 J/kgK. The best compatibility experiment results with simulations were obtained for lb_z = 3 W/mK. The comparison of the results obtained from the numerical analysis and experiment is shown in Fig. 4 and 5.

Comparing thegraphsin Fig.4 and 5,the agreement of the numerical simulations results with experiment can be seen. On the basis of this comparison the correctness of the assumed computational model, material properties and methods for model calibration is confirmed.

3.2. Sampling and verification of the thermal conductivity parameter along the lamination stack

In order to determine the equivalent thermal conductivity along the lamination stack, similar to that described in section 3.1, experiment was conducted, which then was modeled and solved numerically. A method and procedure for experiment were the same as in the case of determination the thermal conductivity parameter across the lamination stack. During the experiment temperature at the measuring points, shown in Fig. 6, was monitored byPt100 sensors. Steady state thermogram is shown in Fig. 7.

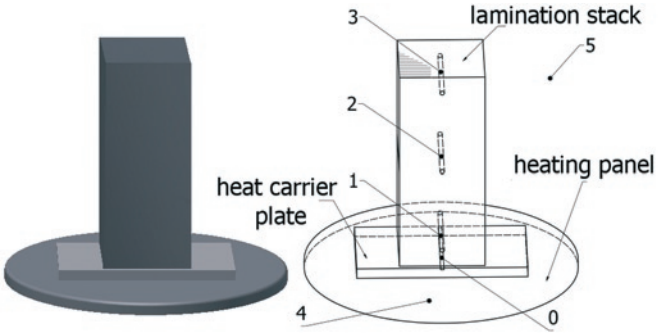

Fig. 6.Thermocouples location: 0-top surface of heat carrier plate, 1,2,3-at holes in the lamination stack 4-heating panel surface, 5-ambient temperature

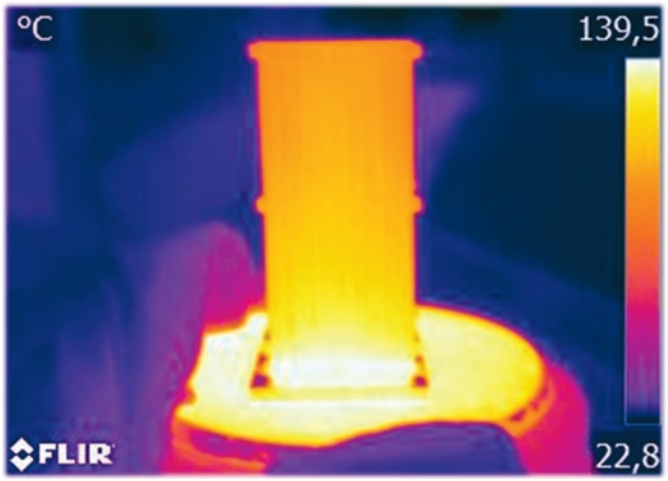

Fig. 7.Steady state thermogram of the thermal conductivity test along the lamination stack

In the numerical simulations thermal conductivity parameter along the lamination stack $\lambda b_{x,y}$ was changed in the range of 20 to 30 W/mK. Specific heat Cp_b as previously was set up at 490 J/kgK. As a result of model calibration, the best simulation compatibility with the experiment results obtained for λb_z=30 W/mK can be observed by comparing the temperature distributions shown in Fig.8 and Fig.9.

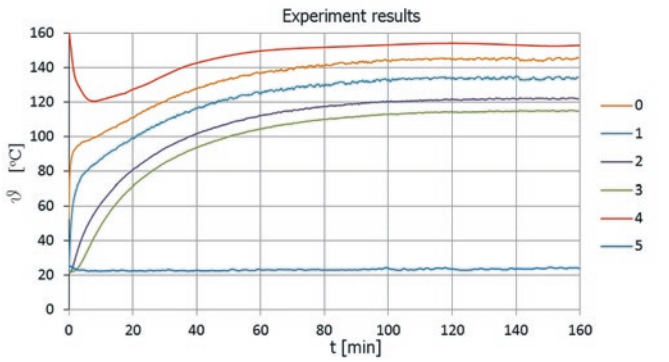

Fig. 8. Temperature distribution at the measuring points 0-5 obtained from laboratory measurements

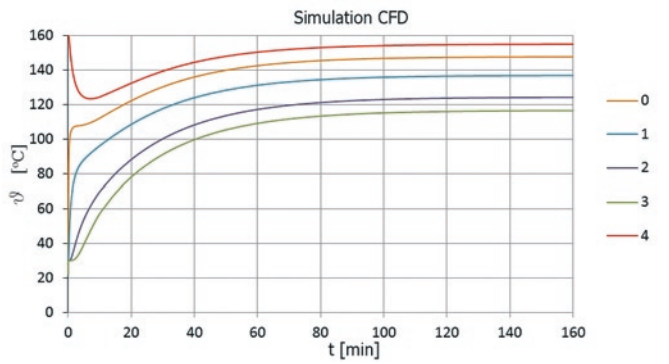

Fig. 9. Temperature distribution at the measuring points 1-3 obtained from numerical simulation

3.3. Accuracy verification of the determination of the slot insulation thermal resistance substitute and coil model parameters replacement

In order to determinethe substitute parameters of slot insulation thermal resistance and thermal properties of electromagnetic circuit model, which is shown in Fig.10, the same as for lamination stack, an experiment was conducted. Also the experiment was modeled and solved numerically.

Fig. 10. Sample of the electromagnetic circuit

A sample of the electromagnetic circuit was prepared according to the most commonly used in manufacture technology stators. Lamination stack was made from laser-cut electrical sheets. The coil windings were made from a round wire ∅0,71 mm. As a slot insulation, a flexible laminate with thickness 0,23 mm was used. Then, the sample was impregnated.

During the experiment the coil winding of the prepared electromagnetic circuit sample was fed with direct current and generated

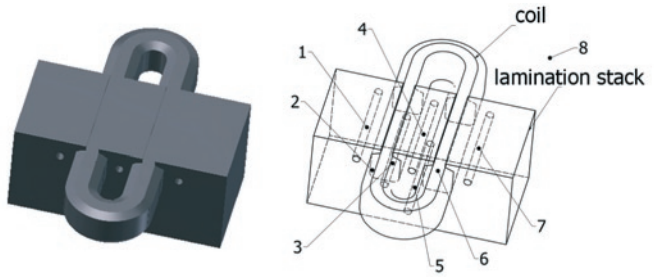

Fig. 11. Thermocouples location: 1,3,4,5,6,7- at holes in the lamination stack, 2-at the bottom of the slot, under slut insulation , 8-ambient temperature

20 W of losses. The temperature was monitoring by Pt100 sensors at the measuring points shown in Fig. 11.

Measuring position has been covered from an air flow to provideheat transfer by natural convection. The study was carried out to achieve a steady state. The steady state thermogram is shown in Fig. 12.

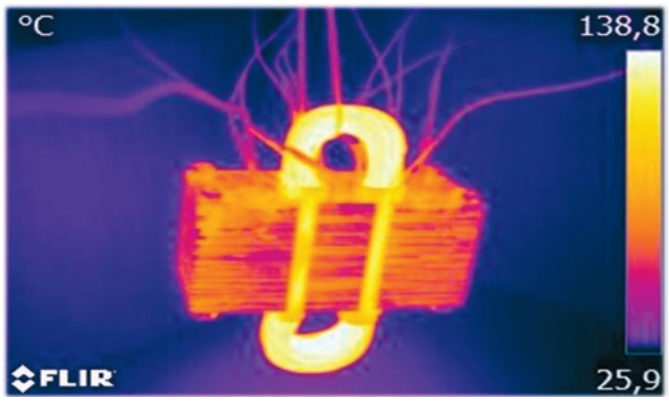

Fig. 12.Thermogram of the sample of electromagnetic circuit

As boundary conditions for the numerical simulation, the same parameters which were measured at the time of conducting research, were set up. The initial temperature of the sample which was equal ambient temperature (~ 21°C), the power supplied to the coil (~ 20 W), and the material properties of lamination stack determined as was described above were determined. The heat exchange to the environment, as in 3.1 and 3.2, includes radiation and convection phenomenon.

A key step in the construction of the numerical model was to develop a model of the winding and slot insulation. Winding was modeled as a monolith. Modeling the slot insulation as a solid causes formation of a thin structure which has an impact on mesh size, and finally the computational time. During the analysis of the spatial model of the whole machine it will increase the number of elements that will make it impossible to carry out effective calculations. Moreover, there is difficulty in determining the effect of slot insulation adhesion to lamination stack and winding, and influence of the applied impregnation and gaps filled with air for final values of the thermal parameter of such insulation. Because of that, in the calculation model a solid model of the slot insulation was replaced by equivalent slot insulation contact thermal resistance parameter $Rc_{\dot{z}}$, calculated on the basis of the known heat flow through the surface of the insulation and temperature drop obtained in steady-state [14, 16]. This alternative method for determining the equivalent thermal resistance of slot insulation is commonly used to determine the thermal parameters of computational models, however, concerns the complete electromagnetic circuit [5, 6], not as in this study a representative sample.

$$Rc_z = \frac{\Delta T}{\dot{Q}/A} \quad (1)$$

In the calculation model, the following thermal properties were set up:

- For the lamination stack:

  Cp_b=490 J/kgK,

  lb_z=3 W/mK,

  lb_{xy}=30 W/mK.
- For the winding:

  Cp_u=380 J/kgK,

  lu_{xy} =190 W/mK,

  lu_z =0,45 W`/mK,

  $Rc_{\dot{z}}$ = 0,0073 Km^2/W.

The equivalent thermal conductivity of the coil across winding-was determined by using the Richter formula, which is valid for the coil with round wires tightlywound and adjacent to each other with the assumption that all voids are filled with varnish.

$$lu_z = cl \quad (2)$$

The c coefficient depends on the ratio of the diameter ***d*** of the wire without insulation and insulated wire diameter ***d'***. For the wire used in the sample winding with a diameter *d* =0,7 1 and *d'*=0,789, Richter's factor takes the value *c* =4,5. With the assumed thermal conductivity of the wire insulation l_i=0,1 W/mK equivalent thermal winding conductivity across winding lu_ztakes the value 0,45 W/mK.

Temperature distribution obtained from laboratory measurements is shown in Fig.13 and obtained by numerical simulation is shown in Fig.14.

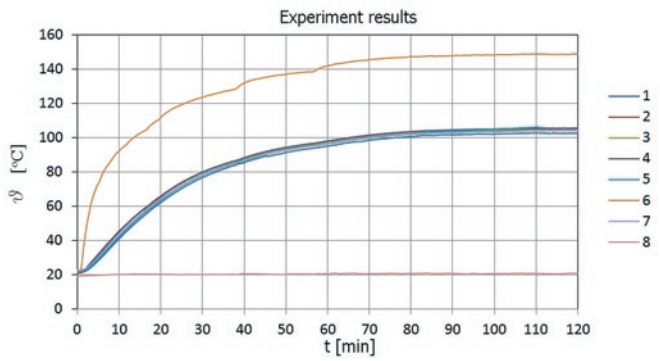

Fig. 13. Temperature distribution of the electromagnetic circuit sample obtained from laboratory measurements

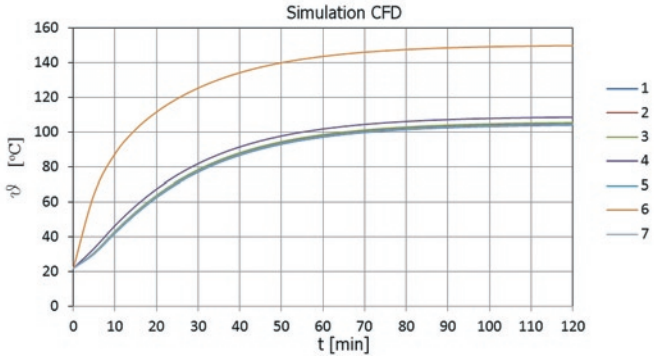

Fig. 14. Temperature distribution of the electromagnetic circuit sample obtained from numerical simulation

Comparing the temperature distribution obtained by numerical simulations and experiment, convergence can be seen. That confirms correct assumption of the calculation model and method of determining the replacement valuesof material properties. Calibrated model of the electromagnetic circuit can be further used to develop a complete electrical machine model.

4. Conclusion

Spatial modeling software allows at the design phase to obtain a virtual machine models. These models are then used for strength and flow calculation which base on the finite element method. However, in the electrical machines analysis it is necessary to select a suitable strategy for construction of computational model. The appropriate simplifications and implementation of adequate parameters are important for correct calculations.

In this paper the possibility of proper preparing of calculation model of the most complicated structure of the electrical machine, which is the electromagnetic circuit, was pointed out. Lamination stack modeling as a body with a thermal conductivity determined by the calibration base on the experiment results, and monolithic coil model with the slot insulation replacement by the substitute thermal contact resistance parameter which is experimentally determined, led to development ofthe effective computational model of electromagnetic circuit. The comparison of the temperature distributions logged during the experiments (Fig. 8 and 13) and the one obtained from numerical calculations (Fig. 9 and 14) conducted with the parameters assumed from the calibration, it can be confirmed that the method of model construction and calibration is correct. The proposed spatial simplified model of the electromagnetic circuit and method of calibration can be used to develop a computational model of the complete electrical machine which will allow for the efficient design of electrical machines with greater reliability using the finite element method.

In the works with similar content, descriptions of different ways of modeling and calibrating computational models and problems associated with them can be find. In the most of the papers, the possibility of use the calculation based on Lumped Parameter Modelingis described [1, 4-8, 10, 12, 13, 15].

References

1. Almandoz G, Poza J, Ugalde G, SanAndres U. Design of Cooling Systems Using Computational Fluid Dynamics and Analytical Thermal odels. IEEE Transactions on Industrial Electronics 2014; 8(61): 4383–4391.
2. Będkowski B, Madej J. The potential of 3D FEM and CFD methods for cooling systems analysis of electrical machines – the premises. Zeszyty Problemowe – Maszyny Elektryczne - Electrical Machines – Transaction Journal 2012;
3. Bennion K. Presentation: Electric Motor Thermal Management. Washington: National Renewable Energy Laboratory, 2012.
4. Boglietti A, Cavagnino A, Lazzari M, Pastorelli M. A simplified thermal model for variable-speed self-cooled industrial induction motor. IEEE Transactions on Industry Applications 2003; 4(39): 945–952, http://dx.doi.org/10.1109/TIA.2003.814555.
5. Boglietti A, Cavagnino A, Staton D. Solving the more difficult aspects of electric motor thermal analysis in small and medium size industrial induction motors. IEEE Transactions on Energy Conversion 2005; 3(20): 620–628.

6. Boglietti A, Mejuto C, Mueller M, Shanel M, Staton D. Evolution and Modern Approaches for Thermal Analysis of Electrical Machines. IEEE Transactions on Industrial Electronics 2009; 3(56): 871-882, http://dx.doi.org/10.1109/TIE.2008.2011622.
7. Coia Y, Colli V D, Marignetti F. Design of axial flux PM synchronous machines through 3-D coupled electromagnetic thermal and fluid-dynamical finite-element analysis. IEEE Transactions on Industrial Electronics 2008; 10(55): 3591–3601.
8. Cheng M, Sun X. Thermal analysis and cooling system design of dual mechanical port machine for wind power application. IEEE Transactions on Industrial Electronics 2013; 5(60): 1724–1733.
9. Głowacz A, Głowacz A, Głowacz Z. Recognition of monochrome thermal images of synchronous motor with the application of quadtree decomposition and backpropagation neural network. Eksploatacja i Niezawodnosc – Maintenance and Reliability 2014; 16(1): 92–96.
10. Hendershot J R, Miller T J E. Design of brushless permanent-magnet motors. Oxford: Magna Physics Publishing and Clarendon Press, 1994.
11. Kuchynkova H, Hajek V. Measurement of temperature of electrical Machines using thermovision camera. Zeszyty Problemowe – Maszyny Elektryczne - Electrical Machines – Transaction Journal 2010; 87: 139-134.
12. Leksell M, Nategh S, Wallmark O, Zhao S. Thermal Analysis of a PMaSRM Using Partial FEA and Lumped Parameter Modeling. IEEE Transactions on Energy Conversion 2012; 2(27): 477-488.
13. Mebarki A, Mejuto C, Mueller M, Shanel M, Staton D. Thermal modelling investigation of heat paths due to iron losses in synchronous machines. Proc. 4th IET International Conference on Power Electronics, Machines and Drives 2008: 225–229.
14. Ozisik, M N. Heat Transfer - A Basic Approach. New York: McGraw Hill, 1985.
15. Staton D A. Thermal computer aided design - Advancing the revolution in compact motors. Proc. International Electric Machines and Drives Conference 2001: 858–863, http://dx.doi.org/10.1109/iemdc.2001.939420.
16. Thomas L C. Heat Transfer – Professional Version, 2nd Edition. Tulsa, Oklahoma: Capstone Publishing Company, 1999.

Bartłomiej BĘDKOWSKI
Jerzy MADEJ
Department of Mechanical Engineering Fundamentals
Faculty of Mechanical Engineering and Computer Science
University of Bielsko-Biała
ul. Willowa 2, 43-309 Bielsko-Biała, Poland
E-mail: bartekbedkowski@wp.pl, juma@ath.bielsko.pl

Article citation info:
ZHOU J, HUANG N, SUN X, XING L, ZHANG S. Network resource reallocation strategy based on an improved capacity-load model. Eksploatacja i Niezawodnosc – Maintenance and Reliability 2015; 17 (4): 487–495, http://dx.doi.org/10.17531/ein.2015.4.2.

Jian ZHOU
Ning HUANG
Xiaolei SUN
Liudong XING
Shuo ZHANG

NETWORK RESOURCE REALLOCATION STRATEGY BASED ON AN IMPROVED CAPACITY-LOAD MODEL

STRATEGIA REALOKACJI ZASOBÓW SIECIOWYCH OPARTA O UDOSKONALONY MODEL PRZEPUSTOWOŚCI-OBCIĄŻENIA

Network resource reallocation is a common way to help restore performance of network systems subject to cascading failures. Majority of current network resource allocation strategies either give little regard to or make impractical assumptions about the relationship between capacity and load of network nodes, despite this relationship is closely related to the propagation of network failures. In this work we present and verify an improved nonlinear network capacity-load model based on the actual relation between network capacity and load. According to the verified model and realistic dynamic characteristics of network loads, we propose a new network resource reallocation strategy for networks under attacks from the perspective of maintenance. The strategy aims to effectively reallocate new capacity to network nodes after cascading failures occur. Both theoretical analysis and empirical studies are performed on three typical types of complex networks. Results show that the proposed network resource reallocation strategy is more efficient in mitigating devastating impact of cascading failures on network performance, in comparison to other three existing network resource reallocation strategies.

Keywords: *network reliability, maintenance, resource reallocation, cascading failures, capacity-load relationship.*

Realokacja zasobów sieci jest powszechnym sposobem, stosowanym w celu przywrócenia działania systemów sieciowych objętych awariami kaskadowymi. Większość współczesnych strategii alokacji zasobów sieciowych kładzie mały nacisk lub czyni niepraktyczne założenia dotyczące zależności między przepustowością i obciążeniem węzłów sieci, choć zależność ta jest ściśle związana z rozchodzeniem się awarii sieci. W niniejszej pracy przedstawiono i zweryfikowano udoskonalony nieliniowy model przepustowości-obciążenia sieci na podstawie rzeczywistej relacji między przepustowością sieci i jej obciążeniem. Na podstawie zweryfikowanych modelu i realistycznych cech dynamicznych obciążeń sieciowych, proponujemy nową strategię realokacji zasobów dla sieci poddawanych atakom z perspektywy utrzymania ruchu. Celem strategii jest skuteczna realokacja nowej przepustowości węzłom sieci po wystąpieniu kaskadowych awarii. Przeprowadzono zarówno teoretyczne analizy, jak i badania empiryczne na trzech typowych rodzajach sieci złożonych. Wyniki pokazują, że proponowana strategia realokacji zasobów sieci jest bardziej skuteczna w zwalczaniu niszczącego wpływu kaskadowych awarii na przepustowość sieci w porównaniu do pozostałych trzech wykorzystywanych strategii realokacji zasobów sieciowych.

Słowa kluczowe: *niezawodnośćsieci, utrzymanie ruchu, realokacja zasobów, awarie kaskadowe, zależność przepustowość/obciążenie.*

1. Introduction

Cascading failure is a common phenomenon in complex network systems, especially in some real-world infrastructure networks, such as transportation systems, power grids and the Internet. It could lead to a sharp degradation of network performance and even collapse the whole network. For example, an initial disturbance happening on August 14, 2003 in Ohio, USA eventually brought about a disastrous blackout which affected millions of people for up to 15 hours [12]. A similar case occurred in Buenos Aires on November 7, 2012, in which the crippled critical power grids triggered large negative effects over one million households, resulting in prolonged chaos in many important departments [15]. Massive cascading failures also take place in communication, social and economic network systems [7, 33]. Due to the devastating effects of cascading failures over the entire networks, it is of great significance to study characteristics of cascades as well as relevant mitigation strategies aiming to protect real-world infrastructure networks.

Optimal resource allocation has been used as a usual way to improve the network robustness to cascading failures [10, 22, 31]. Specifically, overloads (or congestion) on network nodes (edges) are one of the main reasons for triggering cascading failures in networks in reality. For instance, overloads (currents or voltages) on substations or buses in power grids often happen. Hereby, the optimal allocation of limited network capacity resource for reducing the occurrence of overload failures has been one of the hot topics in the complex network study [11, 21, 29, 32, 35, 37]. Lee and Hui [21] proposed a dynamic reallocation scheme based on nodes' willingness to share resources, upon which networks could achieve a better performance. Xia and Hill [35] presented an algorithm that adjusts flow rate and

capacity distribution to maximize the system utility and the utilization ratio of capacity. Wang et al. [32] introduced an idea of cost-based attacks on complex networks and investigated the problem of optimal limited network defence resource distribution for minimizing attacks' damage to infrastructure networks. However, most of current resource allocation strategies are only attempt to optimally allocate resource for initial network construction, ignoring reallocating the subsequent resource after networks are established, and do not take the occurrence of cascading failures under dynamics of network loads into account. In addition, most of prior resource reallocation strategies are still lack of considering essential dynamic characteristics of real-world infrastructure networks which have important impacts on network reliability. Particularly, the practical relationship between capacity and load of infrastructure network nodes is closely related to overload failures in networks.

Considerable research efforts have been carried out to investigate the underlying mechanism of cascading failures in complex networks and network reliability [3, 5, 8, 14, 16, 38, 39]. Crucitti et al. [5] proposed a dynamic flow redistribution scheme for analyzing the cause and process of cascading failures in different complex networks. While most of previous research assumed constant [14, 24], random [17, 33], or linear [5, 20] relationship between capacity and load of nodes in network cascading simulation, Kim and Motter [18] found that there is a nonlinear capacity-load relationship actually exists in different complex infrastructure networks such as air transportation network, highway network, power-grid network and Internet router network. Consequently, prior research on complex infrastructure networks based on the three assumptions about capacity-load relationship mentioned above are inconsistent with real situations to some extent. Dou et al. [8] further researched the nonlinear relationship and presented a capacity-load model (hereinafter referred to as the C-L model) against cascading failures. However, the model has some limitations. For example, it did not identify reasonable ranges of model parameters or give an adequate explanation about the meaning of those parameters. More recently, Fang et al. [10] tackled the issue of capacity-load relationship by introducing the optimization of link capacity allocation. They found that cascade-resilient network systems tend to have a nonlinear capacity-load relation. But they just focused on the link capacity resource used for initial network construction without considering the optimal allocation of subsequent node capacity resource.

To overcome these limitations, in this paper we propose an improved nonlinear C-L model based on the capacity-load relationship of real-world infrastructure networks. Building upon this model and from the perspective of maintenance, we then put forward a new network capacity resource reallocation strategy which takes the subsequently-added network capacity as well as dynamics of network load into consideration. By conducting comparative experiments with three existing capacity resource reallocation strategies, we demonstrate the validity and feasibility of our proposed strategy in mitigating severe influence of cascading failures caused by intentional attacks on complex infrastructure networks.

The rest of this paper is organized as follows: in section 2, the improved nonlinear C-L model is proposed; in section 3, the novel resource reallocation strategy is introduced with theoretical analysis; in section 4, the process of simulating cascading failures in complex networks is described; in section 5, the improved C-L model is verified on two general networks which are subjected to different kinds of attacks, and the simulation results are analyzed; verification of performance of the novel resource reallocation strategy, and comparison with other three existing strategies are presented in section 6. Finally, conclusions as well as directions for future research are given in section 7.

2. The improved C-L model

We assume that the betweenness centrality [13] of network node i at time t represents its load $L_i(t)$ which can be calculated using the algorithm presented in [30]. Node capacity signifies the maximum load that a node could handle without congestion. Crucitti, et al. [5] assumed that because of the limited cost in practice, capacity C_i of node i is linearly proportional to its initial load $L_i(0)$ in real-life networks, as shown in the following widely-used linear C-L model (1):

$$C_i = \alpha \times L_i(0),\ i = 1,2...N,\ \alpha \geq 1 \tag{1}$$

where α is the tolerance parameter, and N is the total number of network nodes.

As mentioned above, nevertheless, different real-world infrastructure networks possess a rather similar nonlinear capacity-load relationship supported by empirical data, which could be simply described as the formula: $C - L \sim L^{\alpha}$, where C represents capacity and L represents load [18]. Accordingly, we propose an improved nonlinear C-L model through curve fitting, intending to match the real data curves. Under our improved C-L model, the description of relationship between network node's capacity and load matches better the actual situations in infrastructure networks which are shown in [18]: heavily loaded network nodes have smaller unoccupied portions of capacity, whereas lightly loaded nodes present larger unoccupied portions of capacity. Our improved C-L model is illustrated in Eq.(2).

$$C_i = \alpha \times \left(L_i(0) + L_i(0)^{1-\mu}\right),\quad i = 1,2...N,\ \alpha \geq 1,\ 0 < \mu < 1 \tag{2}$$

The item $\alpha \times L_i(0)^{1-\mu}$ in the improved C-L model (2) is set to describe the nonlinear characteristic of node capacity and load. α is the tolerance parameter of networks, indicating that the network node capacity is within a realistic cost constraint. Besides, it could also reflect the robustness level of different networks. μ is the nonlinear coefficient, the range of which is set with the consideration of specific situations in real-life networks. By adjusting its value, the corresponding nonlinear relationship between network node's capacity and load could be flexibly adjusted in simulation. In practice, it is more reasonable for us to reference to the data collected from real-world network systems to set these parameters.

Fig. 1 shows an example of the capacity (C)-load (L) relation of network nodes under normal condition in a log-binned scale. The results presented are obtained by applying C-L model (1) and C-L model (2), respectively, in which $\alpha = 1.1$, $\mu = 0.8$. The dashed line, assuming $C = L$ of each network node, is shown in the figure for comparison.

As shown in Fig. 1, the blue curve with symbol '+' (represents the results under the improved C-L model (2)) illuminates the nonlinear capacity-load relationship where the proportion of unoccupied node capacity is larger for nodes with smaller capacity. The smaller a node's capacity, the higher unoccupied proportion of that node's capacity. This nonlinear characteristic is closer to real-world situations in infrastructure networks [20], in contrast with the simulation results under the linear C-L model (1) (represented by the red curve in Fig. 1). In brevity, the improved nonlinear C-L model (2) could better describe the practical flow behavior of real-life infrastructure networks, upon which further analysis of network reliability could be carried out.

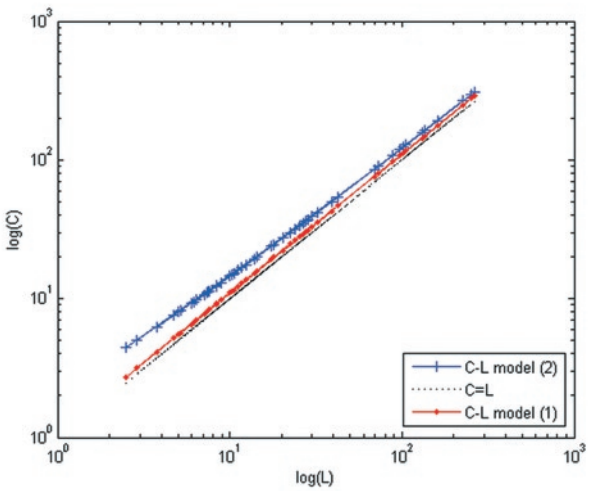

Fig. 1. A comparison between two C-L models' simulation results

3. The proposed resource reallocation strategy

When an infrastructure network system broke down and its performance dropped, depending on the available budget and cost, people usually reallocate some new network resource to a part of important network nodes to maintain the performance of this network (i.e., upgrade those nodes, such as enlarging the capacity of substations in power grids and routers in the Internet). By this way, people intend to restore network performance to some extent to meet the requirements about certain network services. For some real-life infrastructure networks, e.g., power grids, network components upgrade as discussed here is more declined to be taken as a strategic action to maintain network systems, which could work in the long run. While for some other network applications, e.g., the Internet, this action could be adopted as a response to address emergencies as we do in this paper.

In this section, based on the proposed nonlinear C-L model (2), we propose a new capacity resource reallocation strategy (*Cnlinr*) for efficiently reallocating the subsequently-added network capacity against cascading failures. The core part of this new reallocation strategy is described in Eq.(3), which decides the amount of new capacity that every node in the network is reallocated:

$$C_{\Delta i} = \theta \times \left(\frac{L_i(0)}{C_i}\right)^{\eta} \times \left(\frac{L_i(T)}{C_i}\right)^{\gamma} \times \left|L_i(T) - C_i\right| \tag{3}$$

where $0 < \theta \le 1, \eta \ge 1, 0 < \gamma \le 1$, $C_{\Delta i}$ is the subsequent capacity added to arbitrary node *i*, C_i is the initial capacity of node *i*. $L_i(0)$ is the initial load of node *i*, and $L_i(T)$ is its final load at time *T* when network *G* stays stable again after cascades occurred. θ is the scale parameter, and η, γ are nonlinear coefficients. These three arguments, giving a certain degree of flexibility, are used to modify the reallocation proportion of subsequent capacities adding to each network node. By comparing simulation results, we could find a proper combination of the three parameters θ, η and γ for a better capacity reallocation effect in improving performance of damaged networks. The total capacities C_{iall} of network node *i* after capacity resource reallocation are: $C_{iall} = C_i + C_{\Delta i}$.

Specifically, the scale parameter θ in Eq.(3) is used to control the total amount of newly added capacities. The role played by this parameter is mainly for coordinating with the other two model parameters η and γ. Meanwhile, its size could be tuned based on the available capacity resource, signifying the limitation of cost in practice. The second item in Eq.(3), $L_i(0)/C_i$, is the initial load to capacity ratio of node *i*, denoting the nonlinear C-L relationship when the network is under a normal condition, which has a profound influence on the spread of cascades. Consequently, the ratio is highly referred for reallocating new network capacities and the particular scope of parameter η emphasizes the importance of this ratio. The third item $L_i(T)/C_i$ actually reflects the following steady state of node *i* after cascading failures occur from its load viewpoint. Thus, the ratio should also be taken into account in determining the new capacity reallocation proportion. The range of designed parameter γ is set to control the impact of this ratio, $L_i(T)/C_i$. The last item, $\left|L_i(T) - C_i\right|$, in Eq.(3) is the difference between steady load $L_i(T)$ after cascades and corresponding initial capacity C_i of node *i*. This item presents the changes of node load after the dynamic redistribution of network flows resulted from cascades.

According to [18], in many real-world infrastructure networks, the larger a node's load is, the higher proportion of occupied node's capacity is. As a result, the network nodes with larger loads are prone to be overloaded (malfunctioned). Moreover, load-based intentional attacks as well as other attacks, aiming at heavily loaded nodes, would bring a severely adverse influence on network performance if those important nodes break down. Consequently, by taking the redistribution of node loads and its relationship with corresponding node capacities before and after failure propagation into account, we tend to nonlinearly reallocate more subsequent capacity resource to the nodes with larger loads, as illustrated in Eq.(3) above.

Constrained by some real-world factors, e.g., available investment cost, subsequently-added network resource that can be used for reallocation are limited. Hence, different resource reallocation strategies' effects on improving network performance might be very different. In section 'Verification of proposed resource reallocation', we compare our new proposed resource reallocation strategy with other three existing reallocation strategies by simulating cascading failures in scale-free networks, random networks as well as small-world networks. These three types of complex networks are widely-recognized topologies of typical networks nowadays, including the World-Wide-Web, the Internet, social network, the electrical power-grid network, highway network, air transportation network, etc [2, 9, 26, 34]. Simulation results illuminate that the new capacity resource reallocation strategy proposed in this paper could efficiently defend against cascades triggered by intentional attacks on network nodes.

According to related research works [1, 27, 36], some properties of real-life infrastructure networks are independent of sizes of network systems, for example, the relative size of the largest clusters in networks. Thus, for shortening simulation time, network sizes in the simulations presented in this paper are selected but still representative.

4. Cascading process

In this paper, we model a complex network as an undirected, weighted, self loop-free as well as single edge graph *G* with *N* nodes and *E* edges. Single edge graph means that there is only one edge possibly existing between two connected network nodes. For instance, *G* can represent a power grid with *N* stations and *E* transmission lines. Mathematically, it is depicted by an adjacency matrix $\{w_{ij}\}_{N\times N}$ with $w_{ij} \in [0, 1]$ representing the weight (communication efficiency) associated with the edge between node *i* and node *j*. $w_{ij} = 0$ implies that there is no edge between node *i* and node *j*; $w_{ij} = 1$ implies that the edge between node *i* and node *j* works in a perfect condition. We as-

sume that the smaller the entry w_{ij} is, the less efficient communication along the edge between node *i* and node *j* is.

At the initial time of simulation $t = 0$, we set $w_{ij} = 1$ for all existing edges in the network, assuming that those transmission edges all work perfectly. Also, we assume that all network loads are only transmitted along the most efficient paths between a pair of nodes. We use e_{ij} to depict the efficiency of the most efficient path [19] between node *i* and node *j* in the network, which is defined as follows:

$$e_{ij} = \left(\sum \frac{1}{w_k} \right)^{-1} \tag{4}$$

where w_k represents the communication efficiency of edge, as introduced above, involved in the most efficient path between node *i* and node *j*.

Furthermore, network efficiency $E(G)$ defined in Eq.(5) is used to measure the performance of network G [19]:

$$E(G) = \frac{1}{N(N-1)} \sum_{i \neq j \in G} e_{ij} \tag{5}$$

The simulation process of cascading failures in this work is structured as follows: First set up network G, according to the assumptions above, initial node load will not exceed node capacity, and network load distribution along with the most efficient paths will not change. Based on Eq.(5), network efficiency $E(G)$ will remain stable at this stage, i.e., its value will not change, which means that network G is in a steady state. Then the removal (breakdown) of one network node gives rise to the dynamic redistribution of network loads, triggering more overloaded (congestion) nodes. In the next seciton two strategies are explained for choosing the node to be removed. One node removal will lead to alterations of some edges' transmitting efficiencies, i.e., the corresponding entries in $\{w_{ij}\}_{N \times N}$ decrease. As a consequence, the composition and efficiency e of some of the most efficient paths in the network would change, which in turn causes the redistribution of network loads. The above process repeats until all the loads of remaining nodes are below their capacity. At this time, network G stays steady on a lower performance level, which means that network efficiency $E(G)$ eventually converges to a relatively stable value in the cascading simulation. We calculate each edge's weight (transmitting efficiency w) by applying the following iterative rule (6) at every time step t in the simulation [5]:

$$w_{ij}(t+1) = \begin{cases} w_{ij}(0) \times \dfrac{C_i}{L_i(t)}, & L_i(t) > C_i \\ w_{ij}(0) \quad , & L_i(t) \leq C_i \end{cases} \tag{6}$$

where j represents the first neighbor nodes of network node i. As seen in the Eq.(6), the matrix $\{w_{ij}\}_{N \times N}$ is recalculated based on the real-time relationship between node's capacity and load in each simulation step. Through cascading simulations, we can get the overall changing trends of network efficiency $E(G)$, upon which we could observe and further analyze the whole cascading process in the network.

The above cascading failure model based on the complex network theory is relatively comprenhensive and abstract, which has the advantage of using graph theory techniques to model cascading dynamics in real-world infrastructure systems and providing a good understanding of dynamics of cascades. Therefore, it has been recognized to offer a universal perspective and a useful way to research on cascading process on power grids [4, 6, 10].

5. Verification of improved C-L model

In this section, we execute cascading simulations on BA scale-free networks [9] and ER random networks [34]. BA network model is a widely-adopted one to describe scale-free networks, which possesse a power-law distribution of node degree. Note that $P(k)$ represents the distribution probability of network nodes with degree k, $P(k) \sim k^{-\gamma}, \gamma \approx 3$. Similarly, ER network model, proposed by Erdos and Renyi, is a typical model for constructing random networks, whose load distribution and degree distribution all follow the Poisson distribution. Two representative triggering strategies are used here: load-based intentional attack where a network node with the largest load is removed; and random failure where one node chosen at random will be removed from the network. By analyzing the cascading process and the difference generated by adopting the existing linear C-L model (1) and the improved C-L model (2), the performance and feasibility of our improved nonlinear C-L model (2) is validated.

5.1. Simulation on BA scale-free network

The simulation process of an intentional attack on a BA network is as follows: At first, initial network capacities are allocated to network nodes according to the nonlinear C-L model (2). Then the node with the largest load is removed, causing the dynamic redistribution of network loads which is accompanied with a cascade of overload failures. Meanwhile, the weight of each edge and network average efficiency $E(G)$ at every simulation time step are calculated until network G reaches a steady state again. The same process is repeated for the linear C-L model (1). Moreover, the similar cascading simulations are performed for both of the considered C-L models under a random failure where the node initially removed is chosen at random. To minimize random errors, simulation results under random failures correspond to the average of results over four failure triggers.

Fig. 2 and Fig. 3 illustrate the evolution of network efficiency $E(G)$ after intentional attack on the node with the heaviest load in a BA network ($N = 100$, $E = 500$) under C-L models (2) and (1), respectively. Parameters used are $\mu = 0.3$ and $\alpha = 1.01, 1.05$. Apparently, the changing trends of network efficiency $E(G)$ under two C-L models are quite different. The collapse factor Cp shown in the figures means the rate of decline in network efficiency caused by cascading failures. Cp is the ratio of the difference between initial efficiency $E(0)$ and steady efficiency $E(T)$ after cascades spread to initial network efficiency $E(0)$, as the following equation (7) shows. This factor could clearly illuminate the degradation of network efficiency caused by cascading failures:

$$Cp = (E(0) - E(T)) / E(0) \tag{7}$$

We define that a range of ± 2 % on the steady value of network efficiency $E(G)$ is the error band of network efficiency in this paper. Transition time T_r is the time when network efficiency remains stable again within the error band after cascades take place, which manifests that the network reaches the stationary state. Values of T_r obtained in the cascading simulations on BA networks subject to intentional attacks are shown in Table 1. The unit of T_r is the simulation time step.

Table 2 shows experimental results of T_r and decrease extent of collapse in network efficiency (ΔEd) in the simulations on the BA network ($N = 100$, $E = 500$) which is subjected to random failures. ΔEd is calculated according to the following equation (8):

$$\Delta Ed = (E_{\Delta 1} - E_{\Delta 2}) / E_{\Delta 1} \tag{8}$$

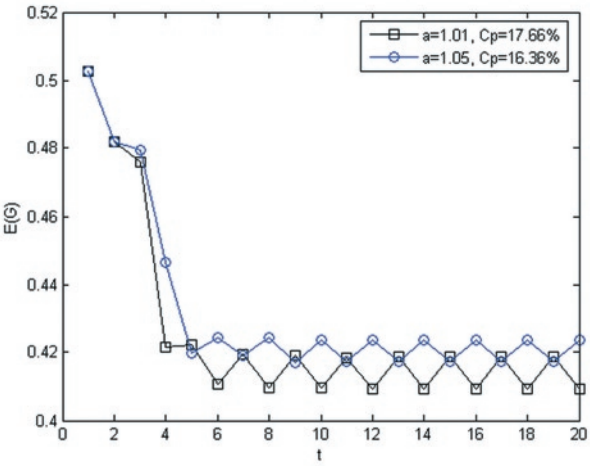

Fig. 2. Changing curves of BA network efficiency under C-L model (2)

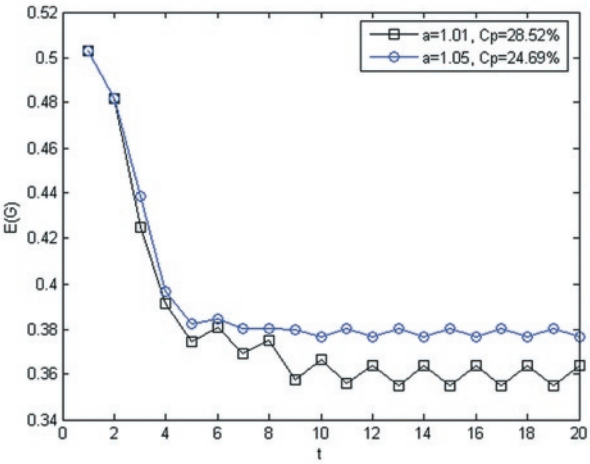

Fig. 3. Changing curves of BA network efficiency under C-L model (1)

Table 1. Transition time T_r of BA networks under two C-L models

	α	μ	Transition time T_r	
			Network 1	Network 2
Linear C-L model (1)	1.01 (1.05)	*	9 (5)	5 (7)
Nonlinear C-L model (2)	1.01 (1.05)	0.3	4 (5)	5 (5)
	1.01 (1.05)	0.5	4 (4)	4 (5)

Network 1: N = 100, E = 500. Network 2: N = 200, E = 1000.

Table 2. Decrease extent ΔEd and T_r under two C-L models

	α	μ	T_r	ΔEd
Linear C-L model (1)	1.01 (1.05)	*	6 (6)	33.76%
Nonlinear C-L model (2)	1.01 (1.05)	0.5	5 (6)	5.33%
	1.01 (1.05)	0.8	5 (5)	12.22%

where $E_{\Delta 1}$ is the decline rate of network efficiency caused by cascading failures when $\alpha = 1.01$, and $E_{\Delta 2}$ is the drop of network efficiency when $\alpha = 1.05$.

Table 3. Decrease extent ΔEd and T_r on ER networks

	α	μ	Network 1		Network 2	
			T_r	ΔEd	T_r	ΔEd
Linear C-L model (1)	1.01 (1.05)	*	5 (6)	27.9%	7 (6)	14.54%
Nonlinear C-L model (2)	1.01 (1.05)	0.8	4 (5)	6.64%	5 (6)	10.17%

Table 4. Decrease extent ΔEd and T_r on ER networks

	α	μ	Network 1		Network 2	
			T_r	ΔEd	T_r	ΔEd
Linear C-L model (1)	1.01 (1.05)	*	7 (2)	63.25%	7 (2)	68.76%
Nonlinear C-L model (2)	1.01 (1.05)	0.5	6 (3)	35.23%	5 (2)	21.79%

Network 1: N = 100, p = 0.101, Network 2: N = 200, p = 0.0503. p is the probability that each edge is included.

5.2. Simulation on ER random network

Using the similar procedures, we perform cascading simulations on ER random networks [34] which are subjected to intentional attacks as well as random failures, respectively. Simulation results of decrease extent of drops in network efficiency (*ΔEd*) and transition time T_r in the cascading process on ER networks under different C-L models are listed in Table 3 (under intentional attacks) and Table 4 (under random failures).

5.3. Results analysis

According to the above cascading simulations on different kinds of networks, the following observations can be made:

(1) As the tolerance parameter α increases (1.01 to 1.05), the network efficiency $E(G)$ is reduced by 13.43% for the BA scale free network using the linear C-L model (1) (Fig. 3). Under the same condition, as shown in Fig. 2, the collapse rate of network efficiency is declined by 7.36% (for $\mu = 0.3$) and 5.33% (for $\mu = 0.5$) when adopting the nonlinear C-L model (2). This implies that increasing the capacity of each network node in the same proportion may not greatly enhance the network performance. It is consistent with the existing findings [23, 25], which verifies the feasibility of the proposed nonlinear C-L model (2). Simulation results on other BA networks with different scales and ER networks present the similar characteristics.

(2) As illustrated in tables 1-4, transition time T_r under the improved nonlinear C-L model (2) is shorter than that under the linear C-L model (1). It demonstrates that cascading failures triggered by intentional attacks or random failures spread rapidly on the two kinds of experimented networks. After cascades occur, network efficiency $E(G)$ will finally stay stable at a lower level. It is in compliance with the current findings [28, 40], which further verifies the feasibility of the proposed nonlinear C-L model (2).

6. Verification of proposed resource reallocation strategy

When a network which is subjected to intentional attacks reaches a new stationary state, i.e., network efficiency stays at a lower level within error band after cascades occurred, we reallocate subsequent network capacities of the same amount to network nodes using our proposed resource reallocation strategy and other three existing reallocation strategies. By analyzing the upward trends of network efficiency as well as eventual steady-state values, we compare effectiveness of these four resource reallocation strategies in restoring network performance against cascading failures, and accordingly verify the performance of our proposed one.

6.1. Simulation method

The three existing resource reallocation strategies [11] for comparison are summarized as follows: (i) the newly added capacity of each node is linearly proportional to the node's degree (***CDlinr***); (ii) the newly added capacity of each node is linearly proportional to its initial load (***CLlinr***); (iii) each node's newly added capacity is equal (***Ceql***). The corresponding equations are as below:

$$C_{\Delta i} = b \times D_i, \quad i = 1,2...N \tag{9}$$

$$C_{\Delta i} = b \times L_i(0), \quad i = 1,2...N \tag{10}$$

$$C_{\Delta i} = c, \quad i = 1,2...N \tag{11}$$

where $C_{\Delta i}$ is the new capacity reallocated to node i, b is the scaling coefficient, D_i in Eq. (9) denotes the degree of node i, and c in Eq. (11) is a constant, signifying the new capacity added to each node.

Fig. 4 shows the averaged relationship between the newly added capacity (C') and initial load ($L(0)$) of each node in the network, which is subjected to an intentional attack, in a logarithmic scale after reallocating equal capacity resource to network nodes based on the four reallocation strategies. The dotted black line (assuming $C' = L(0)$) is the reference line.

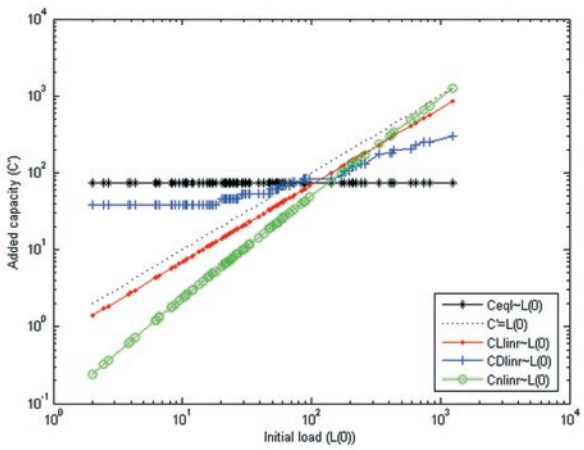

Fig. 4. The relation between added capacity and initial load of each node

As shown in Fig. 4 (the green curve with circles), the proposed new reallocation strategy (*Cnlinr*) reallocates more subsequent capacities to the nodes with larger loads than the ones with smaller loads nonlinearly. It is based on the dynamics of network load redistribution and the corresponding relations with node capacity.

Fig. 5 shows the main steps of subsequent capacity resource reallocation simulation on different networks undergoing cascades which are caused by intentional attacks.

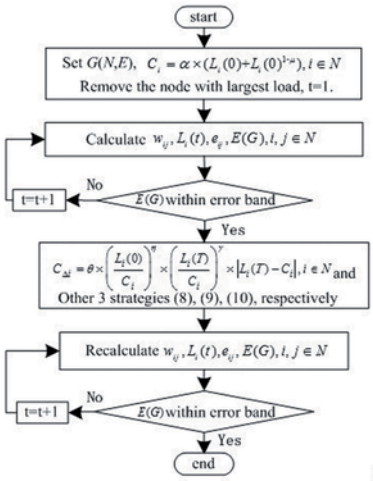

Fig. 5. The simulation steps of reallocating new capacities

Specifically we first use the method introduced in section 'Cascading process' to simulate the cascading process triggered by an intentional attack on network G, adopting the improved nonlinear C-L model (2). When network G reaches a new stationary state after cascades spread, we reallocate subsequent capacity resource of the same amount to network nodes according to the four resource reallocation strategies, respectively. Then we simulate the dynamic redistribution of network loads ensued as mentioned before, and calculate the shortest paths in the network and network efficiency $E(G)$ at every time step, until $E(G)$ ascends to a higher level and remains relatively stable again. It means that network G relaxes to a steady state. By this way, the overall changing trends of network efficiency of scale-free networks, random networks and small-world networks which were subjected to intentional attacks, after reallocating subsequent capacity resource, can be obtained.

The application of our proposed capacity resource reallocation strategy is briefly presented as follows: as we get real-time information of each network node's load and capacity (e.g., voltage and capacity of substations in power grids) in real-life infrastructure networks, a proper combination of model parameters in Eq.(3) can be determined through the above described simulations. For this reason, we can obtain a theoretical reallocation proportion of newly-added capacities for each network node, which can provide guidance in designing robust infrastructure networks, along with mitigating cascading failures in reality.

6.2. Simulation results and analysis

Fig. 6 illuminates the evolution trends of network efficiency $E(G)$ after reallocating new resource to nodes based on the four strategies for a BA network (N = 100, E = 500) subject to cascading failures triggered by intentional attacks. The first three values of each trend curve are stable values of network efficiency when networks reach steady states after cascading failures occur. The corresponding relative increments of network efficiency (ΔR) are listed in Table 5. ΔR is calculated based on equation (12), where $E(T)$ is the steady value of network efficiency after cascades spread, E_f is the final stable value of network efficiency after reallocating new capacities. Parameter values used are μ = 0.5, γ = 0.3, θ = 0.8, η = 2, and α = 1.01, 1.05. ΔC is the ratio between the overall newly added capacities and initial capacities in all.

$$\Delta R = (E_f - E(T)) / E(T) \tag{12}$$

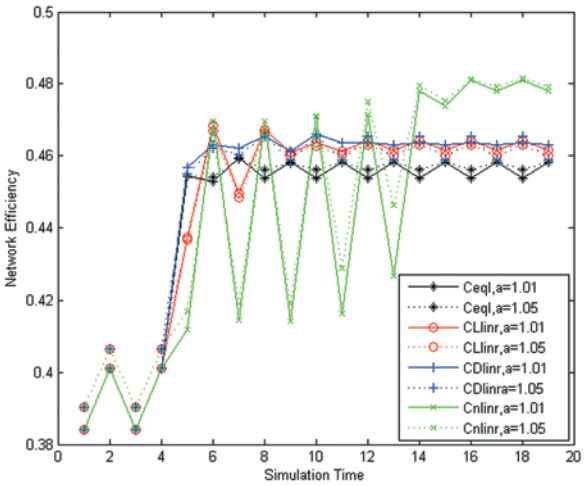

Fig. 6. Rising trends of BA network efficiency after resource reallocation

Table 5. Relative increment ΔR of network efficiency under four strategies

	Ceql	*CLlinr*	*CDlinr*	*Cnlinr*	*ΔC*	*α*
ΔR	18.19%	20.55%	20.68%	24.87%	43.99%	1.01
	17.13%	18.28%	18.41%	23.1%	37.07%	1.05

It can be seen from Fig. 6 that the changing curve (with green crosses) of network efficiency under the proposed resource reallocation strategy is obviously different from others. Initially, it fluctuates severely, and then does cost a longer time to reach a stable level with higher final value (see details in Table 5). We also performed simulations on BA networks with different scales and got the similar conclusion that the proposed resource reallocation strategy (***Cnlinr***) can enable the network efficiency of BA networks to be upgraded the most.

Fig. 7 illustrates the comparative results for an ER network (N = 100, p = 0.101) subject to an intentional attack on the node with the highest loads. Similar to Fig. 6, the first three values of those curves are final network efficiency when networks stay stable again after cascading failures occurred. In the cascading simulations, α = 1.05, μ = 0.5, γ = 0.3, θ = 0.6, η = 2.3, and ΔC = 20.35% is the overall increments of new capacities in each of the four resource reallocation strategies. The values of the factor 'rise' presented in the figure are equal to ΔR.

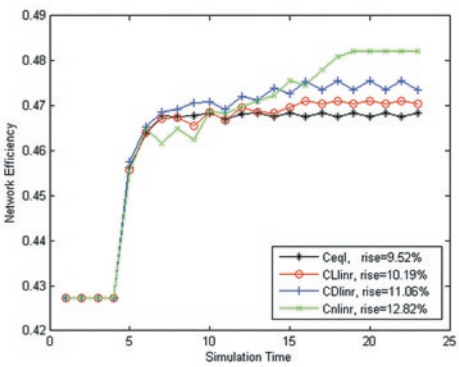

Fig. 7. Rising trends of ER network efficiency after resource reallocation

As shown in Fig. 7, aside from the longer time is taken for network efficiency to stay stable, the proposed resource reallocation strategy (the green curve with crosses) could make the ER network suffering intentional attacks get the largest improvement in the network efficiency, by comparison to results under other three reallocation strategies. Additionally, similar conclusions are obtained in simulations on other ER networks with different scales, which further testify the suitability of the proposed resource reallocation strategy.

We continue to validate the proposed resource reallocation strategy by conducting similar network capacity reallocation simulations on another type of networks called small-world networks. It is a type of network between regular network and random network with short average path length and high clustering coefficient. We choose WS small-world model [1] to generate small-world networks, which is a widely-accepted model with a probability parameter P. In the test network, N = 100, P = 0.5 which is the probability that each initial edge is reconnected. After reallocating subsequent resource based on four strategies separately, the dynamic redistribution of network loads follows. The corresponding four rising trends of network efficiency are obtained, as shown in Fig. 8. Similarly, the first three values of each curve in the figure are the final steady-state network efficiency after cascades spread triggered by attacks intentionally. The values of parameters used in the simulations are: α = 1.04, μ = 0.3, γ = 0.33, θ = 0.66, η = 1.9, ΔC = 24.97%. The values of factor 'rise' listed in Fig. 8 present the values of ΔR as mentioned above. Other WS networks with different scales are also tested and similar findings are obtained.

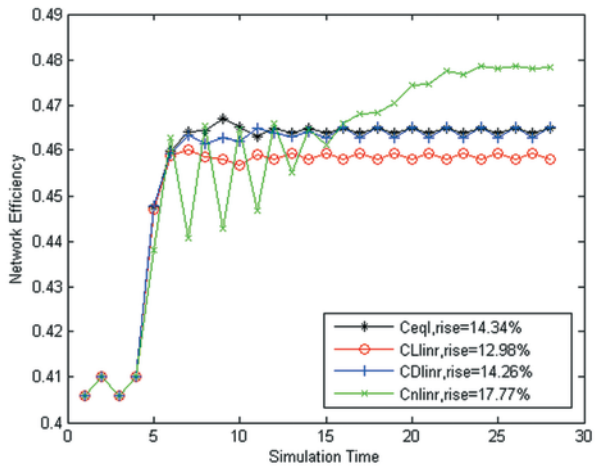

Fig. 8. Rising trends of WS network efficiency after resource reallocation

It can be seen from Fig. 8 that except for the initial fluctuation, the green curve with crosses obtained by adopting our proposed strategy has the largest final value of network efficiency among all curves with the same initial efficiency values. It strongly verifies the performance of our proposed resource reallocation strategy again.

In summary, as compared with the other three existing reallocation strategies, the changing curves of network efficiency for different networks subject to intentional attacks under the proposed new reallocation strategy may fluctuate more drastically, and reach steady states slower in the cases studied. Nevertheless, the corresponding steady-state values of network efficiency under our proposed reallocation strategy are the highest, indicating that network performance can be restored the best after being damaged by cascading failures.

As illuminated in Eq.(3), under the proposed new reallocation strategy, the new subsequent capacity resources are reallocated to network nodes based on not only initial node's capacity but also real-time features of networks, i.e., the distribution of node's load before and after failure propagation, as well as the nonlinear Capacity-Load

relationship. In comparison, the other three strategies reallocate new capacities of the same amount just according to some fixed network properties without combining certain real-time key information of networks. The simulation results demonstrate the effectiveness of the proposed new resource reallocation strategy (*Cnlinr*) in improving the network efficiency against cascading failures triggered by intentional attacks.

7. Conclusion

In this paper, we first propose an improved C-L model based on the realistic, nonlinear relationship between capacity and load of network nodes in many real-life infrastructure networks. We demonstrate its feasibility by simulating cascading failures on two typical types of networks, namely, scale-free networks and random networks, considering both intentional attacks and random failures. The proposed C-L model presents the practical flow behavior of network systems under normal condition, which could be used as a basis for analyzing network failures and their impacts on network performance. According to this improved nonlinear C-L model and some important dynamic characteristics of infrastructure networks, we further propose a network capacity resource reallocation strategy for network systems suffering intentional attacks for the purpose of maintenance. Experimental results are obtained by simulating the proposed resource reallocation strategy on three widely-recognized types of networks, in comparison to other three existing resource reallocation strategies. These comparative results show that our proposed strategy could reallocate subsequently-added capacity more efficiently by identifying important network nodes as well as subsequently reallocating more new capacity to them. As a result, the proposed reallocation strategy could bring about a more marked improvement of network performance after it drops due to cascades. Further, our proposed capacity resource reallocation strategy could effectively reduce damages on infrastructure networks caused by cascading failures, which is of great importance to maintain real-world infrastructure networks with the consideration of limited investment cost. Findings from this research have theoretical importance and could be practically useful for improving the reliability-based design of real-life infrastructure networks, along with defense of cascading failures in them from economic perspective.

Some hypotheses have been made in the cascading simulations, e.g., we assume only one network node is initially removed from the network after it is attacked or breaks down, and the amount of new subsequent capacities is not particularly regulated in resource reallocation simulations. However, they are not necessarily the case for many infrastructure networks in practice. Therefore, one direction of our future work is to relax these assumptions. Besides, we mainly verify the performance of the proposed capacity resource reallocation strategy subject to intentional attacks. The study of its performance for random failures will be another direction of further research.

Acknowledgement

This work was supported by the National Natural Science Foundation of China (61304220) and the Beijing Natural Science Foundation (4143064).

References

1. Albert R, Jeong H, Barabási A L. Error and attack tolerance of complex networks. Nature 2000; 406(6794): 378-382, http://dx.doi.org/10.1038/35019019.
2. Alipour Z, Monfared M A S, Zio E. Comparing topological and reliability-based vulnerability analysis of Iran power transmission network. Proceedings of the Institution of Mechanical Engineers, Part O: Journal of Risk and Reliability 2014; 228(2): 139-151, http://dx.doi.org/10.1177/1748006x13501652.
3. Buldyrev S V, Parshani R, Paul G. Catastrophic cascade of failures in interdependent networks. Nature 2010; 464(7291): 1025-1028, http://dx.doi.org/10.1038/nature08932.
4. Correa G J, Yusta J M. Grid vulnerability analysis based on scale-free graphs versus power flow models. Electric Power Systems Research 2013; 101: 71-79, http://dx.doi.org/10.1016/j.epsr.2013.04.003.
5. Crucitti P, Latora V, Marchiori M. Model for cascading failures in complex networks. Physical Review E 2004; 69(4): 045104, http://dx.doi.org/10.1103/PhysRevE.69.045104.
6. Cupac V, Lizier J T, Prokopenko M. Comparing dynamics of cascading failures between network-centric and power flow models. International Journal of Electrical Power & Energy Systems 2013; 49:369-379, http://dx.doi.org/10.1016/j.ijepes.2013.01.017.
7. Dorogovtsev S N, Mendes J F. Evolution of networks. Advances in physics 2002; 51(4): 1079-1187, http://dx.doi.org/10.1080/00018730110112519.
8. Dou B L, Wang X G, Zhang S Y. Robustness of networks against cascading failures. Physica A: Statistical Mechanics and its Applications 2010; 389(11): 2310-2317, http://dx.doi.org/10.1016/j.physa.2010.02.002.
9. Erdös P, Rényi A. On the evolution of random graphs. Publ. Math. Inst. Hungar. Acad. Sci 1960; 5:17-61.
10. Fang Y P, Pedroni N, Zio E. Comparing Network-Centric and Power Flow Models for the Optimal Allocation of Link Capacities in a Cascade-Resilient Power Transmission Network. IEEE Systems Journal, IEEE 2014; PP(99): 1-12.
11. Ghamry W K, Elsayed K M. Network design methods for mitigation of intentional attacks in scale-free networks. Telecommunication Systems 2012; 49(3): 313-327, http://dx.doi.org/10.1007/s11235-010-9375-2.
12. Glanz J, Perez-Pena R. 90 Seconds That Left Tens of Millions of People in the Dark New York Times. The New York Times 26 August 2003, p.1.
13. Goh K I, Kahng B, Kim D. Universal behavior of load distribution in scale-free networks. Physical Review Letters 2001; 87(27): 278701, http://dx.doi.org/10.1103/PhysRevLett.87.278701.
14. Holme P, Kim B J. Vertex overload breakdown in evolving networks. Physical Review E 2002; 65(6): 066109, http://dx.doi.org/10.1103/PhysRevE.65.066109.
15. Http://www.chinasmartgrid.com.cn/news/20121129/404779.Shtml. (2012, accessed 1 July 2014).
16. Huang N, Hou D, Chen Y, Xing L D, Kang R. A network reliability evaluation method based on applications and topological structure. Eksploatacja i Niezawodnosc-Maintenance and Reliability 2011; 3: 77-83.
17. Kim D H, Kim B J, Jeong H. Universality class of the fiber bundle model on complex networks. Physical review letters 2005; 94(2): 025501, http://dx.doi.org/10.1103/PhysRevLett.94.025501.
18. Kim D H, Motter A E. Resource allocation pattern in infrastructure networks. Journal of Physics A: Mathematical and Theoretical 2008;

41(22): 224019, http://dx.doi.org/10.1088/1751-8113/41/22/224019.
19. Latora V, Marchiori M. Efficient behavior of small-world networks. Physical review letters 2001; 87(19): 198701, http://dx.doi.org/10.1103/PhysRevLett.87.198701.
20. Lee E, Goh K I, Kahng B, Kim D. Robustness of the avalanche dynamics in data-packet transport on scale-free networks. Physical Review E 2005; 71(5): 056108, http://dx.doi.org/10.1103/PhysRevE.71.056108.
21. Lee K, Hui P. High-performance distribution of limited resources via a dynamical reallocation scheme. Physica A: Statistical Mechanics and its Applications 2008; 387(26): 6657-6662, http://dx.doi.org/10.1016/j.physa.2008.08.023.
22. Li P, Wang B H, Sun H, Gao P, Zhou T. A limited resource model of fault-tolerant capability against cascading failure of complex network. The European Physical Journal B-Condensed Matter and Complex Systems 2008; 62(1): 101-104, http://dx.doi.org/10.1140/epjb/e2008-00114-1.
23. Madar N, Kalisky T, Cohen R, ben-Avraham D, Havlin S. Immunization and epidemic dynamics in complex networks. The European Physical Journal B-Condensed Matter and Complex Systems 2004; 38(2): 269-276, http://dx.doi.org/10.1140/epjb/e2004-00119-8.
24. Moreno Y, Pastor-Satorras R,Vespignani A. Critical load and congestion instabilities in scale-free networks. Europhysics Letters 2003; 62(2): 292, http://dx.doi.org/10.1209/epl/i2003-00140-7.
25. Pastor-Satorras R, Vespignani A. Epidemics and immunization in scale-free networks. Handbook of graphs and networks: from the genome to the internet 2005; 111-130.
26. Reeves J, Ramaswamy A, Locasto M, Bratus S, Smith S. Intrusion detection for resource-constrained embedded control systems in the power grid. International Journal of Critical Infrastructure Protection 2012; 5(2): 74-83, http://dx.doi.org/10.1016/j.ijcip.2012.02.002.
27. Sahinoglu Z, Tekinay S. On multimedia networks: self-similar traffic and network performance. Communications Magazine, IEEE 1999; 37(1): 48-52, http://dx.doi.org/10.1109/35.739304.
28. Serazzi G, Zanero S. Computer virus propagation models. Performance Tools and Applications to Networked Systems. Springer 2004: 26-50, http://dx.doi.org/10.1007/978-3-540-24663-3_2.
29. Shi M C, Pang S P, Zou X Q. An LCOR model for suppressing cascading failure in weighted complex networks. Chinese Physics B 2013; 22(5): 058901, http://dx.doi.org/10.1088/1674-1056/22/5/058901.
30. Tao Z, Liu J G, Wang B H. Notes on the algorithm for calculating betweenness. Chinese Physics Letters 2006; 23(8): 2327, http://dx.doi.org/10.1088/0256-307X/23/8/099.
31. Wang B, Kim B J. A high-robustness and low-cost model for cascading failures. EPL (Europhysics Letters) 2007; 78(4): 48001, http://dx.doi.org/10.1209/0295-5075/78/48001.
32. Wang X, Guan S, Lai C H. Protecting infrastructure networks from cost-based attacks. New Journal of Physics 2009; 11(3): 033006, http://dx.doi.org/10.1088/1367-2630/11/3/033006.
33. Watts D J, A simple model of global cascades on random networks. Proceedings of the National Academy of Sciences 2002; 99(9): 5766-5771, http://dx.doi.org/10.1073/pnas.082090499.
34. Watts D J, Strogatz S H. Collective dynamics of 'small-world' networks. Nature 1998; 393(6684): 440-442, http://dx.doi.org/10.1038/30918.
35. Xia Y, Hill D. Optimal capacity distribution on complex networks. EPL (Europhysics Letters) 2010; 89(5): 58004, http://dx.doi.org/10.1209/0295-5075/89/58004.
36. Zhang H, Lan X, Wei D, Mahadevan S, Deng Y. Self-similarity in complex networks: from the view of the hub repulsion. Modern Physics Letters B 2013; 27(28), http://dx.doi.org/10.1142/S0217984913502011.
37. Zhang S, Liang M G, Jiang Z Y, Li H J. Queue Resource Reallocation Strategy for Traffic Systems in Scale-Free Network. International Journal of Modern Physics C 2013; 24(03), http://dx.doi.org/10.1142/S0129183113500137.
38. Zhou J, Huang N, Sun X L, Wang K L, Yang H Q. A New Model of Network Cascading Failures with Dependent Nodes. Reliability and Maintainability Symposium, 2015: 1-6, http://dx.doi.org/10.1109/rams.2015.7105077.
39. Zio E, Sansavini G. Modeling interdependent network systems for identifying cascade-safe operating margins. Reliability, IEEE Transactions on 2011; 60(1): 94-101, http://dx.doi.org/10.1109/TR.2010.2104211.
40. Zou C C, Towsley D, Gong W. Email virus propagation modeling and analysis. Report for the Department of Electrical and Computer Engineering. University of Massachusettes, Amherst, USA, 2003.

Jian ZHOU
Ning HUANG
Xiaolei SUN
Shuo ZHANG
School of Reliability and Systems Engineering, Beihang University
No.37, Xueyuan Road, Haidian District, Beijing, 100191, China
Science & Technology on Reliability & Environmental Engineering Laboratory
No.37, Xueyuan Road, Haidian District, Beijing, 100191, China

Liudong XING
Department of Electrical & Computer Engineering, University of Massachusetts Dartmouth, 285 Old Westport Road, MA 02747-2300, Dartmouth, USA

E-mail: zhoujian977@126.com, hn@buaa.edu.cn, cny258sxl@163.com, zhangshuolt@163.com, lxing@umassd.edu

Article citation info:
PŁONKA S, ZABORSKI A. Operational wear of the neck of spindle coating in cooperation with yarn. Eksploatacja i Niezawodnosc – Maintenance and Reliability 2015; 17 (4): 496–503, http://dx.doi.org/10.17531/ein.2015.4.3.

Stanisław PŁONKA
Andrzej ZABORSKI

OPERATIONAL WEAR OF THE NECK OF SPINDLE COATING IN COOPERATION WITH YARN

ZUŻYCIE EKSPLOATACYJNE SZYJKI OKŁADZINY WRZECION PRZĘDZALNICZYCH PRZY WSPÓŁPRACY Z PRZĘDZĄ

The article presents results of research on the operating time of the neck of spindle coating with collapse balloon crown of a ring spinning frame in cooperation with yarn under industrial conditions in the form of histograms. Adopting the change of the diameter of the cylindrical part of the neck of spindle coating is the wear criterion Δd≥0,5 mm. The assessment of the spindle neck operating time was performed in cooperation with a mixture of fibres: 70÷80% wool fibres with the addition of 10÷20% of polyester fibres, which causes the greatest wear. The research included measurements with the use of the metric method of the wear of the neck coating of a spindles made of the EN AW-2024 alloy (AlCu4Mg1), which were subjected to finishing operation with abrasive cloth, grain number 80, and then 150 and polished with desilted sandpaper and, in the second variant - they were subjected to burnishing. In addition, roundness deviations of the cylindrical part of the neck of spindle coating were measured at equal distances from face of the crown, using a Talyrond 365 roundness tester. Next, on the basis of the roundness outlines obtained, an outline of the cylindricity of the neck of spindle coating burnished before and after the operating time was prepared. Also, measurements of the topography of the surface of the neck of spindle coating were performed before and after the operating time. An analysis of the cylindricity outline and the surface topography confirms that the outer surface of the surface layer along the length and circumference of the neck of spindle coating in cooperation with yarn is subject to uneven wear. The assessment of the topography of the wearing surface and micro-photographs of the side surface of the helical groove lead to the conclusion that the wear of the neck of spindle coating made of the AlCu4Mg1 occurs mostly as a result of abrasive wear.

***Keywords**: ring spinning frame, collapse balloon spindle, operational wear.*

W artykule zamieszczono wyniki badań czasu pracy szyjki okładziny wrzecion z nasadką antybalonową przędzarki obrączkowej przy współpracy z przędzą, w warunkach przemysłowych, w postaci histogramów. Przyjmując jako kryterium zużycia zmianę średnicy, części walcowej, szyjki okładziny Δd≥0,5 mm. Ocenę czasu pracy szyjki przeprowadzono przy współpracy z mieszanką włókien: 70÷80% włókien wełny z dodatkiem 30÷20% włókien poliestrowych, powodującą największe zużycie. Badania objęły pomiary, metodą metryczną, zużycia szyjki okładziny wrzecion wykonanych ze stopu EN AW-2024 (AlCu4Mg1) poddanych obróbce wykończeniowej przez szlifowanie płótnem ściernym o numerze ziarna 80, a następnie 150 oraz polerowanie papierem ściernym odmulonym, jak również w drugim wariancie - operacji nagniatania. Ponadto wykonano pomiary odchyłki okrągłości części walcowej szyjki okładziny, w równych odległościach od czoła nasadki, za pomocą okrągłościomierza Taylrond 365. Następnie na podstawie uzyskanych zarysów okrągłości sporządzono zarys walcowości szyjki okładziny wrzeciona nagniatanej przed i po czasie eksploatacji. Wykonano również pomiary topografii powierzchni szyjki okładziny wrzecion przędzalniczych, przed i po okresie eksploatacji. Analiza zarysu walcowości i topografii powierzchni potwierdzają, że powierzchnia zewnętrzna warstwy wierzchniej, na długości i obwodzie szyjki okładziny, przy współpracy z przędzą ulega nierównomiernemu zużyciu. Ocena topografii powierzchni zużycia oraz mikrofotografii powierzchni bocznej rowka śrubowego skłaniają do stwierdzenia, że zużycie szyjki okładzin wrzecion ze stopu AlCu4Mg1 następuje przede wszystkim w wyniku zużycia ściernego.

***Słowa kluczowe**: przędzarka obrączkowa, wrzeciono z nasadką antybalonową, zużycie eksploatacyjne.*

1. Introduction

In ring spinning frames for collapse balloon spinning, there are parts, which come into direct contact with the yarn (the fibre stream), including guides, collapse balloon crowns, necks of spindle coating etc. [5]. The working surface of these parts should meet at least three conditions:

- it should be characterised by a low coefficient of friction in cooperation with yarn, which mostly depends on the stereometric structure of this surface, which results from the production method [11];
- it should not generate electrostatic loads and it should not develop electrostatic charges in the yarn;
- it should be sufficiently resistant to wear and accidental impact.

The results of the research presented in this article are continuation of work on the wear of metal-yarn tribological pairs. In the study [8], observations and measurements of wear of the neck of spindle coating with collapse balloon crown, made of the EN AW-2024 (AlCu4Mg1) alloy which were subjected to finishing operation with abrasive cloth, grain number 80, and then 150 and polished with sandpaper. The wear of the neck of spindle coating was assessed under industrial conditions in cooperation with two kinds of fibre mixtures: 70÷80% of

(*) Tekst artykułu w polskiej wersji językowej dostępny w elektronicznym wydaniu kwartalnika na stronie ***www.ein.org.pl***

wool fibres with the addition of 30÷20% of polyester fibres and 90% of wool fibres with the addition of 10% of polyamide and 100% of wool fibres. In the study [9], wear of the neck of spindle coating subject to two kinds of finishing: in the first variant burnishing and in the second variant - burnishing and next hard anode oxidation and grinding with PS 20 corundum sandpaper, grain number 600. The wear of the neck of spindle coating was assessed under industrial conditions in cooperation with three kinds of fibre mixtures (the composition of mixtures is presented in Table 1 [9]). On the basis of the performed research and observations, it was concluded that the greatest wear of the neck of spindle coating occurs in cooperation with a yarn, which is a mixture of: 70% of wool fibres with the addition of 30% of polyester fibres.

Therefore, the aim of the research and the results published was to define the influence of the finishing, e.g. grinding, polishing and burnishing on the operating time of the neck of spindle coatings made of the EN AW-2024 alloy (AlCu4Mg1) in cooperation with the mixture of fibres: 70÷80% of wool fibres with the addition of 30÷20% of polyester fibres.

2. Methodology of assessment of the wear of the neck of spindle coating with collapse balloon crown

160 spinning spindles were made and installed on the G-7A ring spinning frame (Fig. 1), in which the neck of coating was finished by:

- grinding with corundum sandpaper HTJ – 13 – 3, grain number 80, and next with grain number 150 and polished with desilted sandpaper with the following parameters: v_c=3,11 m/s and the unit pressure p_n≈0,015 MPa.
- burnishing with a disc with d_k=40 mm and the surface rounding radius with an axial section r_k=9 mm, with the clamping force of F_n=0,30 kN, the feed rate f_n=0,10 mm/r, the burnishing rate of v_n=2,07 m/s and lubrication with machine oil 10 [10, 12].

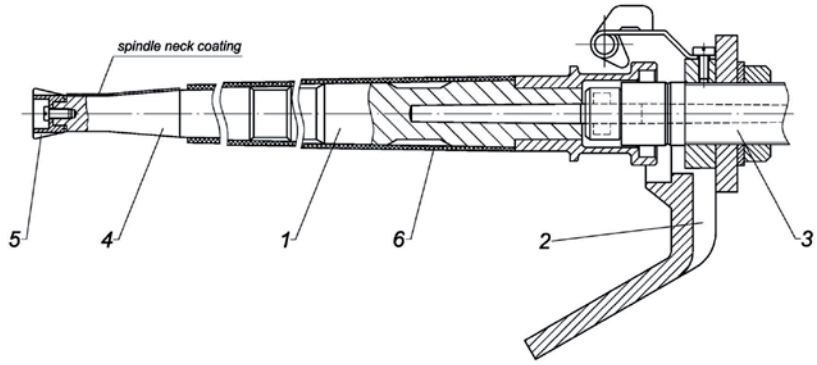

Fig. 1. A complete spindle with collapse balloon crown of the PG-7A ring spinning frame: 1 – spindle coating, 2 – brake, 3 – bearing insert, 4 – spindle neck made of the AlCu4Mg1 alloy, 5 – crown, 6 – bobbin [8, 9]

Tests of the wear of the necks of spindle coating with collapse balloon crown in cooperation with yarn were conducted using the metric method [2] on a ring spinning frame under production conditions. Wear measurements while spinning mixtures, as described in Table 1, were performed at 3-month time intervals using a specially adapted micrometer with a range from 0 to 25 mm with an elementary graduation of 0,002 mm. The wear value Δd was defined as a difference between the initial diameter and the lowest value of the diameter of 5 measurements of the cylindrical part of the neck of coating. The diameter was measured every 60° at a distance of 9 mm from face of the crown. Due to the fact that 5 to 7,5% of all spindle coatings undergo wear in the form of the helical groove, a change in the diameter of the neck of spindle coating was adopted as the criterion of wear - and also of the spindle replacement Δd≥0,5 mm.

Table 1. Types of yarn spun on the ring spinning frame, their characteristics and percentage of their processing time

Type of processed material	Linear mass of the yarn, tex	The number of yarn turns per 1 metre, 1/m	The number of spindle rotations, rpm	Percentage time of their processing, %
Polyester 30% + wool 70%	100; 125	390; 360	9500÷10000	77.6
Polyester 20% + wool 80%	150	280	8500	22.4

Moreover, to assess the wear of necks of spindle coatings, measurements of the roundness deviations (scanning the diameter of the neck of coating) were performed using the Taylrond 365 roundness meter by the Taylor Hobson company, equipped with a measuring tip ended with a ball with a radius of R_k=0,5 mm. Roundness deviations were measured at a distance of 1÷16 mm from the crown at cross-sections at distances of 0,5 mm before and after the operating time of the spindle. Next, as a result of employing a strategy of obtaining roundness outlines, an outline of the cylindricity of the spindle neck burnished before and after the operating was prepared [1].

The shape of the helical groove was measured in the perpendicular direction to the groove using the Form Talysurf 120 contour measurement system by the Taylor Hobson company, equipped with a wide-range head with a measuring tip with a roundness radius of r_p=20 μm. The outline of the shape of the groove was determined at the following distances from face of the crown: 1,0 mm and next every 2,0 mm up to the distance of 17,0 mm, and next at the following distances: 20,0; 25,0; 30,0 and 35,0 mm.

To assess the influence of yarn movement to the roughness of the surface of the neck of spindle coating also measurements of the surface topography at a distance of approx. 9 mm below the crown were carried out. The following parameters of 3D surface roughness were considered [6, 13, 14] (before and after the operating time of the spindles): amplitude parameters of the surface – arithmetical mean height of the surface S_a, root mean square height of the surface S_q, maximum peak height of the surface S_p, maximum pit height of the surface S_v, maximum height of the surface S_z, skewness of the surface S_{sk} and the kurtosis of the surface S_{ku} and spatial parameters: core height S_k, reduced peak height S_{pk}, reduced dale height S_{vk}, material ratio (peaks ratio of the area of the material) S_{mr1}, material ratio (dales ratio of the area of the material) S_{mr2}, volume of the material S_{a1} and volume of deep dales S_{a2}. Moreover, for the surface of the neck of spindle coating after the burnishing operation before and after operation, comprehensive characteristics of the stereometric structures of the surface including: a topographic map of the surface, an isophyse map, a histogram of the distribution of surface ordinates and the areal material ratio curve. The selected 3D roughness parameters were measured using the New Form Talysurf 2D/3D 120 contour measurement system by the Taylor Hobson company using Ultra Surface 5.21 and TalyMap Platinium 5.1.1 software. During roughness measurements, value of the sampling length l_r=0,25 or 0,80 mm was used (the sampling length was selected automatically by the software), the number of registered points N_x=10000, the sampling step Δ_x=0,308 μm, the fillet radius of the diamond gauging point r_{tip}=2,0 μm, the pressure

of the gauging point F_{kp}=1,0 mN, the feed rate of the gauging point v_{os}=1,0 mm/s and a Gaussian filter. Topography measurements were performed to surfaces with the following dimensions 3,08 mm×3,0 mm at 5 μm distances.

Microhardness measurements were conducted using the Vickers method on oblique microsections made at an angle of 4º30´ (0,0785 rad), using a microhardness tester by the Leitz Wetzlar company with the indenter load of 0,49 N.

With the use of a scanning electron microscope (SEM) *Jeol-J7*, traces of wear of the side surface of the helical groove were observed following the period of yarn friction against the neck of spindle coating, which was approx. 21 600 hours.

3. Wear of the neck of spindle coating with collapse balloon crown during the spinning process

During the operation of a spindle yarn moving at a speed of 25÷35 m/min, as a result of local friction caused by insufficiently smooth movement ("skipping") from one notch of the crown to the neighbouring one (Fig. 2a), and often as a result of yarn being "held" by one of the crown's notches, excessive wear of the neck of spindle coating occurs. This wear is manifested by the formation of approx. 2 mm-wide and over 1 mm-deep helical grooves in approx. 5 to 7,5% cases (Fig. 2b) after cooperation with yarn for at least over 10 thousand hours. These grooves prevent smooth movement of yarn over the neck of coating and, as a result, cause a greater number of cases of breaking the yarn.

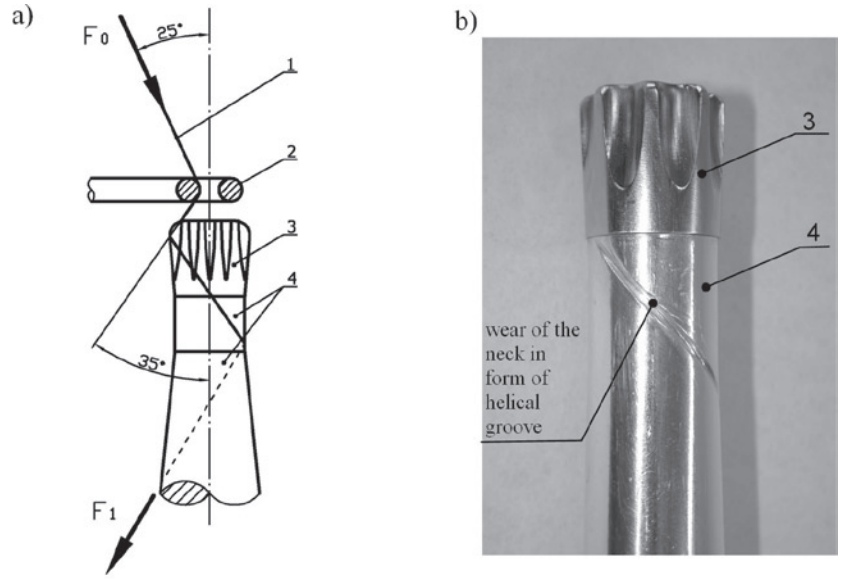

Fig. 2. The spindle neck coating from the AlCu4Mg1 alloy with spindle crown for collapsed balloon spinning: a) yarn movement from rollers feeding yarn onto the guide, and next onto the crown and the neck coating; b) wear of burnished spindle neck coating in the form of a helical groove after an operating time of approx. 21 600 hours: 1 – yarn, 2 – guide, 3 – crown, 4 – spindle neck coating made of the AlCu4Mg1 alloy [8, 9]

The wear of the neck of coating is enhanced by dead particles (of grass, bark, straw) found in the stream of fibres, especially in wool, and quite often dust particles stuck to wool fibres [7].

A histogram of the operating time of the neck of spindle coating with collapse balloon crown after grinding and polishing, in cooperation with yarn being a mixture of 70÷80% of wool fibres with the addition of 30÷20% of polyester fibres, is presented in Figure 3. The necks of spindle coating after burnishing are presented in Figure 4. Histograms of the operating time of the necks of spindle coating were identified by means of the following distributions: normal, exponential, Weibull and logarithmic-normal distribution. The most advantageous fit was obtained for the logarithmic-normal distribution. The hypothesis about the compliance between empirical and theoretical distribution for both cases was verified using a chi-square test at the significance level of 0,05.

It results from histograms, that the average operating time τ of grinded and polished necks of spindle coatings, in cooperation with yarn being a mixture of 70÷80% wool fibres with the addition of 10÷20% of polyester fibres, was τ=9591 work hours. The operating time of burnished necks of spindle coating was extended by approx. 27,3% and it was τ=12211 work hours. This should be explained by a greater hardness of the near-surface zone of the surface layer obtained by burnishing, as compared to the hardness of the near-surface zone of grinded and polished neck and a considerably greater thickness of this layer, in addition to a flat peak structure of the surface with a large share of material carrying capacity.

The influence of the finishing method of the necks of spindle coating and the operating time on the wear Δd is presented in Figure 5. The necks of spindle coating, which were finished by burnishing, were characterised by lower wear. During the first phase of abrasive wear, it should be explained by a more advantageous contour of irregularities of burnished surfaces, lower values of roughness parameters and a larger share of material-carrying capacity. During the second phase (after grinding off irregularities), it can be explained by greater hardness of the near-surface area of the top layer by approx. 400 MPa, as compared to the hardness of this zone of grinded and polished neck and a significantly greater thickness of this layer equal to approx 80 μm (Fig. 6) and its internal compression stresses [3, 4, 12].

The shape of burnished cylindrical surface of the neck of spindle coating situated directly under the crown before and after an operating time of approx. 21 600 work hours is presented in Figure 7. Before the operation, the cylindrical part of the neck of coating was characterised by roundness deviation within the range of 3,37÷9,88 μm at the individual cross-sections while the cylindricity deviation was 17,21 μm. During the operating time of approx. 21 600 work hours, the roundness deviation increased along the neck of coating from approx. 26,5 to approx. 162,0 times and it fell within the range of 261,69÷769,30 μm, while the cylindricity deviation was 849,71 μm [9].

The results of measurements of selected 3D roughness parameters of the necks of burnished spindle coating before and after the operating time are presented in Table 2.

The values of parameters of 3D surface roughness, such as S_a, S_q, S_p, S_v, S_z of the neck of spindle coating for five measurements after the burnishing operation, are almost identical, while the values of the other parameters are very similar. For burnished surfaces, the S_{sk} skewness of the surface falls within the range of 0,205÷0,453, while the kurtosis falls within the range of S_{ku}=3,10÷4,35, which shows that the distribution of ordinates of surface peaks is close to a normal distribution (S_{sk}=0, S_{ku}=3). The movement of the stream of fibres (yarn) over the neck of coating of a burnished spindle makes its surface glossy after a very short contact with the yarn and the values of roughness parameters, such as S_a and S_q were generally reduced. While roughness parameters, such as S_p and S_z increased significantly, while the values of the other parameters were similar. In general, in 5 to 7,5% of cases, as a result of imperfections of the crown-manufacturing process (generally improper rounding of the notch or tooth), one from teeth of the crown holds the yarn significantly longer than the other ones and its contact with surface of the neck is much longer. As a result,

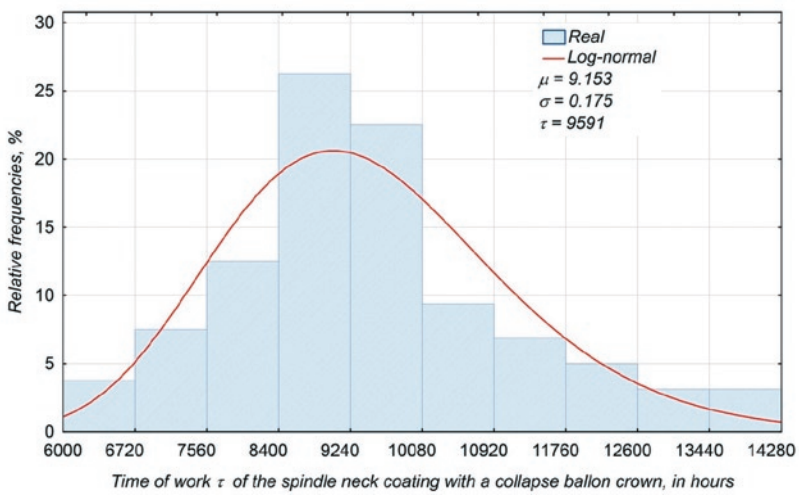

Fig. 3. A histogram of the operating time of grinded and polished necks of spindle coating made of the AlCu4Mg1 alloy in cooperation with yarn [8]

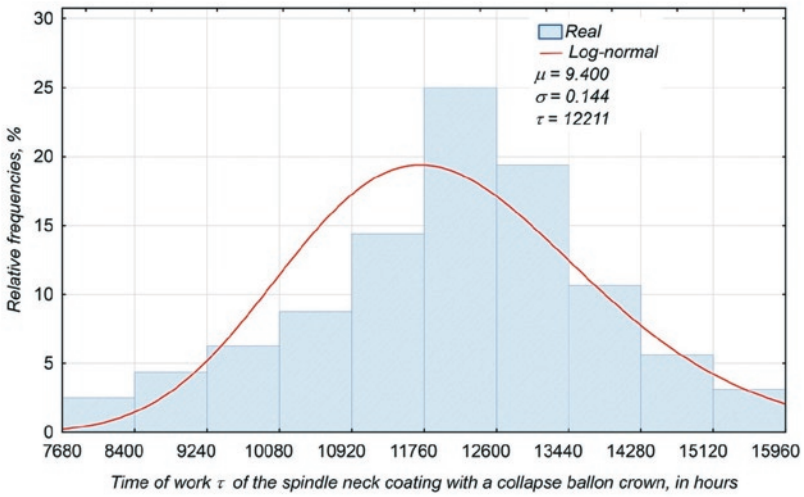

Fig. 4. A histogram of the operating time of burnished necks of spindle coating made of the AlCu4Mg1 alloy in cooperation with yarn

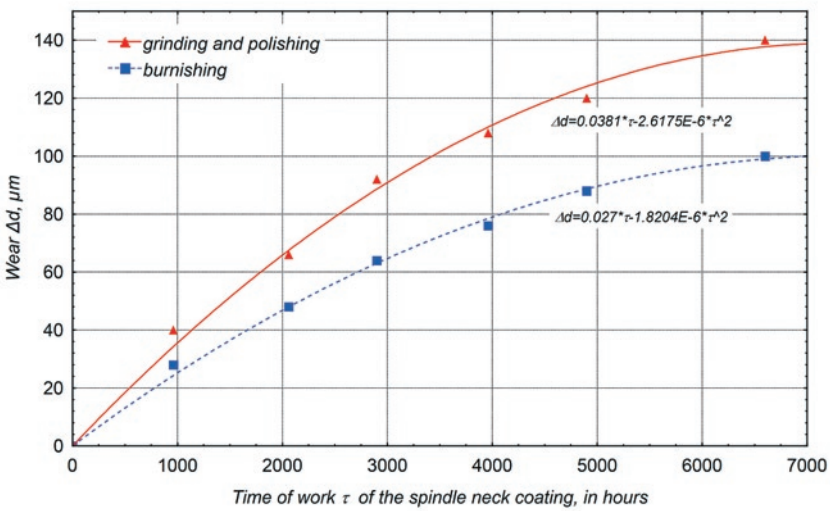

Fig. 5. The influence of the operating time on the wear of the neck of spindle coating with collapse balloon crown for two finishing methods the AlCu4Mg1 alloy in cooperation with yarn [8]

the majority of the measured 3D roughness parameters of the neck of coating increased significantly after approx. 21 600 work hours. For example, the root mean square height of the surface S_q of the neck of burnished spindle coating before operation ranged from 0,351 to 0,377 μm, while after a period of cooperation with yarn of 21 600 work hours, it was – S_q=0,446÷0,723 μm. The maximum height of surface peaks before the operation was S_p=1,33÷1,38 μm, while after the cooperation period with yarn, it was approx. 21 600 work hours – S_p=2,64÷6,16 μm. The S_{sk} and S_{ku} roughness parameters changed the most. The skewness of the surface S_{sk} of the neck of burnished coating fell within the range from 0,205 to 0,453 before the operation, while the kurtosis S_{ku} – ranged from 3,10 to 4,35, while after the period of cooperation with yarn of approx. 21 600 work hours (for worn surfaces) – S_{sk}= – 1,86÷0,999, and S_{ku}=6,95÷15,30. For considerably worn surfaces near a helical groove, the skewness of the surface S_{sk} increased from 2,20 to 4,87 times (the mode of surface peak ordinate distribution distinctly shifts downwards), while the kurtosis S_{ku} – from 1,60 to 2,24 times (which increases the fuzziness of ordinates). The negative value of the skewness of the surface S_{sk} and a value of kurtosis S_{ku}, which was higher from 3,5 to 4,9 times, occurred for a worn surface with deep scratches, which were probably formed by cutting broken yarn wrapped around the neck of coating with a sharp tool. Figures 8 and 9 present comprehensive characteristics of 3D roughness of the surface of a burnished neck of coating before and after the operation, which include: a topographic map of the surface, an isophyse map, the distribution of surface ordinates and the areal material ratio curve. The surface topography of the neck of spindle coating after burnishing is characterised by flattened peaks, however, after an operating time of 21 600 work hours, the peaks of considerably worn surface are sharp. The maximum peak height of the surface S_p after operation (considerably worn) is approx. 4,5 times greater as compared to the maximum height of peaks after burnishing. The parameters of the areal material ratio curve for the neck of coating after burnishing and operation are significantly higher for a considerably worn surface. The core height S_k is higher by 1,61 to 1,86 times, the reduced peak height S_{pk} is from 2,32 to 2,74 times higher, while the reduced dale height S_{vk} is from 1,64 to 2,07 times higher, as compared to the value of these parameters for the surface of the burnished neck of coating.

For burnished surfaces of the neck of spindle coating, the values of the volume of the material S_{a1}, as well as of the volume of deep dales S_{a2} are similar; however, the values of S_{a1} for the same measurement are always higher by 2,22 to 3,46 times from the value of S_{a2}. For burnished surfaces, after the operating time of 21 600 work hours at a considerably worn place, the values of the volume of the material S_{a1} and the volume of deep dales S_{a2} are over two times higher than the values of these parameters for surfaces before operation. The value of the material volume S_{a1} was lower than the value of the volume of deep dale S_{a2} only in one case. This should be explained by damage to the surface of the neck of coating in the form of a relatively deep scratch.

The parameters of 3D surface roughness of the neck of spindle coating after grinding with abrasive

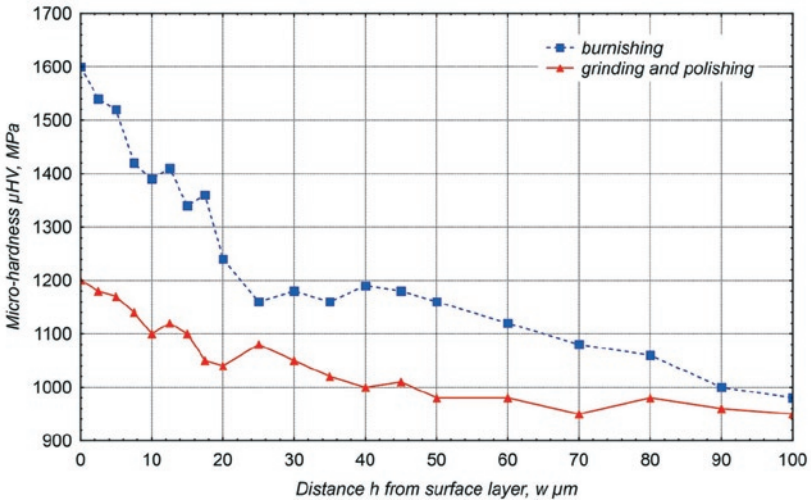

Fig. 6. Distribution of micro-harness in the surface layer of the necks of spindle coating made of the AlCu4Mg1 alloy in depth of the surface layer

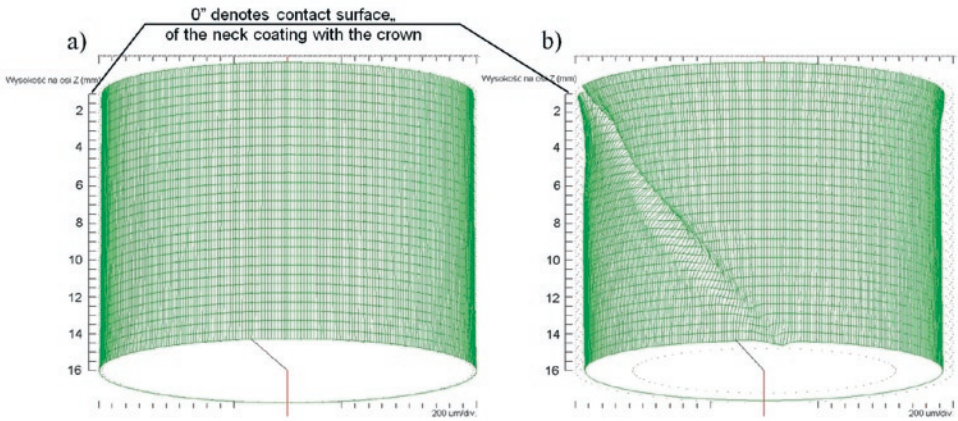

Fig. 7. The shape of the cylindrical part of the spindle neck coating with collapse balloon crown after burnishing: a) before the operation (0 hours in cooperation with yarn); b) after the operation (21 600 hours of cooperation with yarn) [9]

cloth and polishing with desilted sandpaper were the following: S_a=0,50 μm, S_q=0,64 μm, S_p=2,74 μm, S_v=4,03 μm, S_z=6,77 μm, S_k=1,97 μm, S_{pk}=0,07 μm, S_{vk} =0,84 μm, S_{r1}=9,07% and S_{r2}=88,87%. As it can be seen, the values of nearly all roughness parameters after grinding and polishing are significantly higher than after burnishing. Only the S_{pk} parameter after the grinding and polishing operation was several times lower than the value of this parameter for burnished surfaces. After the operating time of approx. 14 400 work hours, on the other hand, as a result of yarn friction against the neck of coating, the following roughness parameters were slightly reduced: S_a, S_q, S_v and S_{vk}, and the following were increased S_p, S_z and S_k [8].

The wear of burnished surface of the neck of coating is uneven, both along the circumference and along the spindle axis (Fig. 7). The movement of the stream of fibres (yarn) along the neck of a burnished spindle coating, if the contact with the yarn is very short, results in its slight wear as regards surface irregularities and is usually manifested by surface glossing. Such a situation occurs when the yarn is on one from the teeth of the crown, and hence at the largest distance from the spindle axis. Then the pressure of the yarn on the neck of coating is the smallest and it lasts the shortest. If the yarn is in cavities of the crown, it fits and adheres to surface of the neck of coating more closely. The yarn pressure on surface of the neck becomes much greater and the time of its contact with surface of the neck is considerably extended. As a result, the intensity of the wear of the neck's surface is greater and cavities are formed; their number for the necks of spindle coatings, which are almost evenly worn, corresponds to the number of teeth on the crown. While for the neck of spindle coating with inappropriately

Table 2. Values of selected 3D roughness parameters of the neck of spindle coating with collapse balloon crown made of the AlCu4Mg1 after burnishing, before and after the operating time

3D roughness parameters	Burnished surface of the neck of coating before operation					Burnished surface of the neck of coating after approx. 21 600 work hours of cooperation with yarn				
	measurement 1	measurement 2	measurement 3	measurement 4	measurement 5	measurement 1	measurement 2	measurement 3	measurement 4	measurement 5
S_a, μm	0,278	0,288	0,298	0,278	0,276	0,530	0,207	0,301	0,227	0,288
S_q, μm	0,359	0,364	0,377	0,358	0,351	0,723	0,267	0,446	0,294	0,374
S_p, μm	1,36	1,38	1,38	1,33	1,36	6,16	2,00	2,50	2,31	2,64
S_v, μm	4,08	3,90	3,99	4,10	3,68	3,13	3,20	4,12	1,69	4,08
S_z, μm	5,44	5,28	5,37	5,43	5,04	9,29	5,20	6,62	4,00	6,72
S_{sk}	0,205	0,350	0,453	0,280	0,399	0,999	0,496	-1,86	0,342	0,620
S_{ku}	4,35	3,10	4,17	4,33	3,58	6,95	4,31	15,30	4,31	4,65
S_k, μm	0,800	0,887	0,924	0,831	0,846	1,49	0,635	0,875	0,700	0,840
S_{pk}, μm	0,468	0,416	0,490	0,477	0,462	1,14	0,362	0,464	0,366	0,514
S_{vk}, μm	0,393	0,313	0,311	0,318	0,367	0,645	0,290	0,948	0,319	0,354
S_{r1}, %	15,5	14,1	14,5	13,9	13,6	13,2	12,3	11,0	11,5	14,3
S_{r2}, %	91,7	91,8	94,7	91,1	93,2	89,1	91,9	91,7	91,1	91,3
S_{a1}, μm^3/mm^2	36,4	29,4	35,6	33,1	31,4	75,6	22,3	25,6	21,1	36,7
S_{a2}, μm^3/mm^2	16,4	12,9	10,28	14,1	12,4	35,1	11,8	39,4	14,1	15,4

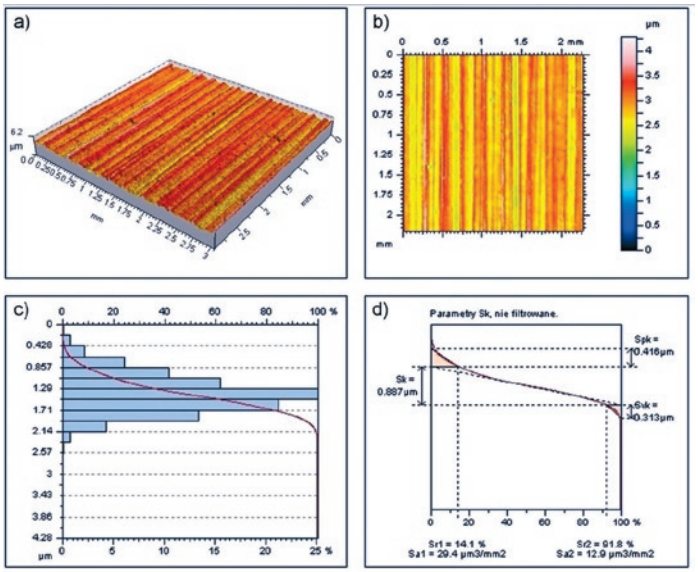

Fig. 8. Image of the stereometric structure of surface of the neck of spindle coating after burnishing: a) topographic map of the surface: S_a=0,288 µm, S_q=0,364 µm, S_p=1,38 µm, S_v=2,90 µm, S_z=4,28 µm; b) isophyse map; c) histogram of surface ordinate distribution; d) areal material ratio curve

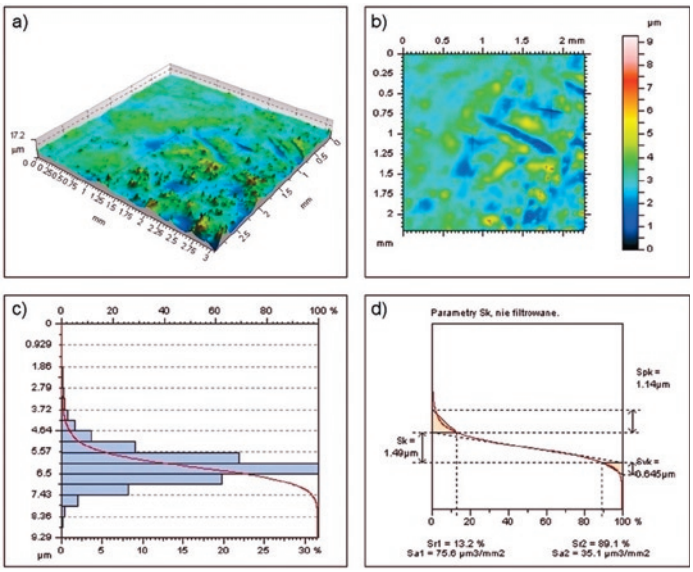

Fig. 9. Image of the stereometric structure of surface of the neck spindle coating after burnishing and after cooperation with yarn for approx. 21 600 hours: a) topographic map of the surface: S_a=0,530 µm, S_q=0,723 µm, S_p=6,16 µm, S_v=3,13 µm, S_z=9,29 µm; b) isophyse map; c) histogram of surface ordinate distribution; d) areal material ratio curve

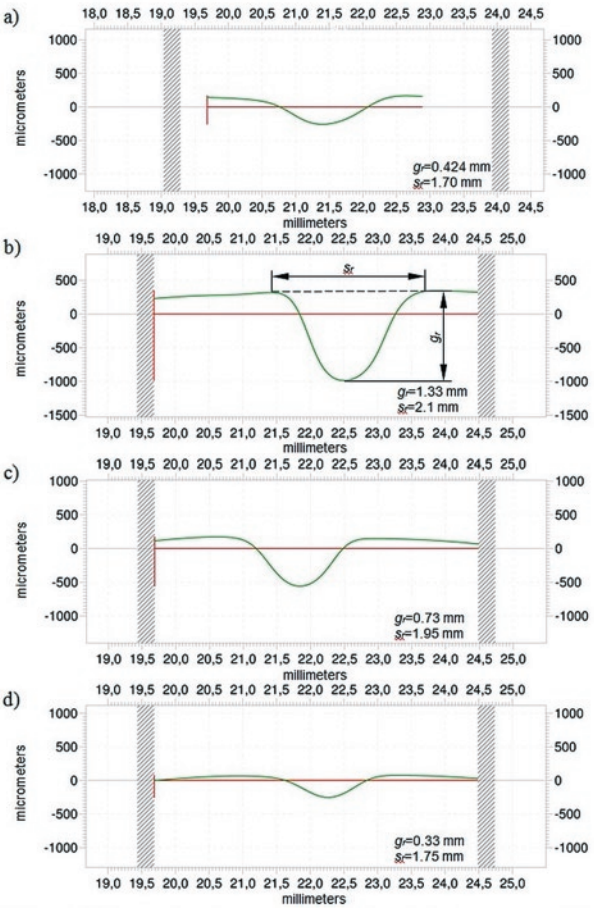

Fig. 10. An outline of the helical groove in a cross-section perpendicular to the outline of the helical groove at a distance of: a) 1,0 mm; b) 9,0 mm; c) 17,0 mm; d) 25,0 mm from face of the crown.

rounded edge of one from the teeth of the crown, the number of cavities at a certain distance from its face is lower by one or two cavities. This is caused by yarn not moving smoothly along the teeth of the crown (the yarn is held by such a tooth). As a result, a helical groove

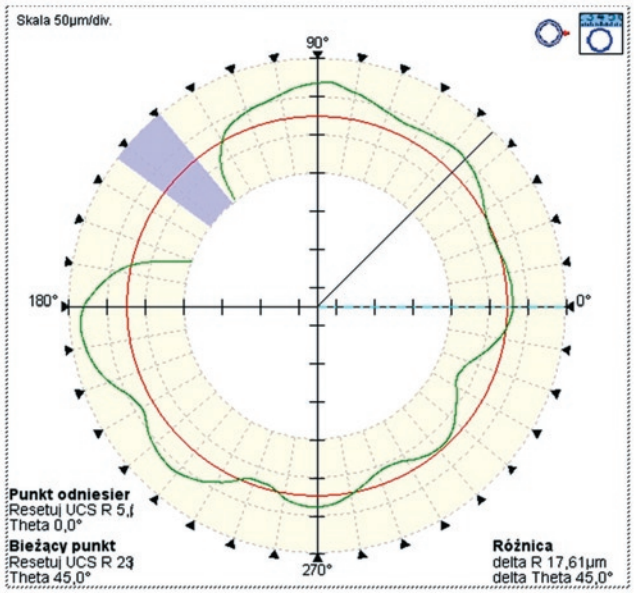

Fig. 11. The shape of burnished neck of spindle coating after an operating time of approx. 21 600 work hours (transverse cross-section at a distance of 9 mm from face of the crown) [9]

is formed along an approx. 45 mm-long section of the neck of coating with a considerable width and variable depth. Figure 10 presents shapes of the groove at a distance of 1,0; 9,0; 17,0 and 25,0 mm from the face of the crown in a cross-section perpendicular to the helical groove outline. The greatest wear in the form of the helical groove with a depth of approx. g_r=1,33 mm and a width of s_r=2,10 mm, in the tested batch of spindles, occurred at a distance of approx. 9 mm from the face of the crown (Fig. 10b). The shape of burnished neck of spindle coating after an operating time of approx. 21 600 work hours in a cross-section perpendicular to axis of the spindle neck at distance of 9 mm from the face of the crown is presented in Figure 11.

Figure 12 presents micro-photographs of the worn surface of the side wall of the helical groove after a period of friction of the yarn against the neck of coating of approx. 21 600 work hours.

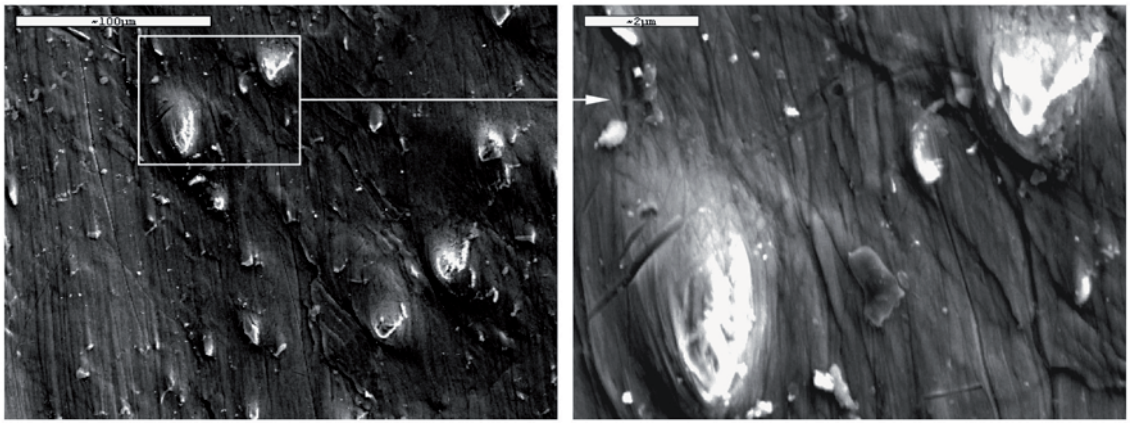

Fig. 12. Micro-photograph of the worn surface of the side wall of the helical groove after cooperation with yarn for approx. 21 600 work hours (at a distance of approx. 9 mm from face of the crown)

The hypothesis that the loss of material along the circumference of the neck of spindle coating with collapse balloon crown in the form of cavities with a helix and, at the same time, a reduction in its diameter, is caused by separating small volumes of the material as a result of continuous impact of yarn fibres and periodical impact of solid particles in the form of grass, bark, straw and often dust particles, which are present in the stream of fibres moving together with it. These particles are pressed against surface of the neck of coating with variable force as a result of variable tension of the yarn caused by its cyclic entering and leaving the notches of the crown and a variable position of the axis of the spindle ended with the crown during the rotational motion. By analogy with the operation of grinding with unrolling sandpaper, it can be adopted that solid particles play the role of micro-blades, which cause cavities of various depths to form over a long period of time.

The number of these cavities at a distance of approx. 9 mm from face of the crown is lower by one or two cavities for the necks of worn spindles than the number of teeth on the crown. In the authors' opinion, abrasive wear is of dominant importance when the friction between the yarn and the surface of the neck of spindle coating with collapse balloon crown occur.

Two groups of factors influence the intensity of this wear: the first one – connected with the stereometric structure of the surface and physical properties of surface layer of the neck of spindle coating and the other one connected with the characteristics of the spinning process, i.e. the type of processed mixture, tension and the rate of yarn movement. The outline of flat peak irregularities of the surface and, in this way, a greater material-carrying proportion increases the contact area with the yarn and with identical spinning conditions, cause lower unit pressure and lower wear. Similarly, an increase in the hardness of the surface layer and compression stresses reduce the wear.

4. Summary

The use of burnishing as the finishing of the neck of spindle coating with collapse balloon crown made of the EN AW-2024 alloy (AlCu4Mg1), resulted in an increase in wear resistance by over 27% in cooperation with yarn being a mixture of: 70÷80% of wool fibres with an addition of 30÷20% of polyester fibres as regards grinded and polished necks of spindle coating. It is caused by a different stereometric surface of burnished surfaces, higher microhardness (by 400 MPa) of the surface layer after burnishing, and internal compression stresses [3, 12]. This wear was manifested by the formation of a helical groove with a variable width and depth, a stroke of approx. 50 mm, over a length of approx. 45 mm of the neck of spindle coating starting form face of the crown. After cooperating with yarn for 21 600 work hours, the greatest wear occurred at a distance of approx. 9 mm from face of the crown and it was characterised by a groove, which was 2,10 mm wide and approx. 1,33 mm deep. This groove prevents smooth movement of the yarn over the neck of coating and, as a result, causes a greater number of cases of breaking the yarn.

The assessment of the surface of the neck of spindle coating with a manufacturing fault at the place of wear shows that after an operating period of 21 600 hours, nearly all roughness parameters were increased, e.g. root mean square height of the surface S_q - over 2,0 times, the maximum peak height of the surface S_p over 4,5 times, the reduced peak height S_{pk} approx. 2,5 times and the reduced dale height S_{vk} from approx. 1,8 to over 2,0 times.

References

1. Adamczak S.: Pomiary geometryczne powierzchni. Zarysy kształtu, falistość i chropowatość. WNT, Warszawa 2008.
2. Kragelsky I.V., Alisin V.V.: Tribology – Lubrication, Friction and Wear, John Wiley & Sons Inc., 2005.
3. Kukiełka L.: Theoretical and experimental foundations of surface roller burnishing with the electrocontact heating. Book of Mechanical Engineering. Technical University of Koszalin 1994.
4. Kukiełka L., Geleta K., Kukiełka K.: Modelling of Initial and Boundary Problems with Geometrical and Physical Nonlinearity and its Application in Burnishing Processes. Steel Research International Special edition, 2012, Publishing Company Wiley – VCH Verlag GmbH&Co. KGaA, Weinheim ISBN 978-3-514-00774-0, pp. 1375-1379.
5. Lawrence C.A.: Fundamentals of Spun Yarn Technology. CRC Press, Leeds 2003, http://dx.doi.org/10.1201/9780203009581.
6. Oczoś K.E., Liubimov V.: Struktura geometryczna powierzchni, Editorial Office of the Technical University Rzeszów 2003.
7. Płonka S., Hajduga M., Jędrzejczyk D.: The Wear Model Prognose of Tribologie Coupe – the Steel Guide – Yarn. Fibres & Textiles in Eastern Europe 2007; 15, 2: 54-57.
8. Płonka S., Hajduga M.: Assesing the Wear of Spindle Neck Coating Made of AlCu4Mg1 Alloy of Ring Spinning Spindles with an Antiballoon Crown, Fibres & Textiles in Eastern Europe 2008; 16, 3: 27-32.

9. Płonka S.: Effect of Surface Treatment on Wear of Spindle-Neck Coating with Collapse Balloon Crown. Fibres & Textiles in Eastern Europe 2013; 21, 1: 48-55.
10. Płonka S.: Metody oceny i wyboru optymalnej struktury procesu technologicznego. Design and Exploitation of Machines 48, Scientific Dissertations 31, Branch of Łodz Technical University, Bielsko-Biała 1998.
11. Płonka S., Przybyło S.: Wpływ struktury stereometrycznej powierzchni warstwy tlenkowej na kinetyczny współczynnik tarcia przędzy. Tribologia - Tribology, 38(2007)6, 151-163.
12. Przybylski W.: Technologia obróbki nagniataniem. WNT, Warszawa 1987.
13. Stout K.J., Blunt L.: Three Dimensional Surface Topography, Penton Press London 2000.
14. ISO 25178-2:2012 (E) – Geometrical product specifications (GPS) – Surface texture: Areal – Part 2: terms, definitions and surface texture parameters.

Stanisław PŁONKA
Department of Manufacturing Technology and Automation
University of Bielsko Biała
43-309 Bielsko-Biała, ul. Willowa 2

Andrzej ZABORSKI
Częstochowa University of Technology
Department of Mechanical Technologies
Częstochowa University of Technology
42-201 Częstochowa, ul. Armii Krajowej 21

E-mail: splonka@ath.bielsko.pl, zaborski@itm.pcz.czest.pl

Article citation info:
LU Z, ZHOU J, LI N. Maintainability fuzzy evaluation based on maintenance task virtual simulation for aircraft system. Eksploatacja i Niezawodnosc – Maintenance and Reliability 2015; 17 (4): 504–512, http://dx.doi.org/10.17531/ein.2015.4.4.

Zhong LU
Jia ZHOU
Naixin LI

MAINTAINABILITY FUZZY EVALUATION BASED ON MAINTENANCE TASK VIRTUAL SIMULATION FOR AIRCRAFT SYSTEM

OCENA OBSŁUGIWALNOŚCI OPARTA NA TEORII ZBIORÓW ROZMYTYCH BAZUJĄCA NA WIRTUALNEJ SYMULACJI ZADAŃ KONSERWACYJNYCH SYSTEMÓW SAMOLOTU

Maintainability is a significant design characteristic of civil aircraft system that has great effect on system availability, life cycle cost and operation safety. A virtual maintenance environment is constructed to support maintainability concurrent design of aircraft system, the evaluation method of maintainability attribute is proposed based on maintenance task virtual simulation or maintainability checklist, and then system maintainability comprehensive evaluation is proposed based on fuzzy theory. A case study, which is maintainability evaluation of a nose landing gear system in civil aircraft, shows the effectiveness of the method presented herein.

Keywords: *maintainability evaluation, virtual simulation, fuzzy theory, aircraft system.*

Obsługiwalność jest ważną cechą konstrukcyjną systemów stosowanych w samolotach cywilnych, która ma ogromny wpływ na gotowość systemu, koszty eksploatacji i bezpieczeństwo pracy W przedstawionych badaniach stworzono wirtualne środowisko eksploatacji wspierające łatwość obsługi systemów lotniczych; zaproponowana metoda oceny atrybutu obsługiwalności oparta jest o wirtualną symulację zadań konserwacyjnych lub listę kontrolną obsługiwalności. Następnie zaproponowano kompleksową ocenę obsługiwalności systemu opartą o teorię zbiorów rozmytych. Studium przypadku, analizujące obsługiwalność systemu podwozia części nosowej cywilnego samolotu, pokazuje skuteczność metody przedstawionej w niniejszym artykule.

Słowa kluczowe: *ocena obsługiwalności, symulacja wirtualna, teoria zbiorów rozmytych, systemy samolotu.*

1. Introduction

Maintainability is a significant design characteristic of civil aircraft system, and it has great effects on daily utilization rate, dispatch reliability, life cycle cost and even operation safety of civil aircraft. Maintainability evaluation is an important design task prescribed in MIL-STD-470B [11]. The purpose of maintainability evaluation is to determine whether the specified maintainability requirements of system can be achieved.

According to MIL-STD-471A [12], the traditional maintainability evaluation is conducted by demonstrating maintenance tasks based on physical prototype in the late phase of system development, which has two types of disadvantages: first, evaluated objects are quantitatively parameters such as *MTTR* (Mean Time To Repair), *MTTRS* (Mean Time To Restore System) and *MTTS* (Mean Time To Service), and qualitative requirements related to maintainability design attributes cannot be evaluated in most situation, thus the evaluation conclusion can hardly provide suggestion about design modification; second, maintenance task demonstration is based on physical prototype or real system, even if design deficiencies are found by evaluation, it is difficult to implement design modification because of cost and time. In a word, the traditional maintainability evaluation lags behind the system development and cannot support the concurrent design of modern aircraft system.

In order to solve the above mentioned problems, many literatures have studied in the field. Wani et al. studied the maintainability factors and attributes in product design and developed a procedure based on a digraph and matrix method for evaluation of maintainability index of mechanical systems [21-22]. Meier et al. presented a model process for implementing maintainability and described the potential roles and benefits of maintainability on various types of projects [9]. Pistikopoulos et al. introduced a system effectiveness optimization framework to properly account for maintainability characteristics at the process design level. In the framework, the problem is formulated as a mixed integer linear programming model whose applicability is demonstrated by a numerical example [15]. Chen et al. discussed and identified a set of maintainability factors in terms of physical design, logistics support and ergonomics; and then, as a specific application of design review, a methodology called Vector Projection Method is applied to evaluate the maintainability of the mechanical system [2]. Tjiparuro et al. consolidated maintainability elements and attributes by reconciling and developing previous research efforts and then proposed an approach to maintainability analysis during conceptual design based on the concept of functional design and maintainability axioms [19]. Slavila et al. presented a maintainability evaluation approach based on fuzzy logic; and fuzzy linguistic variables are employed in order to represent and handle the design data available early in the design process [17]. Li et al. analyzed the tribo-maintainability related design factors from systematic perspective and concluded a more complete set of six factors, and then a fuzzy set based approach was developed to quantitatively evaluate maintainability design as well [6]. Desai et al. presented a systematic methodology of design for maintenance to enhance the maintenance operation of products and systems, human factors are also considered in the methodology [3]. Pedro et al. describe a procedure to obtain maintainability indicators

for industrial devices, they discussed the information obtained through the maintainability assessment process and its computation into several maintainability indicators [13]. ZHOU et al. divided repair time into common and individual repair time, and then proposed a new time characteristics-based maintainability allocation method, which is also applicable to maintainability evaluation [24]. With the development of computer science, virtual reality and digital technology are also used in maintainability analysis and design. Vujosevic proposed the concept of maintainability concurrent design firstly, he presented a computer-aided engineering environment to support maintainability analysis for concurrent design of mechanical system design [20]. Hao et al. developed a maintainability analysis visualization system under the AutoCAD environment, and designers can review their design from the viewpoint of easy maintenance concurrently [5]. Marcelino et al. discussed the design and implementation of a geometric constraint manager that has been designed to support physical realism and interactive assembly and disassembly tasks within virtual environments [7]. Borro et al. developed and integrated a haptic device, which can provide an enhanced sense of real manipulation and can reduce new aircraft engine development costs when conducting maintainability design [1]. Rim et al. proposed a new framework for the evaluation of working conditions by ergonomic and biomechanical analysis using digital models based on XML standard schema, including: products, processes, manufacturing resources and human workers [16]. Peng et al. designed an integrated platform for maintainability design and verification, a case based reasoning method of maintainability design and Extensible Markup Language based representation of maintenance procedure information are presented and used in the platform [14]. Yu et al. provided a fuzzy comprehensive evaluation method for product maintainability evaluation in virtual environment as well. In their research, fuzzy comprehensive evaluation method is used to evaluate product maintainability in virtual maintenance environment at stage of early design [23].

To some extent, the problems of traditional maintainability evaluation have been solved by the above mentioned researches; however, two types of shortages still exist: the one is that the evaluating methods of single maintainability design attribute have not been given, and the other is that maintainability comprehensive evaluation didn't consider detailed maintenance tasks. In order to discover the deficiencies of maintainability design for civil aircraft in the early phase of design, virtual maintenance environment has been constructed in the paper, evaluating methods of maintainability attributes are presented based on virtual demonstration in the virtual maintenance environment, and maintainability comprehensive method is proposed based on fuzzy theory. In this way, the maintainability evaluation can be conducted in the early stage of design, and the concurrent design of maintainability for aircraft system can be realized.

2. The structure of virtual maintenance environment

Virtual maintenance environment is a platform for conducting maintenance task virtual demonstration. Our virtual maintenance environment is built based on the Human Task Simulation Solution of software DELMIA developed by Dassault Systemes, in which digital mockup of civil aircraft system, digital maintenance tools and digital human model are integrated.

In order to realize the virtual simulation of maintenance task more conveniently, we have developed standard tool base and human posture base with DELMIA, from which we can generate maintenance tools with different size and kinds of human posture very quickly. In terms of maintenance task virtual simulation, designers can conduct accessibility and ergonomics virtual evaluation for each maintenance task. Fig. 1 shows the architecture of the virtual maintenance environment.

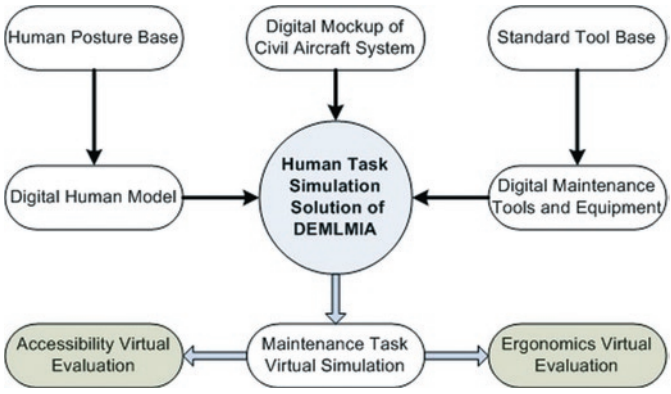

Fig. 1. Architecture of the virtual maintenance environment

3. Evaluation Methods of maintainability design attribute

The factors affecting product maintainability exist in many aspects including design, maintenance personnel, logistic support, operation context, and so on. In design phase, design factors are the main aspect, maintenance personnel and logistic factors also should be considered; and operation context such as aircraft maintenance manual and illustrated part catalog, which are commonly published after design finished, usually needn't to be considered. So, in design phase, we think that the attributes affecting maintainability of civil aircraft system including accessibility, ergonomics, simplicity, modularization, standardization, identification and testability.

Among all of the seven attributes, accessibility and ergonomics are attributes belonging to each maintenance task of the system, and we think that these attributes must be evaluated according to detailed maintenance task simulation. In another word, to these attributes, system value is the function of its all maintenance tasks' values.

In maintainability engineering, system maintenance is composed of several maintenance events, maintenance event is composed of several maintenance tasks, and each maintenance event is generally corresponding to each replaceable unit. With reference to the relationship between system *MTTR* and *MTTR* of each maintenance event [10], the system value of these attributes can be expressed as:

$$V = \sum_{i=1}^{p} \lambda_i V_i \Big/ \sum_{i=1}^{p} \lambda_i \tag{1}$$

where, V is the system value of these attributes, V_i is the ith maintenance event value of these attributes, which is corresponding to the ith replaceable unit of the system, λ_i is the failure rate of the ith replaceable unit, and p is the number of replaceable unit contained in the system. As the basic evaluation element of these attribute is maintenance task, the relationship between attribute value of maintenance event and its maintenance tasks also should be given, it can be expressed as:

$$V_i = \sum_{j=1}^{q_i} t_{ij} V_{ij} \Big/ \sum_{j=1}^{q_i} t_{ij} \tag{2}$$

where, V_{ij} is attribute value of the jth maintenance task in the ith maintenance event, t_{ij} is the time of corresponding maintenance task, q_i is the number of maintenance tasks in the ith maintenance event. Based on equation (1) and (2), we can calculate the system value of these attributes in terms of their value of maintenance tasks.

Other attributes including simplicity, modularization, standardization, identification and testability are attributes of the whole system or

product, to these attributes, we will present evaluation method based maintainability checklist in DOD-HDBK-791AM [4].

3.1. Accessibility and ergonomics evaluation based on maintenance task simulation

In DOD-HDBK-791AM [4], accessibility is defined as a design feature that affects the ease of admission to an area for the performance of visual and manipulative maintenance. According to this definition, to each maintenance task, the accessibility contains two aspects, which are visual accessibility and reachable accessibility. In the following section, we will discuss the evaluation method of the both accessibility for each maintenance task.

1) Visual accessibility evaluation

Visual accessibility of maintenance task shows whether the maintenance personnel can see the corresponding component clearly. The horizontal range of human eyes is 120 degree, and the vertical is 70 degree. Fig.2 shows the visible range of human eyes, which is provided by visual analysis tool of DELMIA.

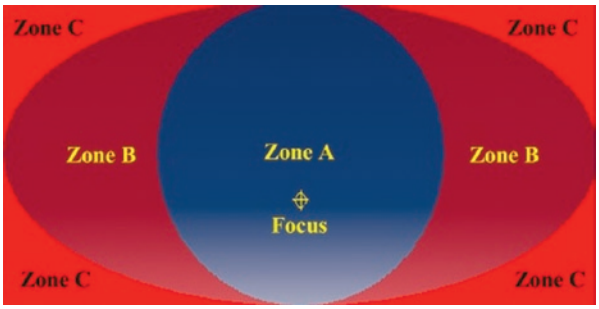

Fig. 2. Visible range of human eyes based on DELMIA

In Fig.2, the range of human vision is divided into three zones, which are zone A, B and C. Zone A's horizontal range is −35 to 35 degrees, zone B's is 35 to 60 degrees or −60 to −35 degrees, and zone C's is greater than 60 degrees or less than −60 degree; the vertical range of both zone A and B is −40 to 40 degrees, and zone C's vertical range is less than −40 degrees or 40 degrees. Fig.3 illustrates the horizontal and vertical range of human vision related to Fig.3.

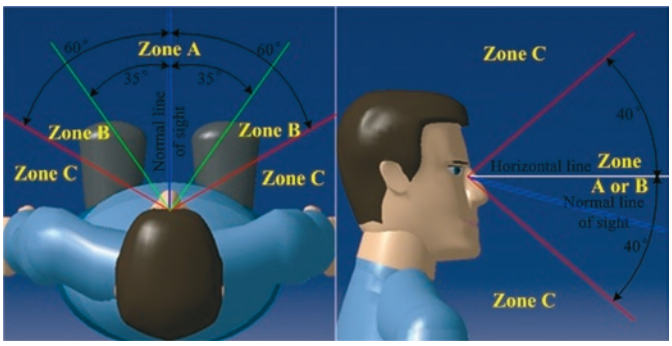

Fig. 3. The horizontal and vertical range of human eyes

We choose typical posture of each maintenance task to conduct visual accessibility evaluation, the attribute values of visual accessibility are expressed by linguistic variable herein, and the values are classified into seven ranks, which are "very satisfied", "satisfied", "a little dissatisfied", "medium", "a little dissatisfied", "dissatisfied" and "very dissatisfied". The evaluation method of visual accessibility is given in Table 1.

2) Reachable accessibility evaluation

The reachable accessibility of each maintenance task is affected by access doors or covers, tools of maintenance and interference of neighboured components. We also take linguistic variable to express the value of reachable accessibility herein. The evaluation method of reachable accessibility is given in Table 2.

In Table 2, special tools are in contrast with standard tools such as spanner, screwdriver, wrenches and pliers, most of which are contained in the standard tool base. According to Table 2, we can make evaluation of each maintenance task based on maintenance task simulation.

3) Ergonomics evaluation based on RULA

The RULA system was developed at the University of Nottingham's Institute for Occupational Ergonomics. It was developed to investigate the exposure of individual workers to risks associated with work-related upper limb disorders. We will use the RULA analysis dialog box of DELMIA to evaluate ergonomics of each maintenance task.

In RULA analysis, risk factors such as number of movements, static muscle work, force, working posture, and time worked without a break are considered to provide a final score that ranges from 1 to 7.

- 1 and 2 indicate that the posture is acceptable if it is not maintained or repeated for long periods of time;
- 3 and 4 Indicate that further investigation is needed and changes may be required;
- 5 and 6 indicate that investigation and changes are required soon;
- 7 indicates that investigation and changes are required immediately.

Determination of score value is detailed described in Dr. Lynn Mc Atamney and Professor E. Nigel Corlett's work [8]. In order to keep the ergonomics value consistent with accessibility value, we still use linguistic variable to denote RULA score; the linguistic variable "very satisfied", "satisfied", "a little dissatisfied", "medium", "a little dissatisfied", "dissatisfied" and "very dissatisfied" denote RULA score 1 to 7 respectively.

Fig. 4 is an illustration instance of using RULA analysis dialog box in DELMIA to evaluate ergonomics of the maintenance task installing wheel in NLG of civil aircraft.

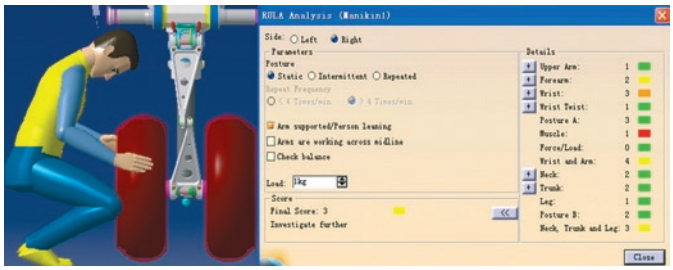

Fig. 4. RULA instance of wheel disassembly

4) Normalization of linguistic variable

In the previous context, the attribute value is expressed by linguistic variable, which can't be calculated by Equation (1) and (2) directly, as it is not numerical and has not been normalized. We use triangular fuzzy number to represent linguistic variables. Triangular fuzzy number is denoted as (v^l, v^m, v^u), where $0 \le v^l \le v^m \le v^u \le 1$, v^m is the most possible value of a linguistic variable or RULA score, v^l is the lower bound and v^u is the upper bound. The operation rules of triangular fuzzy number are given in Equation (3).

$$\begin{aligned} &(v_i^l, v_i^m, v_i^u) \pm (v_j^l, v_j^m, v_j^u) = (v_i^l + v_j^l, v_i^m + v_j^m, v_i^u + v_j^u) \\ &k \times (v^l, v^m, v^u) = (kv^l, kv^m, kv^u) \\ &(v^l, v^m, v^u) / k = (v^l / k, v^m / k, v^u / k) \end{aligned} \tag{3}$$

Table 1. Evaluation rule of visual accessibility

Attribute Value	Rules of Judgement
very satisfied	In the typical posture, the component to be dismantled or installed locates in zone A and the geometric centre of the component is the focus.
satisfied	In the typical posture, the component to be dismantled or installed locates in zone A but the geometric centre is not the focus.
a little satisfied	In the typical posture, the component to be dismantled or installed locates in zone A and B, and the geometric centre is in zone A.
medium	In the typical posture, the component to be dismantled or installed locates in zone A and B, and the geometric centre is in the border between zone A and B.
a little dissatisfied	In the typical posture, the component to be dismantled or installed locates in zone A and B, and the geometric centre is in zone B.
dissatisfied	In the typical posture, most part of the component to be dismantled or installed locates in zone B, and the geometric centre is in zone B.
very dissatisfied	In the typical posture, most part of the component to be dismantled or installed locates in zone C.

Table 2. Evaluation rule of reachable accessibility

Attribute Value	Rules of Judgement
very satisfied	The maintenance task can be finished without opening access doors, without special tools, and the task is not interfered by neighboured components.
satisfied	The maintenance task must be finished with opening access doors or with special tools, but the task is not interfered by neighboured components.
a little satisfied	The maintenance task must be finished with opening access doors and with special tools, but the task is not interfered by neighboured components.
medium	The maintenance task can be finished without opening access doors and without special tools, but the task is interfered by neighboured components slightly.
a little dissatisfied	The maintenance task must be finished either with opening access doors and special tools, and the task is interfered by neighboured components slightly.
dissatisfied	The maintenance task is interfered by neighboured components severely.
very dissatisfied	The maintenance task cannot be finished because of interference of neighboured components.

Triangular fuzzy number can reflect the fuzziness of linguistic variable; Fig. 5 shows the memberships of each linguistic variable that are "very satisfied", "satisfied", "a little dissatisfied", "medium", "a little dissatisfied", "dissatisfied" and "very dissatisfied".

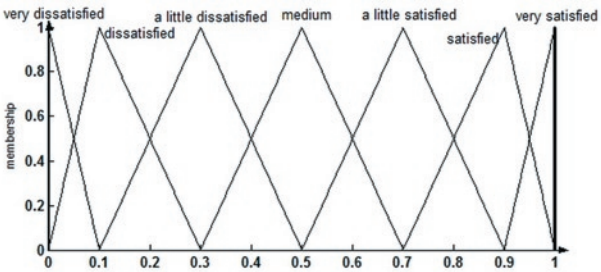

Fig. 5. Membership functions of linguistic variables

According to the membership function, we can get the triangular fuzzy number corresponding to each linguistic variable, which is shown in Table 3.

Table 3. Triangular fuzzy number of each linguistic variable

Linguistic variable	Triangular fuzzy number
Very dissatisfied	(0,0,0.1)
Dissatisfied	(0,0.1,0.3)
A little dissatisfied	(0.1,0.3,0.5)
Medium	(0.3,0.5,0.7)
A little satisfied	(0.5,0.7,0.9)
Satisfied	(0.7,0.9,1)
Very satisfied	(0.9,1,1)

3.2. Evaluation of other attributes based on maintainability checklist

Except for accessibility and ergonomics, other attributes are evaluated based on checklist in our paper. In DOD-HDBK-791AM [4], maintainability checklists are proposed for all these attributes, the evaluation process of each attribute based on maintainability checklist is given step by step as following:

a) To tailor the maintainability checklist in DOD-HDBK-791AM [4], since maintainability checklist in the file is a general one, we must choose the proper items from the checklist according to our researching object;
b) To judge whether the design of our researching object can satisfy the requirement of each item in the tailored maintainability checklist;
c) To calculate the numerical attribute value, which can be acquired by equation (4):

$$V = f(n_s / n_a) \tag{4}$$

where, V is the numerical value of the attribute; n_a is the number of all items contained in tailored maintainability checklist; n_s is the number of items that our researching object satisfied; $f(\bullet)$ is the effectiveness function, which describes the relationship between n_s / n_a and V.

To simplicity, modularization, standardization and testability, we think the result will be "medium" if about 70% items in the tailored checklist are satisfied, and therefore, the effectiveness function of these attributes is expressed as:

$$f(n_s / n_a) = (n_s / n_a)^2 \tag{5}$$

To Identification, as it will affect system safety, all items in the tailored checklist must be satisfied, or else, the result can't be accepted; thus, the effectiveness function of identification is expressed as:

$$f(n_s / n_a) = \begin{cases} 1 & n_s / n_a = 1 \\ 0 & \text{otherwise} \end{cases} \tag{6}$$

d) To convert the numerical attribute value to Triangular fuzzy number.

To keep the evaluation value consistent with accessibility and ergonomics, we should convert the numerical value to triangular fuzzy number.

The linguistic variable set $Y = \{y_1, y_2, y_3, y_4, y_5, y_6, y_7\}$ is also chosen as evaluation set, where y_1 to y_7 denote linguistic variable "very dissatisfied" to "very satisfied". The membership function of each linguistic variable shown in Fig. 5 can be expressed as:

$$\begin{aligned}
y_1(x) &= \begin{cases} -10x+1 & 0 \le x < 0.1 \\ 0 & \text{otherwise} \end{cases} \\
y_2(x) &= \begin{cases} 10x & 0 \le x < 0.1 \\ -5x+1.5 & 0.1 \le x < 0.3 \\ 0 & \text{otherwise} \end{cases} \\
y_3(x) &= \begin{cases} 5x-0.5 & 0.1 \le x < 0.3 \\ -5x+2.5 & 0.3 \le x < 0.5 \\ 0 & \text{otherwise} \end{cases} \\
y_4(x) &= \begin{cases} 5x-1.5 & 0.3 \le x < 0.5 \\ -5x+3.5 & 0.5 \le x < 0.7 \\ 0 & \text{otherwise} \end{cases} \\
y_5(x) &= \begin{cases} 5x-2.5 & 0.5 \le x < 0.7 \\ -5x+4.5 & 0.7 \le x < 0.9 \\ 0 & \text{otherwise} \end{cases} \\
y_6(x) &= \begin{cases} 5x-3.5 & 0.7 \le x < 0.9 \\ -10x+10 & 0.9 \le x < 1 \\ 0 & \text{otherwise} \end{cases} \\
y_7(x) &= \begin{cases} 10x-9 & 0.9 \le x \le 1 \\ 0 & \text{otherwise} \end{cases}
\end{aligned} \tag{7}$$

The conversion equation can be expressed as:

$$(v^l, v^m, v^u) = \sum_{i=1}^{7} y_i(f(\bullet)) \times (v_i^l, v_i^m, v_i^u) \tag{8}$$

where, y_i is the membership function of the ith linguistic variable, (v_i^l, v_i^m, v_i^u) is the triangular fuzzy number of the ith linguistic variable.

4. System maintainability fuzzy evaluation

If each maintainability attribute value is better than "medium", we think the result is acceptable, and then we can conduct comprehensive evaluation of system maintainability, otherwise, the design must be modified. We propose a comprehensive evaluation method of system maintainability based on fuzzy weighted sum.

4.1. Weight calculation

AHP method [18, 23] is used to determine weights of the eight maintainability attributes, which are shown in Fig. 6.

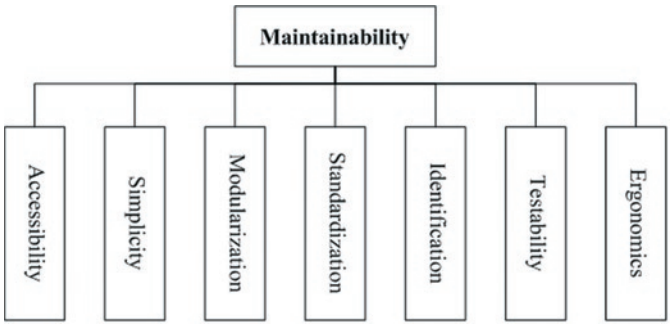

Fig. 6 Maintainability attributes of aircraft system

In AHP method weight of each attribute is acquired by pair-wise comparison matrix C, which is expressed as:

$$C = \left[c_{ij}\right] = \begin{bmatrix} 1 & c_{12} & \cdots & c_{18} \\ c_{21} & 1 & \cdots & c_{28} \\ \vdots & \vdots & \vdots & \vdots \\ w_n / w_1 & w_n / w_2 & \cdots & 1 \end{bmatrix} \tag{9}$$

where, c_{ij} denotes the relative importance bewteen attribute i and j (i, j = 1 to 8) given by experienced designers; the value of c_{ij} has 9 levels shown in table 4, and c_{ij} is the reciprocal of c_{ji}.

Table 4. The assessment rule of relative importance

Value of *cij*	Preference of attribute i to j
1	Equally preferred
3	Moderately preferred
5	Strongly preferred
7	Very strongly preferred
9	Extremely preferred
2, 4, 6, 8	Intermediate levels

The weights vector $W = [w_1, w_2, w_3, w_4, w_5, w_6, w_7, w_8]$ is the unitary eigenvector corresponding to the principal eigenvalue $\lambda_{\max}$ of the pair-wise comparison matrix C. To ensure the consistency of pair-wise comparison matrix, the consistency is evaluated by consistency ratio CR:

$$CR = \frac{\lambda_{\max} - n}{(n-1) \times RI(n)} \tag{10}$$

where, $RI(n)$ is the random consistency index. If CR is not greater than 0.1, the consistency will be accepted.

4.2. Calculation of system maintainability value

The system maintainability value is also denoted by fuzzy triangular number, which is expressed as:

$$(v_s^l, v_s^m, v_s^u) = \sum_{i=1}^{8} w_q \times (v_q^l, v_q^m, v_q^u) \tag{11}$$

where, (v_s^l, v_s^m, v_s^u) is the value of system maintainability, (v_q^l, v_q^m, v_q^u) is the value of the qth maintainability attribute, and w_i is the weight of the qth maintainability attribute.

5. Case study

5.1. Case study of evaluation based on maintenance task virtual demonstration

An example of a NLG system is used to illustrate our approach of accessibility and ergonomics evaluation. The NLG system consists of one shock strut, one drag strut, one lock stay, one Retraction actuator, one lock actuator, two down lock springs, two wheels and four door links, therefore, the maintenance events of the system are replacement of these LRUs. Take wheel replacement as an example, the maintenance event consists of eight maintenance tasks, which are removing cotter pins, removing bolts and nuts, removing wheel fastener, removing wheel, installing a new wheel, installing wheel fastener, installing the bolts and nuts, installing new cotter pins. The virtual simulation of these maintenance tasks is shown in Fig. 7.

Based on the maintenance task virtual simulation and evaluation methods mentioned above, we can determine that the visual accessibility values of all tasks are "satisfied" or "very satisfied". As Fig. 7(b) shown, bolt and nut removing or installing are interfered by wheel rim slightly, thus, their reachable accessibility values are "medium"; and as Fig. 7(c) shown, wheel fastener removing or installing need high torque impact wrench that is a special tool, thus, reachable accessibility values of these tasks are "satisfied" not "very satisfied". Table 5 shows the three attribute values of each maintenance task.

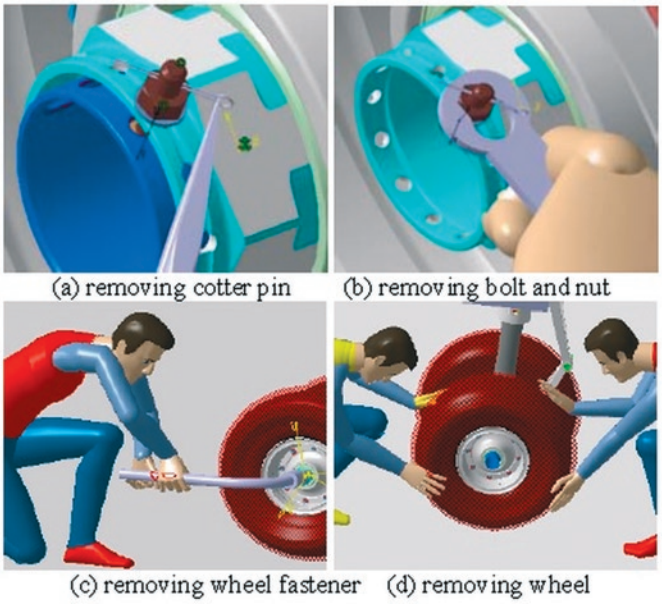

Fig. 7. Maintenance task virtual demonstration of wheel replacement

According to equation (2) and equation (3), we can get the three attribute values of the maintenance event "Replace of wheel", the visual accessibility value is (0.83, 0.96, 1), the Reachable accessibility value is (0.63, 0.79, 0.89), and the Ergonomics value is (0.43, 0.63, 0.83).

We give the three attribute values of other maintenance events directly, which are shown in Table 6. The unit of failure rate is 10^{-6} hours.

According to equation (1) equation (3), we can get the three attribute values of the NLG system, the visual accessibility value is (0.80, 0.94, 1), the Reachable accessibility value is (0.61, 0.77, 0.89), and the Ergonomics value is (0.51, 0.69, 0.88).

5.2. Case study of evaluation based on maintainability checklist

We assume that the tailored simplicity checklist of our aforementioned NLG system is shown in Table 7.

According to equation (5), we can get the numerical value of simplicity:

$$V = (8/10)^2 = 0.64$$

Base on equation (7) and (8), we can get the triangular fuzzy number of simplicity:

$$(v^l, v^m, v^u) = 0.3 \times (0.3, 0.5, 0.7) + 0.7 \times (0.5, 0.7, 0.9) = (0.44, 0.64, 0.84)$$

5.3. Case study of system maintainability fuzzy comprehensive evaluation

We take two types of NLG system as our evaluation object, which are shown in Fig. 8, the left is system A and the right is system B.

System A is just our aforementioned NLG system and most part of system B is similar to system A, the differences exist in two facets:

1) The cabin of NLG system A has four doors that are two front doors and two rear doors, the cabin of system B has only two symmetric doors, thus, system A has four door links and sys-

Table 5. Attribute values of each maintenance task in wheel replacement

Maintenance event	Maintenance task	Number of the task	Time of the task	Visual accessibility value	Reachable accessibility value	Ergonomics value
Replace of wheel	Removing cotter pin	8	0.4 min	Very satisfied (0.9,1,1)	Very satisfied (0.9,1,1)	A little satisfied (0.5,0.7,0.9)
	Removing bolt and nut	8	0.6 min	Very satisfied (0.9,1,1)	Medium (0.3,0.5,0.7)	A little satisfied (0.5,0.7,0.9)
	Removing wheel fastener	1	2.5 min	Satisfied (0.7,0.9,1)	Satisfied (0.7,0.9,1)	Medium (0.3,0.5,0.7)
	Removing wheel	1	2.5 min	Satisfied (0.7,0.9,1)	Very satisfied (0.9,1,1)	Medium (0.3,0.5,0.7)
	Installing a new wheel	1	3 min	Satisfied (0.7,0.9,1)	Very satisfied (0.9,1,1)	Medium (0.3,0.5,0.7)
	Installing the wheel fastener	1	3 min	Satisfied (0.7,0.9,1)	Satisfied (0.7,0.9,1)	Medium (0.3,0.5,0.7)
	Installing the bolt and nut	8	0.8 min	Very satisfied (0.9,1,1)	Medium (0.3,0.5,0.7)	A little satisfied (0.5,0.7,0.9)
	Installing new cotter pin	8	0.5 min	Very satisfied (0.9,1,1)	Very satisfied (0.9,1,1)	A little satisfied (0.5,0.7,0.9)

Table 6. Attribute values of the NLG's all maintenance events

Maintenance event	Number of the LRU	Failure rate of the LRU	Visual accessibility value	Reachable accessibility value	Ergonomics value
Shock strut	1	534	(0.74, 0.91, 1)	(0.52, 0.71, 0.89)	(0.39, 0.55, 0.73)
Drag strut	1	134	(0.75, 0.89, 1)	(0.51, 0.69, 0.88)	(0.45, 0.63, 0.81)
Lock stay	1	167	(0.72, 0.88, 1)	(0.55, 0.69, 0.84)	(0.83, 0.93, 1)
Retraction actuator	1	157	(0.82, 0.95, 1)	(0.45, 0.63, 0.81)	(0.61, 0.72, 0.89)
Lock actuator	1	145	(0.79, 0.94, 1)	(0.39, 0.55, 0.73)	(0.82, 0.95, 1)
Down lock spring	2	33	(0.83, 0.96, 1)	(0.61, 0.72, 0.89)	(0.65, 0.81, 0.92)
Door link	4	211	(0.71, 0.89, 1)	(0.64, 0.81, 0.92)	(0.83, 0.95, 1)
Wheel	2	1894	(0.83, 0.96, 1)	(0.63, 0.79, 0.89)	(0.43, 0.63, 0.83)

Table 7. Tailored simplicity checklist of the NLG system

Item code	Item	Satisfied?
1	The system must be searched for simplified alternatives.	Yes
2	The manual data must be understood by an average person with a junior high school education.	No
3	The function must be performed by a standard or existing part.	No
4	Simplification brainstorming must be attempted.	Yes
5	All function or part must be really necessary.	Yes
6	All wrenching or adjustment locations are visible in prevailing light?	Yes
7	The number of attachments must be minimized.	Yes
8	Adjus Table circuits cannot be further reduced.	Yes
9	Mechanical adjustments must be held to a minimum.	Yes
10	Diagnostic techniques must be simplified?	Yes

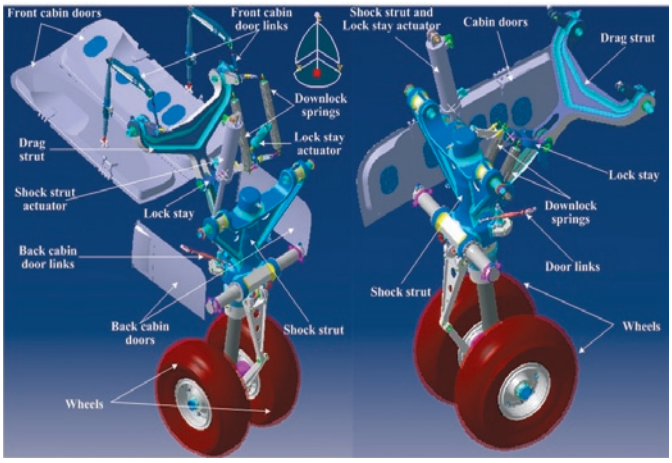

Fig. 8. Two types of NLG system

tem B has two door links. In general, the simplicity of system A is worse than system B, however, the accessibility of system A is better than system B.

2) The system A has an independent lock actuator to lock the NLG when it is in up position; the system B has only one actuator that has both retraction and lock function, so the modularization of system B is better than system A.

The evaluation values of each attribute of the two NLG systems are shown in table 8.

By consulting design experts and maintenance experts, we can get the pair-wise comparison matrix, which is:

$$C = \begin{bmatrix} 1 & 1/2 & 1 & 1/3 & 2 & 3 & 1/3 & 1 \\ 2 & 1 & 2 & 1 & 5 & 5 & 1 & 2 \\ 1 & 1/2 & 1 & 1/2 & 2 & 3 & 1/4 & 1 \\ 3 & 1 & 2 & 1 & 4 & 5 & 1 & 2 \\ 1/2 & 1/5 & 1/2 & 1/4 & 1 & 1 & 1/7 & 1/2 \\ 1/3 & 1/5 & 1/3 & 1/5 & 1 & 1 & 1/6 & 1/2 \\ 3 & 1 & 4 & 1 & 7 & 6 & 1 & 3 \\ 1 & 1/2 & 1 & 1/2 & 2 & 2 & 1/3 & 1 \end{bmatrix}$$

The principal eigenvalue of matrix is 8.078, $RI(8) = 1.41$, according to equation (10), we can get the consistency ratio $CR = 0.0079 < 0.01$, so the consistency is accepted. And we can get the weight vector for all maintainability attributes based on eigenvector of maximum eigenvalue, which is:

$$W = [0.0884, 0.1963, 0.0900, 0.2020, 0.0420, 0.0378, 0.2555, 0.0879]$$

And then, according to equation (11), we can get the system maintainability values of the two NLG system, which are (0.6671, 0.8010, 0.9366) of the NLG system 1 and (0.6865, 0.8160, 0.9420) of NLG system 2. We can know that the maintainability levels of the both NLG systems are between "a little satisfied" to "satisfied", and the maintainability of NLG system A is a little better than system B.

6. Conclusions

In the paper, line maintenance of civil aircraft system is taken as research object, virtual maintenance environment has been constructed for aircraft system, evaluating methods are presented based on maintenance task simulation or maintainability checklist for different types of maintainability design attributes, and the maintainability

Table 8. Evaluation values of each attribute of the two NLG systems

System code	Visual accessibility	Reachable accessibility	Ergonomics	Simplicity
A	(0.80, 0.94, 1)	(0.63, 0.79, 0.89)	(0.51, 0.69, 0.88)	(0.44, 0.64, 0.84)
B	(0.80, 0.92, 1)	(0.60, 0.76, 0.86)	(0.52, 0.67, 0.87)	(0.53, 0.73, 0.92)
System code	Modularization	Standardization	Identification	Testability
A	(0.51, 0.71, 0.90)	(0.70, 0.90, 1)	(0.9,1,1)	(0.69, 0.89, 0.99)
B	(0.65, 0.85, 0.97)	(0.70, 0.90, 1)	(0.9,1,1)	(0.68, 0.88, 0.99)

comprehensive method of aircraft system is proposed based on fuzzy theory.

The contribution of the paper is shown in the following three aspects:

1) A virtual maintenance environment, in which maintenance task virtual simulation can be conducted, has been constructed to support maintainability concurrent design of aircraft system. The evaluation method of maintainability attributes, such as visual accessibility, reachable accessibility and ergonomics are presented according to maintenance task virtual simulation; and the maintainability design deficiencis can be discovered in the early design stage.
2) The comprehensive evaluation method of system maintainability is proposed based on fuzzy theory, as our final evaluation result is given in the form of fuzzy triangular number, we can know the absolute system maintainability level when there is only one candidate design scheme, and we also can choose the best one from several candidate design schemes by comparing their final results.

Acknowledgements

The authors wish to appreciate the support from National Natural Science Foundation of China (61403192) and the Fundamental Research Funds for the Central Universities of China (NS2011008).

References

1. Borro D, Savall J, A Amundarain, et al. A large haptic device for aircraft engine maintainability. IEEE Computer Graphics and Applications, 2004, 24(6):70-74, http://dx.doi.org/10.1109/MCG.2004.45.
2. Chen L, Cai J G. Using Vector Projection Method to evaluate maintainability of mechanical system in design review. Reliability Engineering & System Safety, 2003, 81(2):147-154, http://dx.doi.org/10.1016/S0951-8320(03)00075-9.
3. Desai A, Mital A. Improving maintainability of products through the adoption of a comprehensive design for maintainability method. International Journal of Industrial Engineering-Theory Applications and Practice, 2010, 17(2): 103-114.
4. DOD-HDBK-791AM. Maintainability Design Techniques. U.S. Department of Defense, 1988.
5. Hao J P, Yu Y L, Xue Q. A maintainability analysis visualization system and its development under the AutoCAD environment. Journal of Materials Processing Technology, 2002, 129(1-3): 277-282, http://dx.doi.org/10.1016/S0924-0136(02)00665-9.
6. Li J R, Wang Q H, Shen H Z. Fuzzy evaluation of maintainability with tribological factors at design stage. In Applied Mechanics and Mechanical Engineering, 2010, 20-32: 1027-1033.
7. Marcelino L, Murray N, Fernando T. A constraint manager to support virtual maintainability. Computers & Graphics-Uk, 2003, 27(1): 19-26, http://dx.doi.org/10.1016/S0097-8493(02)00228-5.
8. McAtamney L, Corlett E N. RULA. A survey method for the investigation of work-related upper limb disorders. Applied Ergonomics, 1993, 24(2): 91-99, http://dx.doi.org/10.1016/0003-6870(93)90080-S.
9. Meier J R, Russell J S. Model process for implementing maintainability. Journal of Construction Engineering and Management-Asce, 2000, 126(6): 440-450, http://dx.doi.org/10.1061/(ASCE)0733-9364(2000)126:6(440).
10. MIL-HDBK-472 Notice 1. Maintainability Prediction. USA Department of Defense. U.S. Department of Defense, 1984.
11. MIL-STD-470B. Maintainability Program Requirements for Systems and Equipment. U.S. Department of Defense, 1989.
12. MIL-STD-471A. Maintainability Verification/ Demonstration/ Evaluation. U.S. Department of Defense, 1973.
13. Pedro M D L,Vicente G P D, Luis B M, et al. A practical method for the maintainability assessment in industrial devices using indicators and specific attributes. Reliability Engineering & System Safety, 100 (2012): 84-92, http://dx.doi.org/10.1016/j.ress.2011.12.018.
14. Peng G L, Yu H Q, Liu X H, et al. A desktop virtual reality-based integrated system for complex product maintainability design and verification. Assembly Automation, 2010, 30(4): 333-344, http://dx.doi.org/10.1108/01445151011075799.
15. Pistikopoulos E N, Vassiliadis C G, Papageorgiou L G. Process design for maintainability: an optimization approach. Computers & Chemical Engineering, 2000, 24(2-7): 203-208, http://dx.doi.org/10.1016/S0098-1354(00)00514-7.
16. Rim Y H, Moon J H, Kim G Y, et al. Ergonomic and biomechanical analysis of automotive general assembly using xml and digital human models. International Journal of Automotive Technology, 2008, 9 (6): 719-728, http://dx.doi.org/10.1007/s12239-008-0085-7.
17. Slavila C A, Decreuse C, Ferney M. Fuzzy approach for maintainability evaluation in the design process. Concurrent Engineering-Research and Applications, 2005, 13(4): 291-300, http://dx.doi.org/10.1177/1063293X05059807.
18. Thomas L S. How to make a decision: The analytic hierarchy process. European Journal of Operational Research, 1990, 48(1): 9-26, http://dx.doi.org/10.1016/0377-2217(90)90057-I.
19. Tjiparuro Z, Thompson G. Review of maintainability design principles and their application to conceptual design. Proceedings of the Institution of Mechanical Engineers Part E-Journal of Process Mechanical Engineering, 2004, 218(E2): 103-113, http://dx.doi.org/10.1243/095440804774134280.

20. Vujosevic R. Maintainability Analysis in Concurrent Engineering of Mechanical Systems.Concurrent Engineering: Research and Applications, 1995, 3(1): 61–73, http://dx.doi.org/10.1177/1063293X9500300108.
21. Wani M F and O P Gandhi. Development of maintainability index for mechanical systems.Reliability Engineering & System Safety, 1999, 65(3): 259-270, http://dx.doi.org/10.1016/S0951-8320(99)00004-6.
22. Wani M F and O P Gandhi. Maintainability design and evaluation of mechanical systems based on tribology. Reliability Engineering & System Safety, 2002, 77(2):181-188, http://dx.doi.org/10.1016/S0951-8320(02)00032-7.
23. Yu H Q, Peng G L, Liu W J. A practical method for measuring product maintainability in a virtual environment. Assembly Automation, 2011, 31(1):53-61, http://dx.doi.org/10.1108/01445151111104173.
24. ZHOU D, JIA X, LV C, et al. Maintainability Allocation Method Based on Time Characteristics for Complex Equipment. Eksploatacja i Niezawodność– Maintenance and Reliability, 2013; 15 (4): 441–448.

Zhong LU
College of Civil Aviation,
Nanjing University of Aeronautics and Astronautics
29 Jiangjun Road, Nanjing 211106, China

Jia ZHOU
Department of Aircraft Maintenance
China Eastern Airlines Jiangsu Limited
Nanjing 211113, China

Naixin LI
College of Civil Aviation,
Nanjing University of Aeronautics and Astronautics
29 Jiangjun Road, Nanjing 211106, China

E-mail: luzhong@nuaa.edu.cn, zhou_jia81@126.com, kogdamer@163.com

Article citation info:
BARNAT W. Numerical examination of the influence of headrest use on the body of a soldier in a vehicle loaded with a 25 kg side load. Eksploatacja i Niezawodnosc – Maintenance and Reliability 2015; 17 (4): 513–518, http://dx.doi.org/10.17531/ein.2015.4.5.

Wiesław BARNAT

NUMERICAL EXAMINATION OF THE INFLUENCE OF HEADREST USE ON THE BODY OF A SOLDIER IN A VEHICLE LOADED WITH A 25 KG SIDE LOAD

NUMERYCZNE BADANIE WPŁYWU ZASTOSOWANIA ZAGŁÓWKA NA CIAŁO ŻOŁNIERZA ZNAJDUJĄCEGO SIĘ W POJEŹDZIE OBCIĄŻONYM ŁADUNKIEM BOCZNYM 25 KG*

The issue of specialist vehicle crews' impulse resistance is described in many articles and standardization documents. These publications concern mainly explosives of smaller size. In case of sizeable explosives between 25 and 1000 kg, specialist literature is very poor. In most cases, the existing literature presents the influence of an explosive placed under the vehicle's wheel or body. The following paper focuses on the influence of a 25 kg charge placed on the side of the vehicle on the organism of a soldier staying inside. In this paper the numerical analysis results of the vehicle−explosion mechanical system have been presented. The explosion has1 been modeled using the CONWEP function. The numerical analysis has been carried out in LS-DYNA software. The vehicle has been described by Lagrange elements. The article presents results of numerical calculations for the elements of a combat vehicle's bearing structure charged with an impact generated by an explosion of a big charge placed to the side of the vehicle, at the distance of 5 m from the sideboard, at the height of 1 m. Unfortunately, the method used does not allow for taking into account the phenomena occurring as a result of the wave reflecting off the ground.

***Keywords**: specialist vehicle, explosion, vehicle's movement, FEM analysis.*

Problematyka odporności udarowej załóg pojazdów specjalnych jest opisywana w wielu artykułach i dokumentach standaryzacyjnych. Publikacje te głównie dotyczą małych wielkości ładunków wybuchowych oddziałujących na pojazd. W przypadku dużych ładunków, o wielkości od 25 do 1000 kg, literatura tematu jest bardzo uboga. Istniejące pozycje literaturowe odnoszą się do oddziaływania ładunku umieszczonego pod kołem lub kadłubem pojazdu. W pracy przedstawiono wpływ wielkości ładunku 25 kg umieszczonego z boku pojazdu na organizm żołnierza znajdującego się w nim. Przedsięwzięcie to zrealizowano za pomocą analizy numerycznej układu mechanicznego pojazd-wybuch. Wybuch został zamodelowany funkcją CONWEP. Numeryczną analizę przeprowadzono przy użyciu oprogramowania LS-DYNA. Pojazd został opisany elementami Lagrange'a. W artykule przedstawiono wyniki obliczeń numerycznych elementów struktury nośnej wozu bojowego obciążonej udarem wygenerowanym przez eksplozję dużego ładunku wybuchowego umieszczonego z boku w odległości 5 m od burty pojazdu na wysokości 1 m. Zastosowana metoda nie pozwala na uwzględnienie zjawisk Macha zachodzących podczas odbicia fali od podłoża.

***Słowa kluczowe**: pojazd specjalny, wybuch boczny, analiza MES.*

1. Introduction

Specialist vehicles are exposed to the effects of multiple weapons at enemy's disposal, mainly improvised explosive devices (IED). It results in the fact that contemporary tactical-technical requirements indicate methods of forming military vehicles' armoured bodies in order to provide the crews' high survival capability on the battlefield. Such activities are connected, among others, to providing proper level of protection against mines of different categories (various explosive materials, different masses, various explosive location).

The fundamental issue appears while creating effective crew and internal equipment protection against mines [1, 2], and especially against improvised explosive devices which may contain explosive charges of considerable sizes.

So far, a significant amount of research on human survivability has been conducted. The main driving force behind progress in this domain has been aviation. Military activities in irregular conflicts cause the enemy to make use of materials which are called improvised explosive devices due to their classification method. They may have local or global effect on a vehicle, depending on their size.

In case of an explosion having effect on a vehicle, the results may be classified as:

- knocking the vehicle over [3],
- tossing the vehicle into the air (the crew is affected during both raising and falling) [2, 5],
- armour penetration,
- membrane wave appearance [4, 5].

The main factor of the explosion's impact on the crew is acceleration. The explosion (pressure impulse) affecting the side of a vehicle through construction elements such as seat base or the body (floor) causes perpendicular and longitudinal angular, as well as transverse

(*) Tekst artykułu w polskiej wersji językowej dostępny w elektronicznym wydaniu kwartalnika na stronie ***www.ein.org.pl***

angular accelerations which affect the soldier remaining inside the vehicle. The most exposed to these accelerations are bone structure elements, such as tibias, spine (fragments around pelvis and cervical vertebrae). Research on biomechanical resistance of a human body is being carried on, focusing on many aspects, from car accidents through aviation accidents through explosive charges explosions [6, 7, 10, 12-17]. Such research is being conducted virtually all over the world.

In case of lack of seatbelts (or not fastening them) there exists strong likelihood of head injury against the vehicle ceiling. Such impact may result in injuring cervical vertebrae [13].

Human organism's response has been examined, among others, by Patrick, Kroell and Mertz [9], who concluded that the human organ exposed to G-force damage the most is brain. The authors have demonstrated a relationship between impulse size and its duration.

The following paper focuses on the impact side charges exert on vehicle, or rather on human body. The paper presents results of explosive charges influence on specialist vehicles crews. Additionally, the influence of the headrest used on human body response has been examined.

2. Numerical models description

Usually, in examining soldiers behaviors in armored vehicles LS-Dyna or MSC Dytran software is used. These programs contain explicit implementation of finite element method. They allow for modeling complex phenomena from the range of classical mechanics, flux mechanics, dynamic phenomena, as well as strong discontinuities impact on various structures. For the calculation purposes, Hybrid Dummy III 95% Male [11] model, presented in Fig. 1 has been used. The model had been developed and examined mainly for the purposes of automobile industry. It is used in research on increasing the safety of drivers, passengers, as well as car accident participants.

As has been mentioned before, Hybrid III dummies are used to simulate humans. Thanks to their build, resembling one of a man, the analysis of the results obtained gives full picture of the probability of sustained injuries.

In his book of 1964, J. Grzegorzewski [6] demonstrated that acceleration of 100 g/2ms is lethal. This value was increased to 150 g/2ms by Allem in his 1996 research. The juxtaposition of body injury cases based on the duration is presented in Table 1.

Practically, survivability indexes described in AEP-55 are not exactly indicators. They are defined values created as a result of research on survivability.

Additional research work in NATO [13] concerned tibia injuries resulting from axial force impulse's influence on tibiasin the aspect of age of soldiers exposed to the load. The research has indicated that due to ca. 9 kN axial force influence, the likelihood of injuries for people at the age of 65 amounts to 100%, to 90% for 45-year-olds, and in case of 25-year-olds it decreases down to 25%.

The following paper includes the results of initial numerical analysis of an explosion of a large, side IED charge on a specialist vehicle crew member. In the analyses carried out, a wheeled vehicle of ca. 22 tons has been assumed as the subject of study. The IED charge was placed at the distance X of 5 m from the vehicle, at the height H of 1 m over the ground, as presented in Fig. 2.

Lagrange elements of Shell Quad 4 type were used to model the behavior of vehicle's steel sheets. The elements were given the following mechanical properties: $E = 2.1 \cdot 10^9$ MPa, $\nu = 0.31$. For the description of steel behavior a bilinear elastoplastic model was used. Maximal deformation [10] was assumed as the damage criterion. A general view of vehicle numerical model, as well as the section of the whole layout is presented in Fig. 3. Both the seat with Hybrid 3 dummy and the fastening method are presented in figures below.

Numerical analyses examined two models differing according to the use of headrest (model 1 without any headrest, model 2 with a headrest). For numerical analyses of impulse effect on a crew member Hybryd III dummy was used. The dummy model − 50-centile Hybrid III, implemented separately from vehicle model by LS-DYNA system. The dummy was situated on an inflexible seat with afootrest and pelvic seat belts.

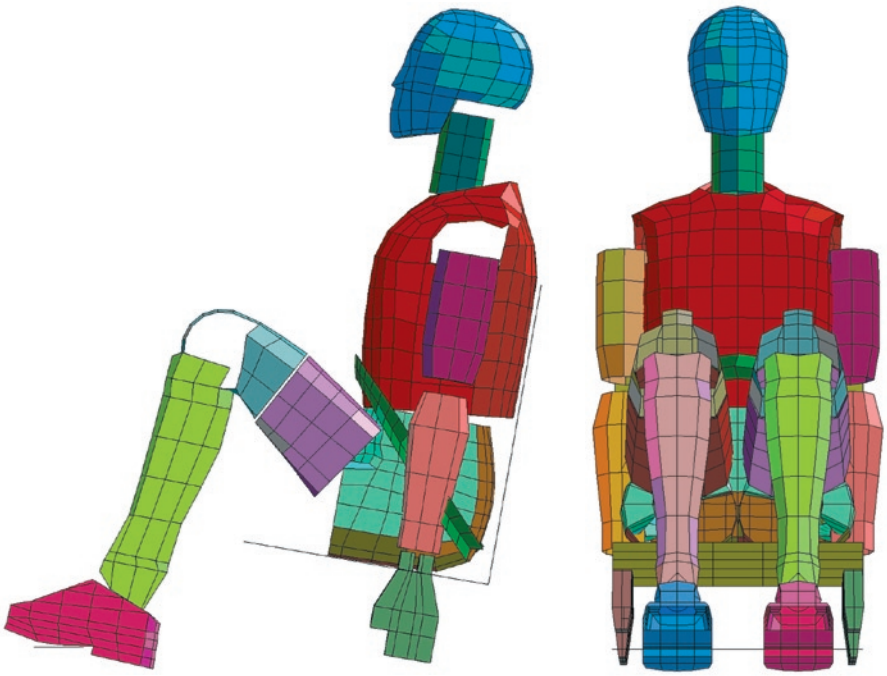

Fig. 1. Hybrid III dummy model

Table 1. Survivability index according to AEP-55 [12]

No.	Body part	Criterion	Permissible value	gravity (significance)
1.	tibia	maximal tibia clenching force value (-Fz)	5.4 kN	10% risk for ASI 2+
2.	thoracic-lumbar region	Dynamic Response Index (DRI)established based on pelvis acceleration Az	17,7	10% risk for ASI 2+
3.	cervical region (neck)	upper neck section clenching force (-Fz)	4 kN (during 0 ms) 1.1 kN (during 30 ms)	Serious (ASI 3) injuries are unlikely
		upper neck section crushing moment bending (+My) stretching (-My)	190 Nm 77 Nm	Serious (ASI 2) injuries are unlikely
4.	internal organs	Central Venous Pressure (CVP)	3.6 m/s	

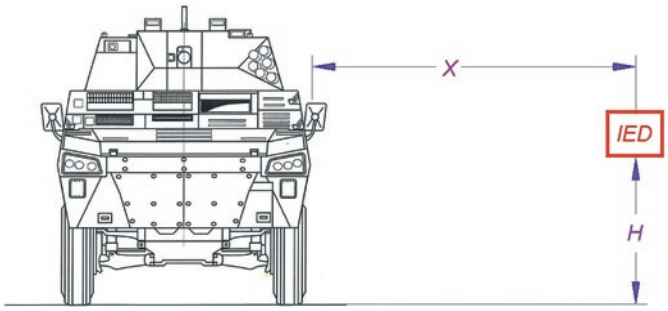

Fig. 2. Charge placement diagram relative to vehicle body

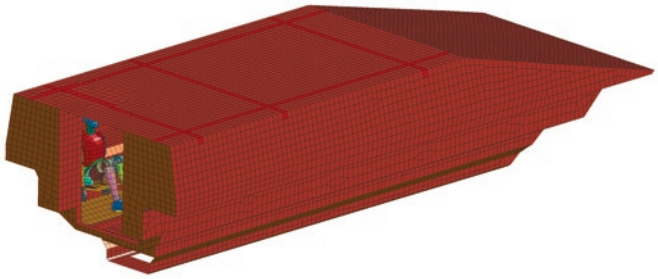

Fig. 3. Numerical vehicle model with a crew member

During numerical analyses, gravity's effect on the numerical model was taken into account.

All military armored vehicle tests are conducted according to appropriate norm, in this case NATO SATANG 4569. One of possible anti-mine resistance tests is examining the effects of TM 57 anti-personnel mine detonation with a 6.34 kg TNT charge. Due to the need for protection against IEDs, whose mass substantially exceeds the one of anti-personnel mines, the analysis conducted focused on a vehicle model loaded with an IED of significantly bigger mass than TM 57 mine.

3. Numerical analyses results

3.1. Numerical analyses results – 25 kg charge without headrest

As a result of the explosion, there appeared pressure wave impact on the side of the vehicle. Fig. 4 presents subsequent phases of vehicle's body movement under the effect of a 25-kg TNT charge.

The dummy's head's movement backwards (especially clearly visible in Fig. 4b), which can damage a soldier's neck is worth mentioning. This movement is caused by the lack of headrest. Additionally, the explosive moved the whole vehicle. Asymmetrical displacement was caused by the vehicle body's asymmetry and the explosive's placement outside of center of gravity.

Analyzing Figs. 4a–d it is worth noticing that Hybryd III's back broke away from the seat. The breaking away took place despite the seat belt use.

The main injury likelihood assessment is conducted as a result of the analyses of physical value course in time, presented in charts below (Figs. 5–8). The maximal values of quantities measured are additionally presented in Table 2.

The way of loading the vehicle entails different effect on a crew member than it has been so fat. Generally, vehicles were examined in the aspect of a load resulting from an explosion of a charge placed under a wheel or centrally. In the case in question, tibia clenching force value equals ca. 141 N (Fig 5.)

In the case in question, the value of maximal pelvis acceleration in vertical direction equaled 3.7 g (Fig. 6).

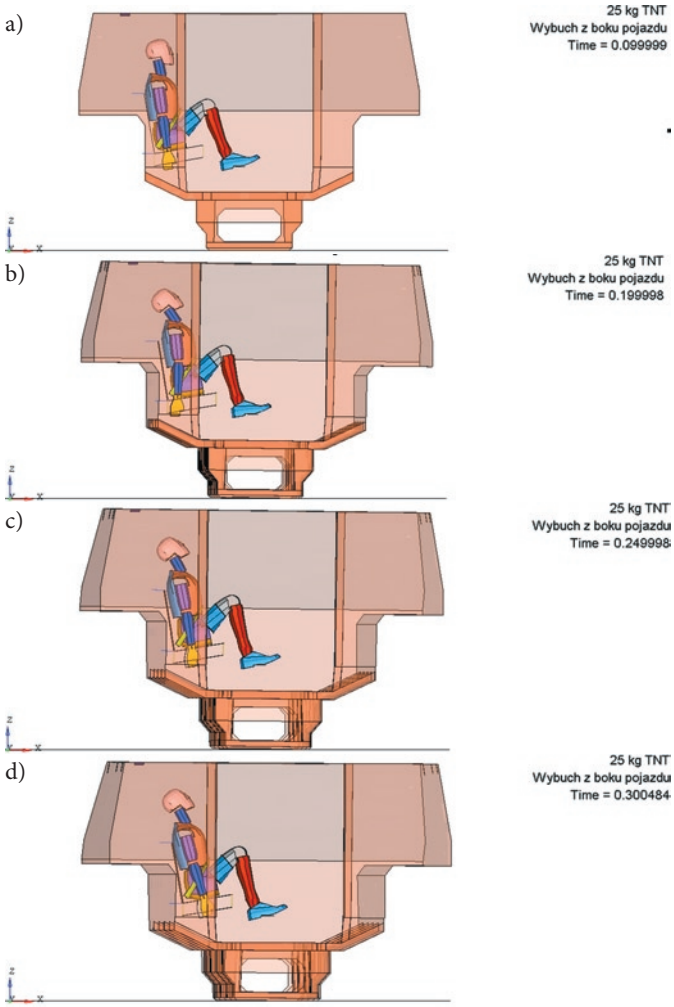

Fig. 4. The manner of vehicle body deformation and explosion's effect on a dummy in different time periods: a) 0s, b) 0.2 ms, c) 0.25 ms, d) 0.3 ms

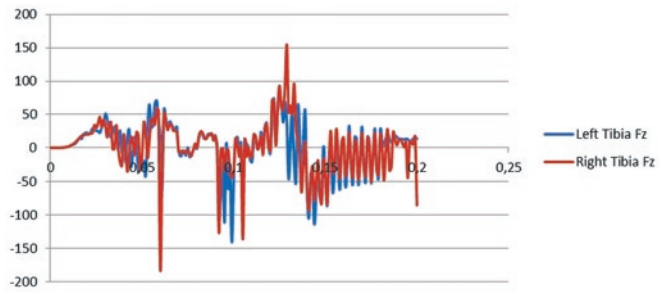

Fig. 5. Chart of longitudinal force in both tibias axis Y [N] axis X [ms]

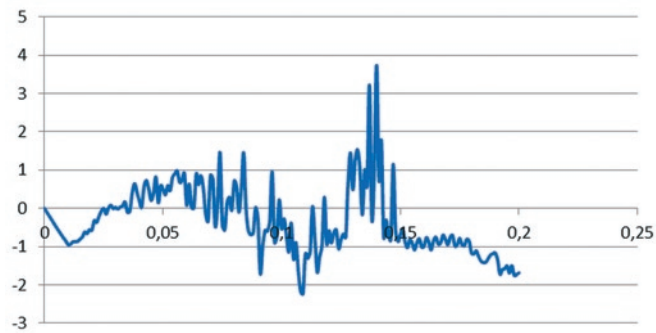

Fig. 6. Pelvis acceleration chart in vertical direction axis Y [N] axis X [ms]

Fig. 7. Chart of longitudinal force in the spine axis Y [N] axis X [ms].

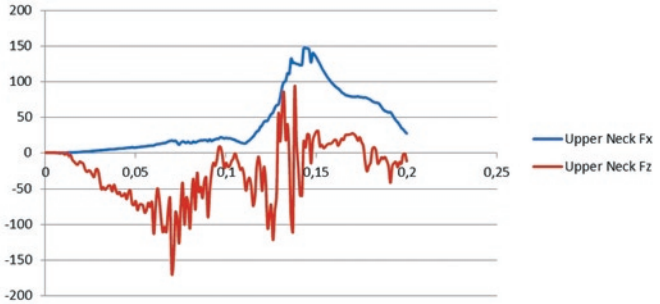

Fig. 8. Chart of longitudinal and transverse forces in the neck axis Y [N] axis X [ms]

Similarly to accelerations in the spine, the value of longitudinal force in the spine does not amount to critical quantities and equals 3750 N (Fig. 7).

Of interest is the chart of forces in the neck. Practically, the values may differ from the ones obtained due to the fictitious force closely related to the system mass. In a real vehicle, a soldier wears a helmet (which may weigh several kilograms with additional gear).
Compared to force values in lower limbs, maximal elongation force value Fz equaled 168 N, and transverse force (shear) Fx 150 N.

3.2. Numerical analyses results – 25 kg charge with headrest

In the model in discussion, additional headrest placed at the back of the vehicle was used. Similarly to the first model, as a result of the explosion there appeared pressure wave affecting the side of the vehicle. Fig. 9. presents subsequent phases of vehicle's body movement (with a headrest mounted to the seat) under the effect of a 25-kg TNT charge.

Compared to the previous model, there has been no backwards deviation of the soldier's head. The use of headrest prevented back of the head's relocation (Fig. 4b). Similarly to the first model, the explosive moved the whole vehicle. Asymmetrical displacement was caused by the vehicle body's asymmetry and the explosive's placement outside of center of gravity.

Analyzing Figs. 9. it is worth noticing that the back of Hybryd III dummy broke away from the seat, as in the first case. The breaking away took place despite the seat belt use.
The main injury likelihood assessment is conducted as a result of the analyses of physical value course in time, presented in charts below (Figs. 10-13). The juxtaposition of maximal values of quantities measured are additionally presented in Table 2.

The way of loading the vehicle entails different effect on a crew member than it has been so fat. Generally, vehicles were examined in the aspect of a load resulting from an explosion of a charge placed under a wheel or centrally. It resulted in large values of forces and perpendicular accelerations, affecting a person.

In the case in question, tibia clenching force value equals ca. 262 N (Fig 10.)

In the case in question, the value of maximal pelvis acceleration in vertical direction equaled 6.2 g (Fig. 11).
Similarly to the accelerations in the spine, the value of longitudi-

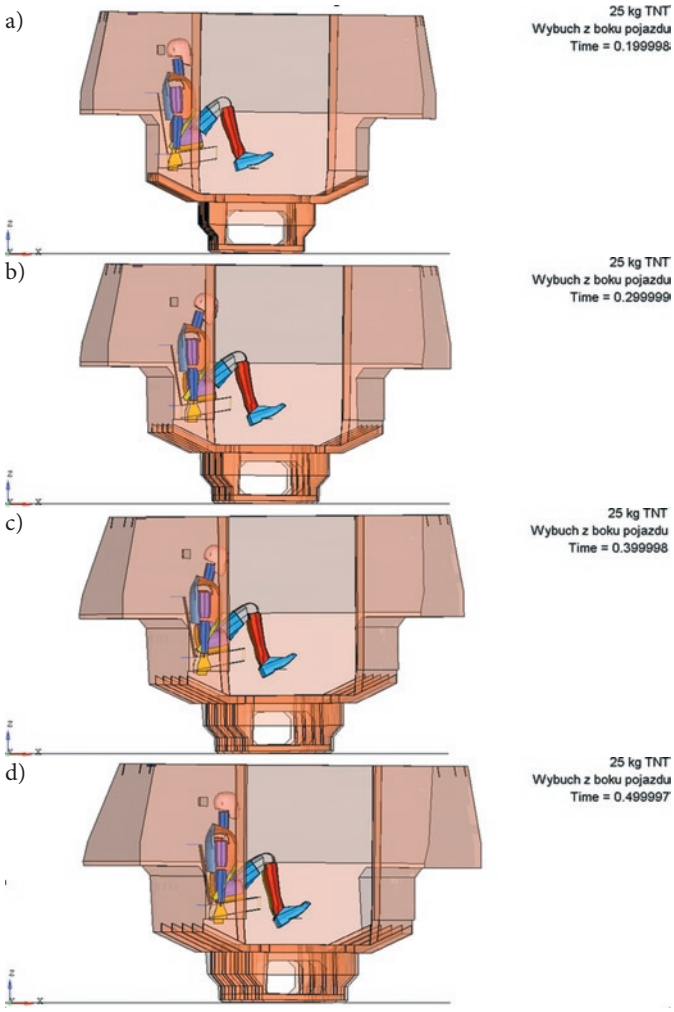

Fig. 9. The manner of vehicle body deformation and explosion's effect on a dummy in different time periods: a) 0.2 ms, b) 0.3 ms, c) 0.4 ms, d) 0.5 ms.

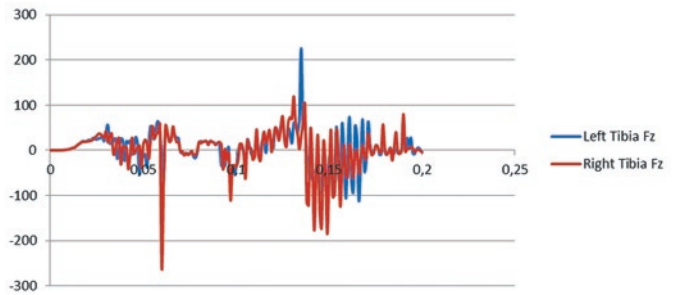

Fig. 10. Chart of longitudinal force in both tibias for the case with a headrest used axis Y [N] axis X [ms].

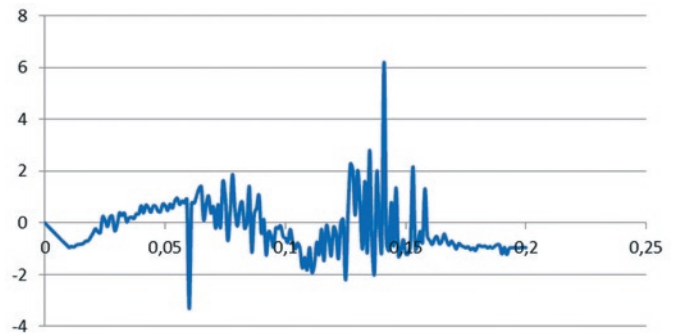

Fig. 11. Pelvis acceleration chart in vertical direction axis Y [N] axis X [ms]

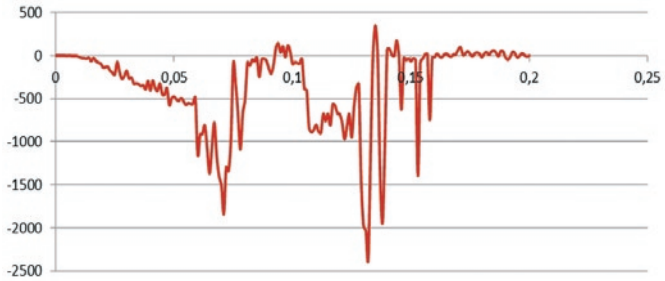

Fig. 12. Chart of longitudinal force in the spine axis Y [N] axis X [ms]

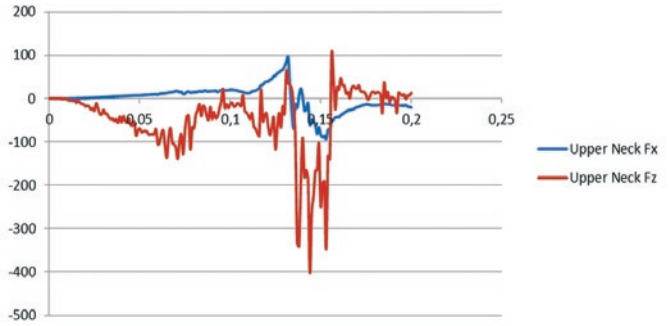

Fig. 13. Chart of longitudinal and transverse forces in the neck axis Y [N] axis X [ms]

Table 2. Maximal values from acceleration and force courses.

	Pelviz Z acceleration [g]	Lumbar Fz [N]	Upper Neck Fz [N]	Upper Neck Fx [N]	Tibia R Fz [N]	Tibia L Fz [N]
25 kg ref.	3,7	-3750	-168	150	-182	-141
25 kg protection	6,2	-2360	-400	100	-262	-225

nal force in the spine does not reach critical quantities and equals 2360 N (Fig. 12). It is worth noticing that the use of headrest contributed to decreasing the value of this force.

As in the previous case, of interest is the chart of forces in the neck. Practically, the values may differ from the ones obtained due to the fictitious force closely related to the system mass. In a real vehicle, a soldier wears a helmet. Compared to force values obtained for the first model, a significant decrease in transverse (shear) force Fx 100 N was noted. Unfortunately, the use of headrest strengthened the effect of elongation force Fz, which equaled 400 N.

4. Conclusions

The article presents one fragment of the analysis of specialist vehicles soldier's protection. Scientific papers to date have not included side influence of large explosives on crew members. The use of finite-element method for numerical analyses allows for limiting the duration of construction process. One should not forget that obtaining satisfactory results does not absolve the constructors of critical approach to the results obtained. Additionally, it is worth noticing that some quantities used to assess the value of human survivability were exceeded. It entails the necessity of modifying the way in which landing forces soldiers are seated.

Proper placement of the explosive charge relative to the vehicle may cause the appearance of numerous unfavorable phenomena from the vehicle protection point of view. In the case of incorporating explosive border value, a knocking over or tossing the vehicle into the air may take place.

Acknowledgement

This study has been supported by the National Centre for Research and Development as a part of a research & development project No DOB-BiO/001/05/2014. This support is gratefully acknowledged.

References

1. AEP-55, Volume 2 for mine threat (Edition 1). Procedure for evaluating the procetion level of logistic and light armoured vehicles, NATO/PfP Unclassified publication 2006.AEP 55, Wydawnictwo NATO,
2. Barnat W. Badania symulacyjne pojazdów wojskowych. Wydawnictwo Wojskowego Instytutu Techniki Inżynieryjnej we Wrocławiu 2014; 241-269.
3. Barnat W. Numerical and experimental investigation on internal membrane pressure wave inside sealed structure. Bulletin of the Polish Academy of Sciences – Technical Sciences 2013; 61, 3; 613-621, http://dx.doi.org/10.2478/bpasts-2013-0064.
4. Barnat W. Wybrane zagadnienia ochrony życia i zdrowia załóg pojazdów przed wybuchem. Military Rok 2011.
5. Barnat W., Nawrat A. The influence the location of large charge on behaviour special vehicles SHIBA and AV (Armoured Vehicle). Studies in Systems, Decision and Control 2, Innovative Control Systems for Tracked Vehicle Platforms, Aleksander M. Nawrat (ed.). Wyd. Springer 2014.
6. Grzegorzewski J. Przyśpieszenia, przeciążenia, nieważkość. Wydawnictwo MON 1964.
7. Krzystała E., Kciuk S., Mężyk A. Identyfikacja zagrożeń załogi pojazdów specjalnych podczas wybuchu, Wydawnictwo Naukowe Instytutu Technologii Eksploatacji 2012.
8. LS DYNA MANUAL 2010.
9. Patrick L., Kroell C., Mertz H. Forces on the human body in simulated crashes. Proceedings of the 9th Stapp Car Crash Conference. Society of Automotive Engineers. Warrendale 1965.
10. Kopczyński A., Rusiński E., Bezpieczeństwo bierne, pochłanianie energii przez profile cienkościenne. Oficyna Wydawnicza Politechniki Wrocławskiej, Wrocław 2010.
11. Test Methodology for Protection of Vehicle Occupants against Anti-Vehicular Landmine Effects. Wydawnictwo RTO/NATO 2007.
12. Tejszerska D. Świtoński E., Gzik M. Biomechanika narządu ruchu człowieka. Instytut Technologii Eksploatacji PIB 2011.

13. Wieremieew. J. Miny wczoraj i jutro. Wydawnictwo Współczesna Szkoła Mińsk 2008.
14. Baskin T.W., Holcomb J.B., Bombs, mines, blast, fragmentation, and thermobaric mechanisms of injury, [in] Mahoney F.P., Ryan J.P., Brooks A.J., Schwab C.W.(ed.): Ballistic trauma. A practical guide. Secondo edition, Ó2005 Springer-Verlag London Limited, pp. 45-66.
15. Pryor J.P., Cotton B., Neck Injury. [in] Mahoney F.P., Ryan J.P., Brooks A.J., Schwab C.W.(ed.): Ballistic trauma. A practical guide. Second edition, Ó2005 Springer-Verlag London Limited, pp. 209-240.

Wiesław BARNAT
Faculty of Mechanical Engineering
Military University of Technology
ul. gen. S. Kaliskiego 2, 00-908 Warszawa, Poland
Email: wbarnat@wat.edu.edu.pl

Article citation info:
DZIUBAK T, SZWEDKOWICZ S. Operating properties of non-woven fabric panel filters for internal combustion engine inlet air in single and two-stage filtration systems. Eksploatacja i Niezawodnosc – Maintenance and Reliability 2015; 17 (4): 519–527. http://dx.doi.org/10.17531/ein.2015.4.6.

Tadeusz DZIUBAK
Sebastian SZWEDKOWICZ

OPERATING PROPERTIES OF NON-WOVEN FABRIC PANEL FILTERS FOR INTERNAL COMBUSTION ENGINE INLET AIR IN SINGLE AND TWO-STAGE FILTRATION SYSTEMS

WŁAŚCIWOŚCI EKSPLOATACYJNE WŁÓKNINOWYCH PRZEGRÓD FILTRACYJNYCH POWIETRZA WLOTOWEGO SILNIKÓW SPALINOWYCH PRACUJĄCYCH W UKŁADACH JEDNO- I DWUSTOPNIOWYCH*

The parameters of basic filter media used in inlet air systems of internal combustion engines of motor vehicles are presented. Performance properties of the air filters defining their basic parameters are discussed. The effects of single and two-stage filtration systems on performance, including filter medium dust capacity are presented. The methods and conditions for testing non-woven fabric filters in single and two-stage filtration systems were developed. Filter separation efficiency and flow resistance characteristic curves for non-woven fabric filters as a function of dust capacity were determined. Dust capacity of tested non-woven fabrics was determined for allowable flow resistance values. The effects of fractional composition of dust downstream of the inertial filter on reduction of dust capacity of non-woven fabrics in two-stage filtration systems were shown.The advantages including improvement in service life and reduction of wear of engine components due to use of inertial filter as the first filtration stage are presented.

***Keywords**: engines, performance, air cleanness, non-woven fabric filter, filter separation efficiency and filtration rate, surface wear, filter durability.*

Przedstawiono parametry podstawowych materiałów filtracyjnych powietrza wlotowego silników pojazdów mechanicznych. Omówiono właściwości eksploatacyjne filtru powietrza i określające je podstawowe parametry. Przedstawiono wpływ warunków filtracji jednostopniowej i dwustopniowejna właściwości eksploatacyjne, a w tym na chłonność materiału filtracyjnego.Opracowano metodykę i warunki badań włóknin filtracyjnych pracujących w warunkach filtracji jednostopniowej i dwustopniowej. Wyznaczono charakterystyki skuteczności filtracji i oporów przepływu włóknin filtracyjnych w zależności od współczynnika chłonności pyłu. Dla dopuszczalnej wartości oporu przepływu wyznaczonowartości współczynnika chłonności pyłu badanych włóknin. Wykazano wpływ składu frakcyjnego pyłu za filtrem bezwładnościowym na zmniejszenie wartości współczynnika chłonności pyłu włóknin pracujących w warunkach filtracji dwustopniowej. Przedstawiono korzyści w postaci wydłużenia czasu eksploatacji i minimalizacji zużycia elementów silnika wynikające z stosowania filtru bezwładnościowego, jako pierwszego stopnia filtracji powietrza.

***Słowa kluczowe**: silniki,eksploatacja, czystość powietrza, włóknina filtracyjna, skuteczność i dokładność filtracji, zużycie powierzchni, trwałość filtru.*

1. Introduction

Modern internal combustion engines operate at higher and higher mechanical and thermal stresses and yet are required to be more reliable and durable. To meet those requirements, it is crucial to ensure high cleanliness of operating fluids, including inlet air.

High cleanliness of inlet air in the internal combustion engines of motor vehicles and machines and thus reduction of friction and improved machine life always was and still is a major operational and design issue, in particular in vehicles operating in heavy dust conditions (approx. 1 g/m^3). The conditions generally apply to special and military vehicles (tanks, land attack vehicles, self-propelled guns and special vehicles) with high-power diesel engines and maximum air demand Q_{Sil}>1 kg/s. E.g. T-72 tank engine air supply system: (cylinder capacity V_{ss} = 38.8 dm^3) at v = 20 km/h on testing ground roads at air dust loading s = 1 g/m^3, introduces over 170 kg of dust at the distance of 1000 km. Passenger car engines (V_{ss} = 1.5 dm^3) at 60 km/h on surfaced roads (s = 10 mg/m^3) introduces over 0.6 kg of dust at the distance of 20 thousand kilometres. The data shows, that the air filters used in special and passenger vehicles must not have the same design and operate in the same way.

Thus, all trucks and special vehicles are fitted with two-stage inlet air filtration system, where the first stage is an inertial filter and the second stage is a paper filter element. Commonly used paper filter elements feature high filter separation efficiency and low dust capacity (k_m = (200 ÷ 240) g/m^2). If the paper filter element is subject to the dust downstream of the inertial filter, its dust capacity is reduced almost four times [10].

Modern production technologies of non-woven fabrics allowed them to be more commonly used as inlet air filter media in motor vehicle engines. Based on the scant data that are available from non-woven fabric manufacturers, the fabrics show significantly higher dust capacity compared to filter papers k_m = (450 ÷ 500) g/m^2 [30]. No data

(*) Tekst artykułu w polskiej wersji językowej dostępny w elektronicznym wydaniu kwartalnika na stronie ***www.ein.org.pl***

are available on separation efficiency, filtration rate and durability of non-woven fabric filter elements, thus relevant tests are required.

2. Contaminants in air and effects on engine's service life

Free air supplied to the internal combustion engines of motor vehicles contains high quantities of the following contaminants [4, 5, 23]:

- natural - over 85% of total contaminants (dust, plant spores, bacteria, salts and gases, e.g. carbon monoxide, sulphur dioxide, sulphur trioxide),
- mineral dust from motor vehicle traffic or wind - road dust,
- exhaust gases from motor vehicles (dust, carbon black, lead compounds, heavy hydrocarbons, particulate matter and gases) [4, 23],
- dust emission by motor vehicles due to wear of friction lining in brakes and clutch plates, tires and pavement [5]
- industrial.

Dust particles can be classified by size [4]:

- total dust – mixture of small solid particles (suspended in the air) standard size <300 μm,suspended dust PM10 – standard size <10 μm,
- fine dust PM2.5 – standard size <2.5 μm,
- nanoparticles PM1 – standard size <1 μm.

Motor vehicles are subject to contaminants, which introduced with air to both piston and turbine engines will result in increased wear of engine components and thus limit their reliability and durability. The most common contaminants affecting machines is the road dust, raised by moving motor vehicles or wind, and introduced with air to engine cylinders. Most naturally occurring dusts, including road dust are polydisperse dusts with different physical and chemical properties. Free air includes contaminants with size composition from (0.001 ÷ 1000) μm. Air dust loading, defining contaminant content (in grams or milligrams) in one cubic meter of air depends on many factors: surface type, climatic conditions, drive system, height, soil type and industrial plant type. Fig. 1 shows air dust loading as a function of operating conditions [2].

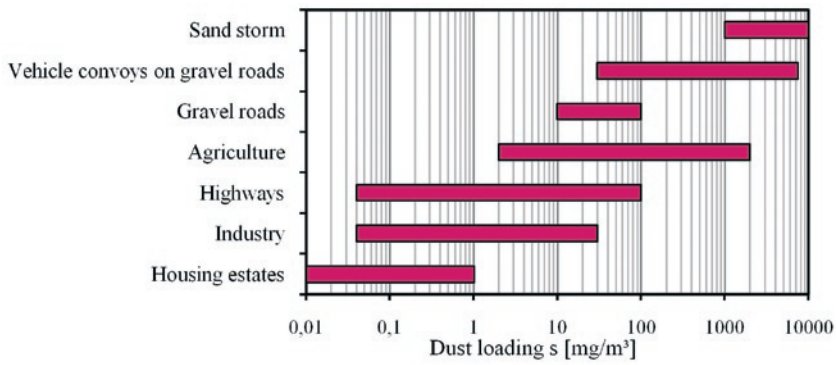

Fig. 1. Air dust loading as a function of operating conditions [2]

Air intakes of internal combustion engine intake systems draw in dust $<d_z$ = (80 ÷ 100) μm with air. Some contaminants that enter the engine cylinders via air supply system are combusted, some are removed with the exhaust gases, and some, mostly the mineral dust (approx. (10 ÷ 20)% settle at the cylinder sleeve walls and are mixed with oil to forms abrasive paste. The dust on the cylinder sleeves enters between the mating surfaces (piston - rings - cylinder) and results in premature wear. During piston movement into the bottom dead centre, the dust with oil is removed to the oil sump, and via the oil lines distributed to all lubricated engine components also resulting in premature wear.

Numerous studies on the effects of contamination of operating fluids on piston engine components wear show that the dust grains with the size corresponding to the minimum thickness of the oil film between mating surfaces cause the highest wear (Fig. 2) [1, 12, 13].

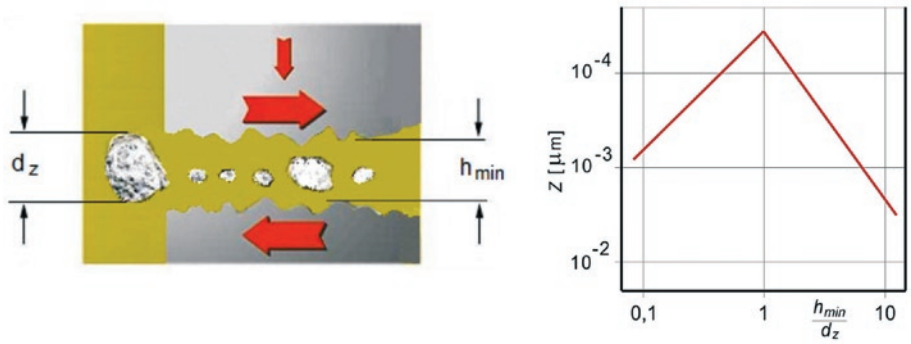

Fig. 2. The effects of the oil film thickness on wear: a) solids acting on the friction pairing, b) relationship between wear Z and ratio h_{min}/d_z [12]

Oil film thickness is not constant but varies depending on the engine operating conditions, mainly its load. Oil film thickness between piston, rings and cylinder is determined by the piston speed, oil viscosity and engine load and its maximum value between the dead centres is between (0.3 ÷ 7) μm [7, 12, 13]. At the dead centres, the piston speed is reduced to zero, which is one of the reasons the oil film thickness is reduced or even eliminated completely, thus resulting in increased wear [7, 13, 18, 19].

The dust particle hardness, depending on its chemical composition also affects the wear rate of mating engine components. The main component of the road dust drawn in with air is silica, with total content in the dust mass of up to 90%. Silica particle hardness in Mohs' scale of hardness is 7, i.e. more than the hardness of components used in the internal combustion engine design. An example of a premature wear of engines in dump trucks used for sand transport, with mileage of approx. (30 ÷ 40) thousand kilometres, due to premature wear of piston, rings and cylinder are shown in [26].

3. Air filter performance parameters

For the air filter to clean inlet air in motor vehicle engines it must feature specific properties, determined by the following parameters: separation efficiency, flow resistance and filtration rate [27].

Filter separation efficiency φ determines filter capacity for qualitative and quantitative retention of particles in the air stream. It is mainly determined as a ratio of the test dust mass m_{PF} retained by the filter to the test dust mass m_{PD} introduced to the filter in the air stream in a unit of time:

$$\varphi = \frac{m_{PF}}{m_{PD}} \cdot 100\% \tag{1}$$

Flow resistance Δp_f is a total pressure difference measured directly at the filter inlet p_{c1} and the filter outlet p_{c2}:

$$\Delta p_f = p_{c1} - p_{c2} \text{ [kPa]}. \tag{2}$$

In special cases, if the inlet and outlet line are at the same level and have the same diameter $D_1 = D_2$, and thus the air flow rate is identical, the flow resistance is expressed as the difference in static pressures as:

$$\Delta p_f = \Delta p_s = p_{s1} - p_{s2} \text{ [kPa]}. \quad (3)$$

Filtration rate is a minimum dust particle size d_{zmin} [μm] retained by the filter for a specific air volume or a maximum dust particle size d_{zmax} downstream of the filter.

Dust capacity k_m is a ratio of the total dust mass m_{CwF}, retained by the filter element at specific Δp_{fdop} value to active surface area of the filter paper F_w at uniform dust distribution along the entire active surface area of the filter paper F_w:

$$k_m = \frac{m_{CwF}}{F_w}, \text{ g/m}^2. \quad (4)$$

Performance of the panel filters used in the inlet air systems of motor vehicle engines depends on the following parameters: air flow rate, dust and filter layer structure. In practice, the air filter performance is usually determined as a function of a single parameter in laboratory conditions, using standard test stands and standard tests with test dust.

In two-stage filters in "multi-cyclone - porous panel filter" configuration, the filter medium is subject to dust, which downstream of the inertial filter (multi-cyclone) shows different size distribution compared to the dust in the inlet air. Depending on the flow conditions of the aerosol inside the cyclone, clean air (cyclone outlet air) contains dust particles <(15÷30) μm. It is both referenced in the literature [1, 16, 17, 22] and result from the single cyclone tests carried out by the authors. The filter element in serial configuration downstream of the multi-cyclone is affected by smaller dust particles. Single-stage filter draws in significantly larger dust particles, up to 80 μm. Thus, the filtration processes in both the former and the latter case can differ. To design a two-stage filter element, the properties of a filter medium corresponding to the operating conditions of the second stage air filter must be known. The performance data can be obtained by experimental tests, although special methods are required to ensure suitable operating conditions of the second stage filtration.

4. Characteristics of inlet air filter media

The most common air filters used in motor vehicles and machines are panel filters, classified by filter medium as surface filters, depth filters and surface-depth filters.

Filter papers (surface-depth medium) are the most commonly used filter media for filtration of operating fluids in motor vehicles. Filter medium manufacturers provide data on some parameters only. Since the filter paper manufacturing companies use different methods to determined those parameters, it is sometimes difficult to compare available data. In general, the filter papers are characterized by the following parameters [8, 11, 14]:

- filter separation efficiency up to φ = 99.99%,
- basis weight – (115 ÷ 240) g/m²,
- bed thickness – (0.3 ÷ 0.9) mm,
- pore size – (40 ÷ 95) μm,
- fibre diameter – (10 ÷ 20) μm,
- dust capacity – up to (200 ÷ 240) g/m²,
- flow resistance,
- air permeability.

In the available national and foreign literature, more and more information are available on basic properties of filter papers with added nano-fibres used as inlet air filters in internal combustion engines of heavy-duty vehicles [11, 14, 15]. The data on filter separation efficiency, filtration rate and dust capacity are available in the literature, but not always include the conditions used to determine these properties. In study [11], mass of dust retained by the filter paper and filter paper with nano-fibres is specified at the point the flow resistance of Δp_w = 7.5 kPa and air flow rate of 1360 m³/h are reached. The element made of PA1885 filter paper, at the point of reaching flow resistance of Δp_w = 7.5 kPa have retained 2415 g of dust, whereas the same paper filter with a layer of nano-fibres have retained over 50% more dust, i.e. 3770 g in the same time period. No surface area of filter medium is specified, and thus no filtration speed and dust capacity can be determined. In study [14], dust capacity of filter paper (k_m = 28 g/m²) and paper with nano-fibre layer (k_m = 78 g/m²) is determined using AC Fine test dust (d_{zmax} = 80 μm). Dust capacity of the same filter media but using sodium chloride particles (dimensions up to d_z = 0,4 μm) is k_m = 4 g/m² and k_m = 21 g/m², respectively. No conditions (flow resistance) at which the dust capacity was determined were specified. The results for filter paper with nano-fibre layer and AC Fine test dust showed almost twofold increase in dust capacity, and in case of sodium chlorine, the dust capacity increased almost four times. Dust capacity of filter paper determined using very fine dust (d_{zmax} = 0.4 μm) was seven times lower compared to large diameter dust (d_{zmax} = 80 μm).

The basic filter medium (depth filter) used in air filters for motor vehicles is a synthetic non-woven fibre. Fibrous woven fabrics feature pore size distribution which is easy to determine and filter separation efficiency, which is easy to adjust by simply changing the spinning parameters. The media allow easy cleaning due to the surface nature of filtration. Woven fabric filters are made of a single type of fibres, different types of fibres or multiple layers of fibres.

Non-woven fabric filters feature higher porosity and thus higher air permeability (lower flow resistance). They also achieve higher filter separation efficiencies, and due to even mass distribution of retained dust at the entire material depth may also achieve higher dust capacities. Random fibre layers are formed by bonding or stitching (mechanical) [6].

The development of fibre forming methods (melt-blown, electrospinning) and low production costs have contributed to more common use of non-woven fabrics as filter medium of panel filter elements in motor vehicles, industrial plants and sanitary plants [6].

Limited publications are available including the test results for non-woven fabrics and dust particle size corresponding to the size of dust particles drawn in by the air filters of motor vehicles (d_{zmax} = 80 μm).

Non-woven fabric tests are carried out on standard test stands, where the tested non-woven fabric forms a flat section enclosed in a tight container. Air filter elements are made of pleated filter medium sheets, both in case of paper filters and non-woven fabric filters. Commonly used test methods does not allow for the effects of filter medium shape on achieved filter separation efficiency and the dust capacity values. Due to air flow, pleated non-woven fabric filters can undergo deformation and deflection, which affect the conditions in which the filter cake is formed and thus affect filter separation efficiency and flow resistance [20].

Filter separation efficiency data available in the literature for fibrous filter media mainly apply to initial separation efficiency. There are limited data available on the characteristics of filter separation efficiency and flow resistance of non-woven fabric filters as a function of retained dust mass. Filter separation efficiency data are sometimes presented as a function of time, without specifying the test conditions (dust loading, flow rate, surface area or filtration velocity). The tests allow to compare different types of non-woven fabrics, although do not give any information on dust capacity, required to determine the service life of a material in specific conditions [21].

In the available studies on non-woven fabric filters, the most common characteristics involve the effects of selected non-woven fabric

parameter (density, fibre packing density) or aerosol (grain size, filtration velocity) on filter separation efficiency [6, 21]. Some sources give the dust capacity of non-woven fabrics, but the values are discrepant. In study [28], the dust capacity of non-calendered non-woven fabric with a thickness of 3.2 mm, determined at a flow rate of 0.3 kPa is k_m = (54.5 ÷ 89.3) g/m², whereas the dust capacity for identical calendered fabric is k_m = (85.5 ÷ 112.3) g/m². In study [8], the dust capacity of a multi-layer non-woven fabric filter is k_m =(900 ÷ 1100) g/ m², without specifying the flow resistance used to determine the dust capacity. As per study [30], the dust capacities of non-woven fabric filters exceed (400 ÷ 480) g/m², although no information on test conditions and test dust used are given.

Filter separation efficiency of non-woven fabric filters can be improved by wetting the fibres with oil to ensure more durable bond between the particles and the fibres to limit re-emission and reduction of filter separation efficiency. Wetting the fibres with oil also reduces the intensity of flow resistance increase as a function of dust mass retained by the filter. As per study [24, 25] wetting the fibres with oil have reduced the intensity of flow resistance increase by half at aerosol flow rate of 0.11 m/s.

The parameters of selected types of non-woven fabric filters manufactured by Korea Filtration Technologies Co. [29] are shown in Table 1, whereas parameters of non-woven fabric filters manufactured by Retop Fibre [30] are shown in Table 2.

Despite high filter separation efficiency (over 99%) and high dust capacity, the non-woven fabric filters are rarely used in inlet air filtration systems in passenger motor vehicles.

Trucks and special vehicles usually operating in high dust loading conditions, are usually fitted with two-stage filtration systems that guarantee long periods between maintenance.The reasoning behind using two-stage filters consists in preliminary separation of large dust particles in the inertia filter and leaving small dust particles in the air d_z<(20÷35) µm and separation of smaller particles d_z = (2 ÷ 5) µm in the panel filter (usually paper filter element with suitable surface area).

The service life of the air filtration systems in engines until the permissible flow resistance value (maximum air flow resistance for specific engine type is determined by the manufacturer and corresponds to 3% decrease in motor power) is reached is much longer than for the panel filter itself in the same dust loading conditions. (Fig. 3). Permissible flow resistance for diesel engines used in trucks and special vehicles is (5 ÷ 7) kPa.

No structural solutions for multi-stage air filters using non-woven fabric filters are available for trucks and special vehicles. It is due to lack of sufficient knowledge on non-woven fabric filter parameters, in particular dust capacity determined in two-stage filtration conditions. Use of non-woven fabrics in inlet air filters in truck engines may significantly reduce the maintenance frequency. The dust capacity of the filter medium in two-stage filtration conditions must be known to design a two-stage air filter. The values in the available literature are given for the paper filters only.

The study shows empirical assessment of filter separation efficiency, dust capacity and flow resistance of selected non-woven fabrics for operating conditions specific to off-road vehicles.

Table 1. Properties of non-woven fabric filters manufactured by Korea Filtration Technologies Co. [29]

Item	Parameters	Units	Non-woven fabric designation			
			AC-1800	AC-3800	AC-301	AC-180
1	Basis weight	g/m²	290	240	210	300
2	Thickness	mm	2.8 ÷ 3.6	3.15 ÷ 3.85	2.43 ÷ 2.86	2.61 ÷ 3.19
3.	Air permeability	cm³/cm²/s	50 ÷ 85	65 ÷ 90	80 ÷ 110	45 ÷ 60
4.	Tensile strength	N/50 mm	>98	>98	>98	>98
5	Bending strength	N/30 mm	1.96 ÷ 3.62	1.96 ÷ 3.62	1.47 ÷ 2.94	1.47 ÷ 3.43
6	Bursting strength	MPa	0.49	0.39	0.59	0.78

Table 2. The properties of non-woven fabric filters manufactured by Retop Fibre [30]

Item	Parameters	Units	Non-woven fabric designation			
			AC-205	AC203S	GH250-OE	GP20T
1	Basis weight	g/m²	220 ± 20	220 ± 20	250 ± 30	130 ± 15
2	Thickness	mm	2.8 ± 0.3	2.8 ± 0.3	5.0 ± 0.5	0.7 ± 0.10
3	Filter separation efficiency	%	≥97	≥96	≥94	≥99.5
4.	Air permeability	dm³/m²/s	≥110	≥1100	≥1600	≥400
5	Pore size	µm	120 ÷ 140	120 ÷ 140	180 ÷ 200	50 ÷ 70
6	Tensile strength	N/50 mm	≥210	≥210	≥130	≥100
7	Dust capacity	g/ m²	≥450	≥450	≥500	≥90
8	Bursting strength	N	>110	>110	>110	>40
9	Temperature resistance	°C	>150	>150	>120	>110

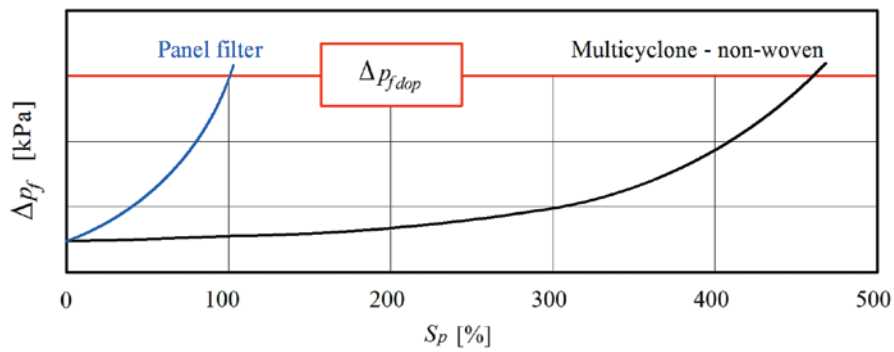

Fig. 3. Flow resistance of the single-stage air filter (porous panel filter) and the two-stage air filter in "multi-cyclone - porous panel filter" configuration depending on vehicle duty S [10].

5. Purpose, test methods and conditions

The purpose of the study was to determine the operating properties of two types of non-woven fabric filters in a single and two-stage filtration system at specific filtration velocity and dust removal rate by ejection from the multi-cyclone's settling tank.

The first stage involved determining the following characteristics: filter separation efficiency and flow resistance of two types of non-woven fabric filters operating in conditions corresponding to the second filtration stage, depending on the dust capacity as:

- filter separation efficiency $\varphi_{w2} = f(k_{m2})$,
- flow resistance $\Delta p_{w2} = f(k_{m2})$.

The scope of tests for the second stage involved determination of the following characteristics: filter separation efficiency and flow resist-

Table 3. AC – 301 and BWF – 02 E200B non-woven fabric filter parameters

Parameter	Unit	Value	
		AC–301	BWF–02 E200B
Basis weight	[g/m²]	210 ± 10%	200 ± 15
Thickness	[mm]	2.34 ÷ 2.86	2.00 ± 0.1
Air permeability	[dm³/m²/s]	800 ÷ 1100 at 120 Pa	> 2300 at 200 Pa
Tensile strength	[N/50 mm]	> 98	–
Bending strength	[N/30 mm]	1.47 ÷ 2.94	–
Flow resistance	[Pa]	–	120 ÷ 130
Components	–	–	Polyester 100%

ance of a non-woven fabric in single-stage filtration system for the fabric that showed better performance in the first stage.

The tests covered two filter elements made of non-woven fabrics available in Poland (Table 3). Non-woven fabric names are given in brackets.

- two-layer AC-301 (AC) non-woven fabric by Korea Filtration Technologies Co.,
- one-layer BWF-02 E200B (B2) non-woven fabric by EkoKarpaty.

Filter elements with tested non-woven fabrics were made based on paper air filter elements for trucks available in serial production. Surface area of non-woven fabric was determined at permissible filtration velocity [1, 8]:

$$\upsilon_{Fdop} = \frac{Q_G}{3600 \cdot F_w} \text{ [m/s]}, \tag{5}$$

where: Q_G – volume flow ratio for air downstream of the filter element [m³/h], see [3], F_w – active surface area of filter medium [m²].

Main stream value is Q_G = 600 m³/h. Ejection dust removal system with an air stream Q_S (value determined based on the following equation for the specific suction rate m_0 = 10%) was used to remove dust from the multi-cyclone's settling tank:

$$Q_S = Q_G \cdot m_0. \tag{6}$$

Assuming the permissible filtration velocity as for the filter papers υ_{Fdop}= 0.08 m/s, surface area of the non-woven fabric filter is F_w = 2.0 m².

The tests were carried out at constant air stream flow through the filter Q_G = 600 m³/h and suction stream Q_s = 60 m³/h, at assumed dust loading at the multi-cyclone inlet s = 1 g/m³, and in a single-stage filtration system at dust loading s = 0.5 g/m³, using PTC-D test dust corresponding to AC-Fine test dust, with size distribution and chemical composition detailed in Fig. 4.

Filter separation efficiency φ_w in tested non-woven fabric filters was determined using mass method at subsequent j cycles, with duration (uniform batching and distribution of test dust) at: t_{1pom} = 3 min – in the initial period i t_{2pom} = 15 min – in further testing period. Filter separation efficiency φ_w of the tested filter element was determined after each j cycle:

- separation efficiency φ_w:

$$\varphi_{wj} = \frac{m_{wj}}{m_{Dj}} \cdot 100\% , \tag{7}$$

where: m_{wj} – mass of dust retained by filter element, m_{Dj} – mass of dust introduced to the filter element (mass of dust at the multi-cyclone outlet) during the cycle:

$$m_{Dj} = m_{wj} + m_{AGj}, \tag{8}$$

where: m_{AG} – mass of dust retained by absolute filter,

- flow resistance:

$$\Delta \text{pwj} = \frac{\Delta h_{wj}}{1000}(\rho_m - \rho_H)g \text{ [kPa]}, \tag{9}$$

where: Δh_w – static pressure drop (in mm H_2O) at U-tube water manometer, ρ_m – manometer liquid density (H_2O) at measurement temperature t_H, ρ_H– free air density in kg/m³, g – local acceleration of gravity.

- dust capacity $k_{m(1-j)}$:

$$k_{m(1-j)} = \frac{m_{w(1-j)}}{F_w} \text{ [g/m²]}, \tag{10}$$

where: $m_{w(1-j)}$ – total mass of dust retained by filter element,

The tests were completed after the tested filter element reached the flow resistance of 5 kPa, which is the commonly used permissible flow resistance for air filters used in motor vehicles.

Filter element tests were carried out on a test stand (Fig. 5) for testing basic characteristics of separation efficiency and flow resistance for air flow rate up to 1500 m³/h at ejector suction rate up to 20% and dust loading up to 3 g/m³.

A measuring line was installed directly downstream of the filter element, from which the end of the U-tube water manometer was connected in the distance of $6D_w$ from the face of a filter element enclosure (where D_w – inner diameter of the outlet line from the tested paper filter element) to measure flow resistance Δp_w (static pressure drop) at the filter element.

The measuring line ends with a filter protecting the measuring orifice plate against dust ingress, which is also a measuring filter to determine the mass of dust flowing through the tested filter element and as a consequence to determine the filter separation efficiency.

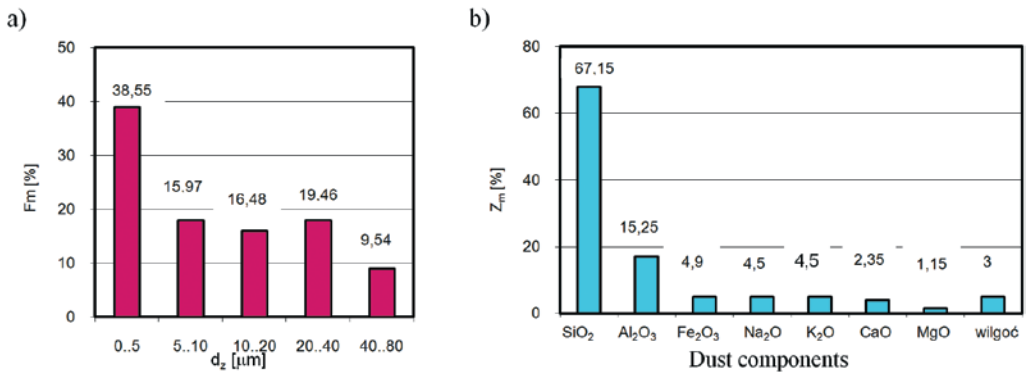

Fig. 4. PTC-D test dust used for testing: a) size distribution, b) chemical composition [27]

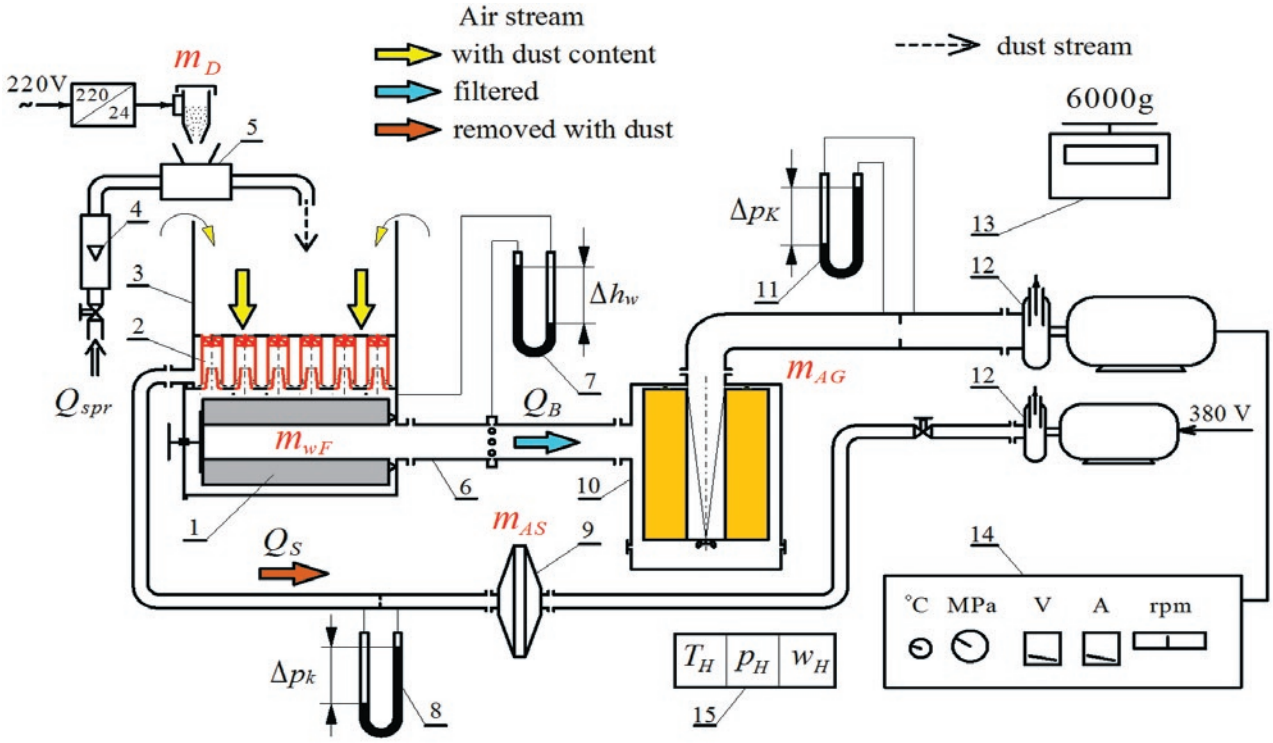

Fig. 5. Test stand diagram: 1 – tested filter element, 2 – dust collector, 3 – dust chamber, 4 – compressed air stream rotameter, 5 – dust feeder, 6 – flow resistance test line, 7 – static pressure drop manometer, filter element, 8 – differential manometer, measuring orifice plate (volume flow rate Q_S), 9 – absolute filter, dust suction line, 10 – absolute filter, main line, 11 – differential manometer, measuring orifice plate (Q_G stream), 12 – suction fans, 13 – weight, 14 – engine and air fan control panel, 15 – pressure, temperature and relative humidity measuring unit

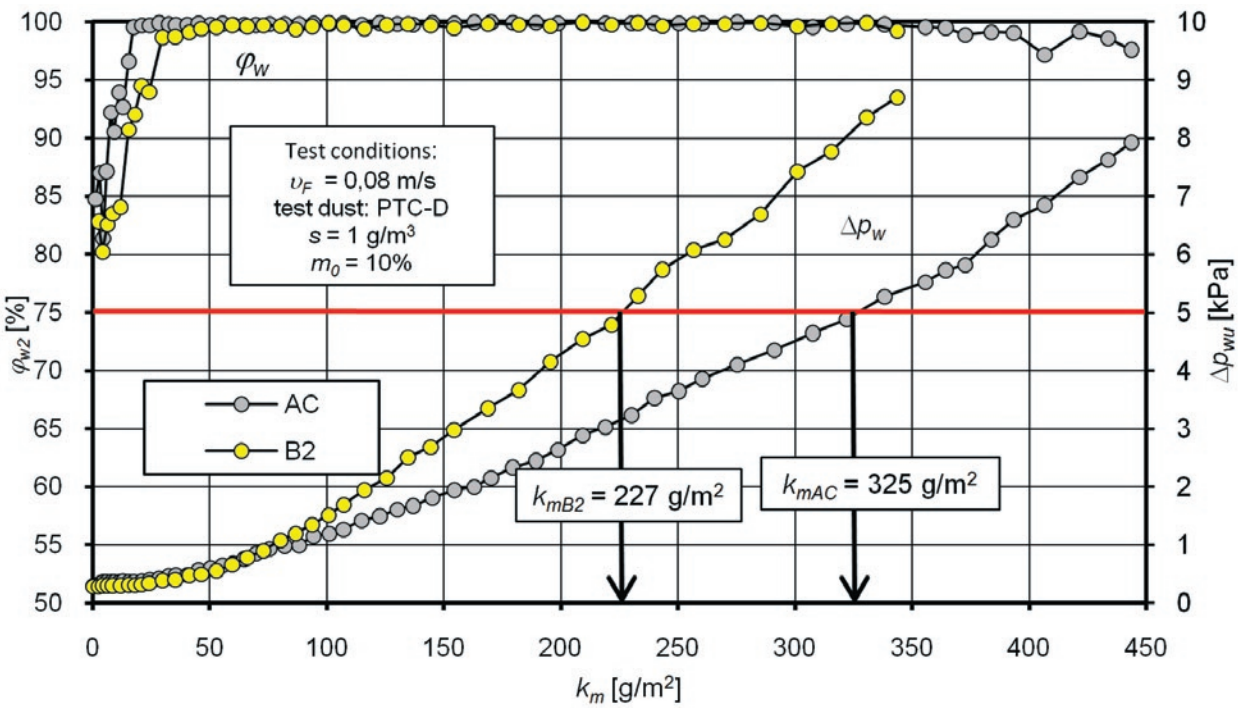

Fig. 6. Characteristics of the filter separation efficiency φ_w and flow resistance Δp_w as a function of dust capacity k_m of systems made of AC and B2 non-woven fabric filters in "multi-cyclone - non-woven fabric panel filter" configuration

6. Test result analysis

Fig. 6 shows filter separation efficiency and flow resistance of filter elements made of AC and B2 non-woven fabrics in two-stage filtration system downstream of the multi-cyclone as a function of dust capacity. Due to the achieved filter separation efficiency, operation time of tested non-woven fabrics can be divided into two periods. The first (initial) period characterized by low filter separation efficiency, which systematically and rapidly increases with the quantity of dust mass retained by the filter paper. The period lasts from the moment the filtration process commences until the specific filter separation

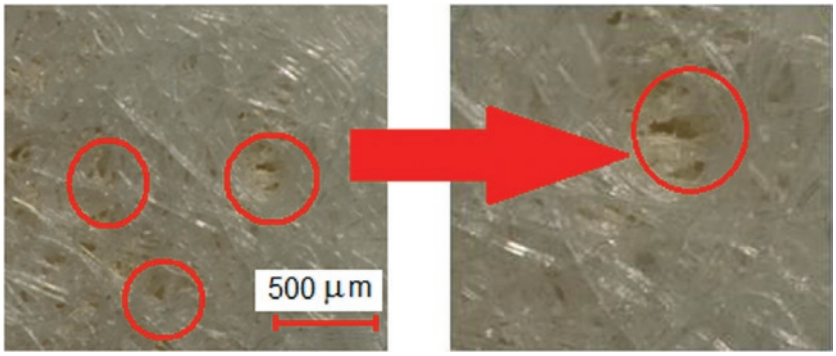

Fig. 7. Visible punctures in non-woven fabric

efficiency is reached by the non-woven fabric. The following main filtration period is characterized by high (over 99%), continuously and slowly increasing filter separation efficiency. In case of tested non-woven fabrics, the interface of both periods was defined as the moment the filter separation efficiency reached 99.5% [8]. After the first measuring cycle, the filter separation efficiency of AC non-woven fabric reached φ_{w2} = 84.8%, and B2 non-woven fabric reached φ_{w2}=80.2% (Fig. 4). The first filtration period (anticipated filter separation efficiency φ_w = 99.5%) for non-woven fabric AC lasted until the dust capacity k_{m2} = 17,3 g/m² was reached For B2 non-woven fabric, the duration of the period was almost twice longer and lasted until the dust capacity of k_{m2} = 35.4 g/m² was reached.

The initial operation period of the non-woven fabric filter is very adverse for two mating parts, since at the same time, a significant quantity of dust with particle size d_z = (2 ÷ 5) µm is introduced to the engine cylinders with air [10]. It may result in premature wear of mating engine parts. New installed non-woven fabric filter element (paper) will not provide the required separation efficiency and filtration rate until a specific mileage. Frequent and unnecessary replacement of the filter element should be avoided.

In the main filtration period, the filter separation efficiency of tested non-woven fabrics is φ_{w2} = (99.5 ÷ 99.97)%. High AC non-woven fabric filter separation efficiency is maintained until the dust capacity of k_{m2} = 364 g/m² is reached. A decrease in filter separation efficiency to the value of (97 ÷ 98)% can be observed in a single measuring point beyond this value, which may indicate depletion of filter medium capacity and/or puncture. Large dust particles and clusters are captured as a result of high flow rate and high pressure difference upstream and downstream of the filter element and forced inside the medium to the outlet side of the filter medium. Fig. 7 shows example points, where the dust was forced through the filter medium. In case of B2 non-woven fabric, the decrease in filter separation efficiency occurred slightly earlier at the dust capacity of k_{m2} = 343 g/m².

With the increase in mass of dust retained by the non-woven fabric filter, the flow resistance of the filter element systematically increases, although the intensity of the increase is higher for the element made of B2 non-woven fabric. After reaching the permissible flow resistance Δp_w = 5 kPa, the dust capacity of AC non-woven fabric is k_{m2} = 325 g/m², and significantly lower in case of B2 non-woven fabric at k_{m2} = 227 g/m² due to lower mass of dust retained by the fabric. It can be explained by lower thickness of B2 non-woven fabric, and thus lower dust capacity. The dust capacity of paper filters in two-stage filtration systems is significantly lower (k_m = 50÷80 g/m²) compared to tested non-woven fabrics.

Fig. 8 shows comparative analysis of AC non-woven fabric filter performance in the single and two-stage system in "multi-cyclone - non-woven fabric panel filter" configuration. Filter separation efficiency and flow resistance of the non-woven fabric filter element in the single-stage filtration system (standard particle size distribution) increases with lower intensity compared to the filter element made of the same AC non-woven fabric in the "multi-cyclone - non-woven fabric panel filter" configuration. It is due to the fact, that the dust downstream of the cyclone does not contain particles >(20 ÷ 35) µm, due to the filtration rate of the mini-cyclones [1, 10, 17, 22]. The filter element is affected by smaller dust particles, which fill all the areas between the fibres, increasing the flow rate and thus intensifying the flow resistance.

Permissible flow resistance Δp_w = 5 kPa was reached by the non-woven fabric filter in the single-stage filtration system at the dust capacity of k_{m1} = 700 g/m², and thus at twice the value compared to

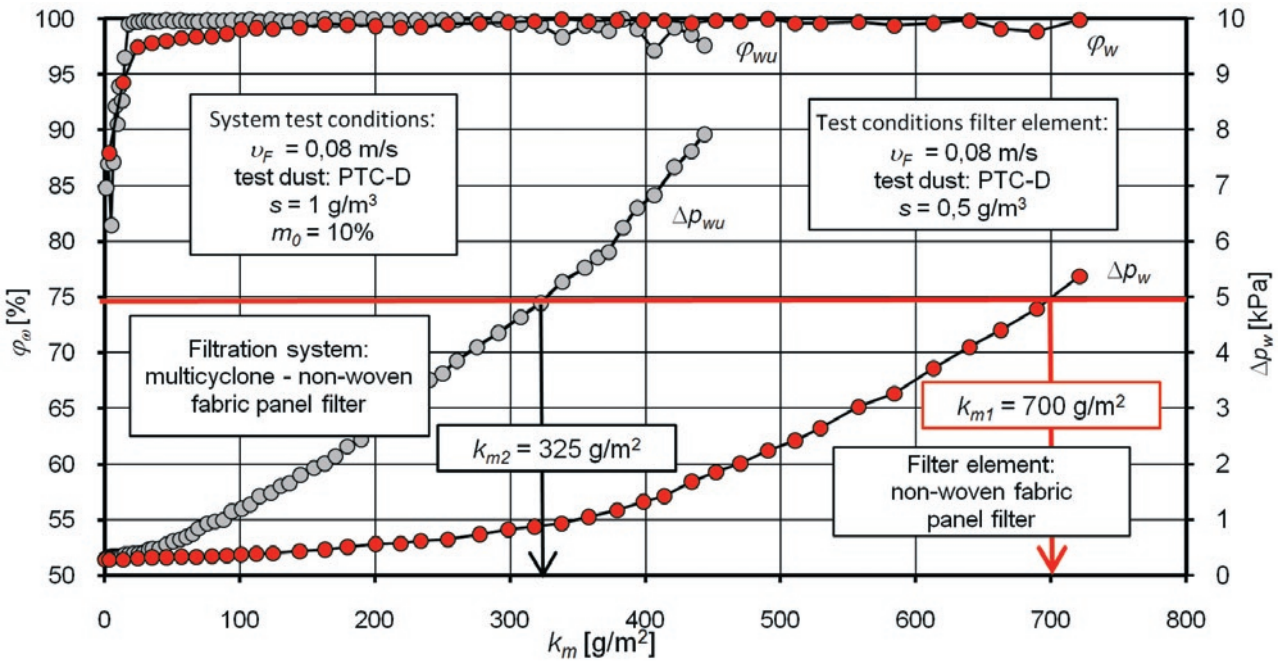

Fig. 8. Characteristic curves of filter separation efficiency φ_w and flow resistance Δp_w of AC-301 non-woven fabric filters in single and two-stage filtration system in "multi-cyclone-non-woven fabric panel filter" configuration

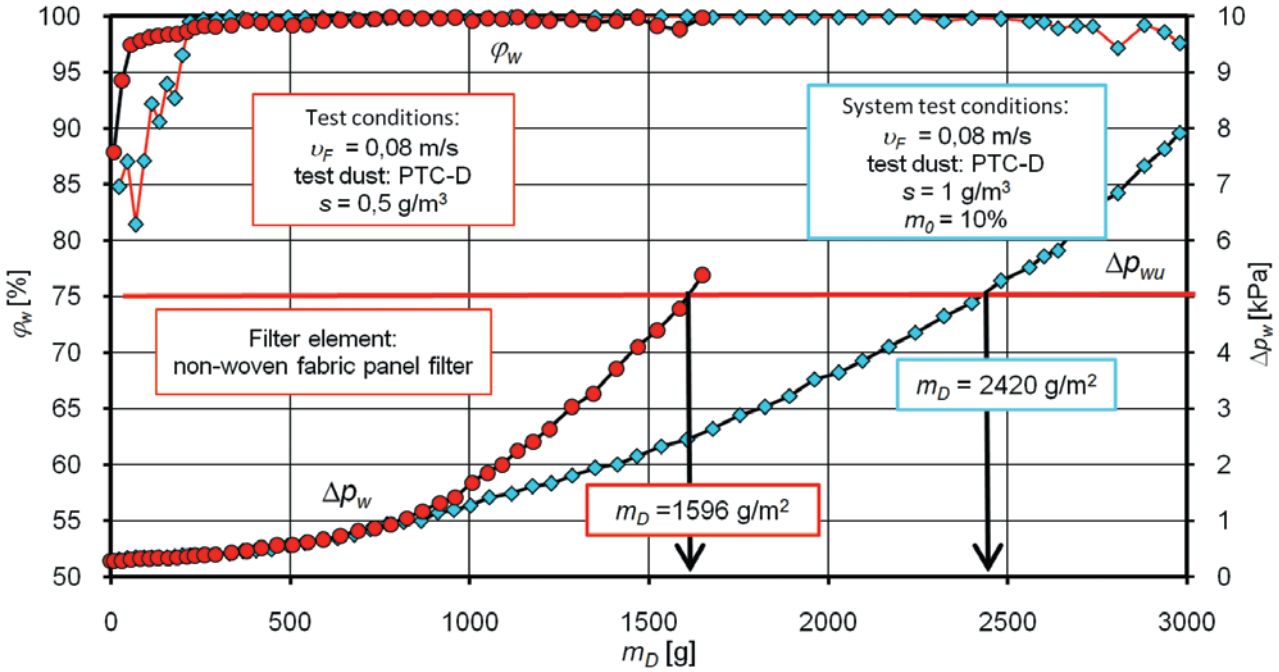

Fig. 9. Characteristics of filter separation efficiency φ_w and flow resistance Δp_w of AC-301 non-woven fabric filters in single and two-stage filtration system in "multi-cyclone-non-woven fabric panel filter" configuration as a function of dust mass mD introduced to the filter

two-stage filtration system – k_{m2} = 325 g/m². The dust capacity of the non-woven fabric subject to dust with size distribution changed by the inertia filter (d_z<20÷35 μm) is lower than the dust capacity of the non-woven fabric subject to the external dust (d_z< 80μm) by 50%. It is consistent with the data available in the studies on filter paper testing [10, 14].

Lower dust capacity of the non-woven fabric subject to dust with size distribution changed by the inertia filter does not mean reduced service life of the two-stage filtration system (shorter mileage) until the permissible flow resistance Δp_{fdop}. is reached. Although more dust (Fig. 9) is introduced with the air to the system, service life of the two-stage filtration system in "multi-cyclone-non-woven fabric panel filter" configuration τ_{p2} is significantly longer. Service life can be calculated from the following equation [1]:

$$\tau_{p2} = \frac{F_c \cdot k_{m2} \cdot k_c}{Q_{Sil\max} \cdot s \cdot (1-\varphi_M) \cdot \varphi_w} \tag{11}$$

where: F_c – total surface area, second stage filtration, k_{m2} – dust capacity of non-woven fabric, k_c – coefficient allowing for the difference between test and actual dust parameters, Q_{max}– volume flow rate via engine, s – average dust loading in drawn in air, φ_M – first stage filter separation efficiency (multi-cyclone), φ_w – filter separation efficiency of non-woven fabric filter.

For the following data: F_c – 2 m², k_{m2} – 325 g/m²; k_c – 1; Q_{max}– 600 m³/h;s – 1 g/m³; φ_M = 0.8; φ_w = 0.99; service time of two-stage filtration system is τ_{p2} = 5.47 h. For the same non-woven fabric in single-stage filtration system, the filter achieves τ_{p2} = 2.37 h, which is half the value compared to the data in Fig. 3.

6. Summary

Non-woven fabrics are more and more commonly used in the inlet air filter systems of modern passenger vehicles. However, no data are available on use of non-woven fabrics as a second filtration stage in multi-stage filters used in trucks and special vehicles, mostly due to the unknown operational properties of non-woven fabric filters, in particular dust capacity. Dust capacity values for non-woven fabrics used as the second filtration stage (downstream of the inertia filter) are lower compared to non-woven fabrics used in single-stage filtration systems. It directly affects the filter service life (time until it reaches permissible flow resistance) and thus vehicle mileage.

The tests of two non-woven fabric filters: AC-301 and BWF – 02 E200B in two-stage filtration system downstream of the multi-cyclone have shown that the dust capacity at determined flow resistance Δp_{fdop} = 5 kPa varies, depending on the parameters of non-woven fabric structure and is k_{m2} = 325 g/m² and k_{m2} = 227 g/ m², respectively. At identical permissible flow resistance, filter papers used as the second filtration stage downstream of the cyclone, achieve the dust capacity of k_{m2} = (50 ÷ 80) g/m² [9] which is several times lower due to the lower thickness of the filter paper.

The tests of AC-301 non-woven fabric filter in single-stage filtration system (PTC-D test dust, standard size distribution up to d_z< 80 μm) have shown that the characteristics of the flow resistance $\Delta p_w = f(k_m)$ vary. Significantly lower intensities of the increase in flow resistance of the non-woven fabric subject to test dust with standard size distribution compared to the non-woven fabric subject to dust from the multi-cyclone (significantly smaller particle size) have been observed.

(Fig. 9). The dust capacity determined for AC-301 non-woven fabric at specific conditions and flow resistance Δp_{fdop} = 5 kPa was k_{m1} = 700 g/m², almost twice as high as achieved in the two-stage filtration system.

Actual service life of the two-stage filter, with a filter medium designed using dust capacity k_{m1} resulting from the non-woven fabric operation in the single-stage filtration system, which is often used when designing filter paper elements, will be halved.

Low (φ_{w2}= (80 ÷ 84)%) filter separation efficiency and presence of large dust particles in the air in the initial, however short operation period may result in a premature wear of mating parts, in particular piston, rings and cylinder. In actual operating conditions, the initial operation period occurs after replacement of the old filter element with a new one.

The filter reaches its highest filter separation efficiency (99.9%) in the end period, when the flow resistance is close to the permis-

sible flow resistance, which is also a criterion for the filter element change. Since high filter separation efficiency is a much-desired property, filter elements should be used as long as possible. An increase in the mass of dust retained at the filter element, not only increases its separation efficiency but also its flow resistance, which in turn may affect motor power and fuel consumption. The manufacturers of modern passenger vehicles recommend filter element change after a specific mileage ((30 ÷ 60) thousand kilometres) and/or based on the flow resistance indication.

References

1. Baczewski K, Hebda M. Filtracja płynów eksploatacyjnych. Radom: MCNEMT, 1991/92.
2. Barbolini M, Di Pauli F, Traina M. Simulation der Luftfiltration zur Auslegung von Filterelementen. MTZ 2014; 11: 53-56, http://dx.doi.org/10.1007/s35146-014-0556-5.
3. Calculating Engine Airflow. www.donaldson.com
4. Chłopek Z. Testing of hazards to the environment caused by particulate matter during use of vehicles. Eksploatacja i Niezawodnosc – Maintenance and Reliability 2012; 2: 160-170.
5. Chłopek Z, Jakubowski A. The examination of the reduction of particulate matter emission from motor vehicle braking system. Eksploatacja i Niezawodnosc – Maintenance and Reliability 2010; 4: 39-36.
6. Das A, Alagirusamy R, Nagendra K R. Filtration characteristics of spun-laid nonwoven fabrics, Indian Journal of Fibre & Textile Research 2009; 34: 253-257.
7. Duchowski J, Collins K. Cleanlines Requirements for Journal Bearing Lubrication. Practicing Oil Analysis Magazine 2000; 7.
8. Durst M, Klein G, Moser N. Filtration in Fahrzeugen. Ludwigsburg: Mann+Hummel GMBH, 2005.
9. Dziubak T. The test stand of air tillers cyclones of vehicles operating in high dustiness condition. Eksploatacja i Niezawodnosc – Maintenance and Reliability 2003; 4: 31-46.
10. Dziubak T, Szwedkowicz S. Experimental research on filtering fibers in a cyclone–porous barrier system. Combustion Engines 2014; 3: 45-55.
11. Extreme Performance Air Filters with ProTura Nanofiber Technology, Kearney: Baldwin Filters, 2014.
12. Fitch J. Clean Oil Reduces Engine Fuel Consumption. Practicing Oil Analysis Magazine 2005; 9.
13. Golloch R, Kessen U, Merker G P. Tribologische Untersuchungen an der Kolbengruppe eines NFZ-Dieselmotors. MTZ 2002; 6: 494-501, http://dx.doi.org/10.1007/bf03226635.
14. Heavy-Duty Air Filter Media Applications. East Walpole: Holingsworth & Vose, 2011.
15. Jaroszczyk T, Fallon S. L, Janikowski E, Kendall O D. Nanofiber Media Performance in Aplication to Motor Vehicle Air Filtration. Nanofibers for the 3td Millennium – Nano for Life. Praga, 2009.
16. Jaroszczyk T. Air Filtration in Heavy-Duty Motor Vehicle Applications. Proc. Dust Symposium III Vicksburg MS, September 15-17. 1987.
17. Jo Y, Tien Ch, Ray M B. Development of a post cyclone to improve the efficiency of reverse flow cyclone. Powder Technology 2000; 1-2: 97-108, http://dx.doi.org/10.1016/S0032-5910(00)00206-0.
18. Koszałka G, Niewczas A. Wear profile of the cylinder liner in a motor truck diesel engine. Journal of KONES 2007; 4: 183-190.
19. Koszałka G. Predicting the durability of the piston-rings-cylinder, assembly of a diesel engine using a piston ring pack model. Eksploatacja i Niezawodnosc – Maintenance and Reliability 2011;. 3: 40-44.
20. Коренев М С, Рузаев И Г. Фильтровальный материал из синтетических волокон для воздухоочистителей. Автомобильная промышленность 1982; 9.
21. Kothari V. K, Das A, Singh S. Filtration behavior of woven and nonwoven fabrics. Indian Journal of Fibre & Textile Research 2007; 32: 214-220.
22. Lim K S, Kim H S, Lee K W. Characteristics of the collection efficiency for a cyclone with diffirent vortex finder shapes. Journal of Aerosol Science 2004; 6: 743-754, http://dx.doi.org/10.1016/j.jaerosci.2003.12.002
23. Merkisz J, Lijewski P, Fuć P, Weymann S. Exhaust emission tests from non-road vehicles conducted with the use of PEMS analyzers. Eksploatacja i Niezawodnosc – Maintenance and Reliability 2013; 4: 364-368.
24. Muller T K, Meyer J, Thebault E, Kasper G. Impact of an oil coating on particle deposition and dust holding capacity of fibrous filters. Powder Technology 2014; 253: 247-255, http://dx.doi.org/10.1016/j.powtec.2013.11.036.
25. Muller T K, Meyer J, Thebault E, Kasper G. Dust capacity increase of air filters by oil pre-treatment. Aerosol Technology 2014.
26. Niewczas A, Wrona J, Wrona R. Zanieczyszczenia oleju smarującego oraz ich wpływ na trwałość silnika spalinowego. Autobusy: technika, eksploatacja, systemy transportowe 2010; 6: 1-5.
27. PN-S-34040, Filtry powietrza. Wymagania i badania. PKN, 1996.
28. Sakthivel S, Ehzil Anban J J, Ramachandran T.: Development of Needle-Punched Nonwoven Fabrics from Reclaimed Fibers for Air Filtration Applications. Journal of Engineered Fibers and Fabrics 2014; 9: 149-154.
29. WIX Filtron, materiały udostępnione przez Filtron, Gostyń, 2013.
30. www.retopfibre.en.alibaba.

Tadeusz DZIUBAK
Sebastian SZWEDKOWICZ
Military University of Technology
Faculty of Mechanical Engineering
ul. Gen. Sylwestra Kaliskiego 2
0-908 Warszawa, Poland
E-mail: tdziubak@wat.edu.pl, sszwedkowicz@wat.edu.pl

Article citation info:
BIAŁAS K, BUCHACZ A. Active reduction of vibration of mechatronic systems. Eksploatacja i Niezawodnosc – Maintenance and Reliability 2015; 17 (4): 528–534, http://dx.doi.org/10.17531/ein.2015.4.7.

Katarzyna BIAŁAS
Andrzej BUCHACZ

ACTIVE REDUCTION OF VIBRATION OF MECHATRONIC SYSTEMS

AKTYWNA REDUKCJA DRGAŃ UKŁADÓW MECHATRONICZNYCH*

In the work presented methods of reduction of vibration of mechanical systems using active elements, as well as examples of the implementation of the active reduction of vibration. Also presents a structural-parametric synthesis, which is defined as the design of active mechanical systems with specific requirements. These requirements apply to the value of the frequency of vibration of these systems. Presented at work considerations relate to illustrate the possible implementation of the physical elements of active using electrical components. In the active subsystems can also be used elements in other environments. To examine their effectiveness should be obtained analysis and check what are the interactions subsystems on the primary system.

Keywords: *analysis, synthesis, reduction of vibration.*

W pracy zaprezentowano metody redukcji drgań układów mechanicznych przy użyciu elementów aktywnych, jak również przykłady realizacji aktywnej redukcji drgań. Przedstawiono również syntezę strukturalno-parametryczna, która rozumiana jest jako projektowanie aktywnych układów mechanicznych o żądanych wymaganiach. Wymagania te dotyczą wartości częstości drgań tych układów. Przedstawione w pracy rozważania dotyczą zilustrowania możliwych realizacji fizycznych elementów aktywnych przy użyciu elementów elektrycznych. W podukładach aktywnych można stosować również elementy z innych środowisk. Aby zbadać ich skuteczność należy dokonać analizy otrzymanych układów oraz sprawdzić jakie są wzajemne oddziaływania podukładów na układ podstawowy.

Słowa kluczowe: *analiza, synteza, redukcja drgań.*

1. Introduction

Vibration belongs to one of the most common phenomena occurring in everyday life. It is defined as a periodical movement of a particle or a system. Such a movement is induced by external factors. Vibration occurs when a system or its part is relocated from a position of balance. The system put out of balance tends to return to its original state. One of the divisions of vibration is done according to the ways of its creation (free, forced and self-excited vibrations).

Most vibrations occurring in machines and devices are harmful and have a negative impact on their technical condition. The harmful effect of vibration is caused by occurrence of the increased stress and the loss of energy, which results in faster wear of the machines. Vibration also has a negative influence on human organism, particularly in the case of low-frequency vibration. That is the reason why many scientists in various research centres carry out investigations relating to the reduction or complete elimination of vibration [5,8,10,14,15,18].

This paper aims to develop a method of searching for structure and parameters, i.e. the structural and parametric synthesis of a mechanical system model with an active reduction of vibration. The goal of such a task is to perform a synthesis understood as a modification – already in the designing phase – of machines' subsystems with reference to the desirable frequency spectrum of the system vibration. This paper applies a non-classical method, i.e. polar graphs and structural numbers. Application of this method makes it possible to perform an analysis without any limitations caused by the type and number of elements of the mechanical system.

2. Methods of reduction of mechanical systems vibration

There are many well-known methods of vibration reduction which can be divided as follows: passive methods, semi-active and active methods.

Passive reduction of vibration consists in the introduction of additional elements such as vibration dampers. The vibration dampers dissipate or store energy. The parameters of passive dampers are subject to no variation in time. In the passive reduction of vibration there is a strong connection between efficiency and vibration frequency as well as there is sensitivity to the changes of parameters.

Semi-active methods consist in the application of semi-active eliminators of vibration. They combine some features occurring in the passive and active elements. The structure of a semi-active subsystem is similar to an active subsystem. The difference between active and semi-active subsystems, however, lies in the fact that the semi-active subsystems demand very little energy. On the other hand, they differ from the passive subsystems in this respect that their parameters may be subject to variation in time. Such changes depend on the current condition of the primary system.

Active reduction of vibration is characterized by the necessity of existence of additional external sources of energy. The energy supplied from the outside counteracts the undesirable vibration. Active subsystems may reduce vibration of the selected parts of machines or devices. The value of their parameters varies in time and depends on the current state of the system. Active subsystems may be constructed from different types of elements: mechanical, electric, pneumatic and hydraulic. The application of active and semi-active methods enables the elimination of limitations occurring in passive methods [1-5, 11, 14, 15, 18].

(*) Tekst artykułu w polskiej wersji językowej dostępny w elektronicznym wydaniu kwartalnika na stronie ***www.ein.org.pl***

3. Synthesis of active mechanical systems

The synthesis presented in this paper is a non-classical method of designing discrete vibrating mechanical systems. As a result of the synthesis the structure and parameters of a system of required properties may be obtained [5,6,8]. The synthesis may also be used for the modification of the existing systems in order to achieve an intended goal. The synthesis consists of two basic stages. In the first stage, which is a designing phase of a new system, the researchers determine requirements concerning the free vibration frequency of the system as well as obtain the structure and parameters of the system constructed only from passive elements (inertial and elastic elements). In the second stage, the reduction of vibration is selected, either passive or active, to fit the existing or obtained system (Fig. 1). The presented method of designing active mechanical systems with vibration reduction by means of polar graphs and structural numbers enables full automation and algorithmisation of calculations during the determination process of dynamic characteristics of the system as well as enables direct tracking of the introduced structural changes irrespective of the complexity of a given system.

In order to obtain the structure and parameters of inertial and elastic elements of a dynamic system two basic methods are applied [8]:

- distribution of characteristic function into continued fraction (3),
- distribution of characteristic function into vulgar fractions (4).

Characteristic functions may include functions in the form of mobility (1) or slowness (2):

$$V(s) = H\frac{c_k s^k + c_{k-1}s^{k-2} + \ldots + c_1 s}{d_l s^l + d_{l-1}s^{l-2} + \ldots + d_0} \tag{1}$$

$$U(s) = H\frac{d_l s^l + d_{l-1}s^{l-2} + \ldots + d_0}{c_k s^k + c_{k-1}s^{k-2} + \ldots + c_1 s} \tag{2}$$

where:

k, l – natural numbers,
c, d – real numbers,
H – any positive real number.

$$V(s) = \frac{c_1}{s} + m_1 s + \cfrac{1}{\cfrac{s}{c_2} + \cfrac{1}{m_2 s + \ldots + \cfrac{1}{\cfrac{s}{c_n} + \cfrac{1}{m_n s}}}} \tag{3}$$

$$U(s) = \frac{c_1}{s} + m_1 s + \cfrac{1}{\cfrac{s}{c_2} + \cfrac{1}{m_2 s}} + \ldots + \cfrac{1}{\cfrac{s}{c_n} + \cfrac{1}{m_n s}} \tag{4}$$

where:

c – elastic elements,
m – inert elements.

In order to design a system with a passive reduction of vibration one should follow the scheme presented in Fig 1. After performing the synthesis consisting in the distribution into continued fraction or vulgar fractions, it is necessary to define the type and value of external excitation affecting the system.

By choosing the passive reduction of vibration a designer determines if passive elements in the form of viscous dampers will be proportional to inertial elements (as illustrated in Fig. 2) or proportional to elastic elements (Fig. 3). It is vital to check the efficiency of the application of passive elements by means of performing the analysis of the obtained system [5, 13].

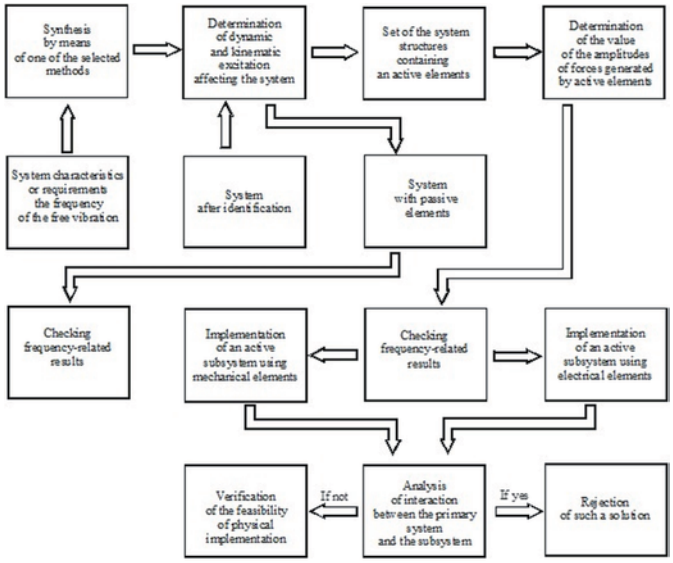

Fig. 1. Idea of synthesis of mechanical systems with reduction of vibration

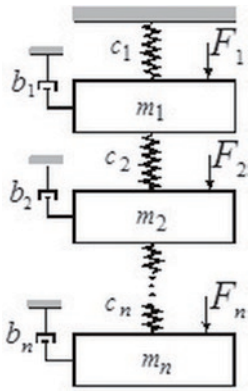

Fig. 2. Model of mechanical system with passive elements proportional to inertial elements

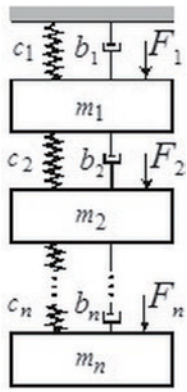

Fig. 3. Model of mechanical system with passive elements proportional to elastic elements

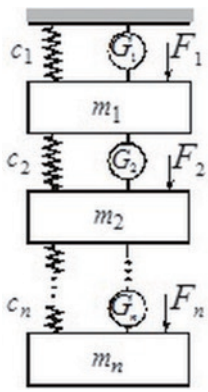

Fig. 4. Model of mechanical system with active elements

Another possibility is the application of active elements in vibration reduction. The synthesis of the systems with the active reduction of vibration has been presented in Fig. 1. The first stage is analogical to the case of the application of passive elements. In the second stage, the structure with active elements and their parameters are selected.

The system with active elements is presented in Fig. 4. Active subsystems are located among inertial elements, which enables the

reduction of the parts of the system pre-defined by the designer in the designing process.

4. System under investigation

The scope of this paper is limited to the description of the active reduction of vibration on the basis of a system with three degrees of freedom having a cascade structure. In order to obtain a system that would meet the requirements concerning the frequency of vibration, one should first define the values of such frequencies (5), then make a characteristic function (6) and perform its distribution into continued fraction (7):

$$\begin{cases} \omega_1 = 10\dfrac{rad}{s},\ \omega_3 = 30\dfrac{rad}{s},\ \omega_5 = 50\dfrac{rad}{s} - \text{resonant frequencies,} \\ \omega_0 = 0\dfrac{rad}{s},\ \omega_2 = 20\dfrac{rad}{s},\ \omega_4 = 40\dfrac{rad}{s} - \text{anti-resonant frequencies.} \end{cases} \tag{5}$$

$$U(s) = \frac{(s^2+\omega_1^2)(s^2+\omega_3^2)(s^2+\omega_5^2)}{s(s^2+\omega_2^2)(s^2+\omega_4^2)}. \tag{6}$$

Function distribution in the form of slowness into continued fraction results in the structure and values of the system with inertial and elastic elements:

$$U(s) = \frac{c_1}{s} + m_1 s + \cfrac{1}{\cfrac{s}{c_2} + \cfrac{1}{m_2 s + \cfrac{1}{\cfrac{s}{c_3} + \cfrac{1}{m_3 s} + \cfrac{1}{\cfrac{s}{c_4}}}}} = \frac{175}{s} + 1s + \cfrac{1}{\cfrac{s}{1325} + \cfrac{1}{1{,}7s + \cfrac{1}{\cfrac{s}{848{,}6} + \cfrac{1}{1{,}6s + \cfrac{s}{268{,}05}}}}} \tag{7}$$

On the grounds of the function distribution it is possible to obtain a polar graph and a mechanical system (Figs. 5, 6).

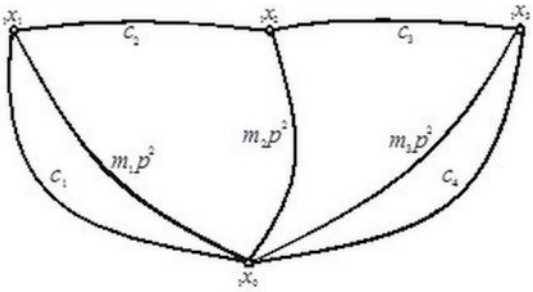

Fig. 5. Polar graph

Symbols in the Fig. 5 represent:

- inert elements

$$m_1p^2 \to m_1 = 1\ [kg],\ m_2p^2 \to m_2 = 1{,}67\ [kg],\ m_3p^2 \to m_3 = 1{,}59\ [kg],$$

- elastic elements

$$c_1 \to c_1 = 175\left[\frac{N}{m}\right],\ c_2 \to c_2 = 1325\left[\frac{N}{m}\right],\ c_3 \to c_3 = 848{,}63\left[\frac{N}{m}\right],\ c_4 \to c_4 = 268{,}05\left[\frac{N}{m}\right].$$

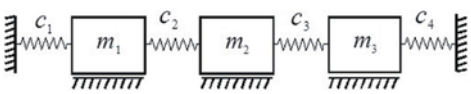

Fig. 6. Model of system obtained by synthesis

Following the diagram presented in Fig.1 it is necessary to define excitations influencing the system. In this case, force F(t) applied to inertial element 3 is exerted upon the system (Fig.7). The polar graph of the system has been presented in Fig.8.

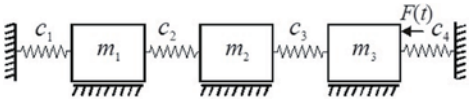

Fig. 7. Model of system (Fig. 6) with dynamic excitation

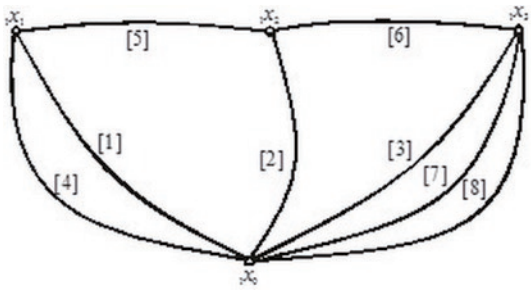

Fig. 8. Polar graph of the system from Fig. 7

The edges of the polar graph (Fig. 8) are numbered in the following way:

$$\left.\begin{matrix} [1] - m_1p^2, \\ [2] - m_2p^2, \\ [3] - m_3p^2, \end{matrix}\right\} \text{ inert elements} \qquad \left.\begin{matrix} [4] - c_1, \\ [5] - c_2, \\ [6] - c_3, \\ [7] - c_4, \end{matrix}\right\} \text{ elastic elements}$$

$$[8] - F(t) \to F(t) = 10\ \sin\omega t\ [N] \text{ dynamic excitation}$$

In order to determine the amplitude of the system vibration (Fig.7), it is possible to use the algebra of structural numbers and its connection with polar graphs [2,4]. In this case the amplitudes will take the following forms (8-10):

$$A_1 = \left| \frac{\underset{z}{Sim}\left(\dfrac{\partial D(\omega)}{\partial [1]}; \dfrac{\partial D(\omega)}{\partial [3]}\right)[8]}{D(\omega)} \right| = \tag{8}$$

$$= \left| \frac{c_2 c_3 F}{\begin{matrix} -m_1m_2m_3\omega^6 + \omega^4\left(m_1m_2c_3 + m_1m_2c_4 + m_1m_3c_2 + m_1m_3c_3 + m_2m_3c_1 + m_2m_3c_2\right) + \\ -\omega^2\left(m_1c_2c_3 + m_1c_2c_4 + m_1c_3c_4 + m_2c_1c_3 + m_2c_1c_4 + m_2c_2c_3 + m_2c_2c_4 + \right. \\ \left. +m_3c_1c_2 + m_3c_1c_3 + m_3c_2c_3\right) + c_1c_2c_3 + c_1c_2c_4 + c_1c_3c_4 + c_2c_3c_4 \end{matrix}} \right|$$

$$A_2 = \left| \frac{\underset{z}{Sim}\left(\dfrac{\partial D(\omega)}{\partial [2]}; \dfrac{\partial D(\omega)}{\partial [3]}\right)[8]}{D(\omega)} \right| = \tag{9}$$

$$= \left| \frac{\left(-m_1c_3\omega^2 + c_1c_3 + c_2c_3\right) F}{\begin{matrix} -m_1m_2m_3\omega^6 + \omega^4\left(m_1m_2c_3 + m_1m_2c_4 + m_1m_3c_2 + m_1m_3c_3 + m_2m_3c_1 + m_2m_3c_2\right) + \\ -\omega^2\left(m_1c_2c_3 + m_1c_2c_4 + m_1c_3c_4 + m_2c_1c_3 + m_2c_1c_4 + m_2c_2c_3 + m_2c_2c_4 + \right. \\ \left. +m_3c_1c_2 + m_3c_1c_3 + m_3c_2c_3\right) + c_1c_2c_3 + c_1c_2c_4 + c_1c_3c_4 + c_2c_3c_4 \end{matrix}} \right|$$

$$A_3 = \left| \frac{\frac{\partial D(\omega)}{\partial [3]}[8]}{D(\omega)} \right| = \tag{10}$$

$$= \left| \frac{\left(m_1 m_2 \omega^4 - \omega^2 \left(m_1 c_2 + m_1 c_3 + m_2 c_1 + m_2 c_2\right) + c_1 c_2 + c_1 c_3 + c_2 c_3\right) F}{\begin{array}{l} -m_1 m_2 m_3 \omega^6 + \omega^4 \left(m_1 m_2 c_3 + m_1 m_2 c_4 + m_1 m_3 c_2 + m_1 m_3 c_3 + m_2 m_3 c_1 + m_2 m_3 c_2\right) + \\ -\omega^2 \left(m_1 c_2 c_3 + m_1 c_2 c_4 + m_1 c_3 c_4 + m_2 c_1 c_3 + m_2 c_1 c_4 + m_2 c_2 c_3 + m_2 c_2 c_4 + \right. \\ \left. + m_3 c_1 c_2 + m_3 c_1 c_3 + m_3 c_2 c_3\right) + c_1 c_2 c_3 + c_1 c_2 c_4 + c_1 c_3 c_4 + c_2 c_3 c_4 \end{array}} \right|$$

The symbols in equations 8-10 present:
$D(\omega)$ – characteristic equation,

$\frac{\partial D(\omega)}{\partial [a]}$ – derivative of structural number in relation to the edge a,

$\underset{z}{Sim}\left(\frac{\partial D(\omega)}{\partial [a]}; \frac{\partial D(\omega)}{\partial [b]}\right)$ – function of simultaneity of structural number, the inverse image of which contains two oriented edges a and b.

A graphic representation of the amplitudes of the analysed system (Fig.7) is shown in Figs. 9-11.

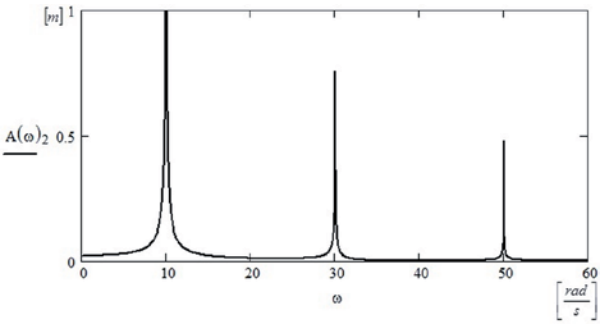

Fig. 9. Diagram of A_1 amplitude of a system with dynamic excitation (Fig. 7)

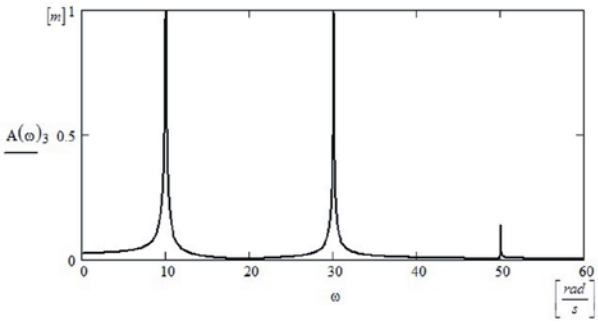

Fig. 10. Diagram of A_2 amplitude of a system with dynamic excitation (Fig. 7)

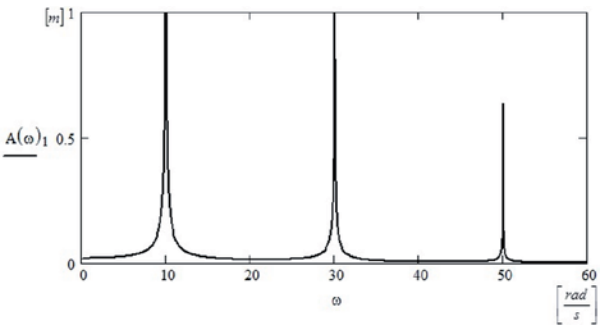

Fig. 11. Diagram of A_3 amplitude of a system with dynamic excitation (Fig. 7)

In order to reduce the system vibration active elements may be applied. The system with the active reduction of vibration has been presented in Fig. 12 and its polar graph in Fig. 13.

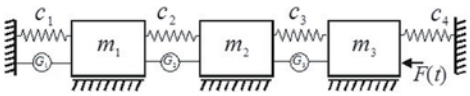

Fig. 12. System of three degrees of freedom with three active elements

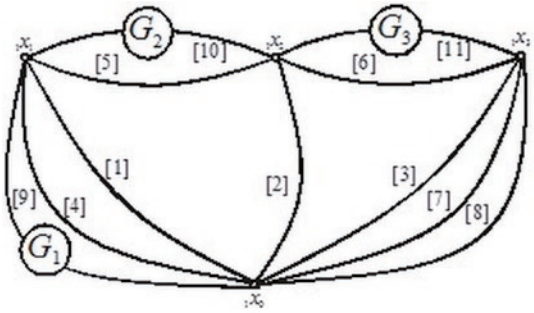

Fig. 13. Polar graph of the systems from Fig. 12

The edges of the graph in Fig. 13 are equivalent to Fig. 8 beyond edges 9-11 which mean the following:

$[9] - G_1 \Rightarrow$ active element 1,

$[10] - G_2 \Rightarrow$ active element 2,

$[11] - G_3 \Rightarrow$ active element 3.

In order to determine the values of forces generated by active elements G_1, G_2 and G_3, it is necessary to solve the following set of equations (11):

$$\begin{bmatrix} \left(\frac{\partial D(\omega)}{\partial([2][3])}\right) & -\underset{z}{Sim}\left(\frac{\partial D(\omega)}{\partial([2][3])}; \frac{\partial D(\omega)}{\partial([1][3])}\right) & -\underset{z}{Sim}\left(\frac{\partial D(\omega)}{\partial([2][1])}; \frac{\partial D(\omega)}{\partial([3][2])}\right) \\ -\underset{z}{Sim}\left(\frac{\partial D(\omega)}{\partial([2][3])}; \frac{\partial D(\omega)}{\partial([1][3])}\right) & \left(\frac{\partial D(\omega)}{\partial([1][3])}\right) & -\underset{z}{Sim}\left(\frac{\partial D(\omega)}{\partial([1][3])}; \frac{\partial D(\omega)}{\partial([1][2])}\right) \\ -\underset{z}{Sim}\left(\frac{\partial D(\omega)}{\partial([2][1])}; \frac{\partial D(\omega)}{\partial([3][2])}\right) & -\underset{z}{Sim}\left(\frac{\partial D(\omega)}{\partial([1][3])}; \frac{\partial D(\omega)}{\partial([1][2])}\right) & \left(\frac{\partial D(\omega)}{\partial([1][2])}\right) \end{bmatrix} \cdot \begin{bmatrix} A_1 \\ A_2 \\ A_3 \end{bmatrix} - \begin{bmatrix} 0 \\ 0 \\ F \end{bmatrix} = \begin{bmatrix} -G_1 \\ -G_2 \\ -G_3 \end{bmatrix} \tag{11}$$

where:

$\frac{\partial D(\omega)}{\partial([2][3])} = -m_1\omega^2 + c_1 + c_2$, $\frac{\partial D(\omega)}{\partial([1][3])} = -m_2\omega^2 + c_2 + c_3$, $\frac{\partial D(\omega)}{\partial([1][2])} = -m_3\omega^2 + c_3 + c_4$,

$-\underset{z}{Sim}\left(\frac{\partial D(\omega)}{\partial([2][3])}; \frac{\partial D(\omega)}{\partial([1][3])}\right) = -c_2$, $-\underset{z}{Sim}\left(\frac{\partial D(\omega)}{\partial([1][3])}; \frac{\partial D(\omega)}{\partial([1][2])}\right)$,

$\underset{z}{Sim}\left(\frac{\partial D(\omega)}{\partial([2][1])}; \frac{\partial D(\omega)}{\partial([3][2])}\right) = 0$.

After solving (11) the values G_1, G_2 and G_3 were obtained.

At $\omega = \omega_1 = 10 \left[\frac{rad}{s}\right]$, the values G_1, G_2 and G_3 are as follows:

$G_1 = 0{,}225 \sin\omega t \ [N]$, $G_2 = -0{,}501 \sin\omega t \ [N]$, $G_3 = -9{,}673 \sin\omega t \ [N]$.

At $\omega = \omega_3 = 30 \left[\frac{rad}{s}\right]$, the values G_1, G_2 and G_3 are as follows:

$G_1 = -2{,}175 \sin\omega t \ [N]$, $G_2 = -4{,}51 \sin\omega t \ [N]$, $G_3 = -13{,}489 \sin\omega t \ [N]$.

At $\omega = \omega_5 = 50 \left[\frac{rad}{s}\right]$, the values G_1, G_2 and G_3 are as follows:

$G_1 = -6{,}975\ \sin\omega t\ \ [N],\ G_2 = -12{,}525 \sin\omega t\ \ [N],\ G_3 = -21{,}12 \sin\omega t\ \ [N].$

Having conducted the synthesis and defined the values of the forces generated by active subsystems, the researchers chose electric elements in the form of a coil with movable core as a physical realisation of such subsystems (Fig.14).

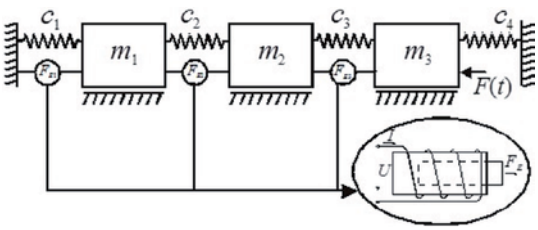

Fig. 14. A model of the system with electric elements

In order to determine the value of electrodynamic force, it is necessary to use the dependence presented below [12,16-18]:

$$F_E = BIL_C \tag{12}$$

where: F_E – electrodynamic force,
B – magnetic flux density,
I – current in the conductor,
L_C – length of the conductor.

The value of electrodynamic force is directly proportional to the intensity of the current flowing in the conductor and to the length of the conductor segment located in a given magnetic field. The values of "F_E" forces are equivalent to the previously determined values of "G" forces. In the above-presented dependence there is an element which can be altered in time, i.e. the current flowing through the conductor "I". Exemplary values of these elements are shown in Table 1.

The next step consisted in the analysis of the impact of the subsystem on the primary system. The analysis is presented in the form of diagrams comparing the amplitudes and deflections of the system without vibration reduction and the system with electric elements reducing vibration (Figs.15-23).

The conducted analysis has resulted in the diagrams showing that an active subsystem does not alter the primary system. The values of free vibration frequency of the system are subject to no alteration, therefore the initial requirements are met by the system.

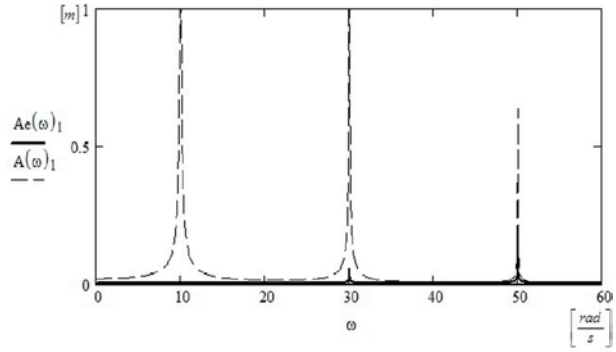

Fig. 15. Diagram of A_1 amplitude and Ae_1 displacement of system with electric elements (Fig. 14) at $\omega = \omega_1 = 10$ rad/s

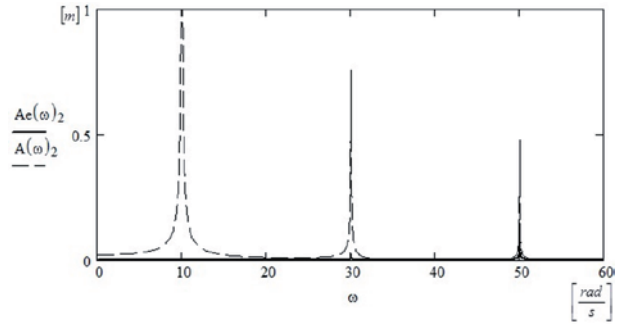

Fig. 16. Diagram of A_2 amplitude and Ae_2 displacement of system with electric elements (Fig. 14) at $\omega = \omega_1 = 10$ rad/s

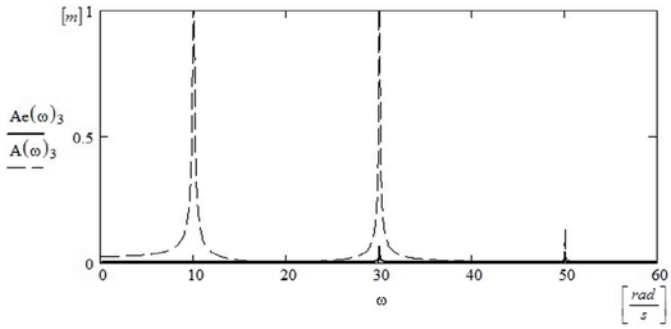

Fig. 17. Diagram of A_3 amplitude and Ae_3 displacement of system with electric elements (Fig. 14) at $\omega = \omega_1 = 10$ rad/s

Table 1. The values of electric elements

Frequency	Magnetic flux density	Current in the conductor	Length of the conductor
$\omega = \omega_1 = 10\ \left[\frac{rad}{s}\right]$	$B_1 = 5{,}825$	$I_1 = 0{,}386$	$L_{C1} = 0{,}1$
	$B_2 = 4{,}346$	$I_2 = 0{,}576$	$L_{C2} = 0{,}2$
	$B_3 = 12{,}731$	$I_3 = 2{,}533$	$L_{C3} = 0{,}3$
$\omega = \omega_3 = 30\ \left[\frac{rad}{s}\right]$	$B_1 = 18{,}11$	$I_1 = 1{,}201$	$L_{C1} = 0{,}1$
	$B_2 = 13{,}04$	$I_2 = 1{,}729$	$L_{C2} = 0{,}2$
	$B_3 = 15{,}03$	$I_3 = 2{,}991$	$L_{C3} = 0{,}3$
$\omega = \omega_5 = 50\ \left[\frac{rad}{s}\right]$	$B_1 = 32{,}43$	$I_1 = 2{,}151$	$L_{C1} = 0{,}1$
	$B_2 = 21{,}73$	$I_2 = 2{,}88$	$L_{C2} = 0{,}2$
	$B_3 = 18{,}81$	$I_3 = 3{,}742$	$L_{C3} = 0{,}3$

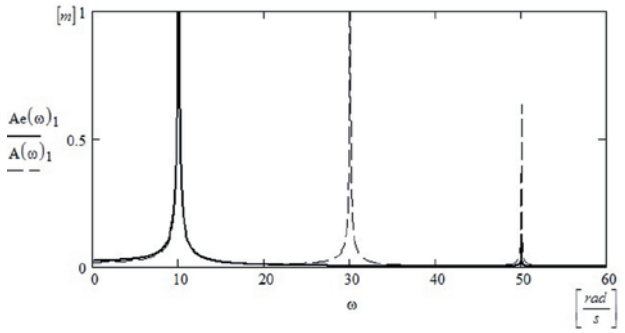

Fig. 18. Diagram of A_1 amplitude and Ae_1 displacement of system with electric elements (Fig. 14) at $\omega = \omega_3 = 30$ rad/s

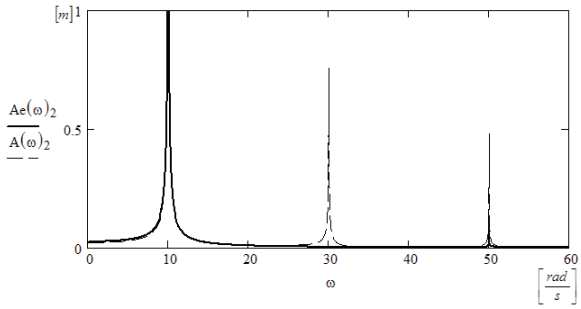

Fig. 19. Diagram of A_2 amplitude and Ae_2 displacement of system with electric elements (Fig. 14) at $\omega = \omega_3 = 30$ rad/s

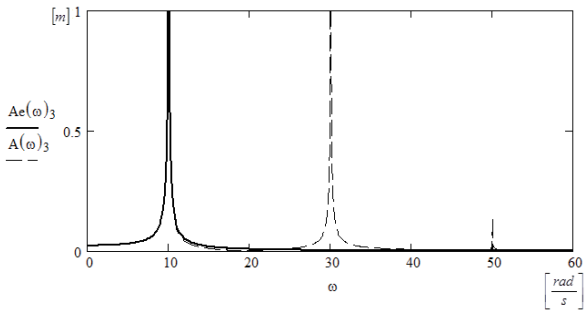

Fig. 20. Diagram of A_3 amplitude and Ae_3 displacement of system with electric elements (Fig. 14) at $\omega = \omega_3 = 30$ rad/s

Another possibility of the application of electric elements presented in the paper is the use of piezoelectric elements [7, 9, 14].

Summary

The paper presents a non-classical method of designing discrete vibrating mechanical and mechatronic systems. The designing consists in the structural and parametric synthesis. As a result of such a synthesis, one obtains a system having pre-defined required properties relating to the frequency values of the system free vibration. Such an approach makes it possible, already in the designing phase, to modify systems irrespective of the number of the degree of freedom possessed by the systems in question.

An important issue brought up in this paper is physical realisability of active subsystems as well as the analysis of mutual relations between the primary system and the subsystem reducing the vibration.

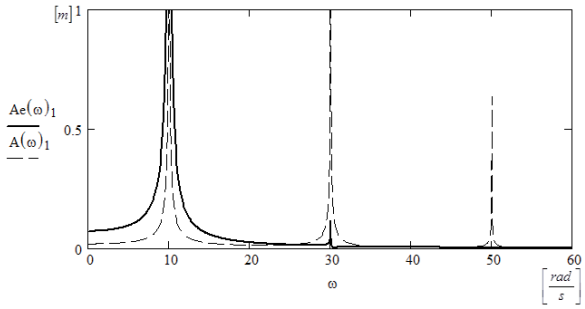

Fig. 21. Diagram of A_1 amplitude and Ae_1 displacement of system with electric elements (Fig. 14) at $\omega = \omega_5 = 50$ rad/s

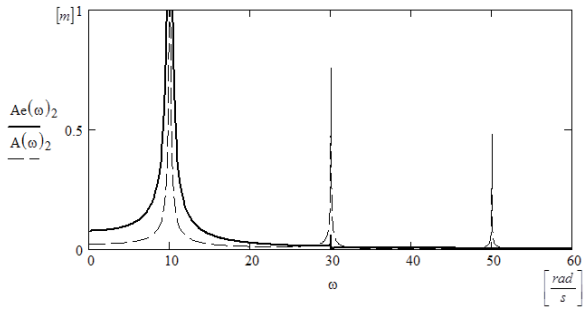

Fig. 22. Diagram of A_2 amplitude and Ae_2 displacement of system with electric elements (Fig. 14) at $\omega = \omega_5 = 50$ rad/s

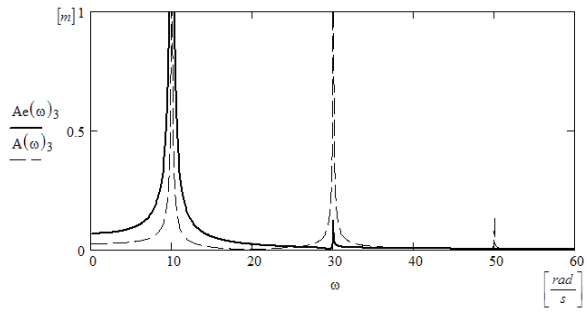

Fig. 23. Diagram of A_3 amplitude and Ae_3 displacement of system with electric elements (Fig. 14) at $\omega = \omega_5 = 50$ rad/s

References

1. Bialas K. Electrical Elements in Reduction of Mechanical Vibrations. Applied Mechanics and Materials 2013; 371: 657-661, http://dx.doi.org/10.4028/www.scientific.net/AMM.371.657.
2. Bialas K. Mechanical and electrical elements in reduction of vibrations. Journal of Vibroengineering 2012; 14 (1): 123-128.
3. Bialas K. Mechanical Subsystem as Implementation of Active Reduction of Vibration. Solid State Phenomena 2013; 198: 657-662, http://dx.doi.org/10.4028/www.scientific.net/SSP.198.657.
4. Bialas K. Passive and Active Elements in Reduction of Vibrations of Torsional Systems. Solid State Phenomena 2010; 164: 260-264, http://dx.doi.org/10.4028/www.scientific.net/SSP.164.260.
5. Białas K., Buchacz A., Dzitkowski T. Synthesis of vibrating active mechanical systems with dumping in view of polar graphs and structural numbers. Gliwice Monograph 230, Silesian University of Technology Press, 2009 (in Polish).

6. Buchacz A. Introduction to synthesis of the torsional vibrating discrete-continuous mechatronic systems by means of the hypergraphs and structural numbers method. Journal of Vibroengineering 2012; 14 (2): 514-519.
7. Buchacz A., Płaczek M.: Damping of Mechanical Vibrations Using Piezoelements, Including Influence of Connection Layer's Properties on the Dynamic Characteristic. Solid State Phenomena 2009; 147-149: 869-875, http://dx.doi.org/10.4028/www.scientific.net/SSP.147-149.869.
8. Buchacz A., Świder J. (red) Computer support CAD CAM, Support for construction of systems reducing vibration and machine noise, Warsaw WNT, 2001 (in Polish).
9. Buchacz A., Wróbel A. Computer-Aided Analysis of Piezoelectric Plates. Solid State Phenomena 2010; 164: 239-242, http://dx.doi.org/10.4028/www.scientific.net/SSP.164.239.
10. Czmochowski J., Moczko P., Odyjas P., Pietrusiak D. Tests of rotary machines vibrations in steady and unsteady states on the basis of large diameter centrifugal fans. Eksploatacja i Niezawodnosc – Maintenance and Reliability 2014; 16 (2): 211–216.
11. Engel Z., Kowal J., Vibro-accoustic processes control, Kraków AGH Press, 1995 (in Polish).
12. Groszkowski J., Manufacturing of electric vibrations, Warsaw PWT, 1958 (in Polish).
13. Jamroziak K., Kosobudzki M. Determining the torsional natural frequency of underframe of off-road vehicle with use of the procedure of operational modal analysis. Journal of Vibroengineering 2012; 14 (2): 472-476.
14. Latalski J. Modelling of macro fiber composite piezoelectric active elements in ABAQUS system. Eksploatacja i Niezawodnosc – Maintenance and Reliability 2011; 4: 72–78.
15. Michałowski S., Active systems in machines construction, Cracow Publication by Cracow University of Technology, Monograph 171, 1994 (in Polish).
16. Onwubolu G. C., Mechatronics Principles and Applications. Elsevier Butterworth-Heinemann 2005.
17. Preumont A., Mechatronics Dynamics of Electromechanical and Piezoelectric Systems. Published by Springer. The Netherlands 2006.
18. Soong T.T., Dargush G.F., Passive energy dissipation systems in structural engineering. Chichester, USA, Wiley 1999.

Katarzyna BIAŁAS
Andrzej BUCHACZ
Institute of Engineering Processes Automation and Integrated Manufacturing Systems,
Faculty of Mechanical Engineering,
Silesian University of Technology,
Konarskiego 18A, 44-100 Gliwice, Poland
E-mail: katarzyna.bialas@polsl.pl, andrzej.buchacz@polsl.pl

Article citation info:
NIWAS R, KADYAN MS, KUMAR J. Probabilistic analysis of two reliability models of a single-unit system with preventive maintenance beyond warranty and degradation. Eksploatacja i Niezawodnosc – Maintenance and Reliability 2015; 17 (4): 535–543, http://dx.doi.org/10.17531/ein.2015.4.8.

Ram NIWAS
MS KADYAN
Jitender KUMAR

PROBABILISTIC ANALYSIS OF TWO RELIABILITY MODELS OF A SINGLE-UNIT SYSTEM WITH PREVENTIVE MAINTENANCE BEYOND WARRANTY AND DEGRADATION

ANALIZA PROBABILISTYCZNA DWÓCH MODELI NIEZAWODNOŚCI SYSTEMU JEDNOELEMENTOWEGO WYKORZYSTUJĄCYCH POJĘCIA POGWARANCYJNEJ OBSŁUGI PROFILAKTYCZNEJ ORAZ DEGRADACJI

This paper presents two reliability models of a single-unit system with the concept of preventive maintenance (PM) beyond warranty and degradation. In both the models, repair of any failure during warranty is cost-free to the users, provided failures are not due to the negligence of users. There is a single repairman who always remains with the system. Beyond warranty, the unit goes under PM and works as new after PM (in both models). In model-1, the unit works as new after its repair beyond warranty whereas; in model-2, the unit becomes degraded. After failure, the degraded unit is replaced by a new one. The failure time of the system follows negative exponential distribution while PM, replacement and repair time distributions are taken as arbitrary with different probability density functions. Supplementary variable technique is adopted to derive the expressions for some economic measures such as reliability, mean time to system failure (MTSF), availability and profit function. Using Abel's lemma, the behaviour of the system in steady-state has been examined. To highlight the behaviour of reliability and profit function, numerical results are considered for particular values of various parameters and repair cost. Profit comparison of both the models is also made to see the usefulness of the concept of degradation.

***Keywords**: probabilistic analysis, reliability, preventive maintenance, warranty, degradation.*

W artykule przedstawiono dwa modele niezawodności systemu jednoelementowego wykorzystujące pojęcia pogwarancyjnej obsługi profilaktycznej oraz degradacji. Oba modele zakładają, że w okresie gwarancyjnym użytkownik nie ponosi żadnych kosztów związanych z naprawą uszkodzeń, chyba że uszkodzenie powstało wskutek zaniedbania ze strony użytkownika. Obsługi są wykonywane przez jedną ekipę remontową, która zawsze pozostaje na stanowisku. Po upływie okresu gwarancyjnego, urządzenie podlega obsłudze profilaktycznej i po jej przeprowadzeniu działa jak nowe (w obu modelach). Model 1 zakłada, że element po naprawie pogwarancyjnej działa jak nowy, natomiast w Modelu 2, element ulega degradacji. Zdegradowany element, który uległ uszkodzeniu, zostaje wymieniony na nowy. Rozkład czasu uszkodzenia jest rozkładem wykładniczym ujemnym, a rozkłady czasu obsługi profilaktycznej, wymiany i naprawy są traktowane jako arbitralne, o różnych funkcjach gęstości prawdopodobieństwa. Zastosowana technika dodatkowej zmiennej pozwoliła na wyprowadzenie wyrażeń dla niektórych miar ekonomicznych, takich jak niezawodność, średni czas do uszkodzenia systemu (MTSF), gotowość i funkcja zysków. Zachowanie systemu w stanie ustalonym badano z wykorzystaniem lematu Abela. Aby przedstawić zachowanie funkcji niezawodności i zysków, analizowano wyniki numeryczne dla poszczególnych wartości różnych parametrów oraz kosztów naprawy. Porównanie zyskowności badanych modeli umożliwiło weryfikację przydatności pojęcia degradacji.

***Słowa kluczowe**: analiza probabilistyczna, niezawodność, obsługa profilaktyczna, gwarancja, degradacja.*

1. Introduction

In modern marketplace, warranty has its own priority in business for manufacturers to protect their benefits and to compete with other manufacturers. By using regenerating point and semi-Markov technique, various researchers including Kadyan et al. [3], Yang and Dhillon [6], Perez Ocon and Ruiz Castro [8], Philip and Cristiano [9] and Yuan and Meng [11] have studied reliability models of one or more unit systems under different sets of assumptions on failure and repair policies. When the failure rate or repair rate or both are time-dependent, the system loses its Markov character and becomes non-Markovian. By introducing one or more supplementary variables, the non-Markovian nature of the process is changed to Markovian. Firstly, Cox [1] used supplementary variable technique in analyzing non-Markovian stochastic process. Singh et al. [10] studied a system having two units in series configuration with controller and Nailwal and Singh [7] analyzed an operating system with inspection in different weather condition by using supplementary variable technique without considering the concept of cost-free warranty. But, warranty assured the customers that the products they are buying perform satisfactorily for a particular period of time and markets the product.

Also, performing PM has become prevalent to improve the condition of the deteriorated product (or system) and reduce the cost of repairing deteriorated product. Kadyan [2] discussed reliability and profit analysis of a single-unit system with preventive maintenance without considering degradation of the unit after its repair.

However, the failed unit does not always work as new after its repair. Due to continuous usage and ageing effect, failure rate of a unit

may increase after its repair. In such a situation, unit works with reduced capacity after its repair and so is called a degraded unit. Kumar et al. [4,5] analysed redundant systems with degradation of the unit after repair without any warranty.

In view of the above observations, here we developed two reliability models of a single-unit system with the concept of PM beyond warranty and degradation. In both the models, repair of any failure during warranty is cost-free to the users, provided failures are not due to the negligence of users such as cracked screen, accident, misuse, physical damage, damage due to liquid and unauthorized modifications etc. There is a single repairman, who always remains with the system. Beyond warranty, the unit goes under PM and works as new after PM (in both the models). In model-1, the unit works as new after its repair beyond warranty whereas; in model-2, the unit becomes degraded. In model-2, the degraded unit is replaced by a new one after its failure. The failure time of the system follows negative exponential distribution while PM, replacement and repair time distributions are taken as arbitrary with different probability density functions. Supplementary variable technique is adopted to derive the expressions for some economic measures such as reliability, MTSF, availability and profit function. Using Abel's lemma ([6] & [9]), the behaviour of the system in steady-state has been examined. To highlight the behaviour of reliability and profit function, numerical results are also considered for particular values of various parameters and repair cost. Profit comparison of both models is made to see the usefulness of the concept of degradation.

2. Notations

λ / λ_1 Constant failure rate of the new unit within/beyond warranty.

λ_2 Constant failure rate of the degraded unit beyond warranty.

λ_m Transition rate with which a unit goes under PM for improvement.

α Transition rate with which warranty of the system is completed.

$\mu(x), S(x) / \mu_1(x), S_1(x)$ Repair rate of the unit and probability density function, for the elapsed repair time x within/ beyond warranty.

$\mu_2(y), S_2(y)$ PM rate of the unit and probability density function, for the elapsed PM time y.

$\mu_3(z), S_3(z)$ Replacement rate of the failed degraded unit and probability density function, for the elapsed replacement time z.

$p_0(t) / p_1(t)$ Probability density that at time t, the system is within/ beyond warranty and in good state.

$p_i(x,t)$ Probability density that at time t, the system is in state S_i, $i=2,4$ and the system is under repair with elapsed repair time x.

$p_3(y,t)$ Probability density that at time t, the system is in state S_3 and the unit is under PM with elapsed PM time y.

$p_5(t)$ Probability density that at time t, the system is operable and in degraded state.

$p_6(z,t)$ Probability density that at time t, the system is in state S6 and the failed degraded unit is under replacement with elapsed replacement time z.

$p(s)$ Laplace transform of function $p(t)$

$S(x) = \mu(x)\, e^{\left[-\int_0^x \mu(x)dx\right]}$

$S_1(x) = \mu_1(x)\, e^{\left[-\int_0^x \mu_1(x)dx\right]}$

$S_2(y) = \mu_2(y)\, e^{\left[-\int_0^y \mu_2(y)dy\right]}$

$S_3(z) = \mu_3(z)\, e^{\left[-\int_0^z \mu_3(z)dz\right]}$

3. State-Specification

The following states of the system are common for both models:

S_0 / S_1 The new unit is operative within/ beyond warranty.

S_2 / S_4 The new unit is in failed state within/ beyond warranty.

S_3 The new unit is under PM beyond warranty.

The remaining states for model-2 are:

S_5 The degraded unit is operative beyond warranty.

S_6 The failed degraded unit is under replacement beyond warranty.

4. Formulation of mathematical model-1

Using the probabilistic arguments and limiting transitions, we have the following difference-differential equations:

$$\left[\frac{d}{dt}+\lambda+\alpha\right]p_0(t)=\int_0^\infty \mu(x)p_2(x,t)dx \tag{1}$$

$$\left[\frac{d}{dt}+\lambda_1+\lambda_m\right]p_1(t)=\alpha\, p_0(t)+\int_0^\infty \mu_1(x)p_4(x,t)dx+\int_0^\infty \mu_2(y)p_3(y,t)dy \tag{2}$$

$$\left[\frac{\partial}{\partial t}+\frac{\partial}{\partial x}+\mu(x)\right]p_2(x,t)=0 \tag{3}$$

$$\left[\frac{\partial}{\partial t}+\frac{\partial}{\partial y}+\mu_2(y)\right]p_3(y,t)=0 \tag{4}$$

$$\left[\frac{\partial}{\partial t}+\frac{\partial}{\partial x}+\mu_1(x)\right]p_4(x,t)=0 \tag{5}$$

Boundary Conditions

$$p_2(0,t)=\lambda\, p_0(t) \tag{6}$$

$$p_3(0,t)=\lambda_m p_1(t) \tag{7}$$

$$p_4(0,t) = \lambda_1 p_1(t) \tag{8}$$

Initial conditions

$p_i(0) = 1$; when $i = 0$

$$p_i(0)=0;\ \text{when } i \neq 0 \tag{9}$$

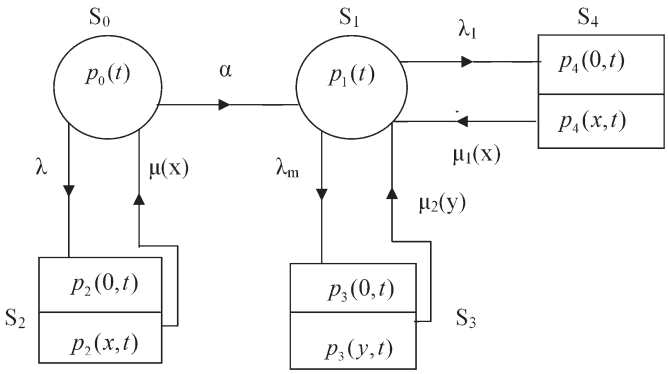

Fig. 1. State transition diagram of the model-1

5 Analysis for model-1

5.1. Solution of the equations

Taking Laplace transforms of equations (1)-(8) and using (9), we obtain:

$$[s+\lambda+\alpha]p_0(s) = 1 + \int_0^\infty \mu(x)p_2(x,s)dx \tag{10}$$

$$[s+\lambda_1+\lambda_m]p_1(s) = \alpha p_0(s) + \int_0^\infty \mu_1(x)p_4(x,s)dx + \int_0^\infty \mu_2(y)p_3(y,s)dy \tag{11}$$

$$\left[\frac{\partial}{\partial x} + s + \mu(x)\right]p_2(x,s) = 0 \tag{12}$$

$$\left[\frac{\partial}{\partial y} + s + \mu_2(y)\right]p_3(y,s) \tag{13}$$

$$\left[\frac{\partial}{\partial x} + s + \mu_1(x)\right]p_4(x,s) = 0 \tag{14}$$

$$p_2(0,s) = \lambda p_0(s) \tag{15}$$

$$p_3(0,s) = \lambda_m p_1(s) \tag{16}$$

$$p_4(0,s) = \lambda_1 p_1(s) \tag{17}$$

Taking integration of equations (12), (13) and (14), we get the following equations:

$$p_2(x,t) = p_2(0,t)\,e^{\left[-sx-\int_0^x \mu(x)dx\right]} \tag{18}$$

$$p_3(y,t) = p_3(0,t)\,e^{\left[-sy-\int_0^y \mu_2(y)dy\right]} \tag{19}$$

and

$$p_4(x,t) = p_4(0,t)\,e^{\left[-sx-\int_0^x \mu_1(x)dx\right]} \tag{20}$$

Using equations (15) and (18), equation (10) yields:

$$[s+\lambda+\alpha]p_0(s) = 1 + p_2(0,t)\int_0^\infty \mu(x)\,e^{\left[-sx-\int_0^x \mu(x)dx\right]}dx = 1 = \lambda p_0(s)S(s)$$

$$p_0(s) = \frac{1}{T(s)} \tag{21}$$

where $T(s) = s + \alpha + \lambda\left(1 - S(s)\right)$ (22)

Using equations (16), (17), (19) and (20), equation (11) yields:

$$[s+\lambda_1+\lambda_m]p_1(s) = \alpha p_0(s) + p_4(0,t)\int_0^\infty \mu_1(x)\,e^{\left[-sx-\int_0^x \mu_1(x)dx\right]}dx + p_3(0,t)\int_0^\infty \mu_2(y)\,e^{\left[-sy-\int_0^y \mu_2(y)dy\right]}dy$$

$$= \alpha p_0(s) + \lambda_1 p_1(s)S_1(s) + \lambda_m p_1(s)S_2(s)$$

$$p_1(s) = \frac{A(s)}{T(s)} \tag{23}$$

Where $A(s) = \dfrac{\alpha}{\left(s + \lambda_1 - \lambda_1 S_1(s) - \lambda_m S_2(s)\right)}$ (24)

Now, the Laplace transform of the probability that the system is in the failed state is given by:

$$p_2(s) = \int_0^\infty p_2(s,x)dx = \lambda p_0(s)\frac{\left(1-S(s)\right)}{s}$$

$$p_2(s) = \frac{\lambda B(s)}{T(s)} \tag{25}$$

Where $B(s) = \dfrac{\left(1-S(s)\right)}{s}$ (26)

Similarly, $p_3(s) = \int_0^\infty p_3(s,y)dy = \lambda_m p_1(s)\dfrac{\left(1-S_2(s)\right)}{s}$

$$p_3(s) = \frac{\left(\lambda_m A(s)C(s)\right)}{T(s)} \tag{27}$$

Where $C(s) = \dfrac{\left(1-S_2(s)\right)}{s}$ (28)

Similarly, $p_4(s) = \int_0^\infty p_4(s,x)dx = \lambda_1 p_1(s)\dfrac{\left(1-S_1(s)\right)}{s}$

$$p_4(s) = \frac{\left(\lambda_1 A(s) D(s)\right)}{T(s)} \tag{29}$$

where $D(s) = \dfrac{\left(1 - S_1(s)\right)}{s}$ (30)

It is worth noticing that:

$$p_0(s) + p_1(s) + p_2(s) + p_3(s) + p_4(s) = \frac{1}{s} \tag{31}$$

5.2. Evaluation of Laplace Transforms of Up and Down state probabilities

The Laplace transforms of the probabilities that the system is in Up State ($p_{up}(t)$) (i.e. Good State) and Down State ($p_{down}(t)$) (i.e. Failed State) at time t are as follows:

$$p_{up}(s) = p_0(s) + p_1(s)$$
$$p_{up}(s) = \frac{\left(1 + A(s)\right)}{T(s)} \tag{32}$$

$$p_{down}(s) = p_2(s) + p_3(s) + p_4(s)$$
$$p_{down}(s) = \frac{\left(\lambda B(s) + \lambda_m A(s) C(s) + \lambda_1 A(s) D(s)\right)}{T(s)} \tag{33}$$

5.3. Steady-State behavior of the system

Using Abel's Lemma ([6] & [9]) i.e.
$\lim_{t\to\infty} F(t) = \lim_{s\to 0} sF(s) = F$ in equations (32) and (33), Provided the limit on the right hand side exists, the following time independent probabilities have been obtained:

$$P_{up} = \frac{1}{\left(1 - \lambda_1 S_1'(0) - \lambda_m S_2'(0)\right)} \tag{34}$$

$$P_{down} = \frac{-\lambda_1 S_1'(0) - \lambda_m S_2'(0)}{\left(1 - \lambda_1 S_1'(0) - \lambda_m S_2'(0)\right)} \tag{35}$$

5.4. Reliability of the system (R(t))

The differential–difference equations for reliability of the system are:

$$\left[\frac{d}{dt} + \lambda + \alpha\right] p_0(t) = 0 \tag{36}$$

$$\left[\frac{d}{dt} + \lambda_1 + \lambda_m\right] p_1(t) = \alpha\, p_0(t) \tag{37}$$

Taking Laplace transform of equations (36) and (37), using (9), we get:

$$\left[s + \lambda + \alpha\right] p_0(s) = 1 \tag{38}$$

$$\left[s + \lambda_1 + \lambda_m\right] p_1(s) = \alpha\, p_0(s) \tag{39}$$

The solution can be written as:

$$p_0(s) = \frac{1}{\left(s + \alpha + \lambda\right)} \tag{40}$$

$$p_1(s) = \frac{\alpha}{\left(s + \alpha + \lambda\right)\left(s + \lambda_1 + \lambda_m\right)}$$
$$R(s) = p_0(s) + p_1(s)$$
$$= \frac{1}{\left(s + \alpha + \lambda\right)} + \frac{\alpha}{\left(s + \alpha + \lambda\right)\left(s + \lambda_1 + \lambda_m\right)} \tag{41}$$

Taking inverse Laplace transform, we get:

$$R(t) = e^{-(\lambda+\alpha)t}\left[\frac{\left(\lambda - \lambda_1 - \lambda_m\right)}{\left(\lambda - \lambda_1 - \lambda_m + \alpha\right)}\right] + e^{-(\lambda_1+\lambda_m)t}\left[\frac{\alpha}{\left(\lambda - \lambda_1 - \lambda_m + \alpha\right)}\right] \tag{42}$$

5.5. Mean time to system failure (MTSF)

$$MTSF = \int_0^\infty R(t)dt$$

$$MTSF = \int_0^\infty \left\{ e^{-(\lambda+\alpha)t}\left[\frac{\left(\lambda - \lambda_1 - \lambda_m\right)}{\left(\lambda - \lambda_1 - \lambda_m + \alpha\right)}\right] + e^{-(\lambda_1+\lambda_m)t}\left[\frac{\alpha}{\left(\lambda - \lambda_1 - \lambda_m + \alpha\right)}\right]\right\} dt$$

$$MTSF = \left[\frac{\left(\lambda - \lambda_1 - \lambda_m\right)}{\left(\lambda - \lambda_1 - \lambda_m + \alpha\right)\left(\lambda + \alpha\right)}\right] + \left[\frac{\alpha}{\left(\lambda - \lambda_1 - \lambda_m + \alpha\right)\left(\lambda_1 + \lambda_m\right)}\right] \tag{43}$$

6. Formulation of mathematical model-2

Equations (1), (3), (4) and (5) defined in model-1 are same for model-2 and remaining equations for model-2 are:

$$\left[\frac{d}{dt} + \lambda_1 + \lambda_m\right] p_1(t) = \alpha\, p_0(t) + \int_0^\infty \mu_3(z) p_6(z,t) dx + \int_0^\infty \mu_2(y) p_3(y,t) dy \tag{44}$$

$$\left[\frac{d}{dt} + \lambda_2\right] p_5(t) = \int_0^\infty \mu_1(x) p_4(x,t) dx \tag{45}$$

$$\left[\frac{\partial}{\partial t} + \frac{\partial}{\partial z} + \mu_3(z)\right] p_6(z,t) = 0 \tag{46}$$

Boundary Conditions

Boundary $p_2(0,t), p_3(0,t)$ and $p_4(0,t)$ are same as defined in model-1 and remaining is:

$$p_6(0,t) = \lambda_2 p_5(t) \tag{47}$$

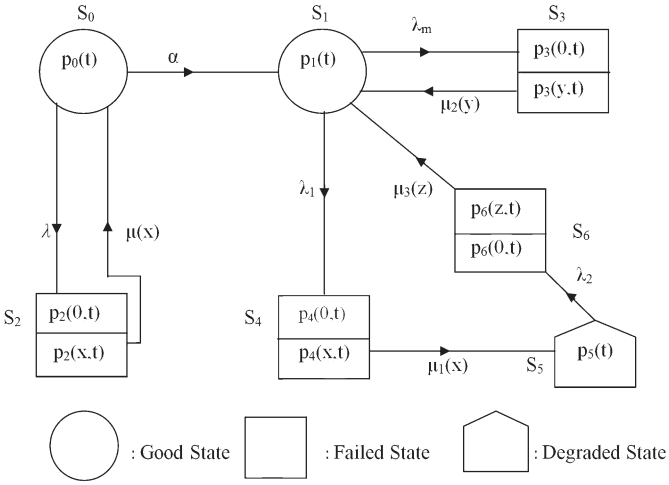

Fig. 2. Transition diagram of the model-2

7. Analysis for model-2

7.1. Solution of the equations

Proceeding in similar way as in model-1, the expressions for $p_0(s)$, $p_2(s)$, $p_3(s)$ and $p_4(s)$ are same as defined in model-1 and remaining expressions are:

$$p_1(s) = \frac{A(s)}{T(s)} \tag{48}$$

Where, $A(s) = \dfrac{\alpha\left(s+\lambda_2\right)}{\left(s+\lambda_1+\lambda_m\right)\left(s+\lambda_2\right)-\lambda_m S_2(s)\left(s+\lambda_2\right)-\lambda_1 S_1(s) S_3(s)}$ (49)

And $T(s)$ is same as defined in model-1.

$$p_5(s) = \frac{\lambda_1 A(s) S_1(s)}{T(s)\left(s+\lambda_2\right)} \tag{50}$$

Now,

$$p_6(s) = \int_0^\infty p_6(s,z)dz = \lambda_2 p_5(s)\frac{\left(1-S_3(s)\right)}{s}$$

$$p_6(s) = \frac{\left(\lambda_2\lambda_1 A(s) S_1(s) E(s)\right)}{T(s)(s+\lambda_2)} \tag{51}$$

where $$E(s) = \frac{\left(1-S_3(s)\right)}{s} \tag{52}$$

It is worth noticing that:

$$p_0(s)+p_1(s)+p_2(s)+p_3(s)+p_4(s)+p_5(s)+p_6(s) = \frac{1}{s} \tag{53}$$

7.2. Evaluation of Laplace Transforms of Up and Down state probabilities

$$p_{up}(s) = p_0(s)+p_1(s)+p_5(s)$$

$$p_{up}(s) = \frac{\left(1+A(s)+\dfrac{\lambda_1 S_1(s) A(s)}{\left(s+\lambda_2\right)}\right)}{T(s)}$$

$$p_{down}(s) = p_2(s)+p_3(s)+p_4(s)+p_6(s) \tag{54}$$

$$p_{down}(s) = \frac{\left(\lambda B(s)+\lambda_m C(s)A(s)+\lambda_1 A(s)D(s)+\left(\dfrac{\lambda_1\lambda_2 S_1(s)A(s)E(s)}{\left(s+\lambda_2\right)}\right)\right)}{T(s)} \tag{55}$$

7.3 Steady-State behavior of the system

$$p_{up} = \frac{\left(\lambda_1+\lambda_2\right)}{\left(\lambda_1+\lambda_2-\lambda_2\lambda_m S_2'(0)-\lambda_1\lambda_2 S_1'(0)-\lambda_1\lambda_2 S_3'(0)\right)} \tag{56}$$

$$p_{down} = \frac{-\lambda_2\lambda_m S_2'(0)-\lambda_1\lambda_2 S_1'(0)-\lambda_1\lambda_2 S_3'(0)}{\left(\lambda_1+\lambda_2-\lambda_2\lambda_m S_2'(0)-\lambda_1\lambda_2 S_1'(0)-\lambda_1\lambda_2 S_3'(0)\right)} \tag{57}$$

7.4. Reliability and mean time to system failure (MTSF)

Reliability and MTSF of this model is same as that of the model-1.

8. Special cases

8.1. Availability of the system for model-1

When repair and PM times follow exponential distribution i.e. $S(s) = \dfrac{\mu}{\left(s+\mu\right)}$, $S_1(s) = \dfrac{\mu_1}{\left(s+\mu_1\right)}$ and $S_2(s) = \dfrac{\mu_2}{\left(s+\mu_2\right)}$

where μ and μ_1 are constant repair rates and μ_2 is constant PM rate. Putting these values in equations (21)-(24), we get:

$$p_0(s) = \frac{1}{I(s)} \tag{58}$$

Where $$I(s) = \frac{\left(s^2+s\left(\mu+\lambda+\alpha\right)+\alpha\mu\right)}{\left(s+\mu\right)} \tag{59}$$

$$p_1(s) = \frac{F(s)}{I(s)} \tag{60}$$

Where

$$F(s) = \frac{\alpha\left(s+\mu_1\right)\left(s+\mu_2\right)}{\left(s+\lambda_1+\lambda_m\right)\left(s+\mu_1\right)\left(s+\mu_2\right)-\lambda_1\mu_1\left(s+\mu_2\right)-\lambda_m\mu_2\left(s+\mu_1\right)} \tag{61}$$

$$p_{up}(s)=p_0(s)+p_1(s)$$
$$\frac{\left(s^3+s^2\left(\lambda_1+\lambda_m+\alpha+\mu_1+\mu_2\right)+s\left(\lambda_1\mu_2+\mu_1\mu_2+\alpha\mu_2+\lambda_m\mu_1+\alpha\mu_1\right)+\alpha\mu_1\mu_2\right)\left(s+\mu_1\right)}{s\left(s^2+s\left(\lambda+\alpha+\mu\right)+\alpha\mu\right)\left(s^2+s\left(\lambda_1+\lambda_m+\mu_1+\mu_2\right)+\left(\lambda_1\mu_2+\mu_1\mu_2+\lambda_m\mu_1\right)\right)} \tag{62}$$

Taking inverse Laplace transform of equation (62), we get:

$$\begin{aligned}p_{up}(t)=&\frac{c_0\mu}{z_1z_2z_3z_4}+\left\{\frac{\left(z_1^{\,3}+c_2z_1^{\,2}+c_1z_1+c_0\right)\left(z_1+\mu\right)}{z_1\left(z_1-z_2\right)\left(z_1-z_3\right)\left(z_1-z_4\right)}\right\}\exp\left(z_1t\right)\\&-\left\{\frac{\left(z_2^{\,3}+c_2z_2^{\,2}+c_1z_2+c_0\right)\left(z_2+\mu\right)}{z_2\left(z_1-z_2\right)\left(z_2-z_3\right)\left(z_2-z_4\right)}\right\}\exp\left(z_2t\right)\\&+\left\{\frac{\left(z_3^{\,3}+c_2z_3^{\,2}+c_1z_3+c_0\right)\left(z_3+\mu\right)}{z_3\left(z_1-z_3\right)\left(z_2-z_3\right)\left(z_3-z_4\right)}\right\}\exp\left(z_3t\right)\\&-\left\{\frac{\left(z_4^{\,3}+c_2z_4^{\,2}+c_1z_4+c_0\right)\left(z_4+\mu\right)}{z_4\left(z_4-z_1\right)\left(z_4-z_2\right)\left(z_3-z_4\right)}\right\}\exp\left(z_4t\right)\end{aligned} \tag{63}$$

Where: $c_2=\left(\lambda_1+\lambda_m+\alpha+\mu_1+\mu_2\right), c_1=$
$=\left(\lambda_1\mu_2+\mu_1\mu_2+\alpha\mu_2+\lambda_m\mu_1+\alpha\mu_1\right), c_0=\alpha\mu_1\mu_2$

and z_1, z_2 are two roots of the equation $\left(s^2+s\left(\lambda+\alpha+\mu\right)+\alpha\mu\right)=0$ and z_3, z_4 are two roots of the equation $\left(s^2+s\left(\lambda_1+\lambda_m+\mu_1+\mu_2\right)+\left(\lambda_1\mu_2+\mu_1\mu_2+\lambda_m\mu_1\right)\right)=0.$

8.2. Availability of the system for model-2

Proceeding in similar way as in model-1, the expressions for $p_0(s)$ is same as that of defined in equation (58) for model-1and remaining expressions are:

$$p_1(s)=\frac{J(s)}{I(s)} \tag{64}$$

Where:

$$J(s)=\frac{\alpha\left(s+\mu_1\right)\left(s+\mu_2\right)\left(s+\mu_3\right)\left(s+\lambda_2\right)}{\left(s+\lambda_1+\lambda_m\right)\left(s+\mu_1\right)\left(s+\mu_2\right)\left(s+\mu_3\right)-\mu_2\lambda_m\left(s+\mu_1\right)\left(s+\mu_3\right)\left(s+\lambda_2\right)-\lambda_1\lambda_2\mu_1\mu_3\left(s+\mu_2\right)} \tag{65}$$

And $I(s)$ is same as defined in equation (59):

$$p_5(s)=\frac{J(s)K(s)}{I(s)} \tag{66}$$

Where $K(s)=\dfrac{\mu_1\lambda_1}{\left(s+\mu_1\right)\left(s+\lambda_2\right)}$ (67)

$$\begin{aligned}p_{up}(s)&=p_0(s)+p_1(s)+p_5(s)\\&=\frac{\left(s^5+b_4s^4+b_3s^3+b_2s^2+b_1s+b_0\right)\left(s+\mu\right)}{s\left(s^2+s\left(\lambda+\alpha+\mu\right)+\alpha\mu\right)\left(s^4+a_3s^3+a_2s^2+a_1s+a_0\right)}\end{aligned} \tag{68}$$

Where $b_4=\left(\lambda_1+\lambda_2+\lambda_m+\alpha+\mu_1+\mu_2+\mu_3\right)$,

$$b_3=\begin{pmatrix}\lambda_1\mu_1+\lambda_1\mu_2+\lambda_2\mu_2+\lambda_1\lambda_2+\lambda_2\mu_1+\lambda_2\mu_3+\lambda_1\mu_3+\lambda_m\mu_1+\lambda_m\mu_3\\+\lambda_m\lambda_2+\mu_1\mu_3+\mu_1\mu_2+\mu_2\mu_3+\alpha\mu_1+\alpha\mu_2+\alpha\mu_3+\alpha\lambda_2\end{pmatrix}$$

$$b_2=\begin{pmatrix}\lambda_1\mu_1\mu_3+\lambda_2\mu_1\mu_3+\lambda_2\mu_1\mu_2+\lambda_2\mu_2\mu_3+\lambda_1\mu_1\mu_2+\lambda_1\mu_2\mu_3+\lambda_m\mu_1\mu_3+\lambda_1\lambda_2\mu_1+\lambda_1\lambda_2\mu_3+\lambda_1\lambda_2\mu_2\\+\lambda_m\lambda_2\mu_1+\lambda_m\lambda_2\mu_3+\mu_1\mu_2\mu_3+\alpha\mu_1\mu_2+\alpha\mu_1\mu_3+\alpha\mu_3\mu_2+\alpha\lambda_2\mu_1+\alpha\lambda_2\mu_3+\alpha\lambda_2\mu_2+\alpha\lambda_1\mu_1\end{pmatrix}$$

$$b_1=\begin{pmatrix}\lambda_1\mu_1\mu_2\mu_3+\lambda_1\lambda_2\mu_1\mu_2+\lambda_1\lambda_2\mu_3\mu_2+\lambda_m\lambda_2\mu_1\mu_3+\alpha\lambda_2\mu_1\mu_3\\+\alpha\lambda_2\mu_1\mu_2+\alpha\lambda_2\mu_2\mu_3+\alpha\lambda_1\mu_1\mu_3+\alpha\lambda_1\mu_1\mu_2+\alpha\mu_1\mu_2\mu_3\end{pmatrix}$$

$b_0=\alpha\lambda_1\mu_1\mu_2\mu_3+\alpha\lambda_2\mu_1\mu_2\mu_3$,

$a_3=\left(\lambda_1+\lambda_2+\lambda_m+\mu_1+\mu_2+\mu_3\right)$

$$a_2=\begin{pmatrix}\lambda_1\mu_1+\lambda_1\mu_3+\lambda_1\lambda_2+\lambda_2\mu_1+\lambda_2\mu_2+\lambda_1\mu_2+\lambda_m\mu_1\\+\lambda_m\mu_3+\lambda_2\mu_3+\lambda_m\lambda_2+\mu_1\mu_3+\mu_1\mu_2+\mu_2\mu_3\end{pmatrix},$$

$$a_1=\begin{pmatrix}\lambda_1\mu_1\mu_3+\lambda_2\mu_1\mu_3+\lambda_2\mu_1\mu_2+\lambda_2\mu_2\mu_3+\lambda_1\mu_1\mu_2+\lambda_1\mu_2\mu_3+\lambda_1\lambda_2\mu_1\\+\lambda_1\lambda_2\mu_3+\lambda_1\lambda_2\mu_2+\lambda_m\mu_1\mu_3++\lambda_m\lambda_2\mu_1+\lambda_m\lambda_2\mu_3+\mu_1\mu_2\mu_3\end{pmatrix}$$

and $a_0=\left(\lambda_1\mu_1\mu_2\mu_3+\lambda_1\lambda_2\mu_1\mu_2+\lambda_1\lambda_2\mu_3\mu_2+\lambda_m\lambda_2\mu_1\mu_3\right)$

Taking inverse Laplace transform of equation (68), we get:

$$\begin{aligned}p_{up}(t)=&\frac{b_0\mu}{z_1z_2z_3z_4z_5z_6}+\left\{\frac{\left(z_1^{\,5}+b_4z_1^{\,4}+b_3z_1^{\,3}+b_2z_1^{\,2}+b_1z_1+b_0\right)\left(z_1+\mu\right)}{z_1\left(z_1-z_2\right)\left(z_1-z_3\right)\left(z_1-z_4\right)\left(z_1-z_5\right)\left(z_1-z_6\right)}\right\}\exp\left(z_1t\right)\\&+\left\{\frac{\left(z_2^{\,5}+b_4z_2^{\,4}+b_3z_2^{\,3}+b_2z_2^{\,2}+b_1z_2+b_0\right)\left(z_2+\mu\right)}{z_2\left(z_2-z_1\right)\left(z_2-z_3\right)\left(z_2-z_4\right)\left(z_2-z_5\right)\left(z_2-z_6\right)}\right\}\exp\left(z_2t\right)\\&+\left\{\frac{\left(z_3^{\,5}+b_4z_3^{\,4}+b_3z_3^{\,3}+b_2z_3^{\,2}+b_1z_3+b_0\right)\left(z_3+\mu\right)}{z_3\left(z_3-z_1\right)\left(z_3-z_2\right)\left(z_3-z_4\right)\left(z_3-z_5\right)\left(z_3-z_6\right)}\right\}\exp\left(z_3t\right)\\&+\left\{\frac{\left(z_4^{\,5}+b_4z_4^{\,4}+b_3z_4^{\,3}+b_2z_4^{\,2}+b_1z_4+b_0\right)\left(z_4+\mu\right)}{z_4\left(z_4-z_1\right)\left(z_4-z_2\right)\left(z_4-z_3\right)\left(z_4-z_5\right)\left(z_4-z_6\right)}\right\}\exp\left(z_4t\right)\\&+\left\{\frac{\left(z_5^{\,5}+b_4z_5^{\,4}+b_3z_5^{\,3}+b_2z_5^{\,2}+b_1z_5+b_0\right)\left(z_5+\mu\right)}{z_5\left(z_5-z_1\right)\left(z_5-z_2\right)\left(z_5-z_3\right)\left(z_5-z_4\right)\left(z_5-z_6\right)}\right\}\exp\left(z_5t\right)\\&+\left\{\frac{\left(z_6^{\,5}+b_4z_6^{\,4}+b_3z_6^{\,3}+b_2z_6^{\,2}+b_1z_6+b_0\right)\left(z_6+\mu\right)}{z_6\left(z_6-z_1\right)\left(z_6-z_2\right)\left(z_6-z_3\right)\left(z_6-z_4\right)\left(z_6-z_5\right)}\right\}\exp\left(z_6t\right)\end{aligned} \tag{69}$$

z_1 and z_2 are roots of the equation $\left(s^2+s\left(\lambda+\alpha+\mu\right)+\alpha\mu\right)=0$ and z_3, z_4, z_5 and z_6 are roots of the equation $\left(s^4+a_3s^3+a_2s^2+a_1s+a_0\right)=0.$

9. Profit analysis of the User

Suppose that the warranty period of the system is (0, w). Since the repairman is always available with the system, therefore beyond warranty period, it remains busy during the interval (w, t). Let K_1 be the revenue per unit time and K_2 be the repair cost per unit time, then the expected profits $H_1(t)$ and $H_2(t)$ for model-1 and 2 during the interval (0, t) are given by

For model-1

Using equation (63), we get the expected profit $H_1(t)$ as:

$$H_1(t) = K_1 \int_0^t p_{up}(t)dt - K_2\left(t-w\right)$$

$$H_1(t) = K_1 \left\{ \begin{array}{l} \dfrac{c_0 \mu t}{z_1 z_2 z_3 z_4} - \left\{ \dfrac{\left(z_1^3 + c_2 z_1^2 + c_1 z_1 + c_0\right)\left(z_1+\mu\right)}{z_1^2\left(z_1-z_2\right)\left(z_1-z_3\right)\left(z_1-z_4\right)} \right\}\left(1-e^{z_1 t}\right) \\ + \left\{ \dfrac{\left(z_2^3 + c_2 z_2^2 + c_1 z_2 + c_0\right)\left(z_2+\mu\right)}{z_2^2\left(z_1-z_2\right)\left(z_2-z_3\right)\left(z_2-z_4\right)} \right\}\left(1-e^{z_2 t}\right) \\ - \left\{ \dfrac{\left(z_3^3 + c_2 z_3^2 + c_1 z_3 + c_0\right)\left(z_3+\mu\right)}{z_3^2\left(z_1-z_3\right)\left(z_2-z_3\right)\left(z_3-z_4\right)} \right\}\left(1-e^{z_3 t}\right) \\ + \left\{ \dfrac{\left(z_4^3 + c_2 z_4^2 + c_1 z_4 + c_0\right)\left(z_4+\mu\right)}{z_4^2\left(z_4-z_1\right)\left(z_4-z_2\right)\left(z_3-z_4\right)} \right\}\left(1-e^{z_4 t}\right) \end{array} \right\} - K_2(t-w) \tag{68}$$

For model-2

Using equation (69), we get the expected profit $H_2(t)$ as:

$$H_2(t) = K_1 \int_0^t p_{up}(t)dt - K_2\left(t-w\right)$$

$$H_2(t) = K_1 \left\{ \begin{array}{l} \dfrac{b_0 \mu t}{z_1 z_2 z_3 z_4 z_5 z_6} + \left\{ \dfrac{\left(z_1^5 + b_4 z_1^4 + b_3 z_1^3 + b_2 z_1^2 + b_1 z_1 + b_0\right)\left(z_1+\mu\right)}{z_1^2\left(z_1-z_2\right)\left(z_1-z_3\right)\left(z_1-z_4\right)\left(z_1-z_5\right)\left(z_1-z_6\right)} \right\}\left(e^{z_1 t}-1\right) \\ + \left\{ \dfrac{\left(z_2^5 + b_4 z_2^4 + b_3 z_2^3 + b_2 z_2^2 + b_1 z_2 + b_0\right)\left(z_2+\mu\right)}{z_2^2\left(z_2-z_1\right)\left(z_2-z_3\right)\left(z_2-z_4\right)\left(z_2-z_5\right)\left(z_2-z_6\right)} \right\}\left(e^{z_2 t}-1\right) \\ + \left\{ \dfrac{\left(z_3^5 + b_4 z_3^4 + b_3 z_3^3 + b_2 z_3^2 + b_1 z_3 + b_0\right)\left(z_3+\mu\right)}{z_3^2\left(z_3-z_1\right)\left(z_3-z_2\right)\left(z_3-z_4\right)\left(z_3-z_5\right)\left(z_3-z_6\right)} \right\}\left(e^{z_3 t}-1\right) \\ + \left\{ \dfrac{\left(z_4^5 + b_4 z_4^4 + b_3 z_4^3 + b_2 z_4^2 + b_1 z_4 + b_0\right)\left(z_4+\mu\right)}{z_4^2\left(z_4-z_1\right)\left(z_4-z_2\right)\left(z_4-z_3\right)\left(z_4-z_5\right)\left(z_4-z_6\right)} \right\}\left(e^{z_4 t}-1\right) \\ + \left\{ \dfrac{\left(z_5^5 + b_4 z_5^4 + b_3 z_5^3 + b_2 z_5^2 + b_1 z_5 + b_0\right)\left(z_5+\mu\right)}{z_5^2\left(z_5-z_1\right)\left(z_5-z_2\right)\left(z_5-z_3\right)\left(z_5-z_4\right)\left(z_5-z_6\right)} \right\}\left(e^{z_5 t}-1\right) \\ + \left\{ \dfrac{\left(z_6^5 + b_4 z_6^4 + b_3 z_6^3 + b_2 z_6^2 + b_1 z_6 + b_0\right)\left(z_6+\mu\right)}{z_6^2\left(z_6-z_1\right)\left(z_6-z_2\right)\left(z_6-z_3\right)\left(z_6-z_4\right)\left(z_6-z_5\right)} \right\}\left(e^{z_6 t}-1\right) \end{array} \right\} - K_2(t-w) \tag{69}$$

10. Numerical analysis

Table 1. Effect of failure rates (λ and λ_1), transition rate (λ_m) and transition rate of completion of warranty (α) on Reliability of the system (R (t))

Time (t)	λ_1 =0.02, α=0.003, λ_m =0.04	λ_1 =0.02, α=0.003, λ_m =0.04	λ =0.01, α=0.003, λ_m =0.04	λ =0.01, λ_1 =0.02, λ_m =0.04	λ =0.01, λ_1 =0.02, α=0.003
	R(t) (for λ =0.01)	R(t) (for λ =0.02)	R(t) (for λ_1 =0.03)	R(t) (for α=0.005)	R(t) (for λ_m =0.05)
10	0.899114	0.814457	0.898175	0.895363	0.898175
11	0.889088	0.797518	0.888004	0.884676	0.888004
12	0.8791	0.780872	0.877867	0.873994	0.877867
13	0.869154	0.764518	0.867771	0.863327	0.867771
14	0.859254	0.748454	0.857722	0.852681	0.857722
15	0.849405	0.732679	0.847724	0.842066	0.847724
16	0.83961	0.717189	0.837782	0.831487	0.837782
17	0.829873	0.701984	0.827901	0.820952	0.827901

Table 2. Effect of repair cost (K_2), PM rate (μ_2) and transition rate by which unit goes for PM (λ_m) on expected profit ($H_1(t)$)

Time (t)	λ=0.01, μ_1=0.1, λ_1=0.02, μ_2=0.3, α=0.003, μ=0.2, λ_m=0.04, K_1=500, W=3	λ=0.01, μ_1=0.1, λ_1=0.02, μ_2=0.3, α=0.003, μ=0.2, λ_m=0.04, K_1=500, W=3	λ=0.01, μ_1=0.1, λ_1=0.02, μ=0.2, α=0.003, W=3, λ_m=0.04, K_1=500, K_2=150	λ=0.01, μ_1=0.1, λ_1=0.02, μ_2=0.3, α=0.003, W=3, μ=0.2, K_1=500, K_2=150
	$H_1(t)$ (For K_2=150)	$H_1(t)$ (For K_2=100)	$H_1(t)$ (For μ_2=0.4)	$H_1(t)$ (For λ_m=0.03)
10	3807.814	4157.814	3808.29	3809.311
11	4135.365	4535.365	4136.008	4137.224
12	4462.205	4912.205	4463.044	4464.464
13	4788.424	5288.424	4789.488	4791.118
14	5114.094	5664.094	5115.411	5117.259
15	5439.274	6039.274	5440.873	5442.942
16	5764.01	6414.01	5765.921	5768.216
17	6088.342	6788.342	6090.592	6093.117

Table 3. Effect of repair cost (K_2), PM rate (μ_2), failure rate of degraded unit (λ_2), transition rate by which unit goes for PM (λ_m) and replacement rate of failed degraded unit (μ_3) on expected profit ($H_2(t)$)

Time (t)	λ=0.01, λ_1=0.02, λ_2=0.03, λ_m=0.04, α=0.003, μ=0.2, μ_1=0.1, μ_2=0.3, μ_3=0.4, W=3, K_1=500	λ=0.01, λ_1=0.02, λ_2=0.03, λ_m=0.04, α=0.003, μ=0.2, μ_1=0.1, μ_2=0.3, μ_3=0.4, W=3, K_1=500	λ=0.01, λ_1=0.02, λ_2=0.03, λ_m=0.04, α=0.003, μ=0.2, μ_1=0.1, μ_3=0.4, W=3, K_1=500, K_2=150	λ=0.01, λ_1=0.02, λ_m=0.04, α=0.003, μ=0.2, μ_1=0.1, μ_1=0.3, μ_3=0.4, W=3, K_1=500, K_2=150	λ=0.01, λ_1=0.02, λ_2=0.03, α=0.003, μ=0.2, μ_1=0.1, μ_2=0.3, μ_3=0.4, W=3, K_1=500, K_2=150	λ=0.01, λ_1=0.02, λ_2=0.03, λ_m=0.04, α=0.003, μ=0.2, μ_1=0.1, μ_2=0.3, W=3, K_1=500, K_2=150
	$H_2(t)$ (For K_2=150)	$H_2(t)$ (For K_2=100)	$H_2(t)$ (For μ_2=0.4)	$H_2(t)$ (For λ_2=0.02)	$H_2(t)$ (For λ_m=0.03)	$H_2(t)$ (For μ_3=0.5)
10	3804.924	4154.924	3805.578	3805.106	3806.008	3804.95
11	4132.078	4532.078	4132.946	4132.232	4133.431	4132.119
12	4458.548	4908.548	4459.667	4458.66	4460.201	4458.61
13	4784.439	5284.439	4785.845	4784.488	4786.421	4784.527
14	5109.836	5659.836	5111.57	5109.851	5112.178	5109.957
15	5434.816	6034.816	5436.915	5434.971	5437.547	5434.976
16	5759.44	6409.44	5761.946	5759.456	5762.59	5759.647
17	6083.764	6783.764	6086.717	6083.809	6087.363	6084.026

Table 4. Expected profit difference ($H_1(t)$-$H_2(t)$)

Time (t)	λ=0.01, λ_1=0.02, λ_2=0.03, λ_m=0.04, α=0.003, μ=0.2, μ_1=0.1, μ_2=0.3, μ_3=0.4		
	K_1	W	$H_1(t)$-$H_2(t)$
10	500	3	2.890131
11	500	3	3.287116
12	500	3	3.657437
13	500	3	3.985432
14	500	3	4.258423
15	500	3	4.457927
16	500	3	4.570277
17	500	3	4.577749

11. Interpretation and conclusion

Table 1 shows that reliability for both the models is same. It is found that reliability of the system decreases with the increase of failure rates (λ and λ_1), transition rate by which unit goes for PM (λ_m) and transition rate of completion of warranty (α) with respect to time and for fixed values of other parameters. Tables 2 and 3 highlight the behaviour of expected profit for model-1 and 2. From table 2, it is observed that expected profit $H_1(t)$ increases with the decrease of repair cost (K_2) and transition rate by which unit goes for PM (λ_m) while with the increase of PM rate (μ_2) with respect to time. From Table 3, it is analyzed that expected profit $H_2(t)$ increases with the increase of PM rate (μ_2) and replacement rate of failed degraded unit (μ_3) while with the decrease of failure rate (λ_2), transition rate by which unit goes for PM (λ_m) and repair cost (K_2) with respect to time. Table 4 shows the expected profit difference ($H_1(t)$-$H_2(t)>0$) which goes on increasing with respect to time. This implies that model-1 is profitable over model-2.

Hence study reveals that after getting PM beyond warranty, a system in which unit works with reduced capacity after its repair will not be economically beneficial to use.

References

1. Cox D R. The analysis of non- Markovian stochastic process by the inclusion of supplementary variables. Proc. Camb. Phil. Soc. 1955; 51: 433-441, http://dx.doi.org/10.1017/S0305004100030437.
2. Kadyan M S. Reliability and profit analysis of a single-unt system with preventive maintenance subject to maximum operation time. Eksploatacja i Niezawodnosc - Maintenance and Reliability 2013;15(2):176-181.
3. Kadyan M S, Promila, Kumar J. Reliability modeling of a single-unit system with arbitrary distribution subject to different weather condition. Int. J. Syst. Assur. Eng. Manag. 2014; 5(3):313-319, http://dx.doi.org/10.1007/s13198-013-0168-3.
4. Kumar J, Kadyan M S, Malik S C. Profit analysis of a 2-out-of-2 redundant system with single standby and degradation of the units after repair. Int. J. Syst. Assur. Eng. Manag. 2013; 4(4): 424-434, http://dx.doi.org/10.1007/s13198-012-0127-4.
5. Kumar J, Kadyan M S, Malik S C. Cost analysis of a two-unit cold standby system subject to degradation, inspection and priority. Eksploatacja i Niezawodnosc – Maintenance and Reliability 2012; 14 (4): 278–283.
6. Nianfu Yang, Dhillon B S. Stochastic analysis of a general standby system with constant human error and arbitrary system repair rates. Microelectron Reliab. 1995; 35(7): 1037-1045, http://dx.doi.org/10.1016/0026-2714(95)90862-K.
7. Nailwal B, Singh S B. Reliability and sensitivity analysis of a operating system with inspection in different weather conditions. Int. J. Reliab. Qual. Safe. Eng. 2012; 19(2):1-36, http://dx.doi.org/10.1142/S021853931250009X.
8. Ocon R P, Castro J E R, Two models for a repairable two-system with phase-type sojourn time distributions. Reliab. Eng. Syst. Safe. 2004; 84: 253-260, http://dx.doi.org/10.1016/j.ress.2003.11.006.
9. Scarf Philip A, Cavalcante Cristiano A V. Modeling quality in replacement and inspection maintenance. Int. J. Prod. Eco. 2012; 135(1): 372-381, http://dx.doi.org/10.1016/j.ijpe.2011.08.011.
10. Singh V V, Singh S B, Ram M, Goel C K. Availability, MTTF and cost analysis of a system having two units in series configuration with controller. Int. J. Syst. Assur. Eng. Manag. 2013; 4(4): 341-352, http://dx.doi.org/10.1007/s13198-012-0102-0.
11. Yuan Li, Meng Xian-Yun. Reliability analysis of a warm standby repairable system with priority in use. Appl. Math. Model. 2011; 35: 4295-4303, http://dx.doi.org/10.1016/j.apm.2011.03.002.

Ram NIWAS
MS KADYAN
Jitender KUMAR

Department of Statistics & O.R.
Kurukshetra University
Kurukshetra, India

E-mail: burastat0001@gmail.com, mskadian@kuk.ac.in, khatkarjitu@gmail.com

Article citation info:
LONKWIC P, RÓŻYŁO P, DĘBSKI H. Numerical and experimental analysis of the progressive gear body with the use of finite-element method. Eksploatacja i Niezawodnosc – Maintenance and Reliability 2015; 17 (4): 544–550, http://dx.doi.org/10.17531/ein.2015.4.9.

Paweł LONKWIC
Patryk RÓŻYŁO
Hubert DĘBSKI

NUMERICAL AND EXPERIMENTAL ANALYSIS OF THE PROGRESSIVE GEAR BODY WITH THE USE OF FINITE-ELEMENT METHOD

BADANIA NUMERYCZNE I DOŚWIADCZALNE KONSTRUKCJI CHWYTACZA PROGRESYWNEGO Z WYKORZYSTANIEM METODY ELEMENTÓW SKOŃCZONYCH*

The article presents the results of experimental and numerical simulations of the braking process of new type CHP 2000 progressive gear roller. The gear which is a main element of the friction drive lift safety during braking is exposed to overloading connected with changeable weight loading the gear. Reliable operation of the braking system of the lift, especially in emergency situations, is the basis for the safe operation of these devices. Presented in this paper progressive gear design solution was subjected to tests on test stand and simulations numerical aimed at confirming the required strength and proper functionality of structures subjected to operational loads. Numerical analysis simulation was gear roller displacement during braking from the neutral position to the maximum displacement and the impact load on the alternating stress levels in the gripper elements. The results of numerical calculations verified by experimental studies, analyzing braking distance. The instrument used was a commercial numerical package for calculations using the finite element method – a program Abaqus®.

Keywords: *friction drive lift, progressive gears, safety, numerical simulation, FEM.*

W artykule zaprezentowano wyniki badań eksperymentalnych oraz symulacji numerycznych procesu hamowania rolki chwytacza progresywnego nowego typu CHP 2000. Chwytacz będący głównym elementem bezpieczeństwa dźwigu ciernego podczas hamowania narażony jest na przeciążenia związane ze zmienną masą obciążającą układ hamowania. Niezawodna praca układu hamowania dźwigu, zwłaszcza w sytuacjach awaryjnych, stanowi podstawę bezpiecznej eksploatacji tych urządzeń. Zaprezentowane w artykule rozwiązanie konstrukcyjne chwytacza progresywnego poddane zostało próbom stanowiskowym oraz symulacjom numerycznym, mającym na celu potwierdzenie wymaganej wytrzymałości oraz właściwej funkcjonalności konstrukcji poddanej obciążeniom eksploatacyjnym. Analizie numerycznej poddano symulację przemieszczenia rolki chwytacza w trakcie hamowaniaz pozycji neutralnej do pozycji maksymalnego przemieszczenia oraz wpływ zmiennego obciążenia na poziom naprężeń w elementach chwytacza. Wyniki obliczeń numerycznych weryfikowano badaniami eksperymentalnymi, poddając analizie długość drogi hamowania. Zastosowanym narzędziem numerycznym był komercyjny pakiet do obliczeń z wykorzystaniem metody elementów skończonych – program Abaqus®.

Słowa kluczowe: *dźwig cierny, chwytacze progresywne, bezpieczeństwo, symulacje numeryczne, metoda elementów skończonych.*

1. Introduction

Passenger and freight lifts are commonly used devices for vertical transport both in public buildings and residential buildings. The universality of this type of construction dictates sanctioned meet the stringent requirements of the building regulations of safety, imposing a strict manner of operation. The basic components of these devices include braking systems, to ensure proper functionality, and above all, the safety of the structure. Despite the high demands placed on these types of devices the current state of the literature on the issues of the construction and operation of the braking and progressive safety gear is not exhaustive. Issues presented in the literature relate to two main lines of research - issues and issues of dynamic load-bearing components of strength. Lifting dynamics issues dealt with, among others, Taplak [16] and Filas and Mudro [6]. In [16], the authors present the issues associated with the use of neural networks to analyze the vibration of the lift, as a result of variable mass of the traffic load. Used neural networks have been used by the authors to assess symptoms of vibration, which show that the failure of the lift or the entire device. The authors of reference [6] described the use of methods reduce the problem of the evaluation of the dynamics of the crane. In their analysis of the lift cab model reduced to a flat system with one vertical degree of freedom. The presented methodology for reducing the authors used to describe a specific mechanism cargo lift, defining the problem mathematically. In addition made an assessment of the lift operating parameters and their effect on the characteristics of the acceleration of the entire system. Issues related to the dynamics of the braking system of the lift, the analysis of the materials and construction of the progressive gears are further discussed in publications [9, 10, 11, 12, 13]. The authors of these studies focused mainly their attention on the analysis of the brake system, compare the construction and operation of the progressive gears European producers to the newly developed solution.

(*) Tekst artykułu w polskiej wersji językowej dostępny w elektronicznym wydaniu kwartalnika na stronie ***www.ein.org.pl***

A different class of problems are lifts used in high-rise buildings, over 40 floors. An example of the analysis of these devices was mentioned in [19] in which the authors have examined issues related to the impact of weight lift car power cords and cables on the work of the crane. In such devices, a significant height requires a compensatory belt, which compensates for the weight of the ropes and wires power, causing relief other components of the lift. The authors describe in an exemplary manner belt compensatory behavior and its impact on the linear model of the lift. Also examine the impact of horizontal displacements countervailing belt natural frequency of the system.

In the process of design and operation of lifts are more widely used numerical tools using the finite element method (MES) [20]. This applies above all stress analysis and optimization of structural elements [5, 7] lifting equipment. Example of using the finite element method to simulate the stresses and displacements of the hook body immediately during braking is shown in [8], in which the results of numerical calculations successfully verified with experimental studies.

The results of the performance tests are presented in the publication [3], where the author presents own research on the application of the coating NiCrBSi-60 applied to the gripper jaws of the wedge and the impact is applied to the coating on the braking parameters with respect to the jaws made from steel C45. A new type of progressive gears, characterized by different performance characteristics with respect to existing solutions used in freight elevators are presented in the work [18]. The authors describe a mathematical model and the structure of your model together with an analysis of the results obtained experimentally. Patent new design solutions progressive roller gear developed for KONE published in [17], in which the original structure was presented progressive roller gear and the characteristics of its activities.

In publications [4, 14] authors describe the use of the finite element method to evaluate the stiffness and the strength of the cabin frame in different types of lifts, including the construction of a progressive gear. The finite element method in the described issues, we used to optimize the design of the support frame, for reduced beam sections of the frame structure, leading to a significant reduction in the weight of the device and determine the coefficients of safety. The results of calculations possible to identify the sensitive areas of the lift frame system on the occurrence of damage.

Presented the results of numerical analysis show a great possibility of using FEM for the design and optimization of structural elements of lifting equipment. In this context, the authors of this article have attempted to extend the issues related to the modeling and simulation of the braking process, based on the author's lift concept of progressive safety gear CHP 2000 presented results of numerical simulations were verified bench test results conducted on the physical model of the structure of the progressive gear.

2. Construction and operation of the braking system and progressive gear

The newly compiled construction of the progressive gears of CHP 2000 type was designed and intended for the lifts with nominal load capacity from 8000 to 20000 N, constituting app. 75% of manufactured devices. Estimated annual production of that type of gears with changeable braking configuration is approximately 2000 sets per year. The braking system consisting of a kinematic connection between CHP 2000 type gears has been presented in Figure 1.

The lift gear is located in the cabin frame under the lift cabin. The release lever *2* is mounted to the gear. The lever ends are connected with the speed limiter line. At the top part of the lift shaft there is the speed limiter which controls the lift operation and at its bottom part there is a weighting agent responsible for proper pull of the speed limiter line. The speed limiter initiates the braking process when the nominal speed of the lift cabin increases by 0.3 m/s. Once the nominal

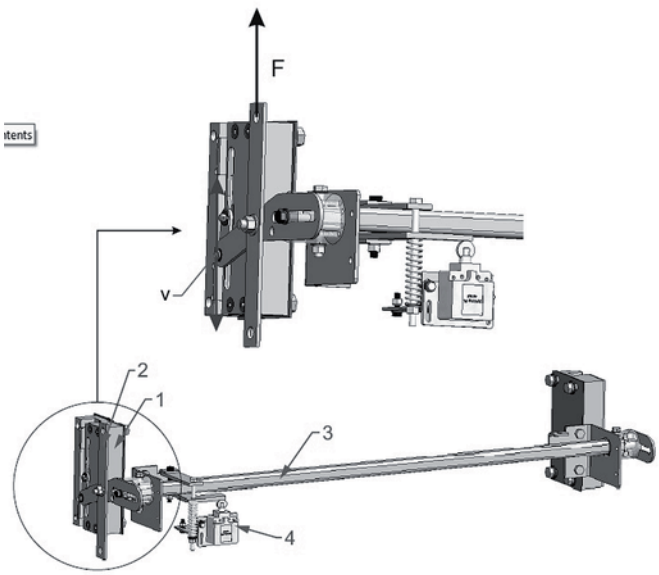

Fig. 1. Kinematic scheme of the friction drive lift braking system. 1 – a gear, 2 – a release lever, 3 – the gears coupler, 4 – controlling and compensating system

speed is exceeded, the speed limiter is blocked, at that time the line via properly selected friction coefficient is blocked as well. During the lift cabin movement with blocked subassys, the lever is dislocated in the direction opposite to the direction of a moving cabin as a result of which the gear braking roller is lifted. The roller is pushed to the guide causing its elastic deformation in the direction of the base plate which is on the other side of the set of Belleville springs as a result of which the energy loss of speeding mass is obtained. Thus, the set of Belleville springs is responsible for creating changeable force which pushes the roller to the guide, dependent on the mass which is transported in the cabin once the braking process is initiated.

CHP 2000 type gear presented in Figure 2 consists of the body *1*, where the cam *5* was located, along the cam the braking roller *2* with knurled surface moves. Between the cam and the body there are the packets of Belleville springs *4* with changeable configuration dependent on the nominal loading capacity of the lifting device. During the operation the gear moves along the lift guide which is located in the gear body between the braking roller and the base plates *3* placed in the opposite sides of the Belleville springs packets.

The changeable setting of the gear is connected with changeable mass which is inside the lift cabin. With respect to the above, the nom-

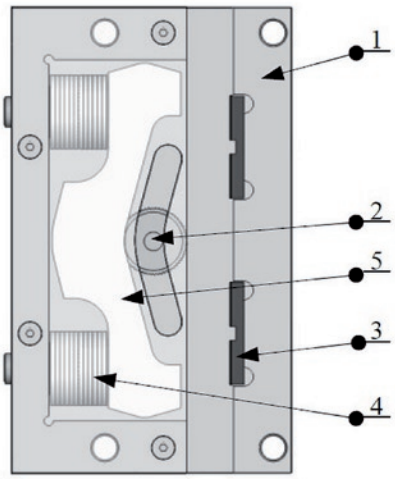

Fig. 2. Diagram of CHP2000 type progressive gears: 1 – a body, 2 – a braking roller, 3 – a braking plate, 4 – Belleville springs, 5 – a cam [11]

inal load is the sum of the weight of progressive gear cab, the cab frame, the cabin door and the nominal load capacity [11].

The design of the progressive safety gear is designed to provide effective braking lifting device. This results in a substantial burden of its individual elements, which depends on the strength of the safety passenger lift. The research will be to examine the strength of the entire team catcher permissible load that may occur during emergency braking.

3. The gear discrete model

Numerical analysis of the hook during emergency braking process was carried out in the case of the maximum static load acting on the elements of the structure. The scope of research included analysis of the steady-state mechanism, so the description of the system is independent of the variable of time. The numerical model of interaction of contact type used in the ABAQUS® defined as Surface-to-Surface, which contact constituting defining the interaction between mating components of the system to normal and tangential direction with friction coefficient of 0.3.

The characteristics of the individual elements of the hook progressive summarized in Table 1. For all of the elements defined by the steel material model elasto-plastic properties of isotropic reinforcement.

Table 1. Elements material features [2]

	Material	Young's Modulus E [MPa]	Poisson's coefficient ν	Yield point Re [MPa]	Resistance limit Rm [MPa]
The braking roller and plates	18HGT steel	210000	0.3	850	1000
The guide	S235JRG2 steel	210000	0.3	235	520
The body, the cam, the remaining elements	C45 steel	210000	0.3	360	610

Boundary conditions attached to the system will enable the simulation of the progressive gear in the process of emergency braking. Model of progressive gear is fully fixed in places mounting screws by blocking in area the holes all degrees of freedom. The guide roller is received, and able to move along the Y axis, and further blocked roll rotatable about an axis Z and X – Figure. 3.

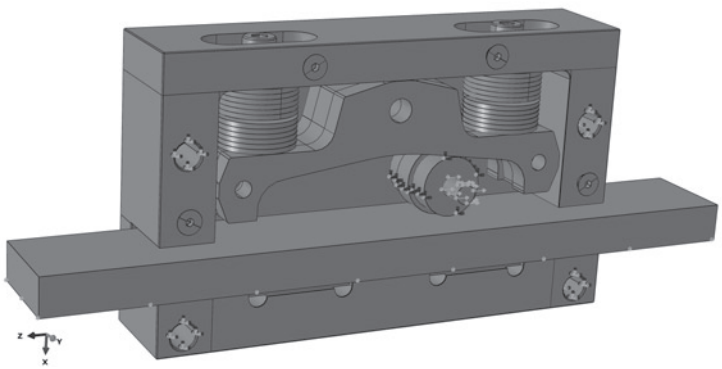

Fig. 3. Boundary conditions

The system works due to the displacement of the braking roller along the path which is determined by the cam and in the opposite direction to Z axis. The cam cooperates with the Belleville springs pressing the roller to the guide, and then respectively the guide is pressed to the base plates in the X axis direction. Elements that map

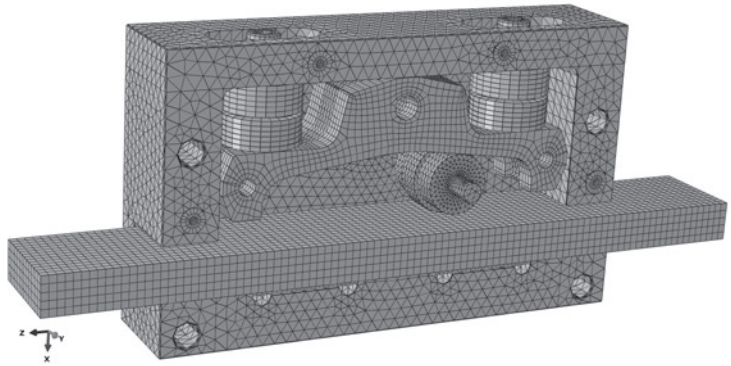

Fig. 4. Finite element mesh used

disc springs are shaped in such a way as to obtain the particular characteristics of elastic deformation by them during emergency braking process.

Discretization of individual elements of the hook was carried out using two types of volume elements: hexagonal - C3D8R and tetragonal type – C3D4 [1]. In both cases the element type has been used first order, and in the case of components used be reduced integrating of eight-node elements [20].

In the case of a four node elements in order to ensure adequate accuracy of the calculations, the high density of the mesh elements of tetragonal (progressive gear roll), as compared to the overall size of the mesh FEM model numerical.

FEM calculations carried out as a static calculation (Static procedure, General) taking into account non-linear problems. The load consisted of the constraint in the form of a displacement of the braking applied to the rollers of the 23.5 mm, acting in the opposite direction to return the Z axis. The total number of finite element numerical model was developed more than 131000.

4. Results of numerical analysis

FEA analysis results are presented on the basis of the gear roller dislocation simulation. In the article the attention is mainly focused on the determination of the stresses level H-M-H (Huber-Mises-Hencky) in the key points of the whole system as well as on the determination of the maximum stresses level and displacements of the guide nodes at the braking stage. The maximum level of stresses is demonstrated by the roller element where R_m resistance limit is reached. The level of stresses in the roller has the nature of nearly symmetrical layout versus its axis, whereas the maximum stress appears in the central part of the subassy which has been presented in Figure 5.

Achieving the level of the breaking of the roller elements R_m=1000 MPa due to the adopted too stringent working conditions of the numerical model of the progressive gear. In a real system roll movement in the analyzed period would be difficult to achieve, at the same time would cause the actual effort of the roller elements below the strength of the material. However, this is one of the critical elements of the progressive gear, who as a result of the emergency braking sustains permanent deformation. Reduced stress levels in the remaining elements of progressive safety gear (excluding items roll) is shown in Figure 6.

Stresses that occur in parts of the outside roller, do not show a level exceeding the limit strength of the material. In addition to the cam and the guide, none of the components does not reach the yield point. Cam suffered a small crossing yield strength (360 MPa) C45 steel. In fact, the force generated by a passenger lift, do not lead to a displacement of the roll to the end of the road, which determines the

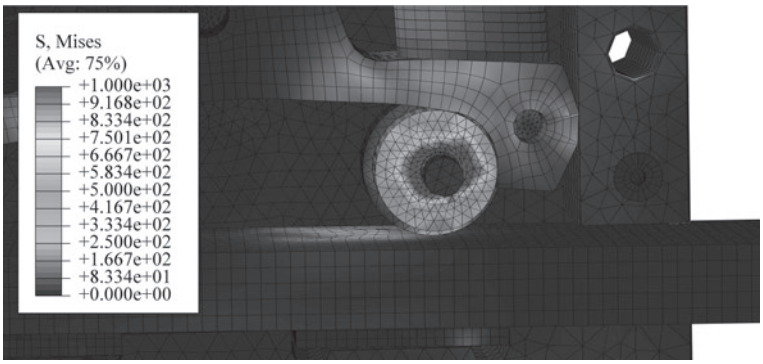

Fig. 5. Stress distribution occurring in the roll replacement [MPa]

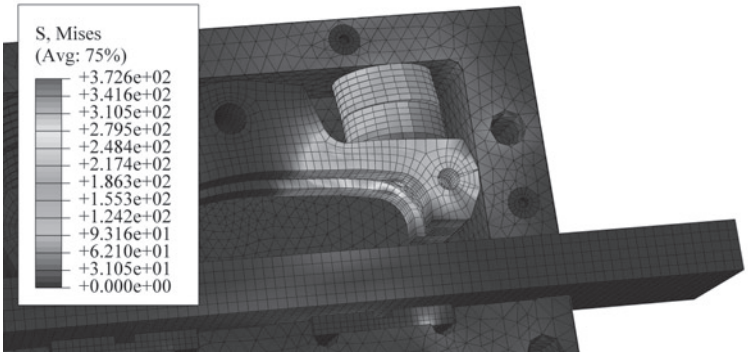

Fig. 6. Stress distribution in other parts of substitute ingredients [MPa]

a)

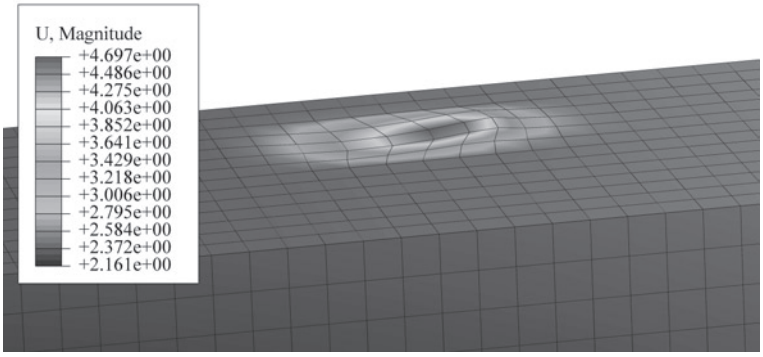

b)

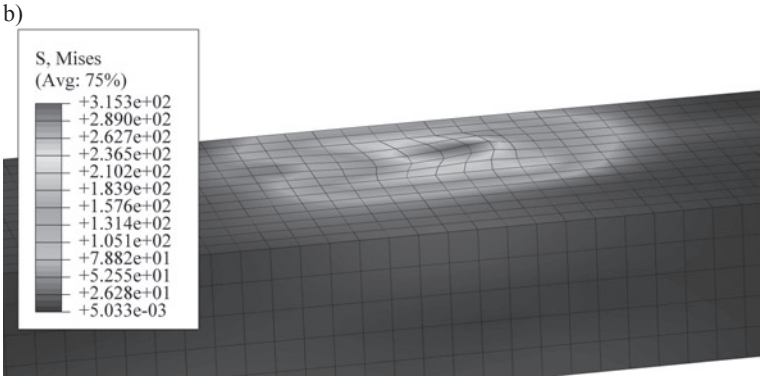

Fig. 7. The results of numerical studies of the guide: a) substitute the stress distribution [MPa], b) the distribution of displacements [mm]

cam. Cam stress level would therefore be much lower than presented in the results of numerical analysis. The most important component of the research was the hook guide. After the performed analysis, numerical and experimental presents the level of the plastic deformation of the guide piece of material, under pressure originating from the roll. FEM studies have shown that exceeded the guide material yield and there was a significant displacement of the nodes. The maximum value of stress at a critical location substitute track was 315.3 MPa, which means exceeding the yield stress of 80 MPa guide. Figure 7 shows the maximum displacement of the tension elements and nodes of the guide.

The maximum displacement nodes at the place pressing of the guide rollers moving was nearly 4.7 mm. The material is permanently laminated to the approximate length of approximately 18 mm, determined on the basis of an area including six nodal displacements of finite elements with an edge length of a single member to be (in the track) of 3 mm.

5. Experimental studies

Experimental studies were carried out on a specially designed position for enabling the free fall test method with variable load traps - Figure 8.

In the design of the test bench guides are placed, after which she moved aggravating frame of progressive gear, coupled with the supervising system of free fall speed. The main task of this system was to initiate the process of braking at speeds above par on the value of 0.3 m/s.

In order to protect against uncontrolled hit the ground test bench, the height at which the system had to be lifted was determined based on the relationship between potential and kinetic energy, determining the amount of free fall. Initiate free fall test system implemented by releasing the lock placed in the frame position. After crossing the speed of 1.25 m/s speed initiated watchdog triggering traps, starting with emergency braking process. After stopping the system under study was performed measurements of braking distances, which was the main parameter of construction associated with the correct evaluation of the work progressive gears.

We also evaluated the technical condition of the structural elements of progressive gears, as among state of the braking rollers and the state of the plastic deformation of the guide, which has been deformed by the roller as a result of braking.

The study confirmed the required bench strength and proper operation of the safety gear developed progressive structure, which is the main element lift safety during emergency braking.

Experimentally determined characteristics of the work progressive gear CHP 2000, defining the relationship of braking distances as a function of load compared with the analogous characteristics of the existing solutions - Figure 9. The present work progressive gear CHP 2000 reaches the lowest value of braking distances in different load cases, compared to previously commonly used in such devices. The resulting performance characteristics translate into significantly to local plastification of the guide, reducing the length of the plastic deformation region. A significant reduction in emergency braking if used design solution improves the safety of use of lifts, which is the main idea of this device design.

The actual level of the plastic deformation of the guide obtained from experimental studies performed on a physical model of the structure is almost progressive gear representation of numerical simulation. The result of the experimental study are shown in Figure 10.

The resulting high that the results of numerical calculations with measurements carried out stand length of the plastic deformation area guide - the difference does not exceed 10 %, providing the basis to confirm the adequacy of the developed numerical model, both in qualitative and quantitative terms. Development

Fig. 8. The test stand: a) general view of the stand for experimental test, b) the progressive gear with the loading system in the neutral position, c) the progressive gear with the loading system at a given load

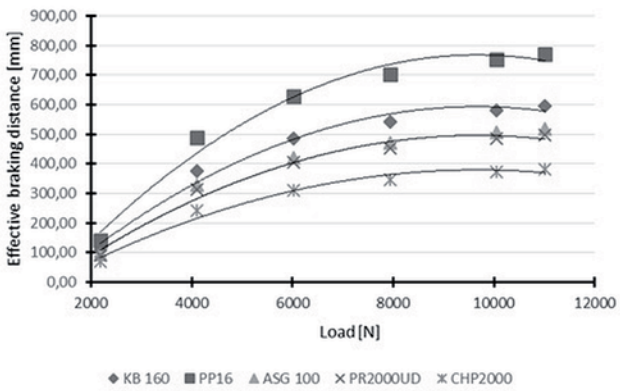

Fig. 9. Performance characteristics of selected types of traps

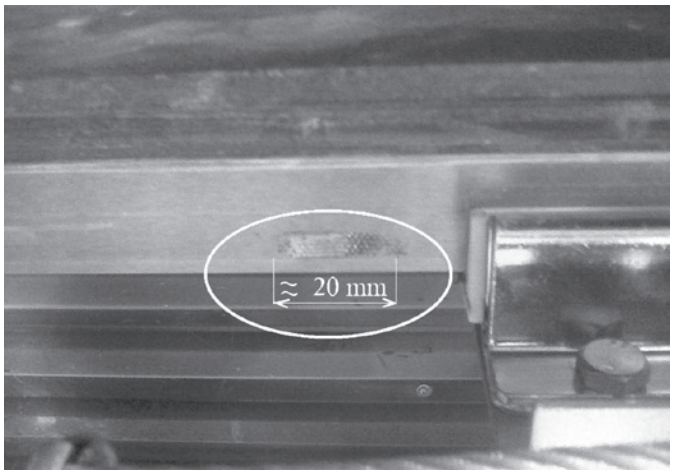

Fig. 10. Area guide plastification observed in the experiment

of experimentally verified numerical models allows while conducting a thorough analysis of the effort and strain individual components of the test device, providing a range of relevant information about the importance of structural and operational. The numerical simulation performed in this case allows an assessment of the gripper elements progressive effort, while the sample bench confirm proper functional-

ity and reliability of structures in braking, as well as exhibit improved structural efficiency of the proposed solution compared to the other devices of this type (Figure 9).

6. Conclusions

The paper presents an original concept of progressive safety gear, which is the primary mechanism for the inhibition of passenger and freight elevators for general use. The developed concept is characterized by a difference of a constructional solution as compared to existing devices of this type. Results of this study confirmed the sufficient strength and reliability of the emergency braking system developed.

Numerical analysis has been carried out strength structural components progressive gear using the finite element method. The performed numerical calculations allowed the evaluation of the degree of effort and strain on the hook mechanism to simulate the load case of emergency braking. The calculation results confirmed the correctness of the designed system, while exhibiting critical elements of the test structure. Proved to be a critical component of the braking roller, which received a reduced stress level close to the breaking point of the material. This means that in the event of emergency braking element is the most vulnerable part of the structure, limiting its strength. The level of effort of the other structural elements of the progressive gear does not endanger the operation of the mechanism.

Performed numerical analysis showed quantitative and qualitative consistency of results with the results of experimental studies conducted on the physical model of the structure. The plastic deformation zone were verified guide progressive gear after emergency braking simulation. Plasticizing FEM simulated testing, resulting in breaking subassembly reflects the nature of the deformation occurring in the way of actual experiment. This is confirmed by the results of experimental studies, in which the guide element area of the plastic deformation of the material obtained due to contact with the surface of the guide roll to a large extent similar to the deformation of the numerical model. The resulting high compatibility with the results of numerical simulations of the experiment indicates a high simulation capabilities similar issues, supporting the important field of research and design processes.

The study of experimental and numerical include important issues concerning the operation of passenger and freight elevators. The devices of this type have a strict conditions laid down building regulations concerning safety requirements to be met by a device that can be put into service. These requirements relate primarily to ensure safety in critical situations to which include lift emergency braking case. As previously mentioned, the crucial element is progressive gear braking system, which directly implement elements of the braking process. The efficiency of this process is primarily determined braking distance, which for safety reasons should be as short as possible, taking into account the different value system load. Conducted research in this area focused on improving therefore the characteristics of these devices, consisting of a crane shorter braking distances. The results presented in the article studies confirm the effectiveness of the proposed solution progressive gear CHP 2000, which also meets the requirements of BS EN 81-1 A3: 2010 [15].

Acknowledgement: *Special thanks and appreciation to NOVA TRADING company from Toruń and Rywal company from Lublin for the financial support owing to which it was possible to perform the research study and tests presented in the compilation.*

References

1. Abaqus HTML Documentation.
2. Banaszek J. Przykłady obliczeń z podstaw konstrukcji maszyn cz. II. Wydawnictwo Uczelniane, 1996; 196-197.
3. Bolin Y. A Surface Composite Coating Elevator Safety Gear Wedge. Advanced Materials Research 2014; 838-841 and 148-151.
4. Feng L. High Speed Elevator Car Frame's Finite Elements Analysis. Advanced Materials Research 2012; 298-303.
5. Ferdynus M. An energy absorber in the form of a thin-walled column with square cross-section and dimples, Eksploatacja i Niezawodnosc – Maintenance and Reliability2013; 15(3): 253-258.
6. Filas J., Mudro M. The dynamic equation of motion of driving mechanism of a freight elevator. Procedia Engineering 2012; 48: 149-152, http://dx.doi.org/10.1016/j.proeng.2012.09.498.
7. Gutkowski W., Latalski J. Structural optimization with member dimensional imperfections. Structural and Multidisciplinary Optimization2005; 30: 1-10, http://dx.doi.org/10.1007/s00158-004-0383-2.
8. Kayaoglu E. Study on Stress and Deformation of an Elevator Safety-Gear Brake Block Using Experimental and FEA Methods. Advanced Materials Research 2011; 308-310 and 1513-1518.
9. Lonkwic P. Analysis of the system dynamics intended to tighten the speed limiter line in the passenger lifts - XIth Scientific & Technical Conference LOGITRANS. Poland, 2014.
10. Lonkwic P. Testing methodology of main progressive gears - XIth Scientific & Technical Conference LOGITRANS. Poland, 2014.
11. Lonkwic P. Using disk spring solver application for prototyping disk spring in passenger lift catchers. Applied Computer Science 2014; 10: 67-74.
12. Lonkwic P., Gardyński L. Testing polymer rollers memory in the context of passenger lift car comfort. Journal of Vibroegineering 2014; 1: 225-230.
13. Lonkwic P., Szydło K. Selected Parameters of the Work of Speed Limiter Line Straining System in a Frictional Lift. Advances in Science and Technology 2014; 8(21): 73-77.
14. Onur Y. A., Imrak C. E. Reliability analysis of elevator car frame using analytical and finite element methods. Building Services Engineering Research & Technology 2011; 33(3): 293-305, http://dx.doi.org/10.1177/0143624411413168.
15. Polish Standard PN-EN 81-1+A3:2010, Safety Regula¬tions Concerning the Structure and Installation of Lifts, Part I. Electric Lifts.
16. Taplak H. The Use of Neural Network Predictors for Analyzing the Elevator Vibrations. Mechanical Engineering 2014; 39: 1157-1170, http://dx.doi.org/10.1007/s13369-013-0632-z.
17. Triboullier F., Levrard J. Elevator safety gear: European Patent EP 1460020 [P], 2008; 10-15.
18. Zhang Z., Tan M., Tian H., Duan K. Research on a New Type of Elevator Safety Catch. Applied Mechanics and Materials 2012; 178-181 and 2837-2840.

19. Zhu W. D.,Ren H.A linear model of stationary elevator traveling and compensation cables. Journal of Sound and Vibration 2013; 332: 3086-3097, http://dx.doi.org/10.1016/j.jsv.2013.01.009.
20. Zienkiewicz O.C., Taylor R.L. Finite Element Method (5th Edition) Volume 2 – Solid Mechanics. Elsevier, 2000.

Paweł LONKWIC
LWDO Lift Service S.A.
ul. Roztocze 6, 20-722 Lublin, Poland

Patryk RÓŻYŁO
Hubert DĘBSKI
Department of Mechanical Engineering
Lublin University of Technology
ul. Nadbystrzycka 36, 20-618 Lublin, Poland

E-mail: plonkwic@gmail.com,
p.rozylo@pollub.pl, h.debski@pollub.pl

Article citation info:
LI X, JIA Y, WANG P, ZHAO J. Renewable warranty policy for multiple-failure-mode product considering different maintenance options. Eksploatacja i Niezawodnosc – Maintenance and Reliability 2015; 17 (4): 551–560, http://dx.doi.org/10.17531/ein.2015.4.10.

Xinyue LI
Yunxian JIA
Peng WANG
Jianmin ZHAO

RENEWABLE WARRANTY POLICY FOR MULTIPLE-FAILURE-MODE PRODUCT CONSIDERING DIFFERENT MAINTENANCE OPTIONS

POLITYKA ODNAWIANIA GWARANCJI DLA PRODUKTÓWO MNOGICH PRZYCZYNACH USZKODZEŃ UWZGLĘDNIAJĄCA RÓŻNE OPCJE OBSŁUGI

Along with the advancement of manufacturing techniques, the quality of the spares for product is likely to be improved during the warranty period. There can be two types of spares, i.e. low-quality spares and high-quality spares for replacement maintenance. And the manufacturers (customers) may have to decide whether or not to provide (buy) the warranty considering upgrading maintenance. This paper presents a renewing warranty policy considering three maintenance options for products with multiple failure modes. The cost and availability models of these maintenance options are proposed. Of these options, upgrading maintenance is taken into account with the assumption that the warrantied item will be upgraded one time during the warranty cycle. After upgrading maintenance, the high-quality spares are used to replace the failed item. By minimizing the ratio between cost and availability of the product, the optimal upgrading opportunity is obtained. In the numerical example, the results of these options are presented. Monte Carlo simulation results are compared with the analytical results to demonstrate the correctness and efficiency of the proposed models considering upgrading maintenance. The renewing warranty policy considering upgrading maintenance policy is compared with the one without considering upgrading maintenance. The results show that the former is better than the latter in some cases. The sensitivity of the cost model and availability model to different parameters is analyzed at last.

Keywords: *multiple failure modes; renewing warranty; preventive maintenance; warranty cost; product availability; upgrading maintenance.*

Wraz z postępem techniki produkcji, wzrasta prawdopodobieństwo, że jakość części zamiennych do produktu ulegnie poprawie w przeciągu okresu gwarancyjnego. Istnieją dwa rodzaje części zamiennych: części zamienne niskiej i wysokiej jakości. Producenci (klienci) mogą być zmuszeni podjąć decyzję czy objąć produkt gwarancją (wykupić gwarancję) zapewniającą konserwację modernizacyjną. W artykule przedstawiono politykę odnawiania gwarancji z uwzględnieniem trzech różnych opcji obsługi produktów narażonych na mnogie przyczyny uszkodzeń. Zaproponowano modele kosztów i gotowości dla omawianych opcji obsługi. Spośród badanych opcji, do dalszej analizy wybrano konserwację modernizacyjną zakładającą, że element podlegający gwarancji zostanie poddany jednokrotnej modernizacji podczas cyklu gwarancyjnego. Po wykonaniu konserwacji modernizacyjnej, uszkodzony element zastępuje się częściami zamiennymi wysokiej jakości. Minimalizując stosunek kosztów do gotowości produktu, uzyskuje się optymalną możliwość modernizacji Przykład numeryczny przedstawia wyniki uzyskane dla omawianych opcji. Wyniki symulacji Monte Carlo porównano z wynikami analitycznymi w celu wykazania prawidłowości i efektywności proponowanych modeli uwzględniających konserwację modernizacyjną. Politykę odnawiania gwarancji uwzględniającą konserwację modernizacyjną porównano z polityką, która takiej konserwacji nie uwzględnia. Wyniki pokazują, że pierwsza z tych opcji jest w niektórych przypadkach korzystniejsza od drugiej. Badania wieńczy analiza czułości modelu kosztów i modelu gotowości na różne parametry.

Słowa kluczowe: *mnogie przyczyny uszkodzeń; odnowienie gwarancji; obsługa profilaktyczna; koszty gwarancji; gotowość produktu; konserwacja modernizacyjna.*

1. Introduction

Warranty is an obligation attached to products that requires manufacturers to provide compensation for customers when the products fail to perform their pre-specified functions during a specified period [20]. Since product warranty can be a powerful incentive in selling a product and a useful way to protect customer from product quality defects, it plays an increasingly important role in commercial transactions and has obtained increasing attention from the manufacturers as well as the customers recently. According to Murthy and Blischke [5], warranty polices can be divided into two classes, i.e. renewing warranty and non-renewing warranty. In a renewing warranty policy, whenever an item fails under warranty, it is replaced by a new item with a new-starting warranty. In contrast, in the case of a non-renewing policy, replacement of a failed item doesn't alter the original warranty [6]. The warranty period for renewing policies begins anew with each replacement, while the replacement item for non-renewing policies will be covered for the remaining time of the item it replaced. Nowadays, most product warranties are non-renewing. But for some high-reliability-required and high-safety-required products (like expensive aviation products), the maintenance in warranty period is considered to be perfect such that the failed product is replaced by a new one. Then the customers are more preferred to choose the renewing warranty policy. However, the period of renewing warranty normally gets longer compared to the non-renewing warranty. Then reducing the warranty servicing cost and improving the product performance

(like availability, mean time between failures, etc.) have become great challenges for both manufactures and customers.

From customer's perspective, product performance is a key factor when a customer is making a buying decision, although cost and availability are both taken into consideration. However, manufacturers are mainly concerned about the profitability and the warranty cost is a key factor to be considered. In order to get to a win-win situation, the warranty policy makers must take some trade-offs between the warranty cost and product performance. In reality, technology development may lead to product improvement, meaning that the spares for replacing failed product are upgraded from low-quality to high-quality. As a result, a question facing the manufacturers (customers) is: whether to provide (accept) upgrading replacement in the warranty or not? In this paper, we focus on the analysis of product cost and availability in the warranty period considering upgrading maintenance. The rest of this paper is organized as follows: Section 2 introduces the relevant work existing in the literature in regarding to product warranty policies. Section 3 outlines the model assumptions and notation, and then proposes three maintenance options including upgrading maintenance. Section 4 is dedicated to development of the mathematical models. A numerical example is given in Section 5 to illustrate our approach.

2. Literature review

Bai and Pham [2] presented discounted warranty cost model for repairable series systems assuming the impact of repair actions on components' failure time was minimal. Huang et al. [9] used a bivariate approach and taken into account periodic preventive maintenance to develop a two-dimensional warranty policy for the repairable product. Park and Pham [12] proposed warranty cost models on the quasi-renewal processes and exponential distribution assuming that a repair service was imperfect for several systems, including multi-component systems. They also [13] introduced two alternative quasi-renewal processes: altered quasi-renewal and mixed quasi-renewal processes to obtain the expected value of warranty cost, covariance of warranty cost and variance of warranty cost for the warranted product. Vahd [19] developed a renewing free replacement warranty policy for a multi-state deteriorating repairable product with N working states and N failure states. Two rectification actions should be done in case any failure has occurred: minimal repair with non-negligible needed time and replacement which was performed instantly. Banerjee and Bhattacharjee [4] analyzed the cost of a new two-dimensional warranty servicing strategy that probabilistically exercised a choice between a replacement and a minimal repair to rectify the first failure in the middle interval. Su and Shen [18] proposed two types of extended warranty policies from the manufacturer's perspective, namely one-dimensional extended warranty policy and two-dimensional non-renewing extended warranty policy. The corresponding warranty cost and profit models were presented to calculate the warranty cost considering minimal repair, imperfect repair combined with minimal repair and complete repair combined with minimal repair for failed component. Bai and Pham [3] presented full-service warranty for repairable multi-component systems under which the failed component(s) or subsystem(s) will be replaced. In addition, a (perfect) maintenance action will be performed to reduce the chance of future system failure, both free of charge to consumers. Chien [7] studied on the effects of a free-repair warranty on a periodic replacement policy with a discrete time process. Sana [16] studied on an imperfect production system with allowable shortages due to regular preventive maintenance for products sold with free minimal repair warranty. Aggrawal et al. [1] used a two dimensional innovation diffusion model to demonstrate product sales cycle, and presented a methodical approach to obtain optimal price and warranty length for a product. The model examined significance of these decision variables and estimates the overall maximum profit for the manufacturer. Exponential distribution has been used to represent the life time distribution of a product and the model has been validated using real life data set.

González-Prida et al. [8] selected the warranty period after the completion of a series of successive repairs on a product. Two stochastic failure models were used: a general renewal process (GRP) model and a non-homogeneous Poisson process (NHPP) model. Both used a Weibull distribution for the life time of the product, allowing the possibility of renewal (GRP) or not (NHPP) when successive repairs were performed. Park et al. [14] proposed a warranty cost model is proposed in consideration of both repair service and replacement service simultaneously upon the system failure to find the optimized warranty period in terms of an expected cost rate during the warranty cycle under the manufacturer's point of view. Xie et al. [21] presented an integrated model to estimate the gross profit for a new durable product to be sold in a fixed sales period at a fixed price. It was assumed that the sales over time can be characterized by a stochastic Bass model in the form of a nonhomogeneous Poisson process and the production system was a make-to-order type of system. Shafiee et al. [17] developed an optimization model to investigate the lengths of the optimal burn-in and warranty period, so that the mean of total product servicing cost was minimized. Jeon and Sohn [10] extracted association rules from warranty data of heavy duty diesel engine in order to find significant patterns of failures along with manufacturing information. They also used Weibull regression to identify influential factors that affect the variation in mean time between failures which were identified from extracted association rules. Liu et al. [11] developed a model based on renewing free-replacement warranty by considering failure interaction among components.

Obviously, lots of literatures focused on optimizing non-renewing policy. On the contrary, only a few researchers studied on renewing policy. However, renewing policy is desirable for both consumers and manufacturers since consumers receive better warranty service compared to the traditional non-renewing policy and manufacturers could attract more consumers to buy their products. In the literatures on renewing warranty policy, the optimization target is always warranty cost and the maintenance actions are only corrective maintenance. Although the warranty cost is a good measure on the overall cost of warranty, it provides little information of the product performance contained in a warranty program. Therefore, it is not sufficient enough to only use warranty cost model. The product availability can provide us a numerical measure of the product performance in the warranty period. These measures are useful for evaluating product performance. So throughout this paper, we consider both the expected cost and product availability for the renewing warranty policy together.

This paper considers three maintenance options including upgrading maintenance. The models proposed in this paper are different from the previous studies on complex system and single component models in the following perspectives:

(1) It is able to handle the multiple failure modes in calculating warranty cost and product availability. In reality, a product normally has several failure modes due to different failure reasons. So the resulting models can be more useful to the warranty policy-makers and customers to make appropriate decisions.

(2) The upgrading maintenance can be considered as a type of preventive maintenance (PM). PM action can sometimes improve the availability or decrease the warranty cost. By adjusting upgrading opportunity, the cost and availability can be optimized.

None of these situations have been considered so far, and thus this model offers warranty policy-maker and customers a useful tool to achieve a win-win situation in terms of minimal warranty cost and best product performance. We believe the models can help warranty policy makers to make optimal decisions with the objective of minimizing the ratio between warranty cost and product availability.

3. Modeling approach

This section develops a new modeling approach and provides some preliminary results. The item being considered in this paper has multiple failure modes as shown in Fig. 1. The failure modes are caused by different failure reasons, which can be chemical, physical or human errors, etc. By collecting failure data during the product life cycle, we can properly find the statistical characteristics of these failure modes. The notations of this paper are as follows:

W_1	warranty period for low-quality item
W_2	warranty period for high-quality item
k_a	failure mode number of low-quality item
k_b	failure mode number of high-quality item
$F_s(\cdot)$	cumulative distribution function of low-quality item
$G_s(\cdot)$	cumulative distribution function of high-quality item
$R_{ai}(\cdot)$	reliability function of the ith failure mode for the low-quality item
$F_{ai}(\cdot)$	cumulative distribution function of the ith failure mode for the low-quality item
$R_{bj}(\cdot)$	reliability function of the jth failure mode for the high-quality item
$F_{bj}(\cdot)$	cumulative distribution functionof the jth failure mode for the high-quality item
f_{ai}	failure density function for the ith failure mode for the low-qualityitem
f_{bj}	failure density function for the jth failure mode for the high-quality item
T	warranty cycle which is a time interval starting from the date of sale and ending at the warranty expiration date
T_0	preventive replacement time period
$\overline{T}_{bm}$	expected operational time between failures
$\overline{D}$	expected downtime
C_a	corrective maintenance cost of low-quality item
C_b	corrective maintenance cost of high-quality item
C_L	downtime loss of the item
T_m	replacement time for the low-quality item
C_p	preventive replacement cost for the low-quality item
T_p	preventive replacement time for the low-quality item
$\tilde{C}_p$	upgrading maintenance cost for the high-quality item
$\tilde{T}_p$	upgrading maintenance time for the high-quality item
T_r	replacement time for the high-quality item

The failure modes are assumed to be independent to each other, so we have:

$$F_s(t)=1-\prod_{i=1}^{k_a}R_{ai}(t)=1-\prod_{i=1}^{k_a}(1-F_{ai}(t)),\ G_s(t)=1-\prod_{j=1}^{k_b}R_{bj}(t)=1-\prod_{j=1}^{k_b}(1-F_{bj}(t)).$$

Due to the renewable nature of the warranty, the restored system will automatically carry a new-starting warranty. Different maintenance options will have influence on warranty cycle, so we consider the following maintenance options:

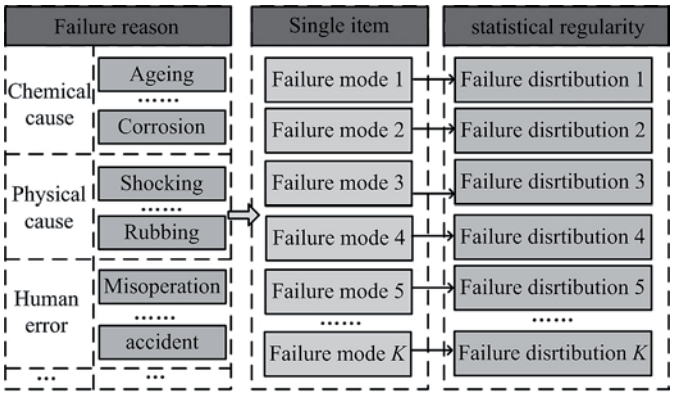

Fig. 1. An item with multiple failure modes

Option I: When an item has failed, it would be replaced by a new low-quality spare in the warranty cycle. Only the low-quality spares are used in the warranty cycle.

Option II: When an item has successfully worked until T_0, a new low-quality spare would be used to replace it. Only the low-quality spares are used in the warranty cycle. After replacement at T_0, the warranty period doesn't renew. And the warranty period renews after the replacement of a failed item.

Option III: When an item has successfully worked until T_0, a new high-quality spare would be used to replace it by upgrading maintenance. Before the upgrading maintenance, the low-quality spares are applied to replace a failed item. After upgrading maintenance, the high-quality spares are used to replace a failed item. After replacement at T_0, the warranty period doesn't renew. But the warranty period renews after the replacement of a failed item.

Option II and Option III can be considered as a type of preventive maintenance. High-quality items normally have higher reliability and lower maintenance cost than low-quality items. They can increase the system availability which will catch more interest from the customers. Under the above maintenance options, manufacturers are responsible for replacing the failed components. After a replacement, the item is in good working condition. Obviously T is a random variable. For Option I and Option II, the value of T depends on W_1. For Option III, the value of T depends on W_1 and W_2. Warranty cycles for different maintenance options are shown in Fig. 2.

For Option I, there is one stage in the warranty cycle. T can be expressed as:

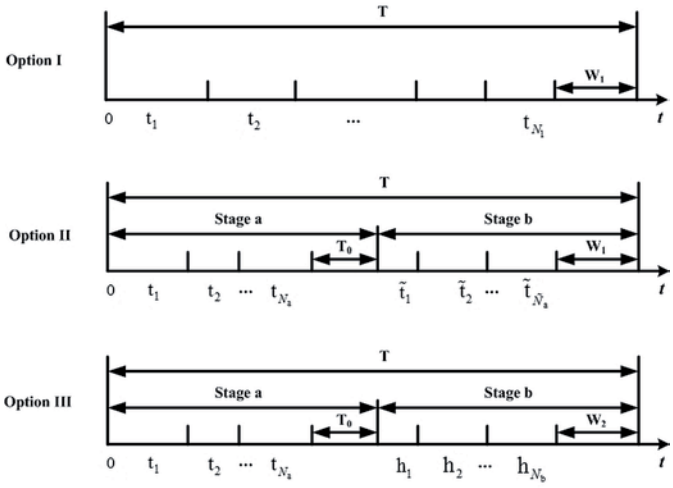

Fig. 2. System failure times for different maintenance options

$$T = t_1 + t_2 + ... + t_{N_1} + \mathrm{W}_1 , \quad (1)$$

where N_1 is the number of failures of the item and t_i (i=1,2,…, N_1) is the corresponding inter-arrival failure times. For Option II, there are two stages in the warranty cycle. T can be expressed as:

$$T = t_1 + t_2 + ... + t_{N_a} + \mathrm{T}_0 + \tilde{t}_1 + \tilde{t}_2 + ... + \tilde{t}_{\tilde{N}_a} + \mathrm{W}_1 , \quad (2)$$

where N_a is the number of failures of the item in stage a, $\tilde{N}_a$ is the number of failures of the item in stage b. t_i (i=1,2,…, N_a) is the corresponding i^{th} inter-arrival failure time in stage a and $\tilde{t}_i$ (i=1,2,…, $\tilde{N}_a$) is the corresponding i^{th} inter-arrival failure time in stage b.

For Option III, there are two stages in the warranty cycle. In stage a, the failed item is replaced by a low-quality item. In stage b, the failed item is replaced by a high-quality item.So T can be expressed as:

$$T = t_1 + t_2 + ... + t_{N_a} + \mathrm{T}_0 + h_1 + h_2 + ... + h_{N_b} + \mathrm{W}_2 , \quad (3)$$

where N_a is the number of failures of the system in stage a. N_b is the number of failures of the system in stage b. t_i (i=1,2,…, N_a) is the corresponding i^{th} inter-arrival failure time of stage a and h_i (i=1,2,…, N_b) is the corresponding i^{th}inter-arrival failure time of stage b.

All warranty claims are valid, all system failures under warranty are claimed, and any warranty service is instant. Take the steady availability of the system as one of the targets, as shown in Eq. 4.

$$\mathrm{A} = \frac{\overline{\mathrm{T}}_{\mathrm{bm}}}{\overline{\mathrm{T}}_{\mathrm{bm}} + \overline{\mathrm{D}}} . \quad (4)$$

The cost for option I can be calculated by Eq.5.

$$\mathrm{TC} = \sum_{i=1}^{k_a} (C_a + C_L T_m) N_{ai} . \quad (5)$$

where N_{ai} is the number of failures of the ith failure mode for the low-quality item within warranty cycle. The cost for option II can be calculated by Eq.6.

$$\mathrm{TC} = \sum_{i=1}^{k_a} (C_a + C_L T_m)(N_{ai} + \tilde{N}_{aj}) + C_{\mathrm{p}} + C_L T_p . \quad (6)$$

where N_{ai}($\tilde{N}_{aj}$) is the number of failures of the ith failure mode for the low-quality item within stage a (stage b). The cost for option III can be calculated by Eq.7.

$$\mathrm{TC} = \sum_{i=1}^{k_a} (C_a + C_L T_m) N_{ai} + \sum_{j=1}^{k_b} (C_b + C_L T_r) N_{bj} + \tilde{C}_{\mathrm{p}} + C_L \tilde{T}_p . \quad (7)$$

where N_{ai} (N_{bi}) is the number of failures of the ith (j^{th}) failure mode for the low-quality (high-quality) item within stage a (stage b). Because the corrective maintenance is replacement, the corrective maintenance cost includes the spare cost and maintenance cost.

4. Analytical model

For a single component, every failure mode will cause the component to fail. We start with the availability model for one component with several failure modes, and then we develop the cost model. Before proposing the models for different options, we give some definitions.

Lemma 1. *For a low-quality item, $p_{ai}(t)$ is the probability that failure mode i causes the component failure before the end of time limit t, so*

$$p_{ai}(t) = P(T_{ai} \le \min(T_{aj}, \forall j, j \in \Omega_1, j \ne i), T_{ai} \le t) = \int_0^t \frac{\lambda_{ai}(u)}{\lambda_{\mathrm{as}}(u)} f_{\mathrm{as}}(u)\mathrm{d}u, \Omega_1 = (1,2,...,k_a). \quad (8)$$

$\lambda_{ai}(u)$ is the failure rate of the ith failure mode and $f_{\mathrm{as}}(u)$ is the probability density function for the low-quality item. Because the failure modes are independent to each other, $\lambda_{\mathrm{as}}(t) = \sum_{i=1}^{k_a} \lambda_i(t)$, $R_{\mathrm{as}}(t) = 1 - F_{\mathrm{s}}(t) = \prod_{i=1}^{k_a} R_{ai}$ and $\lambda_{ai}(t) = \frac{f_{ai}(t)}{R_{ai}(t)}$.

Proof. From the definition of $p_{ai}(t)$, let $Y = \min(T_{aj}, \forall j, j \in \Omega_1, j \ne i)$ we can obtain:

$$p_{bj}(t) = \int_0^\infty P[T_{\mathrm{bj}} \le \min(T_{bj}, \forall j, j \in \Omega_2, j \ne i), T_{\mathrm{bj}} \le t | T_{\mathrm{bj}} = u]\mathrm{d}F_{\mathrm{bj}}(u)$$
$$= \int_0^t P[\min(T_{bj}, \forall j, j \in \Omega_2, j \ne i) \ge u]\mathrm{d}F_{\mathrm{bj}}(u) = \int_0^t \frac{\lambda_{\mathrm{bj}}(u)}{\lambda_{\mathrm{bs}}(u)} f_{\mathrm{bs}}(u)\mathrm{d}t .$$

Lemma 2. Let $p_{bj}(t)$ *be the probability that failure mode j of the high-quality product causes a component failure in t,* $\Omega_2 = (1,2,...,k_b)$ *then:*

$$p_{bj}(t) = \int_0^\infty P[T_{\mathrm{bj}} \le \min(T_{bj}, \forall j, j \in \Omega_2, j \ne i), T_{\mathrm{bj}} \le t | T_{\mathrm{bj}} = u] dF_{\mathrm{bj}}(u)$$
$$= \int_0^t P[\min(T_{bj}, \forall j, j \in \Omega_2, j \ne i) \ge u] dF_{\mathrm{bj}}(u) = \int_0^t \frac{\lambda_{\mathrm{bj}}(u)}{\lambda_{\mathrm{bs}}(u)} f_{\mathrm{bs}}(u) dt . \quad (9)$$

Proof. The proof process is similar to Lemma 1.

4.1. Availability and cost model for Option I

In order to derive the statistical properties of the product availability and cost for Option I, it is necessary to obtain the distribution of N_1. The following lemma gives the probability mass function (pmf) of N_1. Obviously, $N_1 = \sum_{i=1}^{k_a} N_{ai}$. Under the perfect maintenance assumption, the pmf of N_1 is:

$$P(N_1 = n_1) = [F_s(\mathrm{W}_1)]^{n_1} (1 - F_s(\mathrm{W}_1)) \ \forall n_1, n_1 = 0,1,2,... . \quad (10)$$

The proof process is similar to [3].We can formulate the product availability and expected warranty cost for Option I as:

$$A=\frac{\sum_{i=1}^{k_a}E(N_{ai})\int_0^{W_1}tf_{ai}(t)dt+W_1}{\sum_{i=1}^{k_a}E(N_{ai})(\int_0^{W_1}tf_{ai}(t)dt+T_m)+W_1},\ E(C)=(C_a+C_LT_m)\sum_{i=1}^{k_a}E(N_{ai}),\quad(11)$$

where $E(N_{ai})=\frac{p_{ai}(W_1)}{R_{as}(W_1)}$.

Proof. From Eq.11, obviously the product availability and warranty cost can be determined as long as the joint distribution of $N_{ai}(i=1,2,\ldots k_a)$ is known. From Lemma 1, we can obtain the probability that failure mode i causes an item failure before the end of warranty period W_1. Then when the item failed within W_1, the probability that it is caused by failure mode i is $\frac{p_{ai}(W_1)}{F_s(W_1)}$. So the conditional joint distribution of $N_{a1},N_{a2},\ldots,N_{ak_a}$ given $N_1=n_1$ is multinomial as shown by Equation 12:

$$P(N_{a1}=n_{a1},N_{a2}=n_{a2},\ldots,N_{ak_a}=n_{ak_a}\mid N_1=n_1)=\frac{n_1!}{n_{a1}!n_{a2}!\ldots n_{ak_a}!}\prod_{i=1}^{k_a}\left(\frac{p_{ai}(W_1)}{F_s(W)}\right)^{n_{ai}}.\quad(12)$$

According to the properties of multinomial distribution, we can get:

$$P(N_{ai}=n_{ai}\mid N_1=n_1)=\frac{n_1!}{n_{ai}!(n_1-n_{ai})!}\left(\frac{p_{ai}(W_1)}{F_s(W_1)}\right)^{n_{ai}}\left(1-\frac{p_{ai}(W_1)}{F_s(W_1)}\right)^{n_1-n_{ai}}.\quad(13)$$

So the moment generating function of N_{ai} is:

$$E(e^{tN_{ai}})=E[E[e^{tN_{ai}}\mid N_1]]=E[(1-\frac{p_{ai}(W_1)}{F_s(W_1)}+\frac{p_{ai}(W_1)}{F_s(W_1)}e^t)^{N_1}]=\frac{\frac{R_{as}(W_1)}{R_{as}(W_1)+p_{ai}(W_1)}}{1-\frac{p_{ai}(W_1)}{R_s(W_1)+p_{ai}(W_1)}e^t}.\quad(14)$$

Eq.14 shows that N_{ai} follows a geometric distribution:

$$P(N_{ai}=n_{ai})=\left(\frac{p_{ai}(W_1)}{R_{as}(W_1)+p_{ai}(W_1)}\right)^{n_{ai}}\left(1-\frac{p_{ai}(W_1)}{R_{as}(T_0)+p_{ai}(W_1)}\right).\quad(15)$$

So $E(N_{ai})=\frac{\frac{p_{ai}(W_1)}{R_{as}(W_1)+p_{ai}(W_1)}}{1-\frac{p_{ai}(W_1)}{R_{as}(W_1)+p_{ai}(W_1)}}=\frac{p_{ai}(W_1)}{R_{as}(W_1)}$.

4.2. Availability and cost model for Option II

In order to derive the statistical properties of the product availability and cost for Option II, it is necessary to obtain the distributions of N_{ai} and $\tilde{N}_{aj}$. The following lemma gives the probability mass functions (pmf) for Na and $\tilde{N}_a$. Obviously, $N_a=\sum_{i=1}^{k_a}N_{ai}$ and $\tilde{N}_a=\sum_{j=1}^{k_a}\tilde{N}_{aj}$.

For Stage a, under the perfect maintenance assumption, the pmf of N_a is:

$$P(N_a=n_a)=[F_s(T_0)]^{n_a}(1-F_s(T_0))\ \forall n_a,n_a=0,1,2,\ldots.\quad(16)$$

Proof. Let t_1, t_2, …,be the subsequent inter-arrival failure times within T of stage a which follow a distribution F_s. Obviously,

$$N_a=\min\{i:t_i>T_0\}-1.$$

Therefore:

$$P(N_a=n_a)=P(N_a\le n_a)-P(N_a\le n_a+1)=[F_s(T_0)]^{n_a}-[F_s(T_0)]^{n_a+1}.\quad(17)$$

Lemma 3. *For Stage b, under the perfect maintenance assumption, the pmf of $\tilde{N}_a$ for Option II can be expressed as:*

$$P(\tilde{N}_a=\tilde{n}_a)=\begin{cases}1-F_s(W_1\text{-}T_0) & \tilde{n}_a=0\\ F_s(W_1\text{-}T_0)[F_s(W_1)]^{\tilde{n}_a-1}(1-F_s(W_1)) & \tilde{n}_a=1,2,\ldots\end{cases}.\quad(18)$$

Proof. Let $\tilde{t}_1$, $\tilde{t}_2$,... be the subsequent inter-arrival failure times within T of stage b which follow a distribution F_s. Obviously,

$$\tilde{N}_a=\begin{cases}0 & ,\tilde{t}_i\ge W_1-T_0\\ \min\{i:\tilde{t}_i>W_1\}-1, & \tilde{t}_i<W_1-T_0\end{cases}.$$

When $\tilde{t}_1\ge W_1-T_0$, then $\tilde{n}_a=0$ and:

$$P(\tilde{N}_a=\tilde{n}_a)=1-F_s(W_1\text{-}T_0).$$

The PM is perfect, so when $\tilde{t}_1<W_1-T_0$, $\tilde{n}_a>0$ and:

$$P(\tilde{N}_a=\tilde{n}_a)=F_s(W_1\text{-}T_0)[F_s(W_1)]^{\tilde{n}_a-1}(1-F_s(W_1)).\quad(19)$$

Lemma 4. We can formulate the product availability and warranty cost for Option II as:

$$\mathrm{A}=\frac{\sum_{i=1}^{k_a}E(N_{ai})\int_0^{T_0}tf_{ai}(t)\mathrm{d}t+\mathrm{W}_1}{\sum_{i=1}^{k_a}E(N_{ai})(\int_0^{T_0}tf_{ai}(t)\mathrm{d}t+\mathrm{T_m})+\mathrm{T_p}+\mathrm{W}_1}(1-F_s(\mathrm{W}_1-\mathrm{T}_0))$$
$$+\frac{\sum_{i=1}^{k_a}E(N_{ai})\int_0^{T_0}tf_{ai}(t)\mathrm{d}t+\mathrm{T}_0+\sum_{i=1}^{k_a}(\frac{p_{ai}(\mathrm{W}_1\text{-}\mathrm{T}_0)}{F_s(\mathrm{W}_1\text{-}\mathrm{T}_0)}\int_0^{\mathrm{W}_1\text{-}\mathrm{T}_0}tf_{ai}(t)\mathrm{d}t)+\sum_{i=1}^{k_a}E(\tilde{N}'_{ai})\int_0^{\mathrm{W}_1}tf_{ai}(t)\mathrm{d}t+\mathrm{W}_1}{\sum_{i=1}^{k_a}E(N_{ai})(\int_0^{T_0}tf_{ai}(t)\mathrm{d}t+\mathrm{T_m})+\mathrm{T}_0+\mathrm{T_p}+(\sum_{i=1}^{k_a}\frac{p_{ai}(\mathrm{W}_1\text{-}\mathrm{T}_0)}{F_s(\mathrm{W}_1\text{-}\mathrm{T}_0)}\int_0^{\mathrm{W}_1\text{-}\mathrm{T}_0}tf_{ai}(t)\mathrm{d}t+\mathrm{T_m})+\sum_{i=1}^{k_a}E(\tilde{N}'_{ai})(\int_0^{\mathrm{W}_1}tf_{ai}(t)\mathrm{d}t+\mathrm{T_m})+\mathrm{W}_1}F_s(\mathrm{W}_1-\mathrm{T}_0), \quad (20)$$

$$\mathrm{E(C)}=(C_a+C_LT_m)\sum_{i=1}^{k_a}\mathrm{E}(N_{ai})+F_s(\mathrm{W}_1-\mathrm{T}_0)(C_a+C_LT_m)\sum_{i=1}^{k_a}\mathrm{E}(N'_{ai})+C_p+C_L\mathrm{T_p}, \quad (21)$$

where $E(N_{ai})=\frac{p_{ai}(\mathrm{T}_0)}{R_{as}(\mathrm{T}_0)}$ and $E(\tilde{N}'_{ai})=\frac{p_{ai}(\mathrm{W}_1)}{R_{as}(\mathrm{W}_1)}$.

Proof. Obviously, $E(N_{ai})=\frac{p_{ai}(\mathrm{T}_0)}{R_{as}(\mathrm{T}_0)}$, which can be easily proved. For stage b, there are two situations: $\tilde{N}_{ai}=0$ and $\tilde{N}_{ai}>0$. When $\tilde{N}_{ai}=0$, the availability is:

$$\mathrm{A}=\frac{\sum_{i=1}^{k_a}E(N_{ai})\int_0^{T_0}tf_{ai}(t)\mathrm{d}t+\mathrm{T}_0+\mathrm{W}_1-\mathrm{T}_0}{\sum_{i=1}^{k_a}E(N_{ai})(\int_0^{T_0}tf_{ai}(t)\mathrm{d}t+\mathrm{T_m})+\mathrm{T_p}+\mathrm{T}_0+\mathrm{W}_1-\mathrm{T}_0}=\frac{\sum_{i=1}^{k_a}E(N_{ai})\int_0^{T_0}tf_{ai}(t)\mathrm{d}t+\mathrm{W}_1}{\sum_{i=1}^{k_a}E(N_{ai})(\int_0^{T_0}tf_{ai}(t)\mathrm{d}t+\mathrm{T_m})+\mathrm{T_p}+\mathrm{W}_1}.$$

When $\tilde{N}_{ai}>0$, the probability that failure mode *i* causes the item to fail in $\mathrm{W}_1\text{-}\mathrm{T}_0$ is $p_{ai}(\mathrm{W}_1\text{-}\mathrm{T}_0)=\int_0^{\mathrm{W}_1\text{-}\mathrm{T}_0}\frac{\lambda_{ai}(t)}{\lambda_{as}(t)}f_{bs}(t)\mathrm{d}t$. So $\frac{p_{ai}(\mathrm{W}_1\text{-}\mathrm{T}_0)}{F_s(\mathrm{W}_1\text{-}\mathrm{T}_0)}$ is the conditional probability that failure mode *i* causes the item to fail given that the item has failed within $\mathrm{W}_1\text{-}\mathrm{T}_0$. Then the availability is:

$$\mathrm{A}=\frac{\sum_{i=1}^{k_a}E(N_{ai})\int_0^{T_0}tf_{ai}(t)\mathrm{d}t+\mathrm{T}_0+\sum_{i=1}^{k_a}(\frac{p_{ai}(\mathrm{W}_1\text{-}\mathrm{T}_0)}{F_s(\mathrm{W}_1\text{-}\mathrm{T}_0)}\int_0^{\mathrm{W}_1\text{-}\mathrm{T}_0}tf_{ai}(t)\mathrm{d}t)+\sum_{i=1}^{k_a}E(\tilde{N}'_{ai})\int_0^{\mathrm{W}_1}tf_{ai}(t)\mathrm{d}t+\mathrm{W}_1}{\sum_{i=1}^{k_a}E(N_{ai})(\int_0^{T_0}tf_{ai}(t)\mathrm{d}t+\mathrm{T_m})+\mathrm{T}_0+\mathrm{T_p}+(\sum_{i=1}^{k_a}\frac{p_{ai}(\mathrm{W}_1\text{-}\mathrm{T}_0)}{F_s(\mathrm{W}_1\text{-}\mathrm{T}_0)}\int_0^{\mathrm{W}_1\text{-}\mathrm{T}_0}tf_{ai}(t)\mathrm{d}t+\mathrm{T_m})+\sum_{i=1}^{k_a}E(\tilde{N}'_{ai})(\int_0^{\mathrm{W}_1}tf_{ai}(t)\mathrm{d}t+\mathrm{T_m})+\mathrm{W}_1}.$$

Because $P(A)=P(A\mid B)P(B)+P(A\mid\bar{B})P(\bar{B})$, the availability model is proved. Obviously, $\tilde{N}'_a=\sum_{j=1}^{k_b}N'_{ai}=\tilde{N}_a-1$. $\tilde{N}'_a$ is the number of failures after the first failure within stage b. So

$$P(\tilde{N}'_{a1}=\tilde{n}'_{a1},\tilde{N}'_{a2}=\tilde{n}'_{a2},\ldots,\tilde{N}'_{ak_a}=\tilde{n}'_{ak_a}\mid\tilde{N}'_a=\tilde{n}'_a)=\frac{\tilde{n}'_a!}{\tilde{n}'_{a1}!\tilde{n}'_{a2}!\ldots\tilde{n}'_{ak_a}!}\prod_{j=1}^{k_a}\left(\frac{p_{ai}(\mathrm{W}_1)}{F_s(\mathrm{W}_1)}\right)^{\tilde{n}'_{ai}}, \quad (22)$$

$$P(\tilde{N}'_{ai}=\tilde{n}'_{ai})=\left(\frac{p_{ai}(\mathrm{W}_1)}{R_{as}(\mathrm{W}_1)+p_{ai}(\mathrm{W}_1)}\right)^{\tilde{n}'_{ai}}\left(1-\frac{p_{ai}(\mathrm{W}_1)}{R_{as}(\mathrm{W}_1)+p_{ai}(\mathrm{W}_1)}\right). \quad (23)$$

As a result, $E(\tilde{N}'_{ai})=\frac{p_{ai}(\mathrm{W}_1)}{R_{as}(\mathrm{W}_1)}$. According to the property of conditional expectation [15], we can obtain:

$$E(\tilde{N}_{ai}) = 0 \times P(\tilde{t}_1 > \mathrm{W}_1 - \mathrm{T}_0) + P(\tilde{t}_1 \le \mathrm{W}_1 - \mathrm{T}_0)\left[1 \times \frac{p_{ai}(\mathrm{W}_1\text{-}\mathrm{T}_0)}{F_s(\mathrm{W}_1\text{-}\mathrm{T}_0)} + E(\tilde{N}'_{ai})\right]$$
$$= \left[\frac{p_{ai}(\mathrm{W}_1\text{-}\mathrm{T}_0)}{F_s(\mathrm{W}_1\text{-}\mathrm{T}_0)} + \frac{p_{ai}(\mathrm{W}_1)}{R_{as}(\mathrm{W}_1)}\right] F_s(\mathrm{W}_1 - \mathrm{T}_0) \quad (24)$$

And the warranty cost for Option II is

$$\mathrm{E(C)}=(C_a + C_L T_m)\sum_{i=1}^{k_a}\mathrm{E}(N_{ai}) + (1 - F_s(\mathrm{W}_1 - \mathrm{T}_0))(C_p + C_L T_\mathrm{p}) + F_s(\mathrm{W}_1 - \mathrm{T}_0)[C_p + C_L T_\mathrm{p} + (C_a + C_L T_m)\sum_{i=1}^{k_a}\mathrm{E}(N'_{ai})]$$
$$= (C_a + C_L T_m)\sum_{i=1}^{k_a}\mathrm{E}(N_{ai}) + F_s(\mathrm{W}_1 - \mathrm{T}_0)(C_a + C_L T_m)\sum_{i=1}^{k_a}\mathrm{E}(N'_{ai}) + C_p + C_L T_\mathrm{p}$$

4.3. Availability and cost model for Option III

In order to derive the statistical properties of the product availability and cost for Option III, it is necessary to obtain the distribution of N_a and N_b. The following lemma gives the probability mass functions (pmf) for N_a and N_b. Obviously, $N_\mathrm{a} = \sum_{i=1}^{\mathrm{k_a}} N_{ai}$ and $N_\mathrm{b} = \sum_{j=1}^{\mathrm{k_b}} N_{bj}$. For stage a, under the perfect maintenance assumption, the pmf of N_a is:

$$P(N_\mathrm{a} = n_\mathrm{a}) = [F_s(\mathrm{T}_0)]^{n_\mathrm{a}}(1 - F_s(\mathrm{T}_0)) \ \forall n_\mathrm{a}, n_\mathrm{a} = 0,1,2,\ldots \quad (25)$$

For stage b, under the perfect maintenance assumption, the pmf of N_b for Option III is:

$$P(N_\mathrm{b} = n_\mathrm{b}) = \begin{cases} 1 - \mathrm{G}_s(\mathrm{W}_2\text{-}\mathrm{T}_0) & n_\mathrm{b} = 0 \\ \mathrm{G}_s(\mathrm{W}_2\text{-}\mathrm{T}_0)[\mathrm{G}_s(\mathrm{W}_2)]^{n_\mathrm{b}-1}(1 - \mathrm{G}_s(\mathrm{W}_2)) & n_\mathrm{b} = 1,2,\ldots \end{cases} \quad (26)$$

The proof process of Eq. 25 is similar to Eq. 10. And the proof process of Eq. 26 is similar to Eq. 18.

Lemma 5. We can formulate the product availability and warranty cost for Option III as:

$$\mathrm{A} = \frac{E(\sum_{i=1}^{\mathrm{k_a}} N_{ai}\int_0^{\mathrm{T}_0} tf_{ai}(t)\mathrm{d}t + \mathrm{W}_2)}{E(\sum_{i=1}^{\mathrm{k_a}} N_{ai}(\int_0^{\mathrm{T}_0} tf_{ai}(t)\mathrm{d}t + \mathrm{T_m}) + \tilde{\mathrm{T}}_\mathrm{p} + \mathrm{W}_2)}(1 - G_s(\mathrm{W}_2 - \mathrm{T}_0))$$
$$+ \frac{\sum_{i=1}^{\mathrm{k_a}} E(N_{ai})\int_0^{\mathrm{T}_0} tf_{ai}(t)\mathrm{d}t + \mathrm{T}_0 + \sum_{j=1}^{\mathrm{k_b}}(\frac{p_{bj}(\mathrm{W}_2\text{-}\mathrm{T}_0)}{G_s(\mathrm{W}_2\text{-}\mathrm{T}_0)}\int_0^{\mathrm{W}_2\text{-}\mathrm{T}_0} tf_{bj}(t)\mathrm{d}t) + \sum_{j=1}^{\mathrm{k_b}} E(N'_{bj})\int_0^{\mathrm{W}_2} tf_{bj}(t)\mathrm{d}t + \mathrm{W}_2}{\sum_{i=1}^{\mathrm{k_a}} E(N_{ai})(\int_0^{\mathrm{T}_0} tf_{ai}(t)\mathrm{d}t + \mathrm{T_m}) + \mathrm{T}_0 + \tilde{\mathrm{T}}_\mathrm{p} + (\sum_{j=1}^{\mathrm{k_b}}\frac{p_{bj}(\mathrm{W}_2\text{-}\mathrm{T}_0)}{G_s(\mathrm{W}_2\text{-}\mathrm{T}_0)}\int_0^{\mathrm{W}_2\text{-}\mathrm{T}_0} tf_{bj}(t)\mathrm{d}t + \mathrm{T_r}) + \sum_{j=1}^{\mathrm{k_b}} E(N'_{bj})(\int_0^{\mathrm{W}_2} tf_{bj}(t)\mathrm{d}t + \mathrm{T_r}) + \mathrm{W}_2} G_s(\mathrm{W}_2 - \mathrm{T}_0)$$

$$\mathrm{E(C)}=(C_a + C_L T_m)\sum_{i=1}^{k_a}\mathrm{E}(N_{ai}) + G_s(\mathrm{W}_2 - \mathrm{T}_0)(C_b + C_L T_r)\sum_{j=1}^{k_b}\mathrm{E}(N'_{bj}) + \tilde{C}_p + C_L\tilde{T}_\mathrm{p}. \quad (27)$$

where $E(N_{ai}) = \frac{p_{ai}(\mathrm{T}_0)}{R_{as}(\mathrm{T}_0)}$ and $E(\tilde{N}'_{bj}) = \frac{p_{bj}(\mathrm{W}_2)}{R_{bs}(\mathrm{W}_2)}$.

The proof process of Eq. 27 is similar to Eq. 21.

5. Numerical example

In this section, we consider a particular item with two types of spares (high-quality and low-quality) in the warranty renewing cycle. The failure distributions of these spares and the parameters needed for the warranty availability and cost analysis are provided in Table 1. The low-quality spare has three failure modes. However, the high-quality spare has only two failure modes since its quality has been improved by some engineering

Table 1. distributions and parameters

	Failure modes	Failure density function	α	β
Low-quality spare	F11	$f_{a1}(t)=\frac{\alpha_{a1}}{\beta_{a1}}\left(\frac{t}{\beta_{a1}}\right)^{\alpha_{a1}-1}\mathrm{e}^{-\left(\frac{t}{\beta_{a1}}\right)^{\alpha_{a1}}}$	2.42	12.24
	F12	$f_{a2}(t)=\frac{\alpha_{a2}}{\beta_{a2}}\left(\frac{t}{\beta_{a2}}\right)^{\alpha_{a2}-1}\mathrm{e}^{-\left(\frac{t}{\beta_{a2}}\right)^{\alpha_{a2}}}$	2.31	11.37
	F13	$f_{a3}(t)=\frac{\alpha_{a3}}{\beta_{a3}}\left(\frac{t}{\beta_{a3}}\right)^{\alpha_{a3}-1}\mathrm{e}^{-\left(\frac{t}{\beta_{a3}}\right)^{\alpha_{a3}}}$	6.16	18.92
High-quality spare	F21	$g_{b1}(t)=\frac{\alpha_{b1}}{\beta_{b1}}\left(\frac{t}{\beta_{b1}}\right)^{\alpha_{b1}-1}\mathrm{e}^{-\left(\frac{t}{\beta_{b1}}\right)^{\alpha_{b1}}}$	5.14	6.54
	F22	$g_{b2}(t)=\frac{\alpha_{b2}}{\beta_{b2}}\left(\frac{t}{\beta_{b2}}\right)^{\alpha_{b2}-1}\mathrm{e}^{-\left(\frac{t}{\beta_{b2}}\right)^{\alpha_{b2}}}$	2.11	9.21

Table 2. E(C), A and E(C)/A with different T_0

T_0	E(C)	A	E(C)/A
0.5	192.3316	0.9913	194.0241
1.0	164.6387	0.9914	166.0631
1.5	145.5575	0.9910	146.8825
2.0	134.7430	0.9898	136.1375
2.5	131.5604	0.9877	133.2052
3.0	135.4621	0.9846	137.5794
3.5	146.1847	0.9806	149.0747
4.0	163.8199	0.9757	167.8969
4.5	188.8039	0.9701	194.6238

techniques.In this paper, Weibull distribution is applied to model the failure modes. However, any other life time distributions can be used because all integrals and differentiations are manipulated numerically. C_L=100 and W_1=W_2=5.

Fig. 3 shows the warranty cost, product availability and E(C)/A with different W_1 of Option I. T_m=0.29 and C_a=200. When W_1=5, E(C)=138.8441, A=0.9692, and E(C)/A =143.2600.

For Option II, $C_p = 95$ and $T_p = 0.2$. The warranty cost, product availability and E(C)/A with different T_0 of Option II are shown in Fig. 4.

For Option III, $\tilde{C}_p = 80$, $\tilde{T}_p = 0.03$, C_b=250 and T_r=0.05. Fig. 5 shows the warranty cost, product availability and E(C)/A with different T_0. The optimal T_0 is different when the warranty cost is minimal and the product availability is maximal. So we consider E(C)/A to find the optimal T_0. The partial results of E(C)/A with different T_0 is shown in Table 2. We can conclude that when T_0=2.4 years, the renewing warranty policy is optimal and E(C)/A=133.1947.

In order to validate our previous modeling procedure and results, Monte Carlo method is used to obtain simulated results for the purpose of comparing simulated results to analytical results for Option III. Fig. 6 shows the flow chart for the simulation algorithms of Option III.

T_1 (T_3) is the simulated time of stage a (stage b). And T_2 (T_4) is the simulated working time of stage a (stage b). C_1 (C_2) is the simulated warranty cost of stage a (stage b).Fig.7 shows the comparison between the simulated results and the analytical results.

In order to identify the difference between simulated results and analytical results, we apply root-mean-square error (RMSE) method, mean-absolute error (MAE) method, variance-absolute error (VAE) method, mean-average-relative error (MARE) method, and variance-relative error (VRE) method. RMSE, MAE, and VAW belong to absolute error. And MARE and VRE belong to relative error. The relevant equations are:

$$\mathrm{RMSE}=\frac{1}{n}\sqrt{\sum_{w=1}^{n}(\hat{x}_w-x_w)^2},\ \mathrm{MAE}=\frac{1}{n}\sum_{w=1}^{n}|\hat{x}_w-x_w|,\ \mathrm{VAE}=\frac{1}{n}\sum_{w=1}^{n}(|\hat{x}_w-x_w|-\mathrm{MAE})^2;$$

$$\mathrm{MARE}=\frac{1}{n}\sum_{w=1}^{n}\left|\frac{\hat{x}_w-x_w}{x_w}\right|,\ \mathrm{VRE}=\frac{1}{n}\sum_{w=1}^{n}(\left|\frac{\hat{x}_w-x_w}{x_w}\right|-\mathrm{MARE})^2 .$$

where x_w is the simulation result and $\hat{x}_w$ is the analytical result. The results of these errors are shown in Table 3. The error is insignificant, so we can prove that our models are valid.

We change the parameters to analyze the sensitivity of the cost model and availability model of Option III asshown in Fig. 8-9. As can be seen, when α_{a1} and β_{a1} are increasing, the product availability is increasing and the warranty cost is decreasing. When α_{b1} and β_{b1} are increasing, the product availability is increasing and the warranty cost is decreasing. The sensitivity analysis can prove the stability of the models.

Table 3 error analysis between simulated results and analytical results

	RMSE	MAE	VAE	MARE	VRE
Warranty cost	4.4340	26.1987	316.2951	5.6441×10^{-4}	1.5616×10^{-5}
Product availability	9.8000×10^{-4}	4.9771×10^{-3}	2.3249×10^{-5}	1.0031×10^{-4}	4.8317×10^{-7}

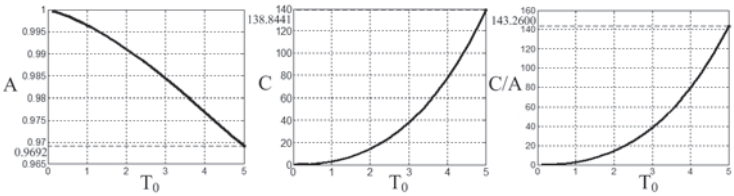

Fig. 3. Results with different W_1 for option I

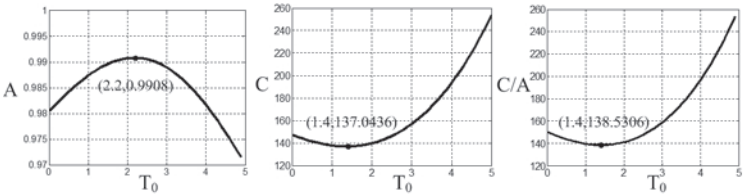

Fig. 4. Results with different T_0 for option II

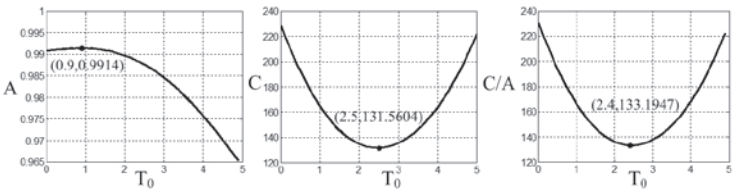

Fig. 5. Results with different T_0 for option III

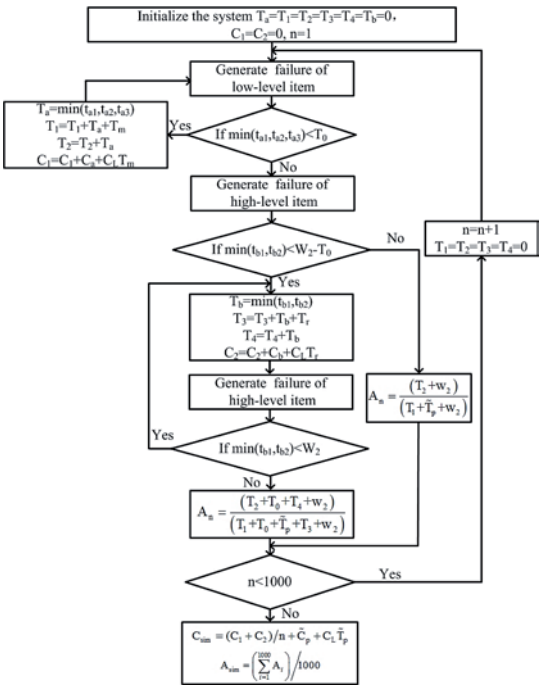

Fig. 6. Simulation flow chart of option III

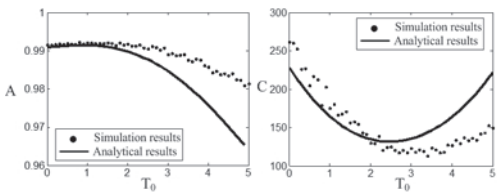

Fig. 7. Simulated results and analytical results for option III

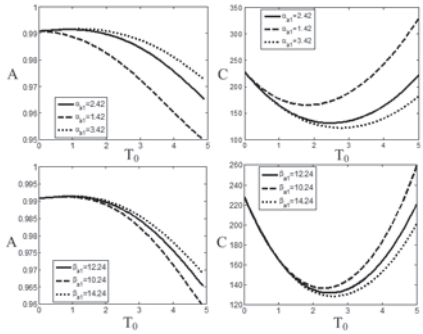

Fig. 8. Product availability and warranty cost analysis with different parameters for low-quality item

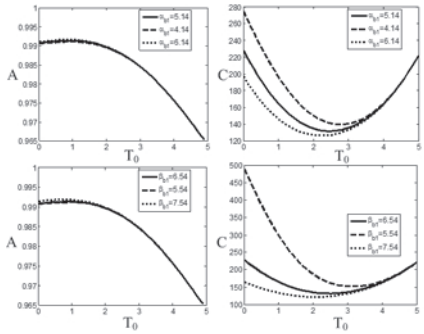

Fig. 9. Product availability and warranty cost analysis with different parameters for high-quality item

6. Conclusions

In this paper, we analyzed three maintenance options in warranty renewing period which includes a new renewing warranty policy considering upgrading maintenance for products with multiple failure modes. The cost and availability models of these maintenance options have been deveoped. For Option II and Option III, the optimal upgrading time T_0 for both warranty cost and product availability can be obtained. The proposed models are illustrated by numerical examples. Monte Carlo simulation method is applied to validate the analytical models of Option III by analyzing the errors between simulation results. Finally, sensitivity analysis for Option III is conducted. We find Option III is better than Option II in some cases. And Option II is better than Option I. As a result, in warranty renewing period, upgrading maintenance can improve the performance and decrease warranty cost in some cases.

There are several potential extensions to the study of the renewing policy considering upgrading maintenance. Firstly, the perfect maintenance assumption can be relaxed. Although this assumption is used widely in practice as well as in warranty and maintenance literature, we believe that more research shall be conducted for the policies considering imperfect maintenance. Secondly, it is needed to consider the case when upgrading maintenance is conducted during the corrective maintenance time. In this paper, we considered upgrading maintenance as a preventive maintenance. Only the low-quality product is working successfully till T_0, then the high-quality spare is used to replace the low-quality product. However, when the corrective maintenance is upgrading maintenance, the models would be different.

References

1. Aggrawal D, Anand A, Singh O, et al. Profit maximization by virtue of price & warranty length optimization. The Journal of High Technology Management Research 2014; 25(1): 1-8 http://dx.doi.org/10.1016/j.hitech.2013.12.006.
2. Bai J, Pham H. Discounted warranty cost of minimally repaired series systems. IEEE Transactions on Reliability 2004; 53(1): 37-42, http://dx.doi.org/10.1109/TR.2003.821945.
3. Bai J, Pham H. Cost analysis on renewable full-service warranties for multi-component systems. European Journal of Operational Research2006; 168(2): 492-508, http://dx.doi.org/10.1016/j.ejor.2004.03.034.
4. Banerjee R, Bhattacharjee M C. Warranty Servicing With A Brown–Proschan Repair Option. Asia-Pacific Journal of Operational Research 2012; 29(03):1-5, http://dx.doi.org/10.1142/S0217595912400234.
5. Blischke W R, Murthy D N P. Product warranty management-I: A taxonomy for warranty policies. European Journal of Operational Research 1992; 62(2): 127-148, http://dx.doi.org/10.1016/0377-2217(92)90242-2.
6. Blischke W R, Murthy D N P. Product Warranty Handbook. Boca Raton: CRC Press, 1995.
7. Chien Y H. The effects of a free-repair warranty on the discrete-time periodic replacement policy. International Journal of Production Economics 2012; 135(2): 832-839, http://dx.doi.org/10.1016/j.ijpe.2011.10.021.
8. González-Prida V, Barberá L, Márquez A C, et al. Modelling the repair warranty of an industrial asset using a non-homogeneous Poisson process and a general renewal process. IMA Journal of Management Mathematics, 2014, http://dx.doi.org/10.1093/imaman/dpu002.
9. Huang YS, Gau WY, Ho JW. Cost analysis of two-dimensional warranty for products with periodic preventive maintenance. Reliability Engineering & System Safety 2015; 134: 51-58, http://dx.doi.org/10.1016/j.ress.2014.10.014.
10. Jeon J, Sohn S Y. Product failure pattern analysis from warranty data using association rule and Weibull regression analysis: A case study. Reliability Engineering & System Safety 2015; 133: 176-183, http://dx.doi.org/10.1016/j.ress.2014.08.015.
11. Liu B, Wu J, Xie M. Cost analysis for multi-component system with failure interaction under renewing free-replacement warranty. European Journal of Operational Research (2015); http://dx.doi.org/10.1016/j.ejor.2015.01.030, http://dx.doi.org/10.1016/j.ejor.2015.01.030.
12. Park M, Pham H. Warranty cost analyses using quasi-renewal processes for multicomponent systems. IEEE Transactions on Systems, Man and Cybernetics, Part A: Systems and Humans2010; 40(6): 1329-1340, http://dx.doi.org/10.1109/TSMCA.2010.2046728.
13. Park M, Pham H. Altered quasi-renewal concepts for modeling renewable warranty costs with imperfect repairs. Mathematical and Computer Modelling 2010; 52(9): 1435-1450, http://dx.doi.org/10.1016/j.mcm.2010.05.028.
14. Park M, Jung K M, Park D H. Optimal warranty policies considering repair service and replacement service under the manufacturer's perspective. Annals of Operations Research 2014:1-16, http://dx.doi.org/10.1007/s10479-014-1740-1.
15. Ross S M. Introduction to probability models. New York: Academic Press, 2014.
16. Sana S S. Preventive maintenance and optimal buffer inventory for products sold with warranty in an imperfect production system. International Journal of Production Research 2012; 50(23): 6763-6774, http://dx.doi.org/10.1080/00207543.2011.623838.
17. Shafiee M, Chukova S, Yun W Y. Optimal burn-in and warranty for a product with post-warranty failure penalty. The International Journal of Advanced Manufacturing Technology 2014; 70(1-4): 297-307, http://dx.doi.org/10.1007/s00170-013-5055-1.
18. Su C, Shen J. Analysis of extended warranty policies with different repair options. Engineering Failure Analysis 2012; 25: 49-62, http://dx.doi.org/10.1016/j.engfailanal.2012.04.002.
19. Vahdani H, Mahlooji H, Eshraghnia Jahromi A. Warranty servicing for discretely degrading items with non-zero repair time under renewing warranty. Computers & Industrial Engineering 2013; 65(1): 176-185, http://dx.doi.org/10.1016/j.cie.2011.08.012.
20. Wang H, Pham H. Reliability and optimal maintenance, Berlin: Springer, 2006.
21. Xie W, Liao H, Zhu X. Estimation of gross profit for a new durable product considering warranty and post-warranty repairs. IIE Transactions 2014; 46(2): 87-105, http://dx.doi.org/10.1080/0740817X.2012.761370.

Xinyue LI
Yunxian JIA
Jianmin ZHAO
Department of Management Engineering
Mechanical Engineering College
Hepingwest road 97#, Shijiazhuang, China

Peng WANG
Reliability Department
Pratt & Whitney AeroPower
4400 Ruffin Road, San Diego, CA, USA

E-mail: oeclxy@hotmail.com, yunxian_jia@hotmail.com, jm_zhao@hotmail.com, pengwang2005@yahoo.com

Article citation info:
DRÓŻDŻ K. Adaptive control of the drive system with elastic coupling using fuzzy Kalman filter with dynamic adaptation of selected coefficients. Eksploatacja i Niezawodnosc – Maintenance and Reliability 2015; 17 (4): 561–568, http://dx.doi.org/10.17531/ein.2015.4.11.

Krzysztof DRÓŻDŻ

ADAPTIVE CONTROL OF THE DRIVE SYSTEM WITH ELASTIC COUPLING USING FUZZY KALMAN FILTER WITH DYNAMIC ADAPTATION OF SELECTED COEFFICIENTS

STEROWANIE ADAPTACYJNE UKŁADU NAPĘDOWEGO Z POŁĄCZENIEM SPRĘŻYSTYM WYKORZYSTUJĄCE ROZMYTY FILTR KALMANA Z DYNAMICZNĄ ADAPTACJĄ WYBRANYCH WSPÓŁCZYNNIKÓW*

In the paper issues related to damping of torsional vibrations in electric drive systems with elastic joint with changeable inertia of the load machine using an adaptive control structure are presented. In order to state variables estimation of a drive system, the extended Kalman filter with a dynamic adaptation of selected coefficients has been applied. Adaptation of selected coefficients of the Kalman filter's covariance matrix ensures an improvement of the state variables and parameter estimation quality of the considered drive system with changeable inertia. The element implementing the adaptation is a fuzzy system, whose input signals are a current estimated value of a time constant of the load machine and a processed signal of an absolute value of difference between the electromagnetic and shaft torques. Theoretical considerations and simulation studies have been verified by tests with laboratory set-up.

***Keywords**: two-mass system, vibrations damping, estimation, Kalman filter.*

W artykule przedstawiono zagadnienia związane z tłumieniem drgań skrętnych w elektrycznych układach napędowych z połączeniem sprężystym o zmiennym momencie bezwładności maszyny roboczej poprzez zastosowanie struktury sterowania adaptacyjnego. W celu odtwarzania zmiennych stanu rozpatrywanego układu wykorzystano zmodyfikowany algorytm rozszerzonego filtru Kalmana z dynamiczną adaptacją wybranych współczynników. Adaptacja współczynników macierzy kowariancji zapewnia poprawę jakości estymacji zmiennych stanu i parametru układu w obecności zmiennego momentu bezwładności. Elementem realizującym wspomnianą adaptację jest system rozmyty, którego sygnałami wejściowymi są aktualna estymowana wartość stałej czasowej maszyny roboczej oraz przetworzony sygnał modułu różnicy pomiędzy momentami elektromagnetycznym i skrętnym. Rozważania teoretyczne i badania symulacyjne zostały zweryfikowane przez testy na stanowisku rzeczywistym.

***Słowa kluczowe**: układ dwumasowy, tłumienie drgań, estymacja, filtr Kalmana.*

1. Introduction

Expectations towards modern drive systems are mainly focused on the precise control of speed and/or position. Examples of the drive systems which have to meet such requirements are servo drives and manipulators of industrial robots [11]. In many mechatronic drive applications there are nonlinear phenomena, changeability of system parameters during operation or oscillations of the electromechanical state variables. In the case of an application of simplified approach for modelling of the drive systems as the one-mass system and the lack of control structure adaptation to changeable operation conditions, these phenomena contribute to the improper operation of the drive system. One of the main causes of the electromechanical state variables oscillations of the drive systems is a finite stiffness of a coupling between the motor and load machine [5]. Therefore, in many cases the adoption of a model of the system as the two-mass system is more appropriate [11]. There are also drive systems where their modelling should take into account a larger number of masses and flexible connections, e.g. conveyors [6].

Issues related to the speed control of the two-mass system initially have been considered in the cases of rolling mills and other heavy industrial drive systems, where high inertia of the motors and long shafts have been cause of torsional vibrations excitation [2, 12, 13]. The development of microprocessor and power electronics technology enabling an effective electromagnetic torque control of the motors caused a visibility of the occurrence of torsional vibrations phenomena in other groups of drives, such as textiles, papers, radio telescopes, robots, cranes, servo drives and others [1, 3, 4, 7, 13, 15]. In order to the damping of torsional vibrations are used, inter alia, mechanical vibration dampers. However, one of the most effective methods is an application of an appropriate control structure. There are many known speed control structures of the two-mass system, which review is presented in [5]. The simplest solutions are based on control structures using PI/PID controllers and basic feedback related to the speed of the motor. In more complex control structures are applied additional feedbacks related to an unmeasurable state variables of the drive system, such as the shaft torque, speed of the driven machine and load torque. In the case of the parameters variability, an adaptive or sliding mode control are applied. This ensures the proper operation of the control structure [13].

In industrial applications of the drive systems, the parameters variability have the greatest impact on their operation quality. In particular the change of value of the load machine time constant T_2. The occurrence of these factors causes the deterioration of the dynamic

(*) Tekst artykułu w polskiej wersji językowej dostępny w elektronicznym wydaniu kwartalnika na stronie ***www.ein.org.pl***

properties of the control structure and to change of assumed trajectory of the speed. In order to ensure the proper operation, the discussed adaptive control is applied [9]. Such type of control is also used in the control of different processes and objects where is parameters variability [8, 14].

The main goal of this paper is to present issues related to the application of a fuzzy Kalman filter in an adaptive control structure of the two-mass system with changeable inertia of the driven machine and the improvement of the estimation quality of the state variables and parameter of the considered drive system.

2. Mathematical model of the plant and the control structure

Object of the research is the drive system with elastic coupling which consists of concentrated masses of the motor and load machine deployed at the ends of the elastic shaft [10]. The commonly used inertia-free-shaft dual-mass system model has been applied [9]. This model is described by the following state equations (in per unit system):

$$\frac{d}{dt}\begin{bmatrix}\omega_1(t)\\ \omega_2(t)\\ m_s(t)\end{bmatrix}=\begin{bmatrix}0 & 0 & \frac{-1}{T_1}\\ 0 & 0 & \frac{-1}{T_2}\\ \frac{1}{T_c} & \frac{-1}{T_c} & 0\end{bmatrix}\begin{bmatrix}\omega_1(t)\\ \omega_2(t)\\ m_s(t)\end{bmatrix}+\begin{bmatrix}\frac{1}{T_1}\\ 0\\ 0\end{bmatrix}[m_e]+\begin{bmatrix}0\\ \frac{-1}{T_2}\\ 0\end{bmatrix}[m_L] \quad (1)$$

where: ω_1 – the motor speed, ω_2 – the load machine speed, m_s – the shaft torque, m_L – the load torque, T_1 – the mechanical time constant of the motor, T_2 – the mechanical time constant of the load machine, T_c – the stiffness time constant.

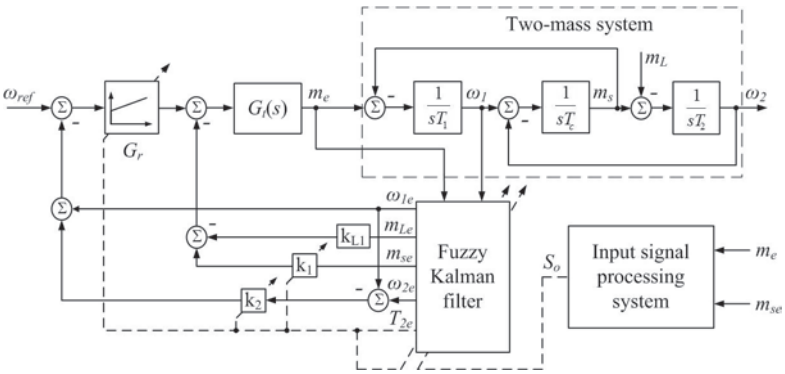

Fig. 1. Schematic diagram of the control structure

The adaptive control structure with PI controller and two additional feedbacks from the shaft torque (k_1) and the speed difference (k_2) has been applied in the research. Schematic diagram of the adaptive control structure is presented in the figure 1. It consists of the optimized electromagnetic control loop, mechanical part of the drive system, extended Kalman filter and PI controller.

The following transfer function of the electromagnetic torque control loop has been assumed:

$$G_t(s)=\frac{1}{0{,}002s+1} \quad (2)$$

The transfer function of the PI speed controller is presented below:

$$G_r(s)=K_p+\frac{K_i}{s} \quad (3)$$

where: K_i, K_p – the integral and proportional gains of the speed controller.

The coefficients of the control structure have been selected on the basis of the current value of the load machine time constant T_2 according to the following formulas:

$$K_i=\omega_r^4T_1T_2T_c \quad (4)$$

$$K_p=4\xi_z\omega_r^3T_1T_2T_c \quad (5)$$

$$k_2=\frac{1}{\omega_r^3T_2T_c}-1 \quad (6)$$

$$k_1=\frac{T_1\left(4\xi_z^2-k_2\right)}{T_2\left(1+k_2\right)}-1 \quad (7)$$

$$k_{L1}=T_cK_I\left(1+k_2\right)+1+k_1 \quad (8)$$

where: ω_r – the reference resonant pulsation, ξ_z – the reference damping factor. The research have been carried out assuming the following values of the reference resonant pulsation and damping factor: ω_r=40 s^{-1}, ξ_z = 0,7.

3. Mathematical model of the extended Kalman filter

In the case of changeable values of the load machine time constant T_2, an extension of the state vector of the considered drive system by using of the parameter T_2 inverse and load torque m_L is required. The assumption of the time constant inverse $1/T_2$ is related to the simplification of calculations concerning linearization of the state equation. In this paper the wide range of changes of the time constant T_2 between T_{2N} and $4T_{2N}$ is assumed. After taking into account of these conditions the state vector takes the following form:

$$\mathbf{x_R}(t)=\left[\omega_1(t)\ \ \omega_2(t)\ \ m_s(t)\ \ m_L(t)\ \ \frac{1}{T_2(t)}\right]^T \quad (9)$$

The extended state and output equations of the considered drive system can be formulated in the following form:

$$\frac{d}{dt}\mathbf{x_R}(t)=\mathbf{A_R}\left(\frac{1}{T_2}(t)\right)\mathbf{x_R}(t)+\mathbf{B_R}\mathbf{u}(t)+\mathbf{w}(t)=\mathbf{f_R}(\mathbf{x_R}(t),\mathbf{u}(t))+\mathbf{w}(t) \quad (10a)$$

$$\mathbf{y_R}(t)=\mathbf{C_R}\mathbf{x_R}(t)+\mathbf{v}(t) \quad (10b)$$

where: $\mathbf{w}$(t), $\mathbf{v}$(t) – white noises occurring in the system.

The matrices of the state, control and output are defined as follows:

$$\mathbf{A_R}\left(\frac{1}{T_2}(t)\right)=\begin{bmatrix} 0 & 0 & \frac{-1}{T_1} & 0 & 0 \\ 0 & 0 & \frac{1}{T_2(t)} & \frac{-1}{T_2(t)} & 0 \\ \frac{1}{T_c} & \frac{-1}{T_c} & 0 & 0 & 0 \\ 0 & 0 & 0 & 0 & 0 \\ 0 & 0 & 0 & 0 & 0 \end{bmatrix},\ \mathbf{B_R}=\begin{bmatrix} \frac{1}{T_1} \\ 0 \\ 0 \\ 0 \\ 0 \end{bmatrix},\ \mathbf{C_R}=\begin{bmatrix} 1 \\ 0 \\ 0 \\ 0 \\ 0 \end{bmatrix}^T \tag{11}$$

The matrix $\mathbf{A_R}$ depends on the parameter T_2. Assuming the parameter variation during operation of the drive system, an update of the matrix $\mathbf{A_R}$ in every calculation step according to the current value of the estimated parameter of the load machine time constant T_2 is required. Input and output vectors of the drive system and Kalman filter are the electromagnetic torque and motor speed:

$$\mathbf{u}=m_e\ ,\ \mathbf{y}=\omega_1 \tag{12}$$

After discretization of the state equation (10) with a sampling period T_s, the estimation of the state variables process using the fuzzy Kalman filter is started. This algorithm can be described in the following steps:

1. State prediction:

$$\hat{\mathbf{x}}_\mathbf{R}(k+1/k)=\mathbf{A_R}(k)\hat{\mathbf{x}}_\mathbf{R}(k/k)+\mathbf{B_R}\mathbf{u}(k) \tag{13}$$

2. Covariance prediction:

$$\mathbf{P}(k+1/k)=\mathbf{F_R}(k)\mathbf{P}(k)\mathbf{F_R^T}(k)+\mathbf{Q}(k) \tag{14}$$

where:

$$\mathbf{F_R}(k)=\frac{\partial \mathbf{f_R}(\mathbf{x_R}(k/k)\mathbf{u}(k))}{\partial \mathbf{x_p}(k/k)}\Big|_{\mathbf{x_R}=\hat{\mathbf{x}}_\mathbf{R}(k/k)} \tag{15}$$

$$\mathbf{F_R}=\begin{bmatrix} 1 & 0 & \frac{-1}{T_1}T_s & 0 & 0 \\ 0 & 1 & \frac{1}{T_2(k)}T_s & \frac{-1}{T_2(k)}T_s & T_s(m_s(k)-m_L(k)) \\ \frac{1}{T_c}T_s & \frac{-1}{T_c}T_s & 1 & 0 & 0 \\ 0 & 0 & 0 & 1 & 0 \\ 0 & 0 & 0 & 0 & 1 \end{bmatrix} \tag{16}$$

3. Calculate of the Kalman gain:

$$\mathbf{K}(k+1)=\mathbf{P}(k+1/k)\mathbf{C_R^T}(k+1)\left[\mathbf{C_R}(k+1)\mathbf{P}(k+1/k)\mathbf{C_R^T}(k+1)+\mathbf{R}(k)\right]^{-1} \tag{17}$$

4. State update:

$$\hat{\mathbf{x}}_\mathbf{R}(k+1/k+1)=\hat{\mathbf{x}}_\mathbf{R}(k/k)+\mathbf{K}(k+1)\left[\mathbf{y}(k+1)-\mathbf{C_R}(k+1)\hat{\mathbf{x}}_\mathbf{R}(k+1/k)\right] \tag{18}$$

5. Covariance update:

$$\mathbf{P}(k+1/k+1)=\left[\mathbf{I}-\mathbf{K}(k+1)\mathbf{C_R}(k+1)\right]\mathbf{P}(k+1/k) \tag{19}$$

6. Return to the first step.

This algorithm requires the selection of coefficients of the **Q** and **R** covariance matrices:

$$\mathbf{Q}=\begin{bmatrix} q_{11} & 0 & 0 & 0 & 0 \\ 0 & q_{22} & 0 & 0 & 0 \\ 0 & 0 & q_{33} & 0 & 0 \\ 0 & 0 & 0 & q_{44} & 0 \\ 0 & 0 & 0 & 0 & q_{55} \end{bmatrix},\ \mathbf{R}=[r]$$

These values have been selected using a genetic algorithm according to assumed objective function:

$$F_1=\frac{\left(\sum_{i=1}^{n}\left|\omega_{i1}-\omega_{i1e}\right|\right)*\left(\sum_{i=1}^{n}\left|\omega_{i2}-\omega_{i2e}\right|\right)*\left(\sum_{i=1}^{n}\left|m_{is}-m_{ise}\right|\right)*\left(\sum_{i=1}^{n}\left|m_{iL}-m_{iLe}\right|\right)*\left(\sum_{i=1}^{n}\left|T_{i2}-T_{i2e}\right|\right)}{n} \tag{20}$$

The above presented objective function takes into account all estimated variables included in the state vector of the considered drive system. Table 1 shows the obtained values of the coefficients of the matrices **Q** and **R**.

Table 1. Values of the coefficients of the matrices Q and R

q_{11}	q_{22}	q_{33}	q_{44}	q_{55}	r
0,037	0,020	2E-5	99,18	61,63	41,84

4. Applied fuzzy system

In the paper the designed fuzzy system which introduces the adaptation of the selected coefficients of the Kalman filter covariance matrix **Q** is presented. The structure of this system is presented in the figure 2. The figure 3 shows the applied membership functions of input variables in the discussed fuzzy system. The calculation of the q_{44} and q_{55} coefficients values of the matrix **Q** is based on the current estimated value of the load machine time constant T_{2e} and the processed signal S_o of the absolute value of difference between the electromagnetic and estimated shaft torques. The value of signal S_o allows to distinguish the static and dynamic state of the considered drive system. In the case of the signal value exceeding the set limit, the fuzzy system retunes the coefficients of the covariance matrix on the values corresponding to the dynamic state of the drive system and specific value of the load machine time constant. Otherwise, the static state is recognized and the analogous retune process is carried out. The signal S_o is the output of the input signal processing system, whose structure is shown in the figure 4. In order to reduce the occurring high frequency disturbances, a low pass filter with a constant value of time constant T_f has been applied in this system. In the research assumed T_f=0,005 s. The designed fuzzy system enables the shaping of a surface of the **Q** matrix coefficients q_{44} and q_{55} changes as a function of T_{2e} and S_o. The shape of the surface depends on the selected values of the coefficients m_i. In the present study, the selection has been carried out using the Pattern Search algorithm according to the following objective function:

$$F_2 = \frac{\left(\sum_{i=1}^{n}\left|m_{iL} - m_{iLe}\right|\right) * \left(\sum_{i=1}^{n}\left|T_{i2} - T_{i2e}\right|\right)}{n} \tag{21}$$

This process has been carried out in two steps because of the large number of parameters. First, the values of coefficients m_9 to m_{16} have been optimized, keeping a constant value of the q_{44}. Next, the values of coefficients m_1 to m_8 have been optimized with variable q_{55}. In the both cases, the optimization algorithm starting points were the values of the Kalman filter covariance matrix coefficients q_{44} and q_{55}. The obtained values of the individual coefficients m_i are presented in the Table 2.

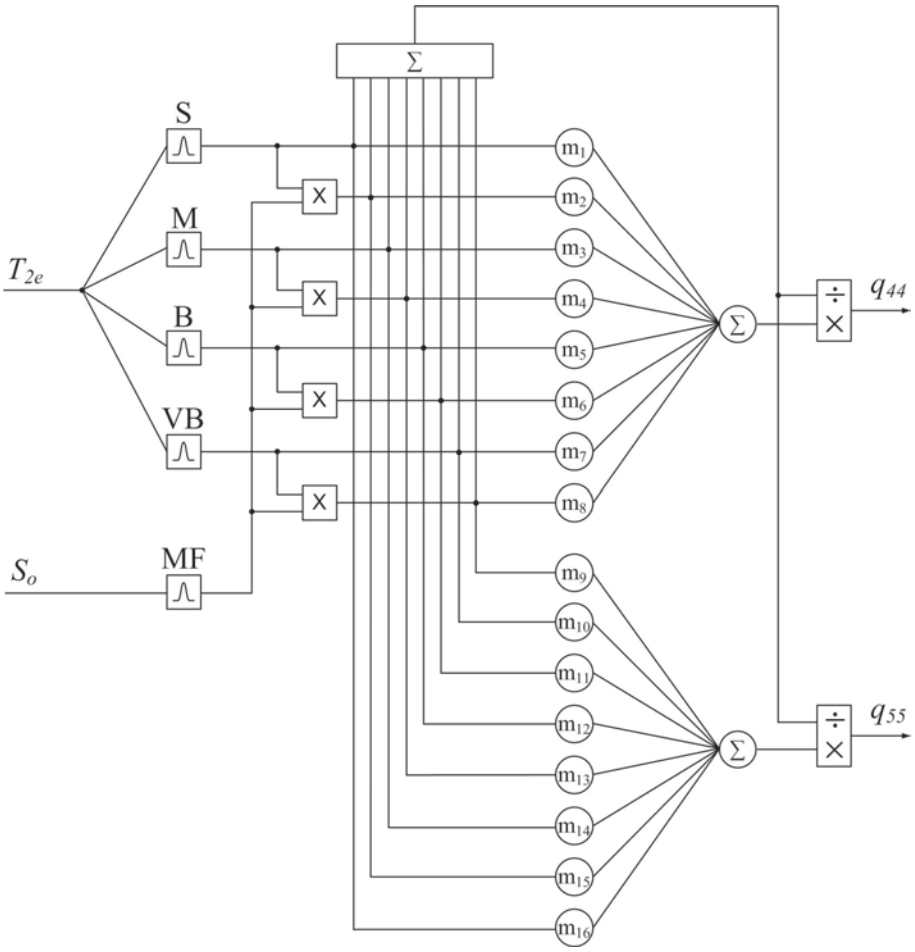

Fig. 2. Structure of the applied fuzzy system

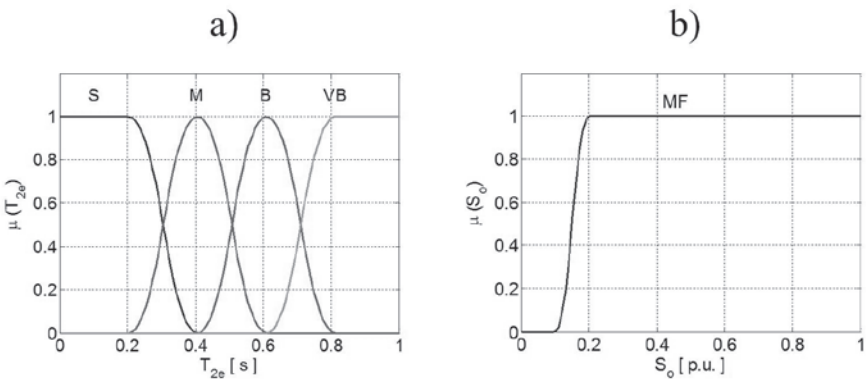

Fig. 3. Applied membership functions

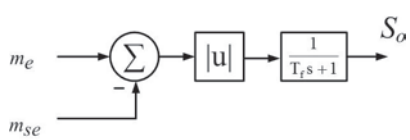

Fig. 4. Structure of the input signal processing system

5. Selected results of the simulation research

In the simulation research initially the extended Kalman filter with fixed coefficients of the **Q** and **R** matrices has been tested in the closed-loop control structure. Different operation conditions of the drive system than in the optimization process were assumed. A system to prevent simultaneous estimation of the load torque and the load machine time constant was applied. The figure 5 shows the selected results of this research. The changes of the load machine time constant during the operation of the drive system in the range of T_{2N} to $4T_{2N}$ were taken into account. The estimation quality of the motor speed, driven machine speed and shaft torque can be considered satisfactory. The analysis of the results showed that the control structure is working correctly. However, the transients of the estimated load torque and the load machine time constant are characterized by undesirable large estimation errors values that can be the cause of excitation of the torsional vibrations. In order to eliminate the discussed drawbacks, the adaptation of the coefficients q_{44} and q_{55} of the matrix **Q** using the designed fuzzy system has been applied. The figure 6 shows the selected results of the research of the closed-loop control structure with the fuzzy Kalman filter. In order to evaluate the estimation quality and comparison of the both methods, the estimation errors of the individuals state variables and parameter have been calculated using following formula:

$$\delta x = \frac{\sum_{i=1}^{n}\left|x_i - x_{ie}\right|}{n}, \; i = 1,.2,..,n \tag{22}$$

where: x – real value, x_e – estimated value, n – number of samples. The calculated values of the estimation errors are presented in the Table 3. An analysis of the obtained results indicates the achievement of a significant improvement of the estimation quality of all estimated variables.

Table 2. The obtained values of the individual coefficients m_i

m_1	m_2	m_3	m_4	m_5	m_6	m_7	m_8
149,21	29,87	208,97	8,11E-4	259,58	5,19	313,45	55,40
m_9	m_{10}	m_{11}	m_{12}	m_{13}	m_{14}	m_{15}	m_{16}
162,60	61426,94	7,34E-4	3624,63	14,61	532,67	13,35	168,83

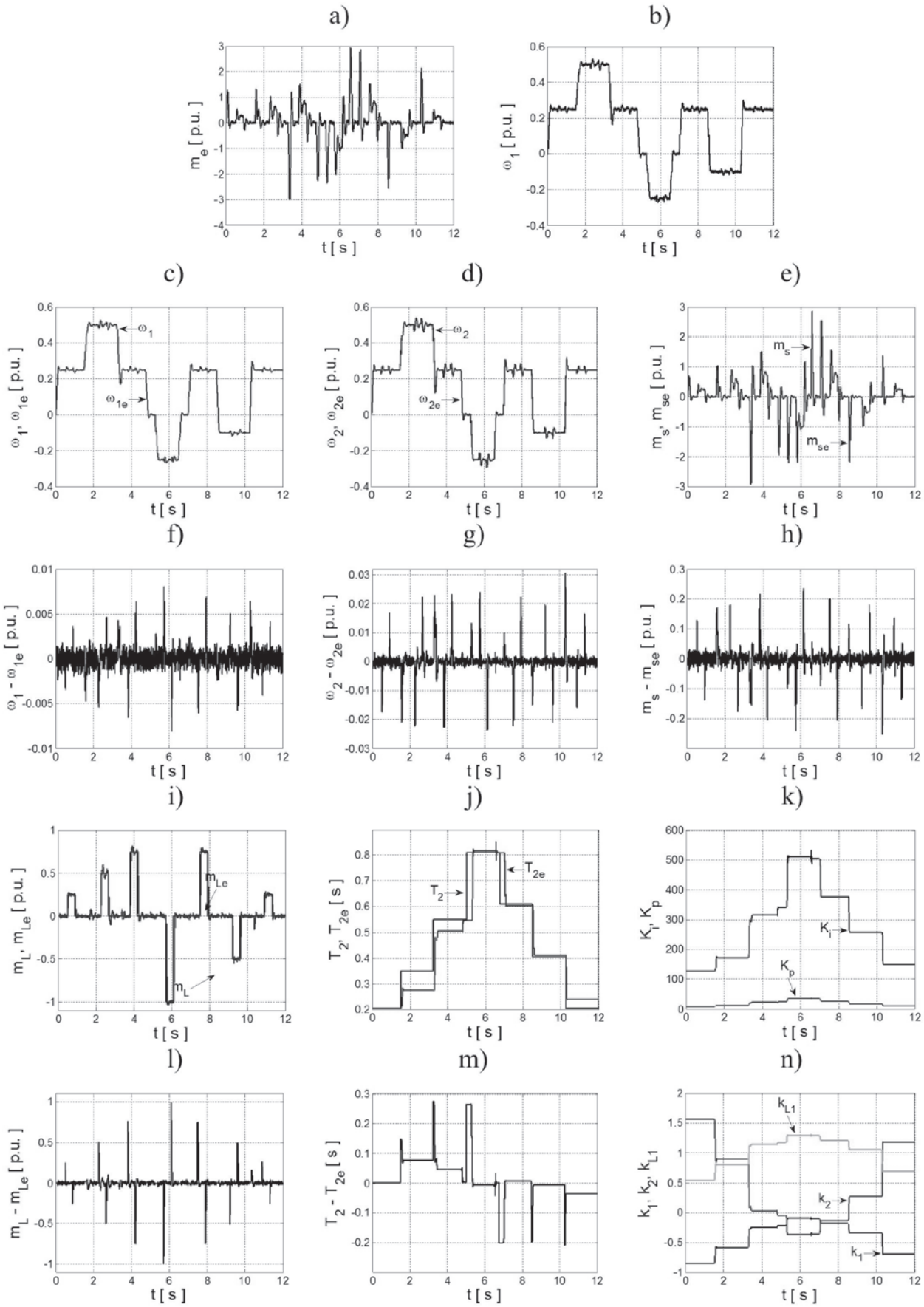

Fig. 5. Simulated transients of: the input signals of the extended Kalman filter – the electromagnetic torque (a) and the motor speed (b), the real and estimated variables and estimation errors of: the motor speed (c, f), the load machine speed (d, g), the shaft torque (e, h), the load torque (i, l), the time constant of the load machine (j, m), the parameters of the control structure (k, n)

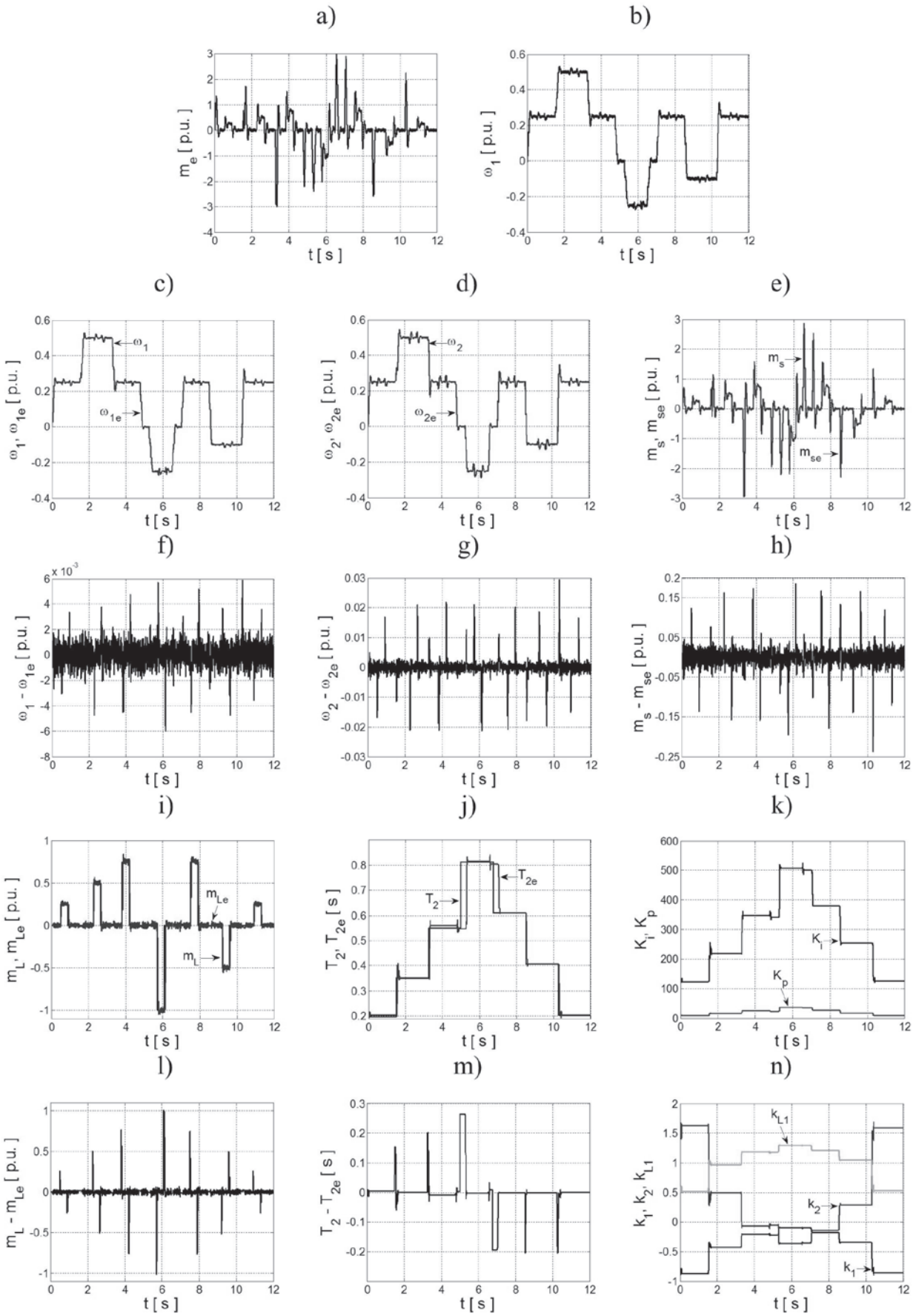

Fig. 6. Simulated transients of: the input signals of the fuzzy Kalman filter – the electromagnetic torque (a) and the motor speed (b), the real and estimated variables and estimation errors of: the motor speed (c, f), the load machine speed (d, g), the shaft torque (e, h), the load torque (i, l), the time constant of the load machine (j, m), the parameters of the control structure (k, n)

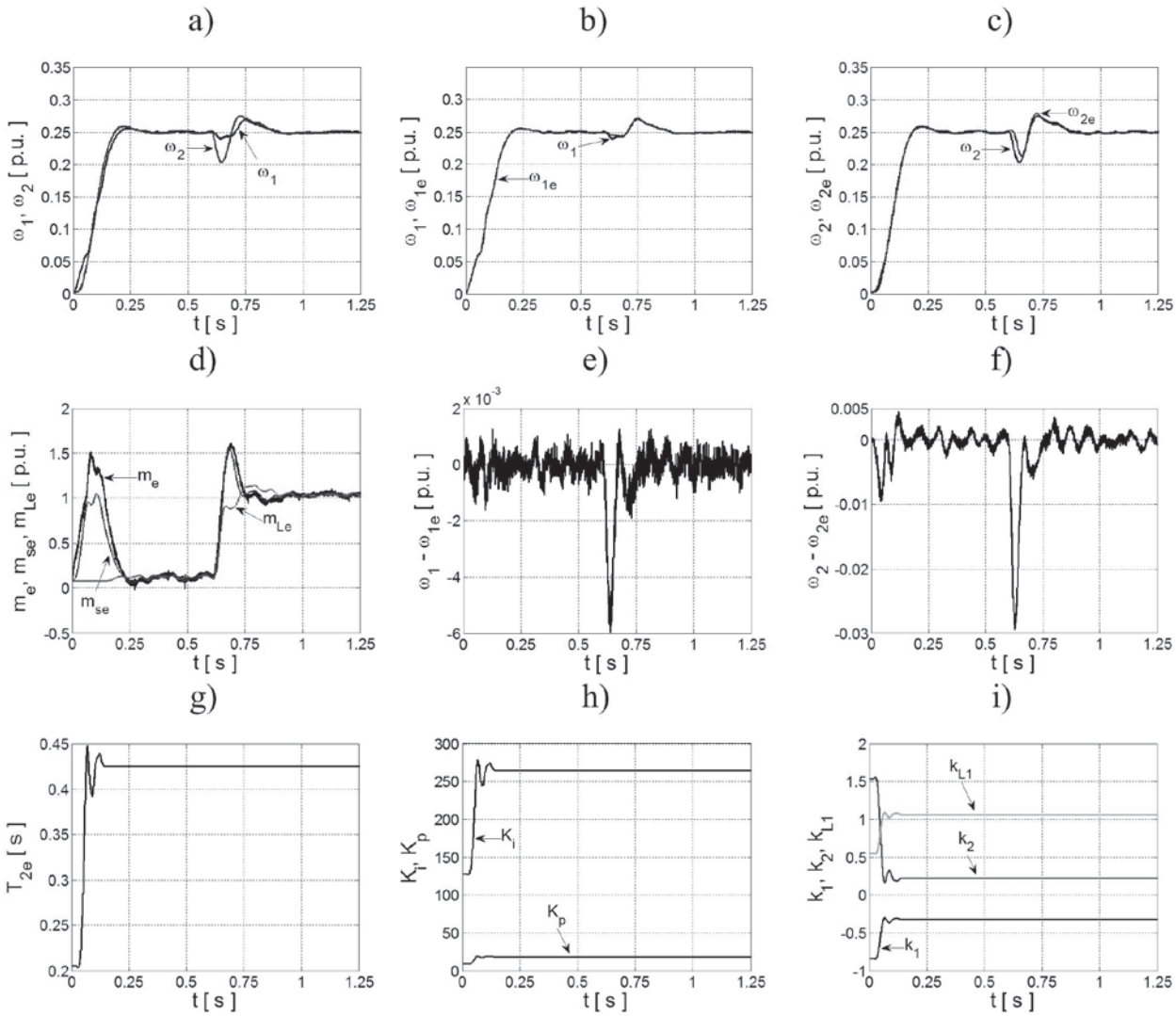

Fig. 7. Experimental transients of: the real and estimated motor speed (b) and load machine speed (c), the electromagnetic, shaft and load torques (d), the estimation errors of the motor speed (e) and the load machine speed (f), the parameters of the control structure (f, g)

6. Selected results of the experimental research

In order to verify of the simulation research, the experimental tests of the proposed solution have been carried out on a laboratory set-up. This system consists of two 500 W DC machines connected by a long elastic shaft. The drive motor is fed by a H-bridge PWM converter. The load of the system has been carried out using a resistance modulator. The control algorithm has been implemented on the dSpace 1103 control platform. The speeds measurements have been realized through two incremental encoders (36000 impulses per rotation). The parameters of the electromagnetic control loop have been tuned in a way that ensures a fast control of this variable. The estimation of the unavailable state variables and parameter T_2 has been realized using the described fuzzy Kalman filter.

The adaptive control structure has been tested for the reference speed $\omega_{ref} = 0{,}25\omega_N$. This value was selected so as to avoid the electromagnetic torque limit. The results are presented in the figure 7. During the starting of the drive system the influence of the system to prevent simultaneous estimation of the load torque and the load machine time constant is visible. The control structure operation starts with the values of the coefficients K_i, K_p, k_1, k_2, k_{L1} selected for incorrect value of the $T_{2e} = 0{,}203$s. Then, at the time of starting the value of T_{2e} is calculated by the fuzzy Kalman filter algorithm and it tends to the real value of T_2 parameter. According to the equations (4)-(8) the coefficients of the control structure are retuned. Analysis of the results indicates the proper operation of the control structure.

7. Conclusion

In the paper issues related to the adaptive control of the two-mass system using the extended Kalaman filter are presented. The mathematical models of the considered drive system, Kalman filter and the control structure have been described. The designed fuzzy system, which task has been the adaptation of the **Q** covariance matrix coefficients q_{44} and q_{55}, has been characterized. The selection way of the fuzzy system coefficients has been presented. The proposed fuzzy Kalman filter has been tested in the case of operation in the closed-loop control structure. The comparative research of the proposed algorithm with the classical extended Kalman filter have been carried out. The significant improvement of the all variables estimation quality has been obtained. The theoretical considerations and simulation studies have been verified in the experimental tests. Based on the extensive investigations, the following conclusions can be formulated:

– the application of the advanced adaptive control structure using the Kalman filters enables the effective damping of the torsional vibrations of the considered drive system with the elastic coupling,

– the introducing of the designed fuzzy system to achieve the dynamic adaptation of the Kalman filter selected coefficients ensures the improvement of the all variables estimation quality in comparison to the classical algorithm. It has a positive impact on the operation of the control structure in the presence of changes of the time constant of the load machine in the wide range,
– the application of the Pattern Search algorithm to optimize the values of the fuzzy system singletons allows obtaining satisfactory results of the observer operation,
– using this algorithm should be pay particular attention to the appropriate form of the objective function.

Acknowledgement

This research work is supported by National Science Centre (Poland) under grant: Robust estimators of the system states and parameters for the drive system with an elastic joint - UMO-2011/01/B/ST7/03500 (2011-2014).

References

1. Brock S, Deskur J, Janiszewski D, Muszyński R. Active damping of torsional vibrations in servodrives. Power Electronics and Electrical Drives. Selected Problems. Wrocław: Oficyna Wydawnicza Politechniki Wrocławskiej 2007: 278-297.
2. Butler D H E, Churches M A, Vergan E R, Anbe Y, Naitoh H. Compensation of a digitally controlled static power converter for the damping of rolling mill torsional vibration. IEEE Transactions on Industry Applications 1992; 28(2): 427-433, http://dx.doi.org/10.1109/28.126752.
3. De Luca A, Schroder D, Thummel M. An Acceleration-based State Observer for Robot Manipulators with Elastic Joints. IEEE International Conference on Robotics and Automation 2007: 3817-3823, http://dx.doi.org/10.1109/robot.2007.364064.
4. Gierlotka K. Układy sterowania napędów elektrycznych z elementami sprężystymi. Gliwice: Zeszyty Naukowe Politechniki Śląskiej 1992; 129(1181).
5. Kamiński M. Implementacja neuronowego estymatora prędkości napędu dwumasowego w układzie FPGA. Przegląd Elektrotechniczny 2010; 2: 225-230.
6. Karolewski B, Ligocki P. Modelling of long belt conveyors. Eksploatacja i Niezawodnosc – Maintenance and Reliability 2014; 2: 179-187.
7. Michael C A, Safacas A N. Dynamic and Vibration Analysis of a Multimotor DC Drive System With Elastic Shafts Driving a Tissue Paper Machine. IEEE Transactions on Industrial Electronics 2007; 54(4): 2033-2046, http://dx.doi.org/10.1109/TIE.2007.895149.
8. Poleszak J. The adaptive control of the injection timing in the diesel engine. Eksploatacja i Niezawodnosc – Maintenance and Reliability 2003; 2: 52-55.
9. Szabat K. Struktury sterowania elektrycznych układów napędowych z połączeniem sprężystym. Wrocław: Prace Naukowe Instytutu Maszyn, Napędów i Pomiarów Elektrycznych Politechniki Wrocławskiej 2008; 61(19).
10. Szabat K, Dybkowski M. Tłumienie drgań skrętnych w układzie dwumasowym z luzem mechanicznym. Przegląd Elektrotechniczny 2010; 2: 376-379.
11. Szabat K, Orłowska-Kowalska T. Adaptive Control of Two-Mass System using Nonlinear Extended Kalman Filter. 32nd Annual Conference on IEEE Industrial Electronics IECON 2006: 1539-1544.
12. Szabat K, Orłowska-Kowalska T. Vibration Suppression in Two-Mass Drive System using PI Speed Controller and Additional Feedbacks - Comparative Study. IEEE Transaction on Industrial Electronics 2007; 54(2): 1193-1206, http://dx.doi.org/10.1109/TIE.2007.892608.
13. Szabat K, Serkies P J. Zastosowanie sterowania predykcyjnego w układzie napędowym z połączeniem sprężystym. Przegląd Elektrotechniczny 2010; 2: 380-383.
14. Świć A, Taranenko W. Adaptive control of machining accuracy of axial-symmetrical low-rigidity parts in elastic-deformable state. Eksploatacja i Niezawodnosc – Maintenance and Reliability 2012; 3: 17-25.
15. Zoller T, Leibfried T, Miri A M. Application of Power Electronics for Damping of Torsional Vibrations. 7th International Conference on Power Electronics and Drive Systems PEDS 2007: 521-525, http://dx.doi.org/10.1109/peds.2007.4487750.

Krzysztof DRÓŻDŻ
Wrocław University of Technology
Faculty of Electrical Engineering
Department of Electrical Machines, Drives and Measurements
Wybrzeże Wyspiańskiego 27, 50-370 Wrocław, Poland
E-mail: krzysztof.drozdz@pwr.edu.pl

Article citation info:
GLOWACZ A. Recognition of acoustic signals of induction motor using FFT, SMOFS-10 and LSVM. Eksploatacja i Niezawodnosc – Maintenance and Reliability 2015; 17 (4): 569–574, http://dx.doi.org/10.17531/ein.2015.4.12.

Adam GLOWACZ

RECOGNITION OF ACOUSTIC SIGNALS OF INDUCTION MOTOR USING FFT, SMOFS-10 AND LSVM

ROZPOZNAWANIE SYGNAŁÓW AKUSTYCZNICH SILNIKA INDUKCYJNEGO Z ZASTOSOWANIEM FFT, SMOFS-10 I LSVM*

A correct diagnosis of electrical circuits is very essential in industrial plants. An article deals with a recognition method of early fault detection of induction motor. The described approach is based on patterns recognition. Acoustic signals of specific induction motor are analyzed patterns. Acoustic signals include information about motor state. The analysis of the patterns was conducted for three states of induction motor using Fast Fourier Transform (FFT), shortened method of frequencies selection (SMoFS-10) and Linear Support Vector Machine (LSVM). The results of calculations suggest that the method is efficient and can be also used for diagnostic purposes.

***Keywords**: acoustic signal, induction motor, feature extraction, classification.*

Prawidłowa diagnostyka obwodów elektrycznych jest bardzo istotna w zakładach przemysłowych. Artykuł zajmuje się metodą rozpoznawania stanów przedawaryjnych silnika indukcyjnego. Opisane podejście jest oparte na rozpoznawaniu wzorców. Sygnały akustyczne określonego silnika indukcyjnego są badanymi wzorcami. Sygnały akustyczne zawierają informację o stanie silnika. Analiza wzorców została przeprowadzona dla trzech stanów silnika indukcyjnego używając FFT, skróconej metody wyboru częstotliwości (SMoFS-10) i liniowej maszyny wektorów wspierających (LSVM). Wyniki obliczeń sugerują, że metoda jest skuteczna i może być również zastosowana dla celów diagnostycznych.

***Słowa kluczowe**: sygnał akustyczny, silnik indukcyjny, ekstrakcja cech, klasyfikacja.*

1. Introduction

The induction motors are used in various industries such as: mining, fuel, metallurgical. These motors have low maintenance and low price. To reduce maintenance costs scientists analyze mechanical properties of materials [18, 20, 25, 30].

They also develop early fault detection methods [1, 5, 6, 10-15]. Especially non-invasive methods are developed such as: acoustic, vibrations, thermal, magnetic [3, 14, 19, 27, 28, 29, 35, 36, 38]. Non-invasive methods are capable to diagnose early faults without disassembly the induction motor. Many of them used patterns recognition and signal processing to identify type of fault.

Incipient faults of motors may change into damages and may stop the production line. The stopped production line causes losses of resources and production time. It increases the cost of operation and maintenance.

This article deals with a recognition method of early faults of induction motor. Proposed method uses Fast Fourier Transform (FFT), shortened method of radio frequencies selection (SMoFS-10) and Linear Support Vector Machine (LSVM).

2. Proposed approach of recognition of acoustic signal of induction motor

The proposed approach of recognition of acoustic signal of induction motor contained two processes: a pattern creation process and an identification process. These processes were needed for proper recognition of acoustic signal (Fig. 1).

The first of them recorded acoustic signal of motor with the help of a sound card and a microphone [22]. Acoustic signal was converted

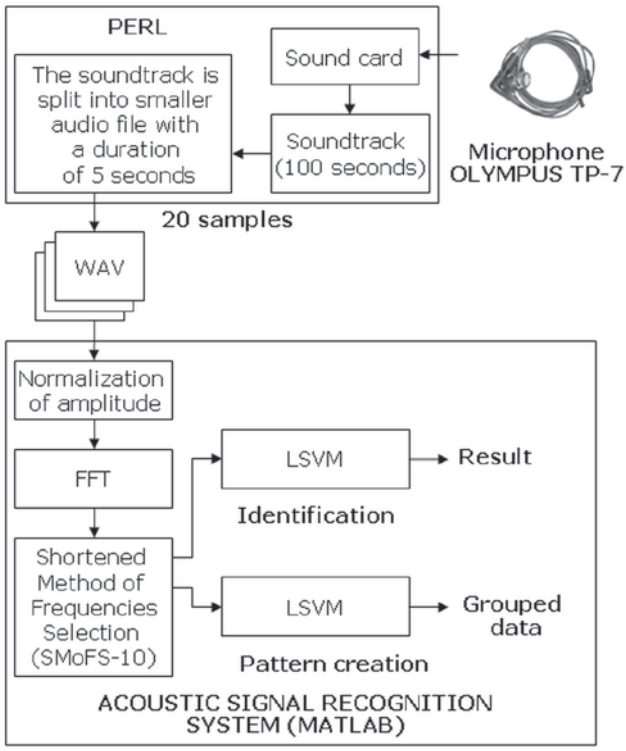

Fig. 1. Process of recognition of acoustic signal of induction motor using FFT, shortened method of frequencies selection (SMoFS-10) and Linear Support Vector Machine

(*) Tekst artykułu w polskiej wersji językowej dostępny w elektronicznym wydaniu kwartalnika na stronie ***www.ein.org.pl***

to soundtrack. Next this signal was converted into smaller audio files with a duration of 5 seconds. After that amplitudes of audio files (recorded acoustic signal) were normalized. Next the radio frequency spectra were calculated by FFT algorithm [8]. These spectra were processed by the shortened method of radio frequencies selection (SMoFS-10). The results of this method were feature vectors containing specific amplitudes of radio frequencies. The shortened method of frequencies selection (SMoFS-10) was discussed in chapter 2.2. Next step was grouping of data. For this purpose, Linear Support Vector Machine (LSVM) algorithm was used. The same methods as above were used in the identification process. Calculated feature vectors were recognized by Linear Support Vector Machine algorithm.

The described approach was based on patterns recognition. Patterns of acoustic signals of specific induction motor were analyzed. For this reason, there were two databases of patterns: training database and test database. The training database of patterns was used in the pattern creation process. All training samples and their classes were known. The test database of patterns was used in the identification process. All test samples were known, but their classes were unknown. Proposed method identified the correct class.

2.1. Measurement and preprocessing of acoustic signals of induction motor

The sound card and the microphone OLYMPUS TP-7 were applied to record acoustic signal of induction motor. Parameters of recorded soundtrack were following: 16-bit depth, number of channels – single channel, sampling rate – 44100 Hz, WAVE PCM audio file. Obtained soundtrack was converted into smaller audio files with a duration of 5 seconds. Afterwards amplitudes of audio files were normalized. Normalization of amplitude divided each point of the signal by maximum value. In that way signals were comparable in the range <-1, 1>. Next the radio frequency spectra were calculated by FFT algorithm. Obtained radio frequency spectra were used by shortened method of frequencies selection SMoFS-10.

2.2. Shortened method of frequencies selection (SMoFS-10)

The shortened method of frequencies selection (SMoFS-10) was based on the radio frequency spectrum. The method had following steps:

1) Calculate the difference of the radio frequency spectra of two states of motor $||F_1|-|F_2||$, where $|F_1|$ - is the radio frequency spectrum of acoustic signal of the first state of motor, $|F_2|$ - is the radio frequency spectrum of acoustic signal of the second state of motor.
2) Select the radio frequencies, which meets following criterion:

$$||F_1|-|F_2||>t \tag{1}$$

where t – threshold of selection of amplitudes of radio frequencies (formula 1), $||F_1|-|F_2||$ – the difference of amplitudes of radio frequencies for two different states of the motor.

Parameter t should be selected properly. This parameter depends on number of analyzed states and number of selected radio frequencies. Too little number of analyzed radio frequencies can cause errors. The differences between the selected radio frequencies can have different values (for example the first difference has maximum amplitude for frequencies 100, 200, 300 Hz; the second difference has maximum amplitude for frequencies 150, 200, 250 Hz; the third difference has maximum amplitude for frequencies 150, 225, 275 Hz in that case states 1 and 3 do not have common radio frequencies). For this reason, the parameter t is selected according to formulas 2 and 3. If the number of radio frequencies (number s) is greater than 10, the method will do loop calculation (formula 3). If the number of radio frequencies is smaller or equal to 10 it finishes its calculations.

$$t = \frac{\sum_{s=1}^{s} || F_1|-|F_2 ||}{s}, \tag{2}$$

$$s \le 10, \tag{3}$$

where t – threshold of selection of amplitudes of radio frequencies (it depends on s and analyzed acoustic signal), s – natural number, number of radio frequencies (initially s=16384, 16384 is the number of all frequencies after usage of FFT algorithm). The amplitudes of selected radio frequencies of acoustic signals of motor are used to create feature vectors. SMoFS-10 method gives feature vector with 1-10 features, where a feature is the amplitude of radio frequency. The feature vector may have 2 features or 8, depending on the analyzed signals and the parameter s (for SMoFS-10 s = 10). Optimalization of parameters s and t depends on the number of analyzed states, their types, disturbances and the type of machine.

Difference between spectrum of acoustic signal of faultless induction motor and spectrum of acoustic signal of induction motor with faulty rotor bar was showed in figure 2.

Selected radio frequencies for differences between spectra of acoustic signals of induction motor were presented (Fig. 3-5). Two radio frequencies were common for analyzed states of induction mo-

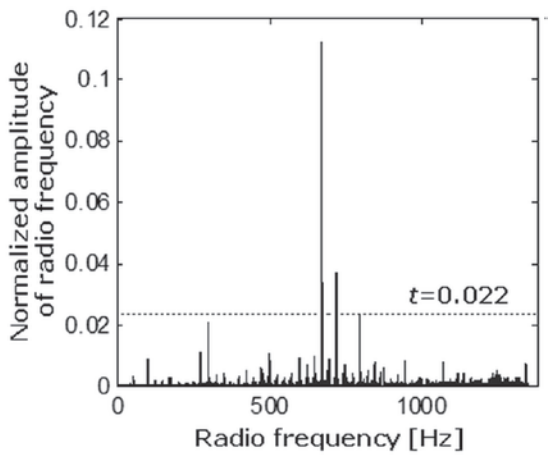

Fig. 2. Difference between spectrum of acoustic signal of faultless induction motor and spectrum of acoustic signal of induction motor with faulty rotor bar

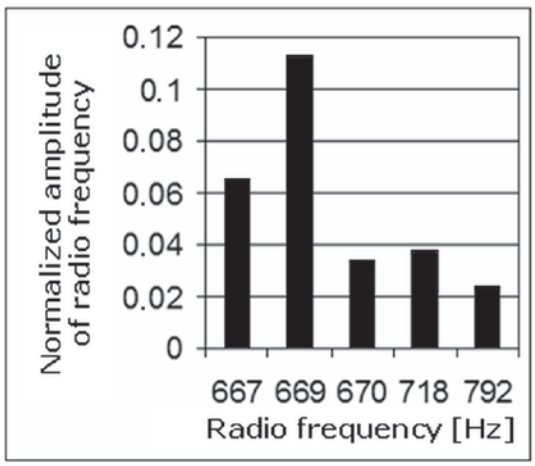

Fig. 3. Selected radio frequencies for difference between spectrum of acoustic signal of faultless induction motor and spectrum of acoustic signal of induction motor with faulty rotor bar with the use of SMoFS-10

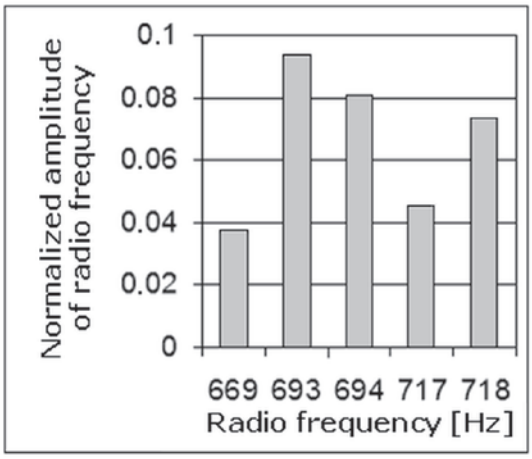

Fig. 4. Selected radio frequencies for difference between spectrum of acoustic signal of faultless induction motor and spectrum of acoustic signal of induction motor with two faulty rotor bars with the use of SMoFS-10

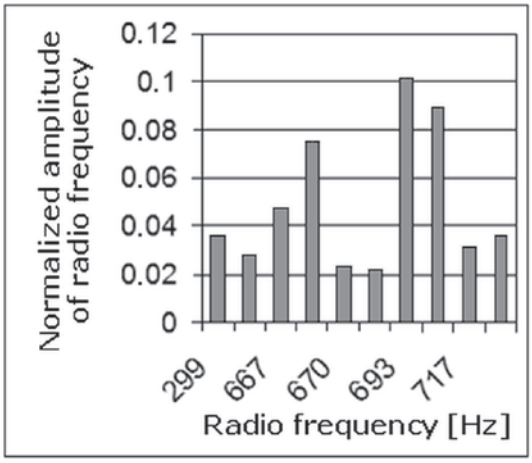

Fig. 5. Selected radio frequencies for difference between spectrum of acoustic signal of induction motor with faulty rotor bar and spectrum of acoustic signal of induction motor with two faulty rotor bars with the use of SMoFS-10

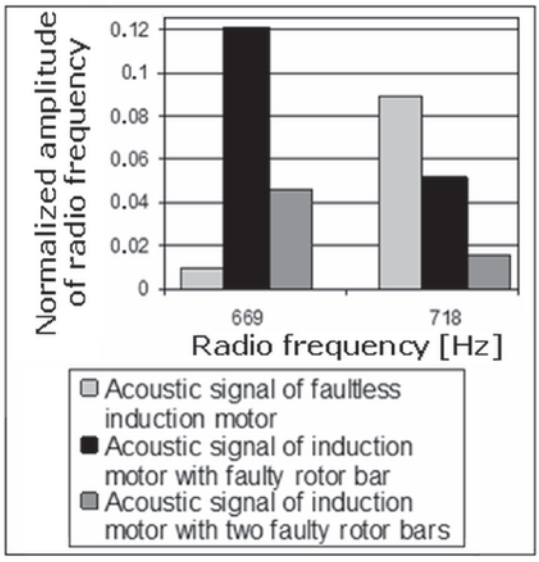

Fig. 6. Selection of common radio frequencies for 3 states of induction motor (669 and 718 Hz) with the use of SMoFS-10

tor: 669 and 718 Hz (Fig. 6). Selected amplitudes of frequencies 669 and 718 Hz were used to form feature vector.

2.3. Linear Support Vector Machine

Last step of signal processing was classification. Scientists proposed many methods of classification in the literature [2, 4, 7, 9, 16, 17, 21, 23, 26, 31-34]. Linear Support Vector Machine (LSVM) classified feature vectors by finding the best hyperplane that separated all vectors of one class from those of the other class. The considered hyperplane had the largest margin between the two classes [24, 37]. There were two more hyperplanes parallel to the separating hyperplane. They cut through the closest training examples (support vectors) on either side. These hyper-planes were called "support hyperplanes". They contained support vectors. A set of vectors $\mathbf{x}_i$ with their categories y_i were training examples.

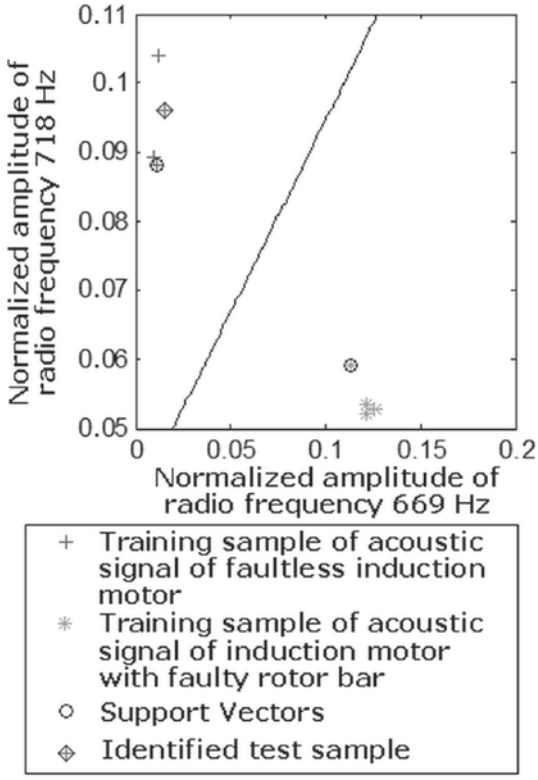

Fig. 7. Identification of test sample (acoustic signal of faultless induction motor) with the use of SMoFS-10, LSVM and training samples of acoustic signal of faultless induction motor and acoustic signal of induction motor with faulty rotor bar

A hyperplane was defined by following formula:

$$<\mathbf{w},\mathbf{x}> + b = 0, \tag{4}$$

where $\mathbf{w} \in R_d$, $\mathbf{x}_i \in R_d$, R_d (datapoints), $y_i = \pm 1$, $<\mathbf{w},\mathbf{x}>$ was the inner product of $\mathbf{w}$ and $\mathbf{x}$, b was real.

Solution of this problem was to find $\mathbf{w}$ and b that minimize $||\mathbf{w}||$ for all training examples $(\mathbf{x}_i, y_i)$,

$$y_i(<\mathbf{w},\mathbf{x}_i> + b) \geq 1. \tag{5}$$

More about Linear Support Vector Machine could be found in literature [24, 37]. Identification of test sample of acoustic signal of faultless induction motor was showed (Fig. 7, 8).

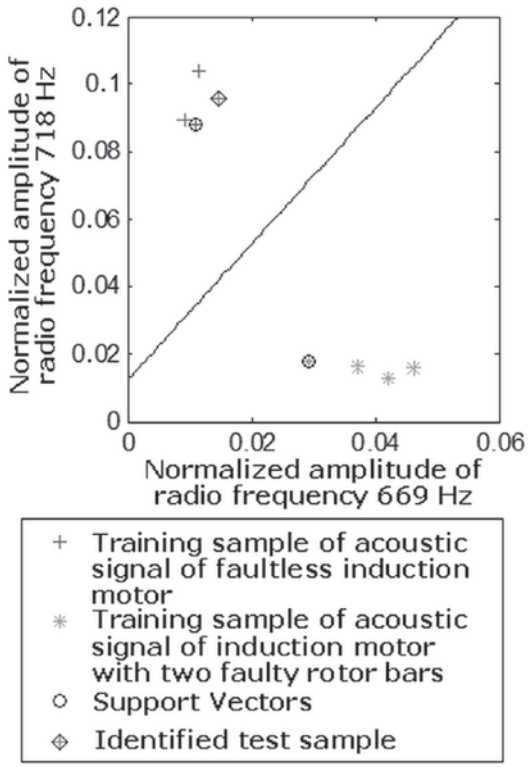

Fig. 8. Identification of test sample (acoustic signal of faultless induction motor) with the use of SMoFS-10, LSVM and training samples of acoustic signal of faultless induction motor and acoustic signal of induction motor with two faulty rotor bars

3. Analysis of acoustic signals of three phases induction motors

Three loaded three phases induction motors were used in analysis. These motors were the same. Open loop control system was used for these motors. Each of them had operational parameters: U_N=220/380 V (Δ/Y), I_N=2.52/1.47 A (Δ/Y), P_N = 0.55 kW, n_N = 1400 rpm, where U_n - nominal stator voltage, I_n - nominal stator current, P_N - motor power, n_N - rotor speed.

The first motor was faultless induction motor. The second motor was induction motor with faulty rotor bar. The third motor was induction motor with two faulty rotor bars (Fig. 9).

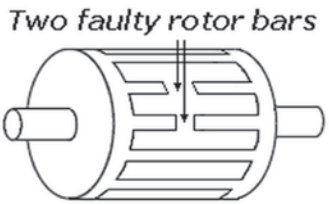

Fig. 9. Squirrel-cage rotor of three phases induction motor with two faulty rotor bars

In the pattern creation process 12 five-second training samples were processed by proposed method of acoustic signal recognition. These training samples were used to group data.

The identification process used 60 samples (20 samples for each class). These samples were used to evaluate efficiency of recognition of acoustic signal. This efficiency was defined as:

$$E = \frac{NoPITS}{NoTS} 100\% \ , \tag{6}$$

where *NoPITS* – number of properly identified test samples of specific class used in the identification process, *NoTS* – number of test samples of specific class used in the identification process, *E* – efficiency of recognition of acoustic signal of specific class.

$$TEoRoAS = \frac{E_1 + E_2 + E_3}{3} \ , \tag{7}$$

where *TEoRoAS* - Total efficiency of recognition of acoustic signal, E_1 - efficiency of recognition of acoustic signal of faultless induction motor, E_2 - efficiency of recognition of acoustic signal of induction motor with faulty rotor bar, E_3 - efficiency of recognition of acoustic signal of induction motor with two faulty rotor bars.

Table 1 presented efficiency of recognition of acoustic signal of three phases induction motor depending on state of induction motor. It also presented total efficiency of recognition of acoustic signal of induction motor.

On the basis of table 1 it can be noticed that *E* was in the range of 90-100 % and *TEoRoAS* was 96.66 %.

Table 1. Results of recognition of acoustic signal of three phases induction motor with the use of SMoFS-10 and LSVM

State of induction motor	*E* [%]
Faultless motor	100
Motor with faulty rotor bar	90
Motor with two faulty rotor bars	100
	TEoRoAS [%]
3 analyzed states of motor	96.66

4. Conclusions

Paper presented method of recognition of acoustic signal of three phases induction motor. This method contained methods of processing such as: FFT, SMoFS-10 and LSVM. SMoFS-10 was also new method of feature extraction. Analysis of acoustic signals showed that proposed solution was good to recognize state of induction motor. Total efficiency of recognition of acoustic signal of induction motor was equal to 96.66 % for 3 analyzed states of motor. Presented method can be used for early diagnostics of specific induction motors (the same size, operational parameters). It can be used for other electric motor when the patterns are properly selected. Moreover method based on acoustic signal can be used together with diagnostics methods based on thermal signals and stator current signals. In this way, it can improve the diagnostics of electrical motors.

Acknowledgments

This work has been financed under AGH researcher grant in 2015 (Adam Glowacz).

References

1. Abramov IV, Nikitin YR, Abramov AI, Sosnovich EV, Bozek P. Control and Diagnostic Model of Brushless Dc Motor. Journal of Electrical Engineering-Elektrotechnicky Casopis 2014; 65 (5): 277-282, http://dx.doi.org/10.2478/jee-2014-0044.

2. Alshayeb M, Eisa Y, Ahmed MA. Object-Oriented Class Stability Prediction: A Comparison Between Artificial Neural Network and Support Vector Machine. Arabian Journal for Science and Engineering 2014; 39 (11): 7865-7876, http://dx.doi.org/10.1007/s13369-014-1372-4.
3. Andonova AV, Hinov NL. Thermographic Analysis of a Bridge Power Converter. Journal of Electrical Engineering-Elektrotechnicky Casopis 2014; 65 (6), 371-375.
4. Augustyniak P, Smolen M, Mikrut Z, Kantoch E. Seamless Tracing of Human Behavior Using Complementary Wearable and House-Embedded Sensors. Sensors 2014; 14 (5): 7831-7856, http://dx.doi.org/10.3390/s140507831.
5. Baranski M. New vibration diagnostic method of PM generators and traction motors - detecting of vibrations caused by unbalance. 2014 IEEE International Energy Conference (ENERGYCON 2014); Book Series: IEEE International Energy Conference: 28-32.
6. Baranski M, Decner A, Polak A. Selected Diagnostic Methods of Electrical Machines Operating in Industrial Conditions. IEEE Transactions on Dielectrics and Electrical Insulation 2014; 21 (5): 2047-2054, http://dx.doi.org/10.1109/TDEI.2014.004602.
7. Dudek-Dyduch E, Tadeusiewicz R, Horzyk A. Neural network adaptation process effectiveness dependent of constant training data availability. Neurocomputing 2009; 72 (13-15): 3138-3149, http://dx.doi.org/10.1016/j.neucom.2009.03.017.
8. Duspara M, Sabo K, Stoic A. Acoustic emission as tool wear monitoring. Tehnicki Vjesnik-Technical Gazette 2014; 21 (5), 1097-1101.
9. Dzwonkowski A, Swedrowski L. Uncertainty analysis of measuring system for instantaneous power research. Metrology and Measurement Systems 2012; 19 (3): 573-582.
10. Glowacz A. Diagnostics of Synchronous Motor Based on Analysis of Acoustic Signals with the use of Line Spectral Frequencies and K-nearest Neighbor Classifier. Archives of Acoustics 2014; 39 (2): 189-194.
11. Glowacz A. Diagnostics of DC and Induction Motors Based on the Analysis of Acoustic Signals. Measurement Science Review 2014; 14 (5): 257-262, http://dx.doi.org/10.2478/msr-2014-0035.
12. Glowacz A, Glowacz Z. Diagnostics of DC machine based on analysis of acoustic signals with application of MFCC and classifier based on words. Archives of Metallurgy and Materials 2012; 57 (1): 179-183, http://dx.doi.org/10.2478/v10172-012-0007-6.
13. Glowacz A, Glowacz Z. Diagnostics of induction motor based on analysis of acoustic signals with application of FFT and classifier based on words. Archives of Metallurgy and Materials 2010; 55 (3): 707-712.
14. Glowacz A, Glowacz A, Korohoda P. Recognition of Monochrome Thermal Images of Synchronous Motor with the Application of Binarization and Nearest Mean Classifier. Archives of Metallurgy and Materials 2014; 59 (1): 31-34, http://dx.doi.org/10.2478/amm-2014-0005.
15. Glowacz Z, Kozik J. Detection of synchronous motor inter-turn faults based on spectral analysis of park's vector. Archives of Metallurgy and Materials 2013; 58 (1): 19-23, http://dx.doi.org/10.2478/v10172-012-0144-y.
16. Hachaj T, Ogiela MR. Application of neural networks in detection of abnormal brain perfusion regions. Neurocomputing 2013; 122 (Special Issue): 33-42, http://dx.doi.org/10.1016/j.neucom.2013.04.030.
17. Jun S, Kochan O. Investigations of Thermocouple Drift Irregularity Impact on Error of their Inhomogeneity Correction. Measurement Science Review 2014; 14 (1): 29-34.
18. Krolczyk GM, Nieslony P, Legutko S. Determination of tool life and research wear during duplex stainless steel turning. Archives of Civil and Mechanical Engineering 2015; 15 (2): 347-354, http://dx.doi.org/10.1016/j.acme.2014.05.001.
19. Krolczyk GM, Krolczyk JB, Legutko S, Hunjet A. Effect of the disc processing technology on the vibration level of the chipper during operations. Tehnicki Vjesnik-Technical Gazette 2014; 21 (2), 447-450.
20. Krolczyk JB. An attempt to predict quality changes in a ten-component granular system. Tehnicki Vjesnik-Technical Gazette 2014; 21 (2), 255-261.
21. Kundegorski M, Jackson PJB, Ziolko B. Two-Microphone Dereverberation for Automatic Speech Recognition of Polish. Archives of Acoustics 2014; 39 (3): 411-420.
22. Kulka Z. Advances in Digitization of Microphones and Loudspeakers. Archives of Acoustics 2011; 36 (2): 419-436, http://dx.doi.org/10.2478/v10168-011-0030-z.
23. Mahmood A, Alsulaiman M, Muhammad G. Automatic Speaker Recognition Using Multi-Directional Local Features (MDLF). Arabian Journal for Science and Engineering 2014; 39 (5): 3799-3811, http://dx.doi.org/10.1007/s13369-014-1048-0.
24. MathWorks – MATLAB and SimuLink for Technical Computing 2015; www.mathworks.com.
25. Nadolny K, Kaplonek W. Analysis of Flatness Deviations for Austenitic Stainless Steel Workpieces after Efficient Surface Machining. Measurement Science Review 2014; 14 (4), 204-212, http://dx.doi.org/10.2478/msr-2014-0028.
26. Nafisi H, Abedi M, Gharehpetian GB. Locating Pd in Transformers through Detailed Model and Neural Networks. Journal of Electrical Engineering-Elektrotechnicky Casopis 2014; 65 (2), 75-82, http://dx.doi.org/10.2478/jee-2014-0011.
27. Paydarnia H, Hajiaghasi S, Abbaszadeh K. Improved Structure of PNN Using PCA in Transformer Fault Diagnostic. Arabian Journal for Science and Engineering 2014; 39 (6): 4845-4851, http://dx.doi.org/10.1007/s13369-014-1004-z.
28. Pleban D. Definition and Measure of the Sound Quality of the Machine. Archives of Acoustics 2014; 39 (1): 17-23.
29. Rusinski E, Moczko P, Odyjas P, Pietrusiak D. Investigation of vibrations of a main centrifugal fan used in mine ventilation. Archives of Civil and Mechanical Engineering 2014; 14 (4), 569-579, http://dx.doi.org/10.1016/j.acme.2014.04.003.
30. Stepien K. Research on a surface texture analysis by digital signal processing methods. Tehnicki Vjesnik-Technical Gazette 2014; 21 (3): 485-493.
31. Swedrowski L, Duzinkiewicz K, Grochowski M, Rutkowski T. Use of neural networks in diagnostics of rolling-element bearing of the induction motor. Smart Diagnostics V 2014; Book Series: Key Engineering Materials; 588: 333-342.
32. Turchenko I, Kochan V, Sachenko A, Kochan R, Stepanenko A, Daponte P, Grimaldi D. Simulation modeling of neural-based method of multi-sensor output signal recognition. 2006 IEEE Instrumentation and Measurement Technology Conference Proceedings; Vols 1-5: 1530-1535, http://dx.doi.org/10.1109/IMTC.2006.328653.
33. Valis D, Zak L, Pokora O. Contribution to system failure occurrence prediction and to system remaining useful life estimation based on oil field data. Proceedings of the Institution of Mechanical Engineers Part O-Journal of Risk and Reliability 2015; 229 (1): 36-45, http://dx.doi.org/10.1177/1748006X14547789.
34. Valis D, Pietrucha-Urbanik K. Utilization of diffusion processes and fuzzy logic for vulnerability assessment. Eksploatacja i Niezawodnosc-

Maintenance and Reliability 2014; 16 (1): 48-55.
35. Umasankar L, Kalaiarasi N. Internal Fault Identification and Classification of Transformer with the Aid of Radial Basis Neural Network (RBNN). Arabian Journal for Science and Engineering 2014; 39 (6): 4865-4873, http://dx.doi.org/10.1007/s13369-014-1030-x.
36. Wu RC, Tsai JI, Chiang CT, Ouyang CS. Detection of induction motor operation condition by acoustic signal. 8th IEEE International Conference on Industrial Informatics (INDIN) 2010: 792-797, http://dx.doi.org/10.1109/indin.2010.5549641.
37. Zhang DZ, Xia BK. Soft Measurement of Water Content in Oil-Water Two-Phase Flow Based on RS-SVM Classifier and GA-NN Predictor. Measurement Science Review 2014; 14 (4), 219-226, http://dx.doi.org/10.2478/msr-2014-0030.
38. Zhao Z, Wang C, Zhang YG, Sun Y. Latest progress of fault detection and localization in complex Electrical Engineering. Journal of Electrical Engineering-Elektrotechnicky Casopis 2014; 65 (1): 55-59, http://dx.doi.org/10.2478/jee-2014-0008.

Adam GLOWACZ
AGH University of Science and Technology
Faculty of Electrical Engineering, Automatics
Computer Science and Biomedical Engineering
Department of Automatics and Biomedical Engineering
al. A. Mickiewicza 30, 30-059 Kraków, Poland
e-mail: adglow@agh.edu.pl

Article citation info:
JAKUBOWSKI R. Evaluation of performance properties of two combustor turbofan engine. Eksploatacja i Niezawodnosc – Maintenance and Reliability 2015; 17 (4): 575–581, http://dx.doi.org/10.17531/ein.2015.4.13.

Robert JAKUBOWSKI

EVALUATION OF PERFORMANCE PROPERTIES OF TWO COMBUSTOR TURBOFAN ENGINE

OCENA WŁAŚCIWOŚCI EKSPLOATACYJNYCHDWUPRZEPŁYWOWEGO SILNIKA TURBINOWEGO Z DWIEMA KOMORAMI SPALANIA

This article presents issues connected with modification of a bypass engine with an additional combustion chamber placed between the high pressure and low pressure turbines. At the beginning, on the basis of scientific literature analysis possible benefits were pointed out which follow from modification of a turbofan aircraft engine. First of all, the attention was drawn to a possibility to limit the gas temperature in the exhaust area of a combustion chamber, which helps to reduce NOx in relation to currently used aircraft engines. Then, a design solution scheme of a two combustor engine was presented. It was discussed how this solution modifies the engine cycle. The assumptions and the adopted limitations in the stage of preparing a numerical model of the engine were presented. The main parameters of the engine operating which were used to estimate its functional qualities were characterized. On the bases of an existing high bypass ratio turbofan engine and the assumptions concerning the influence of the mentioned modification of the engine to its internal characteristics performance properties of a two combustor engine in variable performance conditions were determined: for different speeds and flight altitudes. The results were graphically illustrated in the charts in the form of dependences of thrust, specific thrust, fuel consumption and specific fuel consumption vs. the flight speed for different altitudes. In the discussion of the obtained results performance characteristics for standard a high bypass ratio turbofan engine were referred to. On this basis possible benefits which follow from exploitation of the two combustor engine were shown. This engine is characterized by better performance characteristics in comparison to a conventional turbofan engine in the range of transonic velocity. It was pointed out that despite a little higher specific fuel consumption in take-off conditions it can be more economic in further exploitation cycle, which in the case of the aircraft for which it is dedicated, takes place mostly at a transonic velocity at the altitude of about 11 km.

Keywords: *aircraft engine, turbofan engine, modifications and development of a turbofan engine, characteristics of turbofan engine.*

W artykule przedstawiono zagadnienia związane z modyfikacją silnika dwuprzepływowego o dodatkową komorę spalania usytuowaną pomiędzy turbiną wysokiego i niskiego ciśnienia. Na wstępie, na podstawie analizy literatury, wskazano możliwe korzyści wynikające z zastosowania takiej modyfikacji lotniczego silnika dwuprzepływowego. Przede wszystkim zwrócono uwagę na możliwość ograniczenia maksymalnej temperatury spalin w przekroju wylotowym komory spalania w silniku tego typu, przez co istnieje możliwość istotnej redukcji NOx w odniesieniu do współcześnie eksploatowanych silników lotniczych. Następnie przedstawiono schemat rozwiązania konstrukcyjnego silnika z dwiema komorami spalania. Omówiono, jak takie rozwiązanie modyfikuje obieg silnika. Przedstawiono założenia i przyjęte ograniczenia na etapie przygotowywania modelu numerycznego silnika oraz scharakteryzowano główne parametry pracy silnika, które wykorzystano do oceny jego właściwości eksploatacyjnych. Na bazie danych istniejącego silnika dwuprzepływowego o dużym stopniu dwuprzepływowości oraz przyjętych założeń odnośnie wpływu omawianej modyfikacji silnika na jego charakterystyki wewnętrzne, wyznaczono osiągi silnika z dwiema komorami spalania w zmieniających się warunkach eksploatacji tj. dla różnej prędkości i wysokości lotu. Wyniki zilustrowano graficznie na wykresach w postaci zależności ciągu, ciągu jednostkowego, zużycia paliwa i jednostkowego zużycia paliwa od prędkości lotu dla różnych wysokości. W dyskusji uzyskanych wyników odniesiono się do charakterystyk eksploatacyjnych dla standardowych silników dwuprzepływowych o dużym stopniu dwuprzepływowości. Na tej podstawie wykazano możliwe korzyści wynikające z eksploatacji silnika z dwiema komorami spalania. Silnik ten cechuje korzystniejszy przebieg charakterystyk eksploatacyjnych od klasycznego silnika dwuprzepływowego w zakresie prędkości okołodźwiękowych. Zaznaczono, że pomimo nieco wyższych wartości jednostkowego zużycia paliwa w warunkach startowych, może on być ekonomiczniejszy w całym cyklu eksploatacyjnym, który w przypadku statków powietrznych do których jest dedykowany, odbywa się w zdecydowanej większości czasu z prędkością okołodźwiękową na wysokości ok 11 km.

Słowa kluczowe: *silnik turbinowy, silnik dwuprzepływowy, modyfikacje i rozwój silnika turbinowego, charakterystyki silnika turbinowego.*

1. Introduction

In air-transport two or three shafts high bypass ratio turbofan engines and turboprop engines are the dominant kind of propulsion. Both of the types found their use in aircrafts because of their profitable performance characteristics. First of all, this is low specific fuel consumption, which is about 20% of the value of this parameter for turbojet engines [15, 18].

Turboprop engines are characterized by a lower specific fuel consumption than high bypass turbofan engines. However, a significant limitation of these engines is a lower cruise speed which follows from limitations connected with a significant decrease of propellers per-

(*) Tekst artykułu w polskiej wersji językowej dostępny w elektronicznym wydaniu kwartalnika na stronie ***www.ein.org.pl***

formance when flight speed closes to transonic velocities. Moreover, these propulsion systems make more noise, that is why they are more burdensome for the environment [3, 17].

At present, high bypass turbofan engines are the best solution for long range passenger and transport aircrafts. That is why, further steps have been undertaken by engine manufacturers in order to improve performance properties of these propulsions. Challenges which are put forward are as follows: to decrease fuel consumption, to decrease environmental pollution and noise at maintaining the highest level of reliability in a long-term exploitation [15]. For this reason, the scientists who deal with aircraft engines undertook this research topic.

One of the areas of activities is to find a method of selection of a power unit to an aircraft taking into consideration flying tasks performed by the aircraft. In this respect, works use the methods of optimization and multicriteria optimization in order to determine solutions of the propulsion unit which best meets tactical and technical requirements as for designed aircraft [13, 21, 22].

Another area of research covers the issue of improvement and development of turbofan engines design. The works which deal with this area include: determination of methods of reduction of fuel consumption and emission of pollution to the environment, identification of sources of noise in the engine and possibilities of its limitation, strength tests of selected elements of the engine and whole units in dynamic states, as well as modern materials and manufacturing technologies used in aircraft industry [3, 14, 16, 19, 20].

The research on modification of the cycle of a turbofan engine in order to increase its properties has been carried out for several years. It covers the analysis and energy estimation of the operating cycle of the engine obtained as a result of modifications of the processes taking place in it. Currently, the main streams of modifications of the engine cycle concern additional interstage turbine burning [12, 17], or burning in the additional combustor situated between the high and low pressure turbines in a two-spool engine [5, 7, 9, 10]. The results of these works show that such a solution should be more beneficial from the point of view of energy because in a certain part the heating process should be similar to isothermal process which occurs in the cycle of the highest performance – the Carnot cycle [17]. From the ecological point of view, it is shown that practical implementation of the suggested solutions will enable obtainment of maximal temperature of the engine cycle at maintaining unchanged performance, which should have a beneficial influence of limitation of emission of nitrogen oxides [9, 10].

The engine with an additional combustion chamber between the turbines seems to be a variation which is likely to implement in the future (currently, there is an industrial gas turbine manufactured by ABB). That is why a conception of a two combustor engine and the results of its performance characteristics will be considered. The reference point will be a high bypass turbofan engine on the basis of which simulation calculations of the modified engine will be carried out.

2. A turbofan engine with an additional combustion chamber between the high and low pressure turbines

High bypass turbofan engines are currently produced as two- or three-spool arrangement. In two-spool arrangement the fan and the low-pressure compressor are powered by the high pressure turbine. In three-spool arrangement the fan, the high pressure compressor and the low pressure compressor are powered by separate turbines. The combustion chamber is placed between the high pressure compressor and the high pressure turbine. Energy of the exhaust gases should be enough to power the turbines and to produce the thrust, that is why the temperature of the gases which leave the combustor should be relatively high. Currently, it is about 1700 – 1800 K, which causes that the turbines have to be made of appropriate materials and additionally should be equipped with an advanced cooling system of disks and blades [2, 4, 8, 16, 18]. The cooling system makes the design of the engine more difficult and causes that a large part of the compressed air should be used to cool the turbine's blades, that is why it does not take an active part in producing power in the turbine [2, 4]. As a result, the decrease of temperature and pressure in the turbine is greater in comparison to the work of the engine with similar operating parameters in the case when the turbine does not require cooling. As a result, as it is mentioned in work [2], there is a decrease of the engine's performance.

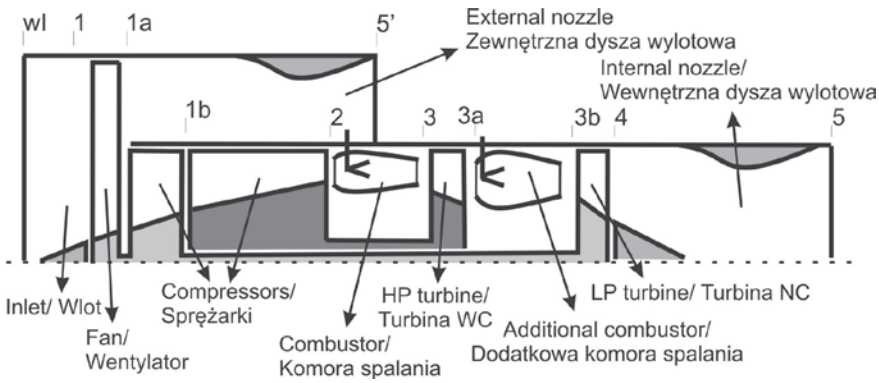

Fig. 1. Scheme of a turbofan engine with an additional combustion chamber between the turbines

The analysis of operation of a two-spool turbofan engine with an additional combustion chamber between the turbines, which scheme is shown in Figure 1, is presented. The additional combustor is placed between the high pressure turbine and the low pressure turbine, due to additional gas heating. It allows limiting the amount of heat added to the main combustor. It was assumed that the temperature of the exhaust gases going out of both combustors would be up to 1300 K. Such a solution allows eliminating the use of advanced systems to cool the turbines, including the internal cooling of the disks and the blades. It also significantly limits the amount of air bleeding of the engine's compressor for cooling purposes [2, 18]. Additional benefits which follow from such a solution are: decreasing the level of complicacy of the design of the disks and blades of the turbine (they are made without internal holes to transport the cooling air), that is why it helps to reduce manufacturing costs and increase the time of reliable work of the unit [11].

3. The analysis of the cycle and performance of the engine with an additional combustor between the turbines

The scheme of the cycle of the engine with two combustors is presented in Figure 2. A significant modification in a description of a numerical model of the cycle is that the total heat added to the engine is a sum of heat added in the main and additional combustors, which is presented as:

$$Q_t = Q_{B\_t} + Q_{IT\_t} \tag{1}$$

where: Q – heat added to the engine,
indexes: t – for total parameters, B – main combustor, IT – additional combustor between the turbines (inter turbines).

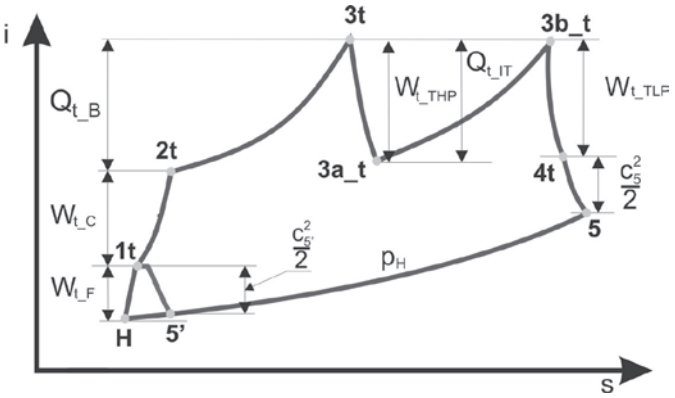

Fig. 2. Enthalpy-entropy diagram of the engine with two combustors, indications: W_t – work, Q_t – heat, c – gases flow velocity, 1,2…5 – indications of the engine's cross-section according to Fig. 1

The heat added in the main combustor is determined from the equation:

$$Q_{B\_t} = \frac{m_{f\_B}}{m_I} h\eta_B = C_p\left(T_{3t} - T_{2t}\right) \tag{2}$$

However, the heat added in an additional combustor is determined as:

$$Q_{IT\_t} = \frac{m_{f\_IT}}{m_I} h\eta_{IT} = C_p\left(T_{3b\_t} - T_{3a\_t}\right) \tag{3}$$

where:

m_{f_B}, m_{f_IT} – mass flow of the fuel in the main and additional combustors,

m_I – mass flow of the air in the entry to the core engine,

h – caloric value of the fuel,

η_B, η_{IT} – thermal efficiency of the combustor and the inter turbine burner,

C_p – specific heat at constant pressure,

T – temperature.

Total mass flow of the fuel in the engine is presented by the equation:

$$\sum m_f = m_{f\_B} + m_{f\_IT} = \left(m_I Q_t\right) / \left(h\left(\eta_B + \eta_{IT}\right)\right) \tag{4}$$

The engine's thrust is calculated as:

$$F = m_5 c_5 + m_I \alpha c_{5'} - m_I\left(1+\alpha\right)V \tag{5}$$

Specific thrust:

$$F_S = \left(\frac{m_5}{m_I} c_5 + \alpha c_{5'} - \left(1+\alpha\right)V\right) \Big/ (1+\alpha) \tag{6}$$

where:

F – thrust,

F_s – specific thrust,

m_5 – mass flow of the core engine exhaust gases at the outlet nozzle,

c_5, $c_{5'}$ – gas velocity in the exhaust area of the internal and external nozzle,

α – bypass ratio,

V – flight velocity.

Specific fuel consumption is determined from the equation:

$$S_f = \sum m_f / F \tag{7}$$

Specific fuel consumption and specific thrust are very important parameters which determine performance properties of an engine. Low specific fuel consumption is of special importance from the point of view of exploitation. This indicator determines the costs which are directly connected with the tasks performed by an aircraft. Low specific fuel consumption causes that less fuel is needed to perform a certain task, which reduces the flight costs, and, on the other hand, at a specified take-off mass of an aircraft it increases the possible commercial weight [13]. Lower fuel consumption also has an ecological aspect, because it causes a limitation of a quantity of exhaust products emitted to the environment [8].

4. Determination of basic design parameters of a turbofan engine with an additional combustor

The data for the GE90-85B turbofan engine were used to define basic design parameters of the engine [23]. This engine's bypass ratio is 8.1, fan pressure ratio is 1.65, low pressure compressor pressure ratio is 1.141, and total pressure ratio of the engine is 40.4.

It was stated in work [7] that the cycle of a two combustor turbofan engine can be optimized in order to meet both criteria: maximum specific thrust and minimum specific fuel consumption. That is why in the analyzed engine with an additional combustor it was assumed that the bypass ratio, the fan and the low pressure compressor pressure ratio are similar to the GE90-85B engine. However, the value of the total compression ratio was determined through optimization of the two combustor turbofan engine cycle regarding the criterion of maximum specific thrust and minimum specific fuel consumption.

The values of the internal engine processes coefficients were assumed on the basis of the data presented in work [23]. The value of coefficients used to describe the processes in the additional combustor were assumed on a lower level than for the main combustor. By this way the pressure loss coefficient is 96% (99% for the main combustor), and the combustion efficiency is 96.5% (99% for the main combustor). Such an assumption follows from the fact that in the additional combustor there would be worse conditions for the process due to a higher flow velocity and that instead of the air a mixture of exhausts and air inflow to the additional combustor.

In calculations of gas properties in the engine control sections a zero-dimensional model presented in works [6,8,18] was used, which was adjusted to the requirements of calculations for the engine with two combustors according to the correlations presented in Part 3. In order to increase precision of the calculation a gas flowing though the engine was assumed as semi-perfect; its model was taken from work [1].

The value of total pressure ratio of the engine with an additional combustor on account of the cycle optimization was assumed to be 26.36 (the GE-90 engine's total pressure ratio is 40.4), which cases that the high pressure compressor pressure ratio is 14 at the assumed values of the compression ratio of the low pressure shaft.

For the selected parameters of the engine work the total temperature and pressure distribution in engine sections are presented in Figure 3. The following performance parameters of the engine were determined: thrust and specific fuel consumption. In take-off conditions the engine's specific thrust is 286.2 Ns/kg, specific fuel consumption

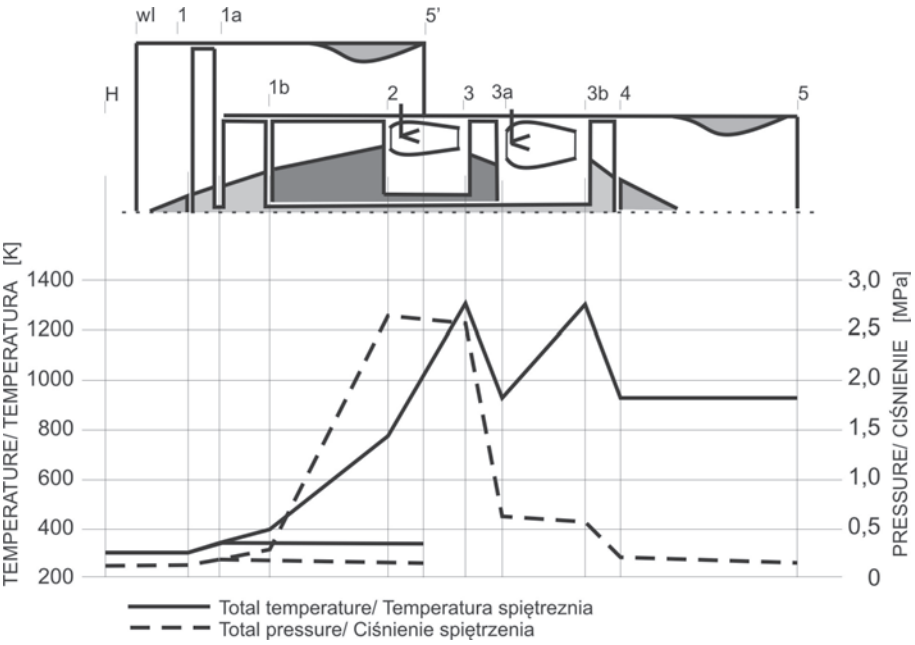

Fig. 3. Diagram of total temperature and pressure distribution in the engine control sections

Table 1. Comparison of basic parameters determined for the two combustor engine and data for the GE90-85B engine [23] for take-off condition

	Two-combustor engine	GE90-85B engine
Total pressure ratio	26.4	40.4
Air mass flow [kg/s]	1350	1350
Thrust [kN]	386.4	375.3
Specific thrust [Ns/kg]	286.2	278.1
Specific fuel consumption [kg/daN/h]	0.344	0.285
Fuel consumption [kg/s]	3.69	2.99

is 0.344 kg/daN/h, thrust is 386.4 kN and fuel consumption is 3.69 kg/s. Comparison of basic parameters of the engine with an additional combustor and the data for the GE90-85B engine are presented in Table 1.

The determined values show that the two-combustor engine has a similar thrust. However, it has a higher specific fuel consumption. This unfavorable effect can be caused by two reasons. Firstly, too low coefficients of the processes in the additional combustor were assumed. This has a significant influence on the increase of the specific fuel consumption, which can be deducted on the basis of the research presented in work [6]. Secondly, the increase of the turbine performance due to elimination of cooling processes was not taken into account. These issues will be analyzed in the next scientific research.

5. Flight performance of a two-combustor engine

A numeric model of an engine was developed in the Matlab environment. It was done in order to determine the influence of flight conditions on a two combustor turbofan engine performance which follow from the area of exploitation of aircraft engines. The parameters which determine performance properties of the engine were defined earlier and they were: thrust, specific thrust, fuel consumption and specific fuel consumption. Changes of the ambient parameters with the altitude were regarded according to the ISA (International Standard Atmosphere) model.

At the stage of developing the model for variable conditions of the flight it was assumed that the pressure ratio of the fan and compressors and expansion of the turbines would not change. It is correct when the engine's operation for constant point of characteristics expressed by corrected parameters. It follows from this assumption that:

– corrected mass flow of the air in the fan and the compressor is constant, i.e. a condition for the fan is fulfilled:

$$m\frac{\sqrt{T_{Ht}(M_a,H)}}{p_{Ht}(M_a,H)} = m_{obl}\left(\frac{\sqrt{288}}{101325}\right) \tag{8}$$

a condition for the high pressure compressor is fulfilled:

$$m_I\frac{\sqrt{T_{1at}(M_a,H)}}{p_{1at}(M_a,H)} = m_{I\_obl}\left(\frac{\sqrt{T_{1at\_obl}}}{p_{1at\_obl}}\right) \tag{9}$$

– corrected rotation speed of the low and high pressure rotors are constant, i.e.

$$\frac{n_{NC}(M_a,H)}{\sqrt{T_{Ht}(M_a,H)}} = const \tag{10}$$

$$\frac{n_{WC}(M_a,H)}{\sqrt{T_{1bt}(M_a,H)}} = const \tag{11}$$

– turbomachinery efficiencies do not change.

On the basis of the assumptions, the mass flow of the inlet air into the engine in the function of velocity and flight altitude was determined from the equation (8), and the mass flow of the air inlet into the core engine was determined from the equation (9). The equations (10) and (11) were used to estimate real rotors speed, and then to determine the temperature value of the gases in the inlet section of the high and low pressure turbines. In order to do it a criterion of constant corrected rotation speed of the high pressure turbine rotor was used:

$$\frac{n_{WC}(M_a,H)}{\sqrt{T_{3t}(M_a,H)}} = const \tag{12}$$

Alike for the rotor of the low pressure turbine:

$$\frac{n_{NC}(M_a,H)}{\sqrt{T_{3bt}(M_a,H)}} = const \tag{13}$$

Equality of the real rotation speed of the compressor or the fan and the turbine on the same spool should be fulfilled. From the combination of equation (10) and (13) as well as (11) and (12) dependences for the temperature of the exhaust gases from the main combustor were related as:

$$T_{3t}(M_a,H) = T_{3t\_obl}\frac{T_{1bt}(M_a,H)}{T_{1bt\_obl}} \tag{14}$$

and the temperature of the exhaust gases from the additional combustor were related as:

$$T_{3bt}\left(M_a,H\right)=T_{3bt\_obl}\frac{T_{Ht}\left(M_a,H\right)}{288} \tag{15}$$

where:

$T_{3t}(M_a, H)$ – total temperature of gas at the combustor's outlet for different flight speeds Ma and altitude H,

$T_{3bt}(M_a, H)$ – total temperature of gas at the additional combustor's outlet for different flight speeds Ma and altitude H,

T_{3bt_obl} – total temperature of gases at the combustor's outlet in design conditions

$T_{Ht}(M_a, H)$ – total temperature of gas in the inlet to the engine which is determined from the equation:

$$T_{Ht}\left(M_a,H\right)=T_H\left(H\right)\left(1+\frac{k-1}{2}M_a^2\right) \tag{16}$$

On the basis of the presented assumptions and the developed numerical model performance of the two combustor turbofan engine versus flight speed and altitude were determined. Some of them are presented in Figure 4.

The presented results of the simulation of the engine's operation were aborted because for the given altitude further increase of the flight speed caused the necessity to exceed permissible gas turbine inlet temperature. The program of controlling the engine should guarantee maintenance of a constant temperature in its further operating range, however, the assumptions accepted at the level of development of the model do not allow continuation of reliable calculations for these conditions of the engine's operation. Characteristics of gases temperature in the outlet section of the main combustor in the function of flight speed and altitude were presented in Figure 5. For the additional combustor the temperature diagram in the outlet section is similar.

On the basis of the determined values of the thrust in the function of the flight altitude it is possible to state that for bigger altitude levels, when the speed reaches about 0.5 Ma, the engine thrust after initial decrease starts increasing. This differentiates the two combustor turbofan engine from a conventional turbofan where thrust characteristics in a whole speed range decrease [18].

It is also reflected in the specific fuel consumption vs. altitude and flight speed performance which for a conventional high bypass turbofan engine is much different when the speed gets close to the speed of sound. In a two combustor engine due to the increase of thrust at higher speeds, specific fuel consumption increases slower. This shows that the performance of a two combustor turbofan engine in flight

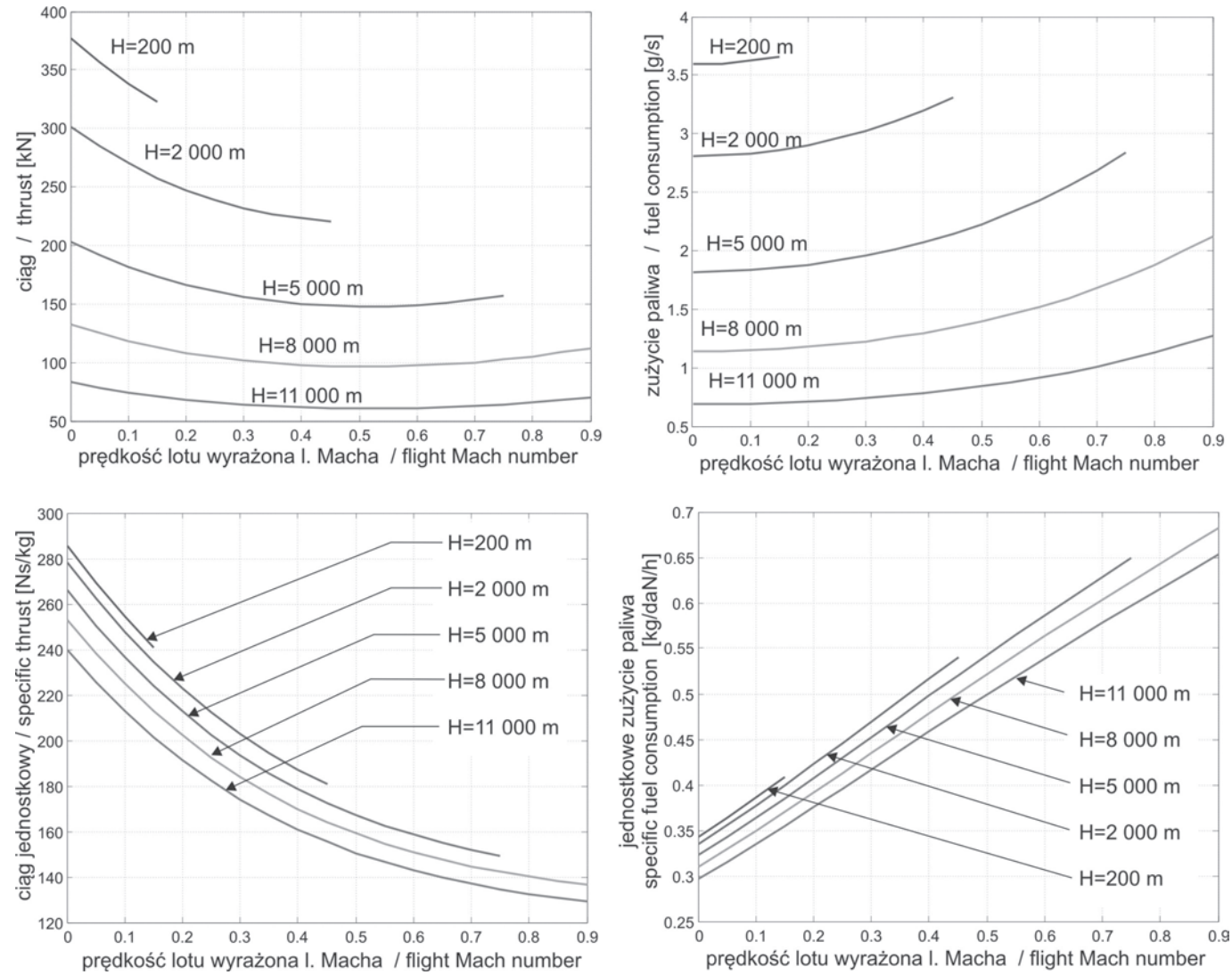

Fig. 4. Dependence of selected performance characteristics of a two combustor turbofan engine for different flight speeds and altitude (H – altitude)

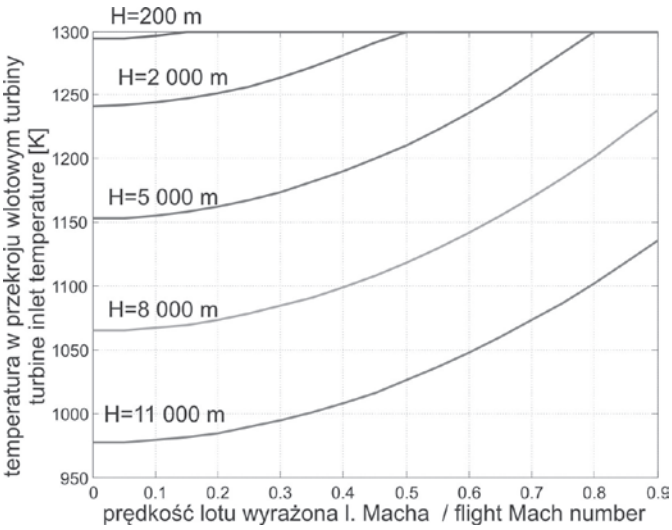

Fig. 5. Gas turbine inlet temperature of a two combustor turbofan engine vs. flight speeds and altitude (H – altitude)

range operating conditions (altitude about 11 km, speed about 0,8 Ma) should be more beneficial than those of a conventional turbofan.

6. Summary and conclusions

The presented analysis showed that the two combustor engine can be an interesting solution of modification of a conventional turbofan engine for airliners. It requires a use of an additional combustor placed between the high and low pressure turbines. However, due to this solution it would be possible to decrease maximal temperature of gases in the high pressure turbine inlet. As a result of this it should be done an increase of reliability and life time of core engine structures, simplification of manufacturing technology of the turbines and reduction of NOx emission.

The results show that the two combustor engine has a smaller value of a total pressure ratio (a smaller compressor) in order to produce the same take-off thrust at the same air flow than conventional turbofan. A smaller pressure ratio causes an increase of a specific fuel consumption in take-off conditions. However, in the range of the flight with high speeds the performance of a two combustor engine are more beneficial that those of a conventional turbofan engine. It shows that this engine can be characterized by lower specific fuel consumption in cruise conditions at speeds close to those at which modern transport and passenger aircrafts fly.

References

1. Guha A. An efficient generic method for calculating the properties of combustion products. Proceedings of the Institution of Mechanical Engineers 2001; A3(215): 375-387, http://dx.doi.org/10.1243/0957650011538596.
2. Horlock J H, Watson D T, Jones T V. Limitations on Gas Turbine Performance Imposed by Large Turbine Cooling Flow. Journal of Engineering for Gas Turbines and Power 2001; 123: 487-494, http://dx.doi.org/10.1115/1.1373398.
3. Huff D L. NASA Glenn's Contributions to Aircraft Engine Noise Research. Journal of Aerospace Engineering 2013; 2(26): 218-250, http://dx.doi.org/10.1061/(ASCE)AS.1943-5525.0000283.
4. Jakubowski R. Modeling and analysis of jet engine with cooling turbine. Journal of KONES Powertrain and Transport 2012; 2(19): 235-243.
5. Jakubowski R. Two-Combustor Turbofan engine Performance Analysis. Journal of KONES Powertrain and Transport 2014; 3(21): 141-148, http://dx.doi.org/10.5604/12314005.1133191.
6. Jakubowski R, Orkisz M. Wpływ zmian procesów przepływowo-cieplnych w silniku turbinowym na jego charakterystyki użytkowe. Eksploatacja i Niezawodnosc - Maintenance and Reliability 2002; 2(14): 4-25.
7. Jakubowski R, Orkisz M, Wygonik P. Preliminary Analysis of Two Combustors Turbofan Engine. Journal of KONES Powertrain and Transport 2013; 2(20):175-180.
8. Lefebvre A H. Gas Turbine Combustion 3th ed. Taylor and Francis Group, 2010, http://dx.doi.org/10.1201/9781420086058.
9. Liew K H, Urip E, Yang S L. Parametric Cycle Analysis of a Turbofan with Interstage Turbine Burner. Journal of Propulsion and Power 2015; (3)21: 546-551, http://dx.doi.org/10.2514/1.2546.
10. Liew K H, Urip E, Yang S L, Mattingly J D, Marek C J. Performance Cycle Analysis of a Two-spool Separate-exhaust Turbofan with Interstage Turbine Burner. Journal of Propulsion and Power 2006; 2(22): 411-416, http://dx.doi.org/10.2514/1.13394.
11. Lin T, Lee J, Lwin T. Integrated approach for rotor blade manufacturing cost estimate. Aircraft Engineering and Aerospace Technology 2011; 4(83): 235-244, http://dx.doi.org/10.1108/00022661111138657.
12. Liu F, Sirignano W A. Turbojet and Turbofan Engine Performance Increases Through Turbine Burners. Journal of Propulsion and Power 2001; 3(17): 695-705, http://dx.doi.org/10.2514/2.5797.
13. Majka A. Multiple objective optimization of the power unit for a very light jet. Aircraft Engineering and Aerospace Technology 2014; 3(86): 234-241.
14. Merkisz J, Markowski J, Pielecha J. Emission tests of the F100-PW-229 turbine jet engine during pre-flight verification of the F-16 aircraft. AIR POLLUTION XXI Book Series: WIT Transactions on Ecology and the Environment 2013; 174: 219-230, http://dx.doi.org/10.2495/AIR130191.
15. Peitsch D. Propelling the future – the meaning of ACARE VISION 2050 for the future development of propulsion systems for aircraft. Combustion engines 2011; 4(147): 3-13.
16. Sieniawski J. Nickel and titanium alloys in aircraft turbine engines. Advances in Manufacturing Science and Technology 2003; 3(27): 23-33.
17. Sirignano W A, Liu F. Performance Increases for Gas-Turbine Engines Through Combustion Inside the Turbine. Journal of Propulsion and Power 1999; 1(15): 111-118, http://dx.doi.org/10.2514/2.5398.
18. Walsh P P, Fletcher P. Gas Turbine Performance 2nd ed. Blackwell Publishing and ASME, 2004, http://dx.doi.org/10.1002/9780470774533.
19. Witek L. Simulation of crack growth in the compressor blade subjected to resonant vibration using hybrid method. Engineering Failure Analysis 2015; 49: 57–66, http://dx.doi.org/10.1016/j.engfailanal.2014.12.004.
20. Witek L, Orkisz M, Wygonik P, Musili D N, Kowalski T. Fracture analysis of a turbine casing. Engineering Failure Analysis 2010; 3(18): 914-923.

21. Wygonik P. Engine and multitask airplane integration: criteria of engine parameters selection. Aircraft Engineering and Aerospace Technology 2013; 6(85): 460-466, http://dx.doi.org/10.1108/AEAT-12-2012-0249.
22. Wygonik P. Selection criteria of internal parameters of turbofan engine for the type of multi-task aircraft mission. Combustion Engines 2013; 154(3): 483-488.
23. http://web.stanford.edu/~cantwell/AA283_Course_Material/GE90_Engine_Data.pdf

Robert JAKUBOWSKI
Department of Aircrafts and Aircraft Engines
Rzeszow University of Technology
Al. Powstańców Warszawy 8; 35-959 Rzeszów, Poland
E-mail: robert.jakubowski@prz.edu.pl

Article citation info:
BRIŠ R, GRUNT O. QRA of accidental events initiated by leaks causing a fire in process industries. Eksploatacja i Niezawodnosc – Maintenance and Reliability 2015; 17 (4): 582–590, http://dx.doi.org/10.17531/ein.2015.4.14.

Radim BRIŠ
Ondřej GRUNT

QRA OF ACCIDENTAL EVENTS INITIATED BY LEAKS CAUSING A FIRE IN PROCESS INDUSTRIES

ILOŚCIOWA OCENA RYZYKA PRZYPADKOWYCH ZDARZEŃ WYWOŁANYCH PRZEZ NIESZCZELNOŚCI POWODUJĄCE POŻARY W PRZEMYŚLE PRZETWÓRCZYM

Risk to safety of personnel in process industries is normally modelled by the application of Event Trees, where the risk is defined as a product of event frequency and its consequences. This method is steady state whilst the actual event is time dependent. For example, gas release is an event comprising the size of gas cloud being released, probabilities of ignition, fire or explosion, fatality, escalation to new releases and fire and/or explosion, and the probability of fatality, all varying with time. This paper brings new perspective, how the risk to safety of personnel could be evaluated in dynamic context. A new approach is presented whereby the time-dependent events and the time-dependent probability of fatality are modelled by means of the analytical computation method based on modeling of different accident scenarios by use of the directed acyclic graph (DAG) and Fault Tree Analysis (FTA) method. Using these methods the modeled scenarios change with relevant probabilities at defined times to configurations with appropriate probabilities of fatalities.The paper uses a realistic example from the offshore industry, where different sizes of leak have different probability characteristics. Specifically small, medium and large leaks are evaluated. Based on the dynamic evolution of the probability of fatality, it is concluded that the most dangerous leak is the large one. Probability of fatality caused by the leak increased very rapidly within first 5 minutes. At the end of 5th minute, there is approximately one order of magnitude difference in the probabilities of fatality associated with the respective leak sizes.

Keywords: *hydrocarbon-related fire risk; offshore industry; time-dependent risk modeling; directed acyclic graph.*

Zagrożenie dla bezpieczeństwa pracowników w przemyśle przetwórczym jest zwykle modelowane za pomocą drzewa zdarzeń, gdzie ryzyko jest zdefiniowane jako iloczyn częstotliwości zdarzenia i jego skutków. Metoda ta dotyczy stanu stacjonarnego, podczas gdy rzeczywiste zdarzenie jest zależne od czasu. Na przykład, ulatnianie się gazu jest zdarzeniem, które wiąże się z wielkością obłoku uwalnianego gazu, prawdopodobieństwem zapłonu, pożaru lub wybuchu, śmiertelnością, eskalacją pod kątem dalszego wycieku i pożaru i/lub wybuchu, oraz prawdopodobieństwem ofiar śmiertelnych, w każdym przypadku zależnie od czasu. Niniejsza praca pokazuje nowe podejście do tego, jak zagrożenie dla bezpieczeństwa pracowników może być rozpatrywane w kontekście dynamicznym. Nowe metoda polega na tym, iż zdarzenia zależne od czasu i zależne od czasu prawdopodobieństwo śmiertelności są modelowane za pomocą analitycznej metody obliczeń opartej na modelowaniu różnych scenariuszy wypadków przez zastosowanie skierowanego grafu acyklicznego (DAG) i metody analizy drzewa błędów (FTA). Dzięki zastosowaniu niniejszych metod, modelowane scenariusze zmieniają się wraz z odpowiednimi prawdopodobieństwami w określonych czasach na konfiguracje z właściwymi prawdopodobieństwami śmiertelności. Artykuł wykorzystuje rzeczywisty przykład z branży morskiej, gdzie różne rozmiary wycieku wykazują różne parametry prawdopodobieństwa. Szczegółowo oceniane są małe, średnie i duże wycieki. W oparciu o dynamiczną ewolucję prawdopodobieństwa ofiar śmiertelnych, należy stwierdzić, że najbardziej niebezpieczny jest duży wyciek. Prawdopodobieństwo ofiar śmiertelnych spowodowanych wyciekiem gwałtownie wzrasta w ciągu pierwszych 5 minut. Na koniec 5. minuty, występuje różnica w przybliżeniu o jeden rząd wielkości w prawdopodobieństwie śmiertelności związanej z odpowiednimi wielkościami wycieku.

Słowa kluczowe: *Ryzyko pożarowe związane z węglowodorami; przemysł morski; modelowanie ryzyka w zależności od czasu; skierowany graf acykliczny*

1. Introduction

Process industry, such as an offshore production, exposes personnel to risk of injury or fatality. Probability of fatality in real practical situations depends on many random events that may occur during a potential accident, which are difficult to quantify at a specific time instant or in the course of a time interval. This results in over- or under-estimation of risk.

After several disasters, Quantitative Risk Assessment methods were applied for evaluation of the risk [13] of injury or fatality due to an accident. All events potentially occurring during the accident are quantified, leading to an estimation of the risk of fatality. The quantification of the risk is very often carried out by the application of Event Trees [6]. Event Trees (ET) are relatively simple and easily understood, but there are some disadvantages of using them, such as:

A hydrocarbon-related incident on a processing plant and the response to it by personnel working in the plant are time-dependent events whilst ET is a steady state method. An incident and the subsequent plant response evolve where the branches of the incident and response sub-events are generated throughout the incident. This should be reflected by actions of personnel, with probabilities on both the incident/plant response side and the personnel side. Such interactions in a time-dependent manner are not possible to represent by Event Trees.

The main body of the ET is used for probabilities of events, whilst the probabilities of fatalities associated with the events are normally included as one cumulative number at the right hand end of the ET. This causes difficulties in finding contributions and sources of event-related fatality probabilities, and, in general, the traceability may be difficult. There is a possibility of constructing an ET which would be large enough to include both the events probabilities and the fatalities probabilities associated with each event, but such an ET would be difficult to modify and manage.

It takes time to build an ET and standard ET are often used. These provide a rapid first application, but tend to be rather coarse and their results may not be of a desired accuracy. ET also tends to be difficult to modify, which makes it time-consuming to explore various design alternatives.

In most cases a method capable of modeling dynamic processes is required. In [1], risk analysis of offshore drilling by using Bow-tie analysis and real time barriers failure probability assessment of offshore drilling operation is shown. The need for better failure analysis of operational barriers in the offshore industry resulted in Barrier and Operational Risk Analysis (BORA) project [16] with methodology of BORA presented in [2].

Risk management by taking into account the time-dependence of the event in the consequence assessment, by means of the application of the approach of the dynamic geoevent was presented in [10].

Another method, Monte Carlo (MC) simulation, was used in [7] to identify the most contributing factors to probability of fatality following hydrocarbon leak occurrence on an offshore platform. In last years, Petri Nets (PN) are frequently used as an alternative to ET method. Given lack of the biggest ET limitation, inability to represent dynamic processes, PN often lead to more desirable model of the risk to personnel in process industries. PN can substitute ET in representation of steady-state system. It is entirely possible to convert ET to PN with little difficulty [11]. As probability of event occurrence in PN can be time-dependent, it is also possible to represent a dynamic industry process by PN model based on steady-state representation in form of an ET model [15]. In [5], combination of PN and MC simulation was used to evaluate production availability of a multi-state, multi-output offshore installation with operational loops, where PN provided the necessary flexibility to describe the realistic aspects of system behavior. In [14] Reliability Block Diagrams (RBD) are used as guidelines to build large PN. RBD-driven PN are shown to be very effective in modeling safety systems.

This paper presents a method whereby the time-dependent events and the time-dependent probability of fatality are modeled by means of an analytical method. A practical example and data from a typical offshore hydrocarbon production facility are used to quantify risk of injury or fatality of working personnel. A "Leak (Small, Medium, Large) in Zone 8"(see description of Zone 8 in Section 2) of a typical offshore hydrocarbon production installation is used as this event represents the highest frequency of potential hydrocarbon accidents on the typical offshore facility. The objective is quantification of probability of fatality of a person working and escaping from the separation and compression Zone 8.

The subject of this paper is complex. It is based, however, on data and experience from actual installations and life threatening incidents. The reader is therefore suggested to develop a "picture in the mind" of the typical installation as shown in Figure 1, and the "incident examples". The application and incident basis as well as the detailed description of hydrocarbon-related incident with leaks are presented in Section 2. Section 3 focuses on the application of the analytical computation method based on modeling of scenarios by the use of directed acyclic graph (DAG) and Fault Tree (FTA) methods. The results of the quantification are presented in Section 4. Section 5 presents conclusions reached in this paper.

2. Application example and incident basis

Figure 1 shows an example of typical offshore production installation consisting of a wellhead platform (WHP), production and riser platform (PRP), and accommodation platform (AP), all connected by bridges. The installation is sub-divided into 10 Zones according to the nature of the plant or activities. Hydrocarbons being produced come up from a reservoir onto WHP in the form of multi-phase fluids, which are piped across the bridge to the PRP, where they are separated into oil, gas, and water and sand. Produced oil and gas are piped through risers and pipelines to a terminal located on-shore. Living quarters are provided on the AP, which is connected to PRP by a bridge. The installation is provided with a standby vessel, which would be located 100m away from the installation.

The main risk on the installation is from potential leaks of the produced hydrocarbons on WHP or PRP. The primary escape and evacuation route from the installation is to the AP, where installation personnel evacuate by free-fall lifeboats. The three lifeboats shown in the Figure 1 are of the minimum capacity of the capacity of the installation. The secondary escape and evacuation route is to the WHP, which is equipped with one free-fall lifeboat. The WHP lifeboat capacity would be based on number of personnel on WHP plus PRP at any one time. Tertiary evacuation capacity is provided on WHP and PRP by life rafts.

In case of evacuation the evacuees are transferred by the lifeboats and life-rafts to the standby vessel. There are 36 personnel on the installation working in two 12-hours shifts. 26 persons are technical, who work in various areas of WHP and RPP and 10 service personnel such as cooks, cleaners, etc.

This paper focuses on the hydrocarbon-related risk, whereas the highest risk is in the wellheads and manifolds area on the WHP (Zone 3) and then in the separation and compression area on the PRP (Zone 8). The various areas are segregated by firewalls, blast walls, plated decks, various rooms and by distances.

Leak frequencies in Zone 8 based on statistical observations may be estimated as follows:

Small leaks 609 per 10000 years,
Medium leaks 234 per 10000 years, and
Large leaks 216 per 10000 years.

A leak in Zone 8 would initiate the following actions:

a) Activation of fire & gas (F&G) system, which in turn would simultaneously activate
b) Alarm,
c) Emergency shutdown of process and electrical systems,
d) Blowdown of hydrocarbon plant inventories (see Note),
e) Start of emergency power generation,
f) Start of fire pumps, and
g) Personnel would make their workplace safe and start to escape.

These actions normally happen within the first 1 minute on the leak detection.

The probability of ignition of the leaking hydrocarbon would be minimized by the shut-down and blowdown, but the leaking hydrocarbon may still ignite immediately or with some delay. Immediate ignition of leaking pressurised gas would result in jet fire, whilst a relatively large gas cloud may accumulate and explode following a delayed ignition. Explosions or prolonged jet fires may damage the plant and structures of the installation. Calculations and trials show that personnel should be able to escape to the lifeboats and evacuate from the installation to the sea within 30 minutes after the start of the leak.

2.1. Problem formulation and application example

It is important to know the possible development/escalation of incidents on the installation, and the implication on escaping personnel in first phases of the accident, as personnel may be trapped or injured by collapsing plant or structures with resultant fatalities. Table 1 summarizes such events with associated probabilities for a person working and escaping from separation and compression Zone 8 on Level 2 of the PRP, related to small, medium and large leaks respectively. P_{is}, P_{im} and P_{il}, P_{fs}, P_{fm} and P_{fl}, and P_{es}, P_{em} and P_{el}, denote the respective probabilities of ignition, hydrocarbon-related fatality and escalation to bridge for small, medium and large releases. P_f denotes the probability of fatality related to the escape to sea by jumping into the sea.

In Table 1 composed of data from [12], as for example, an immediate ignition of a medium release with $P_{im} = 0.03$ may result in an immediate fatality of $P_{fm} = 0.1$. As an alternative, the person may escape unhurt from the leak area behind the nearest fire/blast wall and continue to the PRP-AP bridge, but the bridge may lose support due to the fire damage of PRP. As a result, the escaping person may be trapped by the PRP on fire and the damaged bridge and he/she may need to escape by jumping into the sea the secondary route to WHP. In this case, $P_{im} = 0.03$, $P_{em} = 0.1$ and $P_f = 0.7$.

Personnel escaping on the basis of scenarios described in Table 1 may be exposed to an insufficient condition for evacuation (ICFE), which results in fatality, probability which is to be computed. The objective of this paper is quantification of probability of fatality of a person working and escaping from separation and compression Zone 8. This probability is a time dependent function. We are particularly interested in behavior of the function during initial part of the accident. The initial event of the accident is a hydrocarbon leak and we are considering three sizes of the leak: small, medium and large. As Table 1 illustrates, the leak is detected during the 1st minute, personnel start to escape, but the time of ignition varies (with associated probability) and so also varies the time of fatality with its associated probability.

3. Method

One possibility to find the probability of ICFE is the ET method. ET is an inductive logic methods for identifying the various accident sequences [8], which can generate from a single initiating event. The approach is based on the discretization of the real accident evolution in few macroscopic events. The accident sequences which derive are then quantified in terms of their probability of occurrence. But ETs, which are at present widely used for the estimation of risk, are steady state, whilst the configuration and actions of the systems analyzed may change with time, with associated probabilities of the changes and their outcomes. ET is not a good approach for the characterization of dynamic evolution of time dependencies of the probability of ICFE (resulting in fatality). In this paper we use analytical method for this purpose, based on modeling of scenarios by the use of DAG and FTA as well.

Another possibility to solve the problem is using the direct MC simulation method, which is frequently used to solve dynamic problems [9]. The MC simulation method has formally existed since early 1940's, but only with increasing computer technology and power became widely used. The MC method enables modelling of complex processes without the need of making unrealistic simplifying assumptions, as is inevitably done when using analytical methods. With the increasing availability of fast computers, MC methods become more powerful and feasible. The above-mentioned offshore problem was successfully solved by the MC method in [6, 7].

There are several events which can occur. We do not know when they occur or if they occur at all. But we know probability of their occurrence. We can simulate event occurrence times through these probabilities. It is like we build an offshore platform model and study how the system and personnel reacts on different leak size and different ignition times. As this approach would be obviously too expensive, we construct a virtual model which consists of events and their probabilities and coherences between them. The key part of MC method is to define these events, probabilities and coherences (Table 1).

An example of one MC simulation:

Small leak occurred. Alarm was activated. Installation was shut down and depressurization was started. Leak ignited after either 1 or 2 minutes. Person was behind the firewall and survived the explosion. Person started escaping via stairs to the PRP-AP bridge. He succeeded to reach the Accommodation Platform. All events (type of leak, ignition time, persons surviving explosion) which occurred in our example were generated by random from given probabilities. This sequence of events is just one of possible scenarios generated by small leak. We cannot simulate all of them but enough to get sufficiently accurate results obtained by statistical evaluation. But in some cases the application of the direct MC technique however suffers from slow convergence. If possible, analytical method for exact probability quantification may be used.

3.1. Analytical method for exact probability quantification

Main objective of the analytic method is to find the time evolution of the probability of occurrence of a TOP event during a mission time. One example of the TOP event to be analyzed is shown in Figure 2. The TOP event which in real emergency dangerous situation may be an event causing the ICFE (resulting in fatality) is demonstrated by the use of a DAG, originally described in [3]. A graph is composed of nodes and edges that are numbered. The highest node (TOP node) represents the TOP event, probability of which is to be calculated in a time evolution. Internal and terminal nodes represent source events, which are either sub-events (e.g. failure events on subsystems) or terminal events (input events as random failures or accidents). All of the nodes are bounded by edges. Direction of the graph is not explicitly marked in Figure 2 it is given by itself - by projection to vertical direction. The graph is acyclic which means that two immediately bound nodes are connected just by one edge, i.e. it cannot contain feedback loops.

Nodes are numbered in the increasing order beginning from the highest TOP node. Internal numeration of nodes is such that a node cannot be inferior to a node with a greater number.

As Figure 2 shows, terminal nodes of the DAG are marked by black squares. They represent stochastic behavior of input events mostly given by their probability distribution. Internal nodes (non-terminal) are marked by black circles. They represent stochastic behavior of sub-events. A sub-event occurs in a given time point just in the case when the number of active inferior edges (i.e. number of inferior sub-events or terminal events that occurred at the same time point) reaches at least the number in parentheses, otherwise it does not occur. For example, the sub-event marked by 3(1) occurs just in the case when the number of active inferior edges is at least 1, i.e. when either the terminal event 2 (black square 2) or sub-event 6(3) occurs.

The DAG described above can be compared with Fault Tree (FT) or Success Tree, both are frequently used in PRA (Probabilistic Risk Assessment) methodology, where internal nodes represent logic gates. The DAG is more general representation than FT, because basic gates (AND, OR, etc.) do not require specific description but can be introduced uniformly as internal nodes. Fault tree equivalently constructed to the DAG from Figure 2 is demonstrated in Figure 3.

As a first step of the analysis we have to find the time evolution of the probability of ICFE (TOP event) during a mission time, which was fixed to 300 sec (i.e. 5 min). The ICFE may be reached either by Scenario 1, initiated by ignition within interval 0-1 min (node 2(1) in Figure 2), Scenario 2, initiated by ignition within 1-2 min (node 3(1) in Figure 2), or Scenario 3, initiated by the ignition within 2-5 min

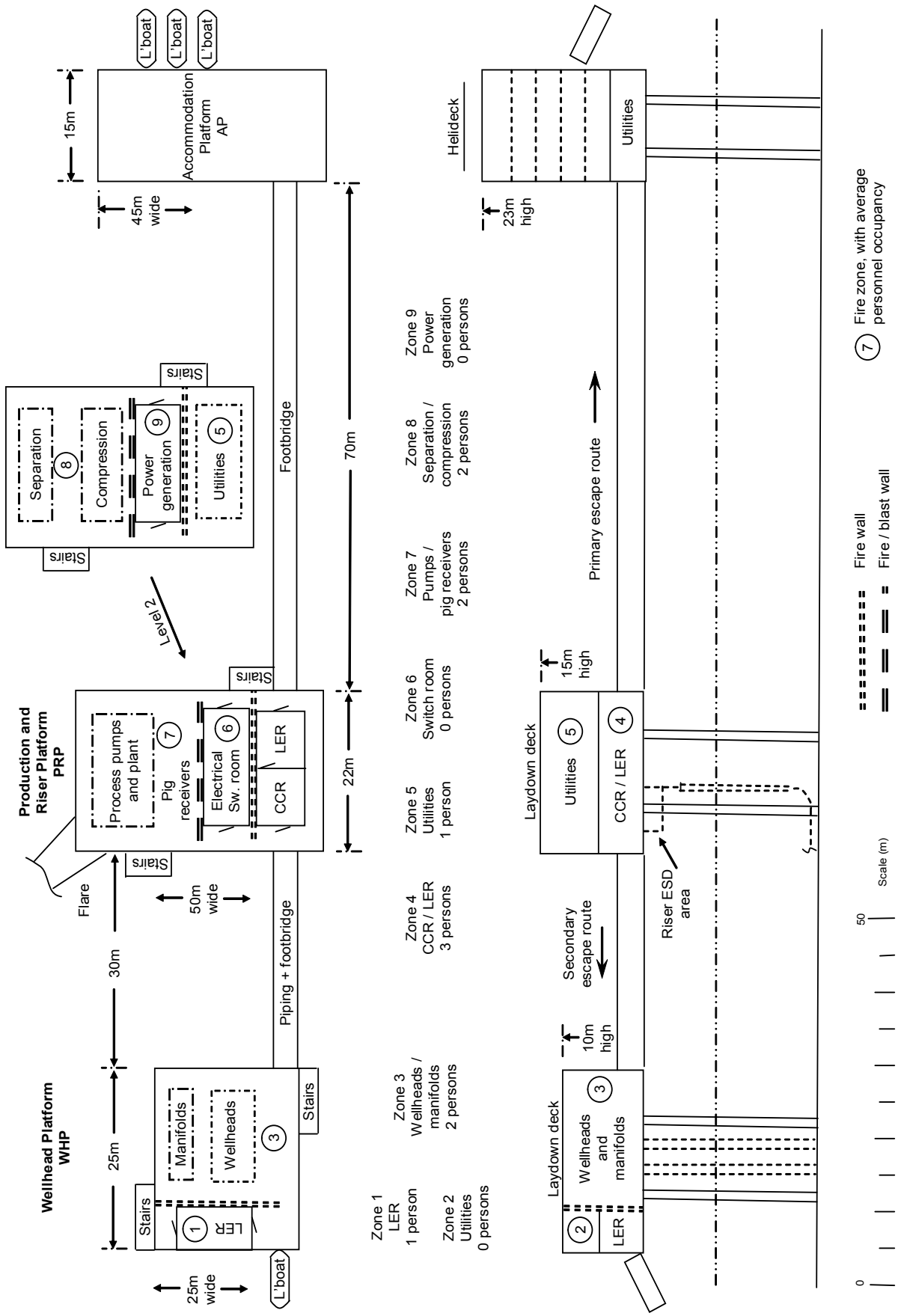

Fig. 1. Typical offshore production installation

Table 1. Person and installation actions at various times [6]

Plant/ Person	0 to 1min	1min to 2mins	2 to 5mins	5 to 8mins	8 to 10mins	10 to 30mins
Plant	-Leak in Zone 8. -Leak detection. -Alarm activated. -Installation shutdown. -Depressurisation starts. -Ignition, Pis=0.004; Pim=0.03; Pil=0.1. -Fire starts.	-Fire continues impinging on flanges and structure. -Installation being depressurised.	-Flanges lose their tightness resulting in escalation to additional fire(s). -Loss of strength of PRP topside resulting in damage of the PRP-AP bridge. Pes=0.05, Pem=0.1, Pel=0.5.			
Person	-Person working in Zone 8. -Making working area safe. -Considering the situation, deciding which way to escape and starting to escape. -Fatality, Pfs=0.05; Pfm=0.1; Pfl=0.3.	-Escaping person located behind the nearest fire/blast wall. -Fatality, Pfs=0.01; Pfm=0.02; Pfl=0.06.	-Escaping via stairs to the PRP-AP bridge. -Person trapped because of the PRP-AP bridge damage and the escalating fires in PRP. -Person escapes to the sea. -Fatality, Pf=0.7.	Escaping person on the PRP-AP bridge. -Person trapped because of the PRP-AP bridge damage and the escalating fires in PRP. -Person escapes to the sea. -Fatality, Pf=0.7.		
Plant	-Leak in Area 8. -Leak detection. -Alarm activated. -Installation shutdown. -Depressurisation starts.	-Ignition, Pis=0.006; Pim=0.04, Pil=0.2. -Fire impinging on flanges and structures. -Installation being depressurised.	-Flanges lose their tightness resulting in escalation to additional fire(s).	-Loss of strength of PRP topside resulting in damage of the PRP-AP bridge. Pes=0.05, Pem=0.1, Pel=0.5.		
Person	-Person working in Zone 8. -Making working area safe. -Considering the situation, deciding which way to escape and starting to escape.	-Escaping person located behind the nearest fire/blast wall. -Fatality, Pfs=0.01; Pfm=0.02; Pfl=0.06.	-Person escaping via stairs to the PRP-AP bridge. -Fatality, Pfs=0.005; Pfm=0.01; Pfl=0.03.	-Escaping person on the PRP-AP bridge. -Person trapped because of the PRP-AP bridge damage and the escalating fires in PRP. -Person escapes to the sea. -Fatality, Pf=0.7.		
Plant	-Leak in Zone 8. -Leak detection. -Alarm activated. -Installation shutdown. -Depressurisation starts.	-Un-ignited leak continues. -Installation being depressurised.	-Ignition, Pis=0.007; Pim=0.05, Pil=0.2. -Fire impinging on flanges and structures. -Installation being depressurised.	-Flanges lose their tightness resulting in escalation to additional fire(s).	-Loss of strength of PRP topside resulting in damage of the PRP-AP bridge. Pes=0.05, Pem=0.1, Pel=0.5.	
Person	-Person working in Zone 8. -Making working area safe. -Considering the situation, deciding which way to escape and starting to escape.	-Escaping person located behind the nearest fire/blast wall.	-Person escaping via stairs to the PRP-AP bridge. -Fatality, Pfs=0.003; Pfm=0.005; Pfl=0.02.	-Escaping person on the PRP-AP bridge.	-Person reaches the AP.	-Embarkation into the lifeboats on the AP. -Lifeboats launched, sailing away from the AP and reaching the standby vessel.

(node 4(1) in Figure 2); see Table 1. All three scenarios are mutually exclusive events. We see further in Figure 2 that terminal nodes 6, 8 and 9 are dependent events, because these events are repeating in both Scenarios 1 and 2 (6 is fatality behind the nearest fire/blast wall, 8 is PRP-AP bridge damage and 9 is fatality caused by escaping person to the sea).

Now we use the assumption that all events occurring in Table 1 follow exponential distribution. For example, ignition probability P_{is} = 0.004 from 0 to 1 min means, that the event "ignition at small leak" is exponentially distributed event which occurs within interval (0,1) with probability 0.004, so that corresponding parameter of failure rate is $\lambda=6.68\times10^{-5}$/s. Table 2 brings failure rates of all events occurring in Table 1 together with their given probabilities. Using the methodology for high-performance computing described in [3], the time evolution of the probability of ICFE (causing fatality) can be computed.

Analytical quantification procedure applied to a graph structure, which considers both independent and dependent (i.e. repeatedly occurring) terminal nodes, is based on combinatorial principle. The probability of TOP event can be obtained upwards resulting from probabilities of inferior terminal nodes. For instance the probability of internal event 3(1) can be computed in two steps:

Step 1 – numerical expression of the probability of occurrence of inferior terminal event 2 and sub-event 6(3), i.e. q_2 and q_6

Step 2 – numerical expression of the probability of occurrence of internal node 3(1) is given as follows:

$$q_3 = q_2.q_6 + (1-q_2)\,q_6 + q_2(1-q_6)$$

In general, we go over all combinations of input events causing occurrence of superior event (here node 3(1)) and summarize probabilities of such combinations. This principle requires summation of numerous different non-negative numbers, which may be one source of inaccuracy. Another source of inaccuracy arises when TOP event is a rare event (e.g. small leak within first minute after the accident appears). In such situation, the algorithm faces the problem of subtraction of two numbers that are very close each to other – an error may be committed at the arithmetic operation. Both these sources of inaccuracy were eliminated in the new computing methodology. Exact quantification procedure for probability of TOP event was developed in [4] displaying very high computational efficiency, as demonstrated in the reference. Original algorithm from [3] based on DAG was radically innovated. The innovative algorithm uses merits of the high-performance language for technical computing – MATLAB.

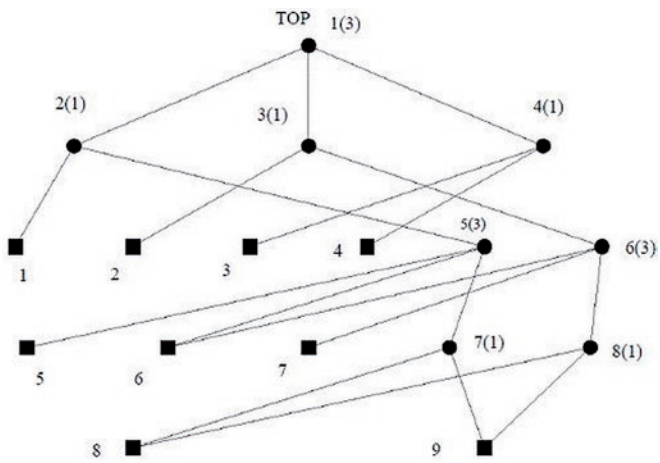

Fig. 2. Example of Directed Acyclic Graph

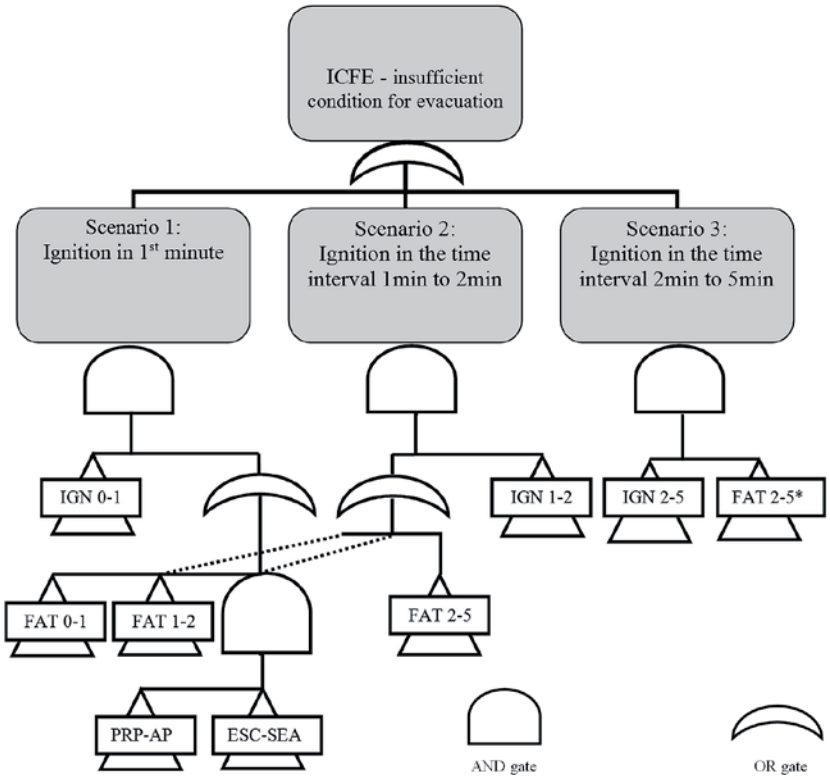

Fig. 3. Fault tree as an equivalent structure to DAG from Fig. 2

Table 2. Data of terminal events

Event	λ_j [s^{-1}] small	λ_j [s^{-1}] medium	λ_j [s^{-1}] large
IGN 0-1	6.68×10^{-5}	5.08×10^{-4}	1.76×10^{-3}
FAT 0-1	5.95×10^{-3}	8.55×10^{-4}	1.75×10^{-3}
FAT 1-2	1.0×10^{-3}	8.37×10^{-5}	1.68×10^{-4}
PRP-AP	1.07×10^{-4}	2.2×10^{-4}	1.0×10^{-3}
ESC-SEA	2.5×10^{-3}	2.5×10^{-3}	2.5×10^{-3}
FAT 2-5	1.67×10^{-5}	3.35×10^{-5}	1.0×10^{-4}
IGN 1-2	1.0×10^{-4}	3.4×10^{-4}	3.7×10^{-3}
IGN 2-5	2.34×10^{-5}	1.71×10^{-4}	7.4×10^{-4}
FAT 2-5*	1.0×10^{-5}	1.67×10^{-5}	6.7×10^{-5}

λ_j ...failure rate of the jth event
IGN 0-1 ...ignition within time interval (0,1) min
FAT 0-1 ...fatality within time interval (0,1) min
FAT 1-2 ...fatality within time interval (1,2) min
PRP-AP ...damage of PRP-AP bridge
ESC-SEA ...fatality due to escaping to the sea
FAT 2-5 ...fatality within time interval (2,5) min for Scenario 2
IGN 1-2 ...ignition within time interval (1,2) min
IGN 2-5 ...ignition within time interval (2,5) min
FAT 2-5 ...fatality within time interval (2,5) min for Scenario 3*

4. Results

4.1. Results of method based on DAG

Using the innovative analytic method described above, two different quantitative risk characteristics can be computed for each size of leak: the time-dependent evolution of the probability of the TOP event during selected first stage of the fire accident and average probability of the TOP event during selected consecutive time intervals. The latter characteristics are particularly useful to evaluate critical height of probability jumps within accident evolution.

It can be seen in Figures 4 and 5 that the probability of ICFE at the end of 5th min is 6.3e-3 for small leak and about one order of magnitude greater for medium leak. There is about 50% chance to survive the fire accident at the same time, for a person exposed to large leak.

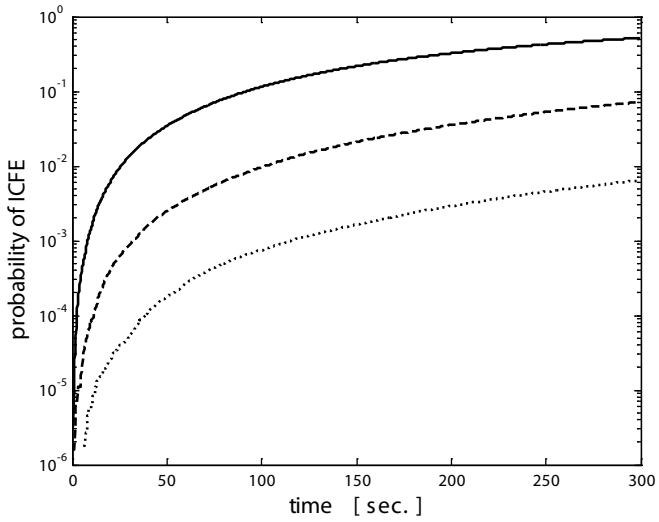

Fig. 4. Probability of ICFE (logarithmic scale) for Large, Medium (middle line) and Small (lower) Leak

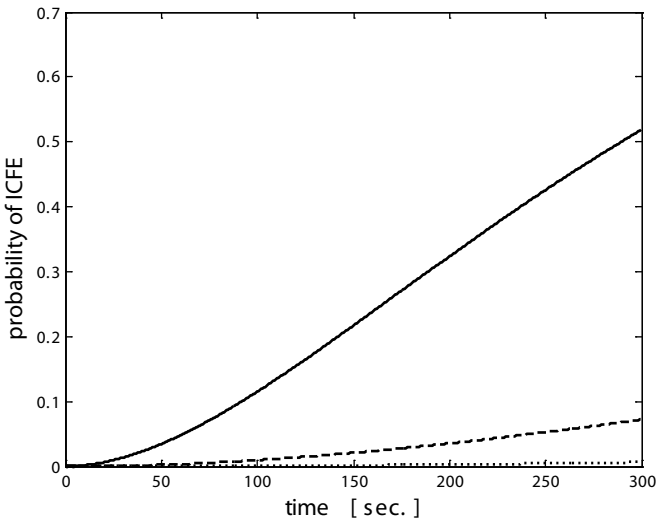

Fig. 5. Probability of ICFE for Large, Medium (middle line) and Small (lower) Leak

Average probabilities of ICFE in the course of consecutive minutes are demonstrated in Figure 6. It may be seen that for small and medium leak the highest jump of probability occurs within 5th minute in comparison with probability jumps in previous minutes. Consequently, we can conclude that 5th minute is most critical time point for safety of personnel. On the other side the probability of fatality in 5th minute for small leak is comparable with the probability in 2nd minute for medium leak and with the probability of fatality in 1th minute for large leak as well.

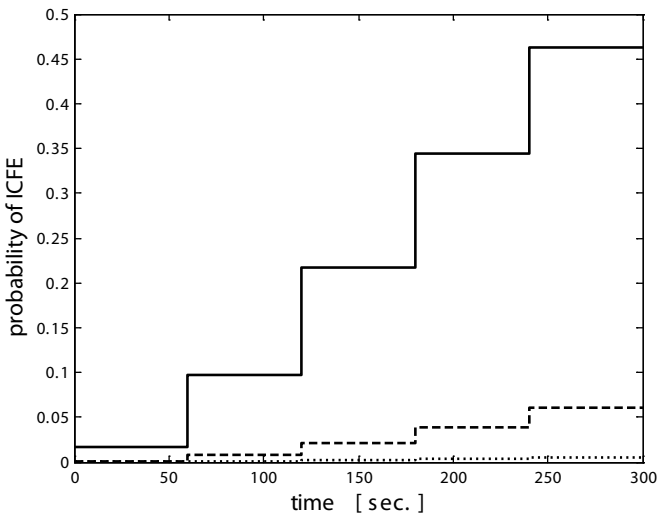

Fig. 6. Average Probabilities of ICFE for Large, Medium (middle line) and Small (bottom) Leaks, per Particular Minute

A large leak is very dangerous, because its associated probability of fatality increases approximately evenly within each minute very rapidly (at about 0.1 per one minute).

4.2. Partial sensitivity analysis

When applying the quantitative risk assessment in practice we often face the problem of lack of data. Using realistic data from [12], shown in Table 1, we were pushed into assuming that all input events follow exponential distribution. Of course, given that used realistic data contain only probability values in prescribed times, the most suitable probability distribution is thus exponential distribution, which is frequently used for modeling of random events in reliability theory. In addition, the source data of Table 1 is unavailable, therefore we are not allowed to verify this assumption.

As an exponential distribution function is determined by its rate parameter λ, we carried out partial sensitivity analysis for small leak to explore to which extent the resulting probability of ICFE is influenced by the parameter. For this reason the qualitative analysis discovering all minimal cuts has been made. Two of them (the most frequent ones) minimal cuts were chosen: C_1={IGN 0-1, FAT 0-1} and C_2={IGN 1-2, FAT 1-2}, that can be considered the most significant contributions to ICFE, if only because they are disjoint sets. Parameter λ of all basic events contained in C_1 and C_2 was modified into two sided 30% interval of λ. Computational results for probability of ICFE assuming lower and upper bounds of λ were obtained within 300 sec time course. Final bounds of probability of ICFE at 300 sec were computed as follows:

Table 3. Probability of ICFE depending on values of λ of two most frequent minimal cuts:

Rate parameters/probabilities	ICFE [s^{-1}]	ICFE change [%]
λ	$6{,}6\times10^{-3}$	0
Lower bound λ	$3{,}5\times10^{-3}$	-47
Upper bound λ	$1{,}0\times10^{-2}$	+53

As shown in Table 3, change of λ parameter led to significant change of ICFE probability. In case of λ value lowered by 30%, corresponding ICFE probability was also lowered by 47%. In case of λ value raised by 30%, corresponding ICFE probability was raised by 53%. Both these results show high sensitivity of ICFE probability to the value of rate parameter λ, therefore stressing the need of correct choice of λ value in FT and DAG models utilizing exponential distribution.

5. Conclusions

This paper demonstrates new approach to evaluate risk of fatality of working personnel in process industries from fire caused by hydrocarbon leak ignition occurring at various times following the leak. The new approach is characterized by its ability to compute time-dependent evolution of probability of personnel fatality, which is impossible by applying steady state methods.

Computed results were obtained by the use of analytical method coming from DAG as a system representation, which was fully innovated using merits of the high-performance language MATLAB.

Despite the fact that obtained results are influenced by addition of new assumptions laid on events occurring in Table 1 (putting them into the framework of exponential distribution), we can conclude that good platform for quantification of probability of ICFE is at our disposal.

Factually, data in Table 1 has been used to compute the time-dependent probability of ICFE for small, medium and large leaks in Zone 8. Based on the dynamic evolution of the probability of ICFE, it can be concluded that the most dangerous leak is the large leak. Probability of fatality following large leak increases very rapidly within first 5 minutes. At the end of 5th minute, person has roughly 50% chance to survive large leak scenario. This can be attributed to ignition of large gas cloud resulting in a fire swiftly escalating outside Zone 8 or outright explosion, both damaging the construction and thus possibly blocking some evacuation routes. On the other hand, small leak scenario is the least dangerous one, as the only danger comes from delayed ignition resulting in an explosion of accumulated gas vapors. The results also demonstrate that at the end of 5th minute, there is approximately one order of magnitude difference in the probabilities of fatality associated with the respective leak sizes.

If we wish to represent the probability for ICFE per annum, we have to multiply these probabilities by leak frequencies in Zone 8 based on statistical observations, see above the Section 2.

Finally, the partial sensitivity analysis showed that the final probability of ICFE is correspondingly influenced by variability of input parameters. Nevertheless by all means the obtained results are of special relevance to draw a comparison between different sizes of leaks.

Future research in this area should be oriented to finding effective measures leading to the risk of personnel fatality reduction, especially in the first minutes after the leak and follow-up fire accident occurrence.

Acknowledgements

This Paper has been prepared in the framework of the IT4Innovations Centre of Excellence project, reg. no. CZ.1.05/1.1.00/02.0070 supported by Operational Programme 'Research and Development for Innovations' funded by Structural Funds of the European Union and the Government of Czech Republic.

References

1. Abimbola M, Khan F, Khakzad N. Dynamic safety risk analysis of offshore drilling. Journal of Loss Prevention in the Process Industries 2014; 30: 74-85, http://dx.doi.org/10.1016/j.jlp.2014.05.002.
2. Aven T, Sklet S, Vinnem, J E. Barrier and operational risk analysis of hydrocarbon releases (BORA-release). Part I, method description. Journal of Hazardous Materials 2006; A137: 689-691, http://dx.doi.org/10.1016/j.jhazmat.2006.03.049.
3. Bris R. Parallel simulation algorithm for maintenance optimization based on directed Acyclic Graph. Reliability Engineering and System Safety 2008; 93: 874-884, http://dx.doi.org/10.1016/j.ress.2007.03.036.
4. Bris R. Exact reliability quantification of highly reliable systems with maintenance. Reliability Engineering and System Safety 2010; 95: 1286–1292, http://dx.doi.org/10.1016/j.ress.2010.06.004.
5. Bris R. Evaluation of the production availability of an offshore installation by stochastic petri nets modeling. 2013 International Conference on Digital Technologies, Zilina, Slovakia: 147-155, http://dx.doi.org/10.1109/dt.2013.6566303.
6. Bris R, Medonos S, Wilkins Ch, Zdráhala A. Time-Dependent Risk Modelling of Accidental Events and Responses in Process Industries. Proceedings of 11th International Probabilistic Safety Assessment and Management Conference and the Annual European Safety and Reliability Conference 2012 in Helsinki, PSAM11-ESREL; 3: 2056-2065.
7. Briš R, Medonos S, Wilkins Ch, Zdráhala A. Time-dependent risk modeling of accidental events and responses in process industries, Reliability Engineering and System Safety 2014; 125: 54-66, http://dx.doi.org/10.1016/j.ress.2013.05.010.
8. Kumamoto H, Henley E J. Probabilistic Risk Assessment and Management for Engineers and Scientists – 2nd ed. New York: IEEE Press, 1996. ISBN 0-7803-1004-7
9. Marseguera M, Zio E. Monte Carlo approach to PSA for dynamic process systems. Reliability Engineering and System Safety 1996; 52: 227-241, http://dx.doi.org/10.1016/0951-8320(95)00131-X.
10. Milazzo M F, Ancione G, Lisi R, Vianello C, Maschio G. Risk management of terrorist attacks in the transport of hazardous materials using dynamic geoevents. Journal of Loss Prevention in the Process Industries 2009; 22: 625-633, http://dx.doi.org/10.1016/j.jlp.2009.02.014.
11. Nývlt O, Rausand M. Dependencies in event trees analyzed by petri nets. Reliability Engineering and System Safety 2012; 104: 45-57, http://dx.doi.org/10.1016/j.ress.2012.03.013.
12. Oil & Gas UK. Fire and Explosion Guidance. The United Kingdom Offshore Oil and Gas Industry Association Limited, Issue 1, 2007.
13. Ramsay C G, Bolsover A J, Jones R H, Medland W G. Quantitative risk assessment applied to offshore process installations. Challenges after the piper alpha disaster. Journal of Loss Prevention in the Process Industries 1994; 7: 295-304, http://dx.doi.org/10.1016/0950-4230(94)80045-6.
14. Signoret J, Dutuit Y, Cacheux P, Collas S, Foleaux C, Thomas P. Reliability block diagrams driven petri nets. Reliability Engineering and System Safety 2013; 113: 61-75, http://dx.doi.org/10.1016/j.ress.2012.12.008.
15. Stroeve S H, Blom H A P, Bakker G J. Contrasting safety assessments of a runway incursion scenario: Event sequence analysis versus

multi-agent dynamic risk modelling. Reliability Engineering and System Safety 2013; 109: 133-149, http://dx.doi.org/10.1016/j.ress.2012.07.002.
16. Vinnem J E, Veire G, Heide B, Aven T. A method for developing and structuring risk activity indicators for major accidents, presented at PSAM7, Berlin, 14-18 June, 2004.

Radim BRIŠ
Ondřej GRUNT
Department of Applied Mathematics
VŠB-Technical University of Ostrava
17. listopadu 15
708 33 Ostrava – Poruba
Czech Republic
Email: ondrej.grunt@vsb.cz, radim.bris@vsb.cz

Article citation info:
WANG Y, ZHAO J, CHENG Z, YANG Z. Integrated decision on spare parts ordering and equipment maintenance under condition based maintenance strategy. Eksploatacja i Niezawodnosc – Maintenance and Reliability 2015; 17 (4): 591–599, http://dx.doi.org/10.17531/ein.2015.4.15.

Yabin WANG
Jianmin ZHAO
Zhonghua CHENG
Zhiyuan YANG

INTEGRATED DECISION ON SPARE PARTS ORDERING AND EQUIPMENT MAINTENANCE UNDER CONDITION BASED MAINTENANCE STRATEGY

ZINTEGROWANY SYSTEM DECYZYJNY DOTYCZĄCY ZAMAWIANIA CZĘŚCI ZAMIENNYCH I UTRZYMANIA RUCHU URZĄDZEŃ W RAMACH STRATEGII UTRZYMANIA ZALEŻNEJ OD BIEŻĄCEGO STANU TECHNICZNEGO

Aiming to optimize the equipment maintenance and the spare parts ordering management jointly, a comprehensive decision model under condition based maintenance (CBM) policy is presented for a single equipment system with continuous and random deterioration. In this model, the equipment deterioration is a continuous Gamma process under a continuous condition monitoring, and the spare parts inventory is controlled by spare parts support probability. Firstly, a spare part support probability model was developed to determine the optimal spare parts stock level S, which is set to meet the requirement of a predetermined stockout probability. Secondly, the equipment replacement and spare parts ordering decision is made to optimize the equipment replacement and spare parts ordering jointly, which is based on the equipment deterioration leveland total operating cost of the system. Thirdly, an integrated decision simulation model is presented for evaluating cost rate, availability and stockout probability. Finally, a numerical example is given to illustrate the performance of this model. The results show that the optimal preventive maintenance threshold obtained from the proposed decision model can satisfy the spare parts support requirements under (S-1, S) inventory control strategy.

Keywords: *spare parts, inventory control, ordering, condition based maintenance, Monte-Carlo simulation.*

Dążąc do jednoczesnej optymalizacji utrzymania ruchu urządzeń i zarządzania zamówieniami części zamiennych, zaproponowano kompleksowy model decyzyjny w ramach strategii utrzymania zależnej od bieżącego stanu technicznego (CBM) przeznaczony dla systemów z pojedynczym urządzeniem i ciągłym oraz losowym zużyciem. W niniejszym modelu, zużycie urządzenia jest ciągłym procesem Gamma z ciągłym monitorowaniem stanu, podczas gdy zapasy części zamiennych są kontrolowane poprzez prawdopodobieństwo wsparcia w zakresie części zamiennych. Po pierwsze, opracowano model prawdopodobieństwa wsparcia w zakresie części zamiennych w celu określenia optymalnego poziomu zapasów części zamiennych S, ustalonej aby spełnić wymogi określonego prawdopodobieństwa braku dostępności. Po drugie, przeprowadzono proces decyzyjny dotyczący wymiany urządzenia i zamawiania części zamiennych w celu jednoczesnej optymalizacji wymiany urządzenia i zamawiania części zamiennych, w oparciu o poziom zużycia urządzenia i całkowity koszt działania systemu. Po trzecie, zaprezentowano zintegrowany symulacyjny model decyzyjny dla oceny poziomu kosztów, dostępności i prawdopodobieństwa jej braku. Zasady niniejszego modelu zilustrowano przykładem numerycznym. Wyniki pokazują, że optymalny próg konserwacji zapobiegawczej uzyskany za pomocą proponowanego modelu decyzyjnego może spełnić wymagania dotyczące części zamiennych w ramach (S-1, S) strategii kontroli zapasów.

Słowa kluczowe: *części zamienne, kontrola zapasów, zamówienia, utrzymanie zależne od bieżącego stanu technicznego, symulacja Monte Carlo.*

1. Introduction

Condition based maintenance (CBM), as one of the most important maintenance method, has been studied extensively in recent years. Based on the analysis of fault mechanism and the test results without disassembly repairing, decision of repair or replace can be made and functional failures can be avoid to a large extend. The advantage of CBM is to supervisory control the working states detect the problems and take corresponding measures in time. It can make an effective prevention before some failures occur, even some serious failures can be prevented or excluded. As a result, it can prevent the occurrence of serious fault, greatly reduce the failure rate and repair costs, improve the usability of equipment, and change the maintenance work from passive to active.

Since the 1990s, research reports on CBM modeling and optimization are growing constantly. Using the CBM, engineers can make a maintenance decision on the basis of equipment deterioration level and the health status from the equipment condition monitoring data. In the current engineering practice, the decision criteria of CBM are mostly based on the engineer's experience or supplier's recommendations. However, the working environments and workloads in different companies are different, and therefore the rationality and scientificity of these decisions criteria has been questioned by researchers. Condition based maintenance modeling and optimization techniques have been studied widely [17]. Grall et al. [2, 5, 6] have studied a class of single equipment system, which is modeled as a continuous deterioration and stochastic process, with a state implementation by non-periodic inspection, and establish an appropriate analytical model. However, these

studies did not take into account the availability of repair spare parts. Dohi et al. [3] proposed an ordering and changing strategy for single equipment system. The decisions on spare parts ordering and system replacement are based on the time. Among them, the delivery time of normal order and emergency orders is a random variable which obeys different distributions. Sheu and Griffith [14] proposed an age replacement policy. In which, the maintenance work includes minor maintenance, and the delivery time of spare parts ordering is random. Sheu et al. [15] studied the age replacement policy like document [14] for single equipment system, which includes impact deterioration system. Alenka [1] studied the joint optimization problem of periodic batch replacement and periodic spare procurement. These studies have only considered the spare parts ordering strategy under planned maintenance system and based on spare parts inventory levels. While the research on joint optimization of spare parts ordering and equipment replacement under CBM strategy is rarely at present. Yoo et al. [19] presented an expected cost model which formulated for the joint spare stocking and block replacement policy using the renewal process. Kawai [7, 8] discussed a decision optimization problem on spare parts ordering and equipment replacement for a Markov degradation system. In which, the decision on spare parts ordering or equipment replacement was given based on the deteriorating state of the system. Y. B. Wang et al. [18] discussed spare parts allocation optimization in a multi-echelon support system based on multi-objective particle swarm optimization method. In fact, most of the degradation process of system is continuous, and the system modeling by the application of Markov chain will make the degradation states divided into several intervals for the discrete random process. In addition, the state transition matrix estimation is often more difficult, which characterizes the discrete time in Markov chain.

In this paper, the problem of maintenance strategy is considered for a single equipment system which shutdown will cause more losses, or even lead to disastrous consequences. Therefore, it is necessary to make a preventive replacement of equipment before failure. When the deterioration of the working unit reaches a scheduled preventive maintenance threshold, a prevention replacement will be conducted using spare parts. In view of the continuous monitoring on a single equipment system, this paper will develop a strategy of equipment replacement and spare parts ordering under condition based maintenance. Under this strategy, the replacement action and spare parts inventory control is driven by the unit deterioration. Spare parts inventory control strategy is $(S, S-1)$, and spare parts support meets the given stockout probability.

The rest of this paper is arranged as follows. In section 2, the system description is presented, which includes the analysis of degradation processes and the modeling assumptions. Section 3 describes the development of the spare parts inventory control model. In which, a spare parts support probability model is established to ensure the optimum stock of spare parts S. Then, the equipment maintenance and spare parts ordering model is presented. In section 4, an integrated decision models for equipment maintenance and spare parts inventory is developed. Section 5 gives an example to show the performance of the proposed model. Finally, in section 6, conclusions are drawn from the work.

2. Description of the system

2.1. Notations

In order to establish the comprehensive decision model, the main parameters are defined as follows:

$F_{\alpha,\beta}(t)$	fault cumulative distribution function of the equipment, where α is the shape parameter, and β is the scale parameter.
L	order delivery time, which is a random variable.
$g(l)$	the probability density distribution function of order delivery time.
c_f	the costs per breakdown maintenance, which is assumed to be constant value.
c_{pm}	the cost per preventive maintenance.
c_q	the loss for equipment unit downtime.
c_o	the management cost of the unit spare parts.
M_f	time of each breakdown maintenance, is assumed to be constant value.
M_{pm}	time of each preventive maintenance.
T	time of a working cycle.
ω	stockout probability of spare parts.
η	the maximum allowable stockout probability.
$\xi_{D_{pm}}$	total number of the arrival of spare parts in the cycle $[0,T]$.
SCL	total number of the stockout of spare parts in the cycle $[0,T]$.
$N_{D_{pm}}$	total times of the maintenance in the cycle $[0,T]$, which is the sum of spare parts orders.
$E[N_{D_{pm}}]$	expected number of the replacement in the cycle $[0,T]$.
S^*	optimum inventory number of spare parts.
t_k	arrival time for spare parts k, $k \in [S^*+1, S^*+2, \cdots, \xi_{pm}]$.
I_k	the existing inventory levels after the kth times of preventive maintenance $k \in [1,2,\cdots,N_{pm}]$.
D_{pm}	preventive maintenance threshold.
D_f	failure threshold of the degradation.
$T_{D_{pm}}^{(k)}$	working time of the kth components, $k \in [1,2,\cdots,N_{pm}]$.
$T_{cum}^{(k)}$	system working time when the kth components has been under preventive maintenance, $k \in [1,2,\cdots,N_{pm}]$.
$E[C_m]$	expected costs of equipment maintenance and replacement in the cycle $[0,T]$.
$E[C_q]$	expected cost of downtime loss in the cycle $[0,T]$.
$E[C_o]$	expected cost of spare parts management in the cycle $[0,T]$.
$E[C]$	expected cost of equipment total operating in the cycle $[0,T]$.
$D(T)$	average downtime of equipment in the cycle $[0,T]$.
$A(T)$	average availability of equipment in the cycle $[0,T]$.

2.2. Degradation processes analysis

Generally, there are many kinds of distributions for equipment deterioration. However, Gamma distribution has a strong universality for the traditional exponential, Chi-square and Erlang distribution are all the special cases of the Gamma distribution [4]. Therefore, Gamma distribution is suitable for various forms of distribution. It can be used to represent different failure distributions such as the early failure, occasional failure and exhaustion failure. Therefore, we take Gamma distribution as the form of equipment deterioration in this paper.

The status parameters of equipment is characterized by the random variable $D(t_i)$ at time t_i, where $t_1 < t_2 < \cdots < t_n$, $t_i \in T_h, 1 \le i \le n$. If the incremental $D(t_1)$, $D(t_2) - D(t_1)$, $D(t_3) - D(t_2)$, …, $D(t_n) - D(t_{n-1})$ are independent of each other, $\{D(t), t \in T_h\}$ is called independent increment process [11]. If the distribution of $D(t) - D(s)$ is only rely on $t - s$ for all $0 \le s \le t$, we can say that $\{D(t), t \in T_h\}$ have a stationary increment. The independent increment processes with stationary increments is called stationary and independent increment process.

The Gamma process is time-homogeneous Lévya process, which is a kind of random and continuous process with independent increments [16]. A standard Gamma process $\{\gamma_t, t \in T_h\}$ has a stable, independent and nonnegative increment. If the incremental degradation was expressed as $D(i) = D(t_i) - D(t_{i-1})$ in time $[t_{i-1}, t_i]$, the Gamma process has the following properties:

(a) $D(i)$ is a smooth, independence and nonnegative increment.

(b) $D(i)$ obeys a distribution with probability density of $\text{gamma}(\alpha(t_i - t_{i-1}), \beta)$, where α is the shape parameter, β is the scale parameter, that is:

$$D(i) \sim \frac{d_i^{\alpha(t_i - t_{i-1})-1} \exp(-\beta d_i) \beta^{\alpha(t_i - t_{i-1})}}{\Gamma(\alpha(t_i - t_{i-1}))}. \tag{1}$$

The cumulative failure distribution function of Gamma process can be expressed as:

$$F_{\alpha,\beta}(t) = \Pr(X < t) = \Pr(D(t) > D_f), \tag{2}$$

where, X is the life of the product, D_f is the failure threshold.

The deterioration process of equipment is a continuous Gamma process, and the cumulative failure distribution function is:

$$F_{\alpha,\beta}(t) = \frac{\Gamma\left(\alpha t, \beta(D_f - x_0)\right)}{\Gamma(\alpha t)}, \tag{3}$$

where α is the shape parameter, β is the scale parameter, x_0 means the state parameters of the initial moment.

Park and Padgett [13] gave the Gamma function degradation process, which includes degradation time and amount of degradation, and the failure distribution function.

2.3. General assumptions

We suppose that the following assumptions are satisfied.

(1) Working period T is always greater than the order delivery time L, and T is a fixed value.

(2) The downtime loss is generated by equipment maintenance or lack of spare parts, and it is proportional to the downtime.

(3) Unit spare parts management fee c_o includes its own cost, spare parts ordering cost and spare parts storage cost, while c_o is a constant.

(4) The stocking spare parts do not deteriorate or fault, and the length of the reserve is not effect to the later working life of spare parts.

(5) The spare parts with earlier ordering must arrive earlier than the later one.

(6) In the integrated decision model, the replacement time is greater than zero, and D_{pm} is less than D_f. Obviously, when the replacement time is greater than zero, the stockout probability of spare parts will decrease. While the stockout probability of spare parts will be increased when $D_{pm} < D_f$. In this paper, it is assumed that the number of the optimal spare parts S^* meets the demands of the spare parts support probability in the integrated decision models.

(7) The equipment deterioration is under a continuous condition monitoring. And after preventive maintenance or corrective mantenance, the equipment will resume to a state of "as good as new".

3. Spare parts inventory control model

Spare parts support probability represents the probability of demand of equipment spare parts with satisfaction. Its numerical size is closely related to spare parts inventory and spare parts demand.

There are two main kinds of index of spare parts support probability. One is the fill rate, which is the percentage of spare parts meet the needs of supply at any time; the other is the stockout rate. It is the percentage of the requirement quantity of spare parts, which did not meet the supply at some time. Spare parts support probability model is particularly important in some important equipment spare parts support process. Because the safety and economic behavior will cause serious consequences for once the important equipment downtime due to lack of spare parts. For some important equipment spare parts which usually with high prices and very low demand, spare parts inventory control strategy $(S-1, S)$ is the most optimal support scheme [10, 12, 13]. This article will use spare parts support probability model for the spare parts inventory decision.

3.1. Spare parts support probability models

A single equipment system under CBM strategy is considered in this paper. The degradation process of equipment is a continuous Gamma process. Its failure probability density function is $f_{\alpha,\beta}(t)$, and the cumulative distribution function is $F_{\alpha,\beta}(t)$. The supply of spare parts inventory control strategy is $(S-1, S)$. The meaning of the inventory policy is that the initial inventory level is S, when stocks fall as $S-1$, then a spare part order is request, and the order quantity is 1. S_{OH} is defined as the available inventory of spare parts, S_{DI} is the number of spare parts in transportation, S_{BO} is the number of spare parts for delayed delivery. In the process of the inventory system operation, the relationships among S_{OH}, S_{DI}, S_{BO} and S are as follows:

$$S = S_{OH} + S_{DI} - S_{BO}. \tag{4}$$

Assuming that preventive maintenance threshold value D_{pm} is equal to the failure threshold value D_f, and the replacement time is ignored. Under the inventory strategy, when the equipment degrada-

tion level has reached D_f, a spare part will be withdraw from the inventory for changing spare parts repair, at the same time, a spare part ordering is performed, and the ordering number is 1, the ordering delivery time is L (its probability density function is $g(l)$). The inventory is out of stock when the equipment degradation reaches to the failure threshold and no inventory for prevent replacement.

Because spare parts ordering delivery time $L>0$, under the condition of meeting the requirement of stockout probability η, the initial inventory of spare parts quantity S shall meet the following conditions:

$$\Pr\left(\sum_i^S T_i < L\right) = \int_0^\infty \Pr\left(\varpi_S = \sum_i^S T_i < L \middle| L = l\right) g(l)dl = \int_0^\infty g(l)\int_0^l f_{\varpi_S}(t)dtdl = \omega \le \eta, \tag{5}$$

where, ω is the stockout probability of spare parts by calculation; T_i is the time from using to degradation failure threshold D_f for spare parts; ϖ_S means the sum using time of spare parts, and its probability density distribution function is $f_{\varpi_S}(t)$, the cumulative distribution function is $F_{\varpi_S}(t)$. As the spare parts are of the same type, so the expression of $f_{\varpi_S}(t)$ is:

$$F_S(t) = F_{\alpha,\beta}^{(S)}(t) = L^{-1}\left\{L[F_{\alpha,\beta}(t)]^S\right\}, \tag{6}$$

where $F_{\alpha,\beta}^{(S)}(t)$ is the dispersed S-fold discrete convolution of $F_{\alpha,\beta}(t)$, $L[F_{\alpha,\beta}(t)]$ is the Laplace transform for $F_{\alpha,\beta}(t)$, and S represents spare parts inventory quantity. When the spare parts inventory quantity S fit $\omega_S < \eta < \omega_{S-1}$, the spare parts inventory quantity is the optimal inventory (S^*).

3.2. Model solution

In order to solve the optimal spare parts inventory number to meet the requirements of stockout probability, the spare parts support probability model is established. The Eqs.5 can be solved by iterative method, and the steps are as follows:

Step 1: Initialize the probability density distribution function $f_{\alpha,\beta}(t)$ of components Gamma degradation process. Then, initialize the failure threshold value D_f, the probability density distribution function $g(l)$ of order delivery time L, the maximum allowable stock-out probability υ, and make the counter variable $i=1$.

Step 2: Make $S_i = i$, and calculate the corresponding stockout probability ω_{S_i}.

$$\omega_{S_i} = \int_0^\infty g(l)F_1(l)dl = E[F_1(l)] \approx \lim_{n\to\infty}\frac{1}{n}\sum_{i=1}^n F_{\alpha,\beta}(l_j)l_j = \{t|G(t)=U_j(0,1)\} \tag{7}$$

in which, $G(\cdot)$ is the cumulative distribution function of the delivery time L, $F_{\alpha,\beta}(\cdot)$ is the Gamma failure cumulative distribution function for spare parts in the process of degradation. If the calculated stockout probability $\omega_{S_i} < \eta$, the computation should be end. At this time, $S^*=1$, otherwise, the computation should go to the next step.

Step 3: Calculate the Laplace transform for function $f_{\alpha,\beta}(t)$:

$$L\left[f_{\alpha,\beta}(t)\right] = \int_0^{+\infty} f_{\alpha,\beta}(t)e^{-st}dt = E\left(e^{-st}\right) \approx \lim_{n\to\infty}\frac{1}{n}\sum_{j=1}^n e^{-s\tau_j}, \quad \forall s, \tau_j = \left\{t\middle|f_{\alpha,\beta}(t) = U_j(0,1)\right\}. \tag{8}$$

Step 4: Make $i=i+1$, $S_i = S_{i-1}+1$, and calculate the Laplace transform for function $F_{\varpi_{S_i}}(t)$:

$$L\left[F_{\varpi_{S_i}}(t)\right] = \frac{1}{s}\left\{L\left[f_{\alpha,\beta}(t)\right]\right\}^{S_i}. \tag{9}$$

Step 5: Calculate $F_{\varpi_{S_i}}(t) = L^{-1}\left\{L\left[F_{\varpi_{S_i}}(t)\right]\right\}$.

Step 6: Calculate stockout probability ω_{S_i} when $S_i = i$.

$$\omega_{S_i} = \int_0^\infty g(l)F_{S_i}(l)dl = E[F_{S_i}(l)] \approx \lim_{n\to\infty}\frac{1}{n}\sum_{i=1}^n F_{S_i}(l_j), \quad l_j = \{t|G(t)=U_j(0,1)\}. \tag{10}$$

Step 7: If the calculated stockout probability $\omega_{S_i} < \eta$, then $S^* = i$, and the calculation is end. Otherwise, it should return to step 4.

4. Integrated decision models for equipment maintenance and spare parts inventory

4.1. Model description

In many cases, a system shutdown will cause significant losses, or even lead to disastrous consequences. In order to reduce the risk of shutdown casued by failures, a CBM strategy may be employed. In this paper, it is considered that a system suffers from deteriorating and its condition is monitored under a CBM strategy. Both preventive maintenance and corrective maintenance are involved in the strategy. The role of the preventive maintenance is preventing the replacement before failure. When the deterioration of the work equipment reaches to a predetermined threshold of preventive maintenance, a preventive replacement is implemented by a spare part. Because the equipment deterioration is under a continuous condition monitoring, a corrective maintenance will occur only for spare parts is stockout when the deterioration reaches to the threshold of preventive maintenance. After maintenance, either preventive or corrective, the equipment will restore to a state of "as good as new".

It is supposed that the system is made up of $S+1$ components, in which, one component is working, while the others are as cold redundant. When the working components fault, the redundant parts will replace them one by one. And the spare parts inventory is under $(S-1,S)$ strategy. Which means once preventive replacement (one spare parts needed at one time) is needed when the equipment degrades to the preventive maintenance threshold D_{pm}. Then, a spare part ordering is performed. While the order number is 1, and order delivery time L is a random variable. Here, the redundant components S must fulfill that its stockout probability is less than η within the order delivery time L. The aim of constructing this model is to solve

the optimal D_{pm} with a minimum cost of system total operation, which is based on calculation of S under the prescribed conditions.

4.2. Model construction

Under the CBM strategy, the maintenance decision-making and spare parts ordering are performed based on the equipment degradation and inventory levels in this paper. In addition, the spare parts inventory level is affected by the spare parts order delivery time and the replacement of the equipment. As a result, it is difficult to establish a mathematical model to calculate the system costs. So, a simulation model is used to simulate the system maintenance cycle such as replacement, spare parts ordering and inventory in this paper. And the related fee is estimated through Monte-Carlo simulation method.

4.2.1. Equipment maintenance and spare parts ordering

In one work cycle $[0,T]$, the analysis of equipment maintenance and spare parts inventory are as follows:

(1) Equipment maintenance analysis

- When $0 < T < T_{cum}^{(1)}$, equipment does not need maintenance.
- When $0 < T_{cum}^{(k)} < T$ and $T_{cum}^{(k)} + M_{pm} < T$, if the inventory of spare parts is not zero, equipment preventive maintenance is performed one time; if the inventory of spare parts is zero, then the equipment will be down for lack of spare parts. And the equipment preventive maintenance should be performed after the ordering spare parts arrival.
- When $0 < T_{cum}^{(k)} < T$ and $T_{cum}^{(k)} + M_{pm} > T$, equipment does not need maintenance.

(2) Spare parts inventory analysis

- When a spare part requirement is generated, if the inventory level $I > 0$, then I reduce 1, and maintenance times $N_{D_{pm}}$ increase 1. If the inventory level is zero, the stockout number SCL increase 1.
- When the ordering spare parts arrival to the warehouse, the number of the arrival spare parts increase 1, and the total number of existing inventory I increase 1.

4.2.2. The cost ratio

The total operating cost of the equipment consists of the following three parts: the costs of equipment maintenance and replacement, the downtime costs, and the costs of spare parts management.

The expected costs of maintenance and replacement in the cycle $[0,T]$ can be expressed by:

$$E[C_m] = c_{pm} E\left[N_{D_{pm}}\right]. \tag{11}$$

The expected cost of downtime loss in the cycle $[0,T]$ can be given by:

$$E[C_q] = c_q \left(T - \sum_{k=1}^{N_{D_{pm}}} T_{D_{pm}}^{(k)} \right). \tag{12}$$

The expected cost of spare parts management in the cycle $[0,T]$ can be expressed as following:

$$E\left[C_o\right] = c_o E[N_{D_{pm}}]. \tag{13}$$

Then, the expected total cost $E[C]$ for the equipment operating in the cycle $[0,T]$ can be expressed by:

$$\begin{aligned} E[C] &= E[C_m] + E[C_q] + E[C_o] \\ &= c_{pm} E[N_{D_{pm}}] \quad + c_q (T - \sum_{k=1}^{N_{D_{pm}}} T_{D_{pm}}^{(k)}) + c_o E[N_{D_{pm}}] \end{aligned} \tag{14}$$

Then, the model can be obtained as follows:

(1) The objective function is:

$$\min_{D_{pm}} E(c_{pm} E[N_{D_{pm}}] + c_q (T - \sum_{k=1}^{N_{D_{pm}}} T_{D_{pm}}^{(k)}) + c_o E[N_{D_{pm}}]). \tag{15}$$

(2) The constraint conditions include:

$$\begin{cases} N_{D_{pm}} = \sup\left\{ i \left| \left(\sum_{k=1}^{i} T_{D_{pm}}^{(k)} + \sum_{k=1}^{i} M_{pm} + \sum_{k=S^*+1}^{i} \varphi_k \right) \le T \right. \right\} \\ E\left[\dfrac{\sum_{k=S^*+1}^{\xi \cdot D_{pm}} \partial_k}{\xi D_{pm}} \right] \le \eta \end{cases} \tag{16}$$

where φ_k is the time of spares stockout and ∂_k means the number of spares stockout. The expressions for them are as follows respectively:

$$\varphi_k = \begin{cases} \inf\left\{ t_k \middle| t_k \ge T_{cum}^{(k)} \right\} - T_{cum}^{(k)} & if \quad I_k = 0 \\ \qquad \forall k \in [S^*+1, S^*+3, \ldots, N_{D_{pm}}] & \\ 0 & otherwise \end{cases} \tag{17}$$

$$\partial_k = \begin{cases} 1 & if \quad t_k > S^* E(T_{pm}) \\ 0 & otherwise \end{cases}. \tag{18}$$

4.2.3. Availability

If the average downtime in the working cycle $[0,T]$ can be acquired, the equipment availability can be calculated by:

$$A(T) = \frac{T - D(T)}{T}. \tag{19}$$

Because the equipment downtime includes maintenance time and stockout time, so the expression of average downtime in a work cycle $[0,T]$ is expressed as:

$$D(T) = E\left[\sum_{k=1}^{N_{D_{pm}}} M_{pm} + \sum_{k=S^*+1}^{N_{D_{pm}}} \varphi_k \right]. \tag{20}$$

4.3. Model solution

In order to obtain the optimal preventive maintenance threshold, the smallest operating costs of the system and the systems availability, a Monte Carlo simulation and iterative optimization program flow for the ordering and replacement policy is given as follows:

Step 1: Parameter initialization, that is the system parameters such as α, β, D_f, c_f, c_b, c_o, M_f, and T should be entered into. Then, let $T_0' = 0$, $I_0 = S$, $N_{D_{pm}} = 0$, $\xi_{D_{pm}} = 0$, $SCL = 0$. In which, T_i' means the starting point of the work time for the ith spare parts; T_j means the arrival time for the jth spare parts ordering; I_i means the existing inventory number after the ith maintenance and replacement; SCL means the stockout number of the spare parts.

Step 2: Let $k = 1$, $D_{pm} = D_f - k\Delta D$, where ΔD is the unit deterioration amount. For a certain D_{pm}, we can use the corresponding generated random numbers to simulate a work cycle of the equipment maintenance and replacement and the inventory cycle. Then, the maintenance replacement times $N_{D_{pm}}$, equipment working time $\sum_{k=1}^{N_{D_{pm}}} T_{D_{pm}}^{(k)}$, the arrival spare parts numbers $\xi_{D_{pm}}$, and the stockout number of the spare parts SCL can be acquired. This simulation process is repeated N times, while N should be set large enough.

Step 3: Make $k = k + 1$, if $D_{pm} > \Delta D$, it should return to step 2. Else, it will continue with the next step.

Step 4: For a certain D_{pm}, the values such as the expected maintenance times $E[N_{D_{pm}}]$, working time $E\left[\sum_{k=1}^{N_{D_{pm}}} T_{D_{pm}}^{(k)}\right]$, arrival spare parts number $E[\xi_{D_{pm}}]$, and the stockout number $E[SCL]$ can be calculated within N times simulation during the working cycle $[0, T]$. Accordingly, the systems total running fee, spare parts stockout probability, and system's availability can be worked out. Finally, the optimal threshold value of preventive maintenance can be acquired by decision on the calculated results above.

5. Example analysis

In order to explain the equipment maintenance and spare parts ordering of the integrated decision model, the following numerical example is given. The assignment model parameters are shown in table 1.

In the example, it is assumed that the more serious the equipment deteriorates, the longer the time spent in preventive maintenance. In addition, the equipment maintenance time consuming is increased exponentially with the degree of equipment deterioration [9]. That is:

$$M_{pm} = M_f \exp\left(1 - \frac{D_f}{D_{pm}}\right)$$

Similarly, it is assumed that the more serious the equipment deteriorate, the more costs will spend for preventive maintenance. In addition, the equipment maintenance and replacement cost consuming is increased exponentially with the degree of equipment deterioration. It can be expressed as follows:

$$c_{pm} = c_f \exp\left(1 - \frac{D_f}{D_{pm}}\right)$$

Table 1. Model parameter values

Model variable	Values	Variables description
α	0.7	shape parameter of Gamma deterioration process function
β	0.006	scale parameter of Gamma deterioration process function
D_f	45	failure threshold
η	0.1	the maximum allowed stockout probability
$g(l)$	Logn (0.02, 0.05)	probability density function of L (as lognormal distribution)
c_f	1500	maintenance costs for each fault
c_q	3750	downtime loss in unit time
c_o	1200	management fee for unit spare parts
M_f	0.4	maintenance time for each fault
T	10	time of a work cycle

(1) Spare parts inventory decision

According to the data in table 1, the optimal spare parts inventory level S^* can be worked out by the iterative method offered by this paper. The iterative results are shown in Table 2.

Table 2. The iterative results from the model

Inventory level	Probability of stockout
1	0.6132
2	0.2119
3*	0.0563

From Table 2, it can be seen that $\omega_3 < \eta < \omega_2$. That is when the inventory level $S = 3$, the system probability of stockout can meet the stated probability. So, the optimal spare parts inventory level $S^* = 3$.

(2) Preventive maintenance threshold decision

When the optimal inventory level of spare parts S^* is certain, the model can be commutated by the Monte-Carlo simulation and iterative methods mentioned above. According to the parameters in Table 1, and make D_{pm} as 40,39,…,6,5, with 1000 times simulation, we can acquire the results of the integrated decision model, which is shown in Table 3.

The optimization results of simulation and iterative can be seen from Table 3. When $D_{pm} = 13$, the system total operation cost is minimum, and the spare parts stockout probability ω is less than the maximum allowable value. However, the system availability is not optimal when $D_{pm} = 13$, and the system availability is optimal when

Table3. Results of the integrated model

D_{pm}	$E[C]$	ω	$A(T)$
5	30880.44	0.21618	0.88239
6	29607.95	0.198461	0.894771
7	28561.55	0.18244	0.90516
8	27970.29	0.169532	0.909784
9	27336.67	0.153453	0.914717
10	26839.91	0.13803	**0.918041***
11	26675.81	0.124363	0.91676
12	26624.36	0.109821	0.914296
13	**26607.64****	0.095687	0.910787
14	26705.73	0.082576	0.90459
15	26874.62	0.07073	0.897384
16	27101.41	0.058625	0.88962
17	27527.31	0.047001	0.880479
18	27619.84	0.036678	0.87244
19	27972.22	0.028778	0.862553
20	28337.86	0.022847	0.852379
21	28675.48	0.016327	0.842734
22	28984.62	0.011862	0.83295
23	29216.69	0.007853	0.824186
24	29601.3	0.005604	0.814682
25	29908.11	0.00338	0.805714
26	30196.85	0.001949	0.797351
27	30356.97	0.000976	0.790473
28	30553.85	0.000357	0.783137
29	30800.67	0.000144	0.776247
30	31108.70	0	0.769122
31	31373.56	0	0.761944
32	31451.68	0	0.756873
33	31639.67	0	0.751418
34	31721.76	0	0.747231
35	32027.27	0	0.74094
36	32026.95	0	0.737948
37	32081.98	0	0.734462
38	32226.08	0	0.729654
39	32434.29	0	0.725858
40	32392.65	0	0.722997

$D_{pm} = 10$. This shows that the total operation cost and availability of this system cannot achieve optimal at the same time.

In order to analyses the simulation data more intuitively to make a maintenance decision, Three figures are drawn according to the simulation data, which is shown as Figure 1, Figure 2 and Figure 3.

Fig.1 shows the relationship between the total operating costs C, maintenance costs C_m, cost of downtime loss C_q, costs of spare parts management C_o and preventive maintenance threshold value D_{pm}.

From Fig.1, It can be seen that: (1) there is an optimum preventive maintenance threshold with a minimum costs for total operating; (2) the maintenance costs is increased with the increasing of D_{pm}, which is related to the model assumption that the more serious the equipment deteriorate, the more costs will spend for preventive mainte-

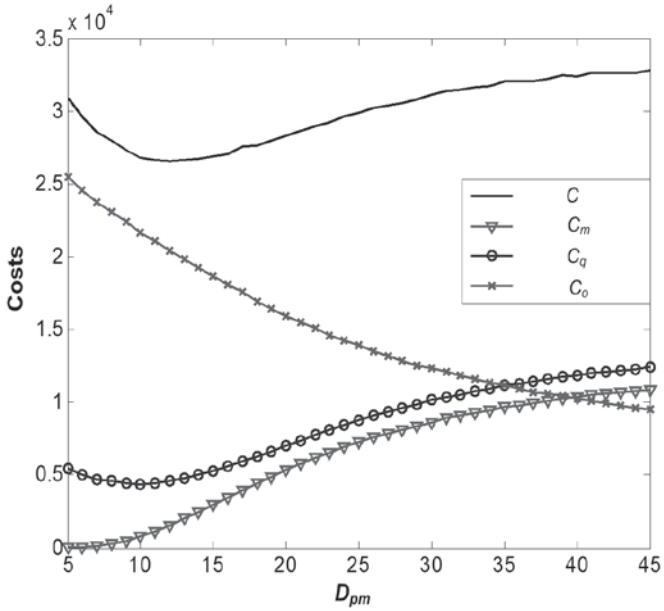

Fig. 1. The corresponding relationship of costs and D_{pm}

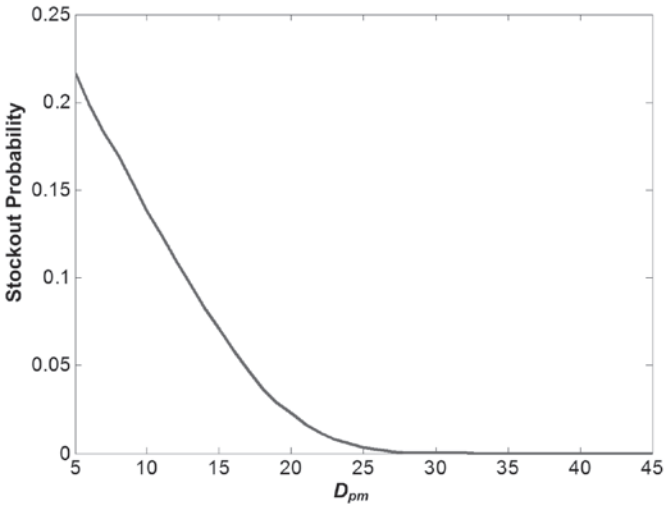

Fig. 2. The corresponding relationship of stockout probability and D_{pm}

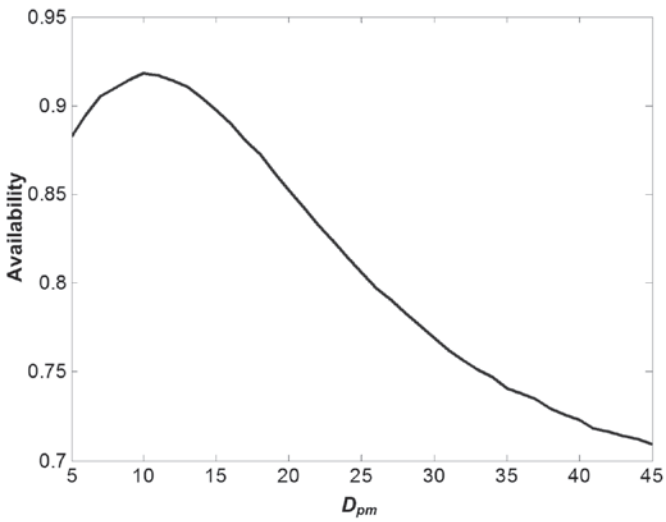

Fig. 3. The corresponding relationship of availability and D_{pm}

nance; (3) there is a firstly drop and later increase process for the costs of downtime loss with the increasing of D_{pm}, which is related to the stockout time increases rapidly when threshold value is too small and the maintenance time increases rapidly when preventive maintenance threshold is too large; (4) the cost of spare parts management is gradually reduced with the increasing of D_{pm}, which is related to that the longer the single equipment working, the less the maintenance times in need during the working cycle.

Fig.2 shows the relationship of the a and D_{pm} when the maximum number of stock S is determined. It can be seen from Fig.2 that the bigger the D_{pm}, the smaller the ω. The reason is that the longer single equipment work, the smaller the stockout probability of the system.

Fig.3 shows the relationship of the system availability and D_{pm}. It can be seen from Fig.3 that the equipment availability is increased with the increasing of D_{pm} at first. When it reaches to a certain value, it will decrease with the increasing of D_{pm} afterwards. It because the maintenance frequency will increase when D_{pm} is too small, and the equipment downtime will increase for the lack of spare parts. While the maintenance time will increase when the D_{pm} is too large, and the equipment availability will decrease correspondingly.

6. Conclusions

In this paper, a spare parts inventory control and integrated decision model is proposed based on the CBM for a class of single equipment system. Firstly, the spare parts support probability model is established to determine the optimum stock of spare parts. And then the system operation and spare parts ordering comprehensive decision-making simulation model is established, which can be used to calculate the running fee rate, system availability and the stockout probability of spare parts. At last, the model is verified by a numerical example. The results show that the optimal preventive maintenance threshold D_{pm} with the decision of target of cost can meet the requirements of spare parts support degree under the $(S-1,S)$ strategy. However, the fee rate and availability cannot achieve an optimal point at the same time.

It is noted that although a Gamma deterioration process is used to develop the spare parts control model, the proposed model may allow other types of distriburion to be incorporated to obtain an optimal stragety for spares controling.

References

1. Alenka B. Alenka. Joint optimization of block-replacement and periodic-review spare-provisioning policy. IEEE Transactions on Reliability 2003; 52(1): 112-117, http://dx.doi.org/10.1109/TR.2002.805790.
2. Dieulle L. Sequential condition-based maintenance scheduling for a deteriorating system. European Journal of Operational Research 2003; 150: 451-461, http://dx.doi.org/10.1016/S0377-2217(02)00593-3.
3. Dohi T. On the optimal ordering policies in maintenance theory: survey and applications. Applied Stochastic Models and Data Analysis 1998; 20(14): 309-321, http://dx.doi.org/10.1002/(SICI)1099-0747(199812)14:4<309::AID-ASM351>3.0.CO;2-R.
4. Gamma distribution [Online].Available: http: // www.brightonwebs.co.uk / distributions / Gamma.asp.
5. Grall A. A condition-based maintenance policy for stochastically deteriorating systems. Reliability Engineering and System Safety 2002; 76: 167-180, http://dx.doi.org/10.1016/S0951-8320(01)00148-X.
6. Grall A. Continuous time predictive maintenance scheduling for a deteriorating system. IEEE Transaction on Reliability 2002; 51: 141-150, http://dx.doi.org/10.1109/TR.2002.1011518.
7. Kawai H. An optimal ordering and replacement policy of a Markovian degradation system under complete observation: part I. Journal of the Operational Research Society of Japan 1983; 26(4): 279-291.
8. Kawai H. An optimal ordering and replacement policy of a Markovian degradation system under complete observation: part II. Journal of the Operational Research Society of Japan 1983; 26(4): 293-307.
9. Liao H T. Maintenance of continuously monitored degrading systems. European Journal of Operational Research 2006; 175: 821-835, http://dx.doi.org/10.1016/j.ejor.2005.05.017.
10. Liu Y, Huang H Z. Optimal replacement policy for multi-state system under imperfect maintenance. IEEE Transactions on Reliability 2010; 59(3): 483-495, http://dx.doi.org/10.1109/TR.2010.2051242.
11. Lin Y L. Application of random process. Beijing, China, Tsinghua university press, pp. 20-30, 2002.
12. Oner K B. Optimization of component reliability in the design phase of capital goods. European Journal of Operational Research 2010; 205(3): 615-624, http://dx.doi.org/10.1016/j.ejor.2010.01.030.
13. Park C. Padgett. Accelerated degradation models for failure based on geometric brownian motion and Gamma process. Life-time Data Analysis 2005; 11: 511-527, http://dx.doi.org/10.1007/s10985-005-5237-8.
14. Sheu S H. Griffith. Optimal age-replacement policy with age-dependent minimal-repair and random lead-time. IEEE Transaction on Reliability 2001; 50: 302-309, http://dx.doi.org/10.1109/24.974128.
15. Sheu S H. Chien. Optimal age-replacement policy of a system subject to shocks with random lead-time. European Journal of Operational Research 2004; 159: 132-144, http://dx.doi.org/10.1016/S0377-2217(03)00409-0.
16. Wang C H. Statistical inference for the process of generalized Gamma. Journal of East China University of Science and Technology (Natural Science Edition) 1995; 21(3): 392-399.
17. Wang L. Theory and application of maintenance decision models and methods. PhD thesis of Zhejiang University, 2007.
18. Wang Y B. Spare parts allocation optimization in a multi-echelon support system based on multi-objective particle swarm optimization method. Ekslpoatacja i Niezawodnosc - Maintenance and Reliability 2014; 16(1): 29–36.
19. Yoo Y K. Optimal joint spare stocking and block replacement policy. International Journal of Advance Manufacture Technology 2001; 18: 906–909, http://dx.doi.org/10.1007/PL00003959.

Yabin WANG
Jianmin ZHAO
Zhonghua CHENG
Zhiyuan YANG
Department of Management Engineering
Mechanical Engineering College
Shijiazhuang 050003, P. R. China

E-mail: wangyabin123@163.com, jm_zhao@hotmail.com,
zszs197466@163.com, yzy_sjz90@126.com

Article citation info:
KSIĄŻKIEWICZ A, JANISZEWSKI J. Low voltage relay contact resistance change influence by short-circuit current. Eksploatacja i Niezawodnosc – Maintenance and Reliability 2015; 17 (4): 600–603, http://dx.doi.org/10.17531/ein.2015.4.16.

Andrzej KSIĄŻKIEWICZ
Jerzy JANISZEWSKI

LOW VOLTAGE RELAY CONTACT RESISTANCE CHANGE INFLUENCE BY SHORT-CIRCUIT CURRENT

ZMIANA REZYSTANCJI ZESTYKOWEJ PRZEKAŹNIKÓW NISKIEGO NAPIĘCIA POD WPŁYWEM DZIAŁANIA PRĄDÓW ZWARCIOWYCH*

Electromagnetic relays are exposed to switching phenomena during its service life. These phenomena may include making of a short circuit, resulting in current flow of significant value for the relay contacts. This current influences the contacts surface and thus the value of the contact resistance, which is an important exploitation parameter for electromagnetic relays.The aim of the study is to analyze the impact of current flow of substantial value on the electric contact resistance of the relay contacts. Significant changes in the resistance after each switching cycle is observed.

***Keywords**: relays, contact materials, contact resistance.*

Przekaźniki elektromagnetyczne w trakcie swojej eksploatacji są narażone na niekorzystne zjawiska łączeniowe. Do narażeń tych można zaliczyć m.in. załączenie obwodu zwartego, co skutkuje przepływem prądu o znacznej wartości przez styki przekaźnika. Przepływ tego prądu, któremu w początkowej fazie może także towarzyszyć łuk elektryczny, wpływa na stan powierzchni styczek, a tym samym na wartość rezystancji zestykowej, będącej istotnym parametrem eksploatacyjnym przekaźników. Celem pracy jest analiza oddziaływania procesów załączania prądu o znacznej wartości na rezystancję zestykową przekaźników. Obserwowane są znaczne zmiany tej rezystancji po każdym cyklu łączeniowym.

***Słowa kluczowe**: przekaźniki, materiały stykowe, rezystancja zestykowa.*

1. Introduction

Electromagnetic relays are commonly used to connect circuitry with moderate values of the switching current (i. e. the medium current circuits) at a voltage not exceeding 1000 V. They are used inter alia as actuators in the building automation systems (eg. KNX, LCN, LonWorks) or in drivers and the programmable relays (Easy, NEED). They differ among themselves with a structure, purpose, and technical parameters. In regard to the contacts of connectors made of different materials, in literature, there are often presented results of research carried out as well in normal operation as in terms of specific exposures. These studies, however, are often focused on the low voltage (<50 V) direct current circuits [8]. Similar research were performed by Morin [16], Neuhaus [17] or Doublet [6], who independently conducted similar work for contacting materials for low voltage direct current circuits. Research related to processes of switching in circuits of medium voltage alternating current are focused on current ranges from a few to several kA [1, 9]. A noticeable is the lack of research in the field of low- and medium current AC switches at currents close to normal and short-circuit working conditions which may occur in low voltage electrical installations, that usually do not exceed 1 kA. Within the scope of modeling simulation studies are being conducted on the heating rail and contact connections with complex shapes, configurations and utilizing a variety of conductive materials [10].

Relays for connecting the receiving circuits are exposed to unfavorable processes. These phenomena may include closing overload and short-circuit currents, which may lead to shortening the life of-relays or, in extreme cases, their total damage. The article describes the impact of switching short-circuit on the change of the contact resistance. Relays with three different contacting materials have been investigated.

Contact resistance of the connector is the important performance parameter. It is important that during the utilisation of the relay this resistance reaches values as small as possible and simultaneously do not differed significantly in time. Among other things, associated with its heating the safe working load of the relay depends on its value [15]. The contact resistance value is dependent on [7, 14]:

– shape resistance R_k,
– tarnish resistance R_n.

The resultant value of contact resistance (transition) is equal to:

$$R_z=R_k+R_n \tag{1}$$

The tarnish resistance R_n is difficult to determine analytically, since it depends on multiple, sometimes random, factors including: temperature, humidity, contact material. The shape resistance R_k mainly depends on the resistivity and hardness of the contact material. To its description the single-point model with elliptical, equipotential current flowlines is often used [5, 7]. The actual contact area is much smaller than the apparent (nominal) surface of the contact point. This model can be considered correct, at low contact pressure forces used in relays.

The value of the contact resistance is affected by the material used for the contact rivet. As used may be the contact points of pure metals, including copper, silver, gold, platinum, palladium, tungsten or molybdenum. More often alloys and sinters, such as silver-copper, silver-cadmium, silver-palladium, silver-cadmium oxide, silver-tungsten, silver-nickel, silver-tin oxide are used [3]. Contacts may be

(*) Tekst artykułu w polskiej wersji językowej dostępny w elektronicznym wydaniu kwartalnika na stronie ***www.ein.org.pl***

covered with an additional layer of material with the aim of improving their certain properties (eg. resistance to material migration). Tin, silver or gold coverages are used. Coverage of the contact with the tin layer leads to a slight increase of the contact resistance relative to the uncoated material. Silver layer has the opposite effect, it reduces the contact resistance transition [19]. At present the most widely used-contact materials, in medium power low-voltage AC relays are sinters of silver with: nickel *AgNi*, cadmium oxide *AgCdO* and tin oxide $AgSnO_2$. The properties of each materials are as follows [3, 23]:

- *AgNi*: exhibits a low material migration, is not resistant to the influence of sulfur and its compounds and is prone to oxides formation,
- *AgCdO*: sulfur-sensitive material, characterized by resistance to welding, its application promotes the process of the electric arc extinguishing, is also resistant to material migration,
- $AgSnO_2$: the material is characterized by high thermal stability and material migration resistance, characterized by a stable contact resistance transition.

Materials made as silver-metal or silver-metal oxide are generally having a high resistance to welding [21]. The frequency and strength of welding during switching increases proportionately to the value of switching current arc, while the arc burning time has no such influence [17]. The force of contact welding does not exhibit the dependence on the static contact pressure force. It is however dependent on the speed of movement of the movable contact. These considerations are valid primarily for contacts made of pure silver [17].

2. Testing set

Miniature relays, using two previously mentioned contact materials, that is, *AgNi* and $AgSnO_2$, were subjected to research. For the later one two types of contacts, full and bimetal, have been tested. Bimetallic rivets are usually made by powder metallurgy technology or in the case of using metal oxides internal oxidation. Full rivets are often produced from the wire made of the contact material and their shape is obtained in the process of cold forging treatment. Electrical diagram of the testing set is shown in figure 1. The system is powered directly from the low voltage power network 230 V_{AC}. The circuit is protected against short circuits and overloads by circuit breakers with a rated operational current 16 A and B, C and D characteristic, and a general purpose fuse gG 16. For each protection device a single switching

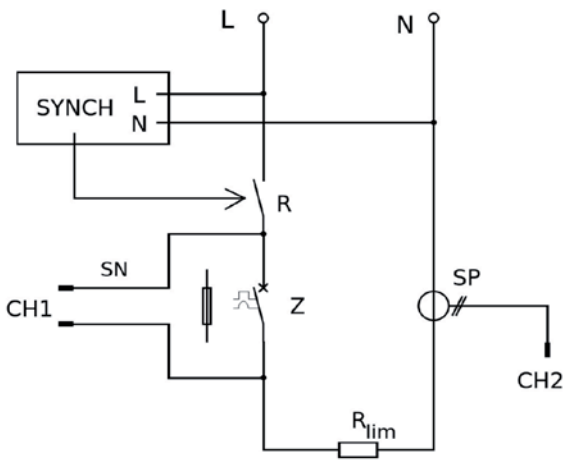

Fig. 1. Testing set electrical diagram: R – tested relay, Z – circuit protection: circuit breaker or fuse, R_{lim} – limiting resistor, SYNCH - synchronizing device, SP – current probe, SN – voltage probe, CH1, CH2 – oscilloscope channels

attempt with each of said contact material was made. By using the synchronizing device the moment of relay switching with the selected voltage phase repeatable testing conditions were obtained. As phase switching the zero crossing voltage was selected. Expected short circuit current was limited by resistor to the value of 320 A (I_m = 453 A). The average value of short circuit current peak for all samples was 413 A. The value lower than the expected may results from limiting it by the circuit protection device.

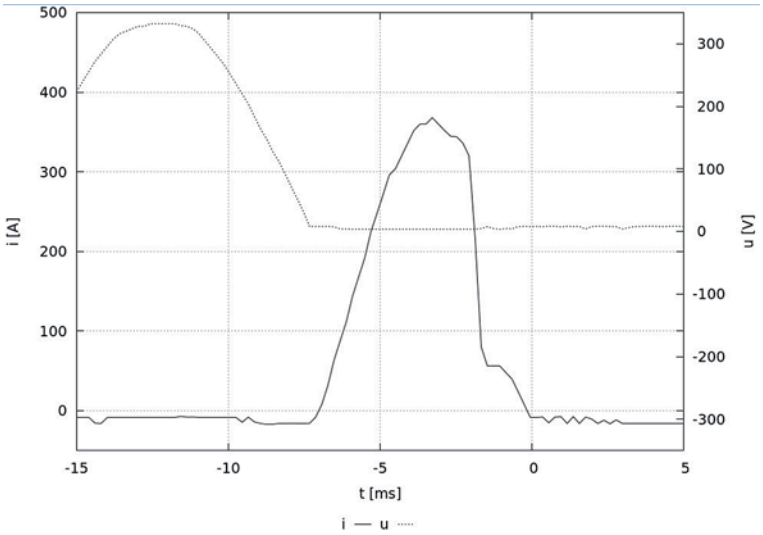

Fig. 2. The oscillogram of current intensity in the test circuit and voltage between contacts of the relay for randomly selected sample

The course of current intensity and voltage between rivets were recorded by oscilloscope using current and voltage probes. An exemplary oscillogram is shown in the figure 2. Relays were connected to the set through a dedicated switching slot. Resistance measurement was performed with four-wire Kelvin method using low resistance meter MI3252 by Metrel. For obtained results taken into account the resistance of the current paths transition of socket and relay was applied, to determine the value of searched contact resistance as closes as possible.

3. The results of measurements

Three types of relays with contacts made of the previously mentioned materials were tested. Each of them has been subjected to one switching trial. Before and after the circuit current switching test the transition resistance was measured. Attempts were performed in two ways, for relays both conditioned and not conditioned. As conditioning the author understands the mechanical processing of contacts by making a specified number of cycles (performed without electrical load). Conditioning of contacts affects the initial value of contact resistance [11]. The number of cycles for conditioning operations amounted to two thousand. For such number of cycles the contact resistance stabilization succeeded, and the differences between consecutive measurements showed little fluctuations. The tests were performed for various commonly used, overcurrent protections. Based on these results an attempt to demonstrate whether there is an additional factor that could affect the outcome was made. Average values of contact resistance for these cases, divided into relays subjected to conditioning and non-conditioned, are shown in table 1. These results do not distinguish between contact resistance values of the applied protection device because there was no such relationship in the applied test.

Changing the value of contact resistance for relays both conditioned and non-conditioned, depending on the contact material, for all tests carried out, is shown in figures 3 and 4. Contact resistance for

two cases after conditioning increased. Only for the AgNi there was a decrease of this value. This may be due to the fact that the material is characterized by the lowest value of the hardness in comparison to other (Tab. 2). Changing the structure of the contact point during switching operations, because of mechanical impact of the movable contact on the stationary one, might be possible due to the lower hardness of the material of the contact. This leads to increase of the actual contact surface area and thereby reduce the contact resistance. In other cases the opposite effect, that are loadless switching operations lead to an increase in contact resistance, was observed. Area of surface deformation of the contact point is dependent on the resistance of the material for welding. The smaller the resistance the greater the contact surface is changed [22]. The working hypothesis to explain the relationship is as follows. Unused contact point is characterized by a certain irregular surface on which micro elevations appear. These micro-elevations, upon first linking may increase the number of contact points, leading to a reduction of contact resistance. During the conditioning the contact surface of the contact point changes by mechanically removing of micro-elevations. After this operation, the surface of the contact point reaches the correct for itself target shape, for which a fair thesis becomes the single point of contact. Along with the change of the surface of the contact point changes its tarnish layer. Because the time between individual stages of research (conditioning – measurement of resistance – switching test – measurement of resistance) was as short as possible, the impact of the tarnish layers on the final result was marginal.

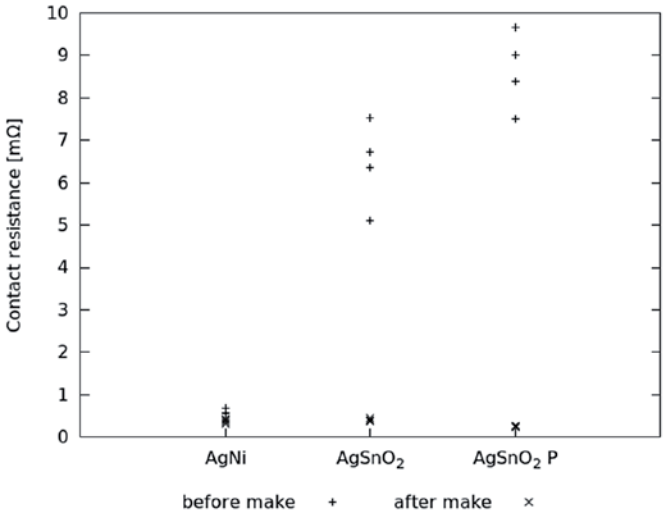

Fig. 4. Change of the contact resistance under the influence of switching the short circuit current; conditioned relays: P – relay with full rivets

Table 2. Selected properties of contact materials used in low-voltage relays [20]

Material	Density	Hardness	Thermal conductivity at 20°C	Electrical conductivity
	[kg/m^3]	[HB]	[W/K·m]	10^{-8}[Ωm]
AgNi	10 300	50	350	1,84
$AgSnO_2$ / $AgSnO_2$ P	9 900	70	307	2,04

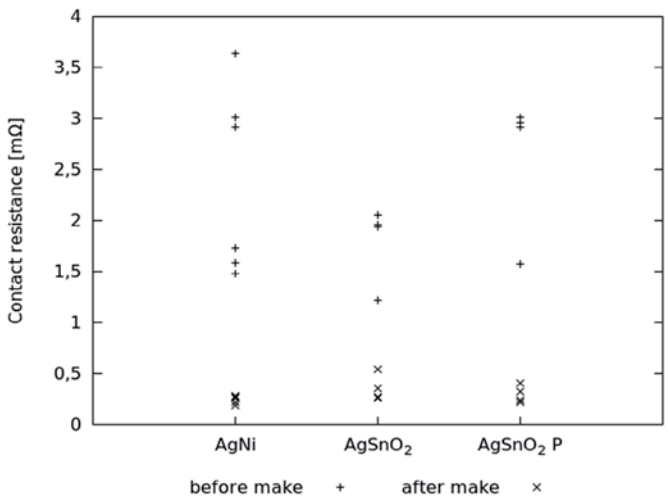

Fig. 3. Change of the contact resistance under the influence of switching the short circuit current; non-conditioned relays: P – relay with full rivets

From Table 1 it also follows that regardless of the initial value of the contact resistance, after attempting to switch short-circuit current, the resistance significantly decreases.

When switching the short circuit current the pre-ignition arc or contact bounce during the conduction of electricity may occur. The fact which phenomenon occurs contributes to contacts welding force [4].

Both of these phenomena affect very negatively on the condition of the contact point and lead to the appearance of the electric arc. With the increase in the value of the switching current intensity increases the loss of mass of the contact point [2, 18, 21]. In addition, the arc can lead to a strong local heating of the arc spot, even above the melting point of the contact material [12]. If at least on the surface of one of the contact points the contact material will be melted and at the same time after contact occurs, there will be welding of contacts [13]. Original contact materials' properties change when the contact area or composition of the material changes [22]. The composition can be altered by the thermal influence of current. These relationships are correct primarily for connecting currents with considerable intensity, on the order of several kilo amperes.

Table 1. Average values of the conditioned and non-conditioned relays contact resistance, before and after the short circuit switch test was performed,

No.	Contact material	The average value of the contact resistance before test	The average value of the contact resistance after test
		[mΩ]	[mΩ]
Non-conditioned relays			
1	AgNi	2,3927	0,2502
2	$AgSnO_2$	1,7909	0,1262
3	$AgSnO_2$ P	2,6162	0,3014
Conditioned relays			
1	AgNi	0,6252	0,3850
2	$AgSnO_2$	6,4300	0,4040
3	$AgSnO_2$ P	8,6381	0,2467
P – *relay with full rivets*			

4. Summary

The occurrence of the short circuit current in the electrical installation is most often the result of an emergency and as such is a unconsolidated event. Based on the results of measurements it can be seen that the short circuit current switching via relay significantly affects the value of its contact resistance. For each of the registered cases there was a decrease of contact resistance values. Its low value can be considered decent, if only because of lower power losses and lower temperature rise of the contact point of the relay during normal use. Conditioning of contacts is substantially affecting the contact resistance. You can not clearly determine whether this operation will result in its increase or decrease. For contacts made of AgNi there was a decrease of this

value, whereas for both contacts performed of $AgSnO_2$ it increased significantly. Regardless of the initial value of contact resistance after the short circuit current switching test this resistance was significantly decreased. Knowledge of contact resistance value under normal operating conditions could be used to indirectly assess the state the contacts surface. In further studies it is expected to develop methods for assessing the state of wear of the surface on the basis of the change in contact resistance.

The research is funded under purpose subsidy for scientific research or development works and the tasks associated with it, for the development of young scientists and doctoral students at the Faculty of Electrical Engineering Poznan University of Technology No. **04/41/DSMK/4133.**

References

1. Borkowski P. Arc erosion of contacts on switching high currents. Archives of Electrical Engineering 2004; 53: 259-287.
2. Borkowski P. Nowoczesne metody badań zestyków elektrycznych. Akademicka Oficyna Wydawnicza EXIT, 2013.
3. Celiński Z. Materiałoznawstwo elektrotechniczne. Oficyna Wydawnicza Politechniki Warszawskiej, 2011.
4. Chen Z.K, Witter G.J. A Study of Dynamic Welding of Electrical Contacts with Emphasis on the Effects of Oxide Contentfor Silver Tin Indium Oxide Contacts. Proceedings of the 56th IEEE Holm Conference on Electrical Contacts 2010; 56: 1-6.
5. Ciok Z. Procesy Łączeniowe w układach elektroenergetycznych. Wydawnictwo Naukowo-Techniczne 1983.
6. Doublet L, Ben Jemaa N, Hauner F, Jeannot D. Make arc erosion and welding tendency under 42 VDC in automotive area. Proceedings of the Forty-Ninth IEEE Holm Conference on Electrical Contacts; 2003:158-162.
7. Holm R. Electric Contacts. Springer-Verlag Berlin Heidelberg GmbH 1981
8. Kharin S.N, Sarsengeldin M. Influence of Contact Materials on Phenomena in a Short Electrical Arc. Key Engineering Materials 2012; 510-511: 321-329, http://dx.doi.org/10.4028/www.scientific.net/KEM.510-511.321.
9. Kolimas Ł. Analysis of the making arcing time during current switching. Przeglad Elektrotechniczny 2008; 84: 72-74.
10. Kolimas Ł. Modelowanie i analiza rozpływu temperatury w torach wielkoprądowych i zestykach. Przegląd Elektrotechniczny 2014; 9: 183-186.
11. Książkiewicz A. Change of electric contact resistance of an electromagnetic relay during switching operations withoutelectric load. 5th International Interdisciplinary Technical Conference of Young Scientists InterTech 2012; 5: 257-260
12. Książkiewicz A, Janiszewski J. Electrical contact temperature change after short-circuit current. Poznan University of Technology Academic Journals. Electrical Engineering 2014; 78: 65–70.
13. Książkiewicz A, Janiszewski J, Batura R. Influence of short-circuit AC currents on electrical contact resistance of low voltage relays. Poznan University of Technology Academic Journals. Electrical Engineering 2012; 70: 99-103.
14. Kulas S. Tory prądowe i układy zestykowe. Oficyna Wydawnicza Politechniki Warszawskiej 2008.
15. Maksymiuk J, Pochanke Z. Obliczenia i badania diagnostyczne aparatury rozdzielczej. Wydawnictwo Naukowo-Techniczne, 2001.
16. Morin L, Jemaa N.B, Jeannot D. Make arc erosion and welding in the automotive area, IEEE Transactions on Components and Packaging Technologies 2000; 23: 240-246, http://dx.doi.org/10.1109/6144.846760
17. Neuhaus A.R, Rieder W.F, Hammerschmidt M. Influence of Electrical and Mechanical Parameters on Contact Welding in Low Power Switches. IEEE Transactions on Components and Packaging Technologies 2004; 27: 4-11, http://dx.doi.org/10.1109/TCAPT.2004.825777.
18. Pons F, Cherkaoui M. An electrical arc erosion model valid for high current: Vaporization and Splash Erosion. Proceedings of the 54th IEEE Holm Conference on Electrical Contacts 2008; 54: 9-14, http://dx.doi.org/10.1109/holm.2008.ecp.15.
19. Sawada S, Shimizu K, Hattori Y, Tamai T, Iida K. Analysis of Contact Resistance Behavior for Electric Contacts with Plating Layer. Proceedings of the 56th IEEE Holm Conferenceon Electrical Contacts 2010; 56: 1-8, http://dx.doi.org/10.1109/holm.2010.5619560.
20. Thurston M. O. Electrical Contacts. Fundamentals, Applications and Technology. Taylor & Francis Group LLC, 2007.
21. Walczuk E, Borkowski P, Księżarek S, Missol W, Rdzawski Z, Durst K. Evaluation of Basic Electrical Parameters of Silver-Based Contact Materials of Different Chemical Composition and Manufacturing Technology. Proceedings of the 56th IEEE Holm Conference on Electrical Contacts 2010; 56: 1-8, http://dx.doi.org/10.1109/holm.2010.5619550.
22. Zhenbiao L, Lichun C, Jiyan Z. The metallurgical researchon contact surface deterioration of AgNi, AgW, AgFe, AgCu contact materials. Proceedings of the Forty-First IEEE HolmConference on Electrical Contacts 1995; 41: 346-349.
23. www.relpol.com.pl, 2014. Relpol. Przekaźniki.

Andrzej KSIĄŻKIEWICZ
Jerzy JANISZEWSKI
Faculty of Electrical Engineering
Poznan University of Technology
Piotrowo 3a, 60-965 Poznan, Poland
E-mail: andrzej.ksiazkiewicz@put.poznan.pl,
jerzy.janiszewski@put.poznan.pl

Article citation info:
KOSICKA E, KOZŁOWSKI E, MAZURKIEWICZ D. The use of stationary tests for analysis of monitored residual processes. Eksploatacja i Niezawodnosc – Maintenance and Reliability 2015; 17 (4): 604–609, http://dx.doi.org/10.17531/ein.2015.4.17.

Ewelina KOSICKA
Edward KOZŁOWSKI
Dariusz MAZURKIEWICZ

THE USE OF STATIONARY TESTS FOR ANALYSIS OF MONITORED RESIDUAL PROCESSES

WYKORZYSTANIE TESTÓW STACJONARNOŚCI DO ANALIZY MONITOROWANYCH PROCESÓW RESZTKOWYCH*

Sustaining high operational efficiency of a machine park requires the use of state-of-art solutions that support both monitoring of residual processes and performing thorough analysis of thereby collected data. What meets the needs of entrepreneurs who strive for high reliability of technological infrastructure is a modern approach to maintenance prediction. The literature of the subject offers numerous studies presenting the use of various statistical models for time series prediction. The objective of this paper is to verify whether tests used in econometrics such as the augmented Dickey-Fuller test and the Kwiatkowski-Phillips-Schmidt-Shin test are suitable for failure prediction. The simulations were performed for one diagnostic parameter, i.e. temperature.

Keywords: *failure prediction, maintenance, stationary tests, ADF, KPSS.*

Utrzymanie wysokiego poziomu efektywności eksploatacyjnej parku maszynowego wymaga stosowania nowoczesnych rozwiązań wspierających monitorowanie procesów resztkowych i poddawania szczegółowej analizie uzyskanych w ten sposób informacji. Naprzeciw oczekiwaniom przedsiębiorców dotyczących utrzymywania wysokiego poziomu niezawodności infrastruktury technicznej wychodzi nowoczesne podejście w obszarze gospodarki remontowo-konserwacyjnej, jakim jest predyktywne utrzymanie ruchu. W literaturze przedmiotu wielokrotnie prezentowano wykorzystanie różnych modeli statystycznych pozwalających na prognozowanie wartości szeregów czasowych. Celem niniejszej pracy było sprawdzenie czy stosowany w ekonometrii rozszerzony test Dickeya-Fullera oraz test Kwiatkowskiego, Phillipsa, Schmidta i Shina mogą zostać użyte do predykcji zdarzeń niepożądanych jakimi są awarie. Symulację przeprowadzono dla wartości jednego parametru diagnostycznego jakim była temperatura.

Słowa kluczowe*: predykcja awarii, utrzymanie ruchu, testy stacjonarności, ADF, KPSS.*

1. Introduction

Meeting contractual obligations is one of the factors that affect operational efficiency of an enterprise. Hence, prompt delivery of a contracted quantity and quality of products is a key task of every company. On the one hand, the use of state-of-the-art manufacturing techniques and advanced production processes enables companies to meet contractual obligations; on the other, it poses problems regarding reliability of production equipment. Consequently, the actions supporting operations taken by a company's maintenance department (production equipment must be kept in constant operational efficiency by controlling technical condition of machines and devices) become increasingly significant. According to Legutko [1], operation is the whole of phenomena, processes and events that occur during the period of existence of a device, from the moment of its construction until its withdrawal from use. When used with respect to maintenance, the term "efficiency" is defined as a property of people or technical objects which determines whether they meet different requirements, e.g. in terms of reliability, economy or quality. Operational efficiency is a quotient of effects produced in a fixed time interval of duration of a given state of an operating object to the costs of achieving these effects. Increasing operational efficiency of machines via failure prediction and restoring full efficiency of a production system, ensures prompt completion of contractual obligations, which – in turn – means higher profits of the enterprise. This is of key importance given the strong competition between enterprises, where constant improvement of manufacturing systems, development of production technologies and production automation solutions are key to success.

The growing interest in predictive maintenance combined with the problem of unused data collected by systems monitoring machine park operations have inspired the present authors to undertake studies aimed at verification the effectiveness of failure prediction by stationary tests. Additionally, on detecting alarming symptoms, residual time of machinery operation was determined, too. Seasonal changes in ambient conditions can have a negative impact on values of observed state parameters and, thus, on the efficiency of predictions made using stationary tests. If this is the case, it is necessary to present assumptions concerning investigated signals (the effect of changes in ambient conditions on observation vector values). Since the simulation assumed maintaining constant ambient temperature conditions, its impact on non-stationarity was not taken into consideration.

2. Effect of maintenance activities on operational efficiency

The observations made in the field of maintenance demonstrate that the dominant trend in most enterprises is to repair machines and devices only after failure, as a result of which the time for response actions exceeds the time for planned operations. This leads to a decrease in operational efficiency. In addition to this, poor condition

(*) Tekst artykułu w polskiej wersji językowej dostępny w elektronicznym wydaniu kwartalnika na stronie ***www.ein.org.pl***

of technical infrastructure leads to lower productivity generating additional losses. The actions taken to improve operational efficiency of enterprises should hence strive to eliminate waste in the form of inefficient work of both machines and maintenance staff. The indicators listed in the standard EN15341 [29] for determining maintenance services efficiency can be useful for verification of the efficiency of implemented improvements [23]. One of the most widely applied indicators is Overall Equipment Effectiveness (OEE) [1, 20, 19]. The considerations of ways of improving the functioning of maintenance and repair sector management also point to connections between operational efficiency level and its selected structure [20, 23].

Maintenance operations are undertaken to:

- maintain specific quality of products/services,
- prolong as much as possible the operation life of production equipment,
- ensure conditions for safe operation of machines and devices,
- reduce production costs as much as possible by limiting production breaks.

The above actions can be implemented following determination of a machine or process state by physical quantities. The behaviour of machines or production processes is modelled by equations of state described by some functions $f(t)$, $t \in T$, where the independent variable t is a time variable, while T is a time interval. The determination of state of a technical object is called diagnosing. Figure 1 shows schematically processes that occur in production and types of diagnosed working and accompanying processes.

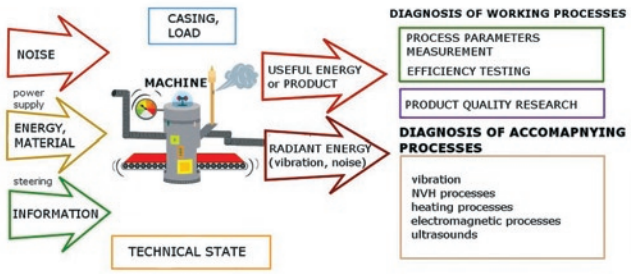

Fig. 1. Schematic representation of processes occurring in a machine and of methods for diagnosing working and accompanying processes [1]

What can occur in operational processes are random events caused, among others, by human error, impact of natural environment and operational environment. With wise modelling of random factors that affect behaviour of machines and production processes, we can increase operational efficiency of such objects [18, 24]. It can therefore be claimed that maintenance is one of the key processes that have a direct impact on increasing operational efficiency.

The efficiency of a machine park depends on operations which provide a basis for_preventive maintenance. This means that decisions concerning machinery maintenance operations are taken based on technical and operational documentation. According to the predictive maintenance approach [4], the moment of maintenance operations in a production process should be scheduled based on machinery condition. For this reason, symptom monitoring, particularly in a non-invasive way, becomes more and more popular. The moments of machine maintenance operations are scheduled based on observation of residual processes using, among others, infrared cameras [37], vibroacoustic sensors [31] and pressure sensors [6]. Residual processes are thermal, frictional, electric and vibroacoustic (vibrations, noise, fluctuation of a working medium in the machine), and can often be a symptom or determinant of wear [5].

3. Stationary processes and system reliability

The behaviour of physical, economic and technical systems is usually described by mathematical models. First, based on historical data, values of structural parameters are determined, and then, following parametric identification, these models can be used to predict the behaviour of systems being described. The behaviour of machines and devices is often predicted by time series models. By predicting future values of system states, we can draw conclusions about a possibility of failure of machines and devices.

Time series can be divided into stationary and non-stationary (see e.g. [2, 11, 7, 27]).

Definition 1. The time series $\{x_t\}_{t \in N_0}$ is said to be strict stationary if for every $m \in N$, any $t_1 < t_2 < ... < t_m$ and every $\tau \in N$ the joint distributions of the probability of m elements of random sequences $x_{t_1}, x_{t_2}, ..., x_{t_m}$ and $x_{t_1+\tau}, x_{t_2+\tau}, ..., x_{t_m+\tau}$ are identical.

Therefore, for stationary time series, the statistical and dynamical properties for any time shift remain unchanged. Given the above, the mean and variance of the elements of the time series $\{x_t\}_{t \in N_0}$ are constant over time.

Definition 2. The time series $\{x_t\}_{t \in N_0}$ is said to be homogeneous non-stationary (homoscedastic) if, by separating a non-random component from the time series, we obtain a stationary series. Homogenously non-stationary series can contain among others a deterministic or stochastic trend; they can have a seasonal or periodic character. Following the application of a differential operator, such series can be reduced to stationary series [2, 11].

Definition 3. The time series $\{x_t\}_{t \in N_0}$ is said to be integrated of order d (defined by $\{x_t\}_{t \in N_0} \in I(d)$) if the series $\left\{\Delta^k x_t\right\}_{t \geq k}$ for $0 \leq k < d$ is non-stationary, while the series $\left\{\Delta^d x_t\right\}_{t \geq d}$ is said to be stationary, where the differential operator Δ is defined as $\Delta x_t = x_t - x_{t-1}$, while $\Delta^{k+1} x_t = \Delta^k x_t - \Delta^k x_{t-1}$ for $k \in N$ (see e.g. [2, 11, 15, 27]).

The stationarity of time series is most often investigated by the augmented Dickey-Fuller test [7], the Kwiatkowski-Phillips-Schmidt-Shin test [16], Philips-Perron test [28] (they are examples of unit root tests also known as stationary tests).

The above tests for time series analysis can be used to investigate reliability of systems and devices. If the results of classical unit root tests confirm the presence of stationarity (static and dynamic properties remain unchanged) and values of the system state are within a fixed range (belong to acceptable interval), then – given the lack of alarming symptoms – it is stated that the system behaves correctly. If it is found (based on the realization state system) that the quality of stationarity is not met, i.e. the system's behaviour contains a linear, polynomial trend (depending on integration degree), it is an alarming symptom. By using the differential operator Δ^d the non-stationary homoscedastic time series $\{x_t\}_{t \in N_0}$ can be reduced to the stationary series $\left\{\Delta^d x_t\right\}_{t \geq d}$ (for more information see [2, 15, 27]). The integration order d defines the degree of a polynomial approximating for deterministic part in a time series (dependence between differentiation and polynomial trend is exhaustively discussed in [15, Section 2.4]). Next, using the least squares method, we determine a deterministic trend in the time series and then, based on prediction of behavior of the time series, we determine the expected time to exceeding acceptable values for a given system (alarming critical values) – residual operation time of a device. The subsequent section presents classi-

cal stationary tests that are employed to determine the moment of taking a decision with respect to device maintenance operations.

4. Stationary tests

Maintenance can be achieved by repairing devices that restore efficiency of technical infrastructure. Maintenance dates are usually scheduled based on technical and operational documentation. The problem occurs when such actions are to be taken based on the real condition of a machine. To obtain information regarding the necessity of repair based on analysis of the diagnostic parameter, we used time series stationary tests.
Below, we present two classical stationary tests: ADF and KPSS.

To perform the augmented Dickey-Fuller test (ADF) [see e.g. 8, 11, 15, 27], it is necessary to consider the time series $\{x_t\}_{t\in N_0}$ with the state equation:

$$\Delta x_t = \theta x_{t-1} + \sum_{i=1}^{k} \Delta x_{t-i} + \varepsilon_t, \tag{1}$$

where $\{\varepsilon_t\}_{t\in N}$ is a sequence of independent random variables with the normal distribution $N\left(0,\sigma^2\right)$. The order of autoregression $k \in N$ should be set such to eliminate correlations between the elements of the series $\{\varepsilon_t\}_{t\in N}$. Then, at the significance level α, we construct a null hypothesis that the time series $\{x_t\}_{t\in N_0}$ is non-stationary (i.e. we take that $\theta = 0$, therefore $\{x_t\}_{t\in N_0} \in I(d)$ and $d \geq 1$). As an alternative hypothesis, we take that the time series $\{x_t\}_{t\in N_0}$ is stationary (i.e. $\theta \in (-2,0)$, therefore $\{x_t\}_{t\in N_0} \in I(0)$). The test statistics:

$$DF = \frac{\hat{\theta}}{S(\theta)} \tag{2}$$

has a Dickey-Fuller distribution, where $\hat{\theta}$ is an estimator of the θ parameter, while $S(\theta)$ denotes the standard deviation of this parameter. The estimator of the θ parameter and standard deviation are determined by the least squares method. Based on the Dickey-Fuller distribution tables, we determine a critical value DF^*. If $DF^* \leq DF$, then at the significance level α there are no grounds to reject the null hypothesis, therefore the elements of the series $\{x_t\}_{t\in N_0}$ are integrated to one or higher (i.e. we take that the series $\{x_t\}_{t\in N_0}$ is non-stationary). If $DF < DF^*$, then on the significance level α we reject the working hypothesis in favour of an alternative hypothesis and take that the series $\{x_t\}_{t\in N_0}$ is stationary. If it is found that the series $\{x_t\}_{t\in N_0}$ is non-stationary, we additionally test the stationarity of the series $\left\{\Delta^d x_t\right\}_{t\geq d}$ for d≥1 in order to determine the degree of a polynomial approximating deterministic part of the series $\{x_t\}_{t\in N_0}$.

The verification of time series stationarity can be done based on the Kwiatkowski-Phillips-Schmidt-Shin test [see e.g. 11, 14, 15, 27] (KPSS test). Therefore, we must consider the series $\{x_t\}_{t\in N_0}$ with the state equation:

$$x_t = \beta t + r_t + \varepsilon_t, \tag{3}$$

where $\{\varepsilon_t\}_{t\in N}$ is a sequence of independent random variables with the normal distribution $N\left(0,\sigma^2\right)$. The process $\{r_t\}_{t\in N_0}$ denotes a random walk process

$$r_t = r_{t-1} + \nu_t, \tag{4}$$

where $\{\nu_t\}_{t\in N}$ is a series of independent random variables with the normal distribution $N\left(0,\sigma_\nu^2\right)$. At the significance level α we construct the null hypothesis that the time series $\{x_t\}_{t\in N_0}$ is stationary (i.e. we take that $\sigma_\nu^2 = 0$, then the elements of the series $\{r_t\}_{t\in N_0}$ are constant and $\{x_t\}_{t\in N_0} \in I(0)$). As an alternative hypothesis, we take that the time series $\{x_t\}_{t\in N_0}$ is non-stationary (i.e. we take that $\sigma_\nu^2 > 0$, then $\{r_t\}_{t\in N_0}$ denotes a random walk process, which causes that the elements of the series $\{x_t\}_{t\in N_0}$ are created as the sum of elements of a stationary $\{\varepsilon_t\}_{t\in N}$ and non-stationary $\{r_t\}_{t\in N_0}$ series). For realization $\{x_t\}_{1\leq t\leq n}$ we use the least squares method to estimate values of parameters of the model (3) and to determine the test statistics:

$$\eta = \frac{\sum_{t=1}^{n} S_t^2}{n^2 S^2(k)}, \tag{5}$$

where $S_t = \sum_{i=1}^{t} \varepsilon_i$, $S^2(k) = \frac{1}{n}\left(\sum_{i=1}^{n} \varepsilon_i^2 + 2\sum_{s=1}^{k} w(s,k) \sum_{t=s+1}^{n} \varepsilon_t \varepsilon_{t-s}\right)$, weights $w(s,k) = 1 - \frac{s}{k+1}$ while k denotes the order of delay. From the tables of the KPSS test, we take the limit value η^*. If $\eta < \eta^*$, then at the significance level α there is no ground for rejecting the null hypothesis, therefore it is taken that the elements of the time series $\{x_t\}_{t\in N_0}$ are integrated in order zero (we take that the series $\{x_t\}_{t\in N_0}$ is stationary). If $\eta \geq \eta^*$, then at the significance level α, we reject the null hypothesis in favour of an alternative hypothesis and take that that the series $\{x_t\}_{t\in N_0}$ is non-stationary.

An algorithm of the proposed approach consisting in assessment of stationarity of time series of temperature is illustrated in Fig. 2.

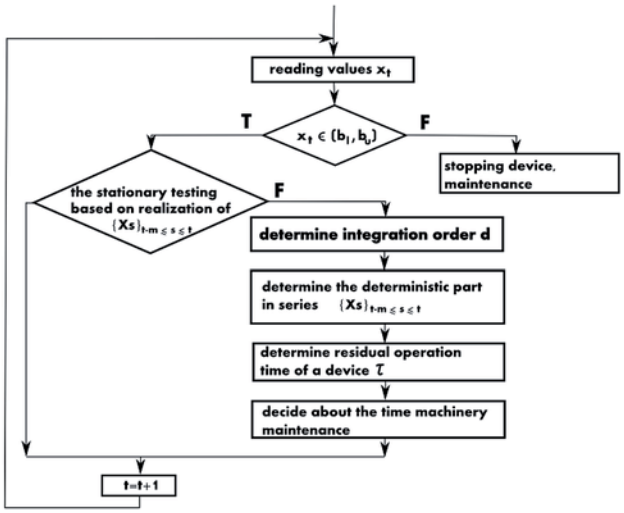

Fig. 2. Algorithm of the proposed approach consisting in assessment of stationarity of time series of temperature (prepared by the authors)

5. Use of stationary tests for analysis of production machinery reliability

Direct reading of device parameters allows us to find whether this device operates correctly (if the parameter value is within the acceptable limit) or not. The use of stationary tests during monitoring of machinery operation enables real-time verification of whether these machines operate correctly. If non-stationarity is detected in a time series by the least squares method, it is necessary to determine a trend in this time series, predicting in this way the behaviour and residual operation time of the device. The moment of determining non-stationarity in the time series is the moment of taking a decision about device maintenance (a maintenance operation date must be scheduled). If the remaining time for production realization does not exceed the residual operation time, then the production maintenance should be done following production process/contractual obligation; otherwise, it is necessary to schedule a maintenance date which does not exceed the residual operation time.

Below, we present the simulations of monitoring correct operation of production machinery by stationary testing. To this end, we used the ADF and KPSS tests. The simulations were performed using the MATLAB programme. The generated numerical values were to represent temperature values read from two sensors. These values were used to create dynamically diagrams for these sensors (Fig. 3).

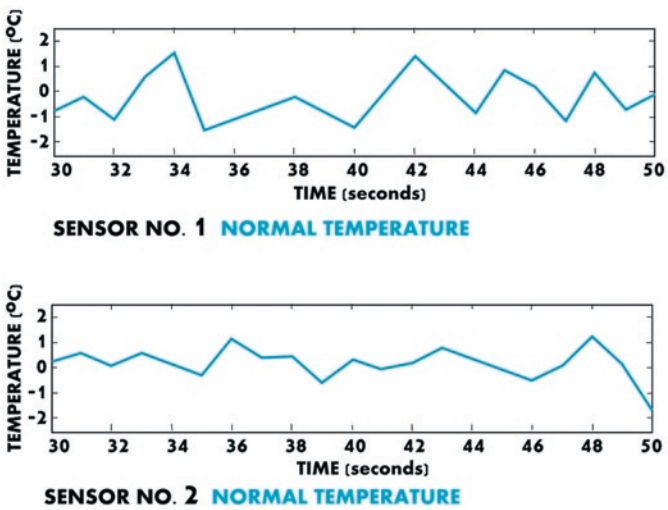

Fig. 3. MATLAB-generated diagrams showing temperatures recorded by two sensors (developed by the authors)

The stationary dynamical testing was conducted based on m -element realization of the series $\{x_s\}_{t-20 \le s \le t}$ for $t \ge m$ (where $m = 20$). If the observed values are within the acceptable interval (b_l, b_u) and the criterion of stationarity is satisfied, then it is concluded that the device is operating correctly. If the ADF test results pointed to non-stationarity, we used the least squares method to determine a trend in this time series $\{x_s\}_{t-20 \le s \le t}$. In addition, we determined the predicted time to exceeding the critical temperature level, the acceptable interval of values being set to (−20°C, 20°C). If the stationary analysis is performed based on short realizations of the time series and the device is placed in a room where atmospheric conditions does not affect its operation, the effect of environment can be omitted. Moreover, the selection of duration should be set adequately to the analyzed problem. Undoubtedly, a value from the previous observation moment is of higher informative significance than a value from the previous year, which is the so-called "data freshness problem".

Figure 3 shows the detection of process non-stationarity, residual time of correct operation of the device and the probability of the zero hypothesis. Based on the realization of $\{x_s\}_{60 \le s \le 80}$ for Sensor 1 by the least squares method, we also determined the state equation:

$$x_{60+t} = 5.35 + 0.492t + \varepsilon_t, \tag{6}$$

where $\{\varepsilon_t\}_{t \in N}$ is a sequence of independent random variables with the normal distribution $N(0, 0.83)$. Based on the results, we predicted subsequent temperature values on Sensor 1 using the equation:

$$x_{80+t} = x_{80} + 0.492t + \varepsilon_t, \tag{7}$$

where $\{\varepsilon_t\}_{t \in N}$ is a sequence of independent random variables with the normal distribution $N(0, 0.83)$ and $x_{80} = 14.12$. The predicted temperature values are determined by the equation:

$$\hat{x}_{80+t} = Ex_{80+t} = x_{80} + 0.492t. \tag{8}$$

The residual time of correct operation of the device is determined as:

$$\tau = \min\{t \in N;\ \hat{x}_{80+t} \notin (-20, 20)\} = 12. \tag{9}$$

Similar results were produced using the KPSS test during the monitoring of temperature reading on Sensor 1. The system user is notified about the exceeding of the critical/acceptable temperature limit by the information displayed under the diagram (Fig. 5). The simulated stationary test results demonstrate that both the ADF and KPSS test are effective methods for failure prediction based on the values of one residual process, i.e. temperature. Besides the ADF and KPSS tests, homogenous non-stationarity can also be investigated using such tests as the Philips-Perron test, Leybourn-McCabe test, Engle-Granger cointegration test, Johansen cointegration test, while non-homogeneous non-stationarity (heteroscedasticity, e.g. for vibration analysis) can be investigated by the Engle's ARCH test, Breusch-Pagan test, White's test, etc.

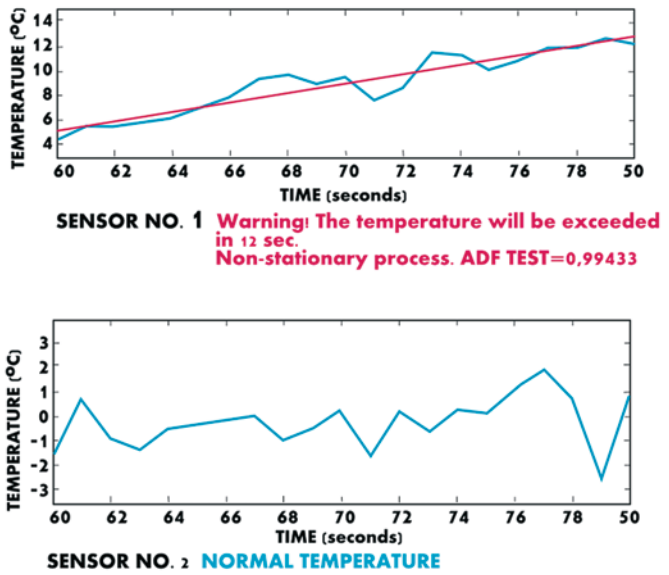

Fig. 4 Notification about process non-stationarity generated due to changes in temperature (developed by the authors)

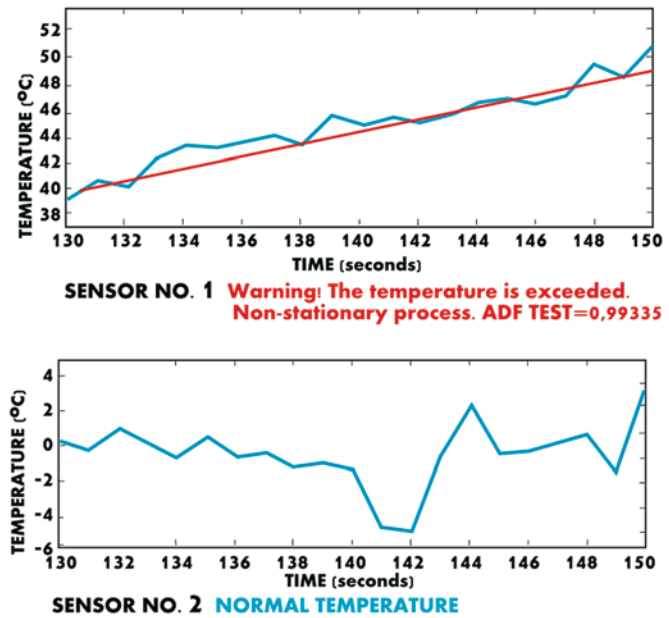

Fig. 5 Notification that the temperature has been exceeded on Sensor 1 (prepared by the authors)

6. Conclusions

The control of a machine park is one of the factors that enable increasing operational efficiency. While the monitoring of diagnostic parameters does not provide a basis for deciding about the necessity of taking maintenance and repair activities, this decision can be taken based on adequate mathematical models for data analysis. One-symptom diagnostics can be performed using statistical stationary tests such as the ADF and KPSS tests, as demonstrated by the MATLAB simulation. The detection of non-stationarity and the determination of a residual operational time of a device can serve as a guideline for maintenance services, signalling that it is necessary to undertake maintenance activities regarding subassemblies or machine components exhibiting alarming changes. This is proved by the simulation results – the alarming changes in the diagnostic parameter, i.e. temperature, were signaled in the programme and, additionally, the predicted time to failure occurrence was announced.

The above statistical tests can be applied for failure prediction due to the fact that they enable analysis of data sets containing values of monitored observation vectors describing machine condition. With the current technologies for recording values of observed parameters and easy access to data storage servers, it is possible to create extensive collections of data. If the collected data are variable and diverse, they are described as *big data* [33].

It must however be stressed that given the multi-symptom machinery diagnostics offering a broad perspective on changing condition of technical infrastructure, the proposed solution should be extended to enable detecting correlations between reduced observation vectors. It is therefore recommended establishing a standard of model development which is based on independent and complete state parameters and fosters optimization of operational efficiency. When developing such model, it should also be taken into account that some measurement results can be random.

References

1. Antosz K, Stadnicka D. Evaluation measures of machine operation effectiveness in large enterprises: study results. Eksploatacja i Niezawodnosc – Maintenance and Reliability 2015; 17 (1): 107–117, http://dx.doi.org/10.17531/ein.2015.1.15.
2. Box G. E. P., Jenkins G.M. Analiza szeregów czasowych. Warszawa: PWN, 1983.
3. Burnos A. Efektywność utrzymania ruchu. Agro Przemysl 2012;2.
4. Carnero MC. Selection of diagnostic techniques and instrumentation in a predictive maintenance program. A case study. Decision Support Systems 2005; 38, http://dx.doi.org/10.1016/j.dss.2003.09.003.
5. Cempel Cz. Diagnostyka wibroakustyczna maszyn. Warszawa: PWN, 1989.
6. Cieślikowski B. Proces diagnostyki układu hydrauliki siłowej w mechanizmie obrotu pługa. Inzynieria Rolnicza 2009; 9.
7. Chow G.C. Ekonometria. Warszawa: PWN, 1995.
8. Dickey D.A, Fuller W.A. Distributions of the estimators for autoregressive time series with a unit root. Journal of the American Statistical Association 1979; 74: 427-431.
9. Dutkowska B. Rosnąca rola systemów CMMS. http://www.utrzymanieruchu.pl/menu-gorne/artykul/article/rosnaca-rola-systemow-cmms/ (dostęp: 12.03.2015r.).
10. Doman M., Doman R. Ekonometryczne modelowanie dynamiki polskiego rynku finansowego. Poznań: Wydawnictwo Akademii Ekonomicznej w Poznaniu, 2004.

11. Hamilton J.D. Time Series Analysis. Princeton: Princeton University Press, 1994.
12. Hetmańczyk M. Predykcyjne utrzymanie ruchu. Inzynieria & Utrzymanie Ruchu Zakładow Przemyslowych 2015: 1, 60-64.
13. Ho T. The government spending and private consumption: a panel cointegration analysis. International Review of Economics & Finance 2002; 10: 95-108, http://dx.doi.org/10.1016/S1059-0560(00)00073-3.
14. Komitet Inżynierii Produkcji PAN. Istota inżynierii produkcji. Warszawa: PAN, 2012.
15. Kozłowski E. Analiza i identyfikacja szeregów czasowych. http://www.kozlowski.pollub.pl/analiza_szeregow.pdf (dostęp: 12.06.2015r.).
16. Kwiatkowski D., Phillips P.C.B., Schmidt P., Shin Y. Testing the Null Hypothesis of Stationary Against the Alternative of a Unit Root. Journal of Econometrics 1992; 54: 159-178, http://dx.doi.org/10.1016/0304-4076(92)90104-Y.
17. Legutko S. Podstawy eksploatacji maszyn i urządzeń. Warszawa: Wydawnictwa Szkolne i Pedagogiczne, 2004.
18. Leszek W., Mazurkiewicz A., Trzos M. Projektowanie eksperymentalnych systemów badawczych w budowie i eksploatacji maszyn. Radom: Biblioteka Problemów Eksploatacji. Instytut Technologii Eksploatacji, 1999.
19. Ljungberg Õ. Measurement of overall equipment effectiveness as a basis for TPM activities. International Journal of Operations & Production Management 2002: 18; 495-507, http://dx.doi.org/10.1108/01443579810206334
20. Loska a. exploitation assessment of selected technical objects using taxonomic methods. Eksploatacja i Niezawodnosc – Maintenance and Reliability 2013; 15 (1): 1–8.
21. Ludwig, B. Predicting the future: Have you considered using the Delphi methodology. Journal of Extension 2005; 6.
22. Mazurkiewicz D. Studium wybranych aspektów diagnostyki eksploatacyjnej transportu taśmowego. Politechnika Lubelska. Lublin, 2011.
23. Mączyński W., Nahirny T. Efektywność służb utrzymania ruchu jako składowa efektywności przedsiębiorstwa. Innowacje w zarządzaniu i inżynierii produkcji / red. R. Knosala. Opole: Oficyna Wydaw. Polskiego Towarzystwa Zarządzania Produkcją, 2012.
24. Młyńczak M. Metodyka badań eksploatacyjnych obiektów mechanicznych. Wrocław: Oficyna Wydawnicza Politechniki Wrocławskiej, 2012.
25. Muchiria P. N, Pintelona L, Martinb H, De Meyerc A. M. Empirical analysis of maintenance performance measurement in Belgian industries. International Journal of Production Research 2010; 20, http://dx.doi.org/10.1080/00207540903160766.
26. Nowicki R., Bate M. Inteligentne podejście w rozpoznawaniu anomalii pracy maszyn napędzanych silnikami elektrycznymi. Zeszyty Problemowe – Maszyny Elektryczne 2013; 2.
27. Osińska M. Ekonometria finansowa. Warszawa: PWE, 2006.
28. Perron P. The great crash, the oil price shock, and the unit root hypoth esis. Econometrica 1989; 6: 1361-1401, http://dx.doi.org/10.2307/1913712.
29. Polska Norma PN-EN 15341:2007 - Maintenance - Maintenance Key Performance Indicators. Warszawa: Polski Komitet Normalizacyjny, 2007.
30. Simões J.M, Gomes C.F, Yasin M.M. A literature review of maintenance performance measurement: A conceptual framework and directions for future research. Journal of Quality in Maintenance Engineering 2011; 2(17), http://dx.doi.org/10.1108/13552511111134565.
31. Sobieski W. Stanowisko laboratoryjne do badania zjawiska kawitacji metodą wibroakustyczną. Diagnostyka 2004; 32: 37-42.
32. Srivastava N.K., Mondal S. Development of a Predictive Maintenance Model Using Modified FMEA Approach. IUP Journal of Operations Management 2014; : 7-16.
33. Tabakow M., Korczak J., Franczyk B. Big Data – definicje, wyzwania i technologie informatyczne. Informatyka Ekonomiczna = Business Informatics 2014; 1.
34. Uhl T., Barszcz T. Informatyczne aspekty projektowania systemów monitorowania stanu maszyn- sprzęt i oprogramowanie. Diagnostyka 2001; 24.
35. Walczak M. System utrzymania ruchu czynnikiem przewagi konkurencyjnej przedsiębiorstwa// Historia i perspektywy nauk o zarządzaniu. Księga pamiątkowa dla uczczenia jubileuszu 40-lecia pracy naukowo-dydaktycznej prof. zw. dra hab. Arkadiusza Potockiego / Mikuła B. [red]. Kraków: Fundacja Uniwersytetu Ekonomicznego w Krakowie, 2012.
36. Yuan Y., Jiang X., Liu X. Predictive maintenance of shield tunnels. Tunnelling and Underground Space Technology 2013; 38, http://dx.doi.org/10.1016/j.tust.2013.05.004.
37. Żabicki D. Zastosowanie kamer termowizyjnych. Monitorowanie i Diagnostyka 2014; 2: 16-19.

Ewelina KOSICKA
Dariusz MAZURKIEWICZ
Mechanical Engineering Faculty
Lublin University of Technology
ul. Nadbystrzycka 36, 20-618 Lublin, Poland

Edward KOZŁOWSKI
Faculty of Management
Lublin University of Technology
ul. Nadbystrzycka 38, 20-618 Lublin, Poland

E-mail: e.kosicka@pollub.pl, d.mazurkiewicz@pollub.pl
e.kozlovski@pollub.pl

Article citation info:
HRYNIEWICZ O, KACZMAREK K, NOWAK P. Bayes statistical decisions with random fuzzy data – an application for the Weibull distribution. Eksploatacja i Niezawodnosc – Maintenance and Reliability 2015; 17 (4): 610–616, http://dx.doi.org/10.17531/ein.2015.4.18.

Olgierd HRYNIEWICZ
Katarzyna KACZMAREK
Piotr NOWAK

BAYES STATISTICAL DECISIONS WITH RANDOM FUZZY DATA – AN APPLICATION FOR THE WEIBULL DISTRIBUTION

ROZMYTO-BAYESOWSKI MODEL PODEJMOWANIA DECYZJI STATYSTYCZNYCH – ZASTOSOWANIE DO ROZKŁADU WEIULLA

In the majority of decision models used in practice all input data are assumed to be precise. This assumption is made both for random results of measurements, and for constant parameters such as, e.g. costs related to decisions. In reality many of these values are reported in an imprecise way. When this imprecision cannot be related to randomness the fuzzy set theory yields tools for its description. It seems to be important to retain both types of uncertainty, random and fuzzy, while building mathematical models for making decisions. In the paper we propose a fuzzy-Bayesian model for making statistical decisions. In the proposed model the randomness of data is reflected in related risks, and fuzziness is described by possibility measures of dominance such as PSD (Possibility of Strict Dominance) and NSD (Necessity of Strict Dominance). The proposed model allows a decision-maker to reflect in his/hers decisions different types of uncertainty. The theoretical results have been applied in the case of reliability data described by the Weibull distribution.

***Keywords**: Bayesian statistics, fuzzy data, possibility measures, reliability, Weibull distribution.*

W większości stosowanych w praktyce modeli decyzyjnych zakłada się, że wszystkie występujące w nich dane wejściowe są podane w sposób precyzyjny. Założenie to dotyczy zarówno losowych wyników pomiarów jak też i stałych parametrów, takich jak np. koszty podjętych decyzji. W rzeczywistości wiele z tych wartości jest podawanych w sposób nieprecyzyjny. Jeżeli taki brak precyzji nie ma charakteru losowego, to teoria zbiorów rozmytych dostarcza narzędzi do opisu tego zjawiska. Wydaje się rzeczą istotną, by przy tworzeniu matematycznych modeli podejmowania decyzji zachować oba typy niepewności: losowość i rozmytość. W pracy proponujemy rozmyto-bayesowski model podejmowania decyzji statystycznych. W proponowanym modelu losowość odpowiada za związane z podjęciem decyzji ryzyko, zaś rozmytość jest opisana przez miary możliwości dominacji, takie jak PSD (Możliwość Ścisłej Dominacji) oraz NSD (Konieczność Ścisłej Dominacji). Zaproponowany model pozwala decydentowi ująć w procesie podejmowania decyzji różne rodzaje niepewności. Rozważania teoretyczne zostały w pracy zastosowane do analizy danych niezawodnościowych opisanych rozkładem Weibulla.

***Słowa kluczowe**: statystyka bayesowska, dane rozmyte, miary możliwości, niezawodność, rozkład Weibulla.*

1. Introduction

Testing statistical hypotheses is one of the most important parts of statistical inference. On the other hand it can be regarded as a part of the decision theory. In the decision theory we assume that decisions (actions belonging to a certain action space) should depend upon a certain state which is uncontrollable and unknown for a decision maker. We usually assume that unknown states are generated by random mechanisms. However, all we could know about these mechanisms is their description in terms of the probability distribution P_θ that belongs to a family of distributions $\{P_\theta : \theta \in \Theta\}$ indexed by a parameter θ (one or multidimensional). In such a case a state space is often understood as equivalent to the parameter space Θ. If we knew the true value of θ we would be able to take a correct decision. The choice of an appropriate decision depends upon a value of a certain utility function that has to be defined on the product of the action space and the state space. If we had known the unknown state we would have been able to choose the most preferred action looking for the action with the highest value of the assigned utility. In practice, we define the expected reward (or the loss) associated with the given action for the given state $\theta \in \Theta$, and then we define the utility $u \in U$ that 'measures' the preference the decision maker assigns to that reward (loss).

In the Bayesian setting of the decision theory we assume that there exists prior information about the true state, and that this information is expressed in terms of the probability distribution $\pi(\theta)$ defined on the parameter space Θ. By doing this we identify each action with probability distribution on a set of possible utilities *U*. According to the Bayesian decisions paradigm we choose the action with the highest value of the expected utility, where expectation is calculated with respect to the probability distribution defined on *U*.

When a decision maker has an opportunity to observe a random variable (or a random vector) *X* that is related to the state θ, such an observation provides him additional information which may be helpful in making proper decisions. In such a case the decision problem is called the statistical decision problem. Comprehensive presentation of the Bayesian decision theory is given in a classical textbook of Raiffa and Schleifer [24], and the Bayesian approach to statistical decision problems may be found in DeGroot [5].

In the statistical decision theory we deal with many quantities which may be vague and imprecise. First, our observation may be imprecise, described in linguistic terms. In such a case we deal with

imprecise (fuzzy) statistical data. Many books and papers have been written on the statistical analysis of fuzzy data. Classical problems of statistical decisions with fuzzy data have been discussed, e.g., in the paper by Grzegorzewski and Hryniewicz [13]. More general approaches, referring to different concepts of fuzzy randomness, are presented in an overview paper by Gil and Hryniewicz [11]. First results presenting the Bayesian decision analysis for imprecise data were given in papers by Casals et al. [2, 3]. In these papers the authors described fuzzy observations using the notion of the fuzzy information system introduced by Zadeh [29] and Tanaka et al. [26]. Other approach, based on the concept of imprecise numbers, has been proposed by Viertl [27]. Further results concerning the decisions based on fuzzy statistical information have been published by Casals [1] and Gil and Lopez-Diaz [12]. Imprecise information about the parameters of the prior distribution have been considered in Hryniewicz [14] and Frühwirth-Schnatter [10]. In the statistical decision theory we may also face practical problems when verified hypotheses are imprecise. This problem was considered by Delgado et al. [6] and by Casals [1]. Finally, the loss function (or the utility function) may be expressed in a fuzzy way, as in the paper by Gil and Lopez-Diaz [12]. Original results on Bayes fuzzy hypotheses testing have been also presented by Taheri and Behboodian [25] who proposed another approach using the posterior odds ratio as the criterion for decision making.

The crucial problem of the fuzzy approach to the Bayes statistical decision analysis is to compare fuzzy risks related to considered decisions. This problem arises from the fact that fuzzy numbers that describe fuzzy risks are not naturally ordered. Thus, the decisions depend upon the method used for such an ordering. Theory of possibility, introduced by Zadeh [29], and based on the fuzzy logic, provides tools for making decisions in the fuzzy environment. We propose to use the possibilistic Necessity of Strict Dominance Index (*NSD*) introduced by Dubois and Prade [8]. Theoretical results are presented in the second, third and fourth sections of the paper. The fifth section is devoted to the application of the proposed methodology for the case of reliability data described by the Weibull distribution.

2. Calculation of the Bayes risks in crisp environment

In the Bayesian approach to statistical decisions we take into consideration potential losses and rewards associated with each considered decision. Let $\theta \in \Theta$ be a parameter describing an element of the state space, and $\delta \in \Delta$ be a decision (action) from a space of possible (admissible) decisions. In the general case of making decisions we usually define a utility function $u(\theta,\delta)$ which assigns a certain utility $u \in U$ to the decision δ which describes a decision maker's level of preference for the decision δ if the true state is described by θ. However, in statistical decisions we rather consider the loss $l(\theta,\delta)$ assigned to decision δ if the true state is described by θ.

Assume now that the decision maker knows the likelihood function $L(\mathbf{x}\,|\,\theta) = L(x_1,\ldots,x_n\,|\,\theta)$ that summarizes the observations of a random sample $(X_1,\ldots,X_n)$. Moreover, we assume that the decision maker has some prior information about possible values of θ. This information, according to the Bayes decision theory is represented by the prior probability distribution $\pi(\theta)$. This information is merged with the information yielded by the random sample. The updated information about the true value of the state θ is calculated using the Bayes theorem, and expressed in the form of the posterior probability distribution:

$$g(\theta\,|\,\mathbf{x}) = \frac{L(\mathbf{x}\,|\,\theta)\pi(\theta)}{\int_{\Theta} L(\mathbf{x}\,|\,\theta)d\pi(\theta)} = \frac{g_n(\theta\,|\,\mathbf{x})}{n(\mathbf{x})} \tag{1}$$

where $\mathbf{x} = (x_1,\ldots,x_n)$, and $g_n(\mathbf{x}\,|\,\theta)$ is the non-normalised posterior distribution. Further analysis is performed in exactly the same way with the posterior probability distribution $g(\theta\,|\,\mathbf{x})$ replacing the prior probability distribution $\pi(\theta)$.

Let $\delta(\mathbf{x}) = \delta(x_1,\ldots,x_n)$ be a decision function which is used for choosing an appropriate decision for given sample values $(x_1,\ldots,x_n)$. The risk function, interpreted as an expected loss incurred by the decision δ, is calculated as:

$$\rho(\delta) = \int_{\Theta}\int_{X} l(\theta,\delta(x_1,\ldots,x_n)) f(x_1,\ldots,x_n\,|\,\theta)\pi(\theta)d\mathbf{x}d\theta \,. \tag{2}$$

Let Δ be the space of possible decision functions. Function δ^* that fulfils the following condition:

$$\rho(\delta^*) = \inf_{\delta\in\Delta} \rho(\delta) \tag{3}$$

we call the Bayes decision function, and the corresponding risk $\rho(\delta^*)$ we call the Bayes risk. Statistical decisions with the risk equal to the Bayes risk are called optimal. In this paper we restrict ourselves to a particular problem of the Bayes decisions, namely to the Bayes test of statistical hypothesis $H_0 : \theta \in \Theta_0$ against the alternative hypothesis $H_1 : \theta \in \Theta_1$, where Θ_0 and Θ_1 are the subsets of the state space Θ such that $\Theta_0 \cap \Theta_1 = \varnothing$. Let us define two functions:

$$H_0(\theta) = \begin{cases} 1, & \theta \in \Theta_0 \\ 0, & \theta \in \Theta_1 \end{cases} \quad \text{and} \quad H_1(\theta) = \begin{cases} 0, & \theta \in \Theta_0 \\ 1, & \theta \in \Theta_1 \end{cases} . \tag{4}$$

Now, let us define loss functions:

$$u(\theta,a_0) = a(\theta)\left[1 - H_0(\theta)\right] \tag{5}$$

that describes the loss related to the acceptance of H_0, and

$$u(\theta,a_1) = b(\theta)\left[1 - H_1(\theta)\right] \tag{6}$$

that describes the loss related to the acceptance of H_1. Functions $a(\theta)$ and $b(\theta)$ are two arbitrary nonnegative functions. In such a case we may consider only two risks: the risk of accepting H_1 when H_0 is true given by:

$$R_1 = \int_{\Theta_1} u(\theta,a_1) g(\theta\,|\,\mathbf{x}) d\theta \,, \tag{7}$$

and the risk of accepting H_0 when H_1 is true given by:

$$R_0 = \int_{\Theta_0} u(\theta,a_0) g(\theta\,|\,\mathbf{x}) d\theta \,. \tag{8}$$

In the following section we present methods for the computation of such a risk in different cases representing situations when different parts of the decision model are described in an imprecise way.

3. Bayes risks for fuzzy statistical data and fuzzy prior information

Let us consider situation when available statistical data are vague and are described by fuzzy random variables. The notion of a fuzzy random variable has been defined by many authors in a different way. One of these definitions, attributed to Kwakernaak [20,21] and – independently – Kruse (see, e.g. Kruse and Meyer [19] for more information), considers the fuzzy random variable $\tilde{X}$ as a fuzzy (vague) perception of an unknown ordinary random variable $X:\Omega \to R$, called an original of $\tilde{X}$. In the presence of fuzzy statistical data the posterior distribution of the state variable θ can be obtained by the application of Zadeh's extension principle to (1). Let $\tilde{x}_i^{\alpha} = \left(\tilde{x}_{i,L}^{\alpha}, \tilde{x}_{i,U}^{\alpha}\right), i = 1,\ldots,n$ be the α-cuts of the fuzzy observations $\tilde{x}_1,\ldots,\tilde{x}_n$. Following Frühwirth-Schnatter [10] let's denote by $C(\tilde{\mathbf{x}})_{\alpha}$ the α-cut of the fuzzy sample which is equal to the Cartesian product of the α-cuts $\tilde{x}_1^{\alpha},\ldots,\tilde{x}_n^{\alpha}$. Frühwirth-Schnatter [10] also proposed a generalization of the fuzzy risk model by allowing fuzziness in the description of the prior information. In such case the probability density function $\pi(\theta,\eta)$ that describes the prior knowledge about the values of the state variable θ may be described as the function of fuzzy parameters $\tilde{\eta}$ denoted by $\pi(\theta,\tilde{\eta})$. Let us denote α-cut of the fuzzy vector $\tilde{\eta}$ by $C(\eta)_{\alpha}$. Thus, the α-contours of the fuzzy posterior probability density are now given by (see [10]):

$$g_{\alpha}^{L}(\theta) = \min_{\mathbf{x},\eta \in C(\tilde{\mathbf{x}})_{\alpha} \times C(\tilde{\eta})_{\alpha}} \frac{f(\mathbf{x}\,|\,\theta)\pi(\theta,\eta)}{n(\theta,\eta)} \tag{9}$$

$$g_{\alpha}^{U}(\theta) = \max_{\mathbf{x},\eta \in C(\tilde{\mathbf{x}})_{\alpha} \times C(\tilde{\eta})_{\alpha}} \frac{f(\mathbf{x}\,|\,\theta)\pi(\theta,\eta)}{n(\theta,\eta)} \tag{10}$$

where $n(\theta,\eta)$ is a normalizing constant. Having these α-contours we can the general methodology for integrating fuzzy functions presented in Dubois and Prade [7] compute the membership functions of fuzzy risks $\tilde{\mathbf{R}}_0$ and $\tilde{\mathbf{R}}_1$. Let us denote by $C\left(\tilde{R}_h\right)_{\alpha} = \left(\tilde{R}_h^{\alpha,L}, \tilde{R}_h^{\alpha,L}\right)$ the α-cuts of the fuzzy risks $\tilde{R}_h, h = 0,1$. The lower and upper bounds of these α-cuts are now calculated from the following formulae:

$$R_h^{\alpha,L} = \int_{\Theta_h} L(\theta,a_h)\, g_{\alpha}^{L}(\theta)\, d\theta,\ h = 0,1 \tag{11}$$

$$R_h^{\alpha,U} = \int_{\Theta_h} L(\theta,a_h)\, g_{\alpha}^{U}(\theta)\, d\theta,\ h = 0,1 \tag{12}$$

The knowledge of these α-cuts is thus equivalent to the knowledge of the membership functions of fuzzy risks $\tilde{R}_0$ and $\tilde{R}_1$, respectively. Further generalization may be achieved by assuming a vague character of utilities (losses). The procedure for finding the α-cuts of $\tilde{\mathbf{R}}_0$ and $\tilde{\mathbf{R}}_1$ is similar, and described in Hryniewicz [15].

Some authors (see, e.g., Viertl [27]) consider lower and upper envelopes for prior and posterior densities. However, such envelopes do not have probabilistic interpretation, as they do not integrate to one (only to "approximately one", as it was stated in Viertl and Hareter [28]. This, unacceptable for many researchers, feature is the consequence of a fact that probability density functions cannot be ordered (in contrast to, e.g., cumulative probability functions, expected values, etc.), and the choice of their „lower" or „upper" representatives requires some additional assumptions. Therefore, the further usage of these envelopes in the Bayesian analysis seems to be debatable.

4. Bayes risks in case of fuzzy statistical hypotheses

In this subsection we present a method proposed in Hryniewicz [15] for the computation of fuzzy risks related to the test of the fuzzy hypothesis $\tilde{H}_0$ against a fuzzy alternative $\tilde{H}_1$. First, let us suppose that all remaining information (i.e. statistical data, prior information, and loss functions) are crisp.

Let $\tilde{H}_h : \theta \in \tilde{\Theta}_h, h = 0,1$ be considered fuzzy statistical hypotheses, where $\tilde{\Theta}_h, h = 0,1$ are the fuzzy sets described by their membership functions $\mu_{\Theta_h}(\theta)$. To simplify the problem let us assume that each fuzzy set $\tilde{\Theta}_h$ may be presented in a form of a fuzzy interval $\left(\tilde{\Theta}_{L,h}, \tilde{\Theta}_{U,h}\right)$, where fuzzy sets $\tilde{\Theta}_{L,h}$ and $\tilde{\Theta}_{U,h}$ have the α-cuts $\left(\Theta_{L,h}^{\alpha,l}, \Theta_{L,h}^{\alpha,U}\right)$ and $\left(\Theta_{U,h}^{\alpha,l}, \Theta_{U,h}^{\alpha,U}\right)$ such that $\Theta_{L,h}^{\alpha,l} \le \Theta_{U,h}^{\alpha,l}$, and $\Theta_{L,h}^{\alpha,u} \le \Theta_{U,h}^{\alpha,u}$. Denote the membership functions of $\tilde{\Theta}_{L,h}$ and $\tilde{\Theta}_{U,h}$ as $\mu_{L,h}$ and $\mu_{U,h}$, respectively. Using the notation of Dubois and Prade [7] we may write the membership functions of the fuzzy risks $\tilde{\mathbf{R}}_h, h = 0,1$ as:

$$\mu_{\tilde{\mathbf{R}}_h}(t) = \sup_{y,z:\, t = \int_u^w u(\theta,\alpha_h) g(\theta|\mathbf{x}) d\theta} \min\left[\mu_{L,h}(y), \mu_{U,h}(z)\right]$$

Finally, let us consider the most general case when we deal with fuzzy statistical data, fuzzy prior information, fuzzy loss function, and fuzzy statistical hypotheses. In this case the fuzzy risks $\tilde{\mathbf{R}}_h, h = 0,1$ are given as an integrals over fuzzy sets from fuzzy functions, i.e.

$$\tilde{\mathbf{R}}_h = \int_{\tilde{\Theta}_h} \tilde{u}(\theta,a_h)\, \tilde{g}(\theta\,|\,\tilde{\mathbf{x}})\, d\theta. \tag{14}$$

Such a fuzzy integral is practically impossible to calculate. However, Hryniewicz [15] proposed its reasonable approximation form above using the following formulae:

$$\mathbf{R}_h^{\alpha,L} = \int_{\Theta_{L,h}^{\alpha,l}}^{\Theta_{U,h}^{\alpha,u}} L_{\alpha}^{L}(\theta,a_h)\, g_{\alpha}^{L}(\theta\,|\,\mathbf{x})\, d\theta\,, \tag{15}$$

$$\mathbf{R}_h^{\alpha,U} = \int_{\Theta_{L,h}^{\alpha,l}}^{\Theta_{U,h}^{\alpha,u}} L_{\alpha}^{U}(\theta,a_h)\, g_{\alpha}^{U}(\theta\,|\,\mathbf{x})\, d\theta\,. \tag{16}$$

When only two hypotheses are considered we have to deal with a relatively simple problem of comparing two fuzzy numbers $\tilde{\mathbf{R}}_0$ and $\tilde{\mathbf{R}}_1$. For doing this comparison Hryniewicz [15] proposed a possibilistic approach introduced by Dubois and Prade [8]. To compare these fuzzy risks he proposed to use the concept of the Necessity of Strict Domi-

nance Index (*NSD*) and Possibility of Dominance Index (*PD*). The *PD* index is defined for two fuzzy sets $\tilde{A}$ and $\tilde{B}$ as:

$$PD = Poss\left(\tilde{A} \geq \tilde{B}\right) = \sup_{x,y:x\geq y} \min\left\{\mu_A(x), \mu_B(y)\right\}, \quad (17)$$

where $\mu_A(x)$ and $\mu_B(y)$ are the membership functions of $\tilde{A}$ and $\tilde{B}$, respectively. *PD* is the measure for a possibility that the set $\tilde{A}$ is not dominated by the set $\tilde{B}$. The *NSD* index is defined as:

$$NSD = Ness\left(\tilde{A} > \tilde{B}\right) = 1 - \sup_{x,y:x\leq y} \min\left\{\mu_A(x), \mu_B(y)\right\}. \quad (18)$$

NSD represents necessity that the set $\tilde{A}$ dominates the set $\tilde{B}$. If *NSD*>0 there exists a strong indication of the acceptance of one hypothesis (say $\tilde{A}$) over another one (say $\tilde{B}$).

Possibilistic indices mentioned above can be used in the evaluation of the undertaken decision in terms of preferences. Cutello and Montero [4] proposed three measures of preference relations. Let be the measure of indifference between alternatives *x* and *y*, $\mu_B(x,y)$ be the measure that the alternative *x* is better than the alternative *y*, $\mu_W(x,y)$ be the measure that the alternative *x* is worse than the alternative *y*. Hryniewicz [15] has noted that in the context of statistical decisions we have the following relations:

$$\mu_I(x,y) = PD - NSD \quad (19)$$

$$\mu_B(x,y) = NSD \quad (20)$$

$$\mu_W(x,y) = 1 - PD. \quad (21)$$

In the next section we show a simple example of this methodology for the case of the lifetime data described by the Weibull distribution.

5. Testing hypotheses for the Weibull distribution using imprecise information

Let *X* be the random variable describing lifetime data. The Weibull distribution, defined by the probability density function (pdf):

$$f(x \mid \gamma, s) = \frac{sx^{s-1}}{\gamma \exp\left(x^s/\gamma\right)}, x > 0, s > 0, \gamma > 0 \quad (22)$$

is frequently used for modeling such data. The parameter *s* determines the shape of the pdf function, and the parameter *γ* determines the spread of variability of *X*. Because of its great applicability in the analysis of reliability (or survival, in a more general setting) classical (non-Bayesian) methods of statistical analysis for the Weibull distribution have been developed by many authors. For more detailed information the reader can be directed to many textbooks, such as e.g. the book by Lawless [22]. The number of papers devoted to the problem of the Bayesian analysis of the lifetime data described by the Weibull distribution is not so high because of difficulties with finding analytical solutions. Comprehensive bibliography of the problem together can be found in the recent paper by Fernández [9]. The reason of these problems stems from the fact that the bivariate conjugate prior distribution for both parameters of the Weibull distribution does not exist. Therefore, indirect methods, such as the method proposed by Kaminskiy and Krivtsov [17], have to be used.

The problem of the statistical analysis of data described by the Weibull distribution becomes much easier if the value of the shape parameter is *s* known. In such case the random variable $Y = X^s$ is distributed exponentially with the scale parameter equal to *γ*. Statistical analysis of lifetime data described by the exponential distribution is well developed, both in the classical (non-Bayesian) and Bayesian sense. For example, in the case of Bayesian there exists the conjugate prior probability distribution for the scale parameter *γ*. This is the inverted gamma distribution defined by the following pdf function:

$$g(y) = \frac{a^b \exp(-a/\gamma)}{\Gamma(b)\gamma^{b+1}}, \gamma > 0, a > 0, b > 0. \quad (23)$$

Note, that the prior distribution for the inverse of the scale distribution $\lambda = 1/\gamma$ is the well known gamma distribution with the same parameters *a* and *b*, respectively. Moreover, in case of the exponential distribution there exists sufficient statistic that summarizes available statistical data. For example in case of type-II censoring this statistic is given by $(w(y), r)$, where $w(y) = \sum_{i=1}^{r} y_{(i)} + (n-r)y_{(r)}$, and $y_{(1)} \leq y_{(2)} \leq \cdots \leq y_{(r)}$. The posterior distribution of *γ* is also the inverted gamma distribution with parameters $a' = a + w(y)$ and $b' = b + r$.

Now let's consider the case that we have only partial knowledge about the value of the shape parameter *s*. Formal description of partial knowledge is still the subject of controversies. Some researchers claim that classical probabilities are sufficient in this case. However, many other researchers present counterexamples showing that some other methods, like imprecise probabilities, Dempster-Shafer belief functions, p-boxes, possibility distributions etc., should be used in order to capture the essence of partial knowledge. In this paper we assume that our knowledge about the value of *s* is described by a possibility distribution, which from a formal point of view is equivalent to the membership function $\mu(s)$ of a fuzzy number $\tilde{s}$. Thus, we assume that we analyze a fuzzy random variable defined as:

$$\tilde{Y} = X^{\tilde{s}}, \quad (24)$$

and the sample information is presented as the *fuzzy number:*

$$\tilde{w}(y) = \sum_{i=1}^{r} \tilde{y}_{(i)} + (n-r)\tilde{y}_{(r)}. \quad (25)$$

Therefore, all results of statistical analyses, either Bayesian or non-Bayesian, will be presented using terms related to fuzzy sets.

Let us consider the problem of the Bayesian estimation of the parameter *γ* in case of type-II censored lifetime data. As natural Bayesian estimators can be considered such statistics like the mode of the posterior distribution or its median. In case of the known *s* it can be done by solving nonlinear equations (see [9]). However, when we have fuzzy data in the form of $\tilde{w}(y)$ this task is rather difficult to do. Much simpler result can be obtained when we use a decision-theoretic approach. When the losses due to erroneous estimation are proportional to $(\gamma_B - \gamma)^2$ then the optimal estimator that minimizes the Bayesian risk is equal to the expected value in the posterior distribution, and in the case of fuzzy data is given by a very simple formula:

$$\tilde{\gamma}_B = \frac{a + \tilde{w}(y)}{b + r - 1}, b + r > 1. \tag{26}$$

The membership function of $\tilde{\gamma}_B$ is similar to the membership function of $\tilde{w}(y)$, except for a linear transformation of the x-axis.

Acquisition of the parameters of the prior distribution is the most important practical problem of the Bayesian approach to statistics. Usually, an expert proposes his/hers evaluations of the moments of the prior distribution, and these values are set equal to their theoretical counterparts, forming equations the parameters of the prior distribution are calculated from. Implementation of this practice in the considered case is rather questionable, as the parameter γ does not have any direct interpretation. Therefore such equations should be constructed using information that is directly related to observed lifetimes or other reliability indices.

The first two moments of the prior distribution of reliability characteristics, such as the reliability function $R(t)$ or the hazard function $h(t)=h_t$, are sometimes recommended for setting the parameters of the prior distribution. In the case of the hazard function h_t Fernández [9] shows that the expected value of the prior distribution of this index is given by $E = E[h_t] = sbt^{s-1}/a$, and its variance is given by $V = V[h_t] = s^2bt^{2s-21}/a^2$. By solving these two equations we can easily find closed formulae for the calculation of a and b:

$$a = a(s) = st^{s-1}\frac{E}{V} \tag{27}$$

$$b = \frac{E^2}{V}. \tag{28}$$

Hence, the Bayes estimator of γ is given as:

$$\gamma(s) = \frac{a(s) + \sum_{i=1}^{r} x_{(i)}^s + (n-r)x_{(r)}^s}{b + r - 1}. \tag{29}$$

However, in the considered case of the fuzzy information about the value of s the Bayes estimator of γ will be described by (29) with s replaced by fuzzy $\tilde{s}$.

Let $\left(s_L^\alpha, s_U^\alpha\right)$ be the α-cut of the fuzzy variable $\tilde{s}$ that represents imprecise information about the value of the shape parameter s. We can find the limiting values of the α-cut of the Bayesian estimator of the parameter γ by solving the following optimization problems:

$$\gamma_{B,L}^\alpha = \inf_{s \in \left(s_L^\alpha, s_U^\alpha\right)} \gamma(s) \tag{30}$$

$$\gamma_{B,U}^\alpha = \sup_{s \in \left(s_L^\alpha, s_U^\alpha\right)} \gamma(s). \tag{31}$$

Unfortunately, $\gamma(s)$ is not a monotonic function of s. However, for consistent possible values of s (either not greater than one or not smaller than one), and usually observed values of x's (smaller than the expected value) $\gamma(s)$ is monotonic. Thus, finding the limiting values according to (27) and (28) does not require special computational efforts.

In a similar, but more complicated, way one can calculated fuzzy risks related to statistical hypotheses about γ and its different functions such as reliability function or hazard rate. For example, consider the important from a practical point of view characteristics such as the reliable life t_R, defined as:

$$t_R = \left(-\gamma \ln R\right)^{1/s}, \tag{32}$$

where R is a specified fraction of survived objects. The Bayes estimator of tR in the case of the gamma prior distribution for $\lambda = 1/\gamma$ with the scale parameter $a_0 = 1/a$ and the shape parameter $b_0 = b$, is given in Martz and Waller[23] as follows:

$$t_{R,B} = \frac{\Gamma\left(b_0 + r - 1/s\right)\left(-\ln R\right)^{1/s}}{\Gamma\left(b_0 + r\right)\left[a_0/\left(a_0 w(y) + 1\right)\right]^{1/s}}. \tag{33}$$

Taking into account the imprecise information about the shape parameter s, and hence, the imprecise values of the parameter a, the limiting values of the α-cut of the fuzzy Bayes estimate of the reliable life are given by the formulae:

$$t_{R,B,L}^\alpha = \inf_{s \in \left(s_L^\alpha, s_U^\alpha\right)} \frac{\Gamma\left(b + r - 1/s\right)\left(-\ln R\right)^{1/s}}{\Gamma(b + r)} \frac{\left[a(s)\right]^{1/s}}{\left[a^{-1}(s)\left(\sum_{i=1}^{r} x_{(i)}^s + (n-r)x_{(r)}^s\right) + 1\right]^{1/s}}, \tag{33}$$

$$t_{R,B,U}^\alpha = \sup_{s \in \left(s_L^\alpha, s_U^\alpha\right)} \frac{\Gamma\left(b + r - 1/s\right)\left(-\ln R\right)^{1/s}}{\Gamma(b + r)} \frac{\left[a(s)\right]^{1/s}}{\left[a^{-1}(s)\left(\sum_{i=1}^{r} x_{(i)}^s + (n-r)x_{(r)}^s\right) + 1\right]^{1/s}}. \tag{34}$$

These values can be computed only numerically using widely accessible routines for finding minima and maxima of continuous functions.

Knowing the fuzzy Bayes estimates of reliability characteristics we can relatively easily find the fuzzy Bayes confidence intervals for these characteristics. In order to do so we have to replace in the respective formulae, that can be found e.g. in the book by Martz and Waller [23], the values of the non-fuzzy estimator with the respective limiting values of the α-cuts: the lower value of the α-cut in the formula for the lower limit of the Bayes confidence interval, and the upper of the α-cut in the formula for the upper limit of the Bayes confidence interval. For the known value of s the limits of the confidence intervals are given by the following formulae:

$$\overline{t}_{R,B}(\gamma) = \left(-\ln R\right)^{1/s} \left\{ \frac{a^{-1}(s)\chi_{\gamma/2}^2(2r + 2b)}{2a^{-1}(s)\left[\sum_{i=1}^{r} x_{(i)}^s + (n-r)x_{(r)}^s\right] + 2} \right\}^{1/s}, \tag{35}$$

$$\underline{t}_{R,B}(\gamma) = \left(-\ln R\right)^{1/s} \left\{ \frac{a^{-1}(s)\chi_{1-\gamma/2}^2(2r + 2b)}{2a^{-1}(s)\left[\sum_{i=1}^{r} x_{(i)}^s + (n-r)x_{(r)}^s\right] + 2} \right\}^{1/s}, \tag{36}$$

where $\chi^2_\beta(k)$ is the quantile of order β from the chi-square distribution with k degrees of freedom. When the shape parameter s is fuzzy the Bayes confidence interval defined by the limiting values (35) and (36) also becomes fuzzy. Its α-cut is in this case defined by the following limiting values:

$$\underline{t}^{\alpha}_{R,B}(\gamma) = \inf_{s\in\left(s^{\alpha}_{L},s^{\alpha}_{U}\right)} \underline{t}_{R,B}(\gamma), \tag{37}$$

$$\overline{t}^{\alpha}_{R,B}(\gamma) = \sup_{s\in\left(s^{\alpha}_{L},s^{\alpha}_{U}\right)} \overline{t}_{R,B}(\gamma). \tag{38}$$

The nested α-cuts (for all $\alpha \in (0,1]$) may be regarded as the *possibility* distribution of the fuzzy Bayes reliable life $\tilde{t}_{R,B}$. Then, we can use the possibilistic methodology described in the fourth section of this paper to compare the fuzzy limits of the Bayes confidence intervals with the reliability requirements for t_R.

6. Conclusions

Statistical methods that use the Bayes approach for the analysis of data are of special importance in the theory and practice of reliability. Because of high reliability of contemporary systems and their elements it is difficult to collect enough data for precise estimation of reliability characteristics using classical statistical methods. Therefore, it is necessary to utilize additional information represented in the form of prior distributions of parameters of the probability distribution of life times. However, it is usually difficult to represent our prior knowledge in a fully precise way. Moreover, the statistical data may be also reported imprecisely. Thus, we should have the methodology for combining random uncertainty with non-random (fuzzy) imprecision in the context of the Bayes reliability analysis. In this paper we have presented a possibilistic approach for making decisions in the case of the fuzzy Bayes reliability analysis.

The results obtained in this paper for the case of the Weibull distribution can be applied not only in the context of reliability. This probability distribution is used for the description of extreme events, and has been also applied in the analysis of some environmental phenomena. In that particular context the combination of imperfectly reported data with imprecise opinions provided by experts is of great practical importance. Therefore, the results presented in this paper can be applied also in this area.

Acknowledgment

The work on this paper has been partially supported by the grant No. N N519316735 of the Polish Ministry of Science and Higher Education.

References

1. Casals M.R. Bayesian testing of fuzzy parametric hypotheses from fuzzy information. RAIRO, Operations Research 1993; 27: 189-199.
2. Casals M.R., Gil M.A., Gil P. On the use of Zadeh's probabilistic definition for testing statistical hypotheses from fuzzy information. Fuzzy Sets and Systems 1986; 20: 175-190, http://dx.doi.org/10.1016/0165-0114(86)90076-X.
3. Casals M.R., Gil M.A., Gil P. The Fuzzy Decision Problem: an approach to the Problem of Testing Statistical Hypotheses with Fuzzy Information. European Journal of Operational Research 1986; 27: 371-382, http://dx.doi.org/10.1016/0377-2217(86)90333-4.
4. Cutello V., Montero J. An Extension of the Axioms of Utility Theory Based on Fuzzy Rationality Measures. In: Fodor J., De Baets B., Perny P. (Eds.) Preference and Decisions under Incomplete Knowledge. Heidelberg: Physica-Verlag, 1999, 33 - 50.
5. De Groot M.H. Optimal Statistical Decisions. New York: McGraw Hill, 1970.
6. Delgado M., Verdegay J.L., Vila M.A. Testing fuzzy hypotheses. A Bayesian approach. In: Gupta M.M., Kandel A., Bandler W., Kiszka J.B. (Eds.) Approximate Reasoning in Expert Systems. Amsterdam: Elsevier, 1985, 307-316.
7. Dubois D., Prade H. Fuzzy Sets and Systems. Theory and Applications. New York: Academic Press, 1980.
8. Dubois D., Prade H. Ranking fuzzy numbers in the setting of possibility theory. Information Sciences 1983; 3: 184-244, http://dx.doi.org/10.1016/0020-0255(83)90025-7.
9. Fernández A.J. Weibull inference using trimmed samples and prior information. Statistical Papers 2009; 50: 119-136, http://dx.doi.org/10.1007/s00362-007-0067-2.
10. Frühwirth-Schnatter S. Fuzzy Bayesian inference. Fuzzy Sets and Systems 1993; 60: 41-58, http://dx.doi.org/10.1016/0165-0114(93)90288-S.
11. Gil M.A., Hryniewicz O. Statistics with Imprecise Data. In: Meyers R. A. (Ed.) Encyclopedia of Complexity and Systems Science. Heidelberg: Springer, 2009, 8679-8690.
12. Gil M.A., Lopez-Diaz M. Fundamentals and Bayesian Analyses of Decision Problems with Fuzzy-Valued Utilities. International Journal of Approximate Reasoning 1996; 15: 203-224, http://dx.doi.org/10.1016/S0888-613X(96)00073-4.
13. Grzegorzewski P., Hryniewicz O. Soft Methods in Hypotheses Testing. In: Ruan D., Kacprzyk J., Fedrizzi M. (Eds.) Soft computing for risk evaluation and management. Heidelberg: Physica Verlag, 2001, 55-72, http://dx.doi.org/10.1007/978-3-7908-1814-7_4.
14. Hryniewicz O. Estimation of life-time with fuzzy prior information: application in reliability. In: Kacprzyk J., Fedrizzi M. (Eds.) Combining Fuzzy Imprecision with Probabilistic Uncertainty in Decision Making. Berlin: Springer-Verlag, 1988, 307-321, http://dx.doi.org/10.1007/978-3-642-46644-1_21.
15. Hryniewicz O. Possibilistic approach to Bayes statistical decisions. In: Grzegorzewski P., Hryniewicz O., Gil M.A. (Eds.) Soft methods in probability, statistics and data analysis. Heidelberg: Physica-Verlag, 2002, 207-218, http://dx.doi.org/10.1007/978-3-7908-1773-7_20.
16. Hryniewicz O. Fuzzy sets in the evaluation of reliability. In: Levitin G. (Ed.) Computational intelligence in reliability engineering. Berlin: Springer-Verlag, 2007, 363-386, http://dx.doi.org/10.1007/978-3-540-37372-8_13.
17. Kaminskiy M.P., Krivtsov V.W. A Simple procedure for Bayesian Estimation of the Weibull Distribution. IEEE Transactions on Reliability 2005; 54: 612-616, http://dx.doi.org/10.1109/TR.2005.858093.
18. Kruse R. The strong law of large numbers for fuzzy random variables. Information Sciences 1982; 28: 233-241, http://dx.doi.org/10.1016/0020-0255(82)90049-4.

19. Kruse R., Meyer M.D. Statistics with Vague Data. Dordrecht: D. Reidel, 1987, http://dx.doi.org/10.1007/978-94-009-3943-1.
20. Kwakernaak H. Fuzzy random variables, Part I: definitions and theorems. Information Sciences 1978; 15: 1-15, http://dx.doi.org/10.1016/0020-0255(78)90019-1.
21. Kwakernaak H. Fuzzy random variables, Part II: algorithms and examples for the discrete case. Information Sciences 1978; 17: 253-278, http://dx.doi.org/10.1016/0020-0255(79)90020-3.
22. Lawless J.F. Statistical models and methods for lifetime data. New York: J. Wiley and Sons, 1982.
23. Martz H.F., Waller R.A. Bayesian Reliability Analysis. New York: J. Wiley & Sons, 1982.
24. Raiffa H., Schleifer R. Applied Statistical Decision Theory. Cambridge: The M.I.T. Press, 1961.
25. Taheri S.M., Behboodian J. A Bayesian approach to fuzzy hypotheses testing, Fuzzy Sets and Systems 2001; 123: 39-48, http://dx.doi.org/10.1016/S0165-0114(00)00134-2.
26. Tanaka H., Okuda T., Asai K. Fuzzy information and decisions in statistical model. In: Gupta M.M., Ragade R.K., Yager R.R. (Eds.) Advances in Fuzzy Sets Theory and Applications. Amsterdam: North-Holland, 1979, 303-320.
27. Viertl R. Statistical Methods for Fuzzy Data. Chichester UK: J. Wiley & Sons, 2011, http://dx.doi.org/10.1002/9780470974414.
28. Viertl R., Hareter D. Generalized Bayes' theorem for non-precise a-priori distribution. Metrika 2004; 59: 263-273, http://dx.doi.org/10.1007/s001840300283.
29. Zadeh L.A. Fuzzy sets as a basis for a Theory of Possibility. Fuzzy Sets and Systems 1978; 1: 3-38, http://dx.doi.org/10.1016/0165-0114(78)90029-5.

Olgierd HRYNIEWICZ
Systems Research Institute
and
Warsaw School of Information Technology
Newelska 6, 01-447 Warsaw, Poland

Katarzyna KACZMAREK
Piotr NOWAK
Systems Research Institute
Newelska 6, 01-447 Warsaw, Poland

E-mail: hryniewi@ibspan.waw.pl,
K.Kaczmarek@ibspan.waw.pl, Piotr.Nowak@ibspan.waw.pl

Article citation info:
ZUO F-J, YU L, MI J, LIU Z, HUANG H-Z. Reliability analysis of gear transmission with considering failure correlation. Eksploatacja i Niezawodnosc – Maintenance and Reliability 2015; 17 (4): 617–623, http://dx.doi.org/10.17531/ein.2015.4.19.

Fang-Jun ZUO
Le YU
Jinhua MI
Zheng LIU
Hong-Zhong HUANG

RELIABILITY ANALYSIS OF GEAR TRANSMISSION WITH CONSIDERING FAILURE CORRELATION

ANALIZA NIEZAWODNOŚCI PRZEKŁADNI Z UWZGLĘDNIENIEM KORELACJI USZKODZEŃ

Reliability analysis is of great importance in engineering practices. However, reliability analysis of mechanical system under considering correlation for multiple failure modes is very difficult. Gear is the key component in many mechanical transmission systems and therefore its reliability analysis is very important. Based on the standards of strength calculation of gears and stress-strength interference theory as well as copula theory, the reliability of gear transmission with three failure modes, including gear bending fatigue, gear flank contact fatigue and flank adhesion, is analyzed. The correlation of the three failure modes is studied and reliability of their correlation is also evaluated based on the selected copula functions. The proposed method can be used to facilitate the design, manufacturing, and maintenance planning of gears.

Keywords: *Reliability analysis; contact stress; bending stress; multiple failure modes; failure correlation.*

Analiza niezawodności ma ogromne znaczenie w praktyce inżynierskiej. Jednakże, analiza niezawodności układu mechanicznego z uwzględnieniem korelacji dla mnogich przyczyn uszkodzeń jest trudnym zadaniem. Koło zębate jest kluczowym elementem w wielu przekładniach mechanicznych i dlatego analiza jego niezawodności jest niezwykle ważna. W oparciu o normy obliczania wytrzymałości kół zębatych i teorię interferencji naprężeń i wytrzymałości, a także teorię kopuł, przeanalizowano niezawodność przekładni zębatej uwzględniając trzy przyczyny uszkodzeń: zmęczenie zginające koła zębatego, zmęczenie stykowe boku zęba i przyczepność boku. Prześledzono korelację trzech przyczyn uszkodzeń i oceniono niezawodność ich korelacji na podstawie wybranych funkcji kopuł. Proponowana metoda może być stosowana w celu ułatwienia projektowania, produkcji i planowania konserwacji przekładni.

Słowa kluczowe: *Analiza niezawodności; naprężenie stykowe; naprężenie zginające; mnogie przyczyny uszkodzeń; korelacja uszkodzeń.*

1. Introduction

Gear is an important component of mechanical transmission. Gear transmission has been recognized as one of the most important mechanical transmission forms because it has a series of advantages, such as broad power and speed ratio in scope, high transmission efficiency, compact structure and so on. In recent years, with rapid development of machine tools, aircrafts, and automobiles, gear transmission has become an extremely important form of mechanical transmission [1, 4, 6, 8].

Reliability of mechanical transmission relies on the most critical component, e.g. gear, of the system [10]. The failure of gears in mechanical transmission will lead to a poor performance, sometimes even serious accidents and subsequently great economic loss. Therefore, developing an effective and accurate fatigue reliability evaluation model for gear transmission has been a hot topic in the gear engineering community [2, 3, 11].

Failure modes of gears are complicated, such as teeth broken, teeth surface pitting, teeth wear, teeth bonding and teeth plastic deformations and so on, because in most cases, gears work under high speed, heavy load and strong impulse conditions. Therefore, multiple failure modes should be considered simultaneously for analyzing reliability of gears. In this paper, the gear transmission of heavy machine tools is analyzed. Tooth bending fatigue, gear contact fatigue and flank adhesion are major failure modes of heavy duty gears. The failures of weak points are dependent of each other, because all the roots (with maximum bending stress) and surfaces (with maximum contact stress) in a gear subject to the same environmental conditions. Thus, the failure dependence of a gear in the transmission system should be considered. Reliability models of gear transmission with common cause failures are developed without the assumption of failure independence [5, 6, 12, 14, 15].

The paper is organized as follows. In Section 2, the strength calculation standards for gears and the copula theory as well as stress-strength interference theory are briefly introduced. Reliability calculation models are developed in Section 3. The proposed method is validated by a gear transmission of heavy machine tools with three failure modes in Section 4. Conclusions are dawn in Section 5.

2. Reliability calculation model

2.1. Stress-Strength Interference (SSI) theory

The stress–strength interference (SSI) model has been widely used for reliability analysis of mechanical components. Mathemati-

cally, the SSI theory presents the failure probability P_f of a mechanical system as the probability that the stress exceeds the strength. The reliability R is the probability that the stress is less than the allowable strength, denoted as [2, 6]:

$$R = P(\sigma_a > \sigma_B) \tag{1}$$

Reliability R of a component can be calculated, if the probability density functions of the allowable strength $f_a(\sigma_a)$ and the actual stress $f_B(\sigma_B)$ are known. The random variable U is a measurement for the distance between the actual stress and the allowable strength:

$$U = \sigma_a - \sigma_B \tag{2}$$

$P_R = P(U > 0)$ is the reliability; $P_F = P(U \le 0)$ is the failure probability.

If the random stress σ_B and allowable strength σ_a are normally distributed respectively with the mean values and standardized deviations $(\bar{\sigma}_B, S_B)$ $(\bar{\sigma}_a, S_a)$, the probability density function of a normal distributed stress can be determined as follows:

$$f_B(\sigma_B) = \frac{1}{S_B\sqrt{2\pi}} e^{-\left[\frac{(\sigma_B - \bar{\sigma}_B)^2}{2S_B^2}\right]} \tag{3}$$

Similarly, the probability density function of the allowable strength can be determined. The random variable U is, likewise, normally distributed. The unreliability for the interference area of the two distributions can be calculated using the following equation:

$$Z = \frac{\bar{\sigma}_a - \bar{\sigma}_B}{\sqrt{S_a^2 + S_B^2}} \tag{4}$$

Then, the reliability can be simply calculated as follows:

$$R = \Phi\left(\frac{\bar{\sigma}_a - \bar{\sigma}_B}{\sqrt{S_a^2 + S_B^2}}\right) \tag{5}$$

2.2. Reliability calculation based on gear bending fatigue

The bending stress of the gear root is the biggest stress in gear transmission process under the alternating bending stress, and the tooth is easy to produce fatigue crack and crack expansion under the alternating bending stress which will lead to tooth bending fatigue fracture. The bending stress can be calculated by [9, 15, 16]:

$$\sigma_F = Y_{Fa} Y_{Sa} Y_\varepsilon Y_\beta \frac{F_t}{b m_n} K_A K_V K_{F\beta} K_{Fa} \tag{6}$$

where m_n is the normal module, Y_{Fa} is the tooth form factor, Y_{Sa} is the bending stress concentration coefficient, Y_ε is the contact ratio factor, Y_β is the helix angle coefficient, F_t is the rated tangential tooth force at transverse pitch, b is the active face width, K_A is the work condition coefficient, K_V is the dynamic load coefficient, K_{Fa} is the load distribution coefficient, $K_{F\beta}$ is the longitudinal load distribution coefficient.

The tooth bending fatigue strength is defined as:

$$\sigma'_{Flim} = \sigma_{Flim} Y_{ST} Y_{NT} Y_{srelt} Y_{Rrelt} Y_X \tag{7}$$

where σ_{Flim} is the experimental gear bending fatigue strength, Y_{ST} is the experimental gear tooth stress concentration coefficient, Y_{NT} is the life coefficient, Y_{srelt} is the relative sensitive coefficient, Y_{Rrelt} is the relative surface condition coefficient, Y_X is the size coefficient.

According to the stress-strength interference theory, the limit state function of bending fatigue is defined as:

$$f(\sigma) = \ln(\sigma'_{Flim}) - \ln(\sigma_F) \tag{8}$$

According to the Eq. (8), the mean of function can be calculated as:

$$\begin{aligned} E\left[f(\sigma)\right] &= E\left[\ln\left(\sigma'_{Flim}\right)\right] - E\left[\ln\left(\sigma_F\right)\right] \\ &= E\left[\ln\left(\frac{\sigma'_{Flim}}{\sigma_F}\right)\right] \end{aligned} \tag{9}$$

where:

$$E\left[\ln(\sigma'_{Flim})\right] = \ln\left[E(\sigma_{Flim})E(\mathrm{Y}_{ST})E(\mathrm{Y}_{NT})E(\mathrm{Y}_{srelt})E(\mathrm{Y}_{Rrelt})E(\mathrm{Y}_X)\right] \tag{10}$$

$$E\left[\ln(\sigma_F)\right] = \ln\left[E(\mathrm{Y}_{Fa})E(\mathrm{Y}_{Sa})E(\mathrm{Y}_\varepsilon)E(\mathrm{Y}_\beta)\frac{E(F_t)}{E(b)E(m_n)}E(K_A)E(K_V)E(K_{F\beta})E(K_{Fa})\right] \tag{11}$$

The variance of the function is as follow:

$$D\left[f(\sigma)\right] = D\left[\ln(\sigma'_{Flim})\right] + D\left[\ln(\sigma_F)\right] \tag{12}$$

Supposed the random variable x is normally distributed, the variance of function $y = \ln(x)$ is:

$$\sigma^2(y) = \left[\left.\frac{dy}{dx}\right|_{E(x)} \sigma(x)\right]^2 = \left[\frac{\sigma(x)}{E(x)}\right]^2 = C^2(x) \tag{13}$$

For multivariable function y composed of multiple independent random variables, the expression is:

$$y = a x_1^{m_1} x_2^{m_2} \ldots x_n^{m_n} = a \prod_{i=1}^{n} x_i^{m_i} \tag{14}$$

$x_1, x_2, \cdots, x_n$ is independent random variables.

According to Eqs. (13) and (14), the variable coefficient of y using the first order Taylor expansion can be expressed as:

$$C_y^2 = \sum_{i=1}^{n} m_i^2 C_{x_i}^2 \tag{15}$$

According to Eq. (12), we have:

$$D\left[f(\sigma)\right] = C^2(\sigma'_{Flim}) + C^2(\sigma_F) \tag{16}$$

According to Eqs. (6), (15), and (16), the variable coefficient of $\sigma'_{F\lim}$ and σ_F can be respectively expressed as:

$$C^2(\sigma_F) = C_{Y_{Fa}}^2 + C_{Y_{Sa}}^2 + C_{Y_e}^2 + C_{Y_b}^2 + C_{F_t}^2 + C_b^2 + C_{m_n}^2 + C_{K_A}^2 + C_{K_V}^2 + C_{K_{F\beta}}^2 + C_{K_{Fa}}^2 \tag{17}$$

$$C^2(\sigma'_{Flim}) = C_{\sigma_{Flim}}^2 + C_{Y_{ST}}^2 + C_{Y_{NT}}^2 + C_{Y_{srelt}}^2 + C_{Y_{Rrelt}}^2 + C_{Y_X}^2 \tag{18}$$

Substituting Eqs. (11) and (17) into the reliability formula, the reliability index for gear bending fatigue strength can be given by:

$$\beta_F = \frac{E(f_\sigma)}{\sigma(f_\sigma)} = \frac{E\left[\ln\left(\frac{\sigma'_{Flim}}{\sigma_F}\right)\right]}{\sqrt{C^2(\sigma'_{Flim}) + C^2(\sigma_F)}} \tag{19}$$

Reliability for gear bending fatigue strength is:

$$R = \Phi(\beta_F) \tag{20}$$

2.3. Reliability design based on contact fatigue

The fatigue life of gears has been studied over many years, and the gear contact fatigue performance is very important from the former studies. Gear tooth contact fatigue is a key characteristic of the gear and affected by design geometry, material, manufacturing methods and other variables. Surface contact fatigue is the common cause of gear failure. It results in damage to the contacting surfaces which can significantly reduce the load-carrying capacity of components, and may ultimately lead to the complete failure of a gear.

Gear contact stress is defined as [16, 17]:

$$\sigma_H = Z_H Z_E Z_e Z_B \sqrt{\frac{F_t}{bd_1}\frac{u+1}{u} K_A K_V K_{H\beta} K_{HA}} \tag{21}$$

where F_t is the rated tangential tooth force at transverse pitch, b is the active face width, K_A is the work condition coefficient, K_V is the dynamic load coefficient, $K_{H\beta}$ is the longitudinal load distribution coefficient, K_{HA} is the transverse load distribution coefficient, Z_H is the nodal field coefficient, Z_E is the elastic coefficient, Z_e is the contact ratio coefficient, Z_B is the spiral angle coefficient, d_1 is the pinion pitch diameter, u is the gear ratio.

Contact fatigue strength of tooth faces is defined as:

$$\sigma'_{Hlim} = \sigma_{Hlim} Z_N Z_R Z_V Z_L Z_W Z_X \tag{22}$$

where σ_{Hlim} is the experimental flank contact fatigue strength, Z_N is the life coefficient, Z_R is the tooth fineness coefficient, Z_V is the velocity coefficient, Z_L is the lubricant coefficient, Z_W is the work harden coefficient, Z_X is the size coefficient.

According to stress-strength interference theory, the limit state function is defined as:

$$g(\sigma) = \ln(\sigma'_{Hlim}) - \ln(\sigma_H) \tag{23}$$

According to Eq. (23), the mean of the function is calculated as:

$$\begin{aligned} E\left[g(\sigma)\right] &= E\left[\ln(\sigma'_{Hlim})\right] - E\left[\ln(\sigma_H)\right] \\ &= E\left[\frac{\ln(\sigma'_{Hlim})}{\ln(\sigma_H)}\right] \end{aligned} \tag{24}$$

where:

$$E\left[\ln(\sigma'_{Hlim})\right] = \ln\left[E(\sigma_{Hlim})E(Z_N)E(Z_R)E(Z_V)E(Z_L)E(Z_W)E(Z_X)\right] \tag{25}$$

$$E\left[\ln(\sigma_{Hlim})\right] = \ln\left[\sqrt{\frac{u\pm1}{u}}E(Z_H)E(Z_E)E(Z_e)E(Z_B)\sqrt{\frac{E(F_t)}{E(bd_1)E(d_1)}E(K_A)E(K_V)E(K_{H\beta})E(K_{HA})}\right] \tag{26}$$

The variances of the function is:

$$\begin{aligned} D\left[g(\sigma)\right] &= D\left[\ln(\sigma'_{Hlim})\right] + D\left[\ln(\sigma_H)\right] \\ &= C^2\left[\ln(\sigma'_{Hlim})\right] + C^2\left[\ln(\sigma_H)\right] \end{aligned} \tag{27}$$

The variable coefficients of σ'_{Hlim} and σ_H are respectively given by:

$$C^2(\sigma'_{Hlim}) = C_{\sigma_{Hlim}}^2 + C_{Z_N}^2 + C_{Z_R}^2 + C_{Z_V}^2 + C_{Z_L}^2 + C_{Z_W}^2 + C_{Z_X}^2 \tag{28}$$

$$C^2(\sigma_{Hlim}) = C_{Z_H}^2 + C_{Z_E}^2 + C_{Z_e}^2 + C_{Z_B}^2 + \frac{1}{4}(C_{F_t}^2 + C_{K_A}^2 + C_{K_V}^2 + C_{K_{H\beta}}^2 + C_{K_{HA}}^2) \tag{29}$$

Substituting Eqs. (26) and (27) into the reliability formula, the reliability index for gear contact fatigue strength can be calculated as:

$$\beta_H = \frac{E(g_H)}{\sigma(g_H)} = \frac{E\left[\frac{\ln(\sigma'_{Hlim})}{\ln(\sigma_H)}\right]}{\sqrt{C^2\left[\ln(\sigma'_{Hlim})\right] + C^2\left[\ln(\sigma_H)\right]}} \tag{30}$$

Reliability for gear contact fatigue strength is:

$$R = \Phi(\beta_H) \tag{31}$$

2.4. Reliability design based on flank adhesion

Generally, we should consider not only contact fatigue strength and bending fatigue strength, but also the scuffing failure during the design of a high speed heavy gear. Flank adhesion damage occurs on gear teeth if they are operated with an inadequate lubricant film

between the teeth. High surface temperatures then arise from the frictional heating, local welding and surface dragging as well as scoring therefore tend to occur. Because flank adhesion failure usually occurs in the sudden onset of high-speed heavy conditions, thereby limiting load capacity and the service life [3, 5, 6, 17].

According to GB/Z 6413, tooth of gear integral temperature θ_S is:

$$\theta_S=\theta_M+1.5\times\left\{0.12\frac{F_t}{b}K_AK_BK_{B\beta}K_{B\gamma}\left(\frac{1}{\upsilon_\Sigma\eta_{ail}}\right)^{0.25}\left(\frac{R_{a1}+R_{a2}}{2Q_{redc}}\right)^{0.25}X_MX_{BE}X_{\alpha\beta}\frac{K_{B\gamma}^{0.75}\upsilon^{0.5}}{|a|^{0.25}}\frac{1}{X_QX_{Ca}}X_\varepsilon\right\} \quad (32)$$

where θ_M is the body temperature, $K_{B\gamma}$ is the twist coefficient of abrasion, X_M is the coefficient of thermal expansion, X_{BE} is the addendum coefficient, $X_{\alpha\beta}$ is the coefficient of pressure angle, X_Q is the contact ratio, X_{Ca} is the addendum modification coefficient, X_ε is the scuffing calculate contact ratio factor, R_{a1}, R_{a2} are the arithmetic average roughness values.

The scuffing temperature limit is defined as:

$$\theta_B=\theta_M+1.5\theta_{fla\,\mathrm{int}} \quad (33)$$

where $\theta_{fla\,\mathrm{int}}$ is flash temperature.

According to the stress-strength interference theory, the limit state function is defined as:

$$g_S=\theta_B-\theta_S \quad (34)$$

According to Eq. (23), the mean and variable of the function are as follows:

$$E(g_S)=E(\theta_B)-E(\theta_S) \quad (35)$$

$$\begin{aligned}D(\theta_{\mathrm{int}})&=D(\theta_M)+1.5^2D(\theta_{fla\,\mathrm{int}})\\&=C_{\theta_M}^2E^2(\theta_M)+1.5^2C(\theta_{fla\,\mathrm{int}})E^2(\theta_{fla\,\mathrm{int}})\end{aligned} \quad (36)$$

where:

$$C_{\theta_{fla\,\mathrm{int}}}=\sqrt{C_{F_t}^2+C_{K_A}^2+C_{K_B}^2+C_{K_{B\beta}}^2+C_{K_{B\gamma}}^2+C_{X_M}^2+C_{X_{BE}}^2+C_{X_{\alpha\beta}}^2+C_{X_\varepsilon}^2} \quad (37)$$

The reliability index for gear flank adhesion can be calculated as:

$$\begin{aligned}\beta_\theta&=\frac{E(g_S)}{\sigma(g_S)}=\frac{E(g_S)}{\sqrt{D(g_S)}}\\&=\frac{E(\theta_{\mathrm{int}s})-E(\theta_{\mathrm{int}})}{\sqrt{D(\theta_{\mathrm{int}s})+D(\theta_{\mathrm{int}})}}\\&=\frac{E(\theta_{\mathrm{int}s})-E(\theta_{\mathrm{int}})}{\sqrt{C_{\theta_{\mathrm{int}s}}^2E^2(\theta_{\mathrm{int}s})+C_{\theta_M}^2E^2(\theta_M)+1.5^2C_{\theta_{fla\,\mathrm{int}}}^2E^2(\theta_{fla\,\mathrm{int}})}}\end{aligned} \quad (38)$$

Reliability of the flank adhesion is:

$$R=\Phi(\beta_\theta) \quad (39)$$

3. Reliability analysis of gears considering failure correlation

Generally, when component has multiple failure modes, the occurrence of any kind of failure mode will lead to component failure [12]. As a result, reliability of component with multiple failure modes can be regarded as a series system, as shown in Fig.1.

It was generally considered that the parts and failure modes of mechanical system are mutually independent. Therefore reliability of a series system is:

$$R_S(t)=R_1R_2\cdots R_n=\prod_{i=1}^{n}R_i(t) \quad (40)$$

where $R_S(t)$ is reliability of the system, R_i is reliability of the ith failure mode.

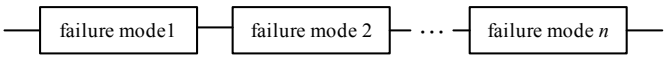

Fig.1. The series system

In practices, for the most engineering systems, their parts work in the same random load environment, and thus their failures are not mutually independent. Correlation is an inherent specialty of complicated mechanical systems, which is one of the greatest issues affecting and restricting mechanical reliability research [2, 6, 7, 10]. If the dependence of system failures is ignored, analysis of system reliability often leads to an excessive error. When we consider the correlation of mechanical components with multiple failure modes, reliability can be shown as:

$$\begin{aligned}R(t)&=P\{\min(T_1,T_2,\cdots,T_n)>t\}=P(T_1>t,T_2>t,\cdots,T_n>t)\\&=1-\sum_{i=1}^{n}P(T_i\le t)+\sum_{1\le i<j\le n}^{n}P(T_i\le t,T_j\le t)+\cdots+(-1)^k\times\\&\quad\sum_{1\le i_1<i_2<\cdots i_k\le n}^{n}P(T_{i_1}\le t,T_{i_2}\le t,\cdots,T_{i_k}\le t)+\cdots+(-1)^kP(T_{i_1}\le t,T_{i_2}\le t,\cdots,T_{i_k}\le t)\\&=1-\sum_{i=1}^{n}F_i(t)+(-1)^k\times\sum_{1\le i_1<i_2<\cdots<i_k\le n}^{n}C(F_{i_1}(t),F_{i_2}(t),\cdots,F_{i_n}(t))\end{aligned} \quad (41)$$

where $F_i(t)$ is a failure probability. $C(F_{i_1}(t),F_{i_2}(t),\cdots,F_{i_n}(t))$ is a copula function. As a useful tool to establish a joint distribution function from its marginal distributions, copula functions are often adopted to study correlation problems. Copulas provide a way of specifying joint distributions if only the marginal distributions are known. In terms of reliability problem with multiple failure modes, we can obtain a multivariate distribution for modeling joint behavior of failure modes using the marginal distributions of each failure mode and the copula function [7, 9, 16, 17].

Let $F_X(x)$ and $F_Y(y)$ denote the marginal distribution functions of variables X and Y, respectively. The joint distribution function $F_{X,Y}(x,y)$ can be expressed as:

$$F_{X,Y}(x,y)=C[F_X(x),F_Y(y)] \quad (42)$$

where $C(u,v)$ is the copula function.

If $F_X(x)$ and $F_Y(y)$ are continuous functions, $C(u,v)$ is unique. Since $F_X(x)$ and $F_X(x)$ are univariate functions and $C(u,v)$ is a copula function, then $F_{X,Y}(x,y)$ is a bivariate joint distribution function with marginal $F_X(x)$ and $F_Y(y)$.

Generally, the Archimedean copula functions are often adopted to build the joint distribution function. An N-dimensional Archimedean copula is given by:

$$C(u_1,u_2,\cdots,u_N)=\varphi(\varphi^{-1}(u_1),\varphi^{-1}(u_2),\cdots,\varphi^{-1}(u_N)) \quad (43)$$

where φ is the generator.

One of the important natural properties of the Archimedean copulas can be represented by the following expression,

$$C(u_1,u_2,u_3)=C[C(u_1,u_2),u_3] \quad (44)$$

$$C(u_1,u_2,u_3,u_4)=C[C(u_1,u_2,u_3),u_4] \quad (45)$$

$$C(u_1,u_2,\cdots,u_{N-1},u_N)=C\left[C(u_1,u_2,\cdots,u_{N-1}),u_N\right] \quad (46)$$

Eqs. (44-46) show that any N-dimensional Archimedean copula could be deduced by a two-dimension copula. In terms of mechanical parts, the failure modes are generally positive correlated, and the joint distribution function could be built by the Gumbel copula function. The expression of the Gumbel copula is as follows [10, 11, 14]:

$$C_G(u,v;\theta)=\exp\{-[(-\ln u)^{\frac{1}{\theta}}+(-\ln v)^{\frac{1}{\theta}}]^{\theta}\} \qquad \theta\in(0,1) \quad (47)$$

4. Numerical example

In this section, we use the proposed method to calculate reliability of a gear transmission for a heavy machine tool. The material of gear is 18Cr2Ni4WA. In accordance to the standard regulations or looking up in figures [13, 15, 16, 17], we get the mean values of each parameter of gear pairs, and the standard deviation of each parameter based on the aforementioned principles. The variable coefficients are shown in Table 1.

According to Table 1, the reliability index β_i, reliability R_i of each failure mode for gear are obtained, shown in Table 2.

According to Table 2, the major failure modes for gear are sorted as bending fatigue failure, flank adhesion failure and contact fatigue failure. Gear bending fatigue is a major failure mode. The more operating torque increases, the more gear bending fatigue strength will be. Therefore, gear tooth bending fatigue is a key characteristic of the gear and affected by geometry, material, manufacturing methods and other variables.

Using Eq. (35), according to the assumption of mutually independent, the reliability of the driving gear and driven gear respectively are:

$$R_1=R_{F_1}R_{H_1}R_{\theta_1}=0.9659$$

$$R_2=R_{F_2}R_{H_2}R_{\theta_2}=0.9748$$

Reliability of gear pair is $R=R_1R_2$ =0.94159.

Table 1. The variable coefficient of gear

variable	variable coefficient	variable	variable coefficient
F_t	C_{F_t}=659.66	X_Q	C_{X_Q}=0.03
Y_{Fa1}	$C_{Y_{Fa1}}$=0.778	X_{BE}	$C_{X_{BE}}$=0.03
Y_{Fa2}	$C_{Y_{Fa2}}$=0.0703	Z_ε	C_{Z_ε}=0.045
Y_{Sa1}	$C_{Y_{Sa1}}$=0.0577	Z_β	C_{Z_β}=0.0478
Y_{Sa2}	$C_{Y_{Sa2}}$=0.0706	Z_F	C_{Z_F}=0.02
Y_ε	C_{Y_ε}=0.0357	Z_N	C_{Z_N}=0.03
Y_β	C_{Y_β}=0.004	Z_R	C_{Z_R}=0.036
Y_{ST}	$C_{Y_{ST}}$=0.0693	Z_V	C_{Z_V}=0.033
Y_{NT}	$C_{Y_{NT}}$=0.033	Z_L	C_{Z_L}=0.033
$Y_{\sigma relt1}$	$C_{Y_{\sigma relt1}}$=0.033	Z_W	C_{Z_W}=0.037
$Y_{\sigma relt2}$	$C_{Y_{\sigma relt2}}$=0.033	Z_E	C_{Z_E}=0.033
Y_{Rrelt1}	$C_{Y_{Rrelt1}}$=0.0351	Z_X	C_{Z_X}=0.033
Y_{Rrelt2}	C_{Rrelt2}=0.0351	Z_H	C_{Z_H}=0.116
Y_X	C_{Y_X}=0.0451	θ_M	C_{θ_M}=0.03
K_A	C_{K_A}=0.033	θ_{ints}	$C_{\theta_{\text{ints}}}$=0.03
K_V	C_{K_V}=0.033	$\sigma_{H\lim}$	$C_{\sigma_{H\lim}}$=0.06
$K_{H\beta}$	$C_{K_{H\beta}}$=0.055	$X_{\alpha\beta}$	$C_{X_{\alpha\beta}}$=0.032
$K_{H\alpha}$	$C_{K_{H\alpha}}$=0.0382	X_M	C_{X_M}=0.027
$K_{F\alpha}$	$C_{K_{F\alpha}}$=0.0382	X_{Ca}	$C_{X_{Ca}}$=0.03

Table 2. The index reliability and the reliability for gear

		β_i	$R_i=\Phi(\beta_i)$
gear bending fatigue failure	driving gear	2.02	$R_{F_1}=0.9783$
	driven gear	2.15	$R_{F_2}=0.9838$
gear contact fatigue failure	driving gear	3.5	$R_{H_1}=0.9935$
	driven gear	2.8	$R_{H_2}=0.9974$
gear flank adhesion failure	driving gear	2.5	$R_{\theta_1}=0.9938$
	driven gear	3.2	$R_{\theta_2}=0.993$

The results obtained by Monte Carlo simulation are $R_{1MCS} = 0.9878$, $R_{2MCS} = 0.9762$, $R_{MCS} = 0.9754$.

where R_{1MCS} is reliability of a driving gear, R_{2MCS} is reliability of a driving gear, R_{MCS} is the reliability of gear pair. All the results are calculated using Monte Carlo simulation.

The relative error is:

$$\varepsilon = \left| R - R_{MCS} \right| / R_{MCS} = 3.4\%$$

According to the properties of the Gumbel copula $C(P_i, P_h)$ $(1 \le i, h \le 3)$, the $C(P_i, P_h, P_t)$ $(1 \le i < h < t \le 3)$ can be obtained:

$$C(P_{1F}, P_{1H}) = 0.2412$$
$$C(P_{1F}, P_{1\theta}) = 0.1262$$
$$C(P_{1H}, P_{1\theta}) = 0.0978$$

$$C(P_{2F}, P_{2H}) = 0.1348$$
$$C(P_{2F}, P_{2\theta}) = 0.0723$$
$$C(P_{2H}, P_{2\theta}) = 0.1527$$

$$C(P_{1H}, P_{1F}, P_{1\theta}) = C(C(P_{1H}, P_{1F}), P_{1\theta}) = 0.045$$

$$C(P_{2H}, P_{2F}, P_{2\theta}) = C(C(P_{2H}, P_{2F}), P_{2\theta}) = 0.032$$

$$C(P_1, P_2) = 0.1264$$

According to Copula theory, reliability of the driving gear and driven gear can be respectively given by:

$$R_1' = 0.9867$$

$$R_2' = 0.9884$$

Reliability of the gear pair is $R' = 0.9851$. The relative error is $\varepsilon = \left| R' - R_{MCS} \right| / R_{MCS} = 0.94\%$.

From aforementioned results, we know that the relative error for mutually independent of failure modes is greater than considers failure correlation. Since this paper only considers three main failure modes, so the difference of relative error is not obvious. When we consider multiple failure modes, the proposed method is superior to traditional methods without considering correlations.

5. Conclusions

This paper has established reliability model with three major failure modes: tooth bending fatigue, gear contact fatigue and gear scuffing failure. From the reliability calculation model, it is concluded that the primary failure mode of gear is the tooth surface contact fatigue failure and secondary failure mode is the gear scuffing failure. Based the copula theory, a reliability calculation method of the gear under considering correlation for multiple failure modes are developed. A comparative analysis has shown that the accuracy and practicality of the proposed model is higher than the model without consider failure correlation. However, correlations widely exist in practical engineering. Therefore, this method provides an effective and reliable approach to assess reliability of engineering systems.

Acknowledgment

This research was supported by the National Science and Technology Major Project of China under the contract number 2013ZX04013-011, and the National Natural Science Foundation of China under contract number 11272082.

References

1. Al-Shareedah E M, Alawi H. Reliability analysis of bevel gears with and without back support. Mechanism & Machine Theory 1987; 22(1): 13-20, http://dx.doi.org/10.1016/0094-114X(87)90071-1.
2. Aoues Y, Chateauneuf A. Benchmark study of numerical methods for reliability-based design optimization. Structural and Multidisciplinary Optimization 2010; 41: 277-294, http://dx.doi.org/10.1007/s00158-009-0412-2.
3. Krantz T, Tufts B. Pitting and bending fatigue evaluations of a new case-carburized gear steel. International Design Engineering Technical Conferences and Computers and Information in Engineering Conference 2007; 4-7, http://dx.doi.org/10.1115/detc2007-34090.
4. Lyu S K, Inoue K, Deng G, et al. Effect of surface treatments on the strength of carburized gears. KSME International Journal 1998; 12(2): 206-214.
5. Li Y F, Mi J, Huang H Z, et al. Fault tree analysis of train rear-end collision accident considering common cause failure. Ekcsploatacja i Niezawodnosc – Maintenance and Reliability 2013; 15(4): 403-408.
6. Madhusekhar D. Reliability based design of a gear box. Journal of Engineering Research and Applications 2009; 4(8): 38-44.
7. Nelsen R B. An introduction to Copulas. Springer Verlag, 2006; 27-32.
8. Noh Y, Choi K, Du L. Reliability-based design optimization of problems with correlated input variables using a Gaussian copula. Structural and Multidisciplinary Optimization 2009; 38(1): 1-16, http://dx.doi.org/10.1007/s00158-008-0277-9.
9. Peng X Q, Liu G, Wu L Y, et al. A stochastic finite element method for fatigue reliability analysis of gear teeth subjected to bending. Computational Mechanics 1998; 21: 253-261, http://dx.doi.org/10.1007/s004660050300.
10. Ramirez-Marquez J E, Coit D W. Optimization of system reliability in the presence of common cause failures. Reliability Engineering and System Safety 2007; 92: 1421-1434, http://dx.doi.org/10.1016/j.ress.2006.09.004.
11. Rao S S, Das G. Reliability based optimum design of gear trains. Journal of Mechanical Design 1984; 106(1): 17-22, http://dx.doi.org/10.1115/1.3258551.
12. Xiao N C, Huang H Z, Li Y F, et al. Multiple failure modes analysis and weighted risk priority number evaluation in FMEA. Engineering Failure Analysis 2011; 18(4): 1162-1170, http://dx.doi.org/10.1016/j.engfailanal.2011.02.004.
13. Yang Q J. Fatigue test and reliability design of gears. International Journal of Fatigue 1996; 18(3): 71-177, http://dx.doi.org/10.1016/0142-1123(95)00096-8.
14. Ye X F, Wang Q, Huang Z Y. Research on probabilistic reliability design of gears. Locomotive & Rolling Stock Technology 2011; 3: 1-5. (In Chinese).

15. Zhang J, Zhang Q, Xu Z Z, et al. A study on the evaluation of bending fatigue strength for 20CrMoH gear. International Journal of Precision Engineering and Manufacturing 2013; 14(8): 1339-1343, http://dx.doi.org/10.1007/s12541-013-0181-0.
16. Zhang Q, Zhang J, Wu C. The evaluation of contact fatigue strength for 20MnCr5 carburized gear. International Journal of Precision Engineering and Manufacturing 2014; 15(1): 117-121, http://dx.doi.org/10.1007/s12541-013-0313-6.
17. Zhang Y M, Liu Q L, Wen B C. Practical reliability-based design of gear pairs. Mechanism and Machine Theory 2003; 38(12): 1363-1370, http://dx.doi.org/10.1016/S0094-114X(03)00092-2.

Fang-Jun ZUO
Le YU
Jinhua MI
Zheng LIU
Hong-Zhong HUANG

Institute of Reliability Engineering
University of Electronic Science and Technology of China
No. 2006, Xiyuan Avenue, West Hi-Tech Zone, Chengdu,
Sichuan, 611731, P. R. China

E-mails: hzhuang@uestc.edu.cn

Article citation info:
SAMBORSKI S, WIECZORKIEWICZ J, RUSINEK R. A numerical-experimental study on damaged beams dynamics. Eksploatacja i Niezawodnosc – Maintenance and Reliability 2015; 17 (4): 624–631, http://dx.doi.org/10.17531/ein.2015.4.20.

Sylwester SAMBORSKI
Jakub WIECZORKIEWICZ
Rafal RUSINEK

A NUMERICAL-EXPERIMENTAL STUDY ON DAMAGED BEAMS DYNAMICS

NUMERYCZNO-DOŚWIADCZALNE STUDIUM DYNAMIKI BELEK Z USZKODZENIEM

This paper focuses on analysis of damage influence on dynamical behaviour of beams. Finite Element Method was used to simulate vibrations of beams under three variants of boundary conditions: a cantilever beam, a simply- supported beam and a symmetrically clamped beam. Analysis of natural frequencies of both intact and damaged beams was performed in order to observe the effect of damage on the beams dynamics. Next, recurrence plot technique was applied. Finally, experimental verification is performed to check the numerical results.

***Keywords**: damage detection, recurrence plot, beam dynamics, free vibration.*

W pracy zaprezentowano analizę wpływu uszkodzenia na dynamiczne zachowanie belek. Do symulacji numerycznych użyto Metody Elementów Skończonych gdzie analizowano trzy warianty zamocowania belek: jednostronne utwierdzenie, swobodne podparcie i obustronne utwierdzenie. Przeprowadzono analizę częstości drgań własnych belki nieuszkodzonej i uszkodzonej a następnie zastosowano metodę wykresów rekurencyjnych aby zaobserwować różnice w ich zachowaniu dynamicznym. W ostatnim etapie przeprowadzono weryfikację eksperymentalną uzyskanych wyników symulacji.

***Słowa kluczowe**: detekcja uszkodzeń, wykresy rekurencyjne, dynamika belki, drgania własne.*

1. Introduction

In many contemporary structures various types of defects can appear leading to significant reduction of the element rigidity and changing its overall mechanical behaviour. A special challenge is detection and localization of hidden defects, which can have many forms depending on the scale of the problem, eg. dislocations, voids or inclusions in microscale [43, 49, 44, 3] to macroscopic defects, such as delamination in laminated composites [31] or welds in metallic materials [53, 50]. The current work is focused on testing the applicability of dynamic vibration-based, as well as the space analysis methods to defect detection and localization in 1D (beam) structures. The vibration-based methods have been widely used in the plates and beams dynamics. For example, Manoach et al. [25, 26, 27, 24, 48] analysed the frequencies and modes of free vibrations in order to identify damage in beam and plates. The most interesting aspect of these papers was introduction of the so-called Damage Index exploiting the information given by the Poincaré maps [19]. The authors of the current study aimed at testing other dynamical methods towards detection and localization of defects in structures, which led them to reach for time series analysis.

Experimental time series, especially nonlinear, can be analyzed by means of the method of delay coordinates, which allows to reconstruct a phase space and Poincaré section. This procedure is precisely described in [2, 32] and can be applied for analysis of experimental signals obtained from different kinds of real processes [12, 5] and numerical simulations [40]. For instance, the delay coordinate technique is used for researching dynamics of robot joints [47] and to analyse nonlinear system with dry friction [40]. Interesting contribution in the field of phase space reconstruction is presented in [7, 8, 36] in which the method of delay coordinates is employed for experimental and numerically generated signals, also with noise. Another example can be an impact and a self-excited oscillator with CoulombAmontons friction [13].

On the basis of delay coordinates method, a recurrence plot technique is introduced to analyse linear or non-linear stationary and also non-stationary time series [30]. The formal concept of recurrences was introduced by Henri Poincaré in his seminal work from 1890 [37], for which he won a prize sponsored by King Oscar II of Sweden and Norway [30]. Therein, Poincaré did not only discover the homoclinic tangl which lies at the root of the chaotic behaviour of orbits, but he also introduced (as a by-product) the concept of recurrences in conservative systems. Even though much mathematical work was carried out in the following years, Poincaré's pioneering work and his discovery of recurrence had to wait for more than 70 years for the development of fast and efficient computers to be exploited numerically. The use of powerful computers boosted chaos theory and allowed to study new and exciting systems. Some of the tedious computations needed to use the concept of recurrence for more practical purposes could only be made with this digital tool [30]. In 1987, [5] introduced the method of recurrence plots (RPs) to visualize the recurrences of dynamical systems. Since that time, scientists have been working in various fields have made use of the RPs. Applications of RPs can be found in numerous fields of research such as astrophysics [52], earth sciences [28], engineering [39, 17, 21, 22, 20, 6, 38], biology [11, 23], cardiology, or neuroscience [29, 30, 46, 51], and otolaryngology [41]. Damage detection of various mechanical structure is also analyzed with the help of the RP [34, 35, 42, 33].

Here, in this paper the applicability of the RPs to identify defect in beam structures were tested and compared with the results of different phase space methods; experimental verification of the results was performed, as well.

2. Research methodology

2.1. Numerical model and assumptions

In numerical analyses three variants of boundary conditions (BC) were considered:

- a cantilever beam (Fig.1),
- a simply-supported beam (Fig.2) and
- a beam encastered at both ends (Fig.3).

3. The methodology of analyzing the beams dynamics based on a comparison of the intact and the damaged beam for each of the three BC variants.

The considered numerical beam models prepared in the ABAQUS/CAE software environment had dimensions equal L × B × H = 800 × 20 × 5mm. One of the possibilities of modelling damage in a beam is changing its local stiffness [10, 14]. Thus, both in the FE analyses and in the experimental part of the research a local thinning of the beam was introduced. For the purpose of testing the usefulness of the RPs method in damage identification process the isotropic aluminum beam was tested so far. Nevertheless, the research on the laminated composite beams is in progress. The accepted material data were as follows: mass density ρ=2720kgm−3, Young's modulus E = 70000GPa and Poisson's coefficient ν=0.33. The BCs for the accepted three beam models can formally be written as u(x = 0) = 0, w(x = 0) = 0, dw/dx(x = 0) = 0, u(x = 0) = 0, w(x = 0) = 0, w(x = L) = 0 and u(x = 0) = 0, w(x = 0) =0, dw/dx(x = 0) = 0, u(x = L) = 0, w(x = L) = 0, dw/dx(x = L) = 0.

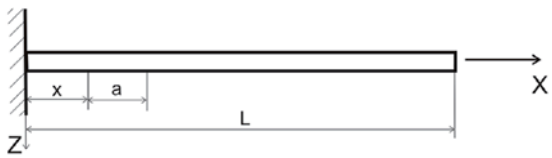

Fig. 1. Cantilever beam model with a defect

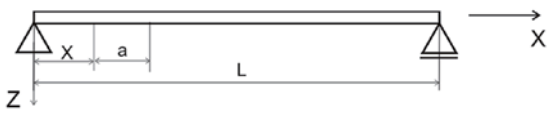

Fig. 2. Simple supported beam model with a defect

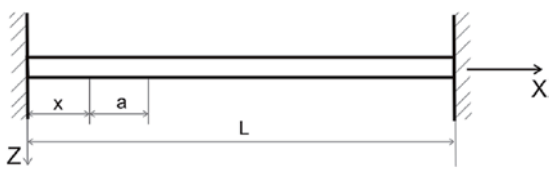

Fig. 3. Clamped-clamped/encastered beam model with a defect

In each case of the BC both damaged and intact beam was analyzed. Such an approach allowed to compare the dynamics of the damaged beams with their undamaged counterparts. In general, for all the models the eigenproblem was solved with the Lanczos algorithm in order to get the frequencies of free vibrations and the respective modes. In the end the elaborated results were collected and compared in order to find the influence of the defect on the dynamical response of the analyzed beam structures. The beam models were composed of the B21 beam-type elements available in the ABAQUS/CAE standard element library [1]. The total number of elements was 40. The defect was modeled as a local thinning of the beam cross-section, as justified above. The weak cross-section had a thickness reduced from the nominal 5mm to 3mm. The defect of the length D=80mm starting at x=40mm from the clamp occupied 10% of the total beam's length. The results obtained with the ABAQUS/CAE were analyzed with the help of different time series analysis and phase space techniques being a background for testing the recurrence plots (RPs) applicability for damage identification. Thus, several scientific approaches were applied simultaneously to find any differences in dynamical output between the intact and the damaged beam.

3.1. Recurrence plots technique

The basic idea of recurrence analysis bases on the delay method where any scalar time series may be used to construct a new time series vector that is equivalent to the original dynamics from a topological point of view. The specific vector in a new space (called the reconstructed space), is formed according to the Takens' theory [45] and can be presented as follows:

$$s_i = (x_i, x_i+d, x_i+_{2d}, \ldots, x_{i+(m-1)d}) \tag{1}$$

where m is called the embedding dimension, d is generally referred as the delay (time delay) or lag. This vector is useful only if parameters m and d are properly chosen. If the delay d is too long, then the coordinates are essentially independent and the proper information cannot be gained from the plot. Whereas the delay d is too short, then the reconstructed states differ not much and the points are scattered around a straight line. The second key embedding parameter m means that we are looking for such dimension of reconstructed phase space to avoid false crossing of the trajectory. If any two points which stay close in the m-dimensional reconstructed space will be still close in the $(m+1)$-dimensional reconstructed space then such a pair of points are called true neighbors, otherwise, they are called false neighbors. One of the most efficient and popular method to choice the time delay d and embedding dimension m are: the average mutual information (AMI) [9] and the false nearest neighbors method (FNN) [18], respectively. In this paper AMI and FNN are used as well.

Recurrence Plot (RP) is an advanced technique of nonlinear data analysis. RP means a visualization of a square matrix, in which the matrix elements correspond to those times at which a state of a dynamical system recurs [30]. The recurrence diagram is expressed by matrix:

$$Ri,j = \mathrm{H}(\varepsilon - |\mathrm{x_i} - \mathrm{x_j}|) \tag{2}$$

where H is the Heaviside step function, ε is a tolerance parameter (threshold),

si and *sj* are a delay vectors (vectors forming the phase space trajectory in the phase space). If the trajectory in the reconstructed phase space returns at time *i* into the neighbourhood of *ε* where it was *j* then M_{ij}=1, other- wise M_{ij}=0. These results are plotted as black and white dots respectively. Detailed description of embedding parameters and much other additional in- formation can be found in [16, 30, 9]. A pattern of RP represents dynamical system behaviour. For instance, periodic motion is reflected by long and non- interrupted diagonals. The vertical distance between these lines corresponds to the period of the oscillation. Irregular motion characterizes the pattern consist of different lengths lines and distance. Here RP technique is used as a method of damage detection in the beams. The embedding parameters: time delay (d) and embedding dimension (m) are estimated first before the recurrence analysis.

3.2. Experimental tests

Experimental verification was performed on the experimental setup presented in Fig.4. The test setup consisted of the Polytec PSV 500

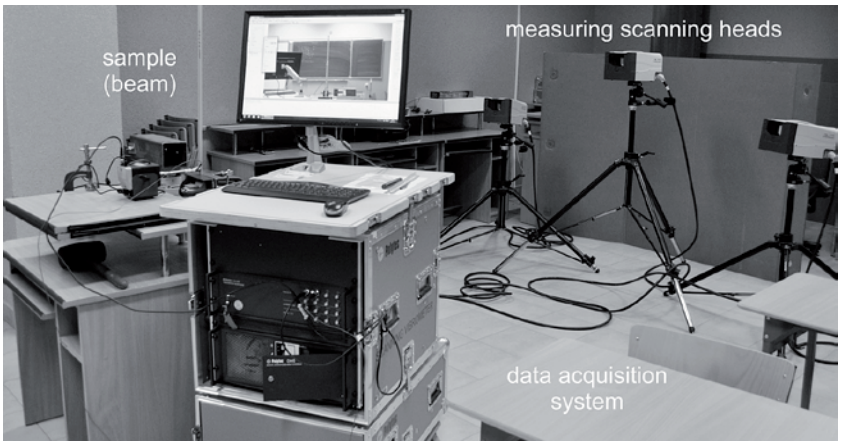

Fig. 4. xperimental standing with 3D Laser Doppler Vibrometer

3D Laser Scanning Vibrometer possessed by Department of Applied Mechanics at Lublin University of Technology.

This sort of vibrometer consists of three in- dependent scanning heads and the data acquisition/visualization unit. Each head is equipped with a laser source; one of them has in addition a video camera. All the three heads have built-in precise transducers able to give dis- placements and velocities of the observed point of the scanned object in time. The three laser beams meet at one point with a defined precision given in microns, what enables highly accurate dynamical measurements, especially around the edges of a specimen. During the measurements a frequency of the laser beam, reflected by the tested object is compared to the one of the sent beam, according to the Doppler effect. Application of the three independent laser scanning heads enables contactless measurements of vibrations of three-dimensional (3D) objects, particularly those having small dimensions. The measurements are simultaneously performed for the three orthogonal spatial directions X, Y and Z. The acquisition/analysis unit is equipped with analog-to-digital data conversion cards. Their task is to collect the measurement data, what is supervised by a dedicated software installed on the PC computer. In addition, the acquisition unit is equipped with an excitation signal generation panel. The laser scanning vibration measurement allows registration of velocities up to 10 m/s in a wide range of frequencies from 0 to 100 kHz. The scanning heads of the PSV500 3D vibrometer enable measurements from 42 cm counting from the object to hundreds of meters [4].

4. Discussion of numerical and experimental results

The first step of the research was the numerical analysis of dynamical behaviour of three beam models differing with boundary conditions (Figs. 1, 2 and 3). Next an experiment was conducted with the Laser Scanning Vibrometer.

4.1. Cantilever beam

The FEA model of the cantilever beam is presented in Fig. 1. In the numerical model the deflection was read at the end point of the beam. The FE simulations gave the eigenfrequencies collected in Tab.1, where the relative differences of the damaged beam's frequencies with respect to the intact one are also presented. In Fig. 5 a direct comparison of free vibration frequencies for both cantilever beams is presented.

Table 1. Eigenfrequencies of the cantilever beam

Eigenfrequency order	Eigenfrequency [Hz]		Relative difference [%]
	intact	damaged	
f_1	6.40	4.43	30.78
f_2	40.11	36.43	9.17
f_3	112.29	108.26	3.59
f_4	219.94	213.44	2.96
f_5	363.36	349.42	3.84

Thus, the reader can see the absolute values of subsequent frequencies; the only slight difference between the frequencies obtained for the damaged beam in comparison with the healthy one is also well seen. Taking into account the frequencies of free vibrations collected in Tab.1 the excitation frequency for the cantilever beam was chosen to be 2 Hz at the sampling frequency of 0.02 s. Such an approach was proposed by Manoach et al. [25, 26, 27]. The load (pressure) was uniformly distributed along the beam. Its value was 1 kPa. The resulting displacement time courses of the beams free end were plotted in Fig. 6. For better visibility of the differences between the damaged and the intact beam a phase plot is shown in Fig. 7. Both the time series and the phase plots show only the difference in vibrations amplitude but the small change in frequency is not observable here. Therefore, the recurrence plot for the delay d=3, embedding dimension m=2 and the neighbourhood ε=0.002 were drawn for the intact and the damaged beam in Fig.8a and b respectively. The former plot obtained for the intact beam (Fig. 8a) pattern characterizes periodic motion. The pattern of the damaged beam (Fig. 8b) reflects also regular vibrations but the amplitude is different from the intact beam output so

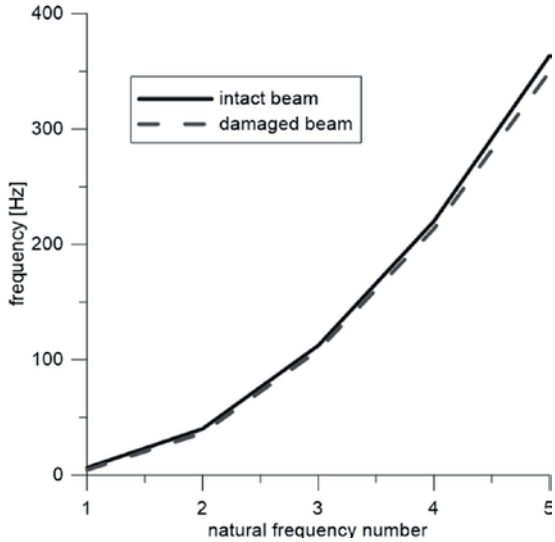

Fig. 5. Comparison of eigenfrequencies for the cantilever intact and damaged beam

it is important to compare both cases in the same neighbourhood size ε.

4.2. Simply supported beam

The simply-supported beam model is presented in Fig. 2. In this case, the displacement (deflection) was measured in the middle of the beam. The eigenfrequencies obtained numerically are given in Tab. 2 and graphically presented in Fig. 9. Again, the frequencies for the intact beam are bigger than those for the damaged beam. Concerning the obtained eigenfrequencies, the excitation frequency was set to 10 Hz, which was in each case less than $f1$, in order to evade the resonance, as the analysis was by assumption linear. For the same reasons the amplitude of the distributed load was set to 10 kPa, what resulted in displacement amplitudes very similar to those obtained for the cantilever beams end; the beam response was sampled every 0.005s.

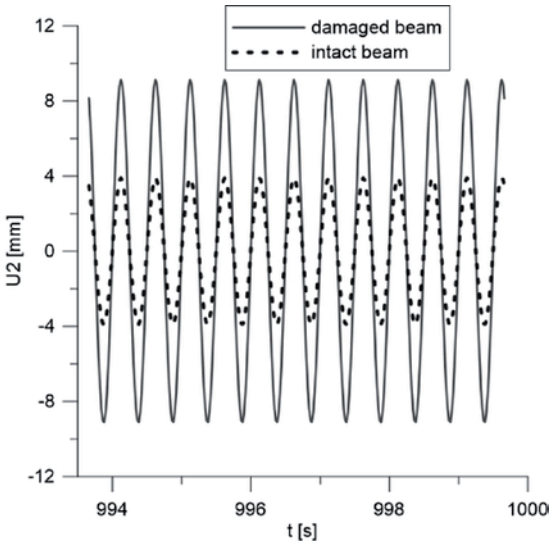

Fig. 6 Displacement time course of intact and damaged cantilever beam forced vibrations at 2Hz

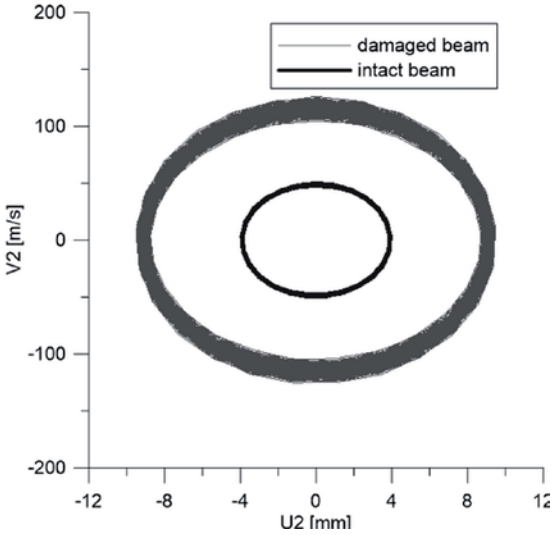

Fig. 7. Phase diagram for the cantilever beam excited at 2 Hz

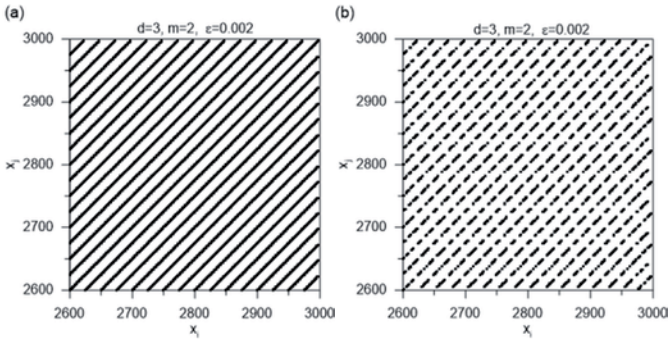

Fig. 8. Recurrence Plot for cantilever intact beam (a) and damaged (b)

The time course (Fig. 10) and the phase plot (Fig. 11) depict the dynamic properties of the simply supported beam. The dynamic behavior of the intact and the damaged structure observed by time series (Fig. 10) and the phase plot (Fig. 11) were very similar to each other but the damaged beam exhibited a bit bigger amplitude of vibrations. The difference between them is more evident in recurrence analysis done for embedding parameters: d=2, m=2 and ε=0.005.

Table 2. Eigenfrequencies of a simply supported beam

Eigenfrequency order	Eigenfrequency [Hz]		Relative difference [%]
	intact	damaged	
f_1	17.97	17.43	3.03
f_2	71.88	65.63	8.70
f_3	161.73	143.71	11.14
f_4	287.49	259.65	9.68
f_5	449.16	416.06	7.37

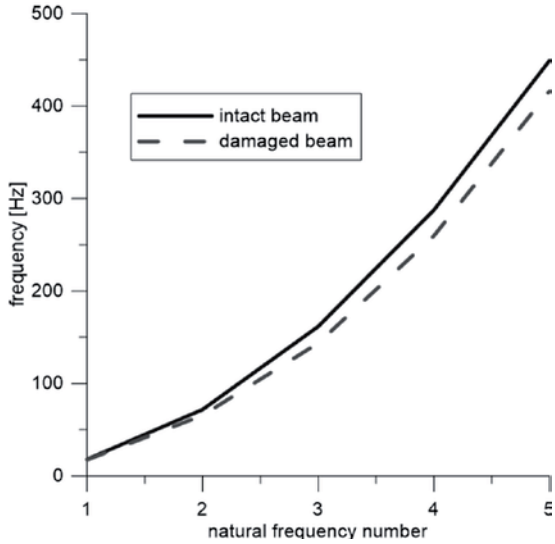

Fig. 9. Comparison of eigenfrequencies for the simply supported intact and damaged beam

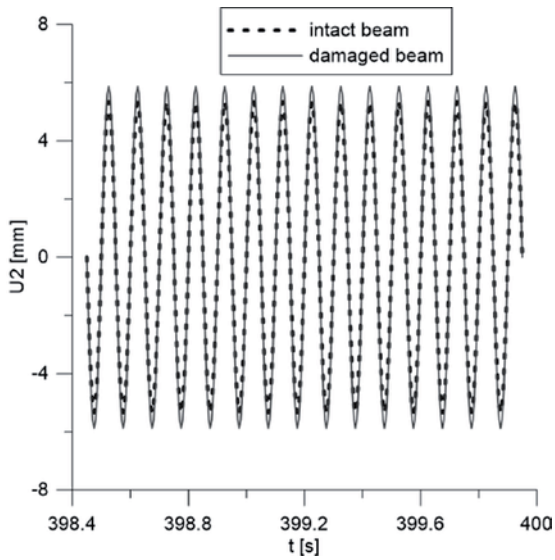

Fig. 10. Displacement time course of intact and damaged simply supported beam forced vibrations at 10Hz

The recurrence plots (Fig. 12) exhibit regular motion of the intact beam while the damaged one manifests a motion with quasi-periodicity that cannot be noticed only through the time series and even the phase plot.

4.3. Clamped-clamped beam

The third model of beam structure was clamped at both ends (Fig. 3). The dimensions of the beam, as well as the size and location of the defect was the same as in the previous two models. However,

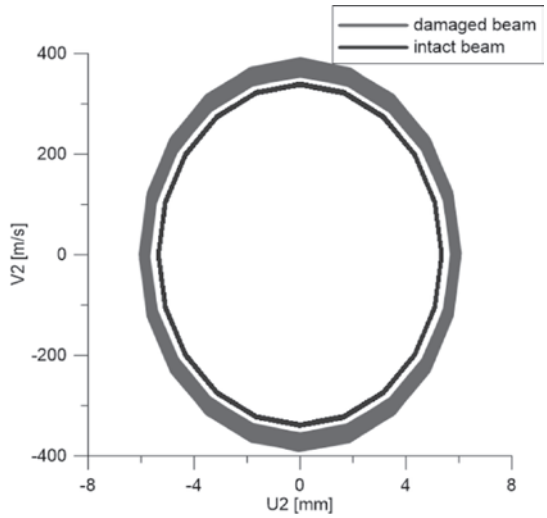

Fig. 11. Phase diagram for the simply supported beam excited at 10 Hz

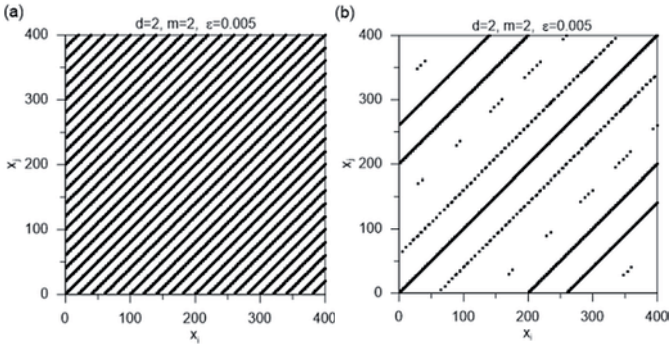

Fig. 12 Recurrence Plot for simply supported intact beam (a) and damaged (b)

Table 3. Eigenfrequencies of the clamped-clamped beam

Eigenfrequency order	Eigenfrequency [Hz]		Relative difference [%]
	intact	damaged	
f_1	40.74	36.82	9.61
f_2	112.30	108.41	3.46
f_3	220.14	213.93	2.82
f_4	363.88	350.43	3.70
f_5	543.52	522.80	3.81

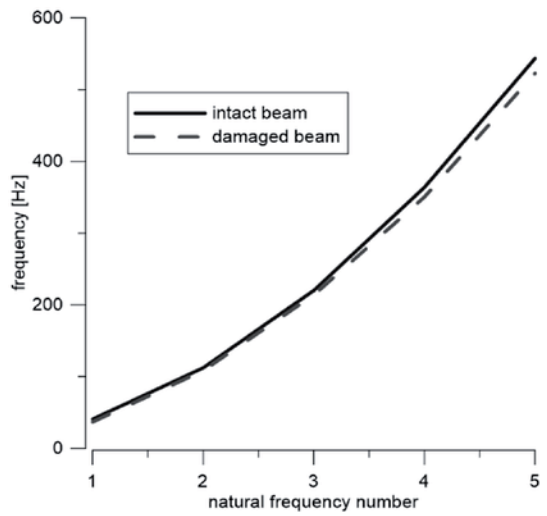

Fig. 13. Comparison of eigenfrequencies for the clamped-clamped intact and damaged beam

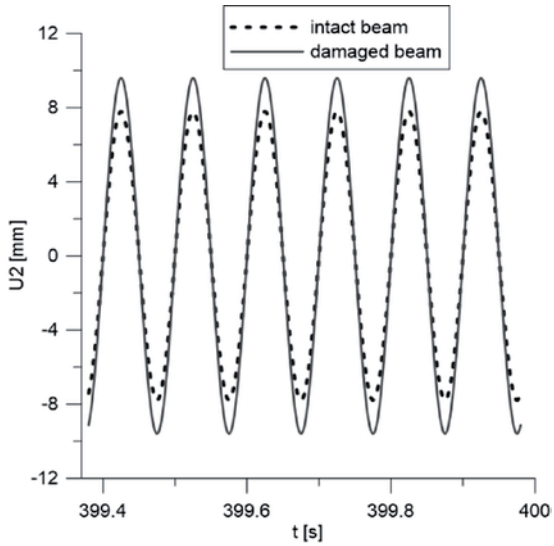

Fig. 14. Displacement time course of intact and damaged clamped-clamped beam forced vibrations at 20 Hz

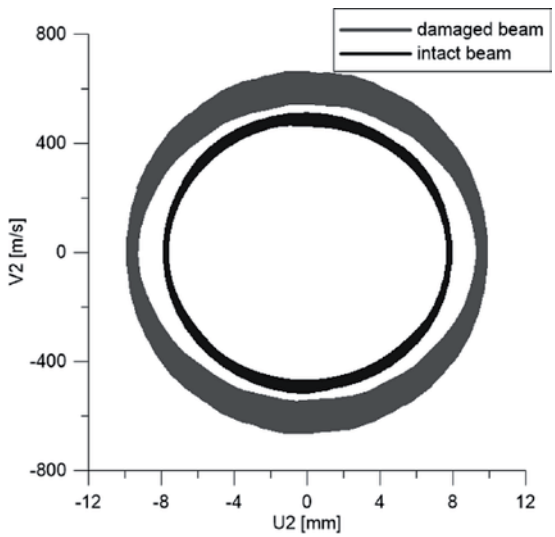

Fig. 15. Phase diagram for the clamped-clamped beam excited at 20Hz

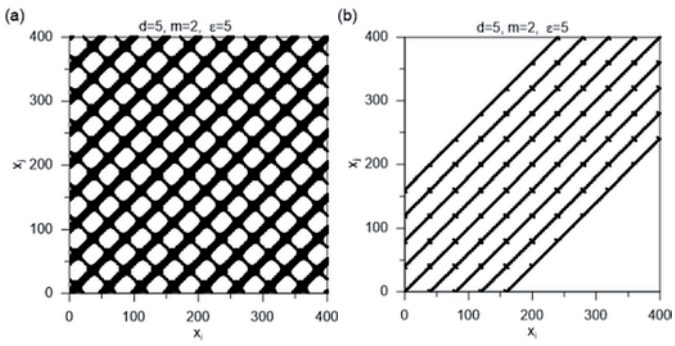

Fig. 16. Recurrence Plot for clamped-clamped intact beam (a) and damaged (b)

for the accepted boundary conditions the beam was much stiffer, what was reflected by its eigenfrequencies collected in Tab.3 and graphically shown in Fig. 13. Also the expected deflections were smaller. For this reason the load amplitude value was chosen to be 1 kPa, what provided approximately the same value of deflection amplitude (measured in the beam's mid-point) compared to the two previous models. The accepted excitation frequency was 20 Hz at 0.005 s sampling. Also in this case the damaged beam was less stiff than the intact one and therefore it had smaller natural frequencies and bigger vibrations

amplitudes, what was reflected by the time series (Fig. 14) and the phase plot (Fig. 15).

The difference in eigenfrequencies was very small specially at first modes that is why simple frequency analysis was not sufficient to detect damages in beams. The recurrence plot technique turned out to give better results provided that embedding parameters are selected properly. Here, for beams clamped at both ends, the embedding parameters were as follows: d=5, m=2 ε=5. Then, the recurrence plots present various pattern depending on the damage existence (Fig. 16). The intact beam (without defect) demonstrates regular RP (Fig. 16a), while irregular pattern is typical for the damaged beam (Fig. 16b). The damaged beam exhibits symptoms of quasi-periodicity.

4.4. Experimental results

The measurements were conducted on a physical aluminum beams, both intact and defected. The BCs provided by the experimental setup in its current form were those given in Fig. 1 – the cantilever beam. The results are collected in Tab. 4. Comparison of the results with those given in Tab. 1 show their good compatibility. Namely, the tendency of subsequent free vibration frequencies for the beam with defect to be smaller than its counterpart obtained for the intact structure was confirmed experimentally. Moreover, the relative differences were the biggest for the first mode, both in simulations and in the experiment. This was of course connected with the applied BCs – clamp at one end. For the higher frequencies the differences were circulating around several percent in both cases. The discrepancies between the numerical results and the experimental ones are now under detailed consideration. The same applies to the experimental setup towards testing the other BCs.

5. Conclusions

Defect detection procedure based on frequency analysis and recurrence plot technique is presented here with quite good results. Since the difference in eigenfrequencies are relatively small especially for lower modes, additional procedure to analyse excited vibrations of identified object is important. The recurrence plots analysis gives a new aspects of the problem. In case of damaged beams recurrence plot pattern is always less regular that let us distinguish intact and damaged structure.

The damaged beams have always bigger amplitude of excited vibrations and smaller natural frequency. That is caused by smaller stiffness of damaged beams comparing to intact beams which do not have any detects. Numerical and experimental results are consistent in this matter.

The difference in the natural frequencies between the intact and damaged beam generally depends on BCs and mode number. Sometimes, it is better to analyse lower modes and sometimes higher ones depending on BCs.

Acknowledgements

Financial support of Structural Funds in the Operational Programme - Innovative Economy (IE OP) financed from the European Regional Development Fund – Project "Modern material technologies in aerospace industry", POIG.01.01.02-00-015/08-00 is gratefully acknowledged.

References

1. Abaqus 6.13: analysis user's manual 2013.
2. Abarbanel HDI Analysis of Observed Chaotic Data. Springer-Verlag, New York 1996.
3. Bathe KJ. Computational fluid and solid mechanics 2003: Proceedings, Second MIT Conference on Computational Fluid and Solid Mechanics, June 17-20, 2003: On the different behaviour of porous ceramic polycrystalline materials under tension and compression stress state, Elsevier, Amsterdam and Boston 2003.
4. Cichon P, Stosiak M. Zastosowanie wibrometru laserowego do pomiaru drgań stołu symulatora liniowego napędu hydrostatycznego. Napędy i Sterowanie 2012; 5: 66–72.
5. Eckmann JP, Kamphorst SO, Ruelle D. Recurrence Plots of Dynamical Systems. Europhysics Letters (EPL) 1987; 4(9): 973–977, http://dx.doi.org/10.1209/0295-5075/4/9/004.
6. Elwakil AS, Soliman AM. Mathematical Models of the Twin-T, Wienbridgeand Family of Minimum Component Electronic Chaos Generators with Demonstrative Recurrence Plots. Chaos, Solitons & Fractals 1999; 10(8): 1399–1412, http://dx.doi.org/10.1016/S0960-0779(98)00109-X.
7. Franca LFP, Savi MA. Distinguishing Periodic and Chaotic Time Series Obtained from an Experimental Nonlinear Pendulum. Nonlinear Dynamics 2001; 26: 253–271, http://dx.doi.org/10.1023/A:1013029607482.
8. Franca LFP, Savi MA. Estimating Attractor Dimension on the Nonlinear Pendulum Time Series. Journal of the Brazilian Society of Mechanical Sciences 2001; 23(4): 427–439, http://dx.doi.org/10.1590/S0100-73862001000400004.
9. Fraser A, Swinney H. Independent coordinates for strange at- tractors from mutual information. Physical Review A 1986; 33(2): 1134–1140, http://dx.doi.org/10.1103/PhysRevA.33.1134.
10. Garc´ıa D, Trendafilova I. A multivariate data analysis approach towards vibration analysis and vibration-based damage assessment. Journal of Sound and Vibration 2014; 333(25): 7036–7050, http://dx.doi.org/10.1016/j.jsv.2014.08.014.
11. Giuliani A, Manetti C. Hidden peculiarities in the potential energy time series of a tripeptide highlighted by a recurrence plot analysis: A molecular dynamics simulation. Physical Review E 1996; 53(6): 6336–6340, http://dx.doi.org/10.1103/PhysRevE.53.6336.
12. Gradisek J, Grabec I, Siegert S, Friedrich R. Stochastic Dynamics of Metal Cutting: Bifurcation Phenomena in Turning. Mechanical Systems and Signal Processing 2002; 16(5): 831–840, http://dx.doi.org/10.1006/mssp.2001.1403.
13. Hinrichs N, Oestreich M, Popp K. Dynamics of Oscillators with Impact and Friction. Chaos Solitons and Fractals 1997; 8(4): 535–558, http://dx.doi.org/10.1016/S0960-0779(96)00121-X.
14. Ismail Z, Kuan KK, Yee KS, Chao OZ. Examining the trend in loss of flexural stiffness of simply supported RC beams with various crack severity using model updating. Measurement 2014; 50: 43–49, http://dx.doi.org/10.1016/j.measurement.2013.12.036.

15. Johnson MA, Moon FC. Nonlinear Techniques to Characterize Prechatter and Chatter Vibrations in the Machining of Metals. International Journal of Bifurcation and Chaos 2001; 2(11): 449–467, http://dx.doi.org/10.1142/S0218127401002171.
16. Kantz H, Schreiber T. Nonlinear Time Series Analysis. Cambridge University Press 1997.
17. Kecik K, Rusinek R, Warminski J. Stability Lobes Analysis of Nickel Superalloys Milling. International Journal of Bifurcation and Chaos 2011; 21(10): 1–12, http://dx.doi.org/10.1142/S0218127411030258.
18. Kennel M, Brown R, Abarbanel H. Determining embedding dimension for phase-space reconstruction using a geometrical construction. Physical Review A 1992; 45(6): 3403–3411.
20. Litak G, Rusinek R Dynamics of a stainless steel turning process by statistical and recurrence analyses. Meccanica 2012; 47(6): 1517–1526, http://dx.doi.org/10.1007/s11012-011-9534-x.
21. Litak G, Kaminski T, Rusinek R, Czarnigowski J, Wendeker M. Patterns in the combustion process in a spark ignition engine. Chaos Solitons and Fractals 2008; 35: 578–585, http://dx.doi.org/10.1016/j.chaos.2006.05.053.
22. Litak G, Syta A, Rusinek R. Dynamical changes during composite milling: recurrence and multiscale entropy analysis. International Journal of Advanced Manufacturing Technology 2011; 56(5-8): 445–453, http://dx.doi.org/10.1007/s00170-011-3195-8.
23. Manetti C, Giuliani A, Ceruso MA, Webber CL, Zbilut JP. Recurrence analysis of hydration effects on nonlinear protein dynamics: multiplicative scaling and additive processes. Physics Letters A 2001; 281(5- 6): 317–323.
24. Manoach E, Trendafilova I. Large amplitude vibrations and dam- age detection of rectangular plates. Journal of Sound and Vibration 2008; 315(3): 591–606, http://dx.doi.org/10.1016/j.jsv.2008.02.016.
25. Manoach E, Samborski S, Mitura A, Warminski J. Vibration based damage detection in composite beams under temperature variations using Poincar´e maps. International Journal of Mechanical Sciences 2012; 62(1): 120–132, http://dx.doi.org/10.1016/j.ijmecsci.2012.06.006.
26. Manoach E, Warminski J, Mitura A, Samborski S. Dynamics of a composite Timoshenko beam with delamination. Mechanics Research Communications 2012; 46: 47–53, http://dx.doi.org/10.1016/j.mechrescom.2012.08.008.
27. Manoach E, Warminski J, Mitura A, Samborski S. Dynamics of a laminated composite beam with delamination and inclusions. The European Physical Journal Special Topics 2013; 222(7): 1649–1664, http://dx.doi.org/10.1140/epjst/e2013-01952-6.
28. Marwan N, Thiel M, Nowaczyk NR. Cross recurrence plot based synchronization of time series. Nonlinear Processes in Geophysics 2002; 9: 325–331, http://dx.doi.org/10.5194/npg-9-325-2002.
29. Marwan N, Wessel N, Meyerfeldt U, Schirdewan A, Kurths J. Recurrence plot-based measures of complexity and their application to heart-rate-variability data. Physical Review E 2002; 66(2), http://dx.doi.org/10.1103/PhysRevE.66.026702.
30. Marwan N, Romano MC, Thiel M, Kurths J. Recurrence plots for the analysis of complex systems. Physics Reports 2007; 438: 237–329, http://dx.doi.org/10.1016/j.physrep.2006.11.001.
31. Muc A, Stawiarski A. Identification of damages in composite multilayered cylindrical panels with delaminations. Composite Structures 2012; 94(5): 1871–1879, http://dx.doi.org/10.1016/j.compstruct.2011.11.026.
32. Nayfeh AH, Balachandran B. Applied Nonlinear Dynamics - Analytical, Computational and Experimental Methods 1995. John Wiley & Sons, Inc., http://dx.doi.org/10.1002/9783527617548.
33. Nichols JM, Trickey ST, Seaver M. Damage detection using multi- variate recurrence quantification analysis. Mechanical Systems and Signal Processing 2006; 20(2): 421–437, http://dx.doi.org/10.1016/j.ymssp.2004.08.007.
34. Nichols JM, Trickey ST, Seaver M, Moniz L. Use of Fiber-optic Strain Sensors and Holder Exponents for Detecting and Localizing Dam- age in an Experimental Plate Structure. Journal of Intelligent Material Systems and Structures 2006; 18(1): 51–67, http://dx.doi.org/10.1177/1045389X06064354.
35. Nomura Y, Morimoto D, Kusaka T, Furuta H. Structural Damage Localization Based on Recurrence Plots of Chaotic Response Attractor. Transactions Of The Japan Society Of Mechanical Engineers Series C 2013; 79(807): 4210–4222, http://dx.doi.org/10.1299/kikaic.79.4210.
36. Piccoli H, Weber H. Experimental Observation of Chaotic Motion in a Rotor with Rubbing. Nonlinear Dynamics 1998; 16: 55–70, http://dx.doi.org/10.1023/A:1008284317724.
37. Poincare H. Introduction. Acta Mathematica 1890; 13(1): 5–7, http://dx.doi.org/10.1007/BF02392506.
38. Rusinek R. Cutting process of composite materials: An experimental study. International Journal of Non-Linear Mechanics 2010; 45: 458–462, http://dx.doi.org/10.1016/j.ijnonlinmec.2010.01.004.
39. Rusinek R. Vibrations In Cutting Process Of Titanium Alloy. Eksploatacja i Niezawodnosc - Maintenance and Reliability 2010; 3: 48–55.
40. Rusinek R, Warminski J. Attractor reconstruction of self-excited mechanical systems. Chaos Solitons and Fractals 2009; 40: 172–182, http://dx.doi.org/10.1016/j.chaos.2007.07.040.
41. Rusinek R, Szymanski M, Warminski J, Zadrozniak M, Morshed K Vibrations in the Human Middle Ear. Medical Science Monitor 2011; 17(12): 372–376, http://dx.doi.org/10.12659/MSM.882123.
42. Sato T, Tanaka Y. Minor Damage Detection Using Chaotic Excitation and Recurrence Analysis. Journal of Earthquake and Tsunami 2011; 05(03): 259–270, http://dx.doi.org/10.1142/S1793431111001054.
43. Sirivedin S, Fenner DN, Nath RB, Galiotis C. Effects of inter- fibre spacing and matrix cracks on stress amplification factors in carbon- fibre/epoxy matrix composites. Part I: planar array of fibres. Composites Part A: Applied Science and Manufacturing 2003; 34(12): 1227–1234, http://dx.doi.org/10.1016/S1359-835X(03)00252-5.
44. Sirivedin S, Fenner DN, Nath RB, Galiotis C. Effects of inter- fibre spacing and matrix cracks on stress amplification factors in carbon-fibre/epoxy matrix composites, Part II: Hexagonal array of fibres. Composites Part A: Applied Science and Manufacturing 2006; 37(11): 1936–1943, http://dx.doi.org/10.1016/j.compositesa.2005.12.022.
45. Takens F. Detecting Strange Attractors in Turbulence. Lecture Notes in Mathematics 1981; 898: 366–381, http://dx.doi.org/10.1007/BFb0091924.
46. Thomasson N, Hoeppner TJ, Webber CL, Zbilut JP. Recurrence quantification in epileptic EEGs. Physics Letters A 2001; 279(1-2): 94–101, http://dx.doi.org/10.1016/S0375-9601(00)00815-X.
47. Trendafilova I, van Brussel H. Non-linear dynamics tools for the motion analysis and condition monitoring of robot joints. Mechanical Systems and Signal Processing 2001; 15(6): 1141–1164, http://dx.doi.org/10.1006/mssp.2000.1394.

48. Trendafilova I, Manoach E. Vibration-based damage detection in plates by using time series analysis. Mechanical Systems and Signal Processing 2008; 22(5): 1092–1106, http://dx.doi.org/10.1016/j.ymssp.2007.11.020.
49. Yu A, Gupta V. Measurement of in situ fiber/matrix interface strength in graphite/epoxy composites. Composites Science and Technology 1998; 58(11): 1827–1837, http://dx.doi.org/10.1016/S0266-3538(98)00048-7.
50. Zahran O, Kasban H, El-Kordy M, El-Samie FA. Automatic weld defect identification from radiographic images. NDT & E International 2013; 57: 26–35, http://dx.doi.org/10.1016/j.ndteint.2012.11.005.
51. Zbilut JP, Koebbe M, Loeb H, Mayer-Kress G. Use of recurrence plots in the analysis of heart beat intervals. In: Computers in Cardiology, 1990: 263–266, http://dx.doi.org/10.1109/CIC.1990.144211.
52. Zolotova NV, Ponyavin DI. Phase asynchrony of the north- south sunspot activity. Astronomy and Astrophysics 2006; 449(1): L1–L4, http://dx.doi.org/10.1051/0004-6361:200600013.
53. Zou Y, Du D, Chang B, Ji L, Pan J. Automatic weld defect detection method based on Kalman filtering for real-time radio- graphic inspection of spiral pipe. NDT & E International 2015; 72: 1–9, http://dx.doi.org/10.1016/j.ndteint.2015.01.002.

Sylwester SAMBORSKI
Jakub WIECZORKIEWICZ
Rafal RUSINEK
Department of Applied Mechanics
Lublin University of Technology
ul. Nadbystrzycka 36, Lublin, 20-618, Poland

E-mail: s.samborski@pollub.pl, j.wieczorkiewicz@pollub.pl, r.rusinek@pollub.pl

INFORMATION FOR AUTHORS

Eksploatacja i Niezawodnosc – Maintenance and Reliability – the journal of the Polish Maintenance Society, under the scientific supervision of the Polish Academy of Sciences (Branch in Lublin), published four times a year.

The scope of the Quarterly

The quarterly *Eksploatacja i Niezawodnosc – Maintenance and Reliability* publishes articles containing original results of experimental research on the durability and reliability of technical objects. We also accept papers presenting theoretical analyses supported by physical interpretation of causes or ones that have been verified empirically. *Eksploatacja i Niezawodność – Maintenance and Reliability* also publishes articles on innovative modeling approaches and research methods regarding the durability and reliability of objects.

The following research areas are particularly relevant to the journal:

1. degradation processes of mechanical and biomechanical systems,
2. diagnosis and prognosis of operational malfunctions and failures.
3. analysis of failure risk/wear,
4. reliability-and-environmental-safety engineering in the design, manufacturing and maintenance of objects,
5. management and rationalization of object maintenance,
6. risk management in the processes of operation and maintenance,
7. the human factor and human reliability in operation and maintenance systems.

Terms and Conditions of Publication

The quarterly *Eksploatacja i Niezawodnosc – Maintenance and Reliability* publishes only original papers written in English or in Polish with an English translation. Translation into English is done by the Authors after they have received information from the Editorial Office about the outcome of the review process and have introduced the necessary modifications in accordance with the suggestions of the referees! Acceptance of papers for publication is based on two independent reviews commissioned by the Editor.

The quarterly *Eksploatacja i Niezawodnosc – Maintenance and Reliability* proceeds entirely online at submission.ein.org.pl

Technical requirements

- After receiving positive reviews and after acceptance of the paper for publication, the text must be submitted in a Microsoft Word document format.
- Drawings and photos should be additionally submitted in the form of high resolution separate graphical files in the TIFF, SVG, AI or JPG formats.
- A manuscript should include: names of authors, title, abstract, and key words that should complement the title and abstract (in Polish and in English), the text in Polish and in English with a clear division into sections (please, do not divide words in the text); tables, drawings, graphs, and photos included in the text should have descriptive two-language captions, if this can be avoided, no formulae and symbols should be inserted into text paragraphs by means of a formula editor; references (written in accordance with the required reference format); author data – first names and surnames along with scientific titles, affiliation, address, phone number, fax, and e-mail address.

The Editor reserves the right to abridge and adjust the manuscripts. All submissions should be accompanied by a submission form.

Detailed instructions to Authors, including evaluation criteria can be found on the journal's website: www.ein.org.pl

Editor contact info

Editorial Office of „Eksploatacja i Niezawodnosc - Maintenance and Reliability"
Nadbystrzycka 36, 20-618 Lublin, Poland
e-mail: office@ein.org.pl

INFORMATION FOR SUBSCRIBERS

Fees

Yearly subscription fee (four issues) is 100 zloty and includes delivery costs. Subscribers receive any additional special issues published during their year of subscription free of charge.

Orders

Subscription orders along with authorization to issue a VAT invoice without receiver's signature should be sent to the Editor's address.

Note

In accordance with the requirements of citation databases, proper citation of publications appearing in our Quarterly should include the full name of the journal in Polish and English without Polish diacritical marks, i.e.,

Eksploatacja i Niezawodnosc – Maintenance and Reliability.

Wydawca:
Polskie Naukowo Techniczne
Towarzystwo Eksploatacyjne
Warszawa

Publisher:
Polish Maintenance Society
Warsaw

Członek:
Europejskiej Federacji
Narodowych Towarzystw
Eksploatacyjnych

Member of:
European Federation of National
Maintenance Societies

Patronat naukowy:
Polska Akademia Nauk
Oddział Lublin

Scientific Supervision:
Polish Academy of Sciences
Branch in Lublin